STUDIES OF TWO–PHASE INTERMITTENT FLOW IN PIPE-LINES

by

Stephen Roy Davies

A thesis submitted for the fulfilment of the requirements
of the degree of Doctor of Philosophy of the
University of London and for the
Diploma of Membership of Imperial College.

Department of Chemical Engineering
and Chemical Technology
Imperial College of Science, Technology
and Medicine
London
England.

June 1992

1 BIBL LONDON UNIV

ABSTRACT

This thesis examines the characteristics of two–phase intermittent flow in pipelines. The overall aim of the research has been to use novel experimental methods to examine the details of intermittent flow and to compare the detailed (as well as the overall) phenomena with predictions.

The importance of pipeline geometry on intermittent characteristics is detailed; with experimental consideration of entrance geometry, pipe diameter, and small risers in the flowline. The importance of geometry on intermittent characteristics is shown to be significant, especially in the economically important case of terrain induced severe slugs.

Novel experimental techniques developed for, and critical analysis of, individual aspects of intermittent flow characteristics are presented. Models developed for representing the shedding process are explained, along with two experiments specifically addressed at these processes. Another important feature of intermittent flow is the entrapment of gas in the slug body. New visual evidence, obtained in the present work, indicates the mechanism of this process. In predicting intermittent flows, it is important to know the slug frequency. Usually, empirical correlations are used for this but, clearly, it would be better if the frequency could be predicted from a physical model. Previous attempts at a physical model are assessed and the interactions that determine slug frequency discussed.

The development of understanding of the mechanisms associated with multiphase flow depends on the design and construction of improved experimental facilities. This thesis describes the construction and commissioning of a multiphase flow facility (WASP), which formed a major part of the present work.

ACKNOWLEDGEMENTS

I would like to thank Professor G. F. Hewitt for his support and patience. In the present work I was encouraged by Professor G. F. Hewitt to experience a wide range of work activities, which have been of value beyond the scope of this work. In the above I was fortunate in having such a supervisor, but there is one aspect of Professor G. F. Hewitt which requires an explicit acknowledgement. He is renowned for his optimism and limitless enthusiasm for multiphase flow. These attributes I found inspiring. I thank him, by recommending any graduate who wishes to enter chemical engineering research to sample his enthusiasm and support.

A significant proportion of the present work was spent working with the excellent technical staff of the Department of Chemical Engineering, Imperial College. Thank you to: Pim Amrit, Peter Arnold, Malcom Dix, Ken Gurney, Terry Stephenson and Richard Wallington for their advice and work. Also, I would like to record a special thank you to Bob King, who made an indispensable contribution to the WASP project with his continuous flow of ideas and guidance.

I would like to thank Dr Lawrence Daniels for his support and patience.

I acknowledge the Underlying Research Programme of the United Kingdom Atomic Energy Authority for the financial support of the work described in this thesis.

TABLE OF CONTENTS

	PAGE
TITLE PAGE	1
ABSTRACT	2
ACKNOWLEDGEMENT	3
TABLE OF CONTENTS	4
LIST OF TABLES	7
LIST OF ILLUSTRATIONS	8
NOMENCLATURE	21
CHAPTER 1 INTRODUCTION	23
CHAPTER 2 THE INTERMITTENT FLOW REGIME	28
2.1 Intermittent Flow Description	29
2.1.1 Horizontal Flow	29
2.1.2 Vertical Flow	29
2.2 Mechanistic Models	32
2.2.1 Horizontal Flow	32
2.2.2 Vertical Flow	33
2.2.3 Inclined Flow	34
2.3 Aspects of Intermittent Flow	37
2.3.1 Propagation Velocity	37
2.3.2 Slug Frequency	41
2.3.3 Slug Region	43
2.3.4 Film/Elongated Region	47
2.3.5 Pressure Drop	50
2.4 Severe Slugging	62
2.4.1 The Mechanism	62
2.4.2 Experimental Studies	62

2.4.3 Theoretical Studies 64

CHAPTER 3 LOW PRESSURE RIG 74

3.1 Basic Equipment 74

3.2 Inlet Section 75

3.3 Pipe Exit 75

3.4 Flow Measurement 76

3.5 Instrumentation 87

3.5.1 Slug Detection 87

3.5.2 Pressure Measurement 90

3.5.3 Flow Visualisation 90

3.6 Data Capture 93

CHAPTER 4 PIPE GEOMETRY EFFECTS ON INTERMITTENT FLOW

4.1 Inlet Mixer Geometry 105

4.1.1 Experimental Method 108

4.1.2 Intermittent Characteristics 109

4.1.3 Stratified–Intermittent Flow 111

4.1.4 Flow Development 112

4.2 Large Diameter Pipe 130

4.2.1 Experimental Facility 130

4.2.2 Instrumentation 131

4.2.3 Results 132

4.3 Small Inclined Section 143

4.3.1 Experiment 143

4.3.2 Visual Observations 144

4.3.3 Slug Frequency 145

4.3.4 Slug Front Velocity 146

4.3.5 Stratified–Intermittent Transition 147

4.4 Terrain Induced Slugs 177

4.4.1 Transition to Severe Slugging 177

4.4.2 TRAC Code 179
4.4.3 Simulations of Schmidt et al (1979) Experiments 182
4.4.4 Simulations of Pots et al (1985) Experiments 187
CHAPTER 5 ASPECTS OF INTERMITTENT FLOW 201
5.1 Slug Tail 201
5.1.1 Tail Hydrodynamics 202
5.1.2 Tail Translational Velocity 209
5.1.3 Pushout Experiments 219
5.2 Slug Body Voidage 240
5.2.1 Experiment 240
5.2.2 Observations 240
5.3 Growth and Decay of Slug Units 249
5.3.1 Experiment 249
5.3.2 Translational Velocity 251
5.3.3 Growth and Decay 256
5.4 Prediction of Slug Frequency 273
5.4.1 Taitel and Dukler (1977) model 274
5.4.2 Slug Frequency Mechanism. 284
CHAPTER 6 HIGH PRESSURE MULTIPHASE FLOW RIG 304
6.1 WASP Facility 305
6.1.1 Facility Equipment 305
6.1.2 Control System and Instrumentation 308
6.1.3 Safety and Facility Documentation 310
6.2 Facility Commissioning 333
CHAPTER 7 CONCLUSION AND RECOMMENDATIONS 338
7.1 Pipeline Geometry 338
7.2 Aspects of Intermittent Flow 339
7.3 Fluid Property Effects 340
REFERENCES 342

LIST OF TABLES

	PAGE
Table 2.3.1 Literature C values.	39
Table 4.3.1 Ruder et al (1988) front criterion for the existence of a slug.	152
Table 4.4.1 Comparison of TRAC calculations with the experimental data and model predictions of Pots et al (1979).	188
Table 6.1.1 Hazard–target interactions pertinent to high pressure air–water experiments on the WASP facility.	329
Table 6.1.2 Attributes associated with why a hazard poses a threat to a target.	330
Table 6.1.3 Attributes associated with how a hazard poses a threat to a target.	331
Table 6.1.4 Attributes associated with where a hazard poses a threat to a target.	332

LIST OF ILLUSTRATIONS

	PAGE
Figure 1.1 Horizontal flow patterns	27
Figure 2.1.1 Horizontal Intermittent Flow	30
Figure 2.1.2 Vertical Intermittent Flow	31
Figure 2.2.1 Intermittent Flow Mechanistic Models	35
Figure 2.2.2 Fernandes (1983) Vertical Intermittent Flow Model	36
Figure 2.3.1 Slug Formation Process (Taitel and Dukler, 1977)	56
Figure 2.3.2 Velocity Distribution in Slug (Kvernvold et al, 1984)	57
Figure 2.3.3 Locus of Constant Slug Hold–up (Barnea and Brauner, 1985)	58
Figure 2.3.4 Velocity Distribution Behind Bubble (Moissis and Griffith, 1962)	59
Figure 2.3.5 Surge Flow (Coney, 1974)	60
Figure 2.3.6 Pressure drop components	61
Figure 2.4.1 Geometry of Riser–Pipe for Severe Slugging	70
Figure 2.4.2 Transition boundaries to severe slugging (Schmidt et al, 1985)	71
Figure 2.4.3 Voidage variation at the riser base (Bendiksen et al, 1982)	72
Figure 2.4.4 Pressure variation at the riser base (Bendiksen et al, 1982)	73
Figure 3.1.1 Schematic of the basic apparatus	78
Figure 3.1.2 Test section flanges	79
Figure 3.1.3 Rig supports	80

LIST OF ILLUSTRATIONS (CONTINUED)

	PAGE
Figure 3.2.1 a) Test section inlet	81
Figure 3.2.1 b) Test section inlet	82
Figure 3.2.2 Inlet section plates	83
Figure 3.3.1 Test section exit	84
Figure 3.4.1 Layout of Air Measurement	85
Figure 3.4.2 Air metering orifice plates	86
Figure 3.5.1 Optical probe principle of operation	95
Figure 3.5.2 Wire probe measurement of liquid height	96
Figure 3.5.3 Wire probe mounting arrangement	97
Figure 3.5.4 Wire probe electronic circuit	98
Figure 3.5.5 Typical wire probe response	99
Figure 3.5.6 Refraction of light beam at pipe–fluid interface	100
Figure 3.5.7 Flow visualisation section	101
Figure 3.6.1 Triangular test signal	102
Figure 3.6.2 Sine test signal	103
Figure 3.6.3 Square test signal	104
Figure 4.1.1 Test section configuration	113
Figure 4.1.2 Variation of slug frequency: Liquid superficial velocity of 0.14 m/s.	114
Figure 4.1.3 Variation of slug frequency: Liquid superficial velocity of 0.18 m/s.	114
Figure 4.1.4 Variation of slug frequency: Liquid superficial velocity of 0.255 m/s.	115
Figure 4.1.5 Variation of slug frequency: Liquid superficial velocity of 0.271 m/s.	115

LIST OF ILLUSTRATIONS (CONTINUED)

PAGE

Figure 4.1.6 Variation of slug frequency: 116

Liquid superficial velocity of 0.32 m/s.

Figure 4.1.7 Variation of slug frequency: 116

Liquid superficial velocity of 0.391 m/s.

Figure 4.1.8 Variation of slug frequency: 117

Liquid superficial velocity of 0.455 m/s.

Figure 4.1.9 Variation of slug frequency: 117

Liquid superficial velocity of 0.52 m/s.

Figure 4.1.10 Variation of slug front velocity: 118

Liquid superficial velocity of 0.14 m/s. (Downstream probe pair)

Figure 4.1.11 Variation of slug front velocity: 118

Liquid superficial velocity of 0.18 m/s. (Downstream probe pair)

Figure 4.1.12 Variation of slug front velocity: 119

Liquid superficial velocity of 0.255 m/s. (Downstream probe pair)

Figure 4.1.13 Variation of slug front velocity: 119

Liquid superficial velocity of 0.271 m/s. (Downstream probe pair)

Figure 4.1.14 Variation of slug front velocity: 120

Liquid superficial velocity of 0.32 m/s. (Downstream probe pair)

Figure 4.1.15 Variation of slug front velocity: 120

Liquid superficial velocity of 0.391 m/s. (Downstream probe pair)

Figure 4.1.16 Variation of slug front velocity: 121

Liquid superficial velocity of 0.455 m/s. (Downstream probe pair)

Figure 4.1.17 Variation of slug front velocity: 121

Liquid superficial velocity of 0.52 m/s. (Downstream probe pair)

Figure 4.1.18 Variation of slug front velocity: 122

Liquid superficial velocity of 0.14 m/s. (Upstream probe pair)

LIST OF ILLUSTRATIONS (CONTINUED)

PAGE

Figure 4.1.19 Variation of slug front velocity: 122

Liquid superficial velocity of 0.18 m/s. (Upstream probe pair)

Figure 4.1.20 Variation of slug front velocity: 123

Liquid superficial velocity of 0.255 m/s. (Upstream probe pair)

Figure 4.1.21 Variation of slug front velocity: 123

Liquid superficial velocity of 0.271 m/s. (Upstream probe pair)

Figure 4.1.22 Variation of slug front velocity: 124

Liquid superficial velocity of 0.32 m/s. (Upstream probe pair)

Figure 4.1.23 Variation of slug front velocity: 124

Liquid superficial velocity of 0.391 m/s. (Upstream probe pair)

Figure 4.1.24 Variation of slug front velocity: 125

Liquid superficial velocity of 0.455 m/s. (Upstream probe pair)

Figure 4.1.25 Variation of slug front velocity: 125

Liquid superficial velocity of 0.52 m/s. (Upstream probe pair)

Figure 4.1.26 Experimental survey of the transition 126

from the stratified to intermittent flow regime.

Figure 4.1.27 Distribution of time between slugs. 127

U_{LS} = 0.271 m/s, U_{GS} = 1.44 m/s.

Figure 4.1.28 Distribution of time between slugs. 128

U_{LS} = 0.271 m/s, U_{GS} = 0.639 m/s.

Figure 4.1.29 Distribution of time between slugs. 129

U_{LS} = 0.255 m/s, U_{GS} = 1.844 m/s.

Figure 4.2.1 Harwell Laboratory 150mm Test Pipeline. 136

Figure 4.2.2 Original Air–Water Mixer. 137

Figure 4.2.3 Mixer Insert. 138

Figure 4.2.4 Stratified to Intermittent Transition Data 139

(Harwell 150 mm Facility)

LIST OF ILLUSTRATIONS (CONTINUED)

PAGE

Figure 4.2.5 Slug frequency data comparison with Gregory and Scott (1969) correlation (D=0.035 m and 0.019 m) 140

Figure 4.2.6 Slug frequency data comparison with Gregory and Scott (1969) correlation (D=0.15 m) 141

Figure 4.2.7 Shedding Factor Data 142

Figure 4.3.1 Test section configuration 154

Figure 4.3.2 Installed inclined pipe section 155

Figure 4.3.3 Slug frequency at 3rd wire probe position U_{LS} = 0.14 m/s. 156

Figure 4.3.4 Slug frequency at 3rd wire probe position U_{LS} = 0.18 m/s. 156

Figure 4.3.5 Slug frequency at 3rd wire probe position U_{LS} = 0.255 m/s. 157

Figure 4.3.6 Slug frequency at 3rd wire probe position U_{LS} = 0.271 m/s. 157

Figure 4.3.7 Slug frequency at 3rd wire probe position U_{LS} = 0.32 m/s. 158

Figure 4.3.8 Slug frequency at 3rd wire probe position U_{LS} = 0.391 m/s. 158

Figure 4.3.9 Slug frequency at 3rd wire probe position U_{LS} = 0.455 m/s. 159

Figure 4.3.10 Slug frequency at 3rd wire probe position U_{LS} = 0.52 m/s. 159

Figure 4.3.11 Slug frequency at 3rd wire probe position and lower pipe for riser configuration. U_{LS} = 0.14 m/s. 160

LIST OF ILLUSTRATIONS (CONTINUED)

PAGE

Figure 4.3.12 Slug frequency at 3rd wire probe position and lower pipe for riser configuration. $U_{LS} = 0.18$ m/s. 160

Figure 4.3.13 Slug frequency at 3rd wire probe position and lower pipe for riser configuration. $U_{LS} = 0.255$ m/s. 161

Figure 4.3.14 Slug frequency at 3rd wire probe position and lower pipe for riser configuration. $U_{LS} = 0.271$ m/s. 161

Figure 4.3.15 Slug frequency at 3rd wire probe position and lower pipe for riser configuration. $U_{LS} = 0.32$ m/s. 162

Figure 4.3.16 Slug frequency at 3rd wire probe position and lower pipe for riser configuration. $U_{LS} = 0.391$ m/s. 162

Figure 4.3.17 Slug frequency at 3rd wire probe position and lower pipe for riser configuration. $U_{LS} = 0.455$ m/s. 163

Figure 4.3.18 Slug frequency at 3rd wire probe position and lower pipe for riser configuration. $U_{LS} = 0.52$ m/s. 163

Figure 4.3.19 Slug front velocity at upstream measurement location. $U_{LS} = 0.14$ m/s. 164

Figure 4.3.20 Slug front velocity at upstream measurement location. $U_{LS} = 0.18$ m/s. 164

Figure 4.3.21 Slug front velocity at upstream measurement location. $U_{LS} = 0.255$ m/s. 165

Figure 4.3.22 Slug front velocity at upstream measurement location. $U_{LS} = 0.271$ m/s. 165

Figure 4.3.23 Slug front velocity at upstream measurement location. $U_{LS} = 0.32$ m/s. 166

Figure 4.3.24 Slug front velocity at upstream measurement location. $U_{LS} = 0.391$ m/s. 166

LIST OF ILLUSTRATIONS (CONTINUED)

PAGE

Figure 4.3.25 Slug front velocity at upstream measurement location. U_{LS} = 0.455 m/s. 167

Figure 4.3.26 Slug front velocity at upstream measurement location. U_{LS} = 0.52 m/s. 167

Figure 4.3.27 Slug front velocity at downstream measurement location. U_{LS} = 0.14 m/s. 168

Figure 4.3.28 Slug front velocity at downstream measurement location. U_{LS} = 0.18 m/s. 168

Figure 4.3.29 Slug front velocity at downstream measurement location. U_{LS} = 0.255 m/s. 169

Figure 4.3.30 Slug front velocity at downstream measurement location. U_{LS} = 0.271 m/s. 169

Figure 4.3.31 Slug front velocity at downstream measurement location. U_{LS} = 0.32 m/s. 170

Figure 4.3.32 Slug front velocity at downstream measurement location. U_{LS} = 0.391 m/s. 170

Figure 4.3.33 Slug front velocity at downstream measurement location. U_{LS} = 0.455 m/s. 171

Figure 4.3.34 Slug front velocity at downstream measurement location. U_{LS} = 0.52 m/s. 171

Figure 4.3.35 Experimental stratified to intermittent transition for the riser and horizontal configurations. 172

Figure 4.3.36 Upstream distance required for exit effects to be no longer operative. 173

Figure 4.3.37 Minimum liquid film height for stable slug (74mm diameter pipe). 174

LIST OF ILLUSTRATIONS (CONTINUED)

PAGE

Figure 4.3.38 Minimum liquid superficial velocity for stable slug (74 mm diameter pipe) 175

Figure 4.3.39 Liquid superficial velocity limit for slug front criterion (74 mm diameter pipe). 176

Figure 4.4.1 Geometry of the Schmidt et al experiment 190

Figure 4.4.2 TRAC voidage prediction of Schmidt et al (1979) experiments. 191

Figure 4.4.3 TRAC voidage prediction of Schmidt et al (1979) experiments. Sensitivity to cell length. 192

Figure 4.4.4 TRAC voidage prediction of Schmidt et al (1979) experiments. Sensitivity to maximum allowable time step. 193

Figure 4.4.5 Voidage vs time at riser base. 194

U_{GS}=0.97 m/s, U_{LS} =0.34 m/s.

Figure 4.4.6 Pressure vs time at riser base. 194

U_{GS}=0.97 m/s, U_{LS} =0.34 m/s.

Figure 4.4.7 Voidage vs time at riser top. 195

U_{GS}=0.97 m/s, U_{LS} =0.34 m/s.

Figure 4.4.8 Pressure vs time at riser top. 195

U_{GS}=0.97 m/s, U_{LS} =0.34 m/s.

Figure 4.4.9 Voidage along test section. 196

U_{GS}=0.97 m/s, U_{LS} =0.34 m/s.

Figure 4.4.10 Voidage vs time at riser base. 196

U_{GS}=0.18 m/s, U_{LS} =0.34 m/s.

Figure 4.4.11 Pressure vs time at riser base. 197

U_{GS}=0.18 m/s, U_{LS} =0.34 m/s.

LIST OF ILLUSTRATIONS (CONTINUED)

PAGE

Figure 4.4.12 Voidage along test section. Time=206 s. 197

U_{GS}=0.18 m/s, U_{LS} =0.34 m/s.

Figure 4.4.13 Voidage along test section. Time=314 s. 198

U_{GS}=0.18 m/s, U_{LS} =0.34 m/s.

Figure 4.4.14 Voidage along test section. Time=330 s. 198

U_{GS}=0.18 m/s, U_{LS} =0.34 m/s.

Figure 4.4.15 Voidage vs time at riser base. U_{GS}=3.4 m/s, U_{LS} =0.34 m/s. 199

Figure 4.4.16 Pressure vs time at riser base. U_{GS}=3.4 m/s, U_{LS} =0.34 m/s. 199

Figure 4.4.17 Voidage vs time at riser top. U_{GS}=3.4 m/s, U_{LS} =0.34 m/s. 200

Figure 4.4.18 Pressure vs time at riser top. U_{GS}=3.4 m/s, U_{LS} =0.34 m/s. 200

Figure 5.1.1 Forces acting on a slug tail (moving co–ordinates). 223

Figure 5.1.2 Definition of y co–ordinate for a circular pipe geometry. 223

Figure 5.1.3 Effect on slug front translational velocity of interfacial shear 224
in slug tail hydrodynamic model.

Figure 5.1.4 Experimental slug tail profile 225

(U_{LS}=0.248 m/s, U_{GS}=2.23 m/s, Frame 5276)

Figure 5.1.5 Experimental slug tail profile 225

U_{LS}=0.295m/s, U_{GS}=1.84 m/s, Frame 134842)

Figure 5.1.6 Representation of characteristics of Equation 5.1.26. 226

Figure 5.1.7 Definition of flow quantities relative to y co–ordinate 227
for a circular pipe geometry.

Figure 5.1.8 Variation of interfacial height calculated from Equation 5.1.44 228
with axial and radial distance

Figure 5.1.9 Slug tail leading point height as a function 229
of boundary layer thickness in the slug body

LIST OF ILLUSTRATIONS (CONTINUED)

PAGE

Figure 5.1.10 Velocity of the leading point of the slug tail as a function of boundary layer thickness for various pipe diameters. 230

Figure 5.1.11 Variation of the leading point velocity with boundary layer thickness for pipe diameter of 0.0762 m. 231

Figure 5.1.12 Variation of the leading point velocity with boundary layer thickness for pipe diameter of 0.1524 m. 232

Figure 5.1.13 Variation of the leading point velocity with boundary layer thickness for pipe diameter of 0.2286 m. 233

Figure 5.1.14 Variation of the leading point velocity with boundary layer thickness for pipe diameter of 0.3048 m. 234

Figure 5.1.15 Variation of the leading point velocity with boundary layer thickness for pipe diameter of 0.381 m. 235

Figure 5.1.16 Test section configuration. 236

Figure 5.1.17 Interface translational velocity as a function of gas superficial velocity. 237

Figure 5.1.18 Pressure and wire probe signal for a gas superficial velocity of 2.8 m/s. 238

Figure 5.1.19 Comparison of experimental interface shedding rate with various slug tail models. 239

Figure 5.2.1 One cycle of the gas entrapment process 243

Figure 5.2.2 Three cycles of the gas entrapment process 245

Figure 5.2.3 Slug front gas entrapment. 6m from test section inlet. 248

Figure 5.3.1 Slug generator on test section. 258

Figure 5.3.2 Operation of slug generator. 259

Figure 5.3.3 Test section configuration. 260

Figure 5.3.4 Artificial slug experimental method. 261

LIST OF ILLUSTRATIONS (CONTINUED)

PAGE

Figure 5.3.5 Slug front translational velocity as a function of gas superficial velocity. 262

Figure 5.3.6 Slug front translational velocity as a function of gas superficial velocity. 263

Figure 5.3.7 Slug tail translational velocity as a function of gas superficial velocity. 264

Figure 5.3.8 Slug tail translational velocity as a function of gas superficial velocity. 265

Figure 5.3.9 Comparison of slug tail and slug front translational velocities for h/D=0.135. 266

Figure 5.3.10 Comparison of slug tail and slug front translational velocities for h/D=0.203. 267

Figure 5.3.11 Comparison of slug tail and slug front translational velocities for h/D=0.270. 268

Figure 5.3.12 Comparison of slug tail and slug front translational velocities for h/D=0.324. 269

Figure 5.3.13 Comparison of slug tail and slug front translational velocities for h/D=0.378. 270

Figure 5.3.14 Comparison of slug tail and slug front translational velocities for h/D=0.473 271

Figure 5.3.15 Comparison of slug tail and slug front translational velocities for h/D=0.554. 272

Figure 5.4.1 Process of slug formation (Taitel and Dukler, 1977) 290

Figure 5.4.2 Slug Initiation (U_{Gs}= 1.84 m/s, U_{Ls}= 0.295 m/s) 291

Figure 5.4.3 Slug Initiation (U_{Gs}= 1.01 m/s, U_{Ls}= 0.411 m/s) 293

Figure 5.4.4 Slug Initiation (U_{Gs}= 1.93 m/s, U_{Ls}= 0.248 m/s) 295

LIST OF ILLUSTRATIONS (CONTINUED)

PAGE

Figure 5.4.5 Slug Initiation (U_{Gs}= 2.91 m/s, U_{Ls}= 0.209 m/s) 298

Figure 5.4.6 Nomenclature for location in t–x plane. 279

Figure 5.4.7 Liquid rebuild profile for Taitel and Dukler (1977) problem. 297

Figure 5.4.8 Variation of slug frequency with time step 298

Figure 5.4.9 Bernoulli term variation along liquid profile. 299

Figure 5.4.10 Sensitivity of slug frequency to stability level. 300

Figure 5.4.11 Variation of equilibrium stratified liquid height with the ratio of interfacial friction factor to gas friction factor. 301

Figure 5.4.12 Sensitivity of slug frequency to the ratio of interfacial friction factor to gas friction factor. 302

Figure 5.4.13 Proposed mechanism for slug initiation frequency. 303

Figure 6.1.1 Calculated time limit on an experimental run for a given pressure and gas flowrate. 316

Figure 6.1.2 Calculated time limit on an experimental run for a given liquid flowrate. 317

Figure 6.1.3 Basic schematic of WASP facility. 318

Figure 6.1.4 View of high pressure air storage tanks and WASP facility test section. 319

Figure 6.1.5 View of test section from the inlet section towards the outlet control hut and dump tank. Other pipes shown are the air supply pipes and liquid return line from the dump tank. 320

Figure 6.1.6 View of oil and water storage tanks at inlet end of the facility, with air control valve located on air supply pipe. 321

Figure 6.1.7 View of inlet mixer located at the inlet to the test section. 322

LIST OF ILLUSTRATIONS (CONTINUED)

PAGE

Figure 6.1.8 View of water storage tank, water flow control valve and magflow meter, and pump in its weather–proof box. Box on brick wall contains control solenoid valves for the rig. 323

Figure 6.1.9 View of air outlet (with silencer) and test section entrance to the facility control hut. 324

Figure 6.1.10 View of the slug catcher/ air–liquid separator located on the top floor of the control hut. 325

Figure 6.1.11 View of visualisation section (in containment box) located on the top floor of the control hut. 326

Figure 6.1.12 View of computer display of facility control system located on ground floor of the control hut. 327

Figure 6.1.13 Visualisation section. 328

Figure 6.2.1 Sample signals from water metering system. 335

Figure 6.2.2 Sample signals from air metering system. 336

Figure 6.2.3 Flow regime data of Mendes–Tatsis et al (1992) 337

NOMENCLATURE

A – cross–sectional area, m/s

D – pipe diameter, m

Fr – Froude number

f – frequency, Hz

f – friction factor

g – nominal gravitational acceleration at the earths surface, m/s^2

h – liquid height, m

l – length, m

p – pressure, Pa

Re – Reynolds number

S – perimeter, m

t – time, s

u,v – velocity, m/s

U,V –velocity, m/s

w – conduit width, m

x – co–ordinate in the axial direction, m

y – co–ordinate in the vertical direction perpendicular to the pipe axis, m

z – co–ordinate in the horizontal direction perpendicular to the pipe axis, m

Greek Letters

α – conduit inclination angle

λ – characteristic value

μ – viscosity, kg/m–s

ν – kinematic viscosity, m^2/s

ρ – density, kg/m^3

σ – surface tension, N/m

τ – shear stress, N/m^2

Subscripts

a – acceleration

b – elongated bubble

f – film

G – gas

i – interfacial, counter

j – counter

L– liquid

m – mixture

s – slug

S – superficial

su – slug unit

TP – two–phase

w – wall

Superscripts

. – rate of change with time

CHAPTER ONE
INTRODUCTION

This thesis is concerned with two–phase gas–liquid flow in horizontal tubes. Such a flow is an example of a multiphase (as distinct from a single phase) flow. Intensive research effort over the last 50 years has taken place into the characteristics of multiphase flow reflecting their considerable industrial importance.

Typical applications in which multiphase flow occurs are found in the nuclear, chemical and oil industries. Example applications are the large sub–sea pipelines that transfer gas and oil from wells to platforms, steam–water flows following postulated accidents in pressurised water reactors, and pneumatic conveyance of granular solids. Of all the types of multiphase flow found in industry the most common and complex are those involving the flows of a gas with one or more liquids.

The basis of any research study is the classification of the subject. Conjoint flow of gas and liquid(s) is often classified according to the geometry of the gas/liquid interface(s) and, if there is more than one liquid phase, the liquid–liquid interface. Each geometry is called a "flow regime" or "flow pattern". The classes of interface geometry that exist depend on the gas and liquid(s) flow rates, physical properties of the fluids and the channel geometry and orientation.

The idealised flow regimes identified for horizontal two–phase gas–liquid flow (the case studied in the work described in this thesis) are depicted in Figure 1.1. The various authors label the flow regimes using different terminology. The flow regimes identified in Figure 1.1 follow the classification of Taitel and Dukler (1976). In bubble flow the gas flows as discrete bubbles in a liquid continuum with the bubble density greater at the top of the pipe. Stratified flow is the complete separation of the gas and the liquid with the liquid flowing at the bottom and the gas on the top. The stratified regime is subdivided into the smooth regime for which the interface is smooth and the stratified wavy regime with an interfacial wave structure. Increasing the gas flow while in the stratified wavy regime increases the size of interfacial disturbances until a disturbance blocks the pipe. The blockage propagates down the pipeline as a "slug" of liquid which

may or may not contain a dispersion of gas bubbles. This regime is known as intermittent flow. On further increase of the gas velocity the gas phase forms a continuous core and the flow is defined as "annular". Here the gas core flowing through the centre of the pipe is surrounded by a liquid film on the circumference of the pipe. The liquid film is thicker at the bottom than at the top due to the effect of gravity.

The intermittent flow regime is the subject of the present work. The irregular liquid loading and pressure variations inherent in the intermittent flow regime pose control problems for operators of process plant. Designers of liquid–gas separation vessels need to be able to predict the "design" slug length for sizing the vessel. In response to these problems research into gas–liquid intermittent flow has concentrated on prediction of pressure drop, length and frequency of the intermittent flow regime units. The present work continues this research with the following general objectives:

1. Pipe geometry effects To investigate the effect of entrance geometry and pipe topography on intermittent flow characteristics and on the stratified–intermittent transition boundary.

2. Aspects of intermittent flow To develop novel experimental and theoretical approaches to individual aspects of intermittent flow.

3. Fluid property effects To study the effect of pressure and liquid properties on intermittent flow characteristics and the stratified–intermittent flow transition.

The experimental part of the present work was carried out on three flow rigs as follows:

1. A low pressure air–water flow rig at Imperial College, designed and constructed to enable development of experimental techniques for the WASP facility experimental programme.

2. A large scale flow facility at the Harwell Laboratory in which experiments could be carried out with tubes of larger diameter and length.

3. A new high pressure multiphase facility (WASP) constructed at Imperial College and capable of operating with multiple phases at pressures up to 50 bar gauge.

The thesis continues with a literature survey on intermittent flow (Chapter 2) and is followed by a description of the Imperial College low pressure facility (Chapter 3). Observations on intermittent flow using that facility are described in Chapter 4 and 5, and similar work on the Harwell Facility is described in Chapter 4. Chapter 4 concentrates on the effect of pipeline geometry on intermittent flow characteristics; with experimental consideration of entrance geometry, pipe diameter, and small risers in the flowline. Under certain circumstances, intermittent flow units can form due to liquid accumulation at changes in pipe inclination from the horizontal. Such "terrain induced" flow is discussed in Chapter 4, where the development and testing of computer models for this kind of intermittent flow are described.

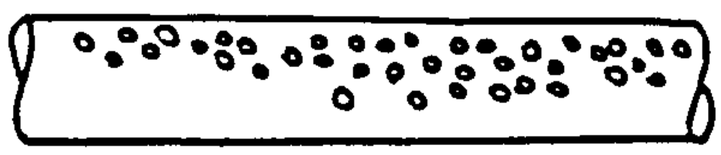
Novel experimental techniques developed for, and critical analysis of, individual aspects of intermittent flow characteristics are dealt with in Chapter 5. In intermittent flow, the slug gathers liquid from the film region ahead of it and sheds liquid from its tail. If the pick-up rate exceeds the shedding rate, then the slug grows. Models developed for representing the shedding process are presented, along with two experiments specifically addressed at these processes. Another important feature of intermittent flow is the entrapment of gas in the slug body. Chapter 5 describes new visual evidence, obtained in the present work, which indicates the mechanism of this process. In predicting intermittent flows, it is important to know the slug frequency. Usually, empirical correlations are used for this but, clearly, it would be better if the frequency could be predicted from a physical model. Previous attempts at a physical model are assessed and an algorithm for a new model presented.

The penultimate Chapter in the thesis (Chapter 6) describes the construction and commissioning of a multiphase flow facility (WASP), which formed a major part of the present work. The proposed experimental programme for the work on intermittent flow is presented. Chapter 7 completes the thesis with a summary of the conclusions of the present work and recommendations for future research in intermittent flow.

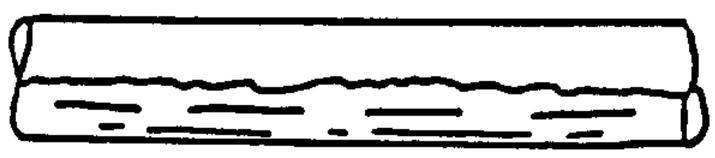
Flow direction

→

Bubble flow



Stratified flow



Intermittent flow



Annular flow

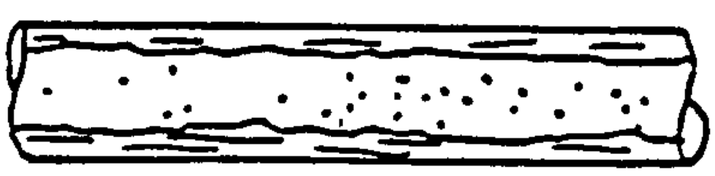


Figure 1.1: Flow regimes in horizontal two–phase gas–liquid flow.

CHAPTER TWO
THE INTERMITTENT FLOW REGIME

Over the past thirty years a number of workers have studied the intermittent flow regime with the objective of understanding the mechanisms involved, and to provide more accurate predictive methods. This Chapter summarises in general the major studies of the intermittent flow regime; the literature on individual flow characteristics is considered in more detail in later chapters.

In the literature two sub classes of the intermittent flow regime , namely "slug" and "plug" flow, are often considered. Criteria for the transition between these sub–classes have been proposed by Barnea et al (1980) and Govier et al (1962). The plug flow pattern is defined by Barnea et al (1980) to be the limiting case of slug flow when the liquid slug is free of entrained gas bubbles. Govier et al (1962) classified the flow regime according to the interface configuration in the gas cavity. Other authors use the term plug and slug interchangeably. In general, it is to be noted that different authors on the subject use different terminology to describe the same phenomena. In this thesis, for both horizontal and vertical conduits, the term "intermittent flow" will be used to describe the whole regime; an "intermittent flow unit" will be defined as consisting of a slug plus an elongated gas bubble with its associated film region. When it is important that the distinction between an aerated and non–aerated slug be made, voidage will be specified.

Section 2.1 defines the intermittent flow regime and Sections 2.2 and 2.3 review literature on phenomological characteristics. Although this thesis is mainly concerned with intermittent flow in horizontal pipelines, vertical intermittent flow is also considered for completeness. The literature on the associated phenomena of terrain–induced "severe slugging" is reviewed in Section 2.4.

2.1 INTERMITTENT FLOW DESCRIPTION

2.1.1 HORIZONTAL FLOW

The horizontal flow pattern is depicted in Figure 2.1.1. We may define an intermittent flow unit of length l_{IU}, which consists of an elongated bubble of length l_b and a liquid slug/plug of length l_s :

$$l_{IU} = l_b + l_s \tag{2.1.1}$$

The elongated bubble interacts with a film of liquid, which is shed from the back of the liquid slug. Depending on the flow conditions, the liquid slug may contain a dispersion of small gas bubbles; here, gas is entrained in the mixing region between the slug and film, and lost at the back of the liquid slug to the elongated bubble. At high gas flow-rates the mixing effect can produce a "frothy" slug.

2.1.2 VERTICAL FLOW

In vertical flow, the flow pattern is as depicted in Figure 2.1.2. Once again a slug unit of length l_{IU} consists of an large bubble of length l_b and a liquid slug/plug of length l_s:

$$l_{IU} = l_b + l_s \tag{2.1.2}$$

The cross–section of the large bubble is nearly the same as that of the pipe or duct and it is surrounded by a film which is shed from the bottom of the liquid slug. Depending on the flow conditions, the liquid slug may contain a dispersion of small gas bubbles. These small bubbles are entrained at the bottom of the large bubble by the mixing process caused by the film entering the liquid slug. Coalescence of these small bubbles then occurs at the front of the next large bubble. In both horizontal and vertical flow one observes trains of intermittent flow units of different lengths, with growth, decay and coalescence of the units taking place in the entry region.

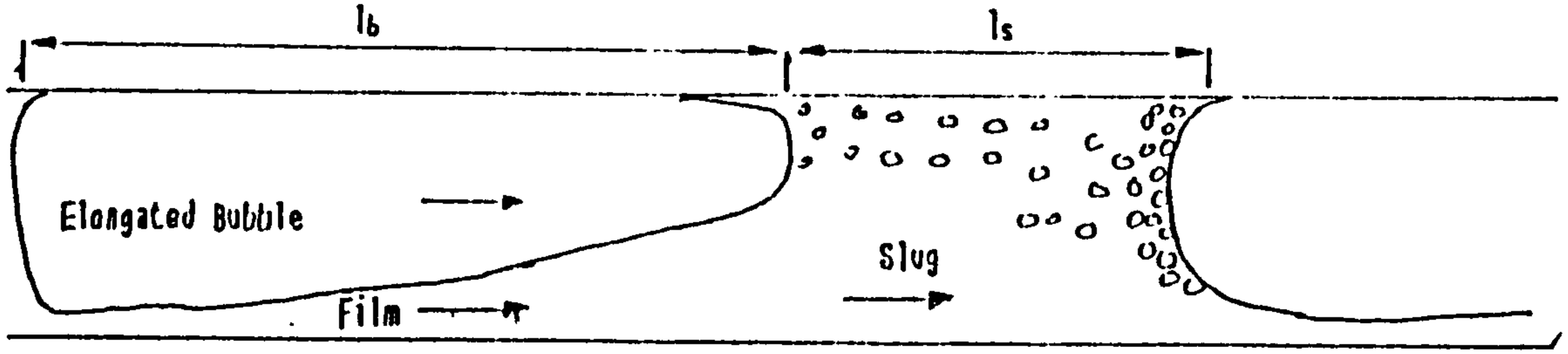


Figure 2.1.1 Horizontal Intermittent Flow.

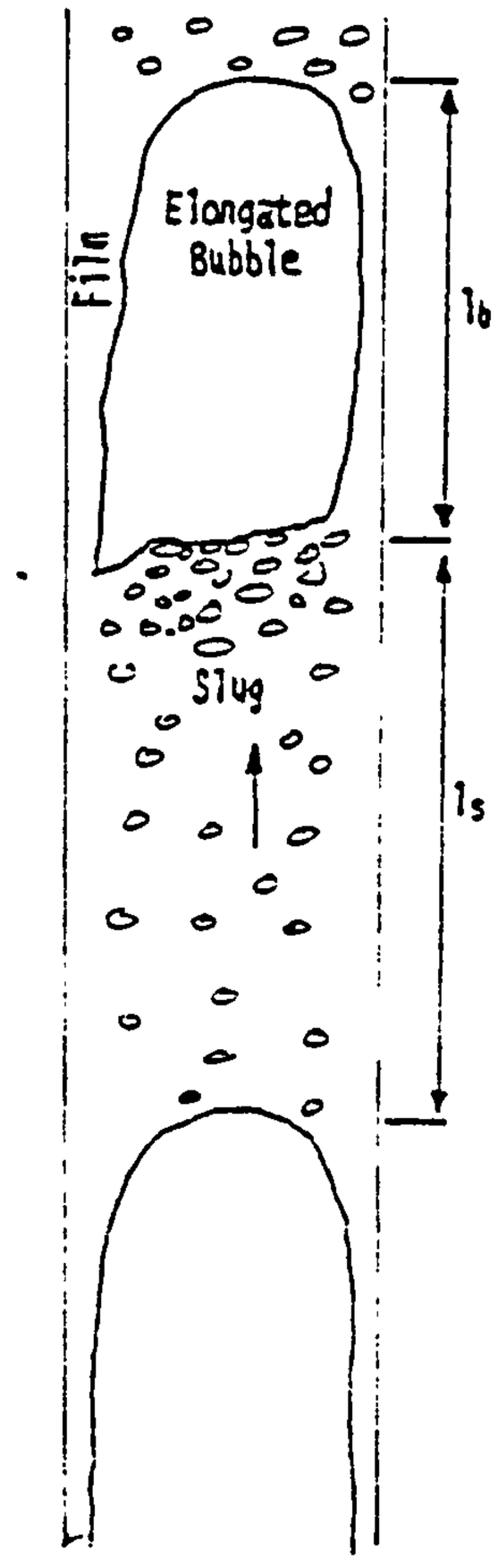


Figure 2.1.2 Vertical Intermittent Flow.

2.2 MECHANISTIC MODELS

This section provides an overview of the mechanistic models developed to represent intermittent flow.

2.2.1 HORIZONTAL FLOW

Figure 2.2.1 provides a pictorial representation of some of the models available for horizontal intermittent flow.

A simple model of intermittent flow was that developed by Kordyban (1961). The model considers a pure liquid slug which "skates" over the film, at the gas velocity without interacting with the film. The pressure drop over the slug unit was calculated taking into account only the shear stress in the slug region. The model has the obvious limitations of assuming the slug to have no entrained gas bubbles and neglecting the force needed to accelerate the liquid film to the slug velocity.

The acceleration of the film was taken into account, albeit by using experimental data, in the work of Vermeulen and Ryan (1971). Once again the slug was assumed to be pure liquid with the total holdup being calculated using the Lockhart and Martinelli correlation. In order to determine the total pressure over a given pipe length, an empirical determination of the slug frequency is required with this model.

Theoretical account was taken of the acceleration of the film by Dukler and Hubbard (1975). The force required to accelerate the liquid film to the slug velocity was considered to contribute an accelerational component to the pressure drop even in steady state incompressible flow. In this model the frictional pressure drop was calculated using the similarity analysis for two–phase frictional pressure drop developed by Dukler et al (1964). Whilst the analysis of Dukler and Hubbard (1975) can give details of all aspects of the intermittent flow unit structure, it still requires the slug frequency and holdup to be specified for given superficial gas and liquid velocities.

The above models consider the flow in the slug body to be equivalent to fully developed pipe flow. Maron et al (1982) considered a continuous destruction of a boundary layer in the mixing region, followed by a recovery process at the back of this region. It was

also assumed that the buoyancy forces were greater than the turbulence effect on the gas bubbles in the slug body. Hence if the gas void fraction,ε_{Gs}, in the slug body is greater than zero, due to the entrainment of bubbles, coalescence of these bubbles occurs at the top wall. Using this model and considering a train of slugs accelerating and decelerating led Maron et al (1982) to suggest that there exists a frequency range for flow stability.

All of the above models require slug frequency to be specified. In order to attain the desired goal of a closed mechanistic model, a non–empirical method of calculating the frequency is needed and Taitel and Dukler (1977) suggested such a method. They assumed that the slug frequency is the reciprocal of the time taken for the stratified layer to reach its equilibrium level, after a slug is formed.

In developed intermittent flow, frequency and intermittent flow unit length are interconnected properties. An attempt was made by Dukler et al (1985) to obtain the minimum stable slug length. The concept of destruction of the boundary layer in the mixing region and reformation of the boundary layer after it , was used. The minimum stable slug length being postulated as the length required for establishing a full velocity profile.

A non–empirical method of calculating the slug holdup is also required for a closed mechanistic model. Barnea and Brauner (1985) related holdup to the gas and liquid superficial velocities by considering the slug body to have a holdup corresponding to the upper limit of dispersed bubble flow at the given total superficial velocity. Although this model for slug voidage is independent of the predictions of all other slug characteristics, it requires a suitable model for the transition from dispersed bubble flow to intermittent flow.

2.2.2 VERTICAL FLOW

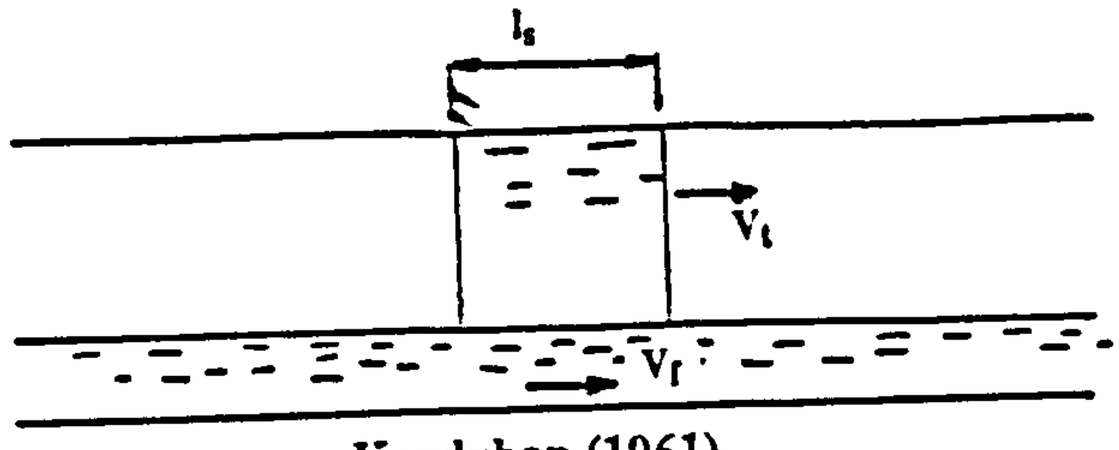
In the 1960s, work was carried out on vertical slug flow, based on the results of Dumitresu (1943) and Davies and Taylor (1950), who considered the rise of bubbles in vertical tubes containing stationary liquids. Griffith and Wallis (1961) derived expressions

for average fluid density and elongated bubble length; and Nicklin et al (1962) obtained expressions for the rise velocity of elongated bubbles in moving streams.

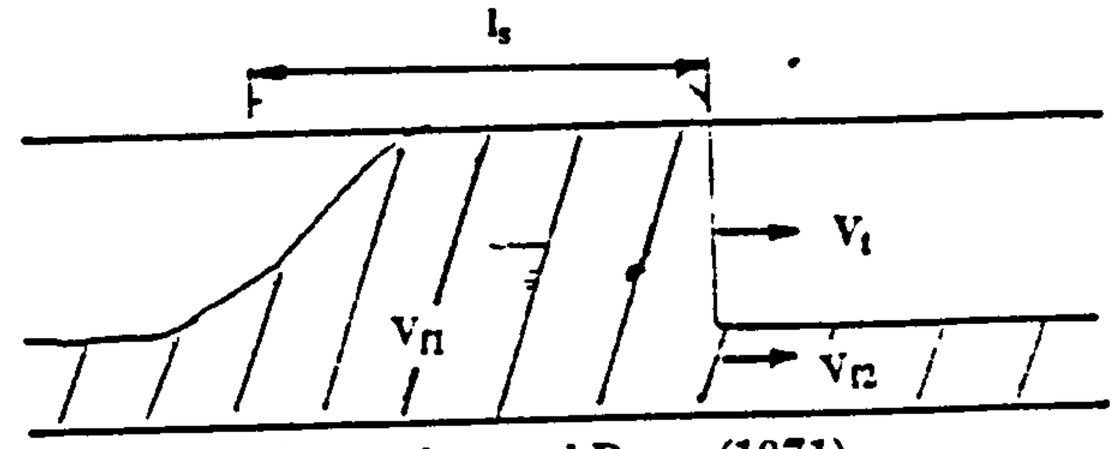
Whilst some aspects of intermittent flow were considered by Dukler et al (1960), as far as the author is aware, it was not until the work of Fernandes et al (1983) that a semi–mechanistic model to predict the detailed structure of the flow was produced. Figure 2.2.2 provides a pictorial representation of the model of Fernandes et al. Though the model of Fernandes et al (1983) predicts many flow details, the calculation of the gas void fraction, ε_{Gs}, in the slug body is carried out indirectly through the use of empirical correlations. Also, for the complete closure of the model, the slug frequency needs to be specified.

2.2.3 INCLINED FLOW

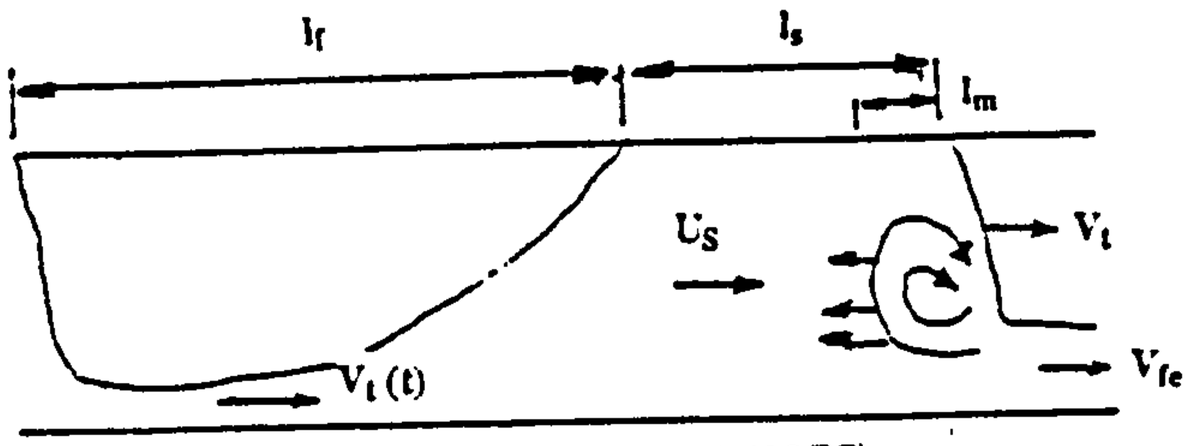
Models for inclined intermittent flow have to take account of the component of gravity parallel to the axis of flow. Bonnecaze et al (1971) produced a model which was a synthesis of earlier models for horizontal and vertical intermittent flow. The model of Dukler and Hubbard (1975) included a gravity term in the equation describing the film. This enables their model to be used for small inclinations.



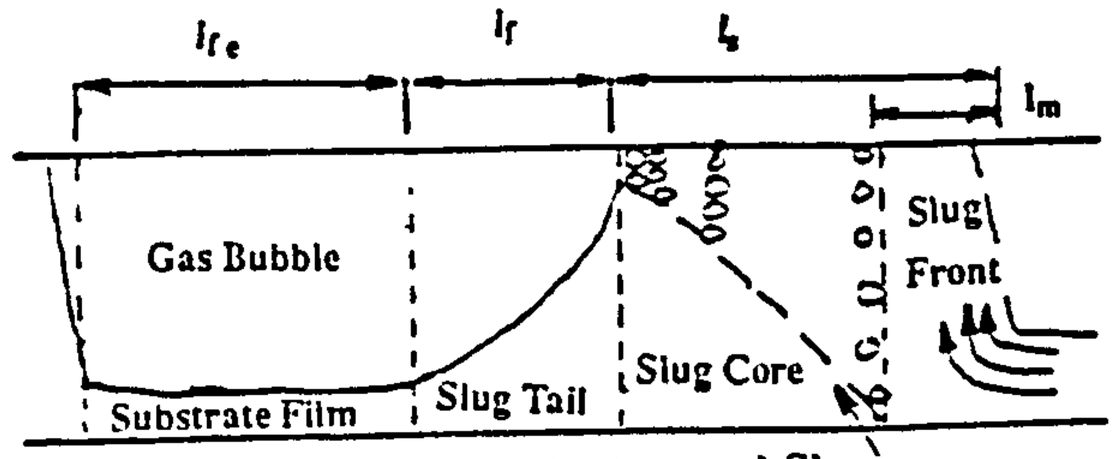
Kordyban (1961)



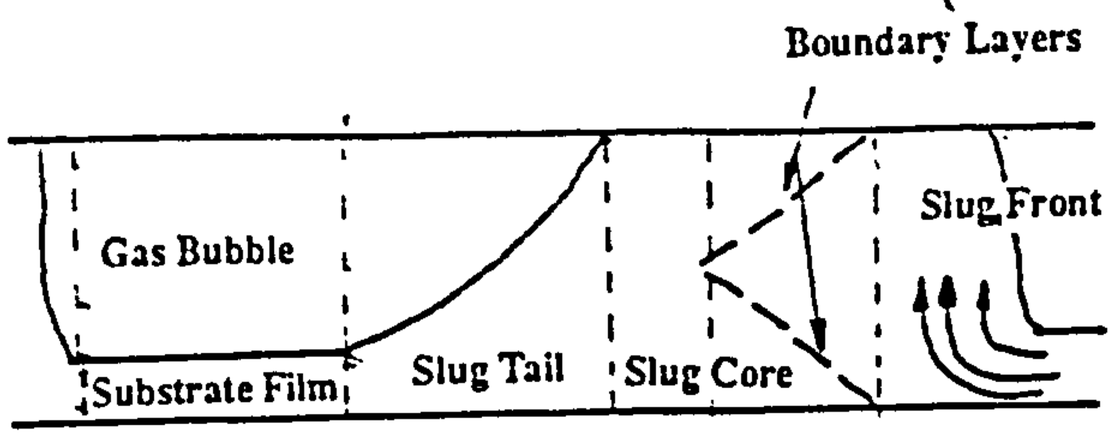
Vermeulen and Ryan (1971)



Dukler and Hubbard (1975)



Maron et al (1982): Aerated Slug



Maron et al (1982): Pure Liquid Slug

Figure 2.2.1 Horizontal Intermittent Flow Models.

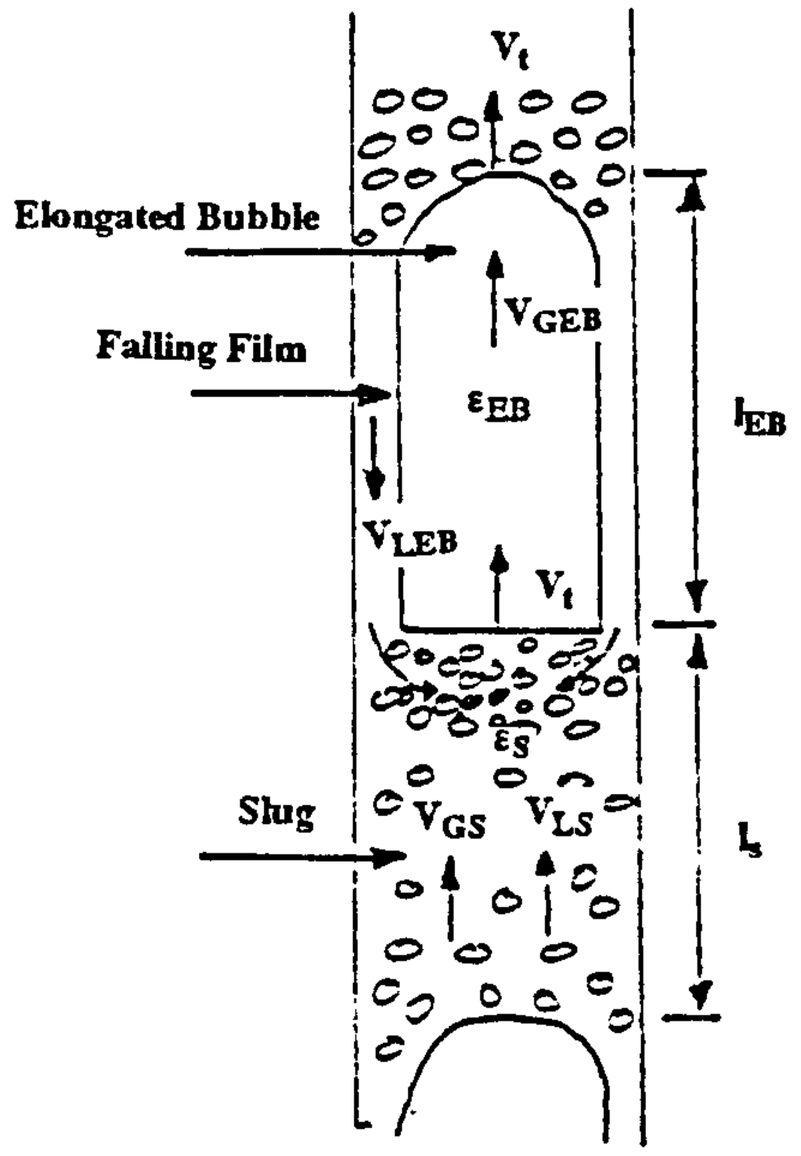


Figure 2.2.2 Fernandes (1983) Vertical Intermittent Flow Model.

2.3 ASPECTS OF INTERMITTENT FLOW

In this section individual aspects of intermittent flow are reviewed. These aspects when combined can form the mechanistic models reviewed above.

2.3.1 PROPAGATION VELOCITY

2.3.1.1 Propagation Velocity: Horizontal Flow

An expression for the translational velocity v_t of a slug can be obtained by considering the volume rate of flow $\dot{V}$ through a plane moving at v_t (Hewitt, 1986). Such a balance yields:

$$\dot{V} = S(U_G + U_L - v_t) = \dot{V}_{Lf} + \dot{V}_{Lb} + \dot{V}_{Gf} + \dot{V}_{Gb} \qquad (2.3.1)$$

where S is the channel cross sectional area, $\dot{V}_{Lf}$ and $\dot{V}_{Lb}$ are the liquid volume rate of flow in the film and elongated bubble respectively, and $\dot{V}_{Gb}$ and $\dot{V}_{Gf}$ are the gas volume rates of flow in the elongated bubble and film respectively. Rearranging the above equation yields:

$$v_t = U_G + U_L - \frac{\dot{V}_{Lf}}{S} - \frac{\dot{V}_{Lb}}{S} - \frac{\dot{V}_{Gb}}{S} - \frac{\dot{V}_{Gf}}{S} \qquad (2.3.2)$$

The earliest model, that of Kordyban (1961), neglected the last five terms of Equation (2.3.2) and assumed that $v_t = U_G$. An improvement was made by Vermeulen and Ryan (1971) who just set the last four terms to zero to give:

$$v_t = U_G + U_L \qquad (2.3.3)$$

Dukler and Hubbard (1975) made the assumption that the gas and liquid are completely separated in the film/elongated bubble region. Hence the liquid volume flow rate $\dot{V}_{Lb}$ in the elongated bubble and the gas volume flowrate $\dot{V}_{Gf}$ in the film are set to zero. This results in the expression for v_t simplifying to:

$$v_t = U_G + U_L - \frac{\dot{V}_{Lf}}{S} - \frac{\dot{V}_{Gb}}{S} \qquad (2.3.4)$$

Hewitt (1986) showed that homogeneous flow through the slug at the total volumetric flowrate of $\dot{V}_{Lf}+\dot{V}_{Gb}$ gave the following relationship between $\dot{V}_{Gb}$, $\dot{V}_{Lf}$ and ε_{GS}, the void fraction in the slug body:

$$\dot{V}_{Gb} = \dot{V}_{Lf}\frac{1-\varepsilon_{Gs}}{\varepsilon_{Gs}} \qquad (2.3.5)$$

which is consistent with Dukler and Hubbards' (1975) assumption of well dispersed bubble flow in the slug. The resulting expression for v_t is :

$$v_t = U_G + U_L - \frac{\dot{V}_{Lf}}{S\varepsilon_{Gs}} \qquad (2.3.6)$$

which is equivalent to the Dukler and Hubbard (1975) expression for mass pick-up rate by the slug:

$$v_t = U_G + U_L + \frac{x}{S\varrho_L\varepsilon_{Gs}} \qquad (x = -\dot{V}_L\varrho_L) \qquad (2.3.7)$$

which can be arranged in the following form:

$$v_t = (1 + C)\,(U_G + U_L) \qquad (2.3.8)$$

where $$C = \frac{x}{\varrho_L S \varepsilon_G (U_G + U_L)} \qquad (2.3.9)$$

and where x is the mass pick–up rate at the slug front which is equivalent to the rate of shedding at the slug tail for steady state intermittent flow.

Values of C quoted in the literature can vary from 0.143 to 0.52. Table 2.3.1 provides a summary of the existing C values. The value of C obtained by Maron et al (1982) for a 2–D channel is a direct consequence of the seventh power law chosen for the turbulent distribution in the slug body. Also it is to be noted that the value of C obtained experimentally by Kvernvold (1984) is higher than the rest, but the Reynolds number range is lower. Hughmark (1965) noticed the following trend in his data; for Re > 400000, C is approximately constant at 0.22, but for lower Reynolds numbers, C is somewhat larger. In contrast, the theoretical expression of Dukler and Hubbard predicts that as Re decreases so does the value of C. Coney (1974) obtained negative C values in his study of the related phenomena of surge flow. The range of C quoted by Jepson (1987) is not calculated from slug flow experiments but, rather, from data on standing hydraulic jumps; Jepson claims that a hydraulic jump is synonymous with a slug front.

Table 2.3.1: Literature C values.

Author	C	Re
Hughmark (1965)	0.22	400000
Gregory (1969)	0.35	29500–13300
Hubbard (1965)	0.25	–
Dukler & Hubbard (1975)	0.021 Ln (Re) + 0.022	300000–400000
Maron et al (1982)	0.143	–
Kvernold et al (1984)	0.52	3000–6000
Jepson (1987)	0.4–0.5	–

2.3.1.2 Propagation Velocity: Vertical Flow

The rise velocity of a non–expanding elongated bubble in a stationary liquid has been investigated both theoretically and experimentally by the following workers; Dumitnesu (1943), Davies and Taylor (1950) and Nicklin et al (1962). The expression obtained is :

$$u_R = 0.35\sqrt{(gD)} \qquad (2.3.10)$$

where u_R is the rise velocity of the elongated bubble.

Griffith and Wallis (1961) studied experimentally the rise of an elongated bubble in a moving liquid. They tried to rationalise their results by splitting the constant of Taylor (1950) into two parts:

$$u_R = C_1 C_2 \sqrt{(gD)} \qquad (2.3.11)$$

one (C_1) to take account of the stationary liquid and the other (C_2) for a function of velocity. They obtained $C_1 = 0.35$ and gave C_2 as a graphical function of Reynolds number of the elongated bubble and film.

Nicklin et al (1962) suggested the following relationship for a single elongated bubble rising in a flowing turbulent liquid:

$$u_R = 1.2(U_G + U_L) + 0.35\sqrt{(gD)} \qquad (2.3.12)$$

The coefficient of 1.2 is believed to be the ratio of the centre line to average velocity of the flow. The experiments of Fernandes et al (1983) suggested a modification to the above expression:

$$u_R = 1.29(U_G + U_L) + 0.35\sqrt{(gD)} \qquad (2.3.13)$$

The difference between 1.29 and 1.2, they suggest, is due to the larger diameter used by Fernandes et al (1983) and the possible interaction of successive elongated bubbles in their experiment. The above expressions apply for elongated bubbles rising in fully developed slug flow. Moissis and Griffith (1962) considered the mean rise velocity (u_R) of elongated bubbles in developing flow as a function of slug length. The velocity u_R is a mean value because of the unstable nature of the elongated bubble front in developing flow. They obtained the following expression:

$$\frac{u_R}{u'_R} = 1 + 8\exp(-1.06\frac{l_s}{D}) \qquad (2.3.14)$$

which is valid for tubes of 1, 2, and 3/4 inch in air–water flows. u'_R is the rise velocity in fully developed flow.

2.3.2 SLUG FREQUENCY

2.3.2.1 Slug Frequency: Horizontal Flow

Gregory and Scott (1969) obtained the following correlation for slug frequency after considering the effects of superficial gas and liquid velocities:

$$f_s = 0.0226\left(\frac{U_L}{gD}\left(\frac{19.75}{U_G + U_L} + U_L + U_G\right)\right)^{1.2} \qquad (2.3.15)$$

while Greskovich and Shrier (1972) rearranged this equation to the following alternative form:

$$f_s = 0.0226\left(\lambda\left(\frac{2.02}{D} + N_{FR}\right)\right)^{1.2} \qquad (2.3.16)$$

where $\lambda = \frac{U_L}{U_L + U_G}$ and $N_{FR} = \frac{(U_L + U_G)^2}{gD}$

Discussion of the effects of U_L, U_G and pipe diameter on slug frequency is given by Greskovich and Shrier (1972) (1971).

As stated earlier Taitel and Dukler (1977) attempted to provide a mechanistic means of obtaining slug frequency. The process they considered is shown in Figure 2.3.1. This can be considered as two stages. After a wave bridges the pipe, there is the time t_1 required to sweep away the liquid in front of the wave and for the level to drop to its lowest level , and the time t_2 for the stratified layer to rebuild to its equilibrium level. Assuming the wave frequency is an order of magnitude greater than the slug frequency, $1/t_2$ can be taken to be the slug frequency. Taitel and Dukler (1977) neglect the effect of wave closures before the equilibrium level is reached, and take no account of the growth of small waves.

2.3.2.2 Slug Frequency: Vertical Flow

There is a lack of information concerning slug frequency in vertical tubes. Vakitotojjar and Javdani (1980) obtained a correlation for the frequency of elongated bubbles:

$$\left|f_s \frac{U_G}{U_L}\right| = 192 U_G + 6.5 \qquad (2.3.17)$$

It must be noted that this correlation is only valid for a CO_2 – water mixture, a single pipe diameter of 0.008 m and a limited range of flowrates.

2.3.3 SLUG REGION

2.3.3.1 Slug Region: Horizontal Flow

The flow phenomena in the slug body are not well understood. The only experimental data available for velocity distribution is that of Kvernvold et al (1984). Laser–Doppler Anemometry (LDA) was used to determine the velocity variation along the bottom of the pipe and at given distance across the pipe in the slug body. The results obtained (see Figure 2.3.2) show a front zone with a large acceleration and velocity profiles develop from an unsymmetrical profile near the slug front, with the highest velocities at the top of the pipe, to a fairly symmetrical profile at the slug end.

The models of Vermeulen and Ryan (1971) and Kordyban (1961) represented the liquid slug as having fully developed flow over its entire length. The work of Dukler and Hubbard (1975), on the other hand consider the slug to consist of a mixing region of length l_m followed by a region of fully developed flow. The length of the mixing region l_m was obtained by using a "velocity head" concept, the velocity head being related to the square of the relative velocity between slug and film. Using this they obtain a simple correlation for the mixing length:

$$l_m = \frac{0.15}{g}(v_s - v_f)^2 \qquad (2.3.18)$$

where v_S is the average velocity of the fluid in the slug body and v_f is the average velocity of the liquid in the film being overtaken by the slug.

Maron et al (1982) used the above correlation for the mixing region length, but assumed boundary layer recovery behind this region. The seventh power law for turbulent flow was used, giving the velocity profile and boundary thickness as:

$$\frac{v_x}{v_i} = 1 - \left(\frac{r}{\delta}\right)^{\left(\frac{1}{7}\right)} \qquad (2.3.19)$$

$$\delta = 1.01 \frac{(x - l_m)}{\left(v_i \frac{(x-l_m)}{v_L}\right)^{0.2}} \qquad (2.3.20)$$

where

x is the axial position from the slug front

r is the co–ordinate in the radial direction

δ is the boundary layer thickness.

Maron et al (1982) considered two cases, that of a pure liquid slug and that of a slug containing dispersed gas bubbles respectively. In the former, boundary layers form at the top and bottom of the duct, but because of the assumption of coalescence of bubbles at the top of the duct, only one boundary layer (at the bottom) is formed for slug voidage < 1.

The gas holdup in the liquid slug is an important parameter in many models. The most widely used means of obtaining the gas holdup in the slug body is the correlation of Gregory et al (1978). Gregory et al (1978) used a capacitance type liquid volume fraction sensor to obtain values of slug void fraction. The experiments were carried out in 0.0258 m and 0.0512 m diameter pipelines of length 30 m. Light oil and air were used as the fluids. Gregory et al (1978) developed a correlation relating the slug gas void fraction to the mixture velocity:

$$\varepsilon_{Gs} = \frac{1}{1 + \left(\frac{v_m}{8.60}\right)^{1.39}} \qquad (2.3.21)$$

where ε_{Gs} is the gas holdup in the slug body and v_m ($v_m = U_L + U_G$) is the mixture velocity in the slug body.

This correlation was derived from data taken in the following flow ranges

$$0.03 < U_L < 2.316 \text{ m/s}$$

$$0.088 < U_G < 10.0 \text{ m/s}$$

for both pipe diameters. A small pipe diameter effect was evident in the data, with the voidage higher for the 0.0258 m pipe at $v_m > 1$ m/s and lower at $v_m < 1$ m/s. The high level of use of this correlation in the past has been based on the lack of an alternative, theoretical or experimental, rather than its strength. The correlation requires development, as Gregory et al (1978) point out, to include diameter and fluid property effects.

Garcia (1980) also used small scale data to relate the slug voidage to the slug body mixture velocity. The correlation derived from the experimental data is :

$$\varepsilon_{Gs} = 0.0735 \frac{v_m}{\sqrt{(gD)}} - 0.1705 \qquad (2.3.22)$$

Further small scale work was carried out by Nydal (1988) who used a gamma densitometer and a capacitance ring probe to study slug voidage for air and water flows at ambient conditions. A 0.032 m internal diameter pipeline was inclined at angles of +10, 0 and –7 degrees during the study. The data obtained had voidage values a lot lower than those of Gregory et al (1978) for similar slug mixture velocities. This difference was attributed to the importance of fluid properties in determining slug voidage. Nydal (1988) also noted, in a review of previous data, that the critical mixture velocity for aerated slugs increases with increasing diameter and the increase in slug voidage with the mixture velocity is also greater for large pipe diameters.

The absence of experimental voidage data at high pressures and large diameters was addressed by Fershneider (1983). The 110 m long 0.146 m internal diameter Boussens facility was used to study intermittent flow for oil and gas at 15 bar at angles of 0 and +4 degrees. A correlation relating the voidage to mixture velocity was presented though the values of the constants C and G were withheld:

$$\varepsilon_{Gs} = \left(1 + \frac{v_m^2 B_o^{2G}}{(1 - \frac{\varrho_G}{\varrho_L}) g D C^2}\right)^{-2} \qquad (2.3.23)$$

where B_0 is the Bond number: $B_o = gD^2(\varrho_L - \varrho_G)/\sigma$

Experimentally based correlations have to be extrapolated with care for fluids, pipe geometries and flow conditions outside the range of construction. Barnea and Brauner (1985) present a physical concept for predicting gas holdup in liquid slugs. Barnea and Brauner (1985) postulate that the maximum concentration of bubbles which can be suspended in a bubbly flow depends on the turbulence level which, for given physical properties, depends on the total superficial velocity $U=U_G+U_L$. Suppose that the bubble concentration is at this maximum value and that we increase U_G and decrease U_L whilst maintaining U constant. This increase in U_G would give a higher void fraction which is greater than the maximum. Thus there is an excess of gas and this forms into large gas bubbles (ie the "film" region) and the slug regions between these large gas bubbles have a void fraction which corresponds to the maximum which can be accommodated at the given value of U. Thus the void fraction (or liquid holdup) in the slug is a function only of U, for given physical properties, as is suggested by the Gregory et al (1978) correlation. The actual value of the maximum void fraction is that pertaining at the transition from dispersed bubble to slug flow. The model of Barnea and Brauner (1985) is illustrated in Figure 2.3.3. Using the transition model of Taitel and Dukler (1976), Barnea and Brauner (1985) were able to predict the Gregory et al (1978) correlation.

2.3.4.2 Slug Region: Vertical Flow

Moissis and Griffith (1962) provide experimental data for the velocity distribution in the slug region in vertical flow. They simulated slug flow by moving a plastic bubble up a tube and measured the total and static pressures to obtain the velocity profiles. The profiles obtained are given in Figure 2.3.4. As expected the velocity is highest nearest the pipe wall just below the simulated bubble, this being due to the liquid falling around the simulated bubble forming a wall jet which persists into the liquid slug region below

the bubble. In the real case, the liquid falls around the bubble in a free falling film, producing the same effect. The velocity profile becomes more symmetrical as the distance increases from the bubble. Mossis and Griffith (1972) also developed a model to describe the velocity profile which had to be adjusted using the experimental data. Walklate and Martin (1983) attempted to measure the liquid velocity profiles in slug flow. A non–disturbing photochromic dye tracing flow visualisation technique was used. The associated cine film provides a good illustration of the characteristic regions of vertical intermittent flow.

In the model of Fernandes et al (1983), the slug region is modelled as two regions, namely a mixing region just below the large bubble and between this and the next large bubble, a fully developed bubble flow region. They used the expression of Zuber and Hench (1962) to obtain the rise velocity of the small bubbles within the fully developed bubble flow region:

$$u_{Gs} = u_{Ls} + 1.53\left(\sigma g\frac{(\varrho_L - \varrho_G)}{\varrho_L^2}\right)^{\frac{1}{4}}(1 - \varepsilon_{Gs})^{\frac{1}{2}} \qquad (2.3.24)$$

This expression is for the rise velocity of a bubble in the presence of a bubble swarm.

The model of Barnea and Brauner (1985) (described for horizontal flow in Section 2.3.4.1 above) for evaluating the slug voidage is also applicable to the vertical geometry. A suitable bubble – slug transition line is required for vertical flow and the line of Dukler et al (1980) may be used for this purpose.

2.3.4 FILM/ELONGATED BUBBLE REGION

2.3.4.1 Film/Elongated Bubble Region: Horizontal Flow

In order to model slug flow the values of the film velocity and the proportion of the tube occupied by the film are required at a point just before the mixing region.

In the early models Kordyban (1961) neglected the film completely, while Vermeulen and Ryan (1971) assumed the film was at rest before being accelerated. Dukler and

Hubbard (1975) used a momentum balance on the film that takes into account wall shear stress, angle of inclination of the pipe, and the hydrostatic pressure effect. This balance neglected the gas shear at the interface. Maron et al (1982) take into account gas shear in their momentum balance on the film, which also includes wall friction and the hydrostatic pressure term. However, Maron et al (1982) consider only a 2–dimensional horizontal duct, which simplifies the algebra.

The rate of liquid shedding from the slug into the film region is required as an initial condition for solving these momentum balances. Dukler and Hubbard (1975) consider the average fluid velocity just before shedding to be v_s. Thus if, at the pipe wall, the velocity is zero, the velocity at the pipe centre must be greater than v_s. Therefore at a certain radius r_s the velocity must be equal to v_s, the slug velocity. Hence for $r > r_s$ the liquid is left behind by the slug and shed into the film region. Using this concept and considering the velocity distribution in turbulent flow, they obtained the following relationship:

$$C = 0.021 \ln \mathrm{Re}_f + 0.22 \qquad (2.3.25)$$

where $\mathrm{Re}_f = \frac{v_s \rho_L D}{\mu}$

where D is the pipe diameter

The term C is the ratio of shedding to the rate of flow in the slug.

Maron et al (1982) considered the shedding rate to be the material contained in the boundary layer(s) at the transition to the film region. The above two methods of obtaining the shedding rate are one dimensional in approach. A two dimensional model might be more appropriate to represent the complex shedding process. Coney (1974) developed such a model for surge flow (see Figure 2.3.5) and considers the effect of boundary layer development during replenishment, and the effect of draining due to gravity.

2.3.4.2 Large Bubble Region: Vertical Flow

Films taken by Nicklin et al (1962) show that the elongated bubble can be considered to consist of a nose region in which the liquid accelerates freely due to gravity and a lower region in which gravity is balanced by wall shear forces and in which the film thickness is constant.

Moissis (1962) carried out a balance on an element of film, considering gravity and wall shear forces, to derive the following expression for film thickness:

$$\delta^* = \frac{f\, v^*_{fe}}{2\,(1-\delta^*)} \qquad (2.3.26)$$

where $\delta^* = \frac{\delta}{D}$ and $v_{fe}^* = \frac{v_{fe}}{\sqrt{gD}}$ are dimensionless quantities

f is a wall friction factor

v_{fe} is the film velocity

δ is the film thickness

The analysis used is similar to that of Nusselt for film condensation. Fernandes et al (1983) assumed the film surrounding the elongated bubble to be falling without interfacial shear. They used the following empirical correlation of Brotz (1954):

$$\delta\left(\frac{g}{v_L}\right) = \left(\frac{3\,\mathrm{Re}_f^{\,2}}{590}\right)^{\frac{1}{2}} \qquad (2.3.27)$$

where Re_f is the Reynolds number of the liquid film defined by:

$$\mathrm{Re}_f = \frac{\delta\, u_{Lb}}{v_L}$$

and δ is the mean film thickness, ν_L is the kinematic viscosity of the liquid, and u_{Lb} is the area averaged velocity of the liquid in the film around the elongated bubble.

BIBL
LONDON
UNIV

Fernandes et al (1983) assumed the net gas flow through the elongated bubble to be zero and to consist of three components. The first component is the gain at the elongated bubble nose from small gas bubbles in the falling film. This term is obtained by calculating the amount of gas bubbles in the slug bottom overrun by the elongated bubble. The second component is the loss due to gas entrainment in the mixing vortex at the liquid slug front. This term is obtained by considering a universal turbulent velocity profile in the elongated bubble and a slug moving at constant velocity. The proportion of gas with a velocity less than that of the slug is considered to be the amount lost. The third component is the return of bubbles from the mixing vortex to the elongated bubble bottom. This term is related to the turbulence fluctuations induced in the mixing region. Fernandes et al (1983) make an estimate of this turbulence by considering the film to be a free annular jet flowing into a stationary pool of its own fluid.

2.3.5 PRESSURE DROP

2.3.5.1 Pressure Drop: Horizontal Flow

Methods of estimating pressure drop in two phase flow can be classified into two types; those that take no account of the flow regime present, and the methods applicable to a specific flow regime.

Models specifically for intermittent flow usually consider the pressure drop across the intermittent flow unit to have the components indicated in Figure 2.3.6. There is the accelerational pressure drop in the mixing region, the frictional pressure drop in the slug body, and the frictional pressure drop in the film region. All models neglect the pressure drop due to the gas in the elongated bubble and for inclined flow a gravity term must be added. Thus the pressure drop over a slug unit is :

$$\Delta p_{IU} = \Delta p_a + \Delta p_{Fs} + \Delta p_{Ff} \qquad (2.3.28)$$

where

Δp_{IU} is the total pressure drop over a intermittent unit

Δp_a is the accelerational pressure drop in the mixing region

Δp_{Ff} is the frictional pressure drop in the film region

Δp_{Fs} is the frictional pressure drop in the slug body.

and over a length l:

$$\Delta p = \frac{\Delta p_{IU} v_s l}{v_t} \qquad (2.3.29)$$

where v_s is the intermittent unit frequency.

Kordyban (1961) and Bonnecaze et al (1971) neglected Δp_{Ff} and Δp_a in their expressions for pressure drop. Bonnecaze et al (1971) included a term to take account of the pressure drop due to gravity acting on the slug body for inclined flows. The expression obtained is:

$$\left(\frac{dp}{dx}\right)_{IU} = \frac{U_L}{U_L + U_G}\left[g\varrho_L \sin\theta + \frac{2\varrho_L f_L (U_G + U_L)^2}{D}\right] \qquad (2.3.30)$$

where

p is the pressure

f is the friction factor

θ is the angle of inclination of the duct

x is the co–ordinate in a direction parallel to the pipe axis.

Vermeulen and Ryan (1971) take into account the pressure drop due to wall friction on the slug and also the effect of film acceleration in their expression:

$$\left(\frac{dp}{dx}\right)_{IU} = \frac{2f\varrho_L U_L (U_L + U_G)}{D} + f_s \varrho_L \varepsilon_f (U_L + U_G) \qquad (2.3.31)$$

Vermeulen and Ryan (1971) use a Blasius type of equation for the friction factor f and, as stated before, assume a liquid slug without bubble entrainment. Dukler and Hubbard (1975) take account of both the liquid velocity in the film region and also of the gas entrainment into the slug body. The resultant expression is:

$$\left(\frac{dp}{dx}\right)_{IU} = \frac{x(U_G + U_L - v_{fe})}{S(l_b + l_s)} + \frac{2f_s(\varrho_L\varepsilon_s + \varrho_G(1-\varepsilon_s))(U_G + U_L)^2(l_s + l_m)}{D(l_b + l_s)} \quad (2.3.32)$$

where

v_{fe} is the velocity of the liquid in the film

l_s is the length of the slug

l_m is the length of the slug mixing region

l_b is the length of the bubble/film region.

x is the mass pick–up rate at the slug front.

Greskovich and Shrier (1971) described a model similar to that of Dukler and Hubbard, using the holdup correlation of Greskovich (1969) and a slug frequency correlation to provide a pressure drop prediction method.

Maron et al (1982) included a frictional pressure drop term for shear forces acting on the film. They also obtained expressions for the wall shear on the slug body and the pressure drop in the mixing region. The expressions obtained for the accelerational

pressure drop and the frictional pressure drops are as follows:

$$\Delta p_a = \frac{\varepsilon_s}{7}(U_L + U_G)(U_L + U_G - v_{fa}) \qquad (2.3.33)$$

$$\Delta p_{Fs} = \int_0^l \frac{\tau}{S} dl \qquad (2.3.34)$$

$$\Delta p_{Ff} = \int_0^{l_f + l_{fa}} \frac{(\tau_i + \tau_{wG})}{S(1 - \varepsilon_s)} dl \qquad (2.3.35)$$

$$\tau = 0.0225 \varrho_L v_t^2 \left(\frac{\nu}{\delta v_t}\right)^{0.25} \qquad (2.3.36)$$

where

τ is the shear stress acting on the slug body

S is the cross–sectional area of the pipe

δ is the thickness of the boundary layer in the slug body

A semi–empirical approach was made by Beggs and Brill (1973). The following pressure gradient equation was derived from a differential mechanical energy balance equation:

$$-\frac{dp}{dx} = \frac{g \sin\theta \, (\varrho_L \varepsilon_L + \varrho_G(1 - \varepsilon_L)) + \frac{f_{TP}(\varrho_L U_L + \varrho_G U_G)(U_L + U_G)}{2D}}{1 - \frac{(\varrho_L \varepsilon_L + \varrho_G(1 - \varepsilon_L))(U_G + U_L) U_G}{P}} \qquad (2.3.37)$$

The two unknowns in this equation, the total liquid holdup fraction ε_L and the two–phase friction factor f_{TP}, were correlated against experimental data. A normalised friction factor was correlated as a function of liquid input and liquid holdup. The liquid holdup was correlated as a function of the angle of inclination of the pipe.

Singh and Griffith (1970) extended the work of Griffith (1961) to provide a simple model of intermittent flow in inclined pipes. The model parameters being determined from experimental data for angles of 5, 10 and 15 degrees. The total pressure drop pre-

dicted by their model being due to the sum of gravity and wall shear stresses on the intermittent flow unit.

Another approach was that of Sen and Ghosal (1982) who obtained an expression for a two–phase multiplier:

$$\Phi_{LO}^{\ 2} = \frac{\Delta p_{TP}}{\Delta p_{LO}} = \frac{4}{3}\left(\frac{U_G + U_L}{U_L}\right)^{0.57}\left(\frac{\varrho_{TP}}{\varrho_L}\right)^{0.5} \qquad (2.3.38)$$

with the two phase density ρ_{TP} being determined using a void fraction given by:

$$\varepsilon_G = 0.833\left(\frac{U_G}{U_L + U_G}\right) \qquad (2.3.39)$$

A comparison of various pressure drop models was carried out by Azzopardi et al (1985) using data culled from the HTFS data bank on two–phase pressure gradients. They concluded that the best results for the models are given by Dukler and Hubbard's (1975) model. Comparison was also made with the empirical analysis of Beggs and Brill (1973), and the HTFS correlation. The models tested performed better than Beggs and Brill (1973) but not as well as the HTFS correlation. It must be noted that the HTFS correlation is based on the data bank, so the latter result is not surprising.

2.3.5.2 Pressure Drop: Vertical Flow

Work on pressure drop in vertical intermittent flow has been carried out by Nicklin et al (1962), Griffith and Wallis (1961) and Fernandes et al (1983).

Nicklin et al (1962) derived a simple expression for a single intermittent unit by applying Bernoulli's equation across a section of flow to the nose of the elongated bubble. Griffith and Wallis (1961) carry out a momentum balance across a intermittent unit to

get:

$$\Delta p_{IU} = \varrho_L g(l_s + l_b) + \frac{4\tau_w(l_s + l_b)}{D} \qquad (2.3.40)$$

taking into account gravity and wall shear stress. They evaluate the wall shear as if the pipe were in fully developed liquid flow at the mixture velocity.

Fernandes et al (1983) take account of the frictional gradient by using the similarity equations developed by Dukler et al (1964) for distributed flow with slip. The expression they obtain for the frictional gradient is:

$$\Delta p_f = \frac{2 f_{TP} \varrho_{TP} u_L^2}{D} \qquad (2.3.41)$$

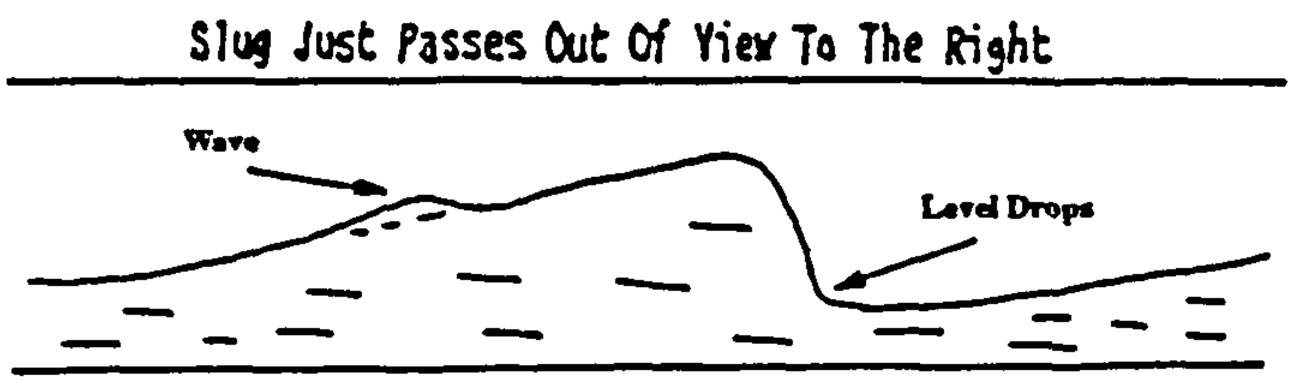


Figure 2.3.1 Slug Formation Process (Taitel and Dukler. 1977)

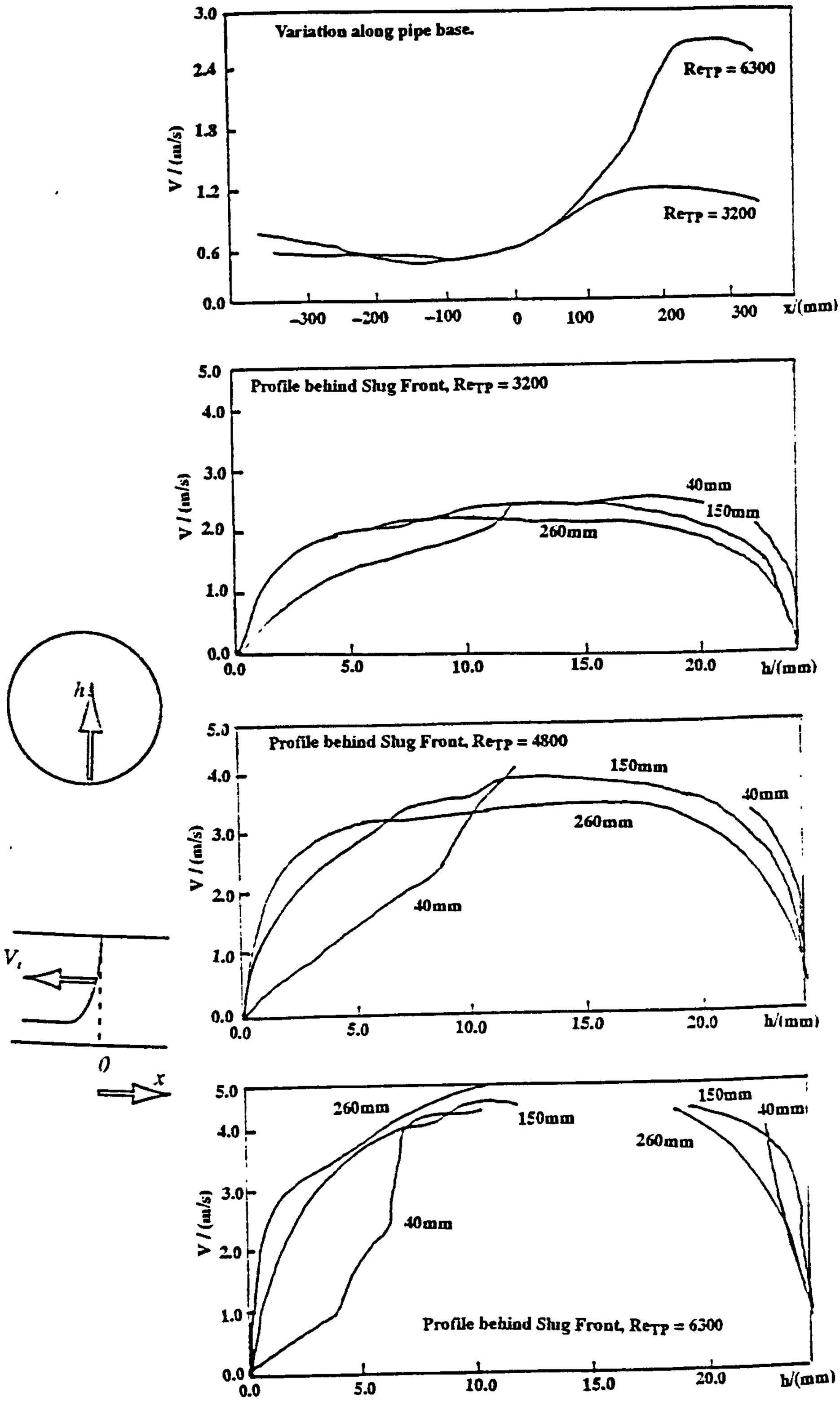


Figure 2.3.2 Velocity Distribution in Slug (Kvernvold et al, 1984)

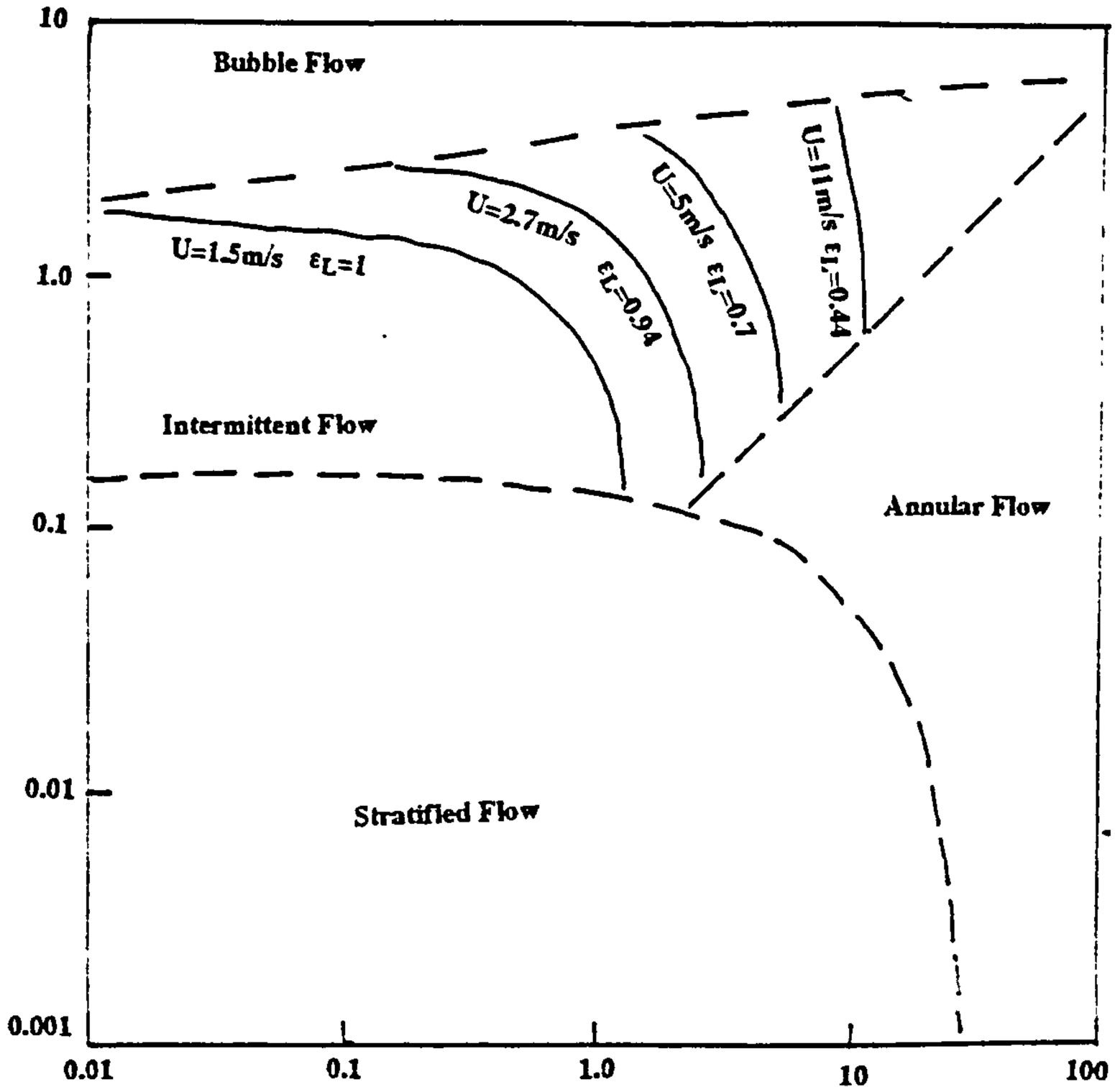


Figure 2.3.3 Locus of Constant Slug Hold-up
(Barnea and Brauner, 1985)

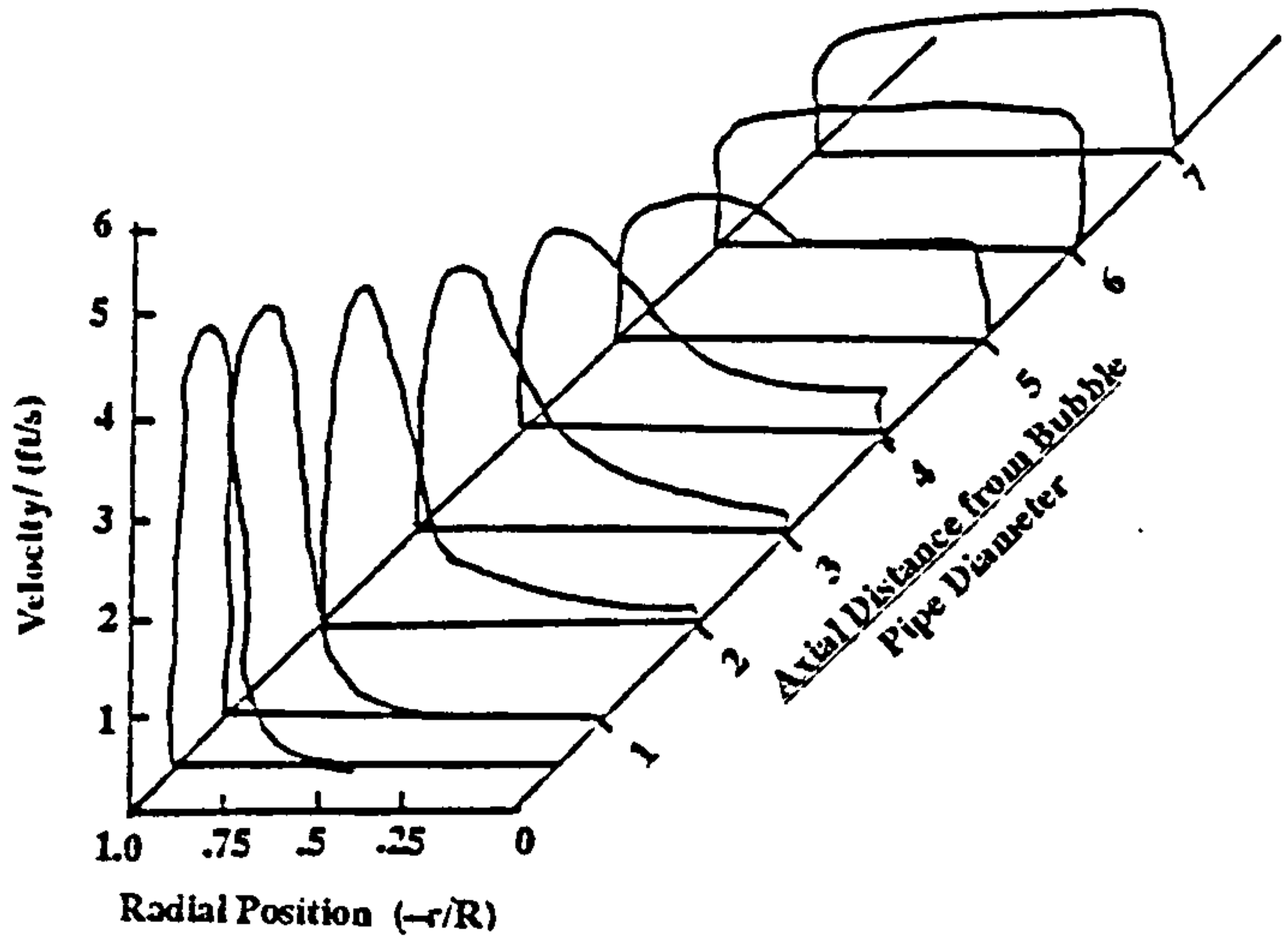


Figure 2.3.4 Velocity Distribution Behind Bubble (Moissis and Griffith, 1962)

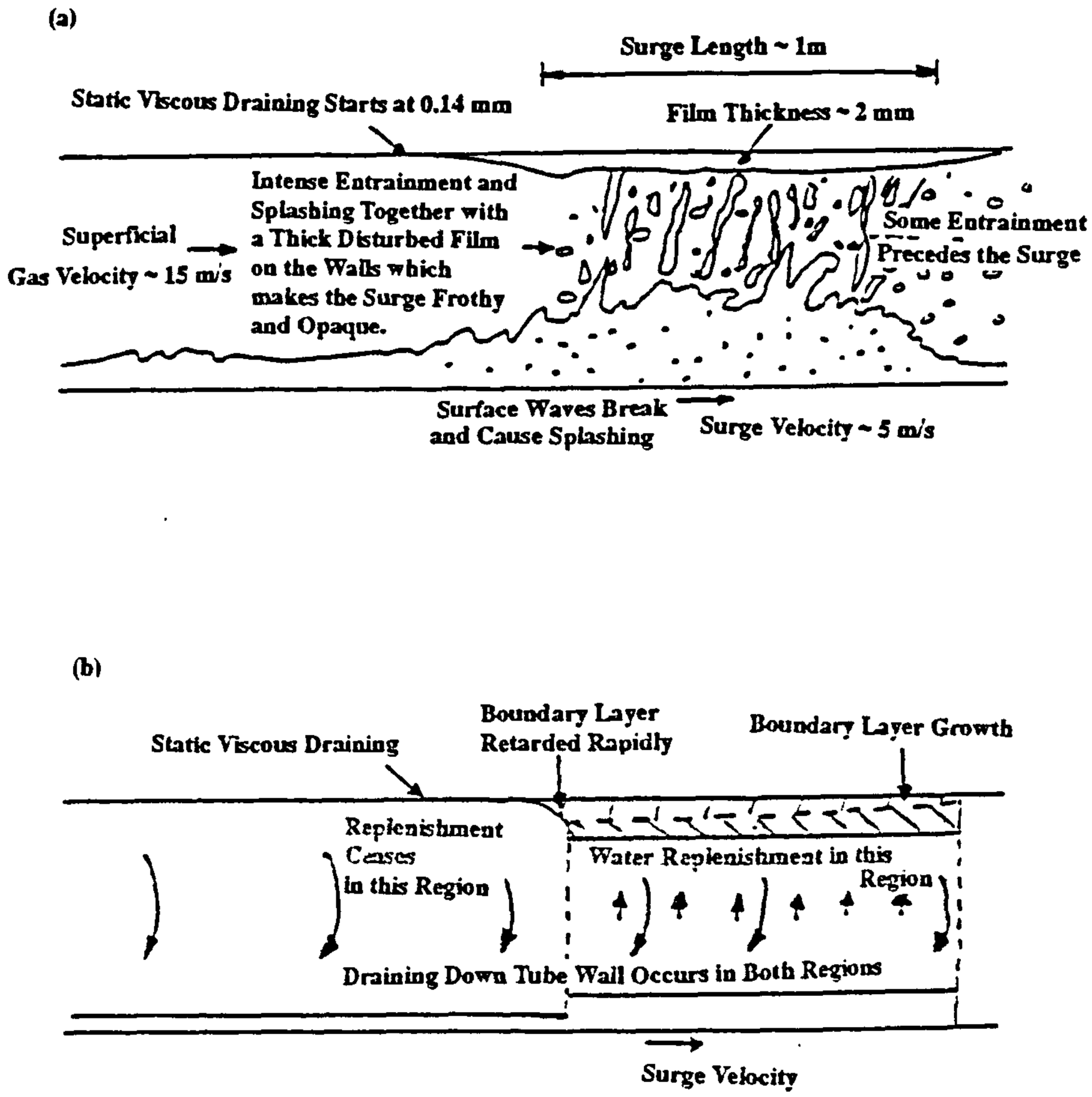


Figure 2.3.5 Surge Flow: Replenishment and Draining Processes (Coney, 1974)
(a) Actual Case
(b) Idealised Picture

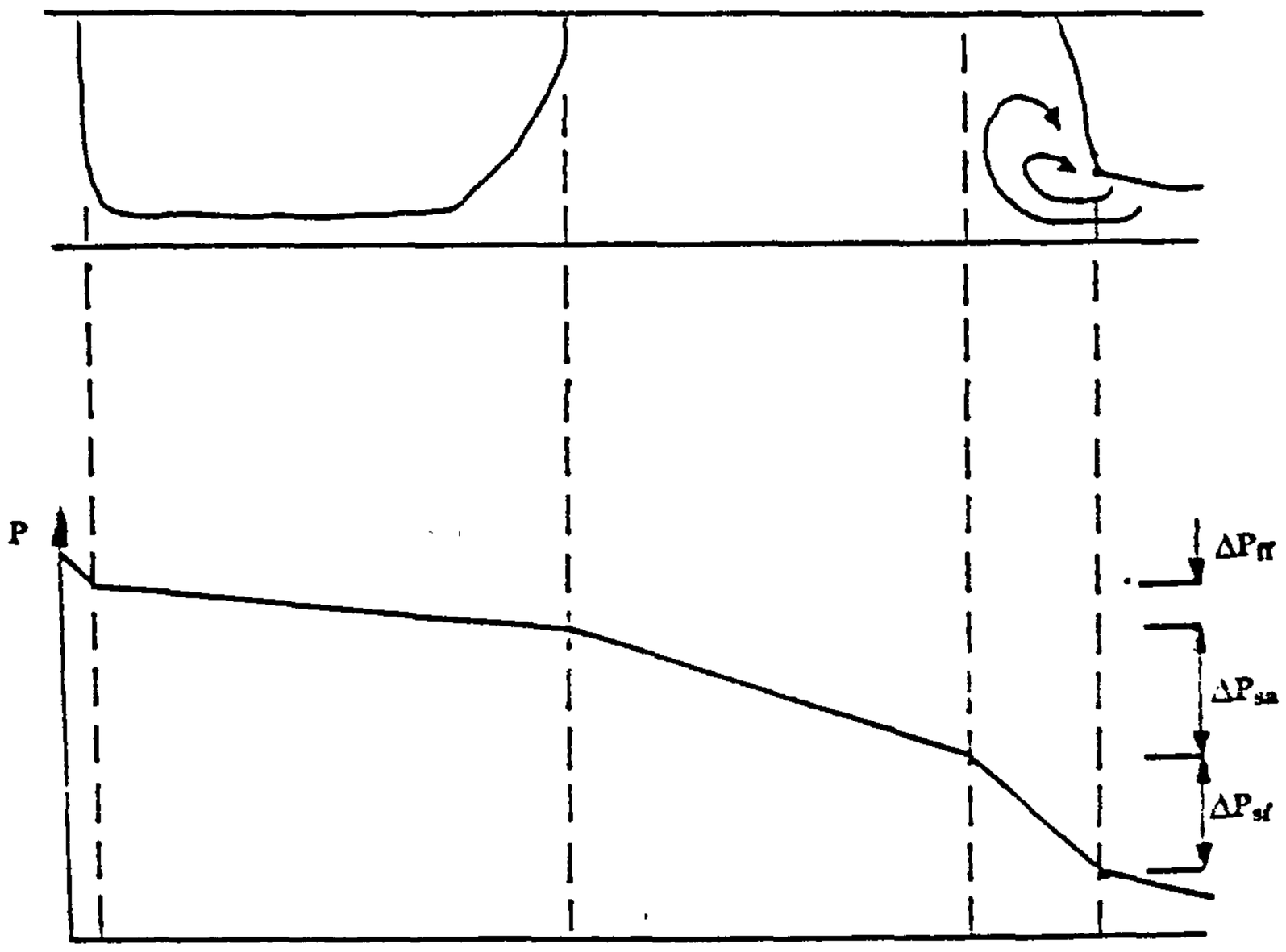


Figure 2.3.6 Pressure Drop Components

2.4 SEVERE SLUGGING

Severe slugging occurs at low liquid and gas flowrates in downward inclined pipelines that are joined to a riser pipe. The following sections review the existing studies of the phenomena.

2.4.1 THE MECHANISM

Consider gas/liquid flow in a pipe system consisting of a downwards declined pipe connected to a vertical or upwards inclined riser (see Figure 2.4.1). At low gas and liquid flowrates, flow in a declined pipe will be stratified and where the declined pipe joins the riser, the pipe may become blocked by liquid. If the rate of hydrostatic pressure build-up in the riser is greater than the pressure build-up in the upstream gas cavity the liquid blockage will grow. The hydrostatic pressure build-up will stop when the slug reaches the top of the riser. When the sum of the hydrostatic pressure in the declined pipe and the gas pressure of any upstream cavity exceed the riser hydrostatic pressure, a liquid slug will be blown out of the riser. The length of the slug produced depends on the supply of liquid in the pipeline, the loss of liquid at the riser top, and the time required for blowout conditions to be reached. The slug length may greatly exceed the riser height.

2.4.2 EXPERIMENTAL STUDIES

Schmidt et al (1979) studied severe slugging in a 30 m long 0.05 m internal diameter transparent pipeline connected to a 15 m vertical riser. Pipeline angles of –5, –2 and +5 degrees from horizontal were used, with the riser vertical in all cases. The fluids used in the equipment were kerosine and air. A flow pattern map was presented for a –5 degree pipeline angle from horizontal. Schmidt et al (1979) also report the use of flow choking at the top of the riser to eliminate severe slugging. The stable flow formed by proper choking was bubble flow. The rate of fall back of the liquid film left in the riser after slug production was found to follow an exponential function of time.

Pots et al (1985) also carried out severe slugging tests in a 0.05 m diameter 30 m long pipeline connected to a 15 m vertical riser. An air buffer vessel, situated at the pipeline

inlet, simulated an extra pipeline length of 120 m. Air was used as the gaseous phase and water or water–glycerine solution, as the liquid phase. Values of slug length, slugging period, liquid production time and relative slug peak velocity were presented for liquid superficial velocities of 0.18, 0.36, and 0.72 m/s. The superficial air velocity was 0.8 m/s referenced to 1.6 bar for all liquid flowrates. Pipe angles of 0, –0.35 and –2 degrees from horizontal were considered. Pots et al (1985) found that while the variation in liquid viscosity has no effect on the onset of severe slugging, increasing viscosity decreases the slug arrival velocity. They also investigated the effect of extra gas lift at the riser base. Though they found that extra gas lift reduces severe slugging severity; however, the amount of gas required for total elimination of severe slugging by gas lift makes this solution to the problem impractical.

Schmidt et al (1985) report work on an experimental facility of a 8.14 m long, 2.54 cm internal diameter pipeline connected to a 3.05 m long riser of the same diameter. The pipeline angle was –1 degree from horizontal and the riser vertical. An air accumulator of 0.011 m^3 simulates an extra flowline length at the air inlet. Water and air form the fluids for the experiments. Schmidt et al (1985) identified three experimental transition boundaries across which severe slugging is dissipated. The first boundary is the transition from stratified flow to slug flow in the inclined pipe. Slugs generated in the inclined pipe were found to flow almost unchanged through the riser pipe, which prevents the generation of a liquid blockage at the riser base. The second condition for which severe slugging could not occur is when the input gas mass flow rate is sufficient for the gas cavity pressure increase rate to overcome the hydrostatic pressure increase rate from liquid fallback and input liquid mass flowrate before the liquid slug reaches the top of the riser. The third method noted for the elimination of severe slugging is to produce normal slug/bubble flow in the riser. Figure 2.4.2 shows these boundaries as located by Schmidt et al (1985) on a flow regime map for a riser pipeline system.

The above workers carried out small scale experiments at near ambient pressure. Fuchs (1987) investigated the effect of system pressure on the terrain slugging mechanism in the high pressure facility operated by SINTEF at Trondheim. Diesel oil and nitrogen

were the respective fluids. A 400 m long, 0.2 m bore pipeline is connected to a 54 m riser. The first 330 m of the pipeline were horizontal with a –2 degree inclination of the last 70 m. Flow regime maps, transient pressure recordings, and transient voidage results are reported at 20 bar, 30 bar, 50 bar and 60 bar. Fuchs (1987) found that as the system pressure increases, the severe slugging region in the flow regime map decreases with the slugs becoming more aerated. Also Fuchs (1987) found that the slug release velocity decreases with increasing pressure and that the riser liquid holdup after blow-out increases with increasing pressure.

Linga (1987) used the same SINTEF two–phase facility as Fuchs (1987) to investigate the effect of topography on severe slugging. A 50 m length of the horizontal pipeline was rotated to form a "bump" in the flowline. Flow regime data, pressure and voidage recordings are reported for the bump configuration at pressures of 30, 50 and 70 bar. In small scale experiments at low pressure, earlier workers reported that the blockage at the low point of the riser was caused by liquid fallback in the riser, stratified flow being the flow regime in the pipeline. The work of Linga (1987) and Fuchs (1987) showed that the blockage was formed by long normal slug units propagating along the pipeline. Linga (1987) found that the bump compacts a train of slugs and that this compact slug train is more effective in blocking the riser low point. Hence the bump introduced by Linga (1987) extends the observed terrain slugging region. Earlier researchers found that by transferring from stratified to slug flow in the inclined pipe severe slugging is eliminated, while Fuchs (1987) and Linga (1987) observed severe slugging with normal slug flow in the inclined pipe. To the author's knowledge this discrepancy has not been explained to date. An explanation of this discrepancy is presented in Chapter 4.

2.4.3 THEORETICAL STUDIES

Models to predict severe slugging need to be able to identify the occurrence of severe slugging and then provide accurate estimates of flow characteristics such as slug length and slugging period.

As mentioned above Schmidt et al (1985) suggested that the boundaries of the severe slugging regime are considered to be the transition from stratified flow to normal slug flow in the inclined pipe, transition to normal slug/bubble flow in the riser, and the transition between severe slugging and semi–severe slugging (riser induced slugs of length less than the riser height). The theoretical derivations available for each boundary will be discussed in turn.

Whilst the transition model applied for transition from stratified wavy to slug flow in an horizontal/slightly inclined pipe is derived from theoretical considerations (Taitel and Dukler (1976)), the application of this model to determine a severe slugging boundary has no theoretical basis. Its acceptance in the literature as a boundary for severe slugging is based on experimental observations in low pressure air–water experiments. These experiments provided the empirical criteria that severe slugging can only occur if stratified flow exists in the inclined pipe, no theoretical proof of this is available in the literature. New thoughts concerning this severe slugging boundary are presented in Chapter 4 as part of the work described in this thesis.

The transition between severe slugging and semi–severe slugging can be defined as the flow condition at which the pipeline gas cavity reaches the riser base just before the liquid slug reaches the riser top. The transition boundary can be obtained by using a severe slugging hydrodynamic model, such as that of Schmidt et al (1979), to experiment and find the highest gas flowrate at a fixed liquid flowrate that will produce severe slugs of length greater than the riser. The hydrodynamic model of Schmidt et al (1979) is discussed later in this section. Bøe (1981) is reported to have developed an explicit expression for locating the boundary between severe slugging and semi–severe slugging in terms of gas and liquid superficial velocities. Bøe (1981) based the analysis on a simplified version of the Schmidt et al (1979) model, neglecting liquid fallback in the riser. Taitel (1986) also used a simplified version of the Schmidt et al (1979) model to obtain a simple relationship for the liquid flowrate above which the front of the gas cavity reaches the riser bottom before the slug front reaches the riser top:

$$U_L = \frac{\varrho_{GO} RT}{\varrho_L g \varepsilon_G l} U_{GO} \qquad (2.4.1)$$

where

U_{GO} is the gas superficial velocity referenced to atmospheric pressure

ρ_{GO} is the gas density referenced to atmospheric pressure

ε_G is the voidage in the pipeline upstream of the riser

l is the length of the pipeline upstream of the riser

R is the universal gas constant

T is the gas temperature.

It is interesting to note that the liquid flowrate depends on the pipeline length l (not the riser length), and hence when defining the boundary in terms of U_{GS} and U_{LS} the pipeline length must be specified as well.

The third boundary of severe slugging corresponds to the transition to normal slug/ bubble flow in the riser. Taitel (1986) carried out a stability analysis on the riser to locate the transition between severe and normal slugging in the riser. It was shown that the net force (per unit area) acting on the liquid in the riser is:

$$\Delta F = \left[(p_s + \varrho_L g h) \left(\frac{\varepsilon_G l}{\varepsilon_G l + \varepsilon_G' y} \right) \right] - [p_s + \varrho_L g (h - y)] \qquad (2.4.2)$$

where

ε_G' is the voidage in the riser

h is the height of the riser

y is the height from the riser base to the highest point in the gas bubble that penetrates the riser.

p_S is the separator pressure.

assuming the pipeline to be in stratified flow upstream of the riser.

The first term on the right hand side of Equation (2.7.2) is the pipeline pressure driving force and the second term is the sum of the force due to the separator pressure and the hydrostatic pressure of the liquid column in the riser. The net force varies with y and the system is in equilibrium when y=0. Taitel (1986) states that the necessary condition for severe slugging is that ΔF increases with y, such that the liquid column is blown out. Thus the condition under which severe slugging cannot occur is given by:

$$\frac{\partial(\Delta F)}{\partial y} < 0 \quad at \quad y = 0 \qquad (2.4.3)$$

$$or \quad \frac{p_s}{p_o} > \frac{(\varepsilon_G/\varepsilon_G')l - h}{p_o/\varrho_L g} \qquad (2.4.4)$$

where p_O is the atmospheric pressure.

Pots et al (1985) assumed that for severe slugging to occur two conditions must be satisfied. Firstly the gas flow in the pipeline upstream of the riser must be arrested and secondly the rate of increase of hydrostatic pressure in the riser must exceed the rate of gas pressure build-up in the upstream pipeline. Such conditions ensure that the riser is full of liquid before the gas pressure can drive the liquid slug into the separator. These conditions in combination with the assumptions of no mass transfer between the phases and a vertical riser lead Pots et al (1985) to suggest the following dimensionless group for the occurrence of severe slugging:

$$\Pi_{ss} = \frac{ZRT/M_w}{gl\varepsilon_G} \frac{\dot{m}_G}{\dot{m}_L} \qquad (2.4.5)$$

where

$\dot{m}_G, \dot{m}_L$ are respectively the gas and liquid mass flowrates

M_w is the molecular weight of the gas

Z is the gas compressibility factor.

Π_{SS} is the ratio between the hydrostatic and gas pressure build–up rates, and Pots et al (1985) state that if $\Pi_{SS} < 1$ then severe slugging will occur.

Schmidt et al (1979) developed an hydrodynamic model based on the following assumptions:

– Pure liquid slug

– Constant gas and liquid mass input

– Constant pressure at the riser top

The hydrodynamic model consisted of four differential equations derived from the gas equation of state, a pressure balance across the slug, a liquid balance, and a volume balance on the gas cavity. Prediction of the experimental data of Schmidt et al (1979) is good, except that increasing divergence is noted in slugging period as the period increases. Also liquid slug length tends to be over predicted as slug length increases. Despite the good agreement with their own data the following deficiencies exit in the model:

– Experimental data used to produce correlation for liquid fallback as well as for validation.

– Applicable to stratified flow regime in the inclined pipe only

– Liquid holdup in the pipeline calculated using the Manning expression for average liquid velocity in open channel flow. Hence the gas velocity is neglected in calculating the liquid holdup.

– the model is unable to calculate the transition to severe slugging

Bendiksen et al (1982) used OLGA, a dynamic one–dimensional two–phase model, to simulate the Schmidt et al (1979) severe slugging experiments. In the OLGA code mass and momentum conservation equations for each phase are implicitly integrated with time. Energy equations are not included in the coding, with temperature profiles along a pipe specified in the input. Slip effects such as different phase velocities and density variations are taken into account in the code. Bendiksen et al (1982) claim good agreement with the experimental results of Schmidt et al (1979). This claim is examined by focusing on one simulated case of voidage and pressure variation at the riser

base during severe slugging, given in Figures 2.4.2 and 2.4.3 respectively for a gas superficial velocity of 0.97 m/s and a liquid superficial velocity of 0.34 m/s. The frequency of pressure variations shown in Figure 2.4.3 indicates slug lengths of the order of 8.5 metres. For the experimental apparatus of Schmidt et al (1979) a fully formed severe slug will be at least the size of the vertical riser, which is 30 m. It is to be noted that pressure variations less than the riser hydrostatic head obtained by Bendiksen et al (1979) are to be expected at the riser base as the slug generated does not exit to a separator at the riser top but continues along some piping to the separator.

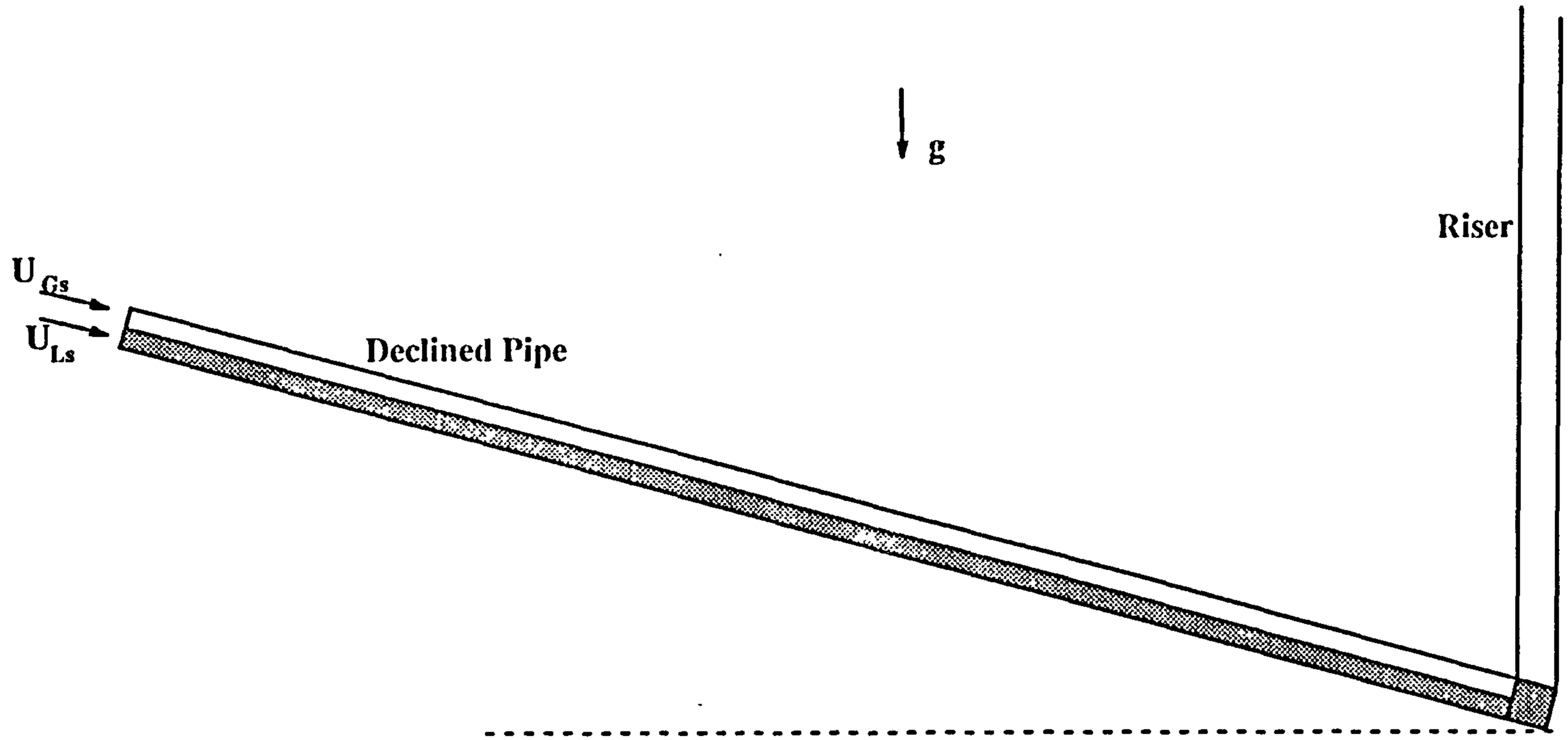


Figure 2.4.1 Geometry of Riser–Pipe for Severe Slugging

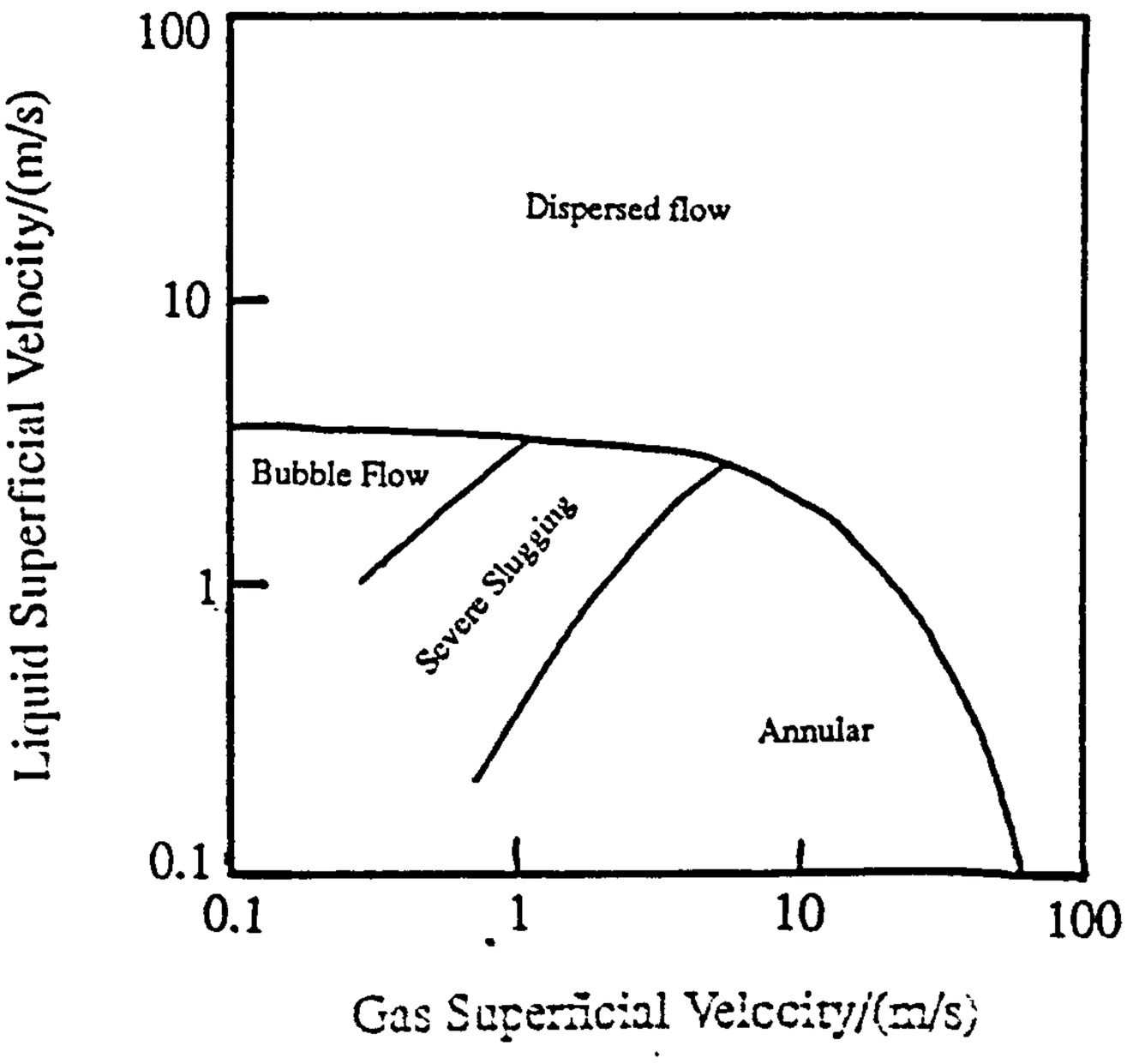


Figure 2.4.2 Transition Boundaries to Severe Slugging (Schmidt et al, 1985)

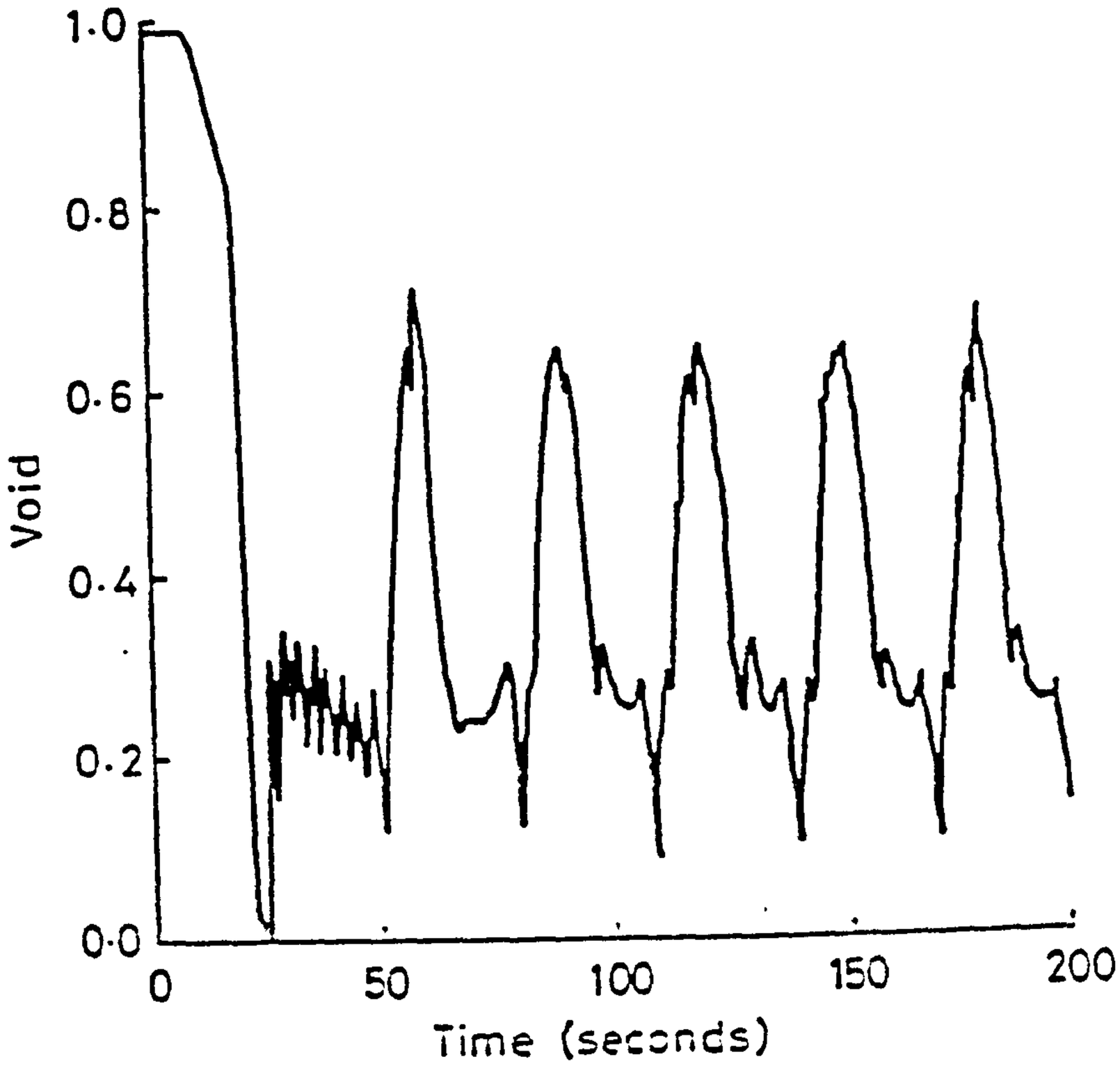


Figure 2.4.3 Voidage Variation at the Riser Base.
(Bendiksen et al. 1982) U_{Gs} = 0.97m/s. U_{Ls}= 0.34 m/s.

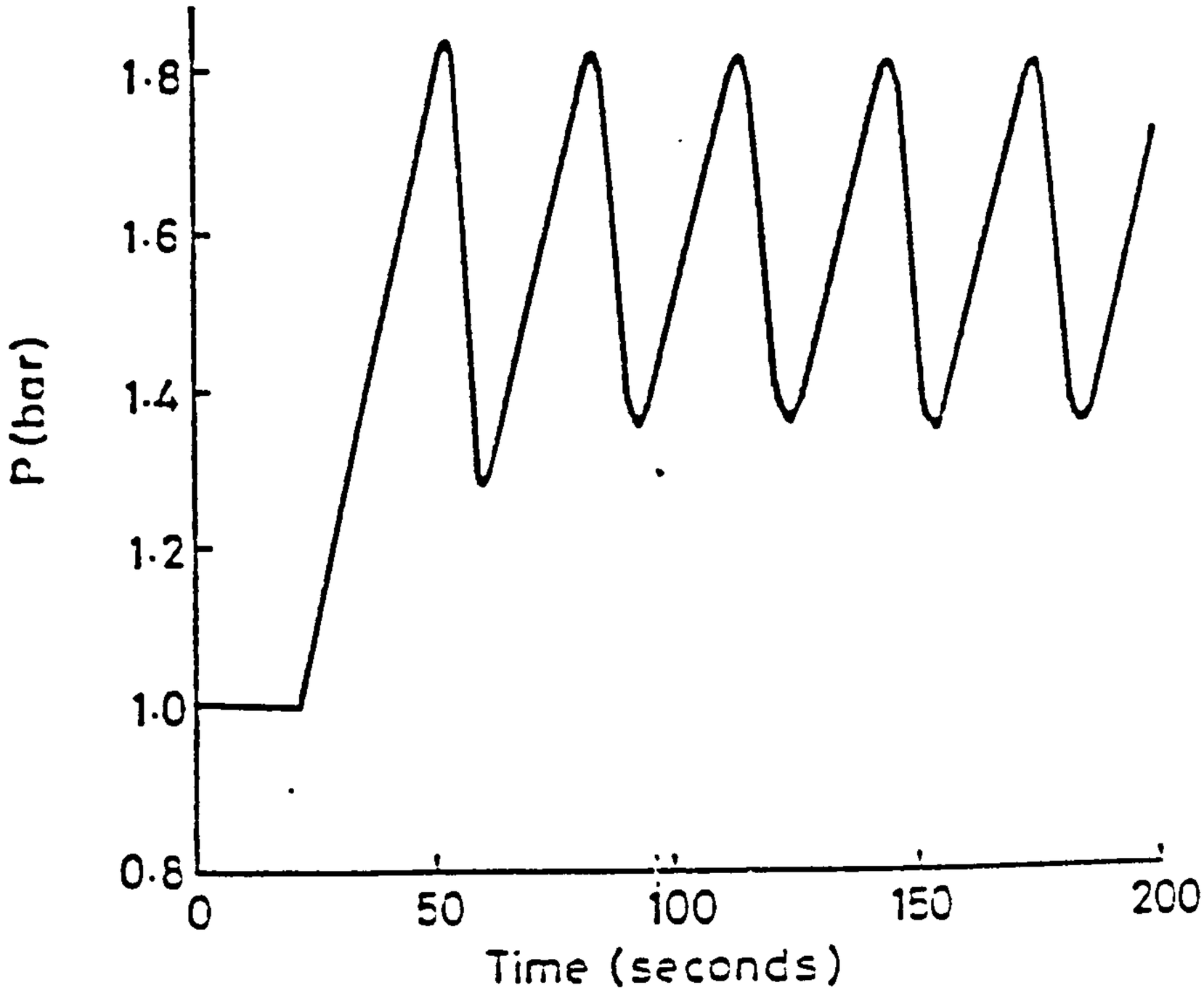


Figure 2.4.4 Pressure Variation at the Riser Base.
(Bendiksen et al, 1982) U_{Gs} = 0.97m/s. U_{Ls}= 0.34 m/s.

CHAPTER THREE

LOW PRESSURE RIG

A low pressure two–phase flow facility was designed, manufactured and constructed to obtain the results described in Chapters 4 and 5. Whilst the geometry of the test section was specific to individual experiments, the main characteristics of the rig were common to all experiments. The equipment is described in this Chapter to avoid repetition.

3.1 BASIC EQUIPMENT

A schematic of the basic apparatus is given in Figure 3.1.1. Water is pumped from a 1 m^3 reservoir tank to the test section by an Ingersoll–Rand 40–100 SM pump, which is capable of providing a maximum flowrate of 400 litres/min. In the inlet section the water mixes with air and then flows co–currently to the pipe exit. The water then returns to the tank and the air is discharged to atmosphere. Air is taken from the site 7.8 bar g (100 psig) compressed air supply and passed through an IMI–Norgan flow regulator and filter. The air is then metered using an orifice plate meter, designed to British Standard number 1042, and enters the inlet section.

The pipe is nominally 10 m in length and consists of flanged sections of 74 mm internal diameter transparent perspex pipe. The flanges, shown in Figure 3.1.2, use a tongue and groove mating to facilitate alignment of tube sections and were machined to an exact internal diameter so that no steps exist at the joint between the flanges. This minimises flow disturbances by reducing mismatch at the flanges. Ring supports hold the pipe, and the whole arrangement is supported as shown in Figure 3.1.3. The supports allow a range of pipe inclinations from + 6 degrees to – 8.5 degrees from horizontal.

Due to the sensitivity of flow regime boundaries to pipeline inclination, see for example the work of Barnea et al (1980), great care was taken to level the pipeline for each specific experiment. This was achieved by attaching a "Roman" level (ie a length of plastic tube filled with water and open at both ends) between two locations on the pipeline base. The supports for the pipeline were adjusted until the water level reached

the same position with respect to the pipeline base for each position. This process was repeated along the whole length of the test section.

3.2 INLET SECTION

An inlet section was designed to control the injection of the gas and liquid at the pipe entrance; the basic concept was to separate the gas and liquid flows entering the tube by means of a plate which was mounted horizontally at various levels and which was thus parallel with the tube axis. The purpose was to reduce interaction in the vertical plane between the two fluids by developing a flow of the two fluids parallel to the pipe axis before the fluids came into contact. The inlet section is shown in Figure 3.2.1 (a) and Figure 3.2.1 (b). It consists of a flanged section of perspex pipe into which the air and water are introduced through two tubes which are opposite each other on the pipe circumference, the air entering vertically downwards and the water entering vertically upwards.

On entering the pipe, the flows of the two fluids are separated by the plate and the flows turn through a right angle and axial flow is established before the two fluids come into contact at the end of the plate. The plate is mounted into slots cut into the entrance section wall and in the end blanking flange of the inlet section (see Figures 3.2.1 a and b). Four sets of slots were available allowing a plate to be placed in a horizontal plane passing through the tube axis or in three other alternative planes parallel to the first (axial) plane and equally spaced between that plane and a parallel plane separated from the first plane by a distance equal to the tube radius. Of course, it was necessary to have four different sized plates for the respective positions, a photograph of the plate being given in Figure 3.2.2 By turning the inlet section through 180 degrees it was possible to have a total of seven different channel sizes for the respective phases.

3.3 PIPE EXIT

Initially a 90 degree bend was chosen to guide the flow from the pipe into the liquid reservoir tank. In the vertical section of the bend (see Figure 3.3.1 a) slugs accelerated

due to gravity; and adversely affected the upstream gas flow. Thus the end section was redesigned to remove this effect.

The bend was removed and a box built around the pipe exit to contain the slugs (see Figure 3.3.1 b). The water drops sharply into the tank providing a well defined outlet condition. Liquid height gradients introduced in the flow upstream by this sharp drop were varied by the use of a weir at the pipe exit.

3.4 FLOW MEASUREMENT

Orifice plates with D and D/2 tappings designed and constructed to the specification of BS1042, were used to measure the gas flowrates. The layout and dimensions of the equipment are shown in Figure 3.4.1. The swirling motion induced in the gas by the pressure regulator and upstream pipe elbows is removed by a 2 m calming length before the orifice plates. Four orifice plates, see Figure 3.4.2, were manufactured to cover a range of flowrates. The orifice hole diameter to pipe diameter ratios of these plates are 0.192, 0.345, 0.537, and 0.695. Flowrate is obtained by noting the pressure drop across the two pressure tappings, the absolute pressure at the upstream tapping, air temperature and the orifice plate size. Equation (7) of BS1042 is used to calculate volume flowrate:

$$Q = 0.01252\, C\, Z\, \varepsilon\, E\, d^2 \sqrt{\frac{h}{\varrho}} \qquad (3.4.1)$$

where $E = \dfrac{1}{\sqrt{(1 - m^2)}}$

$m = (\dfrac{d}{D})^2$

Q is the volume rate of flow (m^3/h)

d is the diameter of the orifice (mm)

D is the internal diameter of the upstream pipe (mm)

ρ is the density of the fluid at the upstream tapping (kg/m^3)

h is the pressure differential (mmH_2O)

C is the basic coefficient

Z is the combined Reynolds number and pipe size correction factor

ε is the expansibility factor

The orifice metering installed allows superficial gas velocities to be measured in the range 0.2 m/s to 14 m/s at 1 bar, 20 degree centigrade. While the uncertainty associated with metering can only determined by measurement using a technique of known greater accuracy, an estimate of the magnitude of the uncertainty can be obtained by considering the sources of error. Each source of error needs to be quantified based on previous experience and all the components combined to provide an estimate of the overall uncertainty.

An estimate of the error in Q was obtained by considering the uncertainty in the following quantities:

$$d, D, \varrho, h, C, Z, \varepsilon$$

It must be noted that the magnitude of the errors in the above quantities depends on the uncertainty associated with the subsidiary quantities used to calculate them. As only an estimate of the magnitude of the uncertainty of the gas flowrate was required it was assumed that the subsidiary quantities used in calculating C, Z, ε were known exactly. Each individual metered gas flowrate has an specific uncertainty associated with it. For example, the estimated accuracies associated with instantaneous gas flowrates of 0.2 m/s and 14 m/s at 1 bar, 20 degree centigrade are respectively $\pm 2.8\%$ and $\pm 1.64\%$.

Water flowrate was measured using a Series 1000 metric 65X rotameter manufactured by the Rotameter MFG Co. Ltd., Croydon. This rotameter enables flow measurement in the range 0.07 m/s to 0.62 m/s superficial liquid velocity. The rotameter was calibrated by measuring with a standard volume the volume of liquid collected in a vessel in a given period. The estimated uncertainty associated with superficial water velocities of 0.07 m/s and 0.62 m/s are respectively $\pm 5.5\%$ and $\pm 0.6\%$.

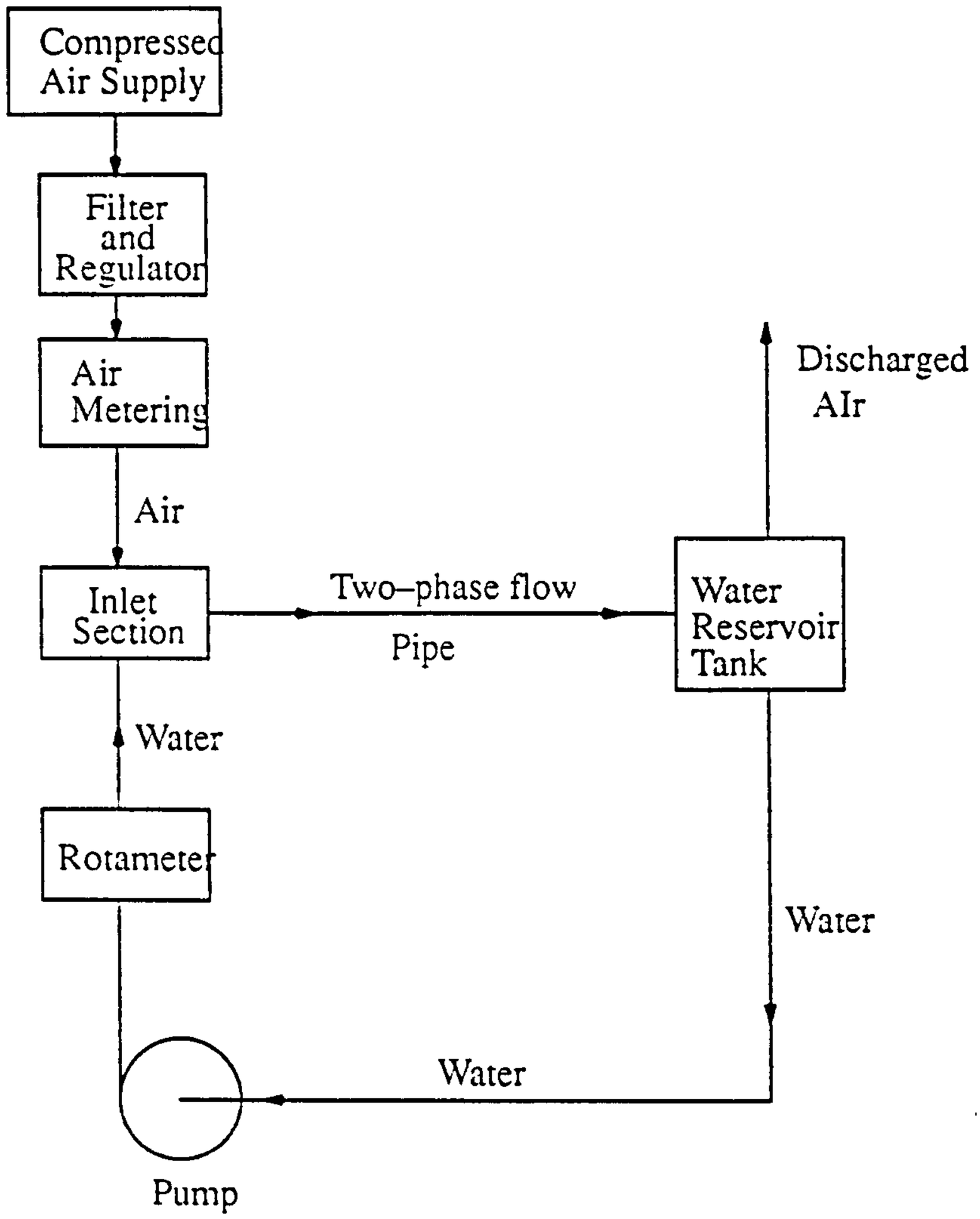


FIgure 3.1.1 Schematic of the basic apparatus.

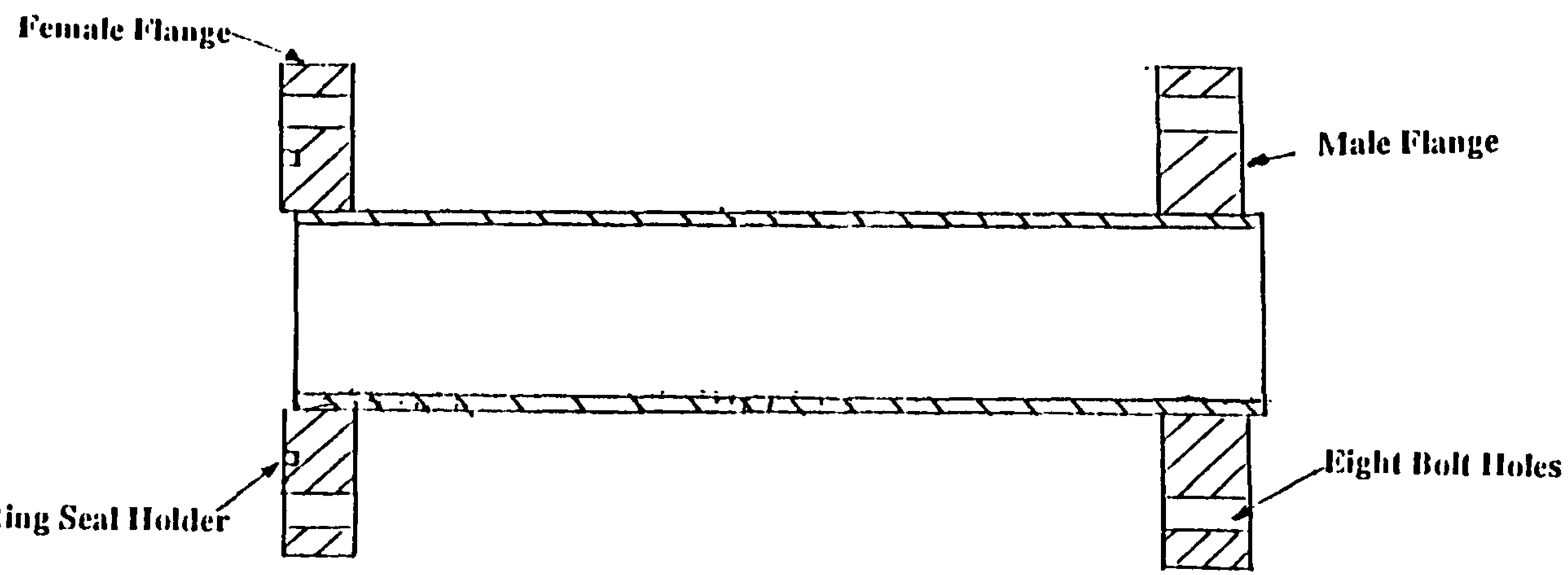


Figure 3.1.2 Test Section Flanges

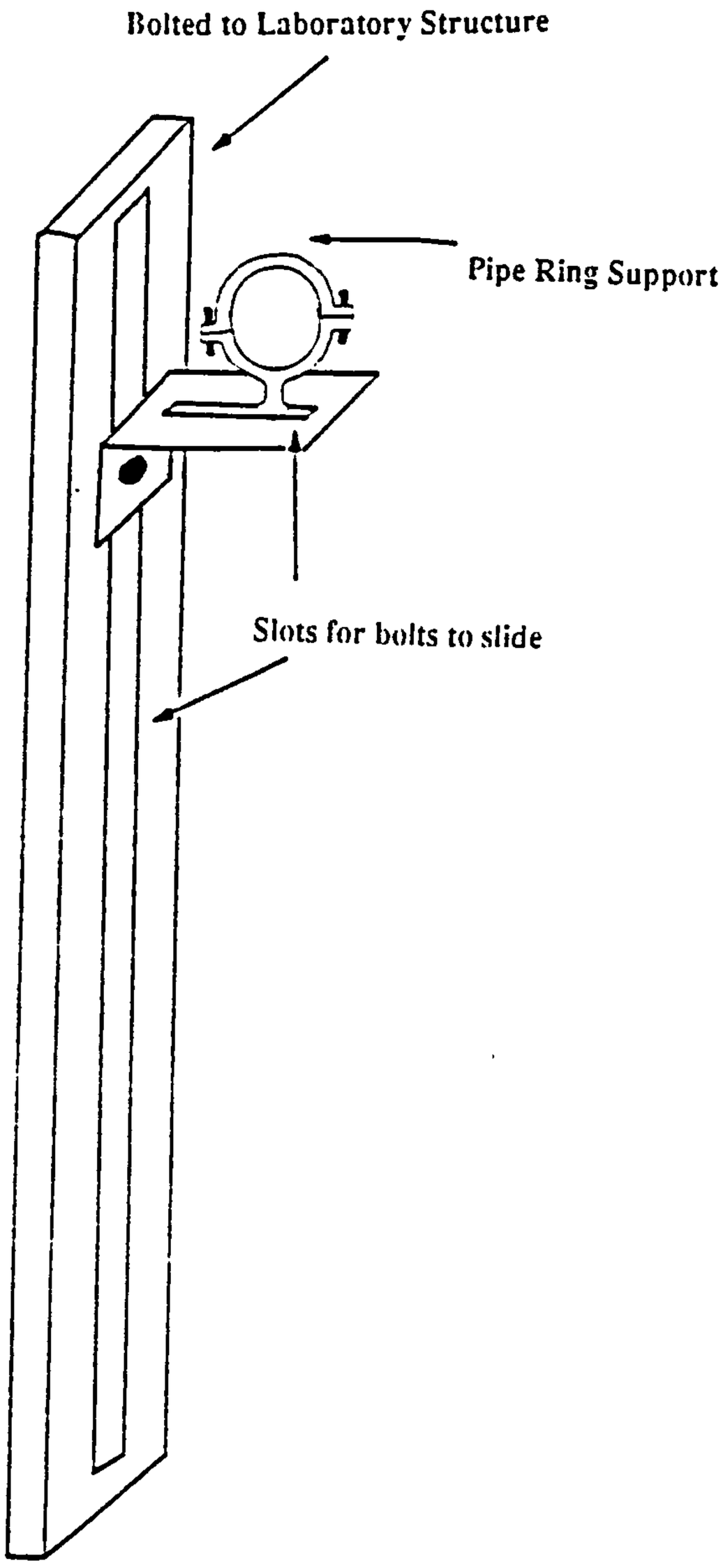


Figure 3.1.3 Rig Supports.

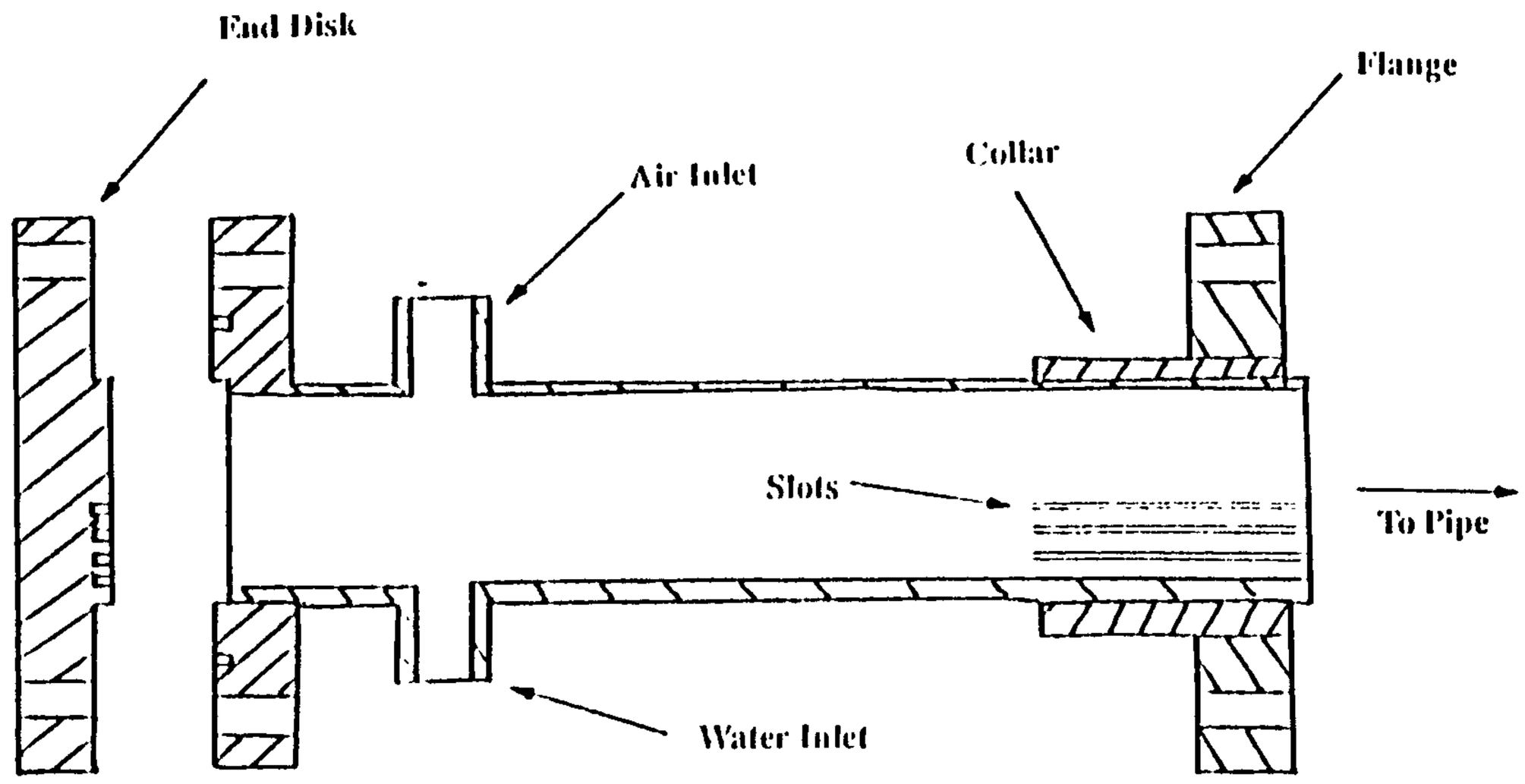


Figure 3.2.1 a) Test Section Inlet.

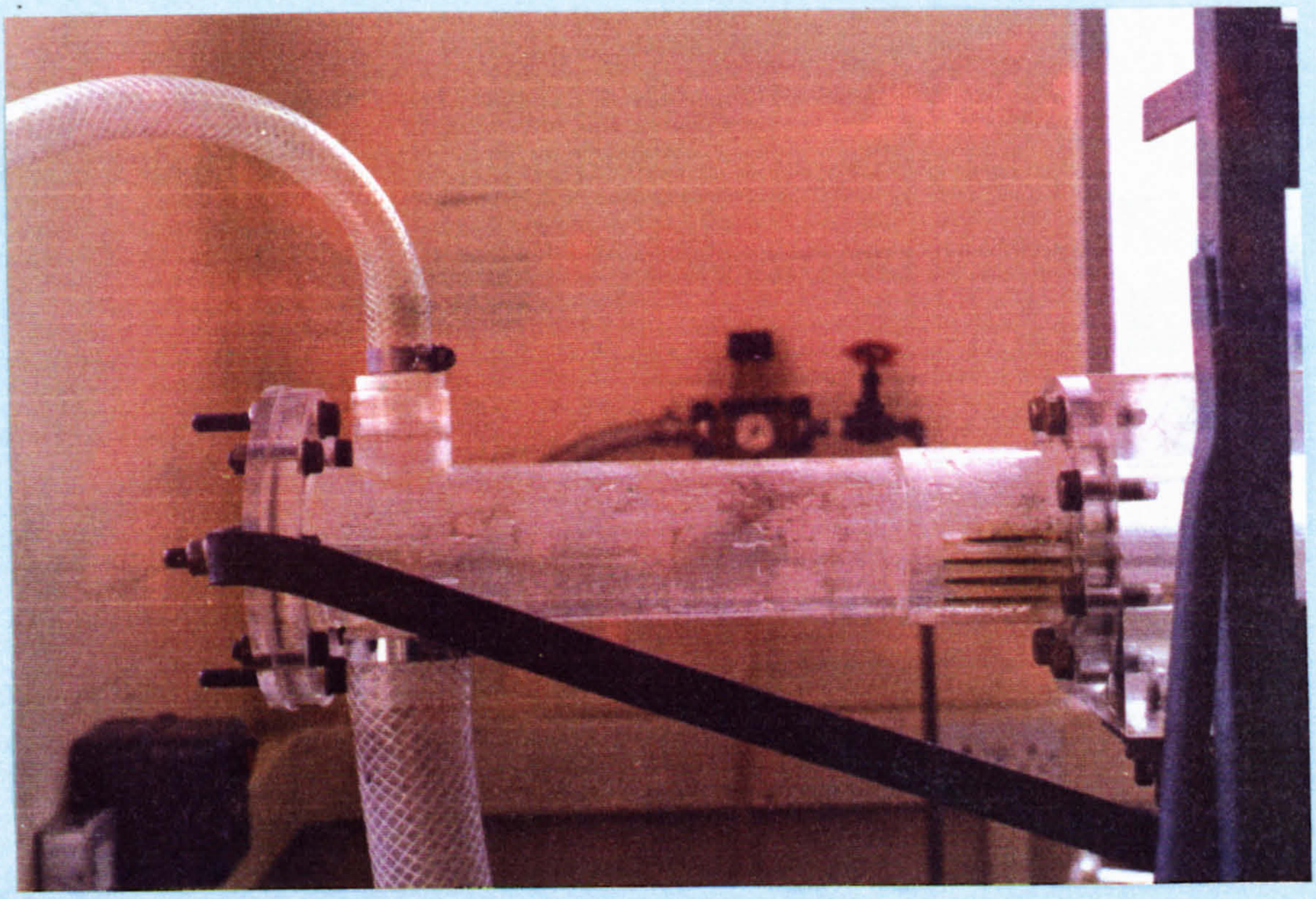


Figure 3.2.1 b) Test section inlet.

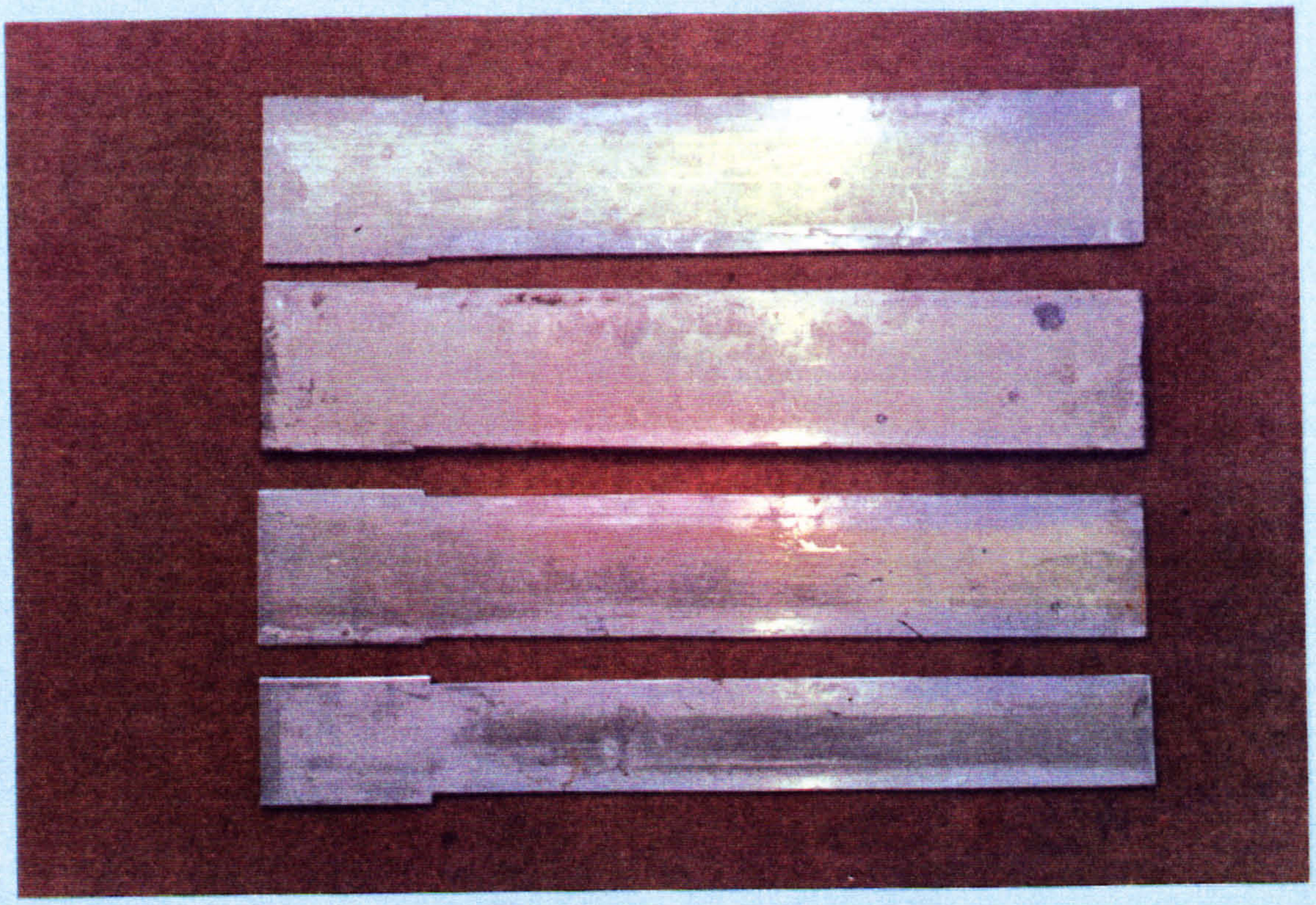
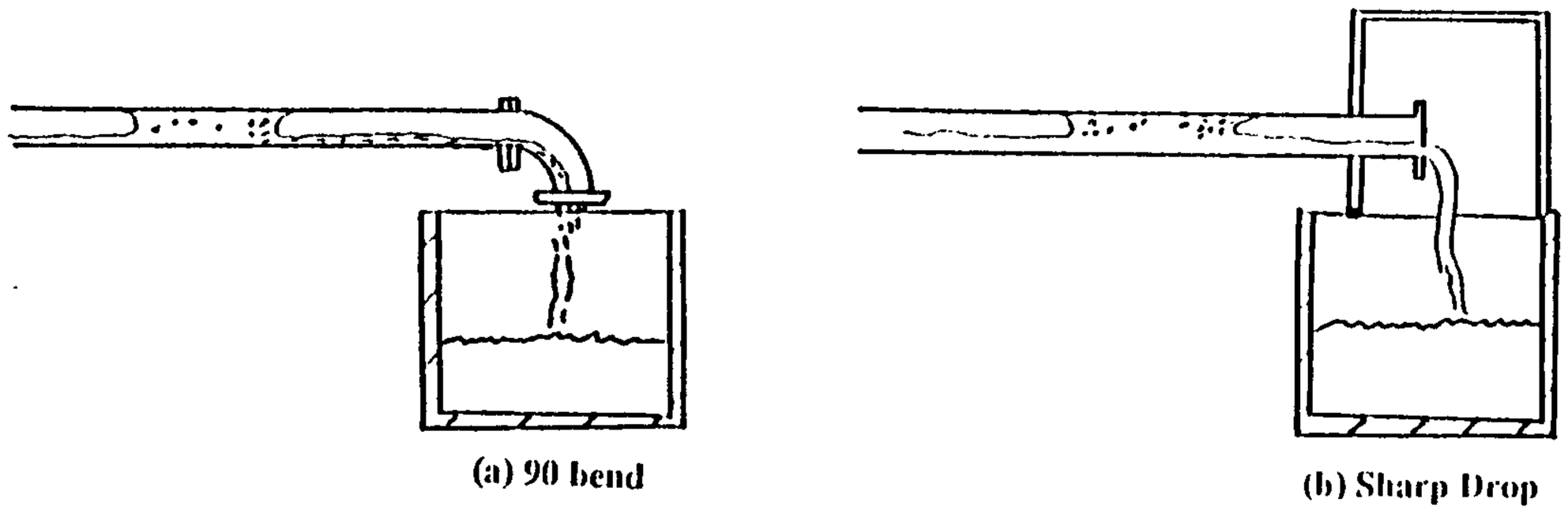


Figure 3.2.2 Inlet section plates



(a) 90 bend

(b) Sharp Drop

Figure 3.3.1 Test Section Exit.

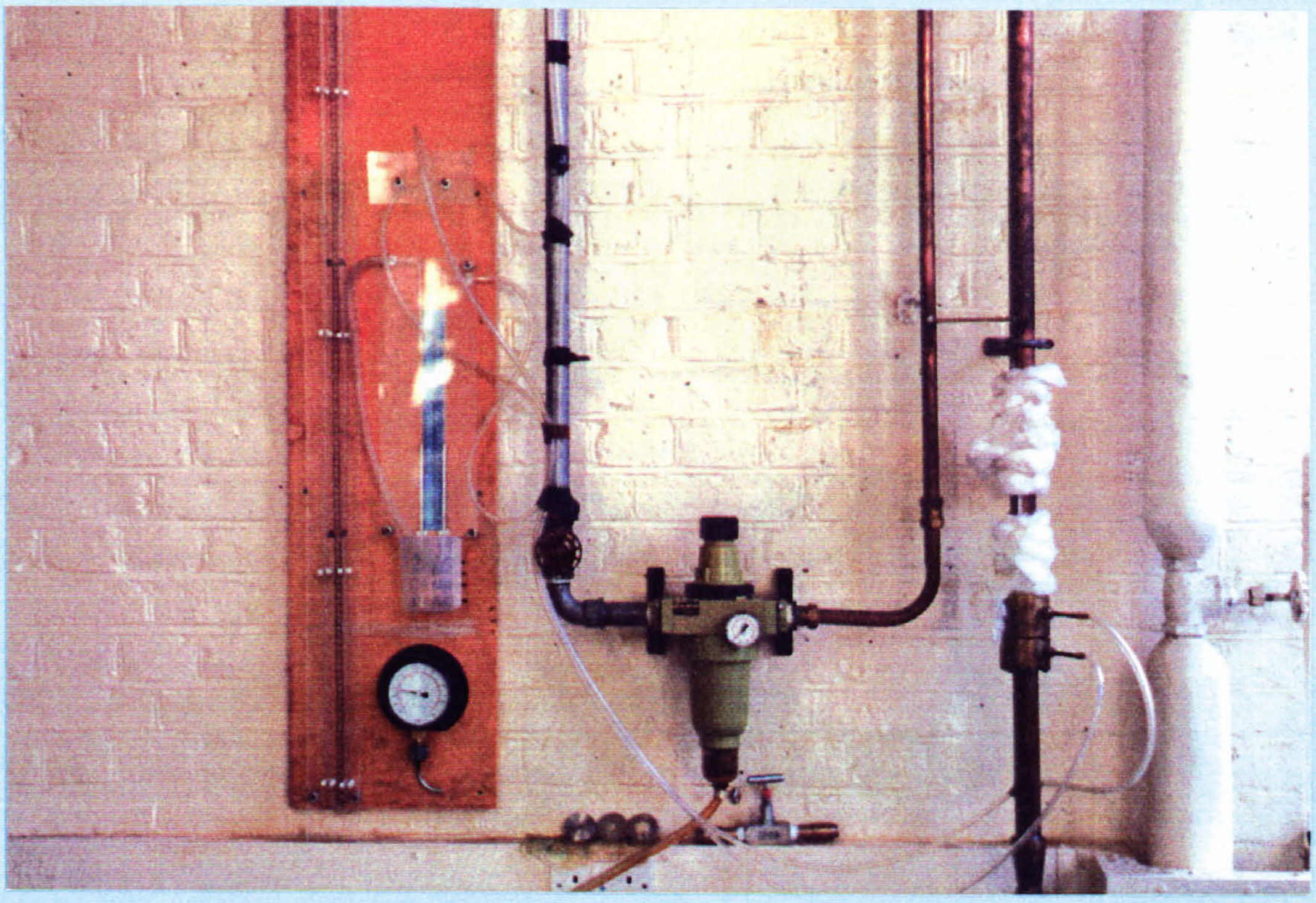


Figure 3.4.1 Layout of air measurement

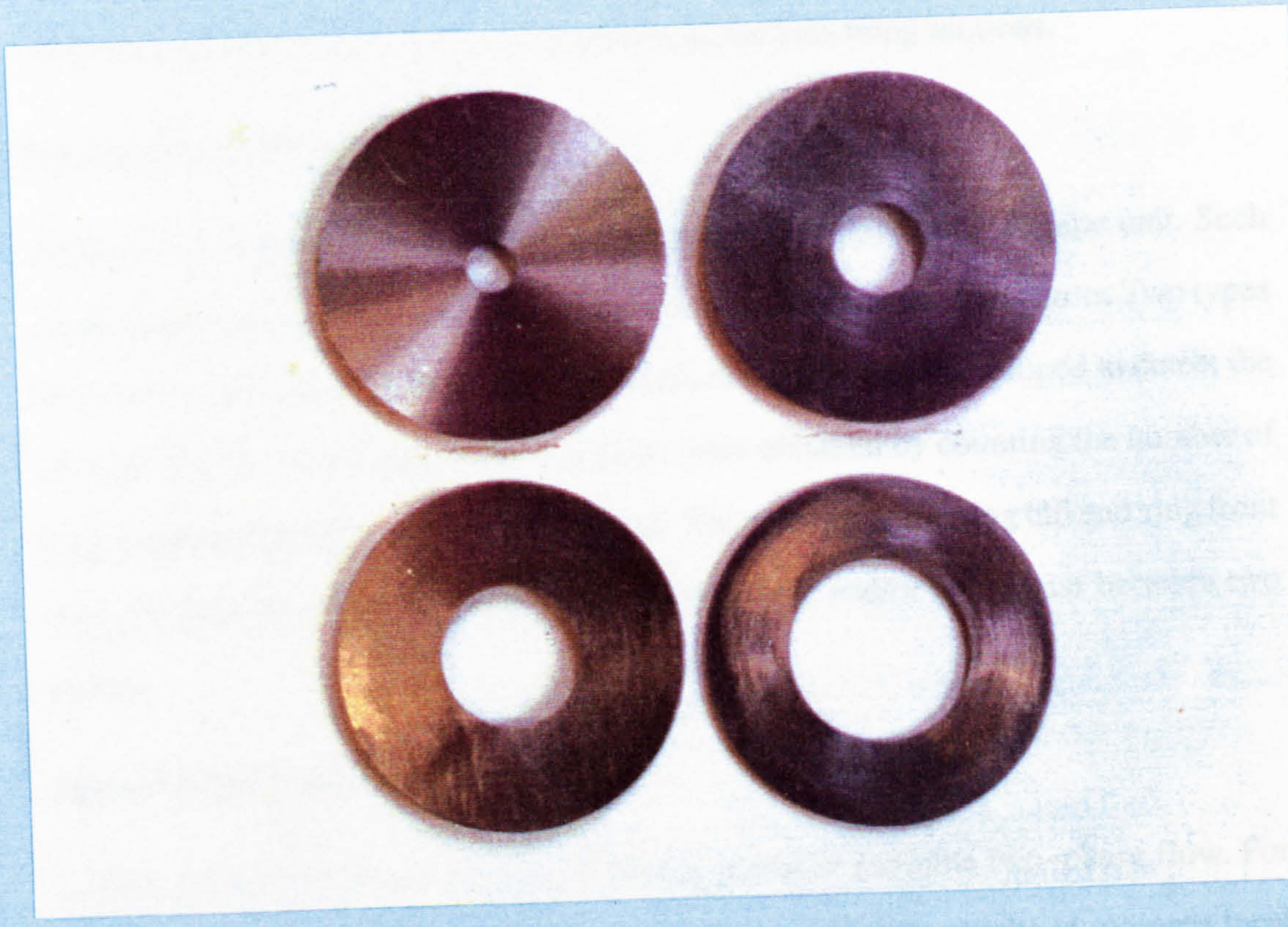


Figure 3.4.2 Air metering orifice plates.

3.5 INSTRUMENTATION

The experimental programme described in this work required identification of discrete intermittent units, pressure monitoring with time and flow visualisation. Techniques used to obtain this information are described in the following sections.

3.5.1 SLUG DETECTION

Probes were required to detect the passage of an intermittent flow regime unit. Such probes being used to obtain frequency and velocity of the intermittent units. Two types of probe, an optical fibre probe and a conductance probe were developed to detect the passage of slugs. The frequency of the slugs were obtained by counting the number of slugs passing a probe in a given time period. The velocity of the slug tail and slug front were obtained by recording the time for the slug front and/or tail to pass between two probes.

Optical Fibre Probes

Optical probes have been used in the past as a tool to examine two–phase flow. For example, Miller and Mitchie (1970) used a 0.3 mm diameter probe to measure local void fraction in two–phase flow. A review on optical probe devices is given by Delhaye (1982).

The probes use the principle, shown in Figure 3.5.1, that incident light passing down the fibre is completely reflected when the probe is in the gas phase. The tip of the probe can be considered to be a prism. Consider a probe of refractive index n_1 surrounded by a medium of refractive index n_2. Descartes law of refraction shows that a light beam with an angle of incidence i_1 will emerge from the probe at an angle i_2 :

$$n_1 \sin i_1 = n_2 \sin i_2 \qquad (3.5.1)$$

which in the case of a glass of n_1=1.62 and an angle of incidence to the probe tip of 45°, there will be refraction only when n_2 is greater than 1.15. Thus if the probe tip was surrounded by air it would reflect light (higher signal) and if surrounded by water refract light (lower signal).

In the work described in this thesis, optical probes manufactured from an optical fibre were used to measure slug frequency and translational velocity. Each probe consisted of an optical fibre bent through 180° to form a tip, approximately 3 mm wide. The fibre is enclosed in a stainless steel tube to protect the probe and ensure its rigidity. This tube is introduced into the test section through a guiding boss mounted on the outer wall of the test section pipe. The boss enables the probe to be located at any position in the vertical plane passing through the pipe center. Four probes were produced.

The light from a source located at one end of the optical fibre is reflected and refracted at the probe tip. The reflected light continues along the fibre and a phototransitor converts the light into an electrical signal. This signal is amplified and passed to the recording equipment detailed in Section 3.6.

It must be noted that while previous work using optical fibres has tried to reduce the size of the sensing tip, such considerations are not critical for the application in this work. Previous workers had to measure the local void fraction in two–phase flows with bubbles of small dimension, while the purpose in this work is only to detect the transition between the gas of the elongated bubble and the liquid of the slug front.

Wire Conductance Probes

The second technique used in determining the characteristics of the two–phase flows was the use of parallel wire probes. These consist of two wires placed at a constant distance apart and spanning the tube from top to bottom. The liquid content is determined by measuring the conductance between the two wires.

While, in principle optical probes can be applied to any fluid system, the application of the second method developed in this work is limited to liquids that conduct electricity. Wire probes have been used by Brown et al (1978) to measure liquid film thickness in annular gas–liquid flows. The details of the theory behind wire conductance probes are presented by Miya (1970) and Brown et al (1978).

Figure 3.5.2 shows the response of the conditioned wire probe signal to water height in a static calibration pipe for the wire probe developed in this work. The technique is

very sensitive to the conductance of the liquid phase. Thus, if the probe is used to determine liquid layer thickness, liquid layer conductance must be measured. However, in this present work the probes are used only to detect the passage of slugs and hence measurement of the liquid phase conductance is not relevant, the requirement being mainly to distinguish between a full and a partially empty tube.

The mounting arrangement of the parallel wire probes is shown in Figure 3.5.3. Two perspex disks, each with a hole in the middle, are mounted opposite each other on the top and bottom of the perspex test section.. Each disk contains four threaded metal rods with an arrangement of nuts to enable the wire to be tensioned and secured. In the centre of each disk the outer surface of the perspex test section is exposed. At this point two 0.35 mm diameter holes have been drilled through the pipe wall at a distance of 3mm apart in a direction normal to the tube axis. Wires pass through the 0.35 mm holes and extend vertically across the entire pipe section, parallel to each other. The separation between the wires is 3mm in the test section. The platinum wires used in the probes were 0.05 mm diameter. Eight wire conductance probes were manufactured for the test section, allowing the distance over which slug translational velocity is determined to vary between 10 cm and 10 m.

Figure 3.5.4 shows a circuit diagram of the electronics developed for the wire probes. An oscillator provides an input sine wave of 50 kHz to the wire probes. The output signal from a wire probe is another sine wave in phase with the input sine wave, but with an amplitude which is dependant on the liquid height. The output sine wave from the wire probe is connected to a conditioner which provides a DC output signal corresponding to the peak voltage of the output sine wave. This DC signal is recorded by the equipment detailed in Section 3.6.

A typical digitised signal obtained by the wire probes with slug flow in the test section is shown in Figure 3.5.5. As can be seen, the signal shows the sharp rise in liquid 'height' at a slug front followed by a gradual drop in liquid height at the slug tail. The local troughs in the signal within the slug body correspond to concentrations of air bubbles.

3.5.2 PRESSURE MEASUREMENT

Some of the experiments detailed in later sections require measurement of the local pressure in the pipeline as a function of time. The pressure was monitored by two transducers linked to the data capture equipment described in Section 3.6. Two Druck flush mounting strain gauge bridge type pressure transducers were located on the test section. A flush mounting transducer has its sensing diaphragm fitted at the tip of the thread connection, enabling flush mounting of the transducers on the pipe circumference at the pipe top. The pressure transducers are threaded into a perspex boss located on the pipeline. Each transducer had an operating pressure range of 0 to 1 bar gauge and was calibrated over the range using a Budenburg dead weight tester.

3.5.3 FLOW VISUALISATION

One of the experimental objectives of the work described in this thesis was to examine the details of intermittent flow. Photographic studies provide an unrivalled technique for examining the mechanisms associated with multi–phase flow. Hence a significant effort was invested in the photographic examination of fast transients associated with intermittent flow. Initially a Milliken high speed motion picture camera was used.

This camera was run at its maximum speed of 400 frames per second using the maximum film size of 4000 frames. Though the author was fortunate at having sole use of the camera and dark room, several problems were encountered with applying the equipment to the test facility.

At the higher gas flowrates investigated, the waves at the interface of the gas and liquid were moving so fast that a blurred film image resulted. While this was not the case at lower gas flowrates it was difficult to ensure that an event such as a slug initiation cycle (or even a part of the cycle) was recorded within the ten seconds filming time. While it was possible to predict when a initiation was about to take place within about 2 seconds, it was not possible to be certain that the event would occur in the filming window due to the random nature of the phenomena. In addition the time lag between shooting a film and viewing the result to see if an event was captured was about a day. The above

resulted in high rates of film and time wastage and hence significant operating cost penalties.

A way around these problems was provided by using the Kodak Ektapro high speed video camera equipment of the Harwell Photographic centre. This equipment allowed a speed of 1000 frames per second which adequately captured the events of interest. In addition at this speed, a recording time of 20 seconds was available and the recording could be played back immediately after recording, reducing operational time and eliminating film wastage. It must be noted that the expense of using this equipment outside its home laboratory limited its use on this project to one day. The resulting video was digitised and then analysed on a personal computer, again reducing the effort involved in examining the mechanisms.

The digital processing equipment used was a Imaging Technologys PCVISION Frame Grabber and its associated software package. The analogue signal from the video recorder was sampled at discrete time intervals and each sample converted to a digital value. This value is then stored in the memory of the frame grabber, with one pixel stored in each memory location. The frame memory is then accessible by the CPU in the personal computer, and can be manipulated by the software.

The above paragraphs have concentrated on the recording equipment used for the visualisation studies. Equally important are the means of lighting and the materials through which the light has to pass. The latter is particularly important when considering light transmission through curved surfaces, such as perspex pipes.

In flow visualisation experiments the potential optical distortion resulting from a curved surface such as a pipe has to be considered. The resulting distortion depends on the difference between the refractive indices of the transmission materials and the viewing angle. For example, if the pipe wall material has a higher refractive index than the surrounding fluid then a beam of light is bent away from the centre of the pipe, see Figure 3.5.6. This is the case with air as the surrounding fluid. Fogwell (1986) noted that no distortion results when looking through a flat surface into a medium of constant

refractive index. He further proposed that since circular pipes have curved boundaries, it is necessary to match the refractive index of the tube material with that of the fluid inside the pipe. In addition it is necessary to fill the volume between the pipe and the flat viewing window with a fluid which has the same refractive index as that flowing inside the pipe. Thus all refractive indices match and distortion is eliminated.

In the experiments of this work two fluids, air and water, coexist in the pipe. There is no solid material with as low a refractive index as air, hence only the refractive mismatch resulting from the interfaces of the pipe material and the water and the pipe material and the fluid outside the pipe can be reduced. Thus it is necessary to obtain a pipe wall material which has a refractive index close to that of water.

Fogwell (1986) examined the refractive indices and transmission spectra of a number of materials one of which was found to have a refractive index close to that of water. Fluorinated ethylene propylene (FEP) whose refractive index is 1.34. It was decided to manufacture a flow visualisation section out of FEP.

A photograph of the complete assembly is given in Figure 3.5.7, this includes an external box containing the flat viewing plate, which also enables the pipe to be surrounded with water. The manufacture of the 3 inch diameter FEP section suitable for optical work required faster quenching than is usually used by the manufacturers of the material. This quick cooling reduces the amount of crystalline structure present in the FEP of a size able to refract visible light. Hence the scattering of light will be reduced, resulting in the reduction of the opacity of the material. Even so, the wall thickness of the FEP tube had to be kept to a minimum as a thick piece of this material passes almost no light.

The fact that the pipe thickness has to be small, which makes the pipe rather flexible, places a limitation on the length of the section that could be installed in the test facility. This in turn means that the flanges of the visualisation section must be designed so as to keep to a minimum the flow disturbance induced. FEP is an awkward material to flange as no commercially available compounds are able to glue the material. This was

overcome by trapping each end of the pipe material between two flanges with a ring of metal stretching the material as the flanges are drawn together by bolts. The ring and flanges were machined so that the transition from outer flange to the ring to the pipe material was smooth.

Various positions for the lighting were tried and the final form chosen was back lighting with a diffuse sheet in front of the back window of the visualisation box.

3.6 DATA CAPTURE

Signals from the instrumentation were recorded by two methods.

A SE Laboratories Ltd Ultra–Violet Recorder Type SE2005 was initially used to record signal time traces. This recorder produces traces by deflecting high intensity beams of light, rich in UV, onto Kodak Linagraph direct print paper at frequencies up to 8 kHz. The principle of operation of the recorder depends on the incident light from a UV lamp being deflected by the movement of a small mirror attached to the galvanometer suspension. This movement is caused by the 'motor' effect when a current is passed through a coil attached to the suspension. The recorder can handle up to 12 channels simultaneously.

Analog signals from the instrumentation were also digitised and stored on an Amstrad PC1512 personal computer. The specification of the Amstrad employed was 512 k bytes of main memory, with a 16 bit 8086 chip operating at 8 MHz and a 20 MByte hard disc. Analog to digital (A/D) conversions were performed by a Scientific Solutions Inc Lab Master data acquisition unit consisting of two boards connected by a ribbon cable, with the mother board installed in an expansion slot of the Amstrad PC1512. The mother board controls the digital logic and the external daughter board contains all the analogue acquisition circuitry. This mother–daughter feature has the advantage of allowing the daughter board to be located near to the source of the signals being acquired rather than having to run these analog signals over a distance and into the noisy PC1512 frame. The A/D unit can handle up to 16 single ended or 8 true differential inputs, and has a resolution of 12 bits with a jumper selectable input range of +/– 10 V or 0 to +

10 V. In the work described in this Thesis the signal voltage range of +/– 10 V was selected. A maximum A/D conversion rate of 30 kHz is possible with the LabMaster module, although the actual conversion rate used is specified in the software. Sampling rates used in this study were 1000 kHz for one channel, 10 kHz for three channels, and 100 Hz for eight channels. The mother board contains an AM9513 system timing controller which controls the timing of the A/D conversion. The AM9513 is a large scale integrated circuit with five general purpose 16 bit counters and an internal oscillator with associated frequency scaling circuitry for dividing frequencies. The internal oscillator is a crystal providing an accurate base frequency of 1 MHz.

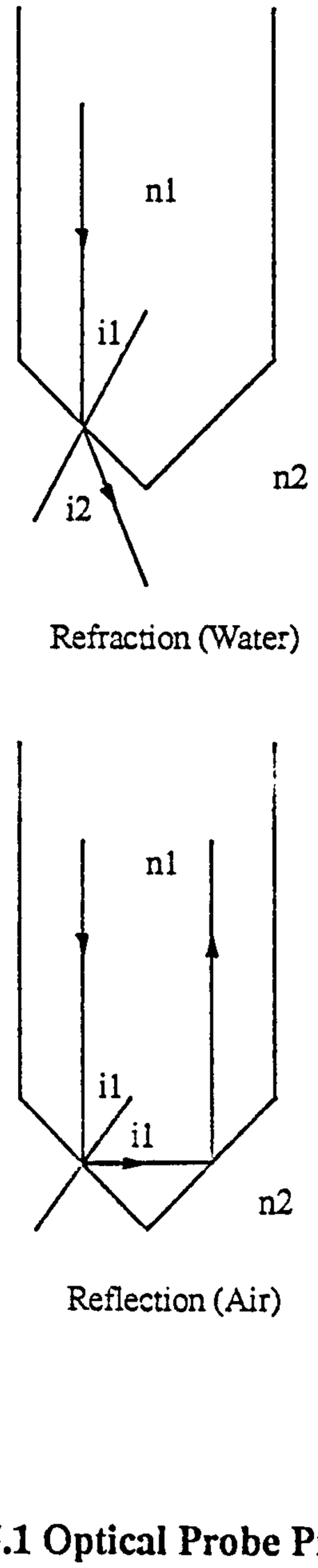
The computer programs associated with the Lab Master module, to control the A/D conversions and to record the data converted, were modified to be application specific. Data obtained from the A/D module was contained in a data buffer prior to being stored on the Amstrad PC1512 hard disc for latter analysis. Computer programs in the basic language were written to interrogate stored data files.

Tests on the computer based data acquisition were carried out to validate performance. An example test which used 3 signals of known characteristics as analog inputs to the A/D convertor is summarised below:

Channel	Input
1	+/– 8 V, Triangular, 10 Hz
2	+/– 8 V, Sine, 10 Hz
3	+/– 8 V, Square, 10 Hz

Sampling frequency: 1000 Hz for 3 channels.

Figures 3.6.1, 3.6.2 and 3.6.3 are the digitised results from channels 1,2 and 3 respectively. As can be seen the results are consistent with the applied signals in form, amplitude and frequency.



Refraction (Water)

Reflection (Air)

Figure 3.5.1 Optical Probe Principle of Operation

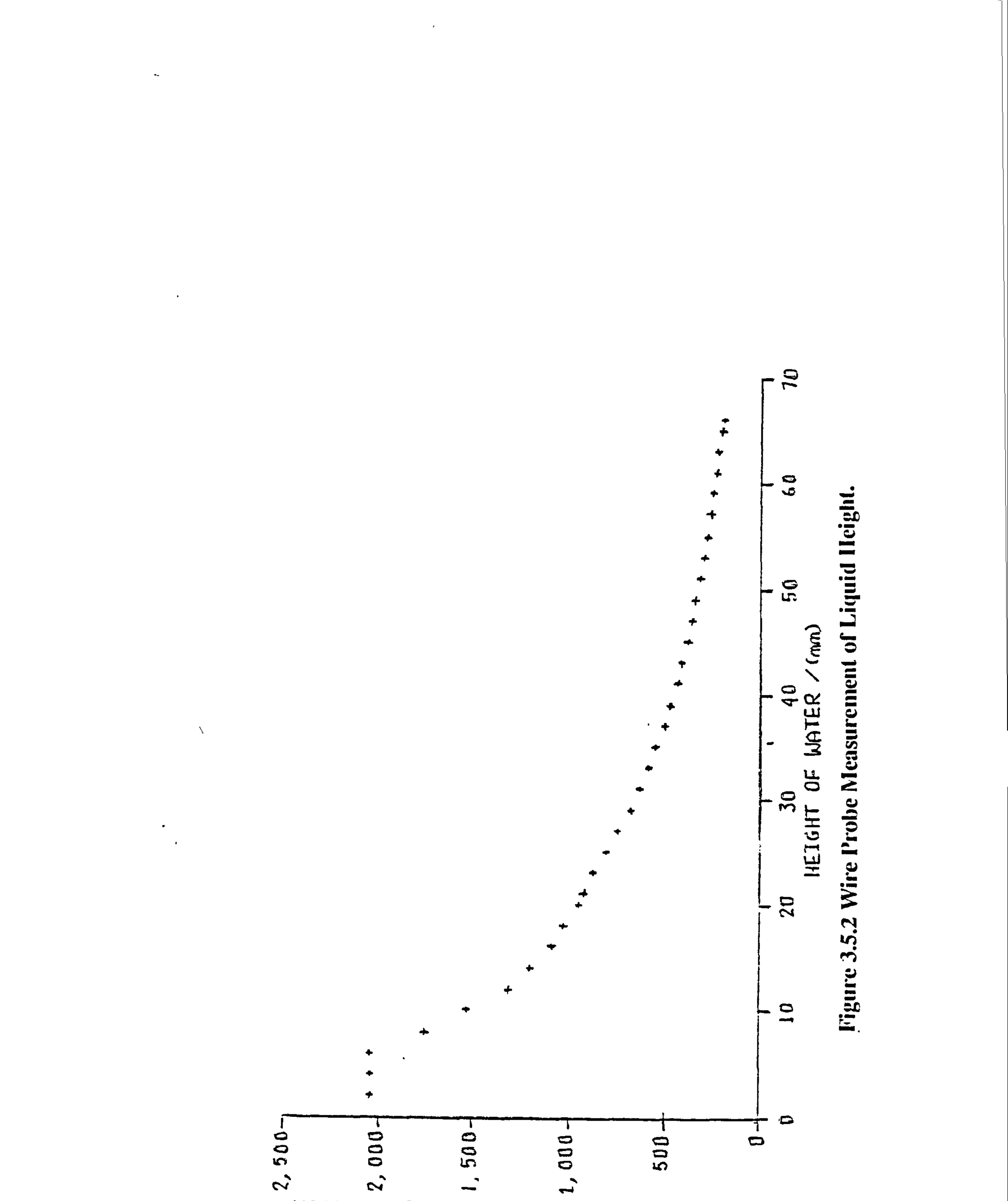


Figure 3.5.2 Wire Probe Measurement of Liquid Height.

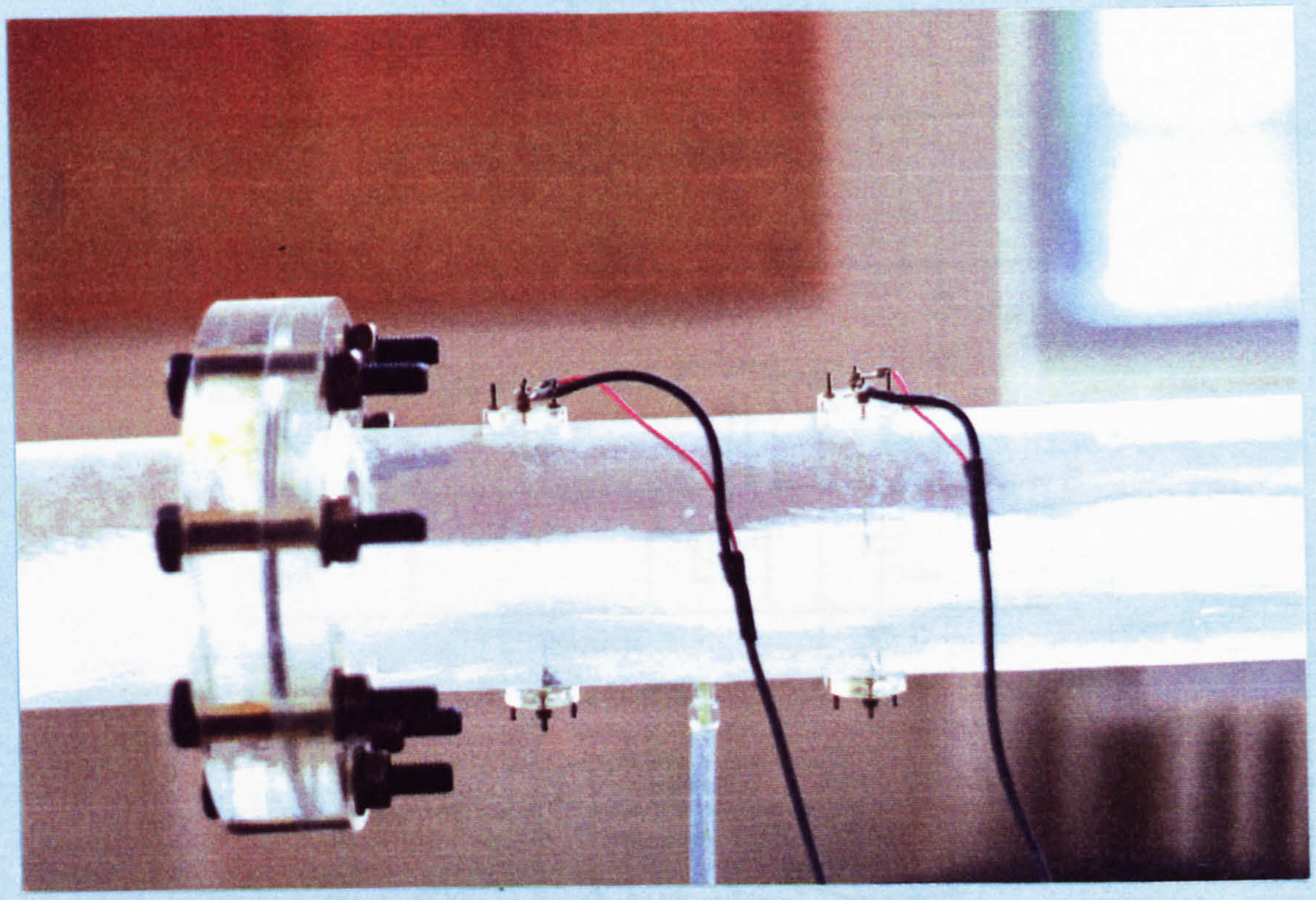


Figure 3.5.3 Wire probe mounting arrangement

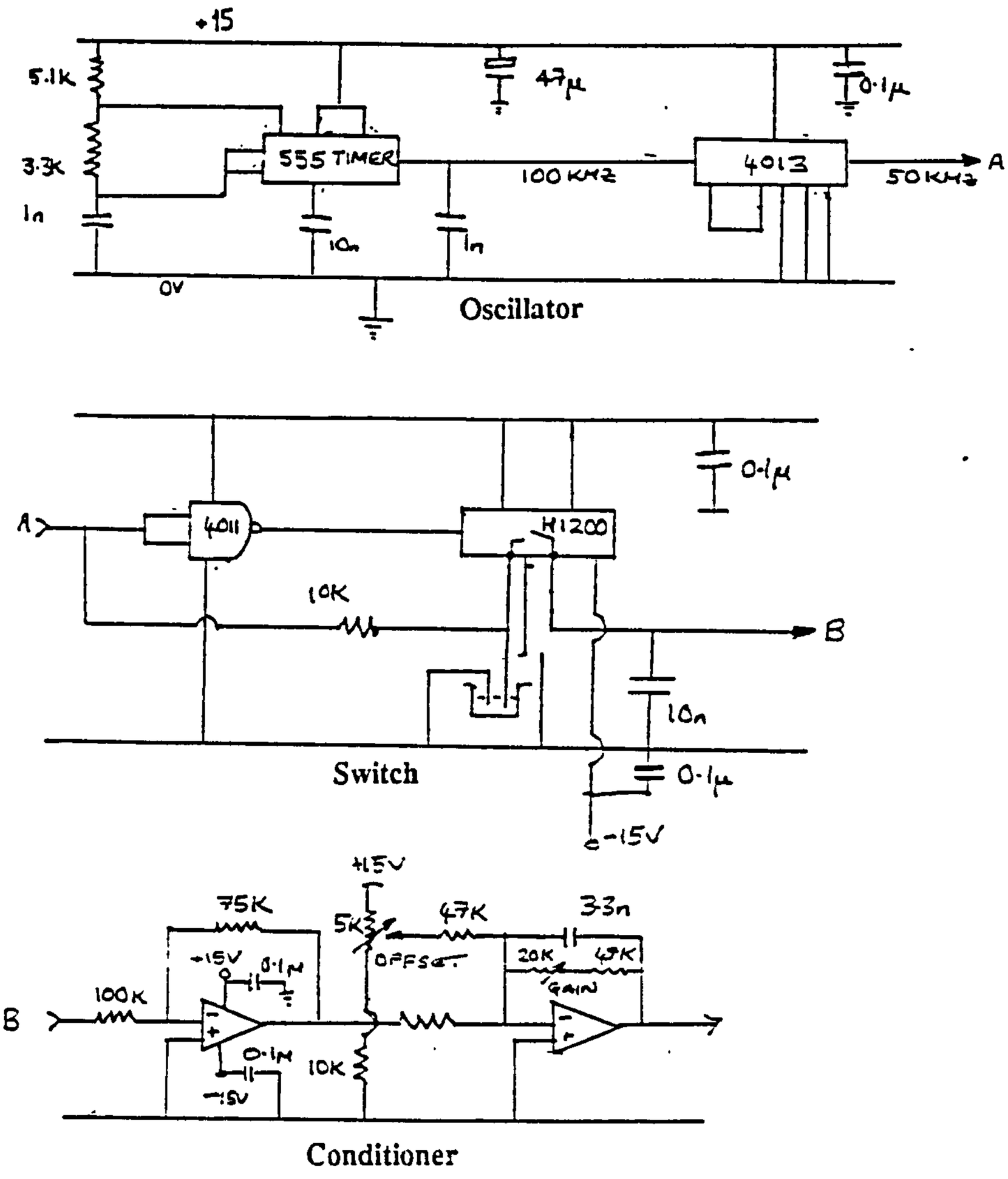


Figure 3.5.4 Wire Probe Electronic Circuit.

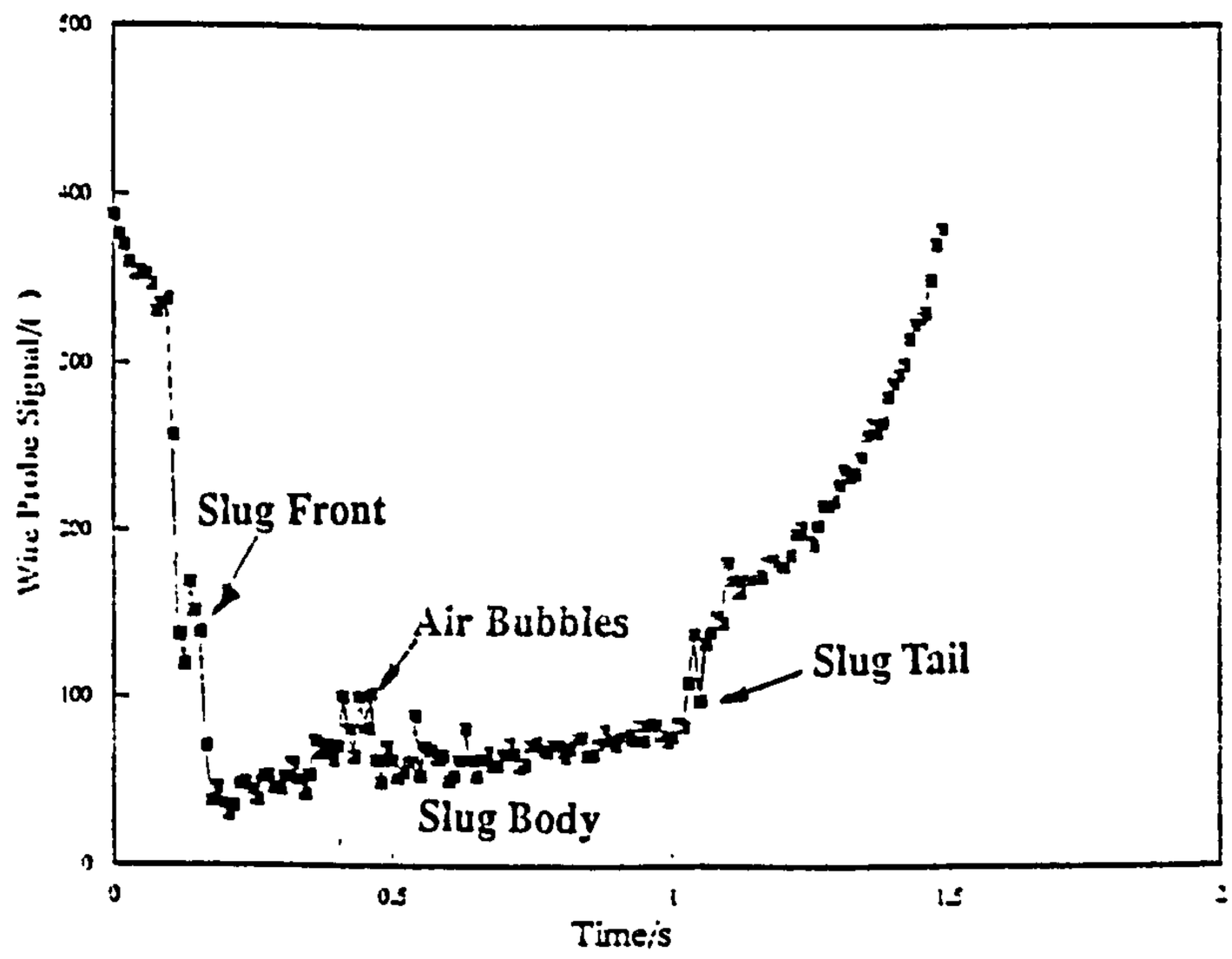


Figure 3.5.5 Typical Wire Probe Response

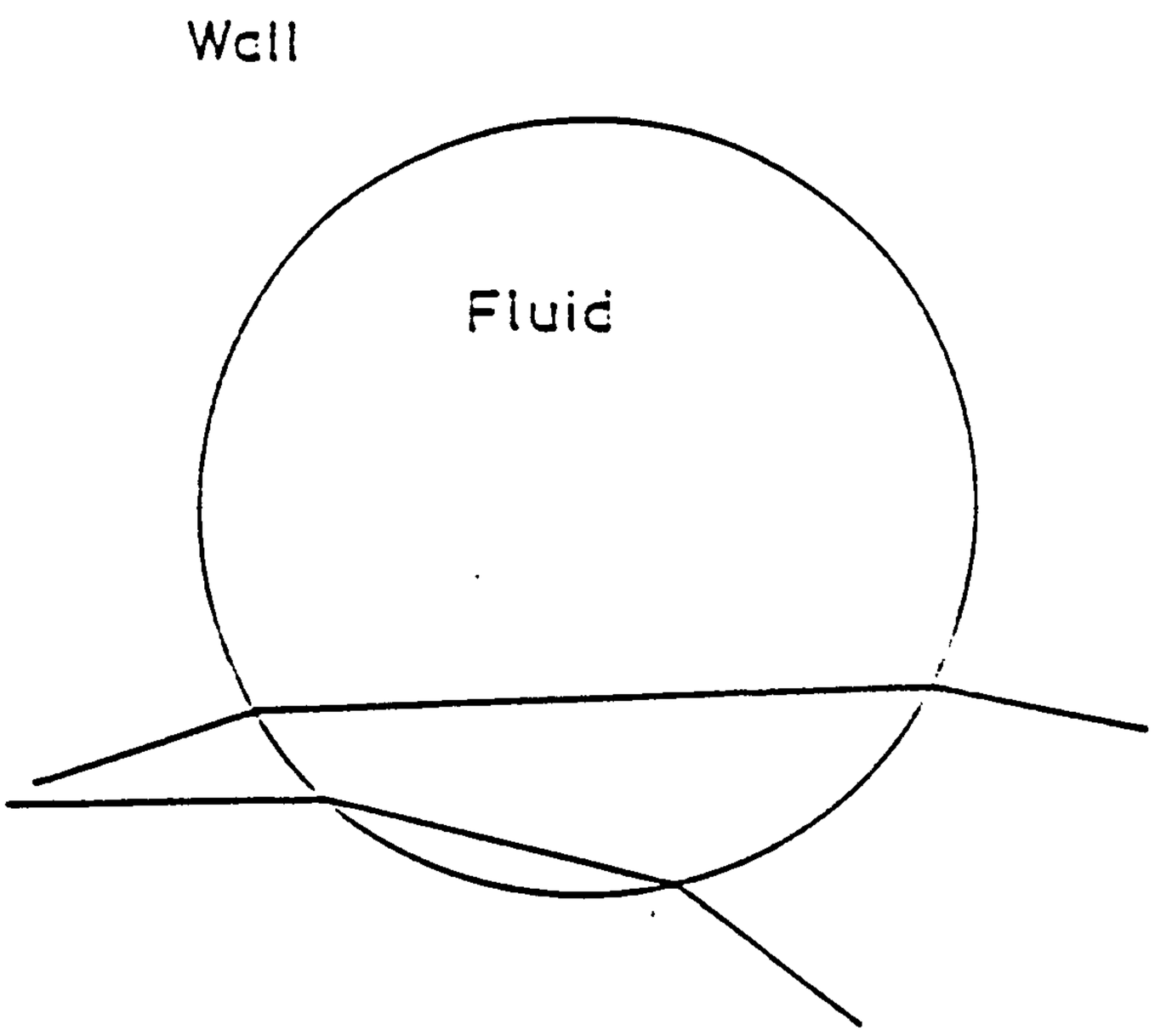


Figure 3.5.6 Refraction of Light Beam at Pipe/Fluid Interface
(Refractive index of pipe wall > refractive index of fluid).



Figure 3.5.7 Flow visualisation section.

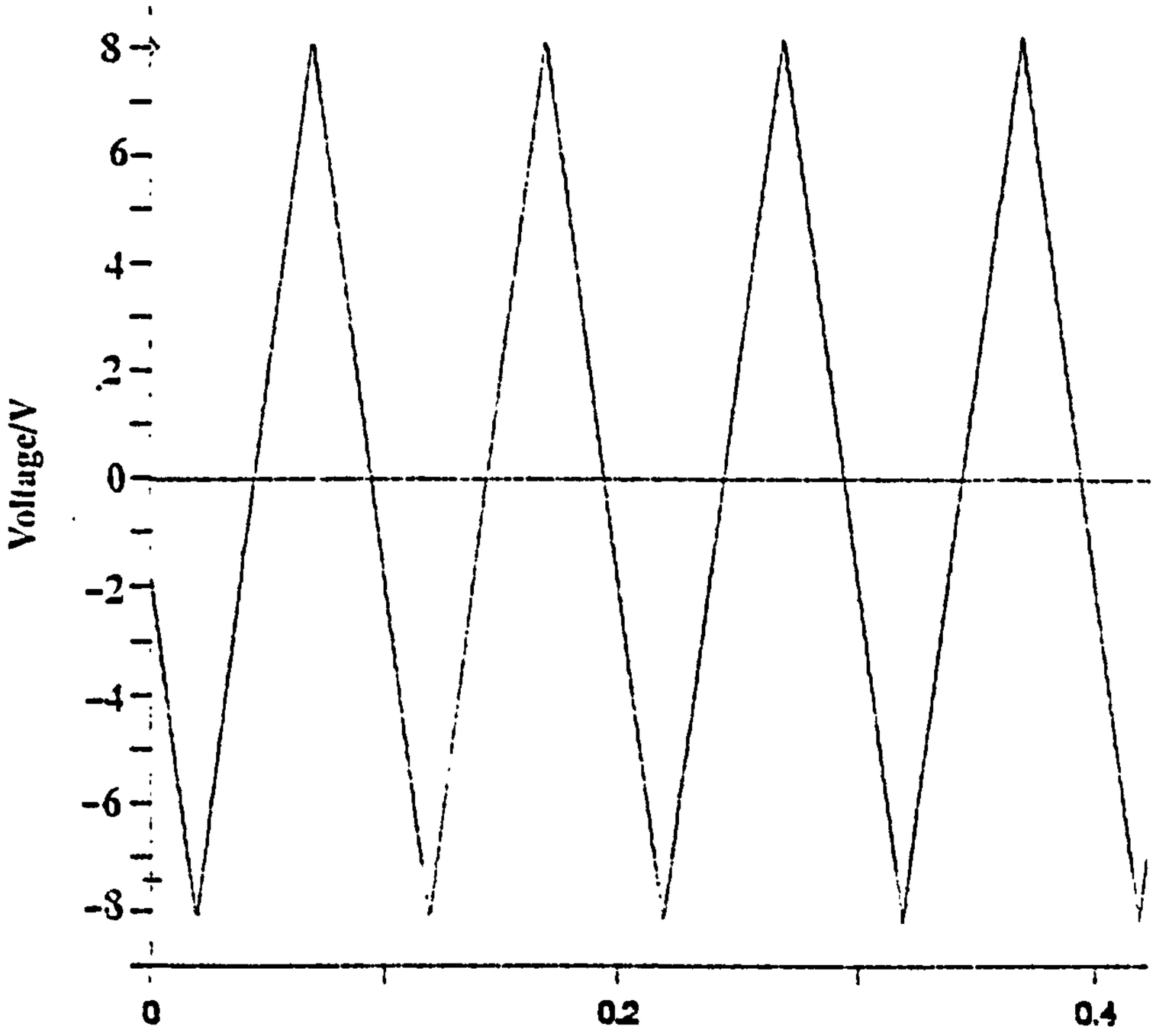


Figure 3.6.1 Triangular Test Signal (±8V, 10 Hz).

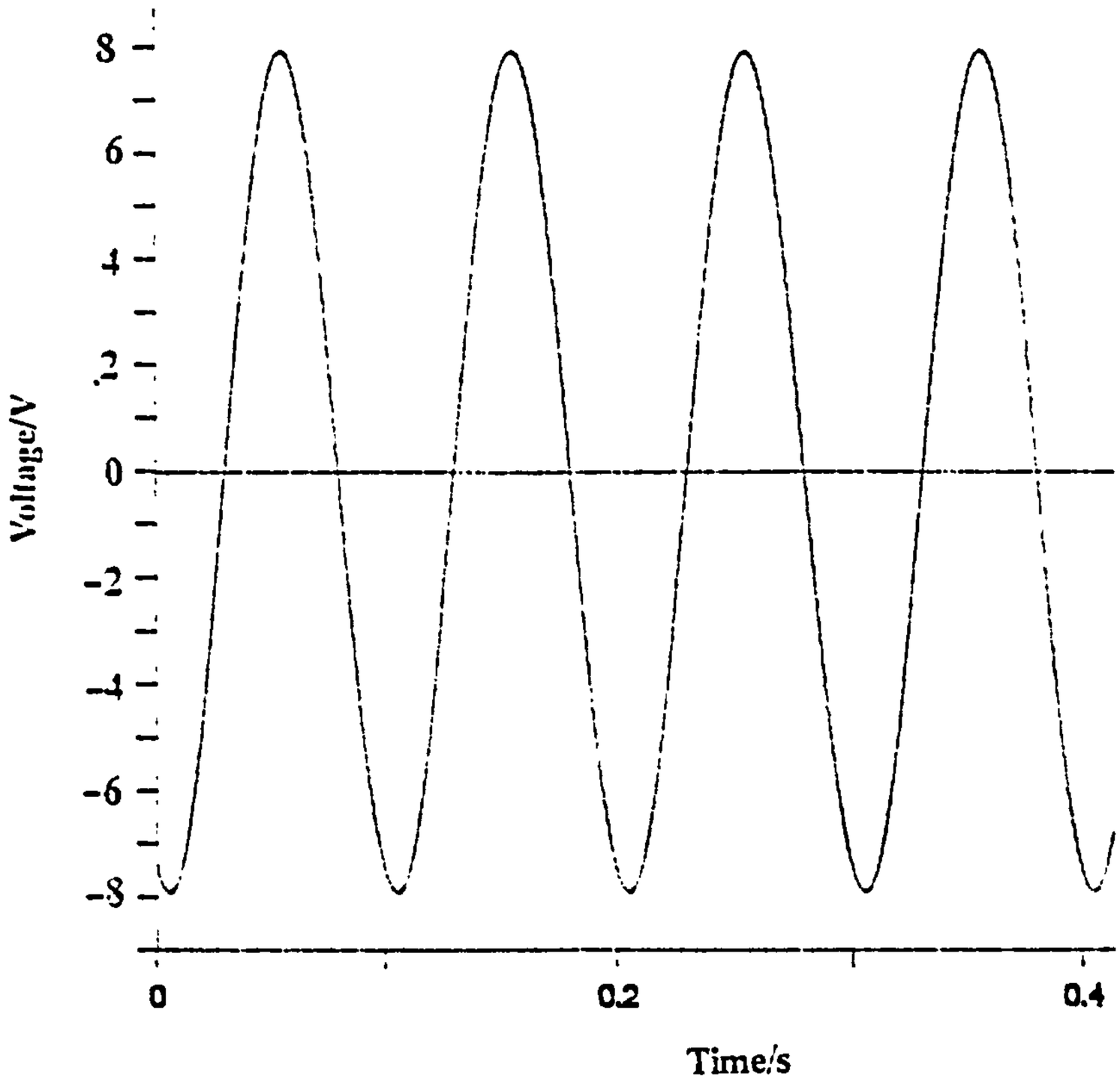


Figure 3.6.2 Sine Test Signal (±8V, 10 Hz).

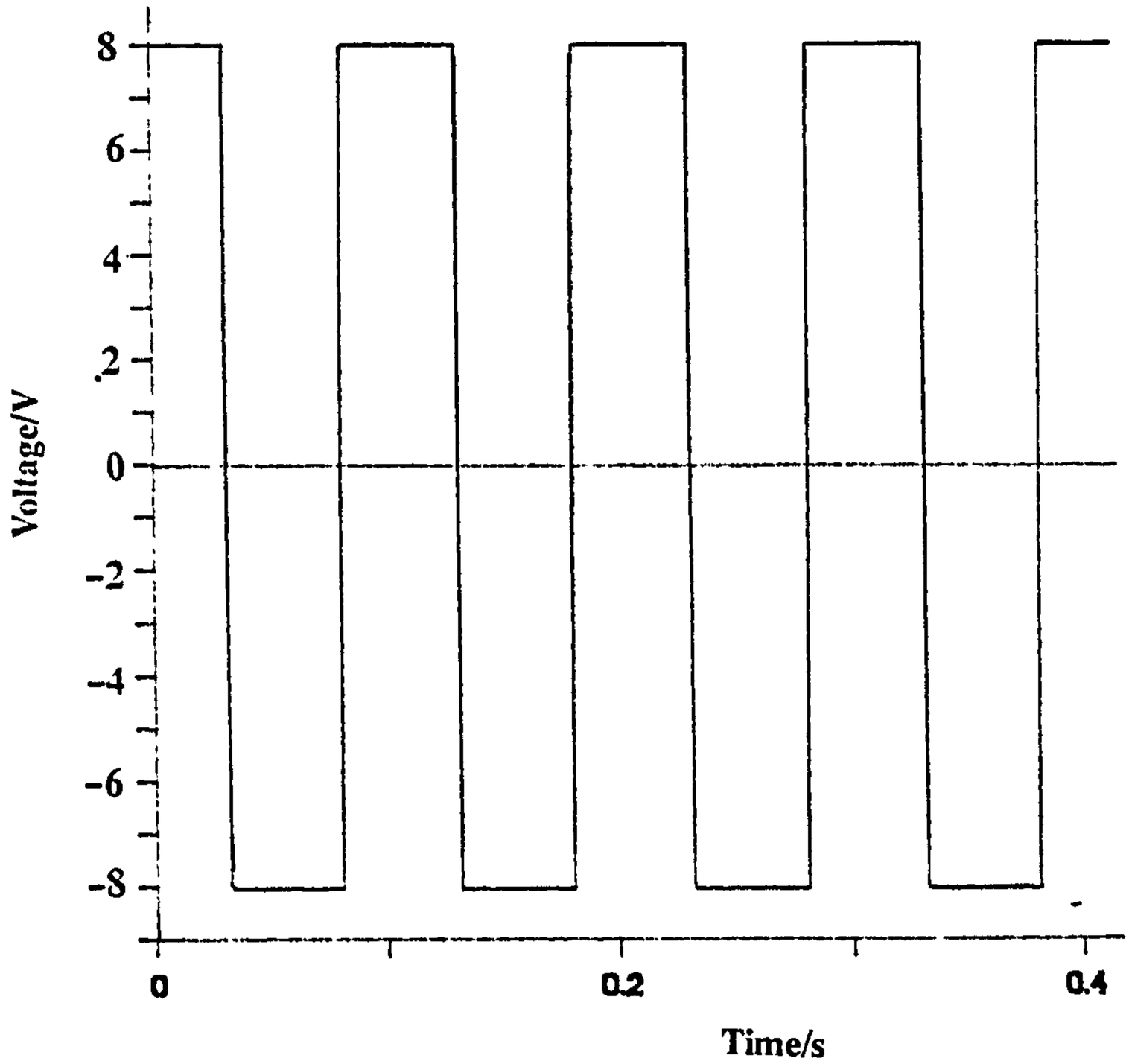


Figure 3.6.3 Square Test Signal (±8V, 10 Hz).

CHAPTER FOUR

PIPE GEOMETRY EFFECTS ON INTERMITTENT FLOW

This Chapter examines how pipeline geometry changes the characteristics of intermittent flow. Section 4.1 considers the effect of two different inlet geometries. The inlet design recommended from this work was installed in a large diameter pipeline. Section 4.2 presents the results obtained from the large diameter pipeline and a discussion of the effects on pipe diameter on the stratified to intermittent transition. The majority of the literature has been concerned with straight horizontal, vertical, or inclined pipelines; Section 4.3 examines the effect on intermittent characteristics of a small inclined pipe located between two horizontal sections. Section 4.4 presents an examination of riser–induced "severe slugging", which is of importance for the off–shore oil industry.

4.1 INLET MIXER GEOMETRY

In the past numerous experimental studies have delineated the intermittent–stratified transition and examined intermittent flow characteristics, but rarely has information on the inlet geometry used in the work been supplied. Even in the rare cases when the inlet geometry has been supplied to readers, only limited investigations of the effect of inlet geometry on the results obtained have been carried out. Though some of the previous workers have determined that the flow was fully developed at their metering position, it does not follow that the results obtained are independent of inlet geometry. To the authors knowledge it has yet to be proven that the characteristics of fully developed intermittent flow are independent of the inlet geometry chosen.

Three examples may be cited of authors who in varying degrees considered the effect of inlet geometry on two phase flow. Weisman et al (1979) considered two inlet devices, a simple horizontal tee and a mixer were the gas is introduced through a central annulus. They noted that an equilibrium situation seemed to be reached after a L/D of 60, and concluded that the flow pattern transition between stratified and intermittent

was not significantly affected by the inlet geometry at the end of their test section. Again limited consideration was given to inlet effects by Lin and Hanratty (1987), with two different test section L/D of 590 and 258. The entry section used was two simple tees with the air introduced in the branch and the water in the run. Some experiments were repeated with the air in the run and water in the branch and it was found that the stratified–intermittent transitions were identical except for low superficial air velocities of 1 m/s or less. A more focussed and detailed study by Bendiksen and Malnes (1985) reported the effect of varying the angle of the inlet section on the transition from stratified to slug flow, showing that the transition was sensitive to inlet geometry. A test section of L/D of 411 was used in their study. No data on slug characteristics was presented and hence no consideration given to the characteristics of the developing and fully developed flow resulting from different inlet sections. The title of the paper of Bendiksen and Malnes (1985) is "Experimental data on hysterisis effects in the transition from stratified to slug flow in horizontal tubes". Bendiksen and Malnes (1985) describe the variation of the transition between intermittent and stratified flow as a function of the interaction between the gas and liquid at the inlet. Hysterisis effects in the transition between stratified and intermittent flow may be investigated by examining the difference between two transition curves; the transition from stratified to intermittent flow and the transition from intermittent to stratified flow for a single inlet geometry. Such a difference may arise from the following mechanism.

A stratified flow with an equilibrium liquid layer height of h_1 and at gas and liquid mass flowrates infinitesimally below the condition at which intermittent flow would occur, takes place in a pipeline. A small increase in either gas or liquid mass flowrate would result in slug formation. Gas and liquid flowrates at the test section inlet are independent of downstream pressure. The pipeline length is such that any slug transit time to the end of the pipe is significantly greater than the stratified layer rebuild time resulting from either slug formation or flowrate changes. Consider an infinitesimal increase in gas mass flow which results in a small interfacial disturbance forming a slug. The slug grows and travels down the pipe, with the pressure in the upstream gas cavity reaching

a higher steady value after the initial pressure transient due to the acceleration of the slug from rest. This pressure increase will result in the gas velocity over the liquid surface decreasing and hence the liquid level rising due to reduced interfacial shear. The flow geometry upstream of the slug will be stratified.After slug formation the gas mass flowrate is reduced to its initial value, and the resulting new stratified equilibrium level h_2 will be above the initial value h_1. If this level h_2 had been reached from the initial stratified flow the increase in liquid mass flowrate necessary would have resulted in slug formation. The exit of the slug from the pipeline releases the gas pressure upstream and the resulting velocity over the liquid interface is greater than that of the initial stratified flow, with a greater liquid height. Hence a new slug is formed despite the fact that the inlet gas and liquid mass flowrates are not sufficient in themselves to cause slug initiation. The perpetuation of the intermittent flow regime at the initial flowrates will depend on the liquid film height on which the slug travels being sufficient to sustain the slugs formed. The liquid film height will be formed from the liquid released from the preceding slug and the flow from the upstream stratified layer.

In previous work some authors have concluded that inlet geometry has a sustained effect on the stratified–intermittent transition while others have concluded that negligible effect was recorded. In view of the different inlet types compared by different authors it is not possible to form a view as to which claim is true. It is not unreasonable to postulate that while the inlet geometries considered respectively by Lin and Hanratty (1987) and Weisman et al (1979) may be physically different the extent of gas–liquid interaction introduced is similar. In comparison it is known that significant differences in gas–liquid interaction were induced by Bendiksen and Malnes (1986) varying the inlet section angle. In the work described in this thesis it was decided to investigate the effect of inlet geometry on not only the stratified to intermittent transition but also on intermittent characteristics, using two inlet geometries that would represent the "worst" and "best" case interactions of the gas and liquid possible at the inlet. The worst case interaction for testing inlet effects on intermittent characteristics and the stratified to intermittent transition is to maximise the number and amplitude of inlet

induced interfacial waves on the stratified layer and the best case is an inlet that minimises the number and amplitude of inlet induced waves on the stratified layer. It was decided after viewing several inlet configurations (including vertical and horizontal tees, a gas annulus with liquid core, a liquid annulus with gas core and bends just downstream of the inlet) that the worst case interaction was with the gas and liquid contacting head on (air and water are introduced through two tubes which are opposite each other on the pipe circumference, the air entering vertically downwards and the water entering vertically upwards) and that the least interaction could be obtained by introducing the liquid and gas parallel to each other from a calming section.

The objectives of the study were as follows:

(1) To measure flow characteristics such as slug front velocity and slug frequency as a function of pipelength in the developing region and in the developed region for each inlet case.

(2) To measure the transition boundary for stratified to intermittent flow for each inlet case as a function of pipelength.

(3) To examine whether the characteristics of fully developed intermittent flow vary with the inlet geometry.

It was recognised at the start of this work that a long pipe would be required to fully satisfy the above objectives. Data obtained on the low pressure facility described in Chapter 3 is presented in this section. The length of the test section in the low pressure facility was less than ideal (L/D = 135) and, as part of the work done for this thesis, a major new high pressure facility with L/D = 540 was designed and constructed.

4.1.1 Experimental Method

The low pressure flow facility described in Chapter 3 was used in the configuration shown in Figure 4.1.1. As can be seen, wire probes were located at three positions in the tube and were used to measure the average slug front velocity between the first and second probe and second and third probes. Time averaged slug frequency was visually recorded at the third wire probe position downstream of the test section inlet. The nom-

inal flow matrix examined consisted of 0.44, 0.64, 1.0, 1.46, 1.86, 2.34, 3.04, 3.75, 4.2, and 5.2 m/s gas superficial velocity and 0.14, 0.18, 0.225, 0.271, 0.32, 0.391, 0.455, and 0.52 m/s liquid superficial velocity.

The transition boundary between intermittent and stratified flow was determined by setting a gas and liquid flowrate in the stratified flow regime and then increasing the liquid flowrate in small steps at constant gas flowrate until intermittent flow was observed at the third wire probe position. At low flowrates, experiments required long observation times (a typical time was 15 minutes) to determine the flow regime. Observation of even a single slug at the third wire probe position was recorded as intermittent flow. The first liquid velocity at which intermittent flow was observed was taken to be the transition velocity at which the transition from stratified to intermittent flow occurred.

The inlet section described in Chapter 3 was used to form first a tee inlet, were the air and water contact head on (see previous page), and, then a plate inlet which separates and diverts both flows parallel to each other before contact. The tee inlet is referred to as "no plate" and the parallel flow inlet as "plate" in the following text. In both inlet configurations the air enters from the top and the water from below.

4.1.2 Intermittent Characteristics

Figures 4.1.2 to 4.1.9 show the variation of slug frequency as a function of gas superficial velocity, with each figure depicting data for one superficial liquid velocity for both the "plate" and "no plate" inlet configurations.

In general the slug frequency increases with increasing liquid superficial velocity, but distinct differences in both the form and magnitude of the slug frequency verses superficial gas velocity curves is noted between the "plate" and "no plate" inlet configurations.

Figure 4.1.2 shows, for a liquid superficial velocity of 0.14 m/s, that for both the "plate" and "no plate" inlets the range of flowrates at which intermittent flow was observed is limited, this being more so for the "plate" configuration, and that any slugs

formed are infrequent. As the liquid superficial velocity increases the gas superficial velocity range over which intermittent flow is observed increases as does the frequency of the slug units. It is noted that at lower superficial gas velocities the slug frequencies for the "no plate" inlet are greater than those of the "plate" inlet and that the opposite is true at higher gas superficial velocities.

It was observed that the initiation of slugs occurred at the inlet for the "no plate" inlet while for the "plate" inlet the position of slug initiation depended on the gas superficial velocity and ranged over the entire length of the test section. In addition it was noted that the frequency of initiation was higher for the "no plate" inlet than for the "plate" inlet reflecting the greater fluid interaction of the "no plate" inlet.

The following mechanisms may explain the results presented in Figures 4.1.2 to 4.1.9. At low gas flowrates slugs are initiated for the "plate" geometry near the inlet within a narrow axial position range. These slugs persist to the end of the pipe so that the slug initiation frequency is equivalent to the slug frequency at the third wire probe position. Similarly a large majority (but not all) of the slugs initiated for the "no plate" inlet persist to the end of the test section. In view of the higher slug initiation frequency of the "no plate" inlet in comparison with the "plate" inlet the frequency of slugs monitored at the third wire probe is greater for the "no plate" inlet at low gas superficial velocities. As the gas superficial velocity is increased the slug initiation frequency dramatically increases for the "plate" inlet and slugs are formed at multiple positions in the pipe. In addition the proportion of slugs initiated for the "no plate" inlet which persist to the third wire probe decreases. Note that the "no plate" slugs have a longer development (or decay) length than slugs of the "plate" geometry which were formed nearer the third wire probe position and in some cases just downstream of that position. These two effects result in the slug frequency measured at the third wire probe being less for the "no plate" inlet geometry than the "plate" inlet at higher gas superficial velocities, with the difference between the two increasing with gas superficial velocity.

Figures 4.1.10 to 4.1.25 show the variation of slug front velocity as a function of gas superficial velocity, with each figure depicting data for one superficial liquid velocity

for both the "plate" and "no plate" inlet configurations. The velocity measurements were taken between wire probe number one and two (indicated as upstream measurement in the Figures 4.1.18 to 4.1.25) and between probes number two and three (indicated as downstream measurement in the Figures 4.1.10 to 4.1.17). In general the slug front velocities noted for the "plate" and "no plate" inlet configuration are close at a given gas and liquid flowrate. The exceptions may correspond to slugs that are travelling over a liquid layer formed from a decayed slug or the inlet stratified flow. The slug front velocity for both "plate" and "no plate" inlets increases with increasing gas superficial velocity.

This near independence of slug front velocity of inlet geometry is to be expected as the average fluid velocity in the slug body is determined by the gas and liquid flowrates at the inlet to the test section. The shedding rate from the tail of each slug can hence be considered to be close and hence the height and velocity of the film on which the next slug travels similar for both inlet geometries. Thus since the velocities of the slug body fluid are similar and the characteristics (such as height and velocity of the film) are similar, it is to be expected that the resulting slug front velocities are close and hence would be independent of inlet geometry in fully developed flow.

4.1.3 Stratified–Intermittent Transition

Figure 4.1.26 shows a experimental survey of the transition from the stratified to intermittent flow regime in terms of gas and liquid superficial velocities for both the "plate" and "no plate" inlet geometry. As can be seen over most of the range of gas superficial velocities the transition to intermittent flow occurs first for the "no plate" inlet geometry. This reflects the greater interaction between the gas and liquid for this geometry. It must be noted that this transition has been determined for a short pipe of length 10 m. Experiments planned for the long facility described in Chapter 6 would need to examine the transition from stratified to intermittent flow as a function of pipelength to determine if the above difference persists.

4.1.4 Flow Development

As stated earlier, the test section length in the low pressure facility is less than ideal. Although the test section is suitable for investigating developing flow it is not long enough to determine fully developed flow characteristics. It was for this reason that the facility described in Chapter 6 was built. A fully developed flow which is truly independent of inlet conditions would exhibit not only insensitivity of slug frequency and velocity to inlet configuration, but also fixed values of statistical properties such as slug length distribution and distribution of time between slugs. Such statistical distributions can be determined from the output of the wire probes as may be illustrated by the results from the low pressure facility.

Data on distributions of time between slugs, as measured in the low pressure (10m tube length) test facility are shown in Figures 4.1.27 to 4.1.29. Each figure shows the distribution of the time between slugs (measured over a period of five minutes only) for the "plate" and "no plate" inlet geometries at one flow condition. Figures 4.1.27 and 4.1.28 again show the significant difference in slug frequency between the "plate" and "no plate" inlets, with significant differences in the form of the distribution of times between slugs. In carrying out further work with the new facility, this form of analysis could be used to investigate the state of development of the flow.

In summary preliminary work has shown that the inlet geometry has a significant effect on slug frequency and the stratified to intermittent transition in the developing flow seen in the 10 m low pressure test section. In future work, experiments using the facility described in Chapter 6 will examine the persistence of these differences as a function of pipelength in developing flow and in the developed flow region.

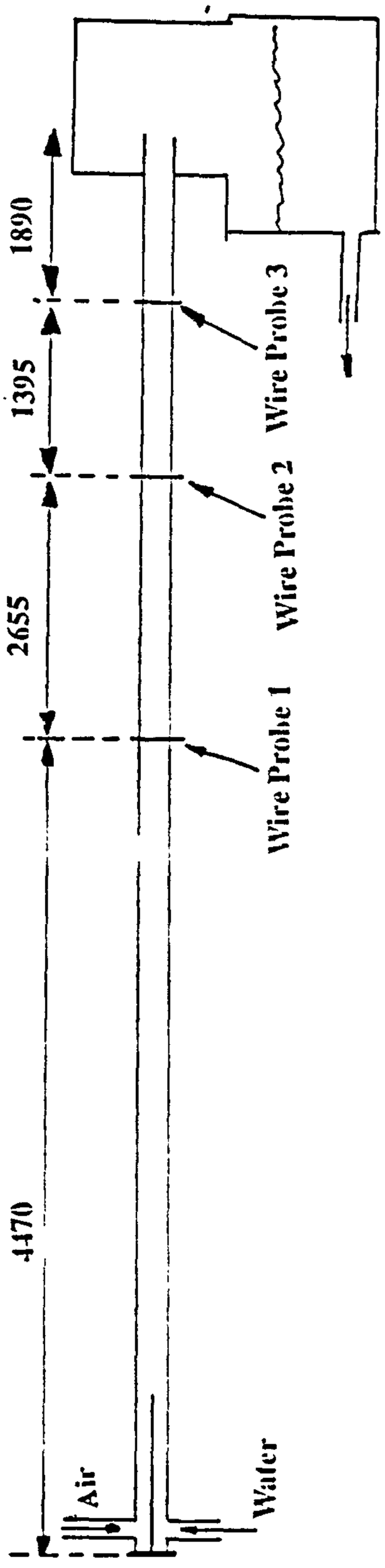


Figure 4.1.1 Test Section Configuration

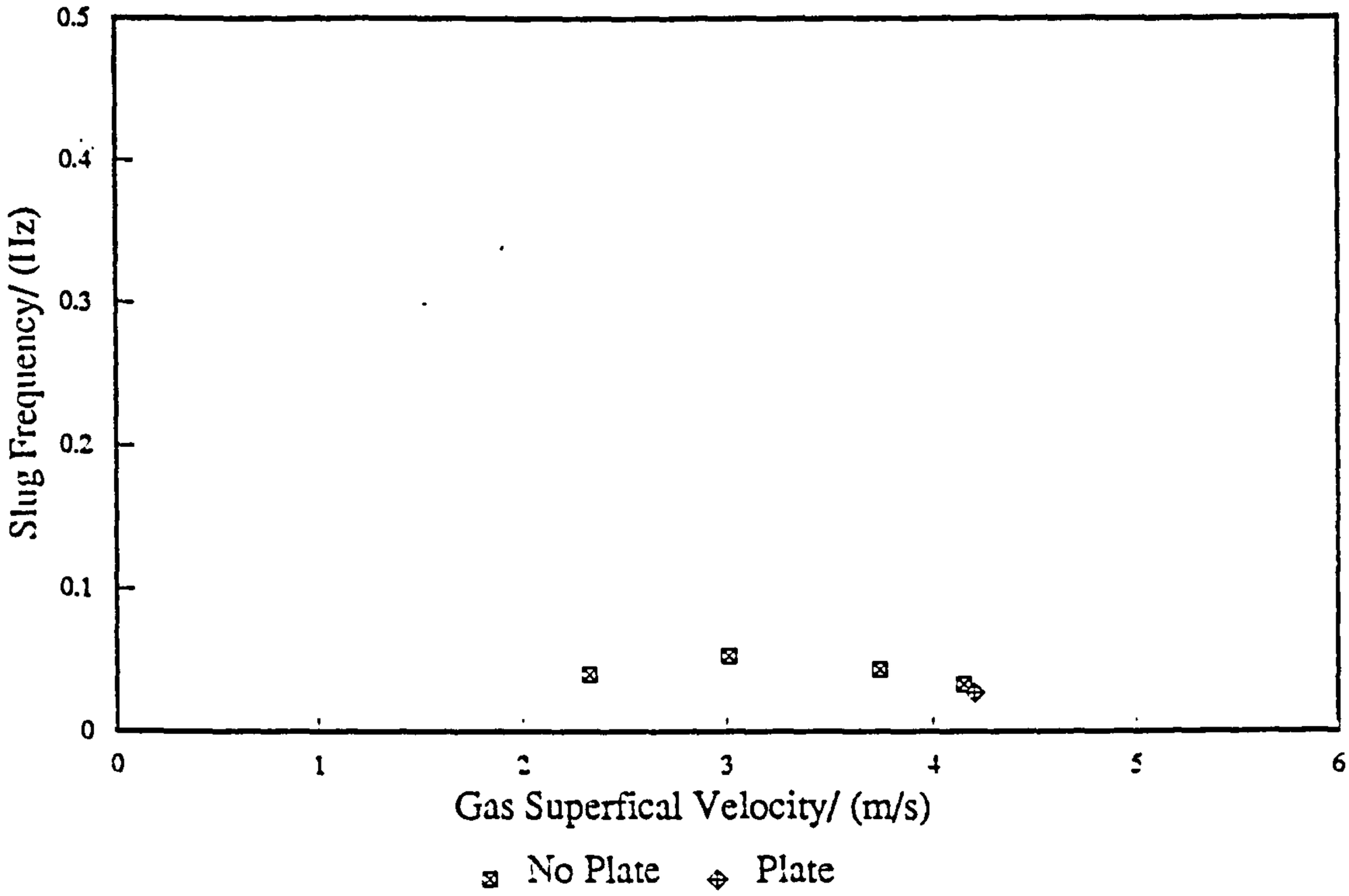


Figure 4.1.2 Variation of Slug Frequency: Liquid Superficial Velocity of 0.14 m/s

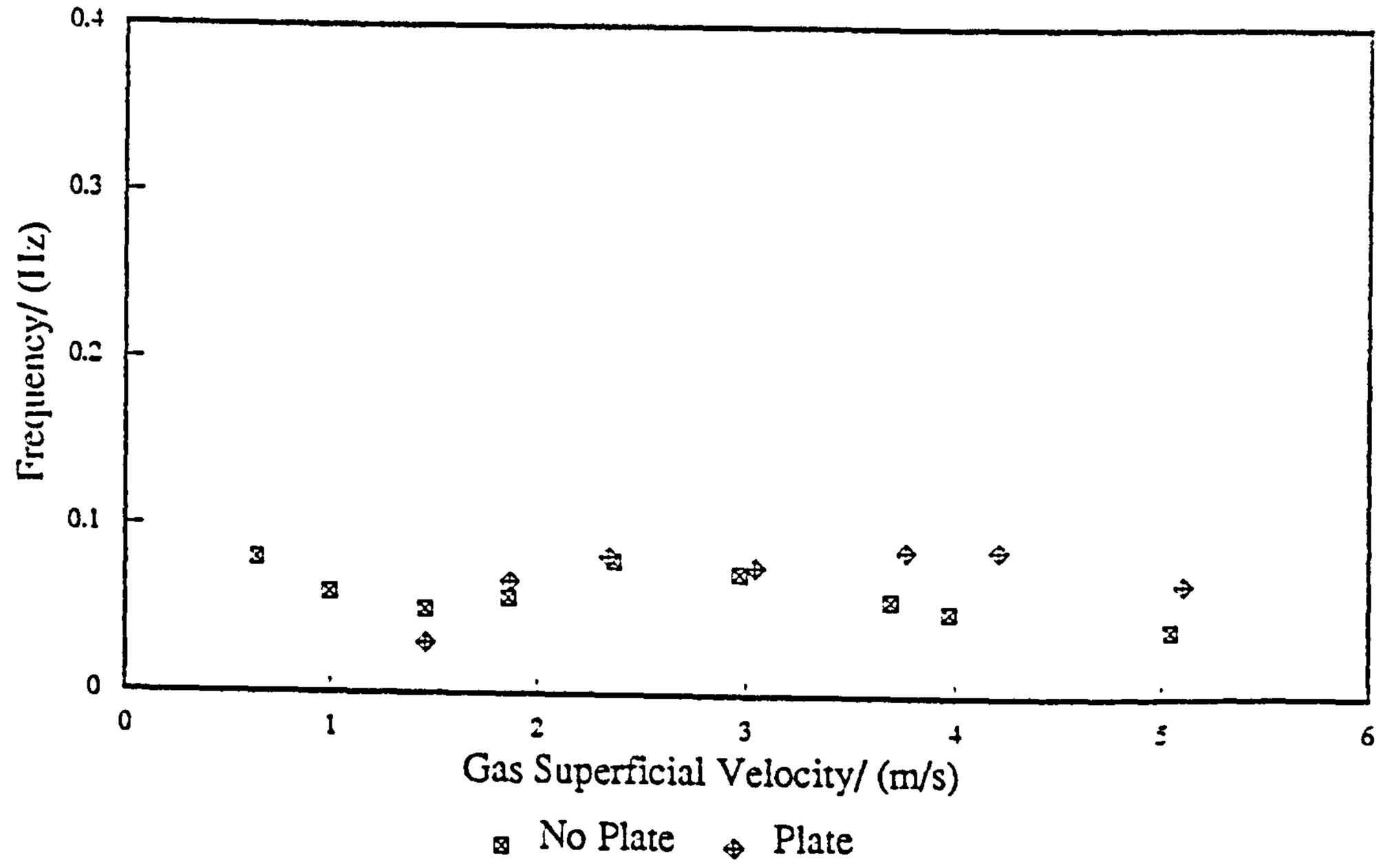


Figure 4.1.3 Variation of Slug Frequency: Liquid Superficial Velocity of 0.18 m/s

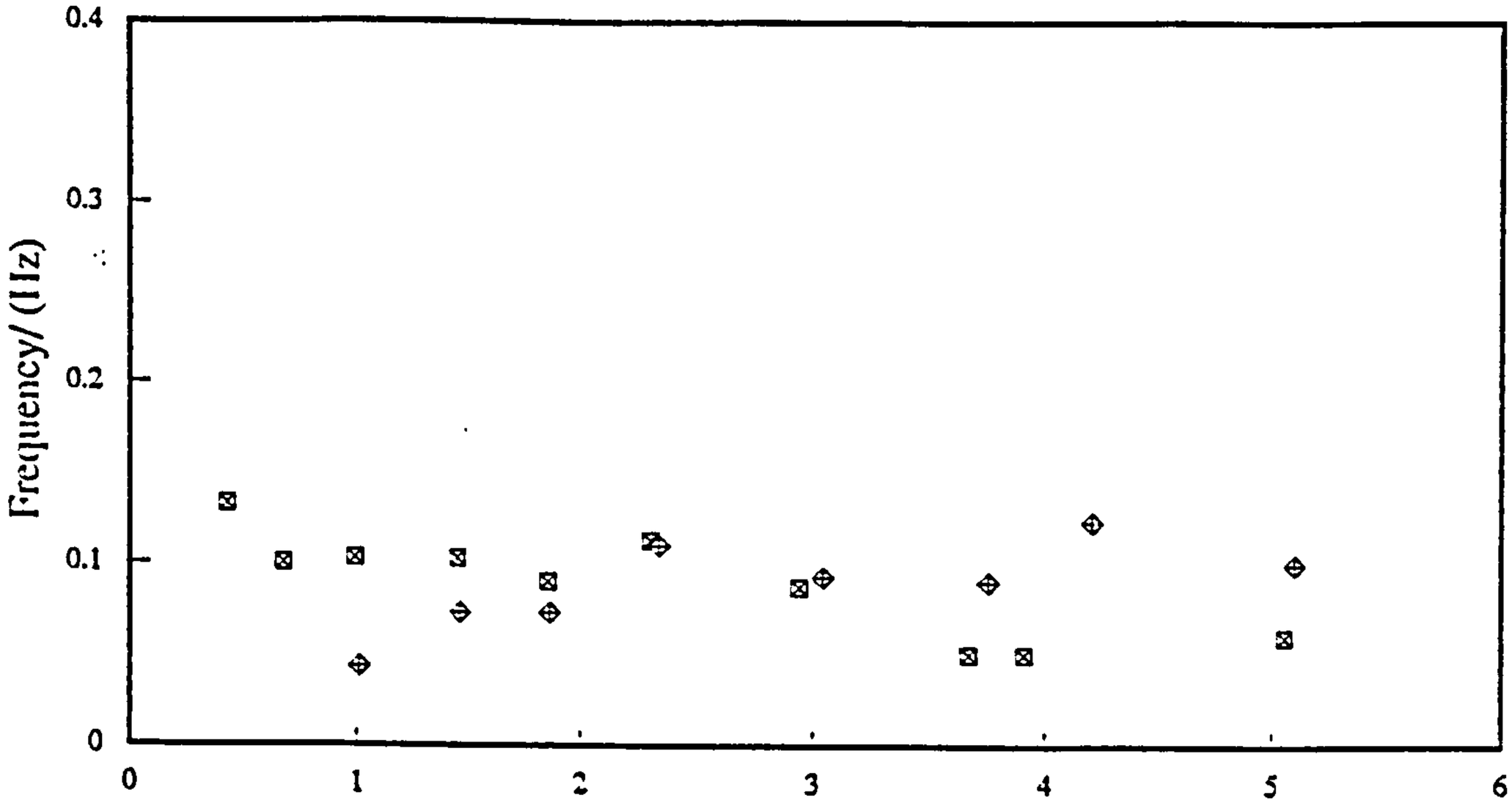


Figure 4.1.4 Variation of Slug Frequency: Liquid Superficial Velocity of 0.255 m/s

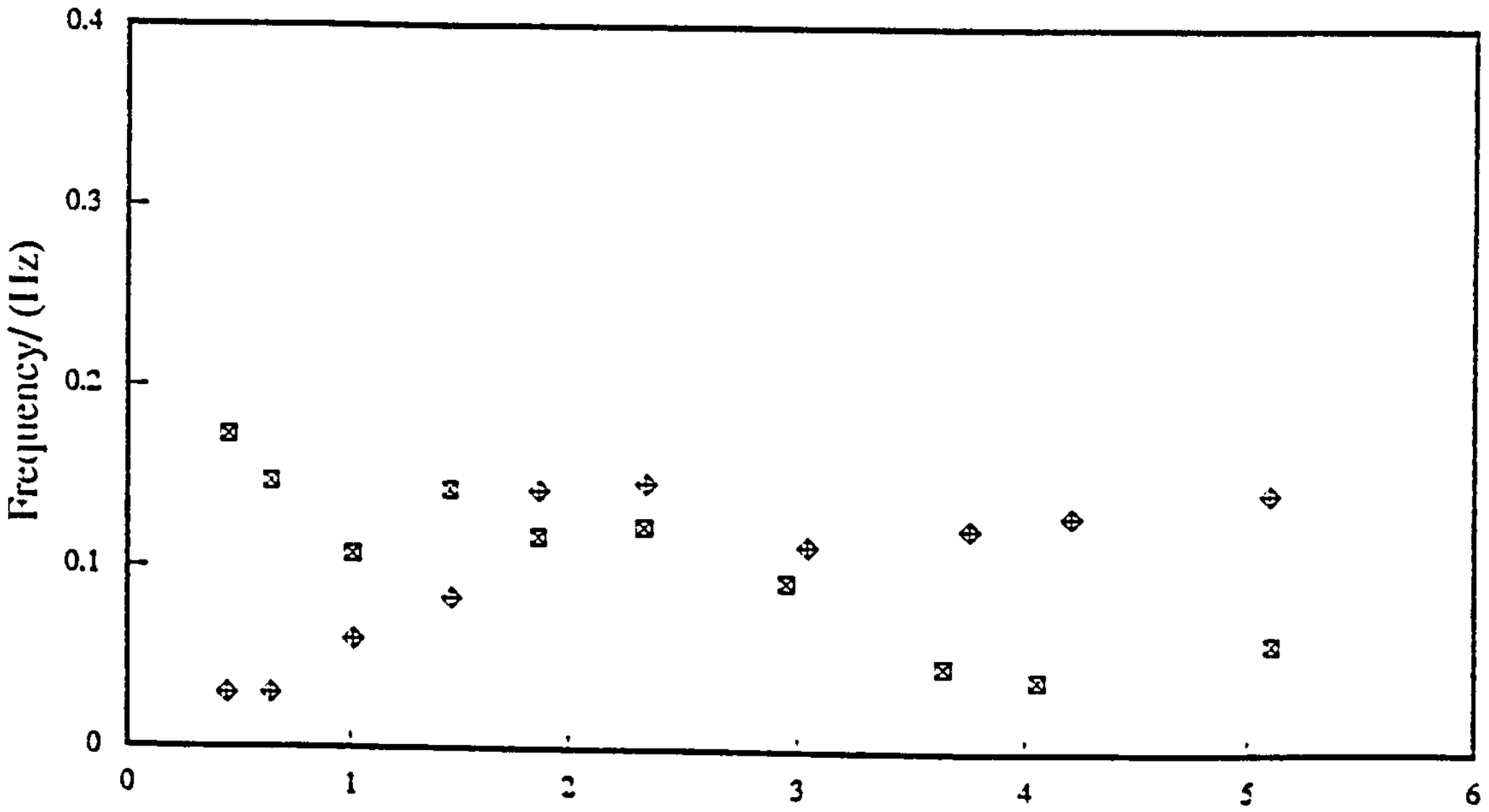


Figure 4.1.5 Variation of Slug Frequency: Liquid Superficial Velocity of 0.271 m/s

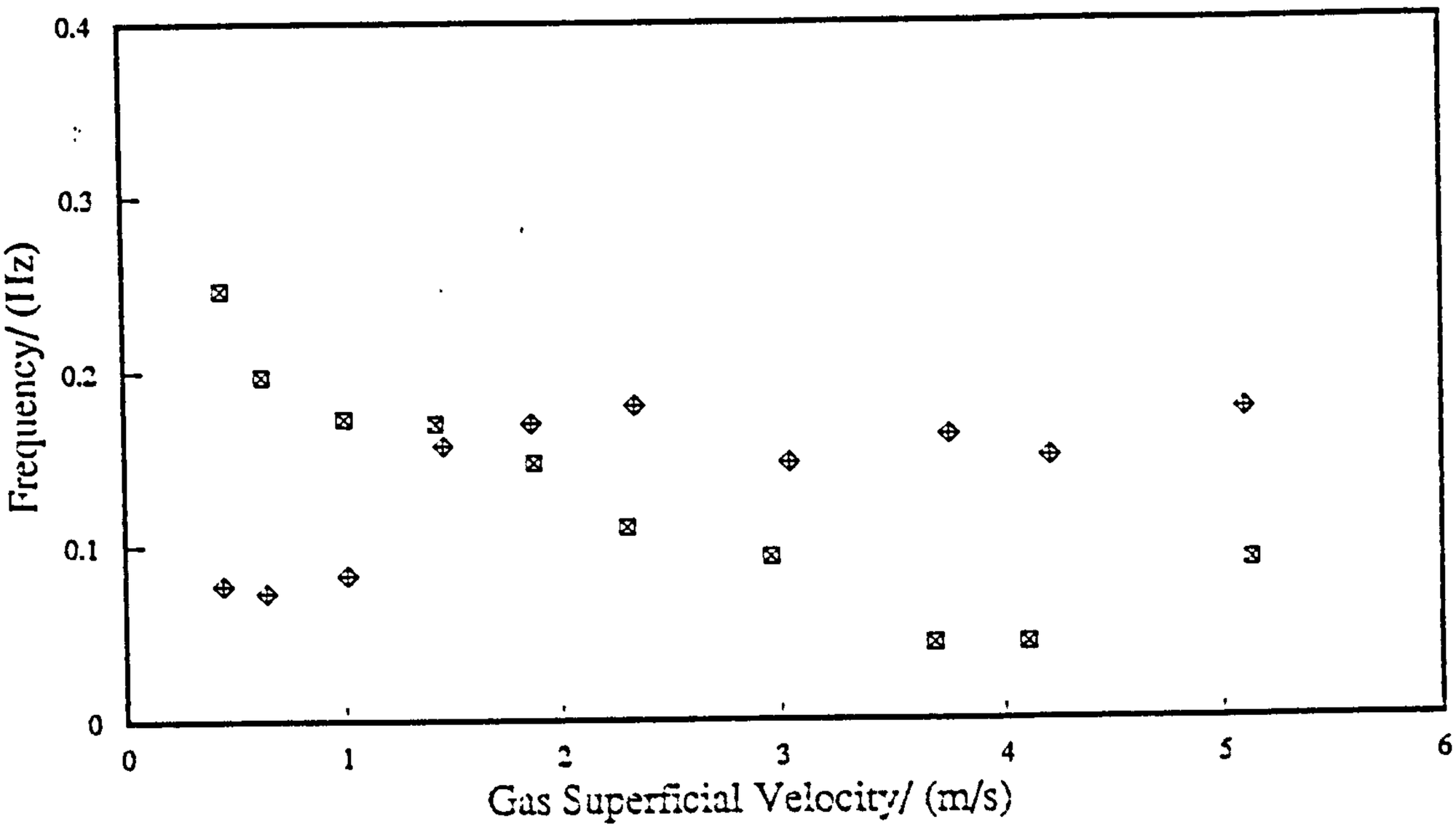


Figure 4.1.6 Variation of Slug Frequency: Liquid Superficial Velocity of 0.32 m/s

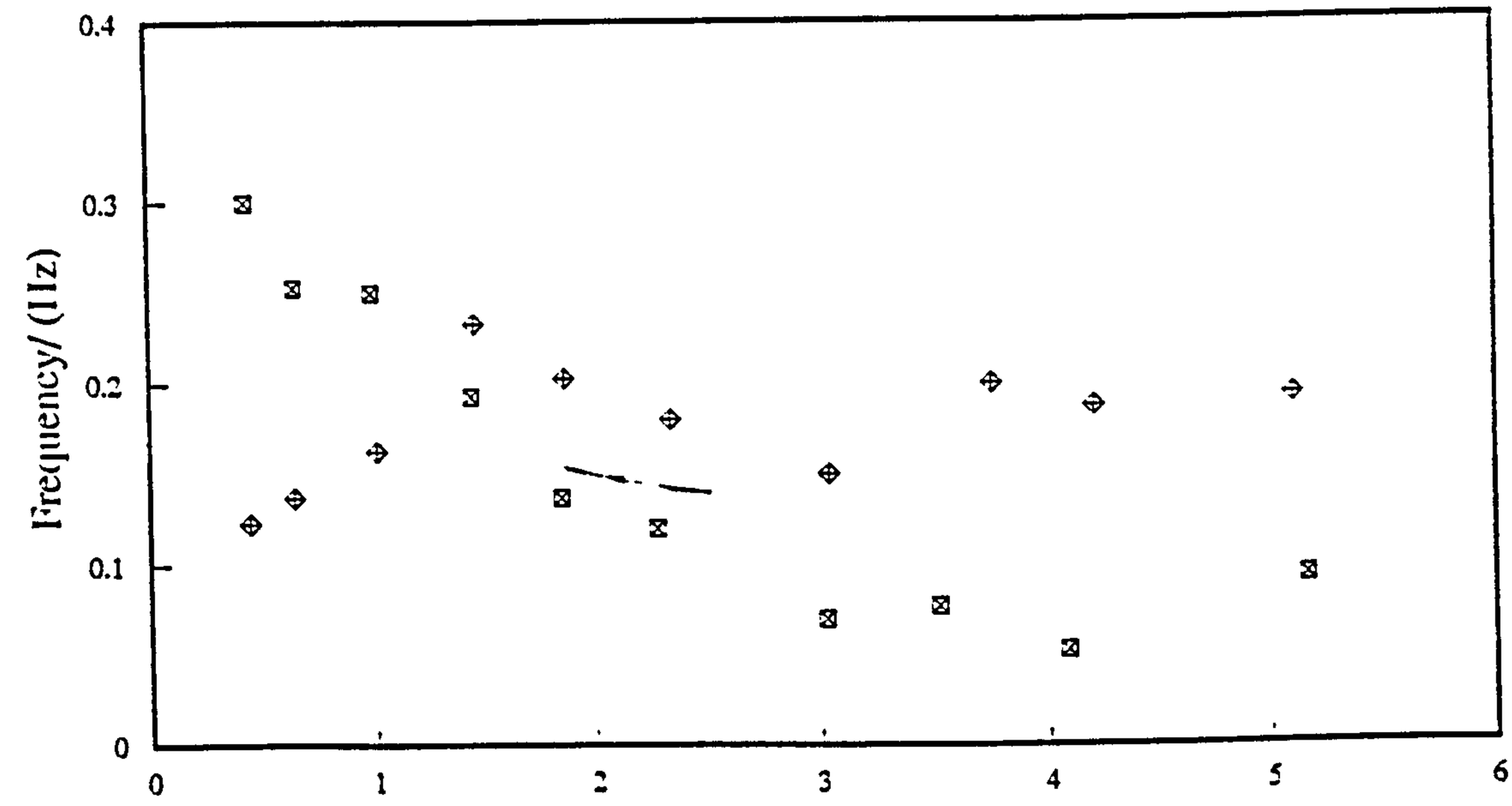


Figure 4.1.7 Variation of Slug Frequency: Liquid Superficial Velocity of 0.391 m/s

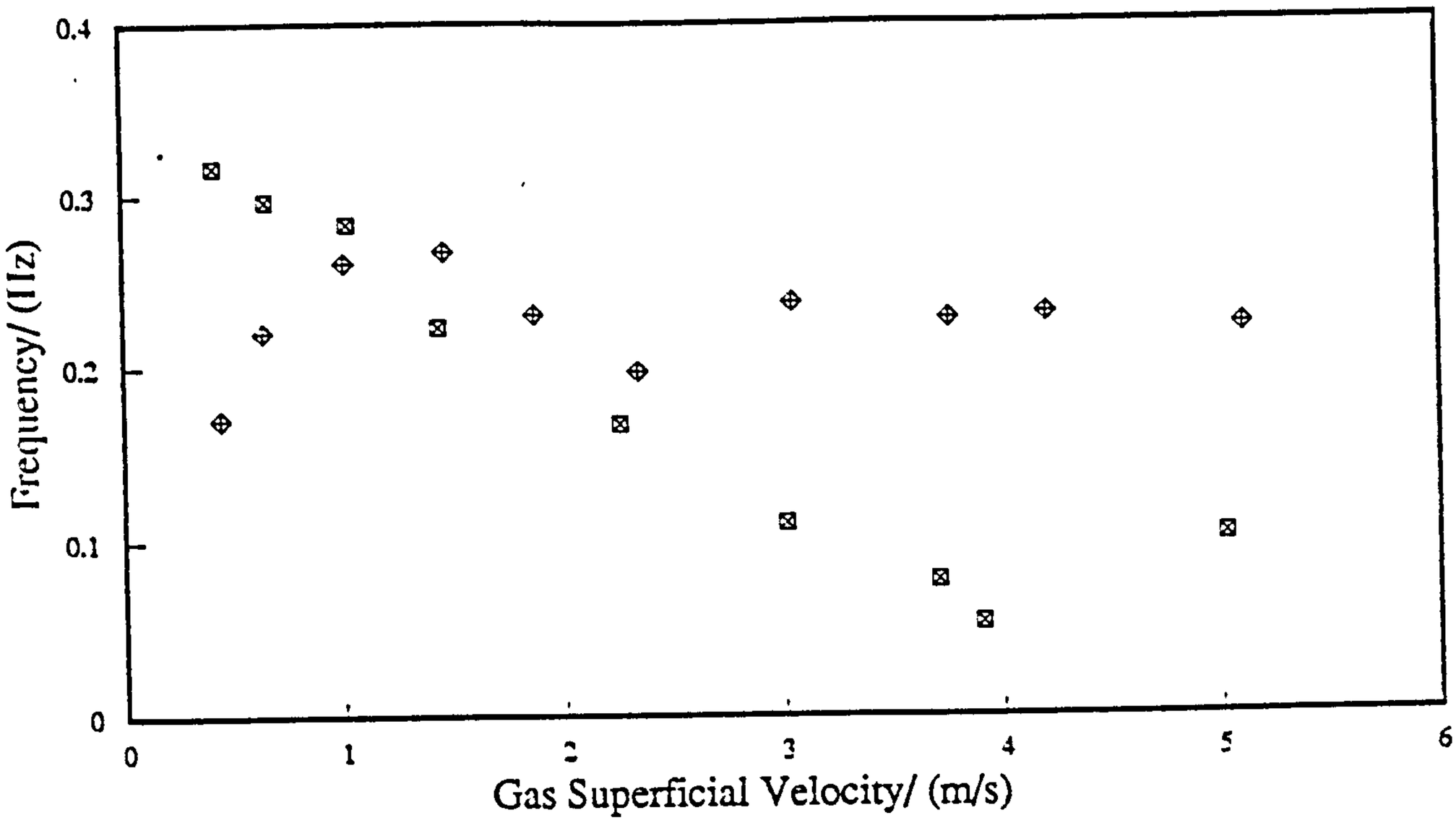


Figure 4.1.8 Variation of Slug Frequency: Liquid Superficial Velocity of 0.455 m/s

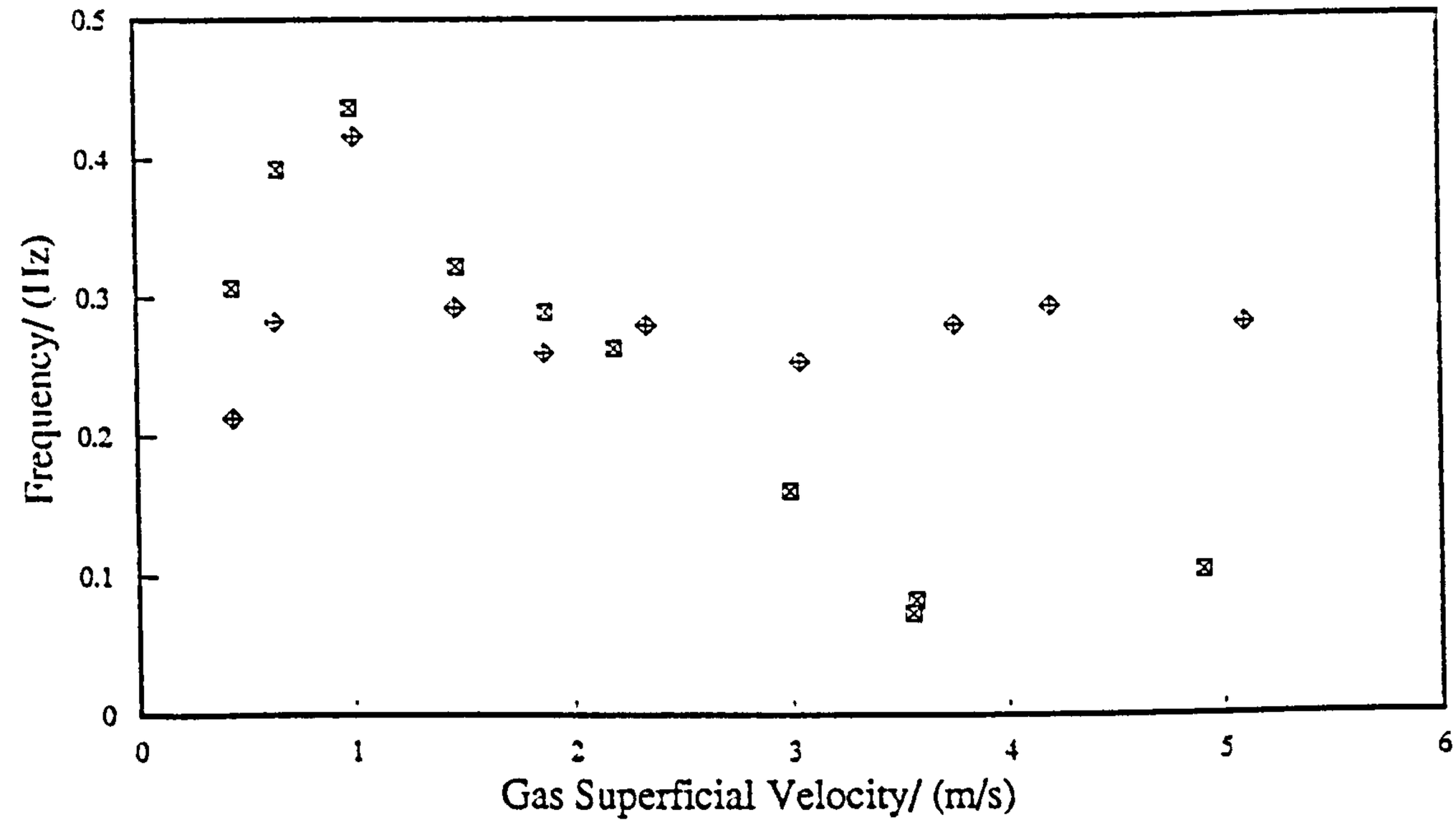


Figure 4.1.9 Variation of Slug Frequency: Liquid Superficial Velocity of 0.52 m/s

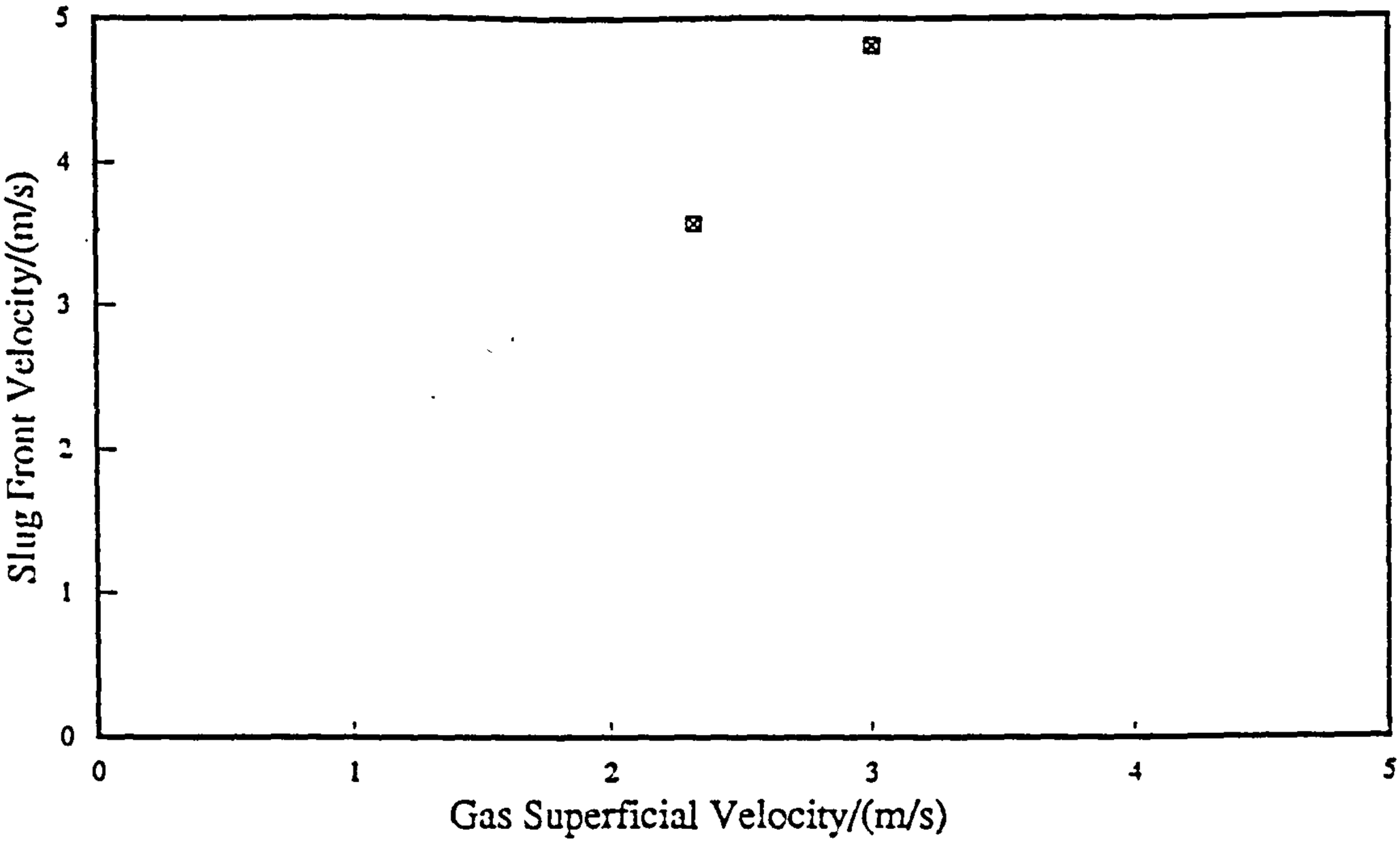


Figure 4.1.10 Variation of Slug Front Velocity
U_{Ls} = 0.14 m./s (Downstream probe pair)

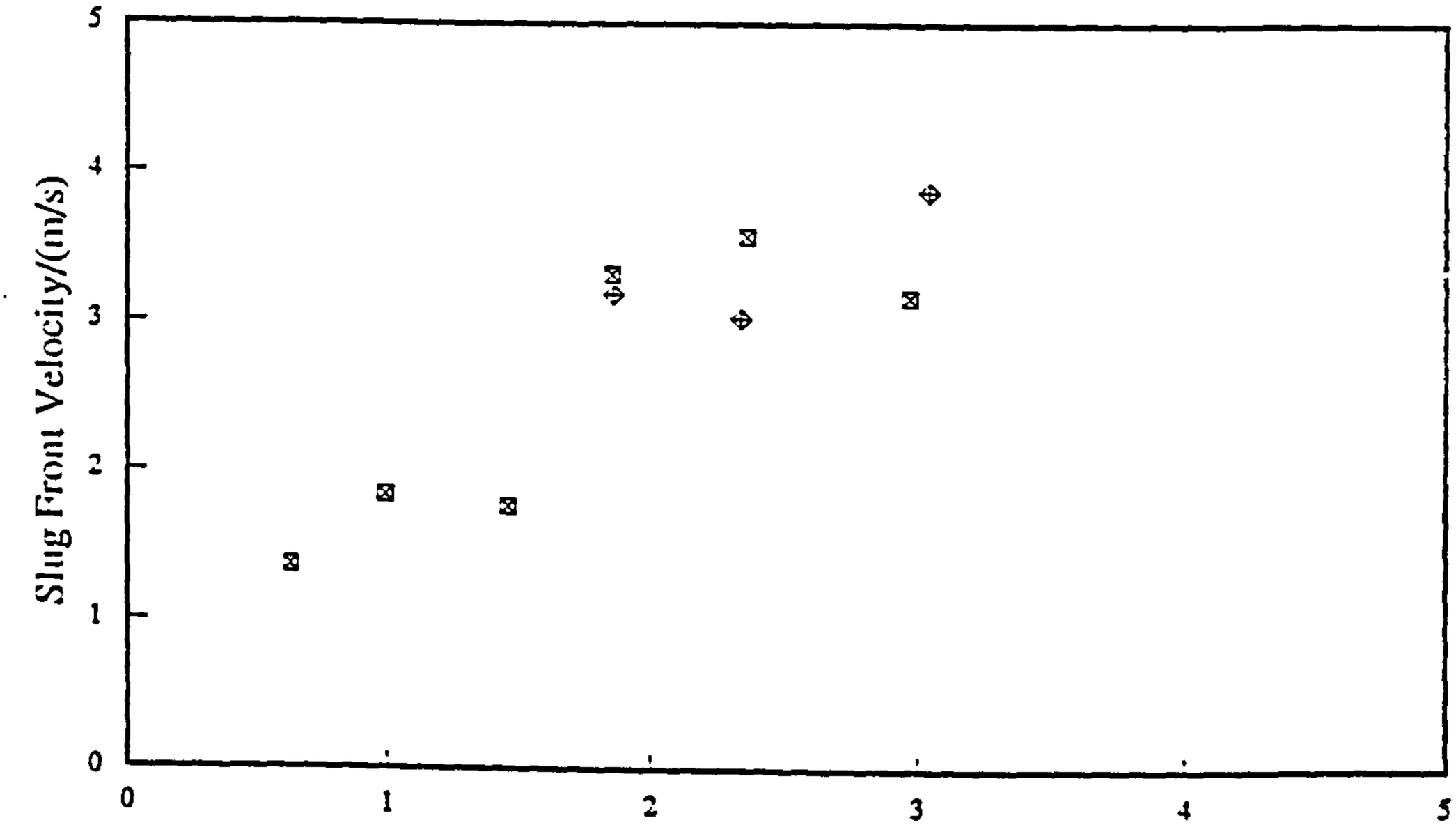


Figure 4.1.11 Variation of Slug Front Velocity
U_{Ls} = 0.18 m./s (Downstream probe pair)

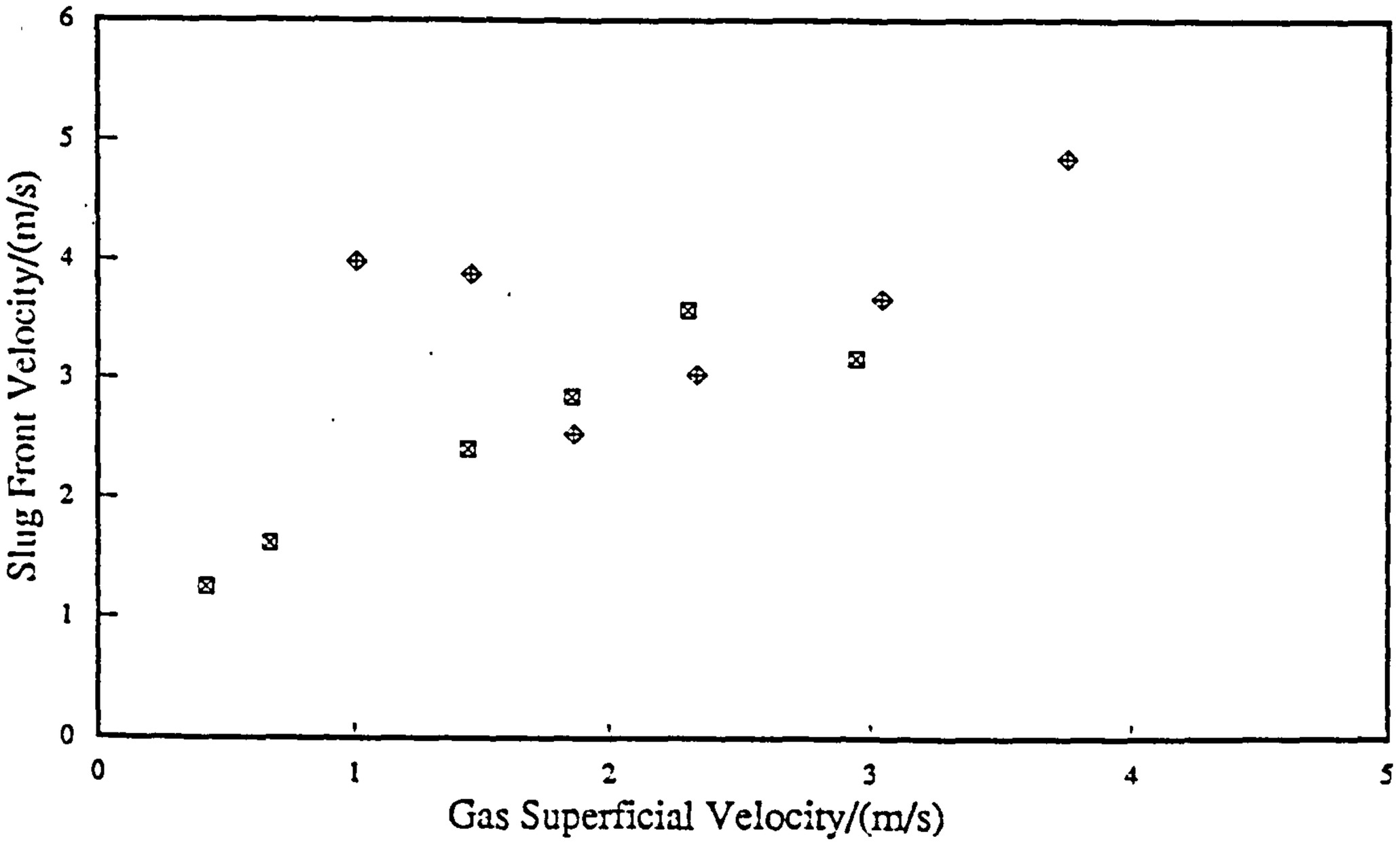


Figure 4.1.12 Variation of Slug Front Velocity
U_{Ls} = 0.255 m./s (Downstream probe pair)

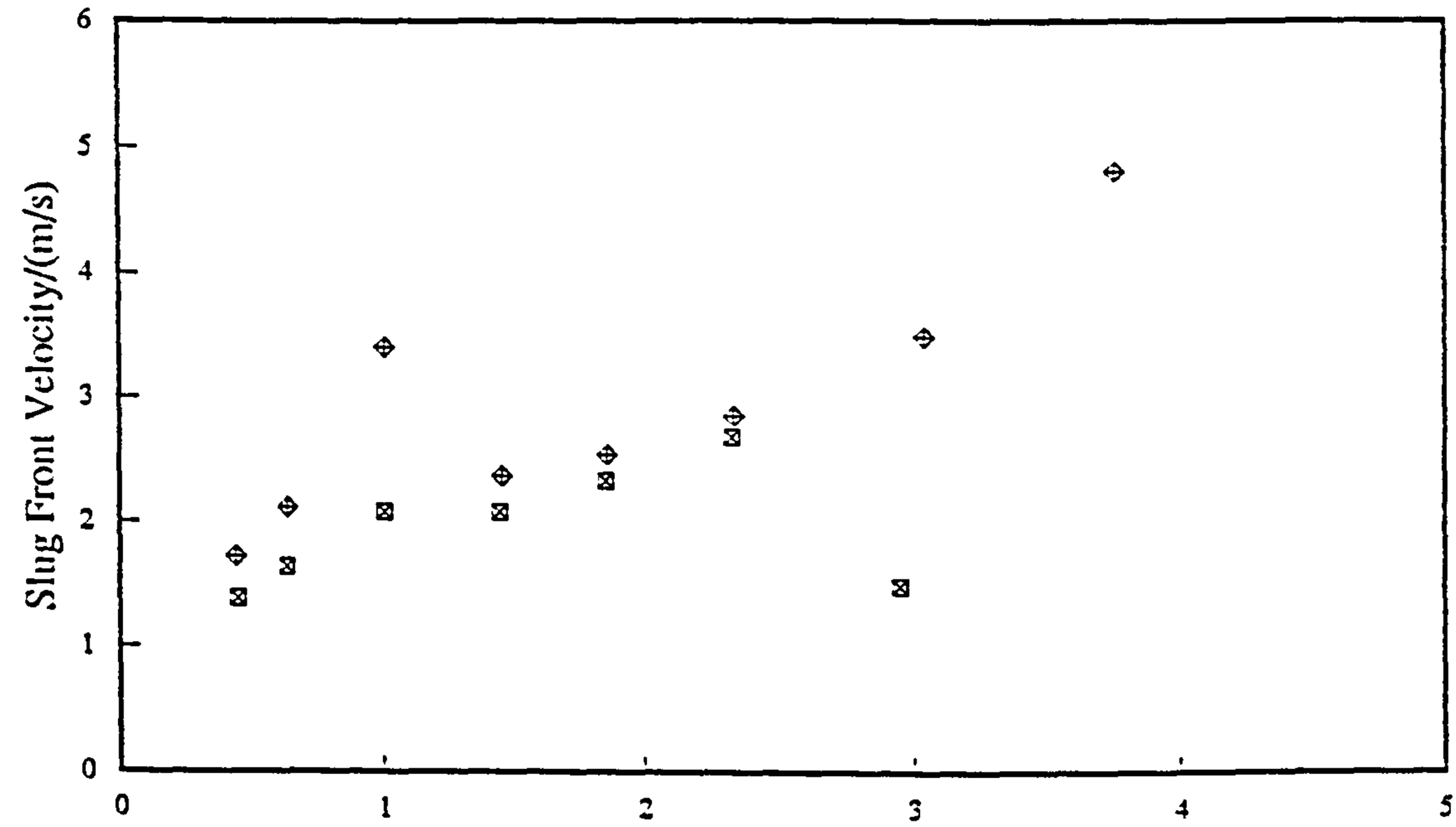
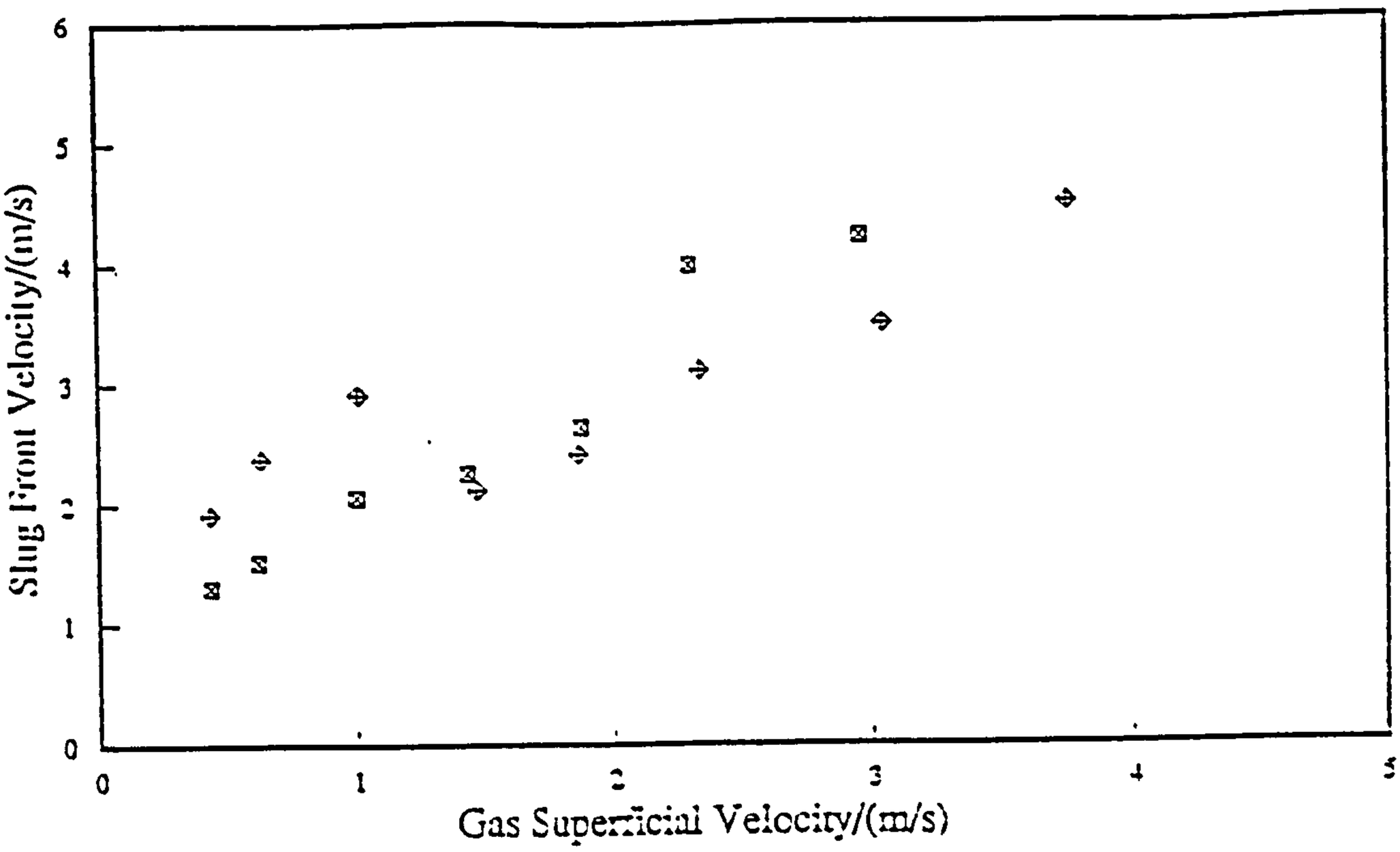
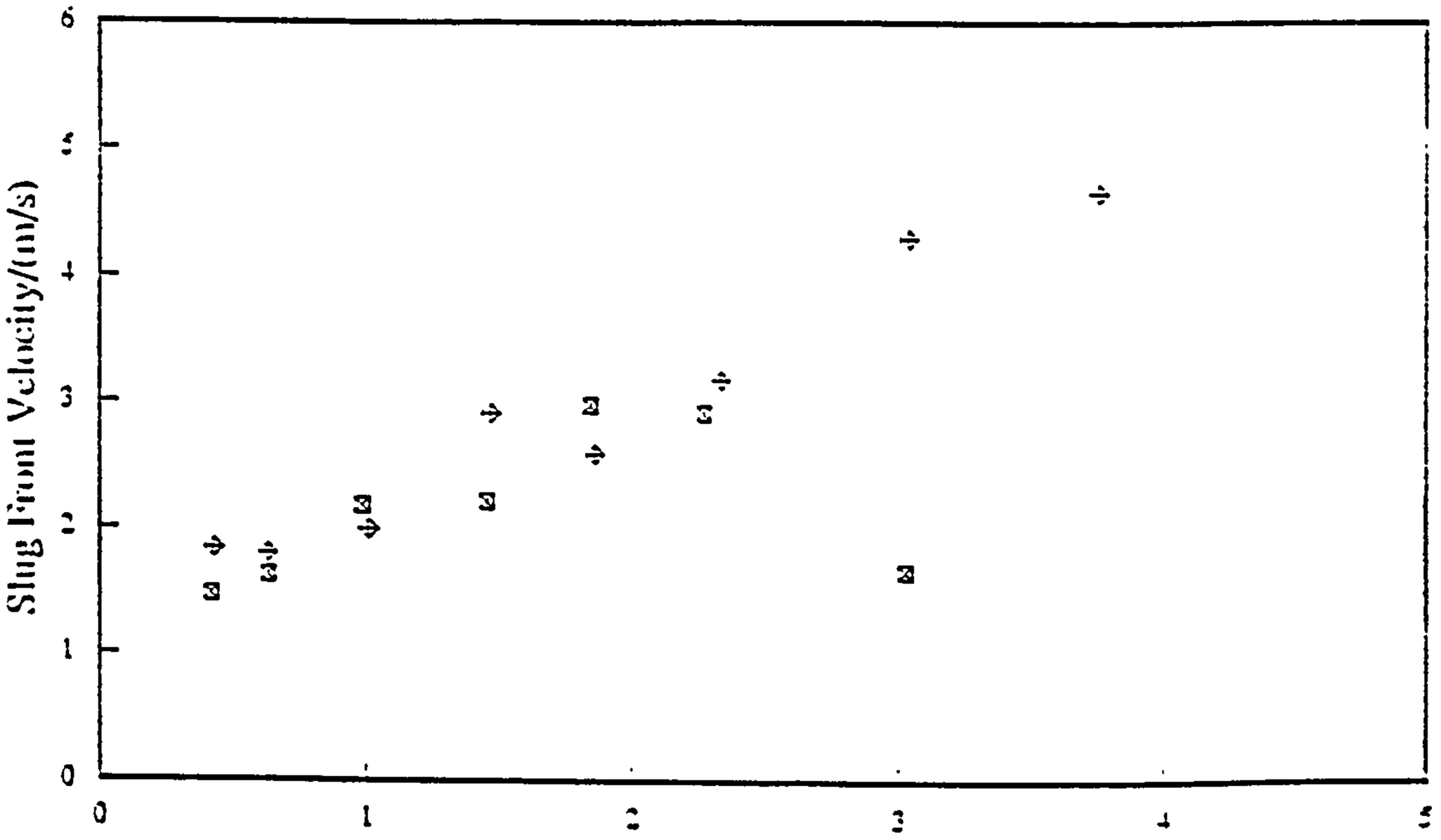


Figure 4.1.13 Variation of Slug Front Velocity
U_{Ls} = 0.271 m./s (Downstream probe pair)



No Plate Plate

Figure 4.1.14 Variation of Slug Front Velocity
U_{Ls} = 0.32 m/s (Downstream probe pair)



No Plate Plate

Figure 4.1.15 Variation of Slug Front Velocity
U_{Ls} = 0.391 m/s (Downstream probe pair)

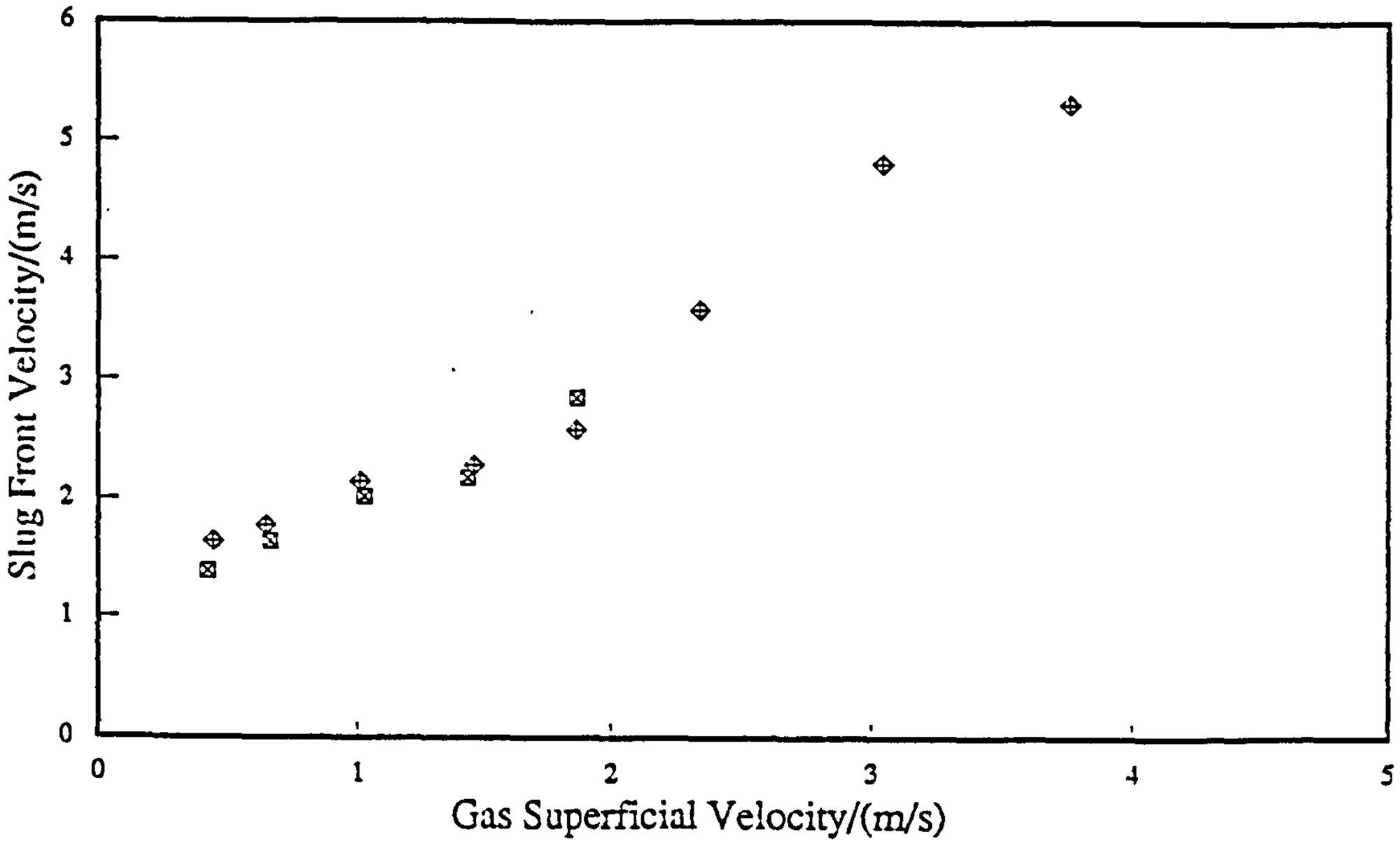


Figure 4.1.16 Variation of Slug Front Velocity
U_{Ls} = 0.455 m./s (Downstream probe pair)

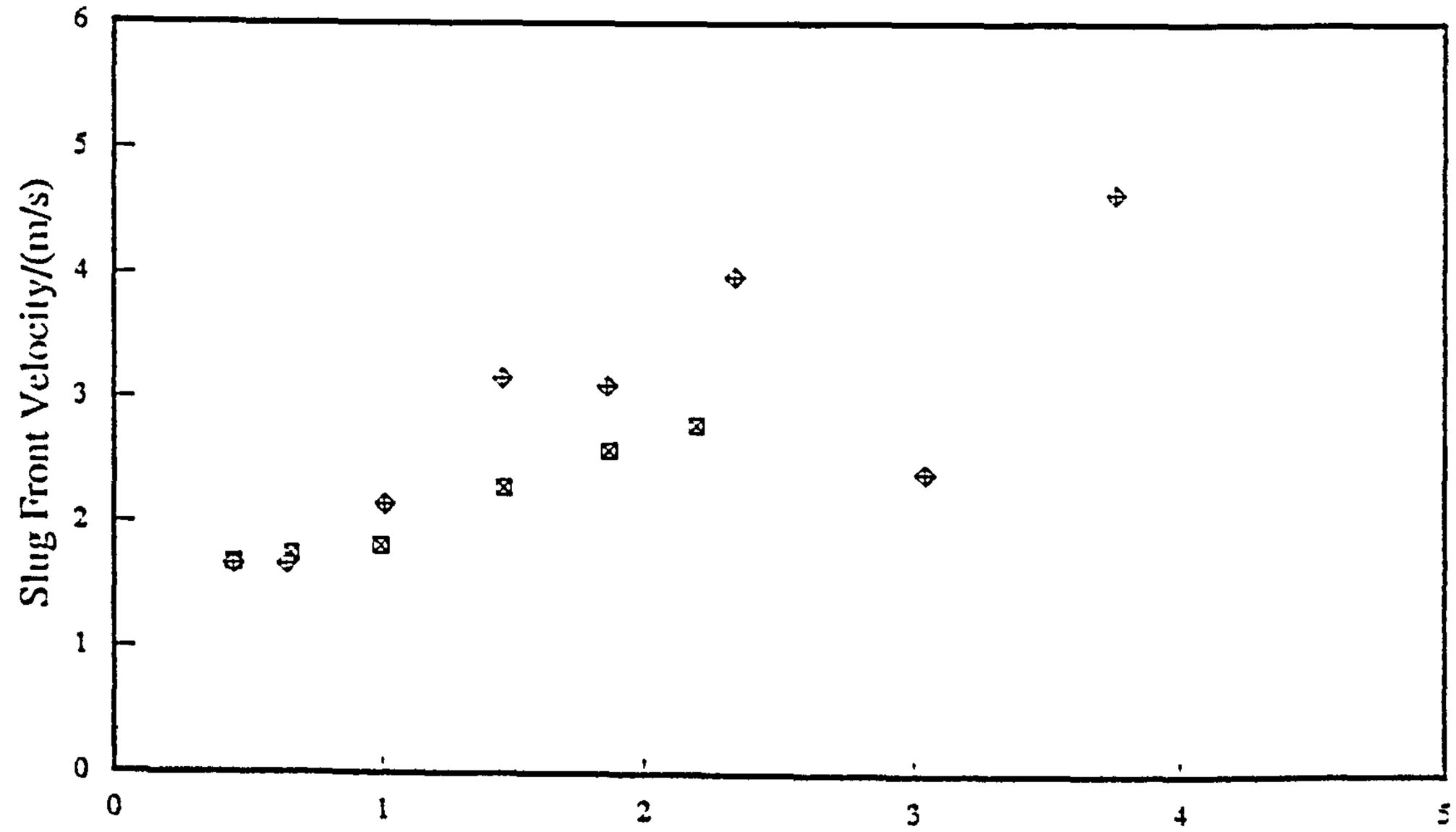


Figure 4.1.17 Variation of Slug Front Velocity
U_{Ls} = 0.52 m./s (Downstream probe pair)

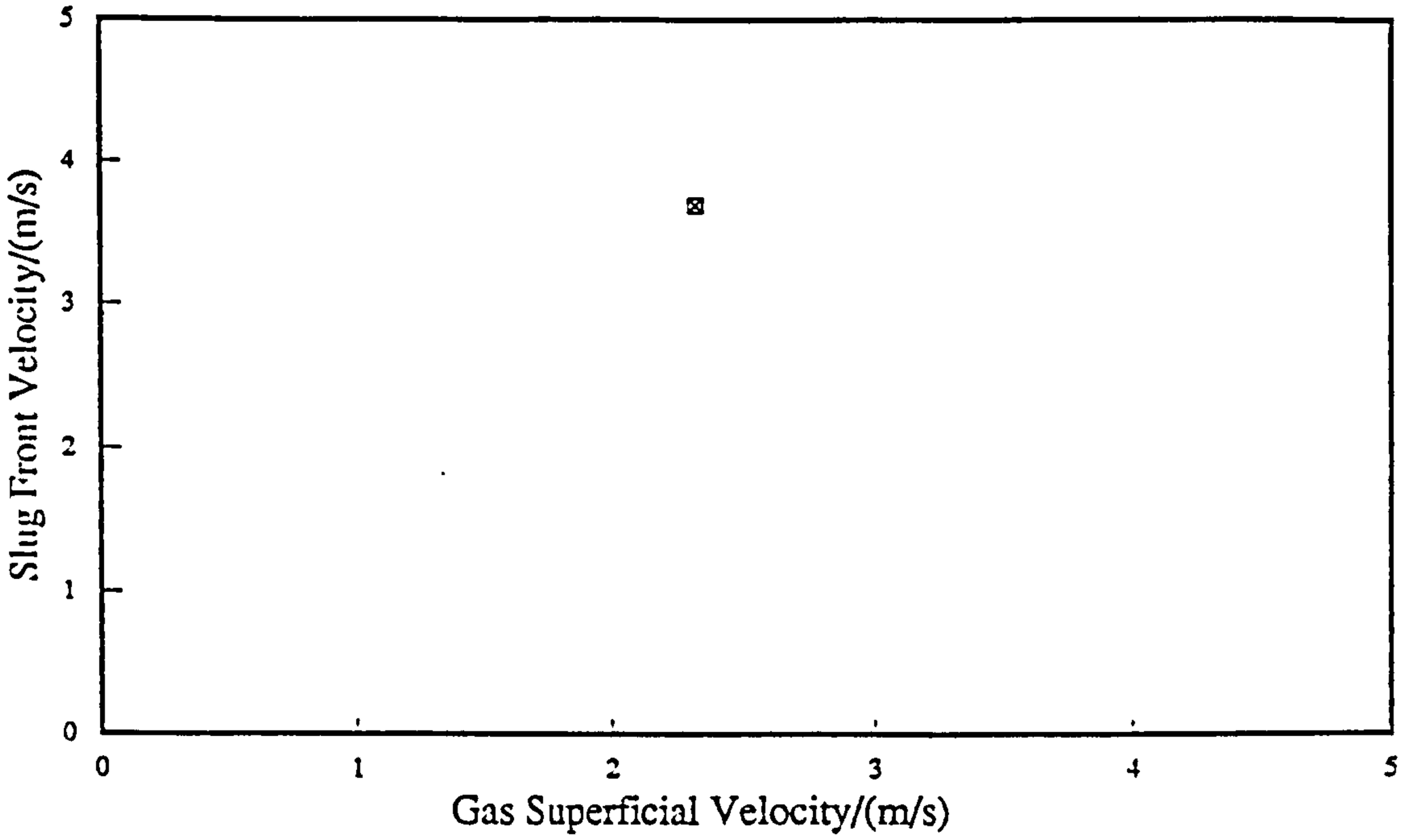


Figure 4.1.18 Variation of Slug Front Velocity
U_{Ls} = 0.14 m/s (Upstream probe pair)

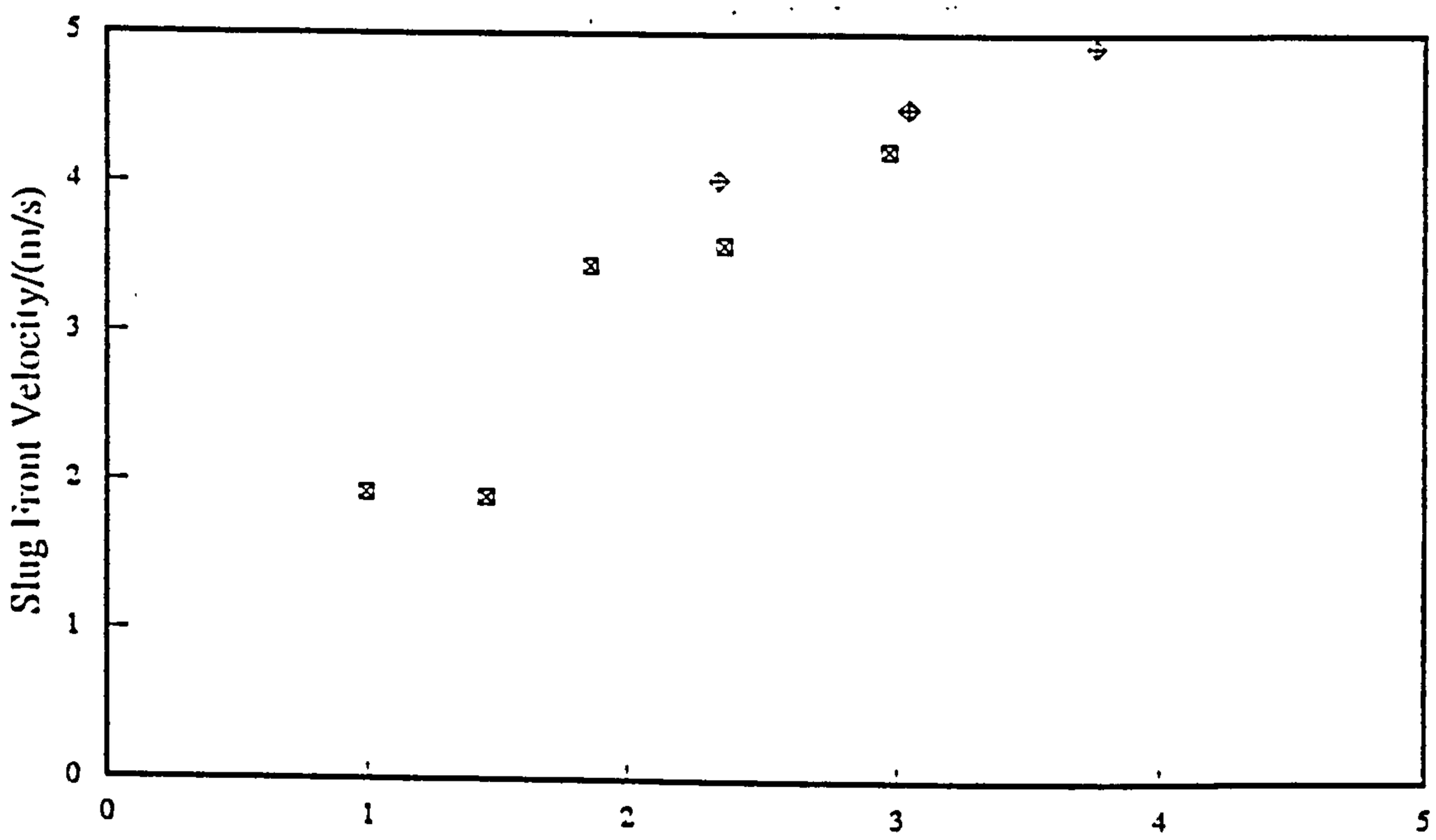


Figure 4.1.19 Variation of Slug Front Velocity
U_{Ls} = 0.18 m/s (Upstream probe pair)

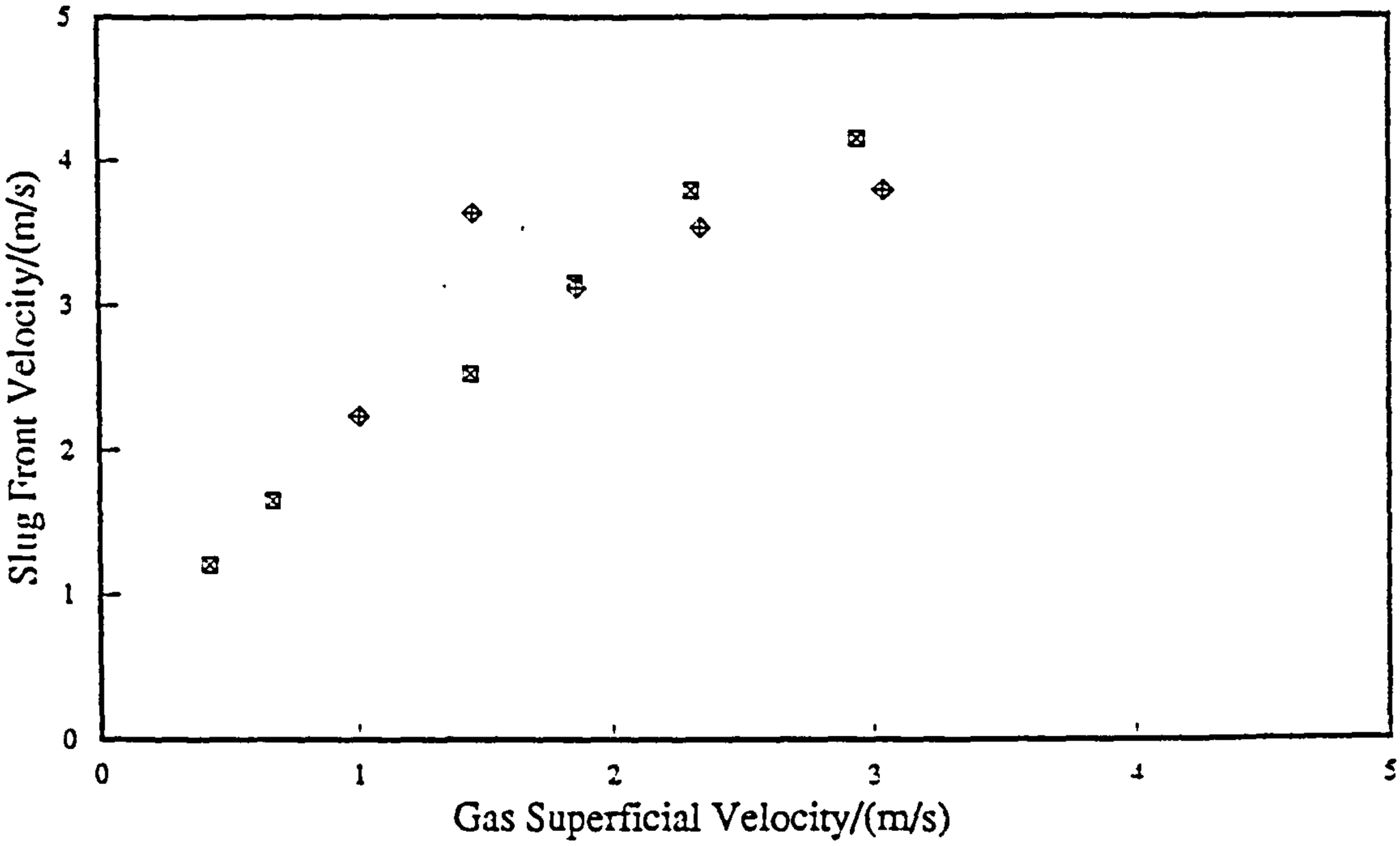


Figure 4.1.20 Variation of Slug Front Velocity
U_{Ls} = 0.255 m./s (Upstream probe pair)

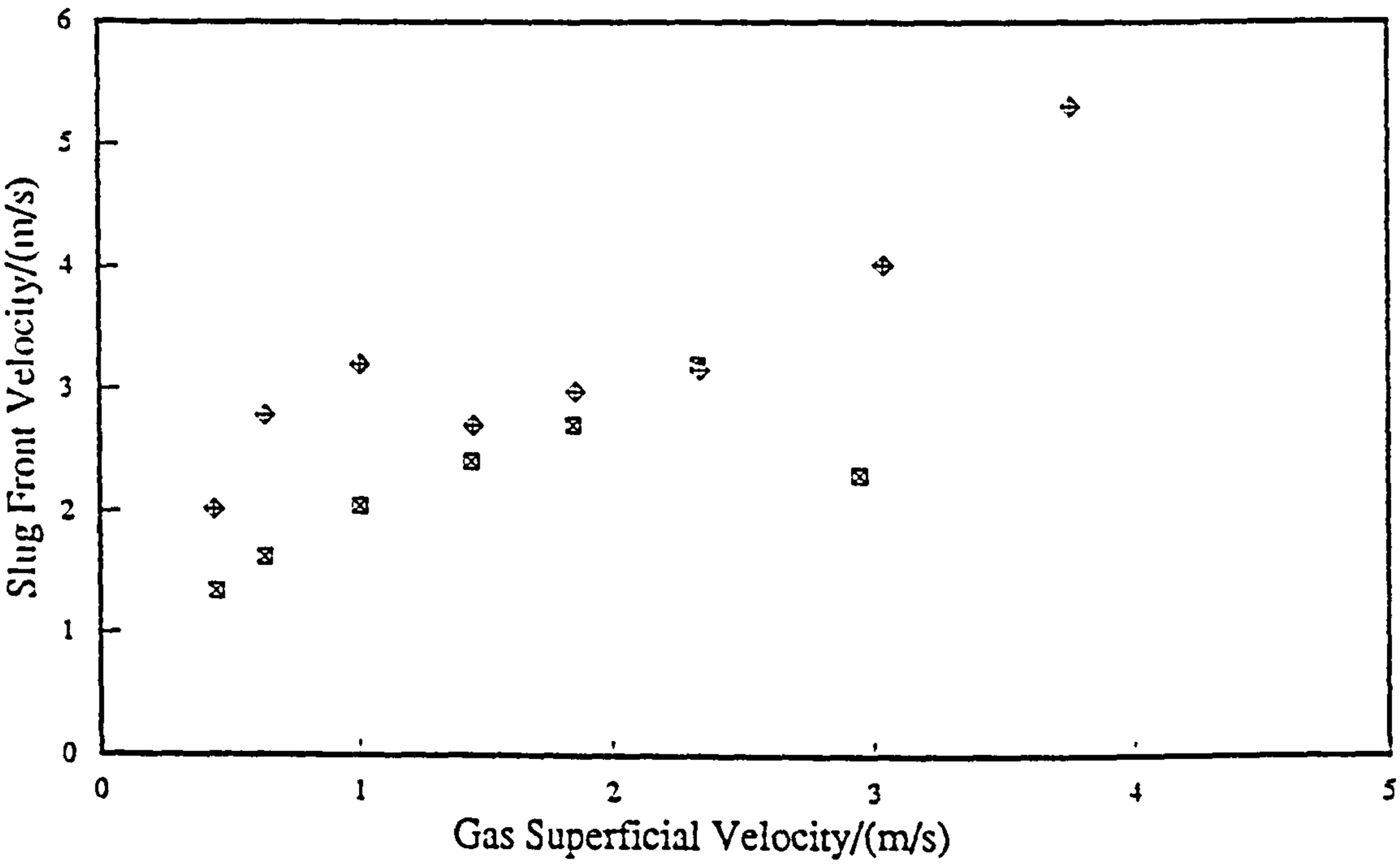


Figure 4.1.21 Variation of Slug Front Velocity
U_{Ls} = 0.271 m./s (Upstream probe pair)

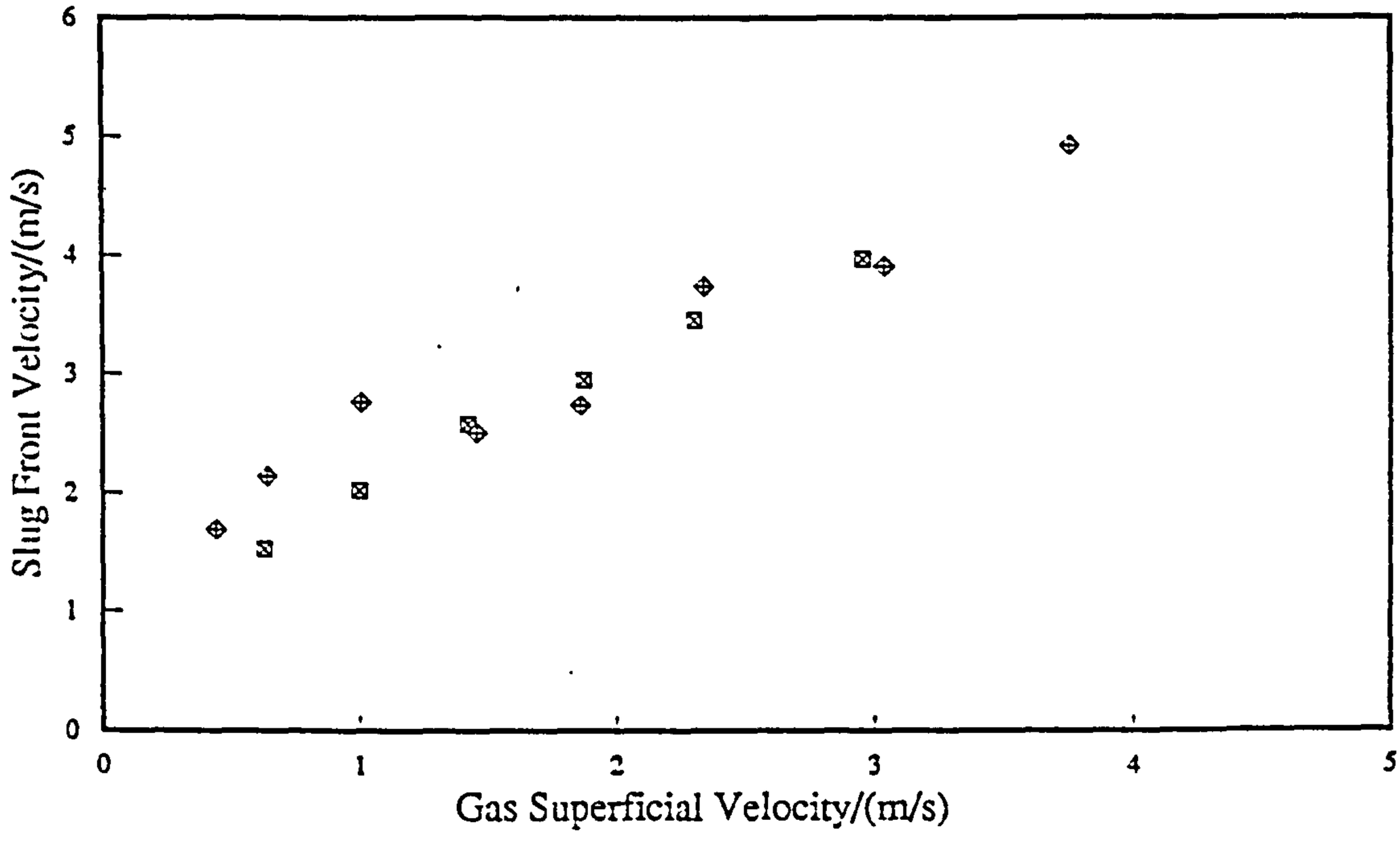


Figure 4.1.22 Variation of Slug Front Velocity
U_{Ls} = 0.32 m./s (Upstream probe pair)

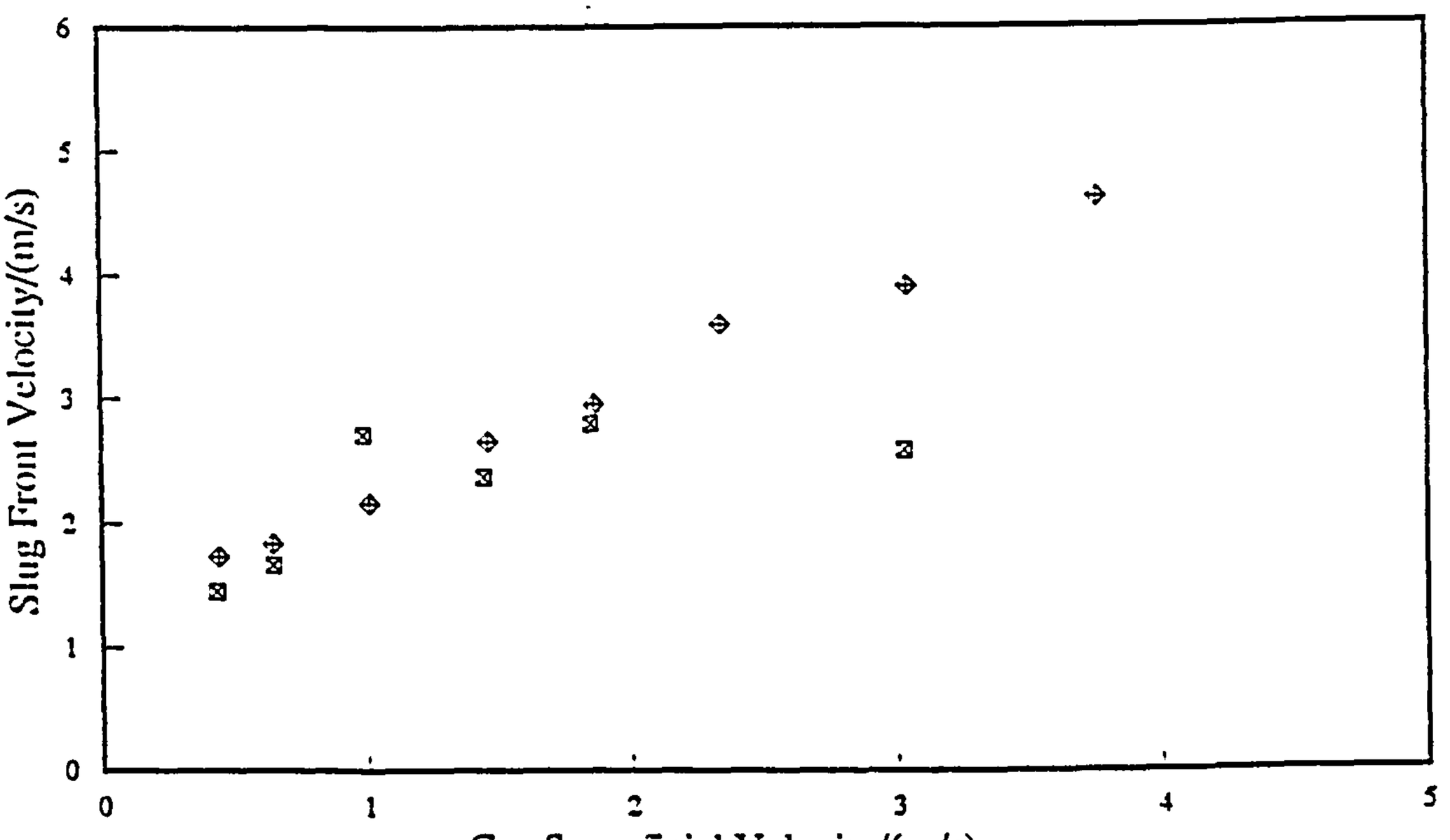


Figure 4.1.23 Variation of Slug Front Velocity
U_{Ls} = 0.391 m./s (Upstream probe pair)

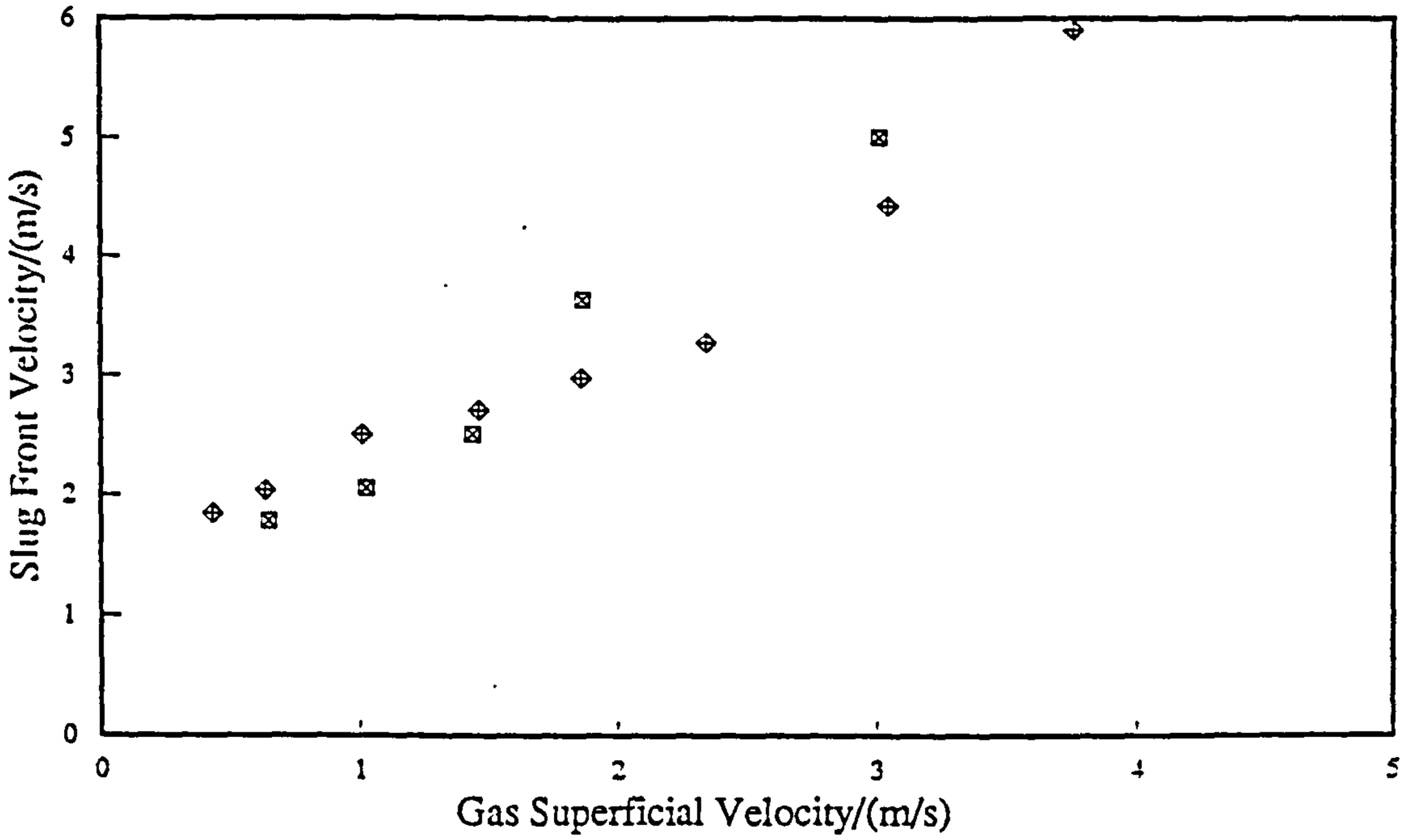


Figure 4.1.24 Variation of Slug Front Velocity
U_{Ls} = 0.455 m./s (Upstream probe pair)

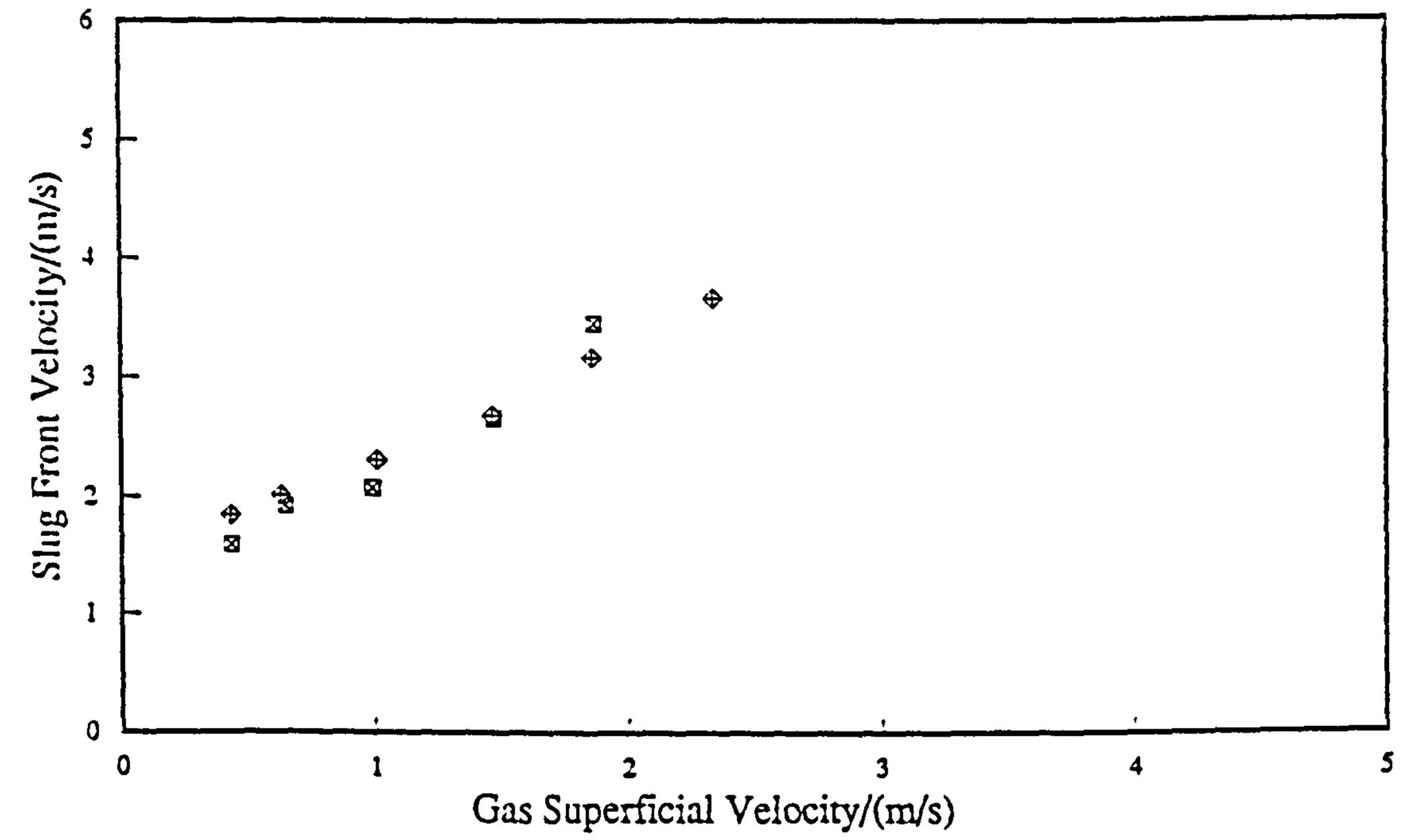


Figure 4.1.25 Variation of Slug Front Velocity
U_{Ls} = 0.52 m./s (Upstream probe pair)

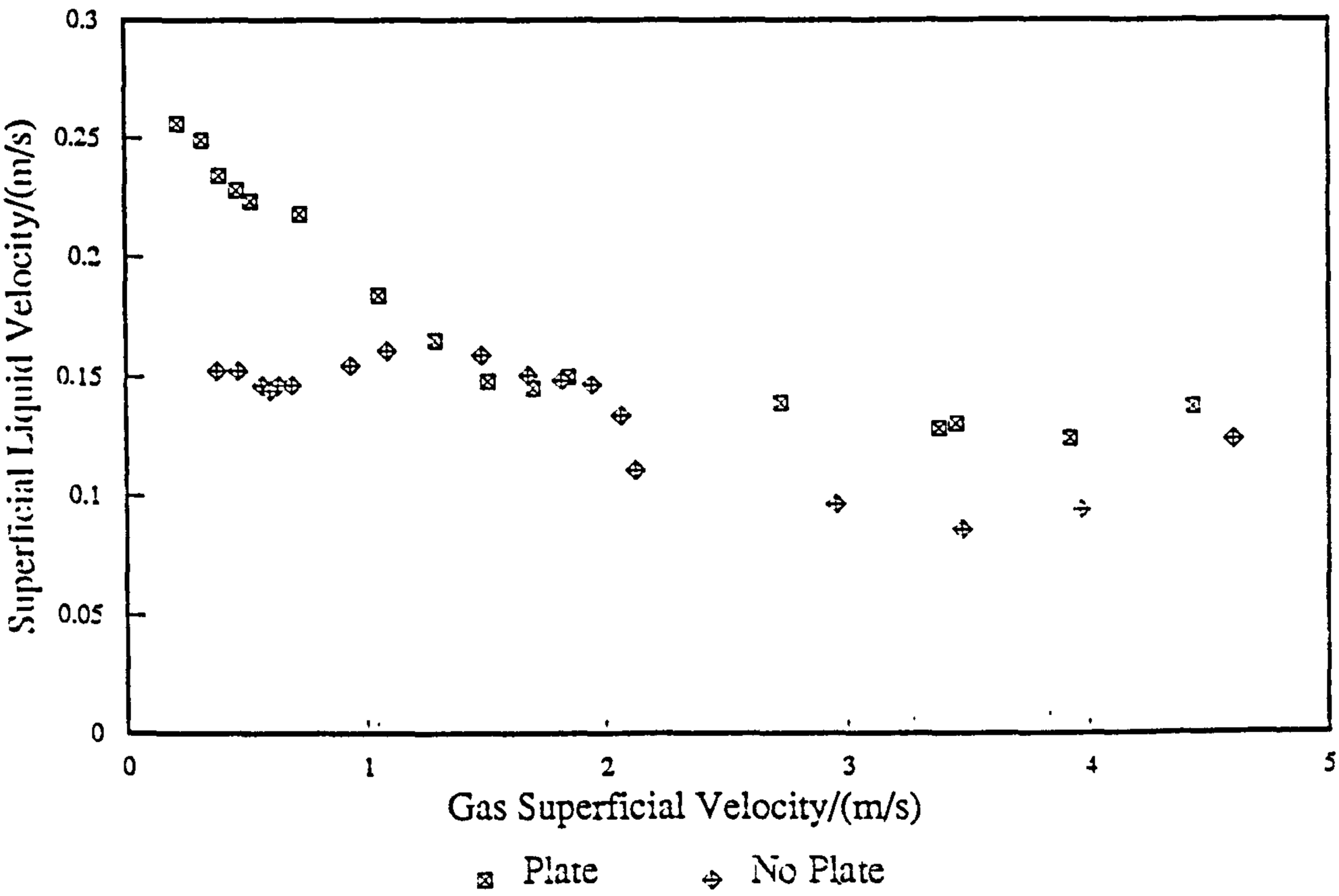


Figure 4.1.26 Experimental Survey of the Transition from the Stratified to Intermittent Flow Regime.

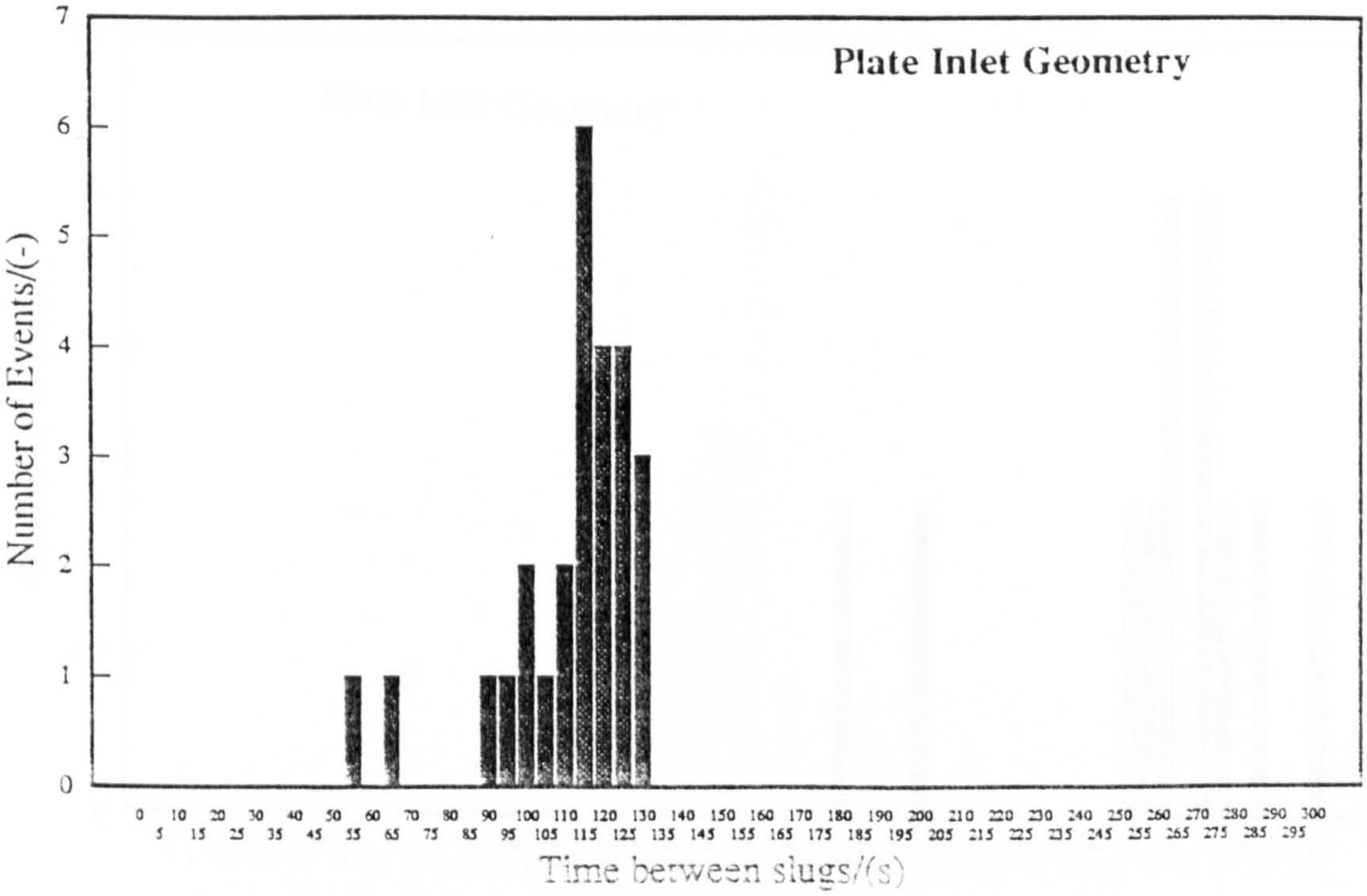
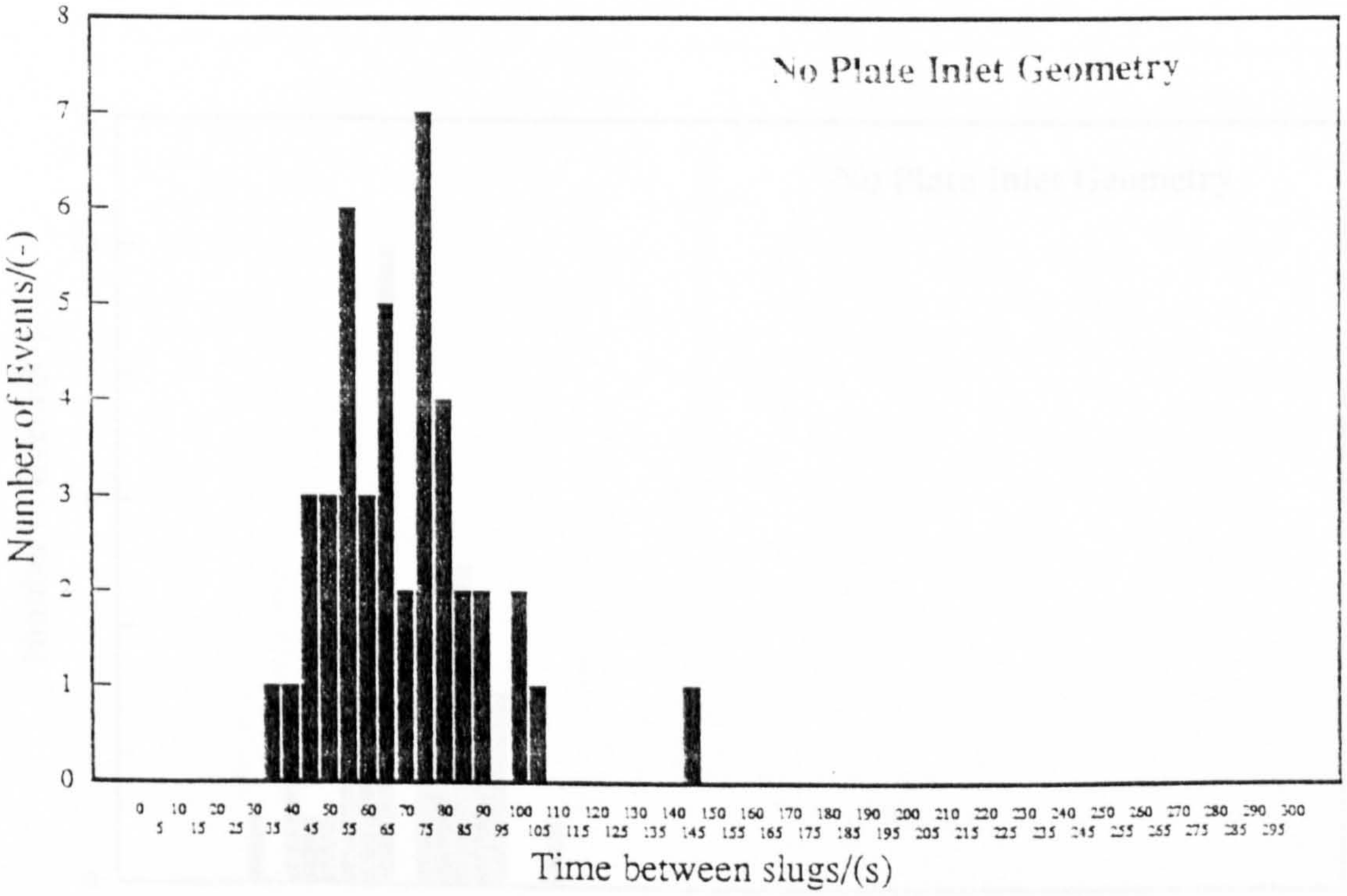


Figure 4.1.27 Distribution of Time between Slugs.
U_{Ls} = 0.271 m/s, U_{Gs} = 1.44 m/s



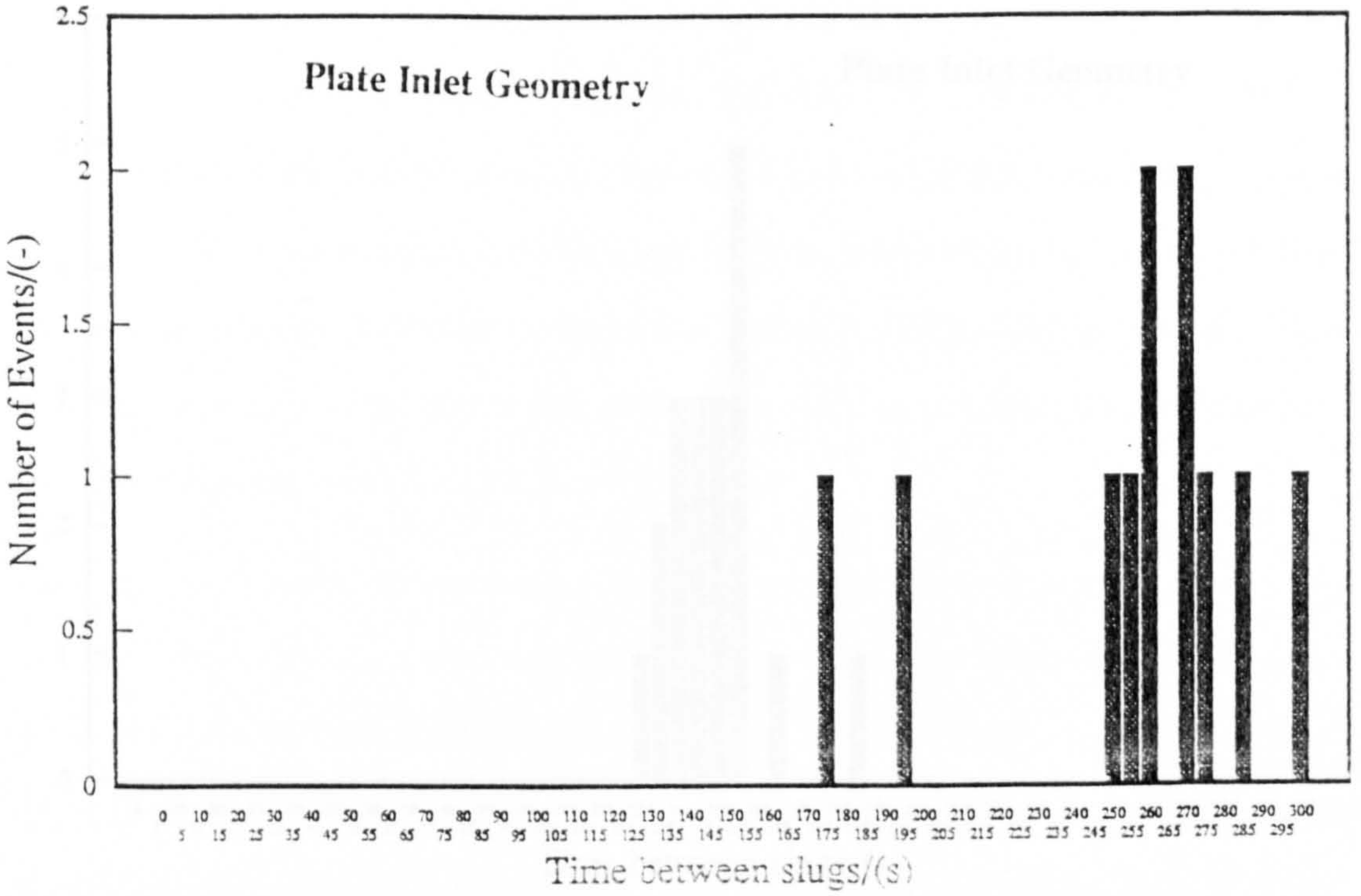
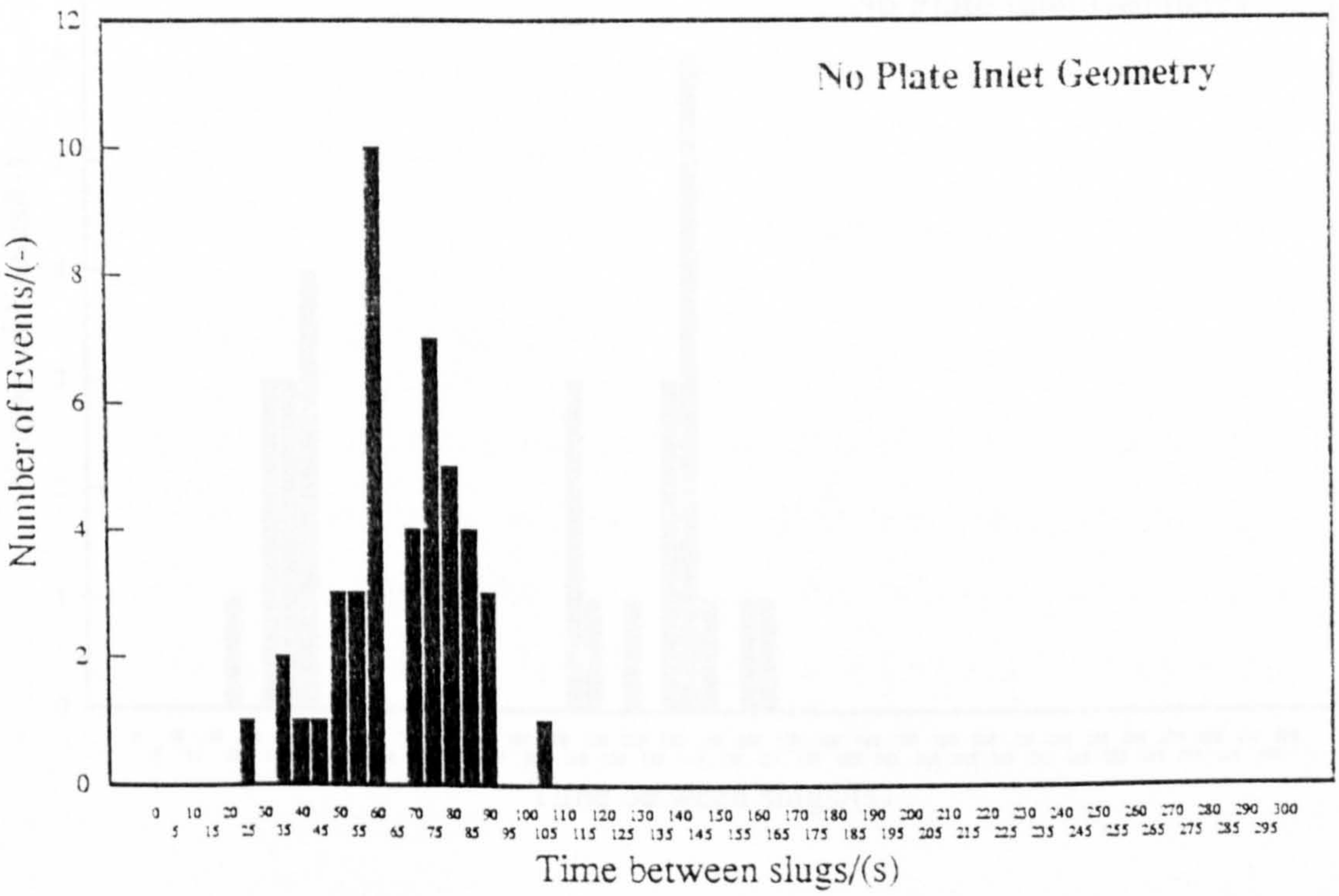


Figure 4.1.28 Distribution of Time between Slugs.
U_{Ls} = 0.271 m/s, U_{Gs} = 0.639 m/s



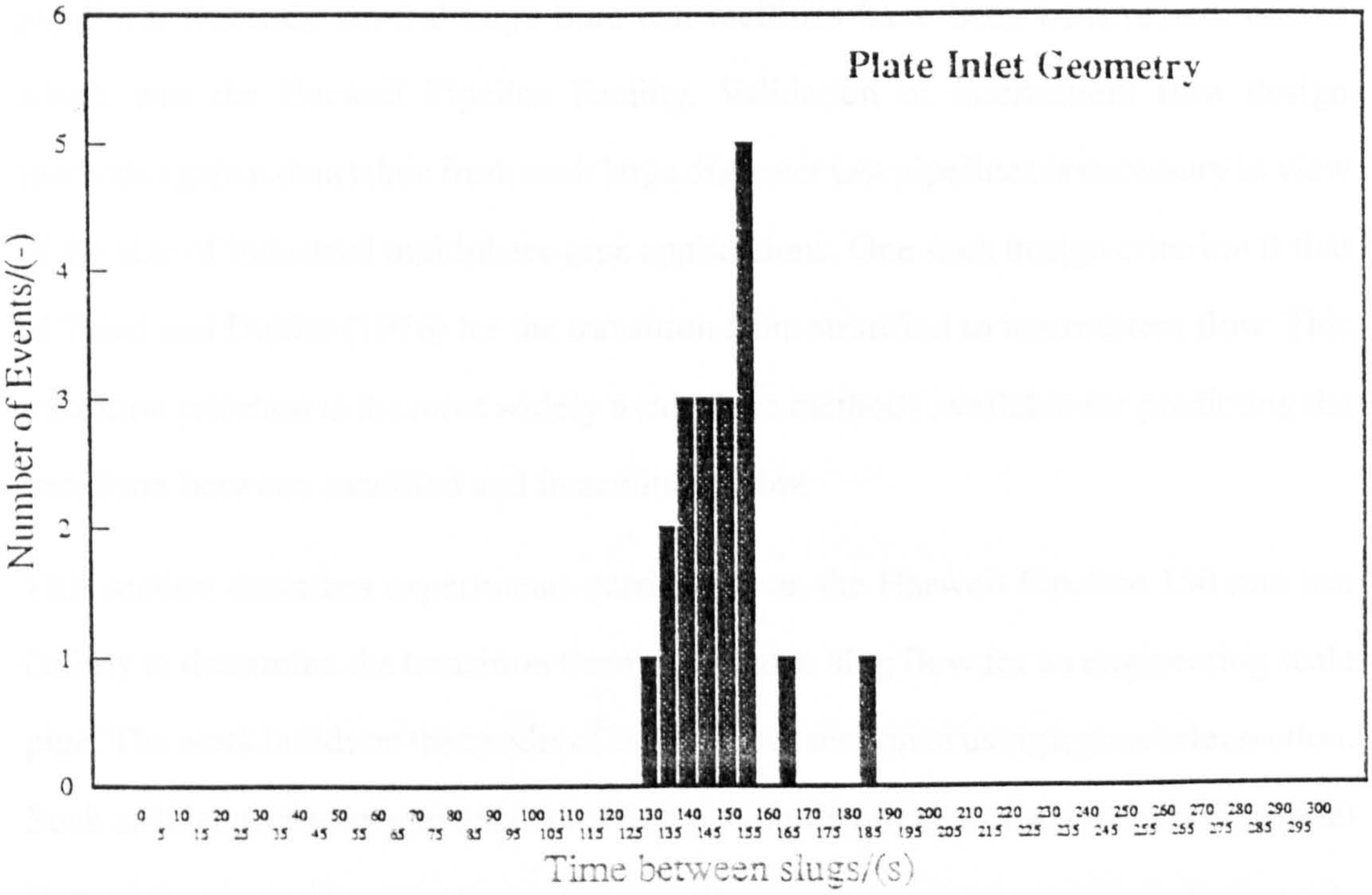
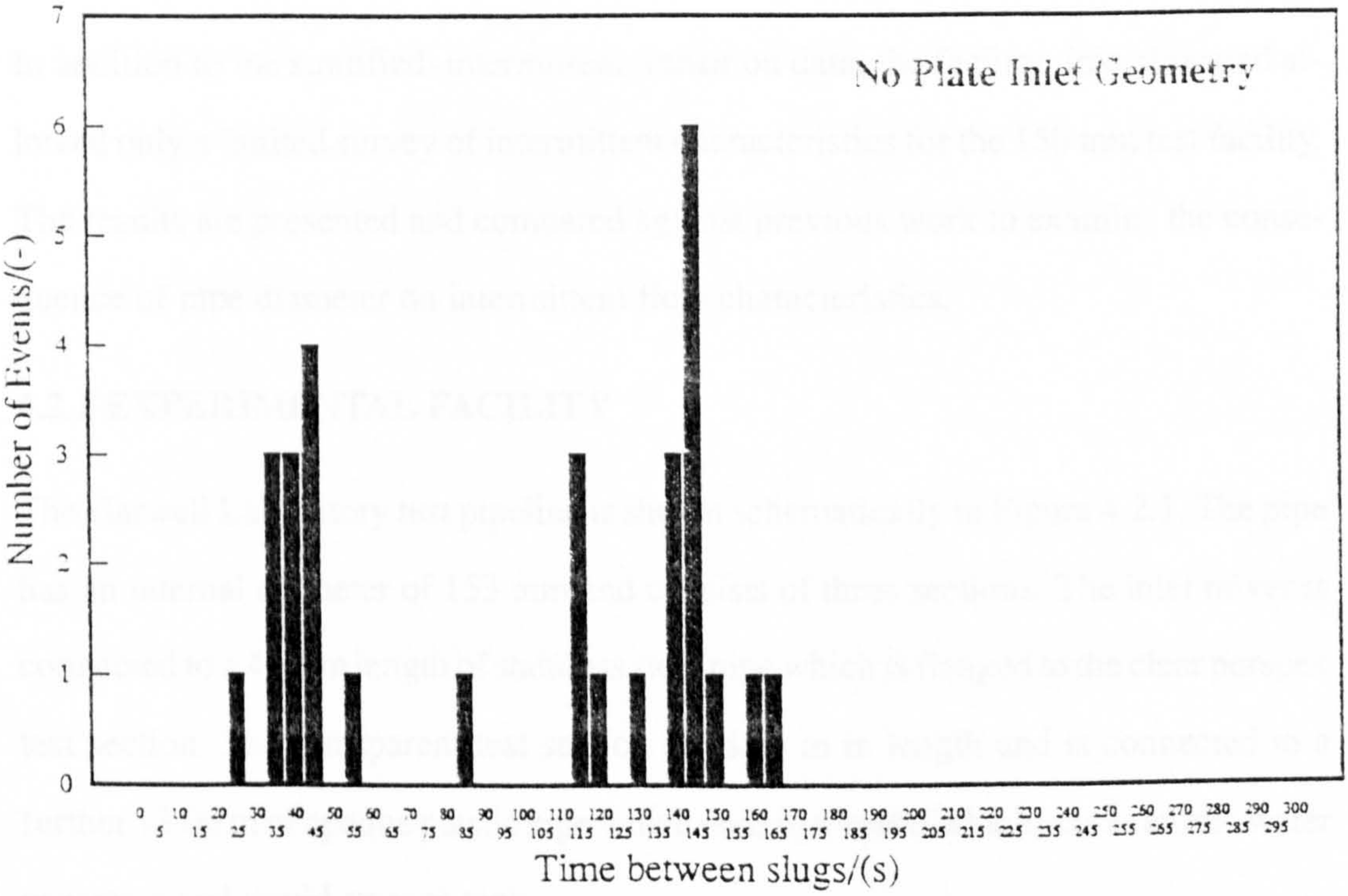


Figure 4.1.29 Distribution of Time between Slugs.
U_{Ls} = 0.225 m/s. U_{Gs} = 1.844 m/s



4.2 LARGE DIAMETER PIPE

In the past, most multiphase flow research has been carried out on small diameter test pipelines. Recently several large bore test facilities have been constructed, one of which was the Harwell Pipeline Facility. Validation of intermittent flow design methods against data taken from such large diameter test pipelines is necessary in view of the size of industrial multiphase pipe applications. One such design criterion is that of Taitel and Dukler (1976) for the transition from stratified to intermittent flow. This transition criterion is the most widely used of the methods available for predicting the transition between stratified and intermittent flow.

This section describes experiments carried out on the Harwell Pipeline 150 mm test facility to determine the transition from stratified to slug flow for an engineering scale pipe. The work builds on the results of the previous section in using a plate inlet section. Such an inlet geometry prevents excessive gas–liquid interaction and results in parallel flow of the gas and liquid at the exit of the inlet section. An inlet section producing parallel flow and only small finite waves is a necessary condition for testing of the model of Taitel and Dukler (1976), which is based on consideration on the Kelvin–Helmholtz instability of a small finite wave on a parallel flow of gas and liquid.

In addition to the stratified–intermittent transition data, the facility time allocated allowed only a limited survey of intermittent characteristics for the 150 mm test facility. The results are presented and compared against previous work to examine the consequence of pipe diameter on intermittent flow characteristics.

4.2.1 EXPERIMENTAL FACILITY

The Harwell Laboratory test pipeline is shown schematically in Figure 4.2.1. The pipe has an internal diameter of 153 mm and consists of three sections. The inlet mixer is connected to a 4.81 m length of stainless steel pipe which is flanged to the clear perspex test section. The transparent test section is 18.65 m in length and is connected to a further 13.06 m of opaque plastic pipe which ends in a vessel which acts as an air–water separator and liquid storage tank.

Demineralised water from the storage vessel is pumped to the inlet mixer by a thyristor controlled pump. The pump can supply water to a maximum liquid superficial velocity of 3 m/s. The water is metered by a magnetic flow meter which is located in a long straight section of pipe upstream of the mixer inlet.

Air is supplied to the mixer from two electrically driven centrifugal fans in series. The fans use atmospheric air to supply up to a maximum air superficial velocity of 40 m/s at a maximum delivery pressure of 1.8 bar absolute. The air on exit from the fans passes through a water cooled heat exchanger and on to a vortex shedding meter. The vortex shedding meter is located upstream of the mixer inlet in a straight section of the pipe. Pressure and temperature are measured by a fast response pressure transducer and a thermocouple.

The air–water mixer used on the facility prior to the work described in this Thesis is illustrated in Figure 4.2.2. The air enters parallel to the mixer axis and the water tangential to the circumference of the mixer. Anti–swirl baffles are fitted between the mixer and the air–water test pipeline.

The mixer insert designed and manufactured for the work reported in this section is shown in Figure 4.2.3. The insert fits inside the existing mixer, the anti–swirl baffles being removed. The mixer now consists of two components, the outer shell in which only water flows and the inner pipe in which air and water flow. Water still enters the pipe section at right angles to the mixer axis. The water then passes parallel to the pipe axis bounded by the pipe walls and the plate. Air is guided to flow parallel to the pipe axis over the plate.

4.2.2 INSTRUMENTATION

A high speed data logger connected to a Tandon personal computer recorded the air velocity, water velocity, pressure, and temperature at the vortex meter, and the pressure and temperature in the test section.

Three 0–50 mbar differential pressure transducers were located at 11.49 m, 16.28 m and 23.46 m downstream of the mixing section. A dead–weight tester was used to cali-

brate the transducers. Signals from the transducers were logged on a pen chart recorder. A Texaco Fast Volume Weight Meter (FVWM) leased to Harwell as part of a another project was used in this work to obtain the translational velocity of slugs. The details of the FVWM are confidential. The instrument consists of two gamma ray sources which irradiate the pipe cross–section at two locations on the pipe. Sodium Iodide detectors collect the gamma rays and the count rates enable the liquid fraction at the two locations to be calculated. The FVWM has a response time of approximately 20 milliseconds. The two stations of the FVWM were located at 24.63 m and 27.60 m from the inlet mixer section. The FVWM was calibrated with the pipe full of liquid and empty of liquid. Signals from the FVWM were recorded and displayed on a dedicated data logger and computer.

4.2.3 RESULTS

4.2.3.1 Mixer section

Prior to installation of the new mixing section considerable swirl in the liquid phase was observed over a wide range of liquid flowrates, despite the presence of anti–swirl baffles. The swirl induced by the tangential water inlet persisted down the test section. Observations of the water flow issuing from the new mixing section indicated that the swirl was imperceptible except at the highest liquid flowrate.

4.2.3.2 Slug–stratified transition boundary

In this work 103 data points were collected in the region of the stratified–slug transition boundary. The gas velocity in the facility was set, with the flow in the stratified regime, and the liquid velocity increased until slugging occurred. This process was repeated for each flow point taken, to ensure that the data obtained corresponded to the transition from stratified to slug flow.

The flow regime was determined by visual observation in the clear pipe section and by examining the pressure traces of the differential transducers. Figure 4.2.4 shows the data collected on the facility to delimit the stratified to slug transition, and compares this data with the theoretical transition boundary calculated from the theory of Taitel

and Dukler (1976). The Kelvin–Helmholtz theory, which provides a stability criteria for waves of infinitesimal amplitude, was extended in a simple way, by Taitel and Dukler (1976), to the case of finite waves on a stratified liquid in a pipe. As can be seen the theoretical transition of Taitel and Dukler (1976) neither predicts the magnitude or the form of the experimental transition boundary. A certain amount of subjective interpretation is implicit in classifying flow regimes, especially at high gas flowrates, but it is felt that the discrepancy can not be explained away by subjective interpretation of the data due to the self–consistency of the experimental data shown in Figure 4.2.4 and the significant difference in the magnitude between the experimental data and the theoretical prediction at low gas flowrates.

The experimental transition boundary shows that the liquid superficial velocity for transition first decreases with increasing gas and then, at approximately 5 m/s, increases with gas superficial velocity. This trend is consistent with that observed in Section 4.1 for the "plate" inlet geometry for the low pressure 74 mm internal diameter facility, in that case the minimum in the transition curve occurred at the lower gas superficial velocity of approximately 3.5 m/s. It was observed in the experiments described in Section 4.1 that slug formation at high gas velocities occurred due to fast travelling roll waves merging with slower roll waves to form a combined roll wave of greater amplitude than the two individual components. Thus, the increase in the gas velocity with increasing pipe diameter at which the transition curve minimum occurs may indicate that a higher gas velocity is required for transition to 3–dimensional roll waves in larger diameter pipes.

4.2.3.3 Intermittent characteristics

Figures 4.2.5 and 4.2.6 present a limited survey of slug frequency and slug translational velocity taken on the 150mm Harwell Pipeline Facility.

Figure 4.2.5 compares slug frequencies with those calculated from the correlation of Gregory and Scott (1969) to investigate the effect of pipe diameter on slug frequency. Gregory and Scott used data obtained on pipes of 0.019 m and 0.035 m internal diameter to construct their correlation. Comparison of the correlation with the 0.15 m bore

Harwell facility data is shown in Figure 4.2.5 for pipe diameters of 0.019 and 0.035 m. Figure 4.2.5 shows that slug frequency decreases with decreasing liquid superficial velocity and if it is assumed that pipe geometry considerations are equivalent for both sets of data, Figure 4.2.5 would show that increasing the pipe diameter decreases the slug frequency at constant superficial velocities. Figure 4.2.6 shows a comparison of the slug frequencies recorded at pressure transducer 1 (upstream) and pressure transducer 3 (downstream) with calculated values from the correlation of Gregory and Scott (1969) for a pipe of 0.15 m bore. It can be seen that in the case of the results for a liquid superficial velocity of 0.77 m/s the upstream and downstream frequencies are equivalent and the correlation of Gregory and Scott (1969) agrees quite well with the experimental data. The data for a liquid superficial velocity of 0.97 m/s shows that the frequency upstream is significantly less than that recorded upstream, and that the correlation does not agree with the experimental data. This discrepancy may result from the flow at 0.97 m/s not being fully developed.

Figure 4.2.7 presents, in terms of the shedding factor C defined by Dukler and Hubbard (1975), the slug translational velocity data recorded .

where $$C = \frac{x}{\varrho_L S \varepsilon_{Gs} (U_G + U_L)} \qquad (4.2.1)$$

and where x is the mass pick–up rate at the slug front.

As can be seen at low gas superficial velocities C tends to 1 and steadily decreases as the gas superficial velocity increases. The values of C presented in the literature are summarised in Table 2.1.1 of Chapter 2. The trend follows that recorded by Hughmark (1965), who found that for Re>400000 C is approximately constant at 0.22 but for lower Reynolds numbers the constant increases. The negative values of C at gas superficial velocities of 4m/s and higher corresponds to gas blow through the slug body. Coney (1974) obtained negative values of C in his study of this phenomena which he labelled "surge" flow.

In summary it has been shown that the theoretical stratified to intermittent transition criteria of Taitel and Dukler does not predict the experimental data obtained in a engineering scale pipeline. This fact is of major importance to designers of multiphase pipelines.

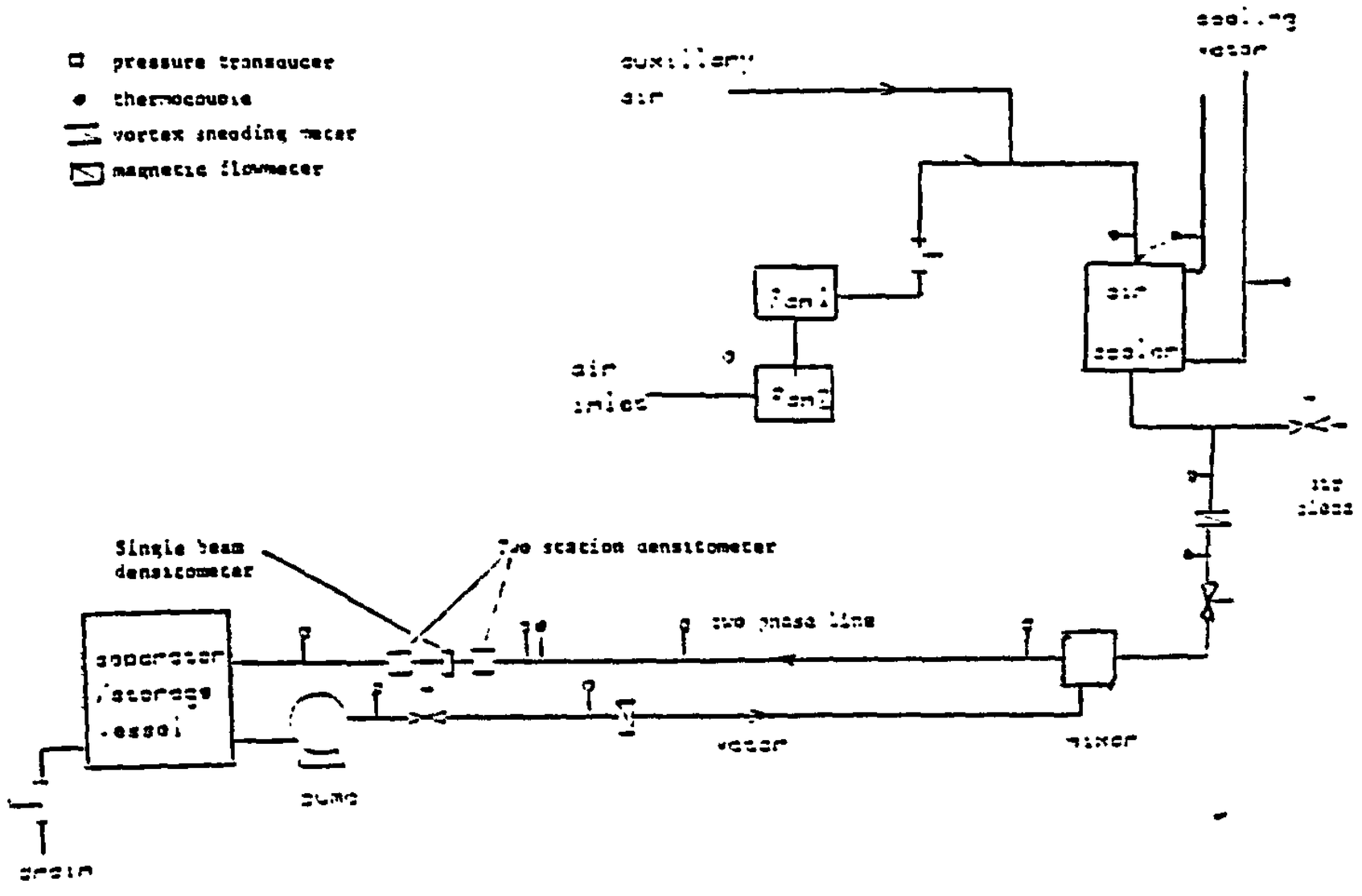
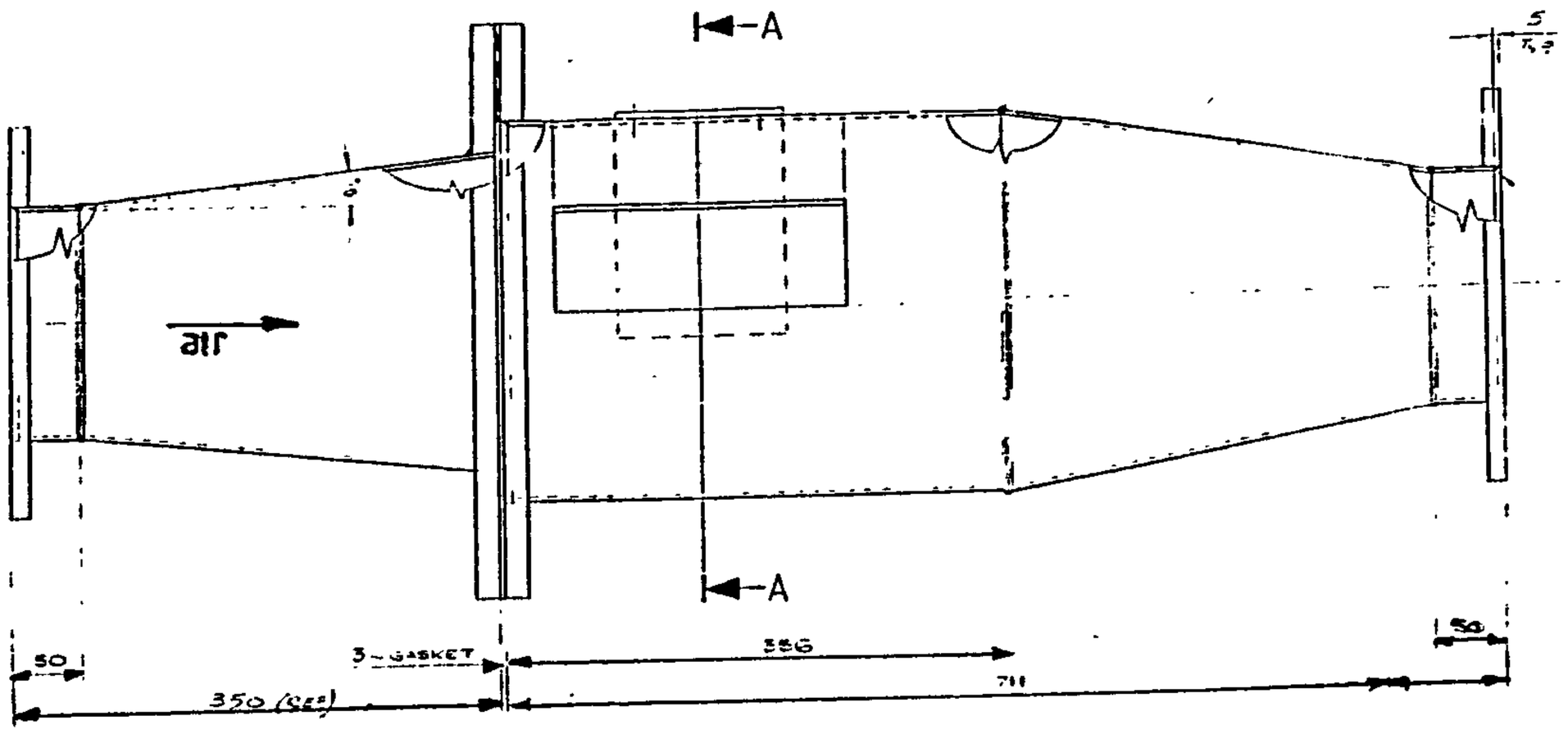


Figure 4.2.1 Harwell Laboratory 150mm Test Pipeline.



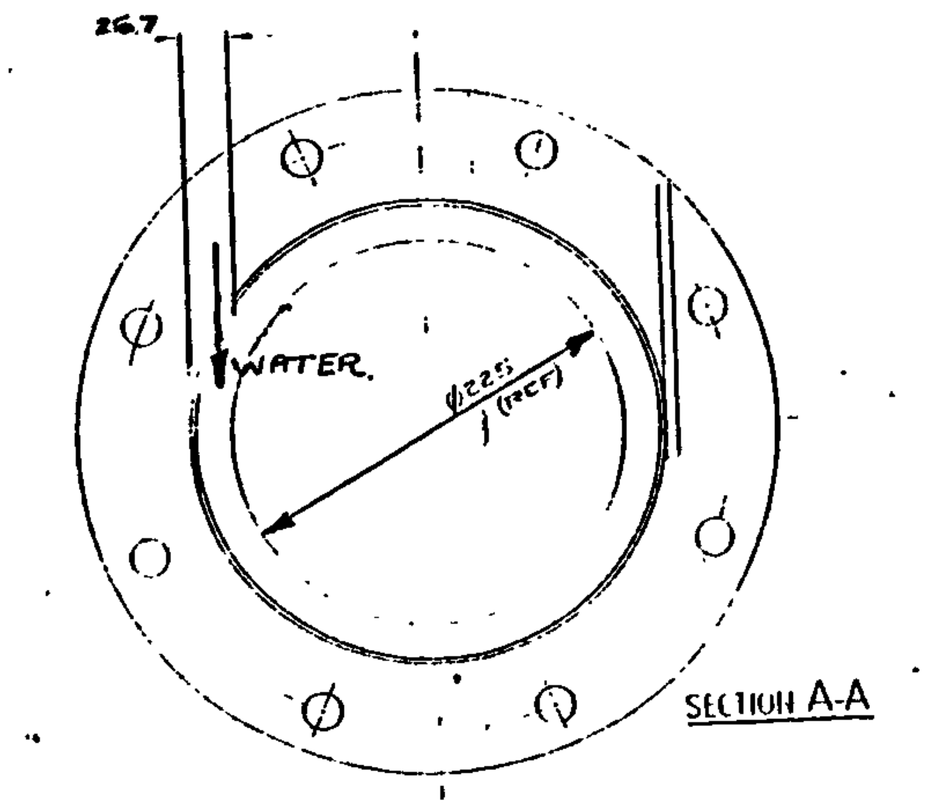
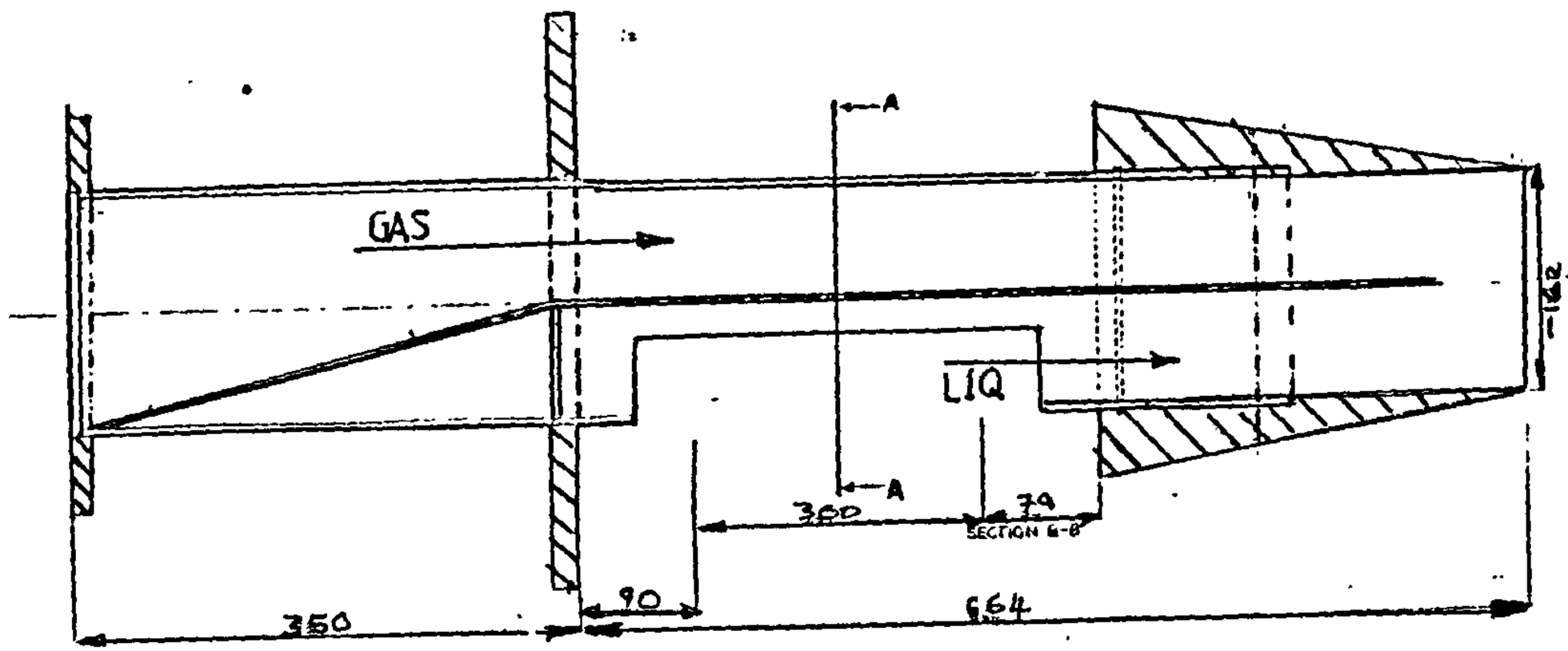
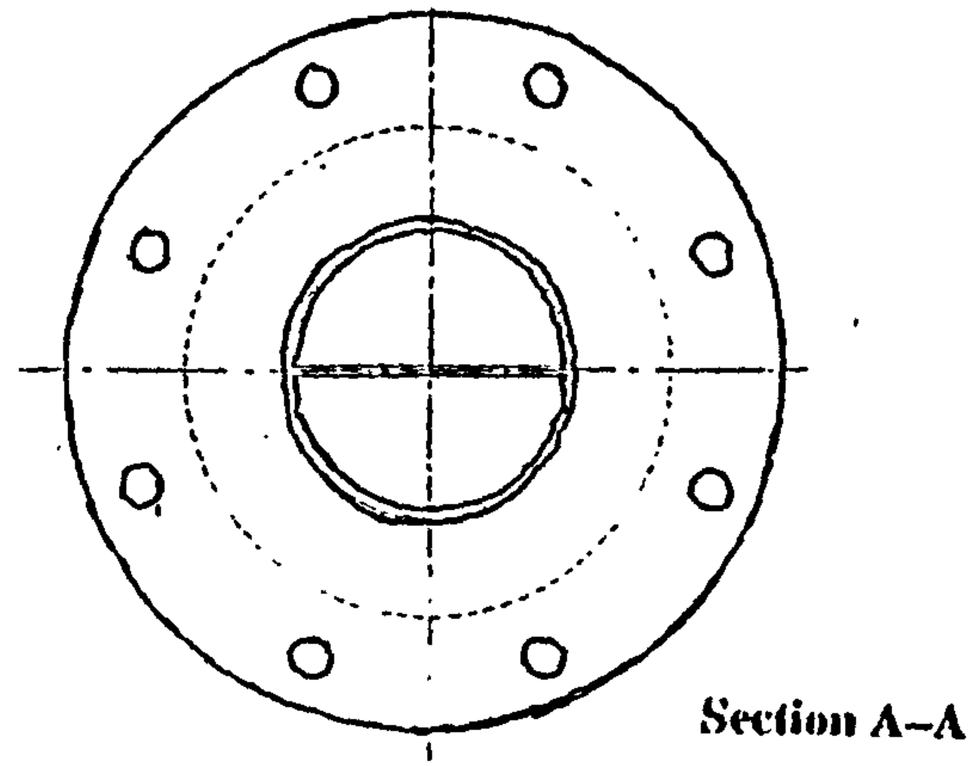


Figure 4.2.2 Original Air–Water Mixer





Section A–A

Figure 4.2.3 Mixer Insert.

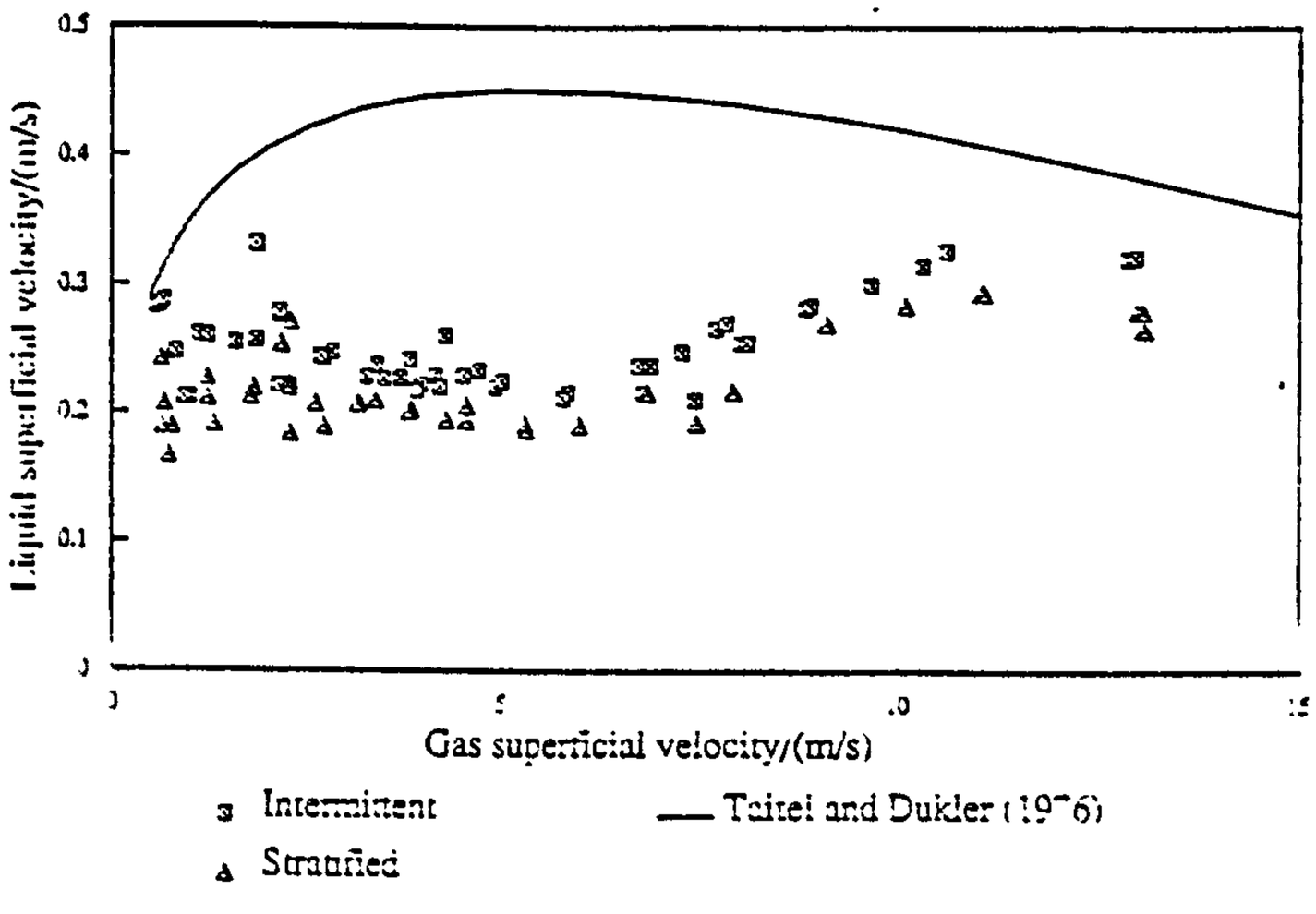


Figure 4.2.4 Stratified to Intermittent Transition Data (Harwell 150mm Facility)

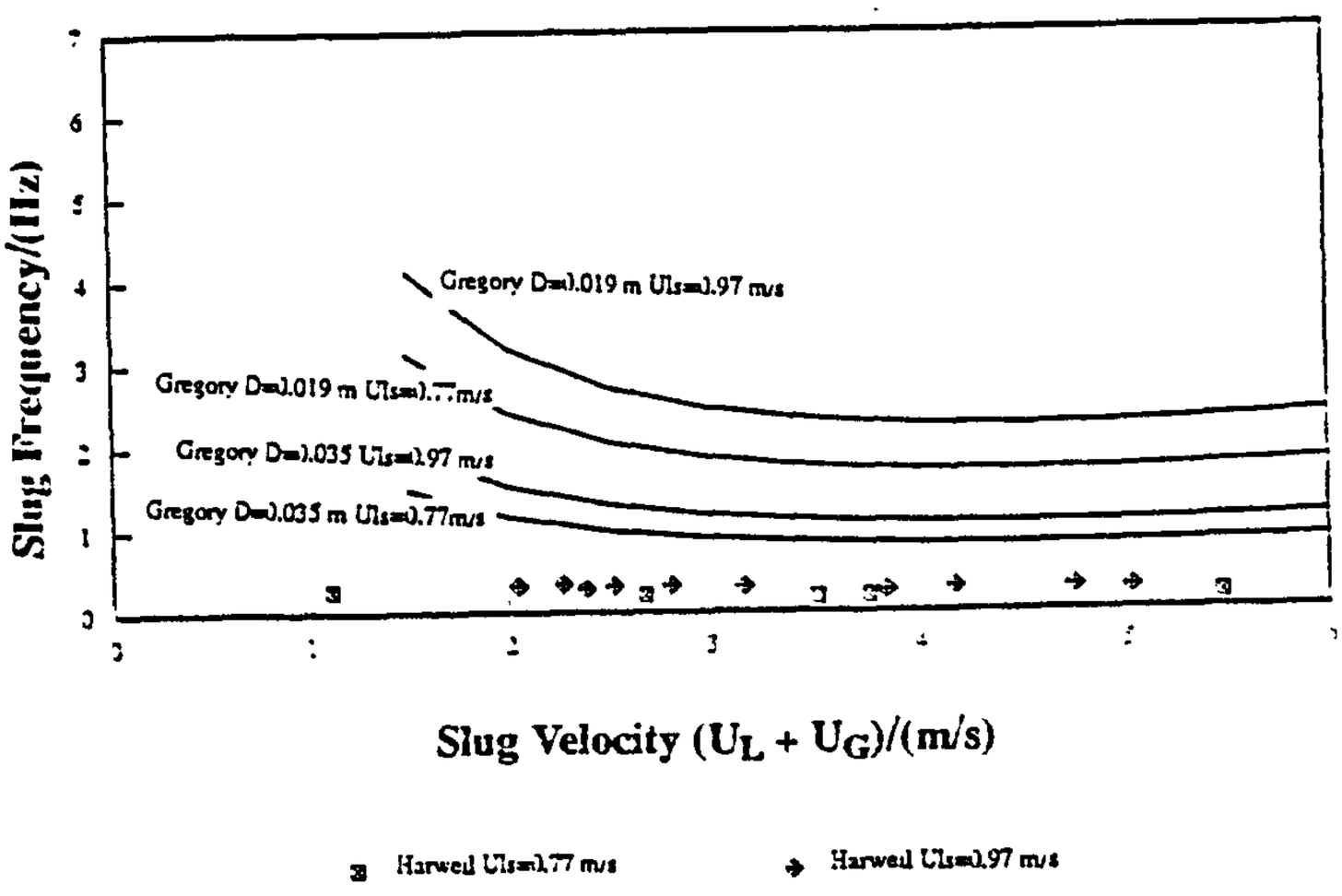


Figure 4.2.5 Slug Frequency Data Comparison
with Gregory and Scott (1969) Correlation (D=0.035 m and 0.019 m)
(Harwell 150mm Facility)

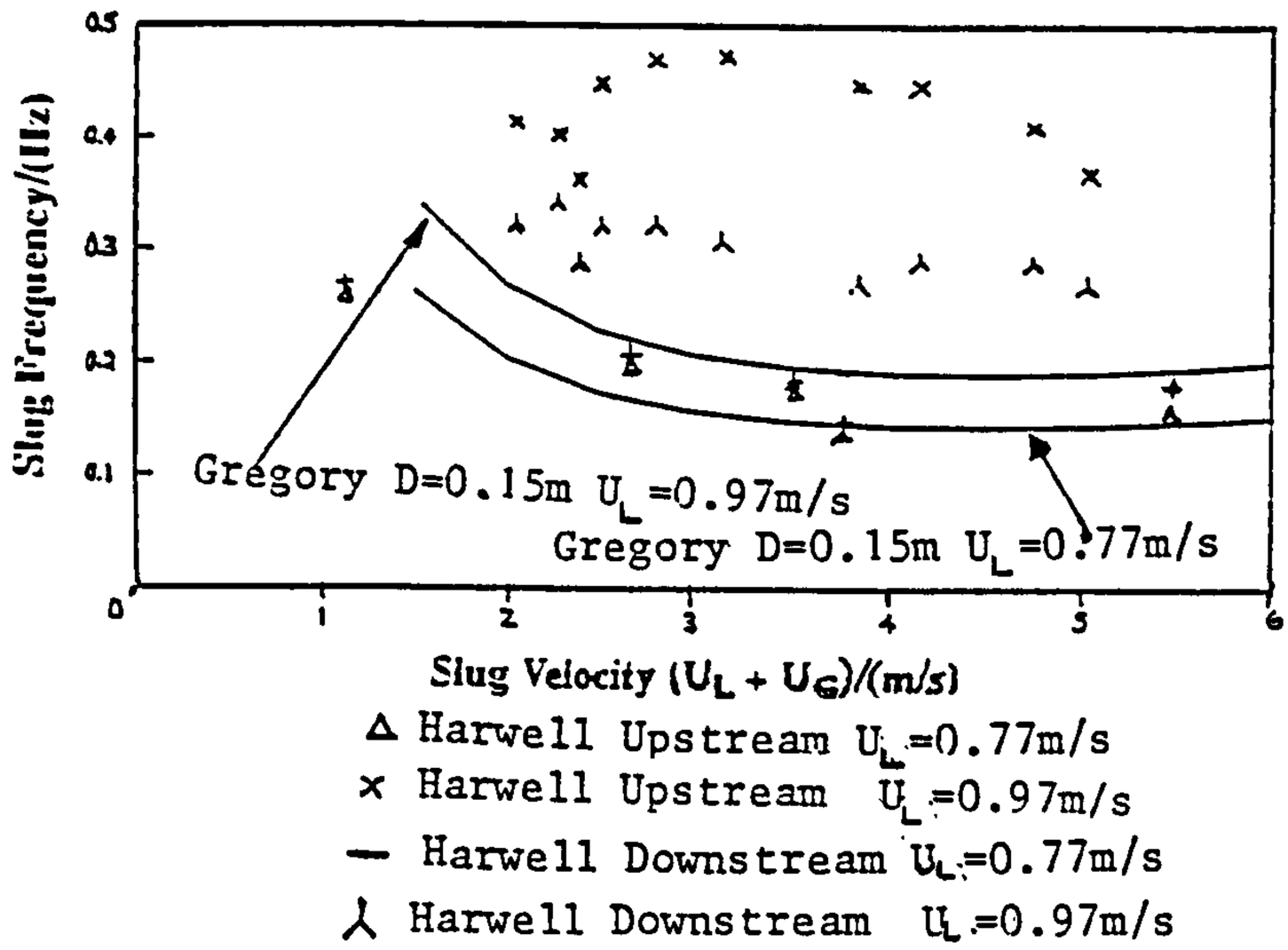


Figure 4.2.6 Slug Frequency Data Comparison with Gregory and Scott(1969) Correlation (D=0.15m) (Harwell 150mm Facility)

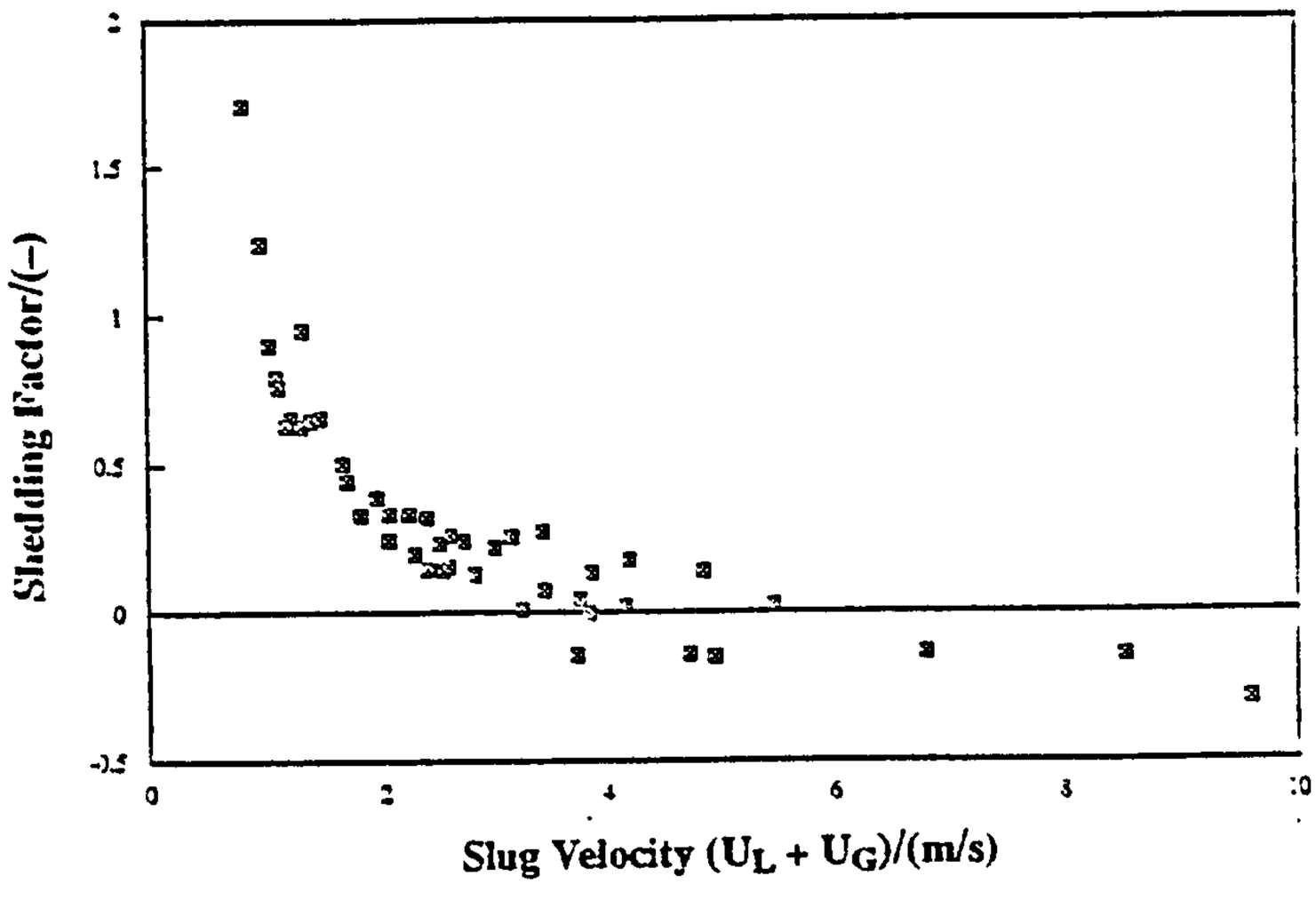


Figure 4.2.7 Shedding Factor Data (Harwell 150 mm Facility)

4.3 SMALL INCLINED SECTION

Most of the literature on intermittent flow has been concerned with straight horizontal, vertical, or very occasionally inclined pipelines. In pipeline systems, however, horizontal sections are often joined by short inclined sections which allow a level change. Here, an investigation is reported into how such a small inclined pipe located between two horizontal pipelines affects the slug frequency and slug front velocity in intermittent flow, and the transition from stratified to intermittent flow. A comparison is made with results from a purely horizontal pipeline.

4.3.1 EXPERIMENT

The air–water flow rig described in Chapter 3 was used for the investigation. The configuration of the test section is given in Figure 4.3.1. A riser section can be inserted in place of the removable pipe section indicated in Figure 4.3.1. The riser results in the pipe centres of the upstream and downstream horizontal pipelines being one diameter apart, with the increase in height being from the upstream (lower) pipe to the downstream (upper) pipe. Figure 4.3.2 shows the installed riser. The distance that separates the start of the riser base from the end of the inlet mixer is 1.68 m. The inlet mixer consisted of a plate located at the pipe centre with the air entering from above and the water from below the plate.

Visual observations were made on the flow in the whole of the test section, the observations being referenced to the horizontal distance from the inlet mixer. Three wire conductance probes were used to measure slug front velocity, and were located at 4470, 7125, and 8520 mm from the air inlet. The frequency of slugs was obtained by noting the number passing a specified point on the test section. The frequency of the slugs at the end of the pipe were measured at the third wire probe, located at 8520 mm from the inlet. With the riser arrangement a frequency analysis was conducted for the lower pipe. Slugs were only counted if they passed a position 100 mm upstream of the riser.

The nominal flow matrix examined consisted of 0.44, 0.64, 1.0, 1.46, 1.86, 2.34, 3.04, 3.75, 4.2, and 5.2 m/s gas superficial velocity and 0.14, 0.18, 0.225, 0.271, 0.32, 0.391, 0.455, and 0.52 m/s liquid superficial velocity.

4.3.2 VISUAL OBSERVATIONS

The presence of the riser section had a profound effect on the flow patterns in the system and the phenomena observed were complex.

At medium gas superficial velocities (such as 2.23 m/s) and at a low liquid superficial velocity (for example 0.14 m/s) slug formation in the lower pipe followed a similar mechanism to that observed in a purely horizontal pipeline. The liquid level increased with distance from the inlet, with the interfacial wave amplitude increasing. Eventually a wave bridged the pipe and formed a slug which was carried up the riser and into the upper horizontal tube. However it was found that much smaller liquid velocities were required for the section including a riser than for a purely horizontal pipe.

At low gas velocity slugs were initiated over the whole liquid velocity range by an additional mechanism. After a slug had been initiated in the lower pipe it travels up the inclined pipe into the upper horizontal pipe, with some of the water in the slug tail draining down the inclined pipe into the lower pipe by the force of gravity. This water produces a wave in the liquid layer in the lower pipe which propagates back towards the inlet section. When the wave reaches the inlet, a slug is initiated which travels up the riser into the upper pipe, with liquid draining from its tail for the process to be repeated.

If the returning wave from the inclined pipe does not produce a slug the first time it reaches the inlet, because of insufficient liquid height in the lower pipe, the wave "rebounds" at the inlet back towards the inclined pipe where it is reflected off the inclined section back to the inlet section. Meanwhile the liquid level has increased in height due to the continuous flow of water into the lower pipe, so a slug is usually initiated. This process is only observed at low superficial gas velocities of 0.44 to 1.00 m/s and low liquid superficial velocities of 0.09 m/s to 0.18 m/s.

At liquid velocities larger than 0.18 m/s slugs were often produced in the middle of the lower pipe, not just by waves growing in size on the stratified layer but due to the returning wave, mentioned in the previous paragraph, meeting the front of the fresh water inlet wave. The resulting combined wave sometimes formed a slug in the middle of the lower pipe. The process of the rebound wave producing slugs did not occur at larger gas flowrates of 1.74 m/s and above.

One of the consequences of the horizontal–inclined–horizontal arrangement was that the water in the upper horizontal pipe flowed in pulses for liquid superficial velocities of 0.09 to 0.225 m/s. At the lower end of the above liquid velocity range the pipe was often dry inbetween pulses, but at higher liquid velocities the pulses/waves were more frequent and resulted in continuous water flow in the upper pipe. The observed flow behaviour in the upper pipe is discussed in the following paragraphs.

At high gas velocities, 3.52 m/s upwards, the waves in the lower section are blown up the inclined section, even at the lowest liquid velocities. At very high gas velocities, for example 5.39 m/s, water droplets entrained in the gas flow at the inclined pipe were blown a long distance down the upper pipe, causing water streaking on the pipe walls. At these high gas velocities any slugs produced in the lower section were broken up by the inclined pipe to produce large roll waves in the main pipe. The larger roll waves catching up and combining with smaller roll waves, sometimes initiating slugs.

At high liquid velocities , such as 0.52 m/s and medium to high gas velocities, a slug produced in the lower pipe is only slightly disrupted by the inclined pipe and continues into the upper pipe.

4.3.3 SLUG FREQUENCY

Figures 4.3.3 to 4.3.10 show slug frequency (at 3rd wire probe location) as a function of gas superficial velocity, with each figure depicting data for one superficial liquid velocity for both the test section with a riser and the straight horizontal tube.

For low gas flowrates (0.44 – 1.0 m/s) the frequency of slugs is higher for the riser arrangement. This is because the riser section fills up to the critical height for slug for-

mation quicker due to the liquid level gradient introduced by the riser, giving rise to a higher frequency of slug initiation. This high frequency of initiation of slugs in the lower pipe is demonstrated further in Figures 4.3.11 to 4.3.18. These plots show a comparison of slug frequency in the lower pipe, 100 mm upstream of the riser, with that at the 3 rd wire probe position in the upper pipe for the riser configuration only. As can be seen the slug frequency in the lower pipe is substantially greater in comparison with the frequency in the upper pipe over most of the flow range considered. Returning to consideration of Figures 4.3.3 to 4.3.10 we see that as the gas flowrate increases the difference in frequency between the test section with a riser and the straight horizontal pipe configuration becomes smaller, until at 2–6 m/s gas superficial velocity the slug frequencies for both configurations are equal to within experimental error. At higher gas flowrates, the enhancement of the liquid level in the lower pipe by the riser is insignificant. In addition, the frequency of slug initiation is controlled by roll wave coalescence for both configurations and hence the recorded slug frequencies are very close to each other. As the liquid flowrate is increased at constant gas flowrate, slug frequency increases for both the riser and horizontal configuration.

4.3.4 SLUG FRONT VELOCITY

Figures 4.3.19 to 4.3.34 show the variation of slug front velocity as a function of gas superficial velocity, with each figure depicting data for one superficial liquid velocity for both the riser and horizontal pipe configurations. The velocity measurements were taken between wire probes number one and two (indicated as upstream measurement in the Figures 4.3.19 to 4.3.26) and between probes number two and three (indicated as "downstream" measurement in the Figures 4.3.27 to 4.3.34). In general the slug front velocities noted for the riser and horizontal configuration are close at a given gas and liquid flowrate. The exceptions may correspond to slugs that are travelling over a liquid layer formed from a decayed slug or over a stratified layer on which slugs had not previously been formed, rather than over liquid shed from the rear of a preceding (still active) slug. The slug front velocity for both riser and horizontal geometries increases with increasing gas superficial velocity.

4.3.5 STRATIFIED–INTERMITTENT TRANSITION

In the riser arrangement the riser section fills up to a higher liquid level than the horizontal arrangement for any liquid flowrate and the same gas flowrate. Thus the stratified to intermittent transition curve for the riser arrangement is expected to be lower than for the horizontal arrangement as slug initiation is dependant on the liquid level in the pipe.

The transition boundary between intermittent and stratified flow was determined by setting a gas and liquid flowrate in the stratified flow regime and then increasing the liquid flowrate in small steps at constant gas flowrate until intermittent flow was observed at the location of the 3rd wire probe. Figure 4.3.35 shows the experimental stratified to intermittent transition for the riser and horizontal configurations. As expected the transition occurs at a lower liquid superficial velocity for the riser at each gas flow condition presented. Both experimental curves exhibit a minimum, as found for the experiments carried out on the Harwell Pipeline (Section 4.2). It is also noted from Figure 4.3.35 that at low gas superficial velocities both curves exhibit an increase in the liquid superficial velocity necessary for transition to intermittent flow with decreasing gas superficial velocity. This rise in liquid superficial velocity occurs at a lower gas superficial velocity for the riser geometry. In contrast, the stratified to intermittent transition criteria of Taitel and Dukler (1976) predicts a small decrease in liquid superficial velocity with decreasing gas superficial velocity at low gas superficial velocities.

The increase in liquid velocity for transition at low gas velocities may imply that the liquid level in part of the pipe is less than that for equilibrium flow, this being caused by outlet effects. The stratified liquid layer falls freely from the outlet end of the pipe into the sump tank. The liquid level may therefore be lower than equilibrium at the outlet and this decrement may persist upstream through an hydraulic gradient. It is interesting to calculate the distance upstream of the end of the tube over which the level is less than that for equilibrium. An analytical treatment of this problem is given by Taitel and Dukler (1987) and this analysis was applied in the present work. The results may

be expressed in terms of the distance upstream of the end of the tube over which the liquid level would be lower than the equilibrium value. For the 74 mm tube, the calculated distances are plotted in Figure 4.3.36. This shows that the upstream distance over which the exit effect causes the liquid level to be below that for equilibrium stratified flow increases with decreasing gas superficial velocity. The distance increases to 10 m (the length of the test section) when the gas velocity falls to about 3.2 m/s. Hence one would expect at gas superficial velocities less than 3.2 m/s to see the liquid superficial velocity necessary for transition from stratified to intermittent to increase with decreasing gas superficial velocity. Unfortunately while this explanation would be satisfactory for the horizontal configuration it is not satisfactory for the test section including the riser since the test–section–induced hydraulic gradient cannot be "felt" in the lower pipe.

It was observed at low gas velocity for the riser geometry that slugs were formed in the lower horizontal pipe at liquid superficial velocities less than the liquid flowrate necessary for slugs to be observed at the third wire probe position. Hence the sharp increase in liquid superficial velocity for transition to intermittent flow for the riser geometry may be explained by considering the stability of slugs at low gas superficial velocity. Here, we will consider two alternative mechanisms for this effect, both suggested by Ruder et al (1989).

Slugs at such low gas superficial velocity contain no gas in the slug body, and so only liquid is gained at the front of the slug and shed at the tail. Such a slug will persist when the gain of liquid at the front of the slug is greater than or equal to the liquid shed at the slug tail.

The volumetric flowrate of liquid (in a frame of reference moving at the slug translational velocity) that the slug gains from the liquid layer in front is given by:

$$\dot{V}_{front} = (V_t - v_L)A_L \qquad (4.3.1)$$

where

V_t is the translational velocity of the slug.

v_L is the velocity of the liquid film.

A_L is the pipe area occupied by the liquid film.

Ruder et al (1989) suggested that the tail can be modelled as a 'Benjamin bubble' (Benjamin, 1968) which gives the following solution for the slug tail translational velocity, V_t:

$$V_t = (U_L + U_G) + 0.542(gD)^{0.5} \qquad (4.3.2)$$

Then, Ruder et al (1989) estimated the minimum height of liquid layer over which unaerated slugs can propagate in a horizontal pipe by equating the volumetric flowrate of liquid (in a frame of reference moving at the slug translational velocity) that the slug gains from the liquid layer at the slug front to the volumetric flowrate of liquid (in a frame of reference moving at the slug translational velocity) that the slug sheds at the tail:

$$(V_t - v_L)A_L = 0.542\left(\frac{\pi D^2}{4}\right)(gD)^{0.5} \qquad (4.3.3)$$

where

V_t is the translational velocity of the slug.

v_L is the velocity of the liquid film.

A_L is the pipe area occupied by the liquid film.

Figure 4.3.37 shows the application of Equation 4.3.3 to investigate the minimum liquid height required for stable unaerated slugs in a 74 mm diameter horizontal pipe. The experimental transition boundary data contained in Figure 4.3.35 is given in terms of liquid superficial velocity instead of minimum liquid height. It is therefore necessary to extend the analysis of Ruder et al (1989) to convert the minimum liquid height calculated from Equation 4.3.2 into a corresponding minimum liquid superficial velocity.

Equation 4.3.3 for given liquid and gas superficial velocities defines a relationship between the pipe area occupied by the liquid in the film region and the liquid film velocity Another relationship between the pipe area occupied by the liquid in the film region and the liquid film velocity can be derived by assuming that the liquid film is in equilibrium just before the slug front.

A force balance on the liquid film (see for example Taitel and Dukler, 1976) gives the following equation:

$$\frac{-\tau_L S_L}{\varrho_L A_L} + \frac{\tau_i S_i}{\varrho_L A_L} + \frac{\tau_G S_G}{\varrho_L A_G} + \frac{\tau_i S_i}{\varrho_L A_G} = 0 \qquad (4.3.4)$$

where

τ_w is the shear stress acting at the wall–liquid interface.

τ_i is the shear stress acting at the gas–liquid interface.

τ_G is the shear stress acting at the gas–wall interface.

S_G is the perimeter of the wall–liquid interface

S_i is the perimeter of the gas–liquid interface

S_L is the perimeter of the wall–liquid interface.

Equation 4.3.4 enables the velocity of the liquid film to be calculated given the area occupied by the liquid film and the gas velocity over the film. The area averaged gas

velocity over the film will be equal to the slug translational velocity in stable flow ; so:

$$v_G = V_t \qquad (4.3.5)$$

and $$A_L = A\left(1 - \frac{v_G}{U_G}\right) \qquad (4.3.6)$$

Equation 4.3.5 and 4.3.6 assume the gas is incompressible.

For specified gas and liquid superficial velocities Equations 4.3.4, 4.3.5 and 4.3.6 allow the liquid film velocity to be calculated. Substituting this value of liquid film velocity, A_L, and U_G into Equation 4.3.3 allows an updated value of the liquid superficial velocity to be obtained. If this new value is equivalent to the original specification of the liquid superficial velocity then one point of a slug stability line has been obtained, expressed in terms of the gas and liquid superficial velocities.

To examine whether the sharp increase in liquid superficial velocity for transition to intermittent flow for the riser geometry may be explained by considering the stability of slugs at low gas superficial velocity, the stability line for the 74mm diameter test section calculated from the above equations is shown in Figure 4.3.38. While a rise in liquid superficial velocity is shown at gas superficial velocities less than 0.5 m/s, the calculated liquid superficial velocities are a magnitude less than the liquid superficial velocities of the experimental transition data. Hence stability considerations derived from the propagation velocity of a slug tail do not explain the observed sharp increase in liquid superficial velocity for transition to intermittent flow for the riser geometry at low gas superficial velocity.

The second necessary condition for the existence of stable slugs suggested by Ruder et al (1989) is based on describing the slug front by a hydraulic jump. The role of hydraulic jumps in slug behaviour was first discussed by Jepson (1987). Ruder et al (1989) provide an analytical framework for this phenomena. Unless the relative velocity between the film and the slug is sufficient for an hydraulic jump, the slug cannot exist. The analytical treatment of this definition by Ruder et al (1989) produced a cri-

terion for the existence of a slug. Namely, for an unaerated slug to exist in a circular pipe it is necessary that the value of $(V_t - v_L)/(gD)^{0.5}$ must be greater than those given in Table 4.3.1 for a given liquid film height. This criterion was not assessed against experimental data by Ruder et al (1989).

Table 4.3.1 Ruder et al (1989) front criterion for the existence of a slug

h/D	$(V_t-v_L)/(gD)^{0.5}$
0.1	0.9459
0.2	0.92
0.3	0.090
0.4	0.9108
0.5	0.9213
0.6	0.944
0.7	0.9937
0.8	1.0778
0.85	1.1444
0.89	1.2106

Application of Equations 4.3.2, 4.3.4, 4.3.5 and 4.3.6 converts the values given in Table 4.3.1 into corresponding liquid and gas superficial velocities. These values are shown in Figure 4.3.39. Figure 4.3.39 shows for a specific liquid superficial velocity the minimum gas superficial velocity for an unaerated slug to exist in a circular pipe. As can be seen the calculated minimum gas superficial velocity decreases with increasing liquid superficial velocity. Also the magnitude of the calculated liquid and gas superficial velocities match the experimental velocities for the increase in liquid superficial velocity for transition to intermittent flow for the riser geometry.

Thus the necessary condition for the existence of stable slugs based on describing the slug front by a hydraulic jump, proposed by Ruder et al (1989), is the more probable explanation of the increase in liquid superficial velocity for transition to intermittent flow for the riser geometry. A more detailed experimental investigation of the behaviour of the liquid slugs for the riser geometry at low gas flowrate is necessary before a definite conclusion can be made.

In summary it has been shown for the 10 m low pressure test section that the insertion of a riser between two horizontal pipes alters the intermittent characteristic of slug frequency and the stratified to intermittent transition. Examination of the results suggests consistency, for the low velocity region, with the criterion of hydraulic jump as a necessary condition for existence of slugs.

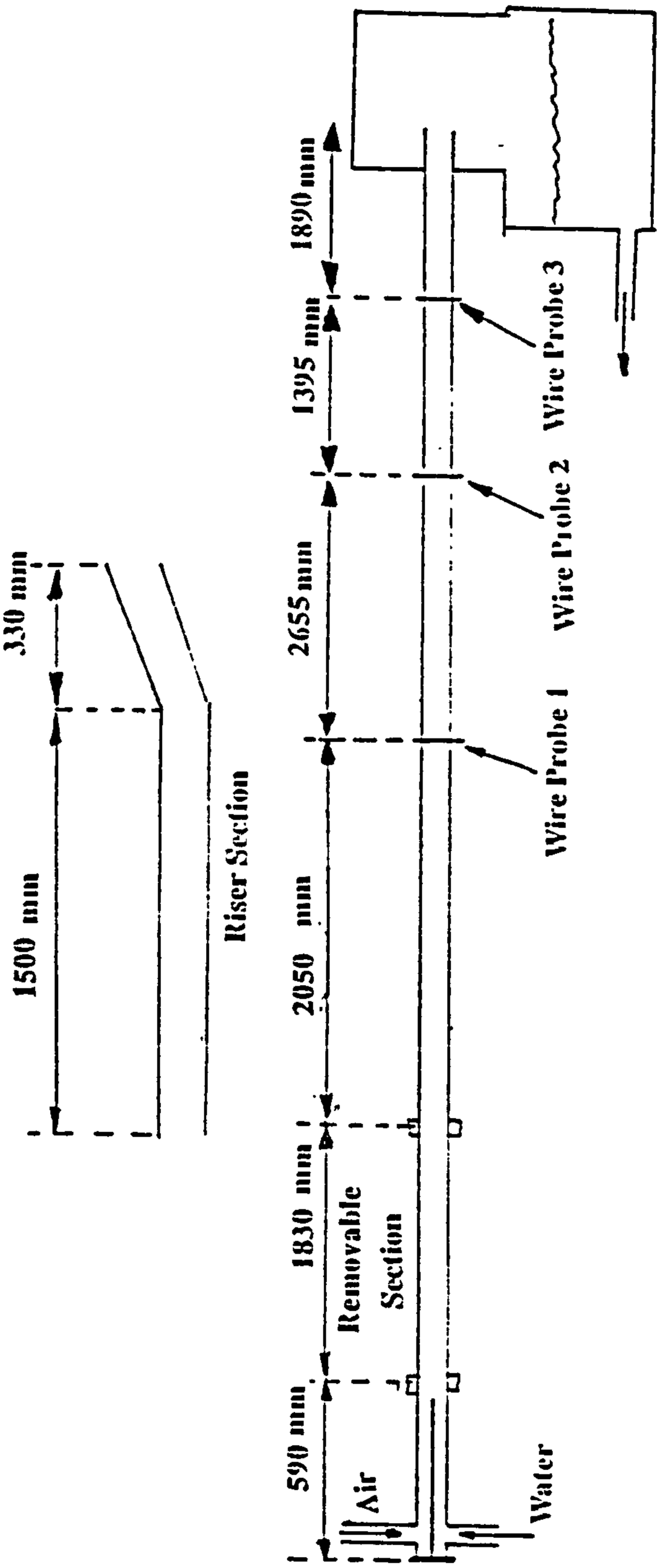


Figure 4.3.1 Test Section Configuration

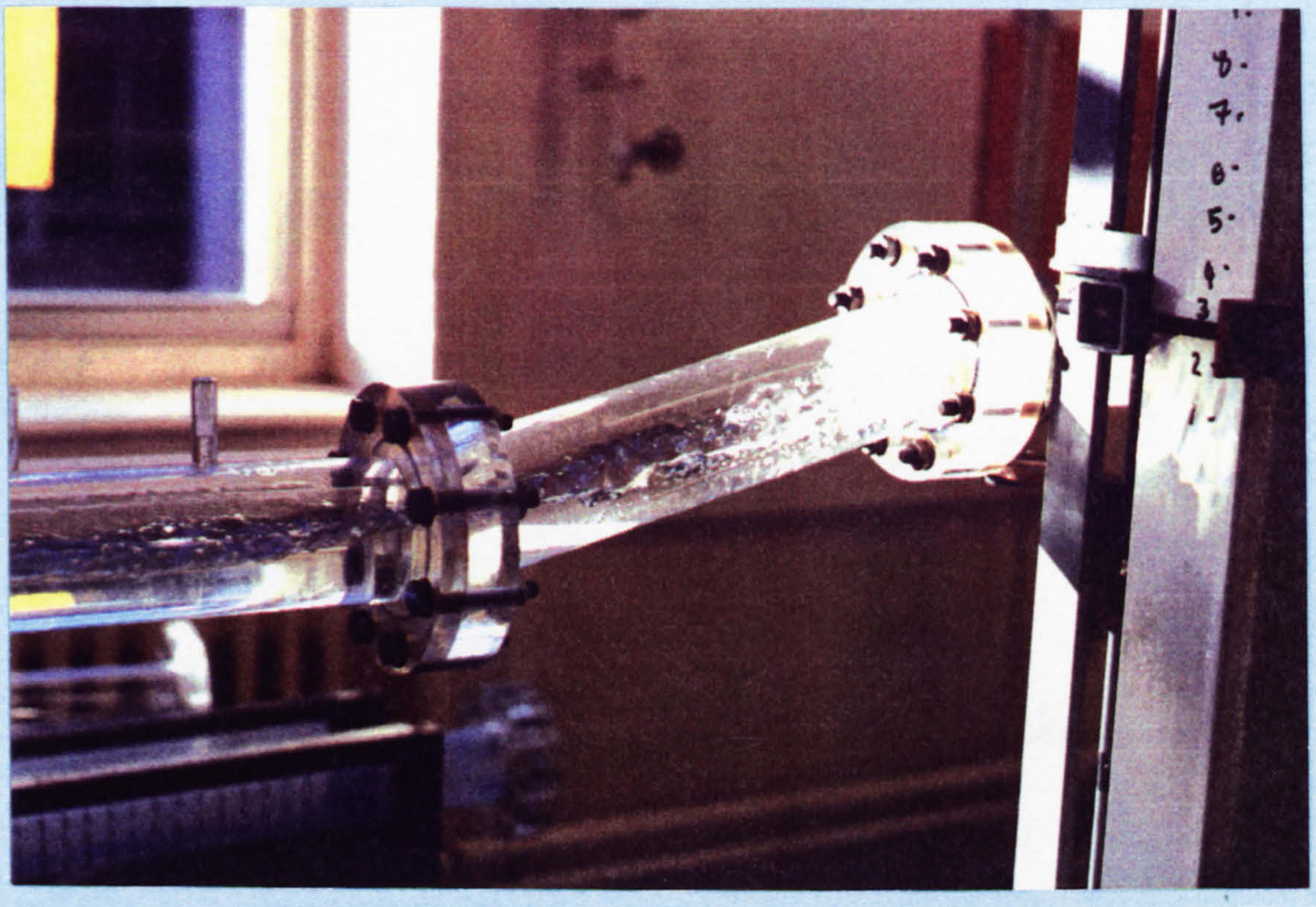


Figure 4.3.2 Installed inclined pipe section.

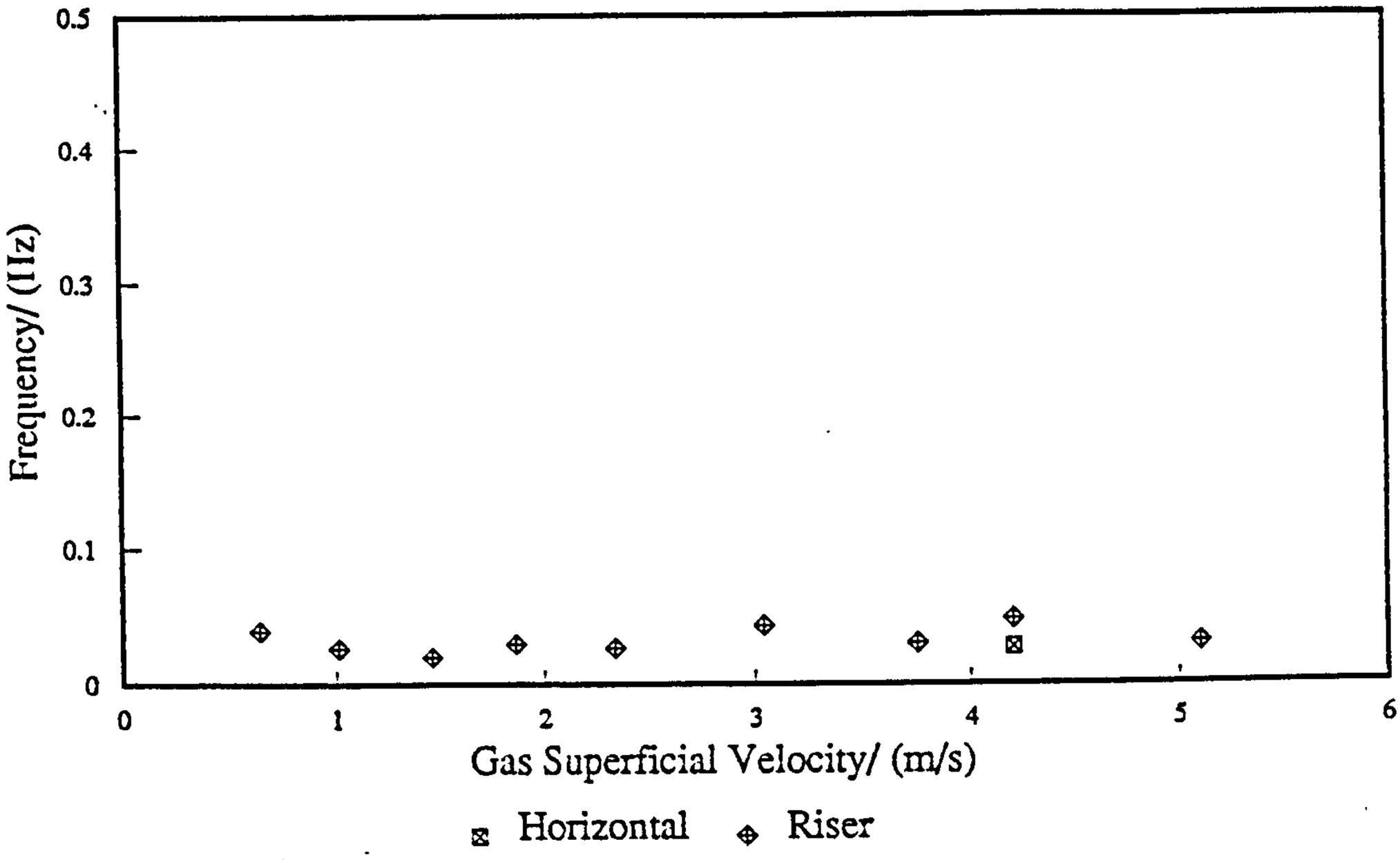


Figure 4.3.3 Slug Frequency at 3rd Wire Probe Position
U_{LS}=0.14 m/s

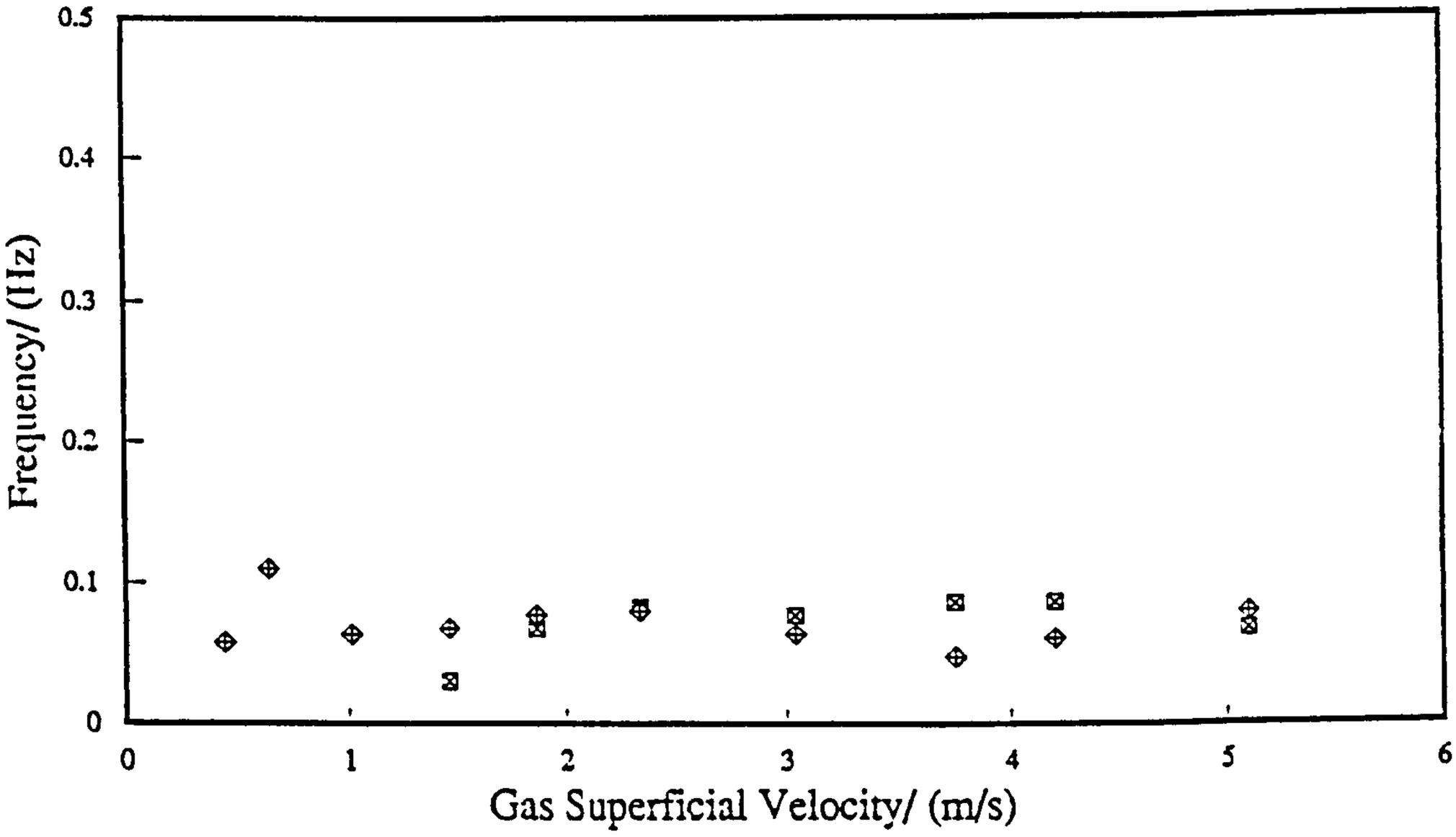


Figure 4.3.4 Slug Frequency at 3rd Wire Probe Position
U_{LS}=0.18 m/s

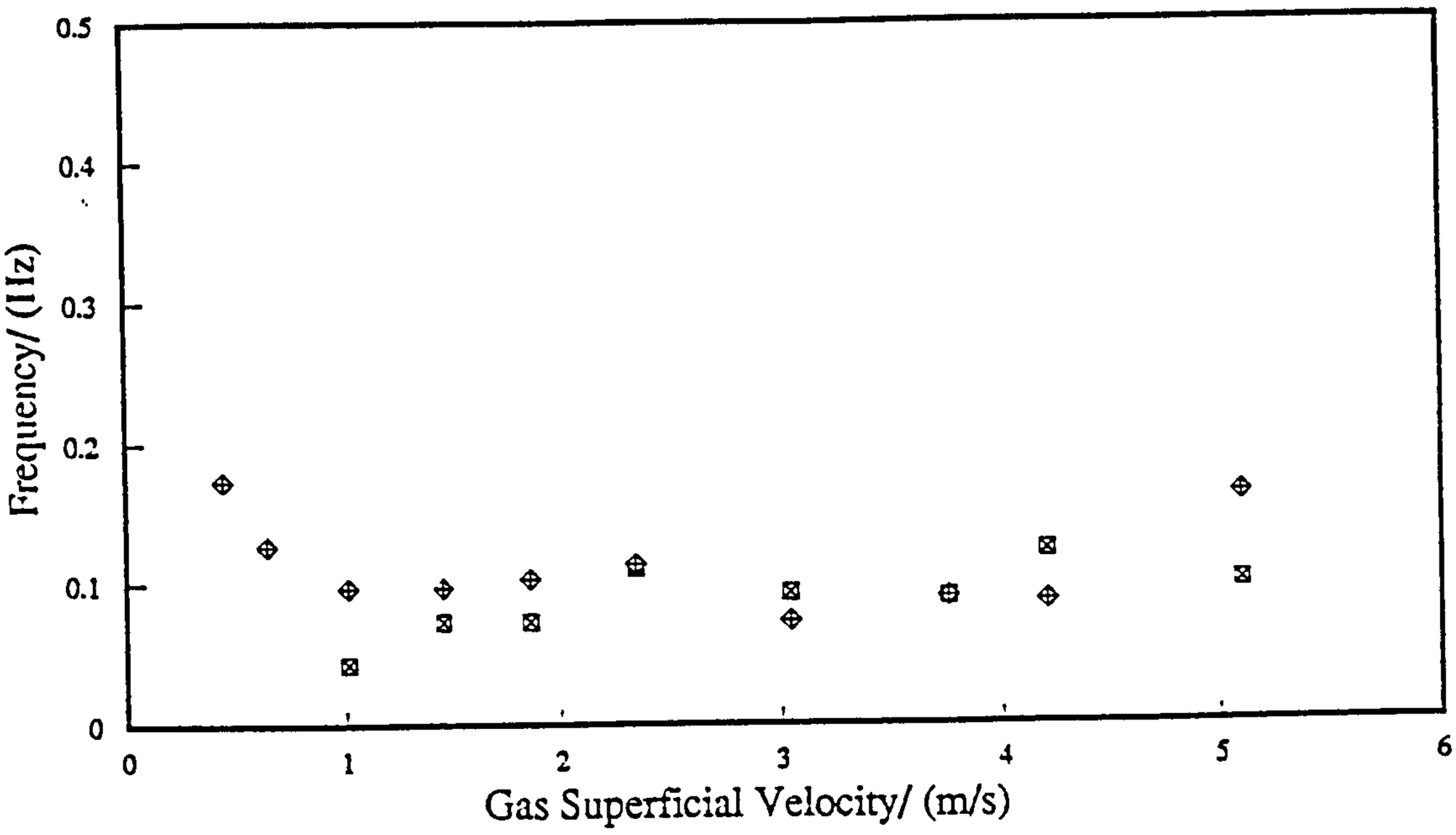


Figure 4.3.5 Slug Frequency at 3rd Wire Probe Position
U_{Ls}=0.255 m/s

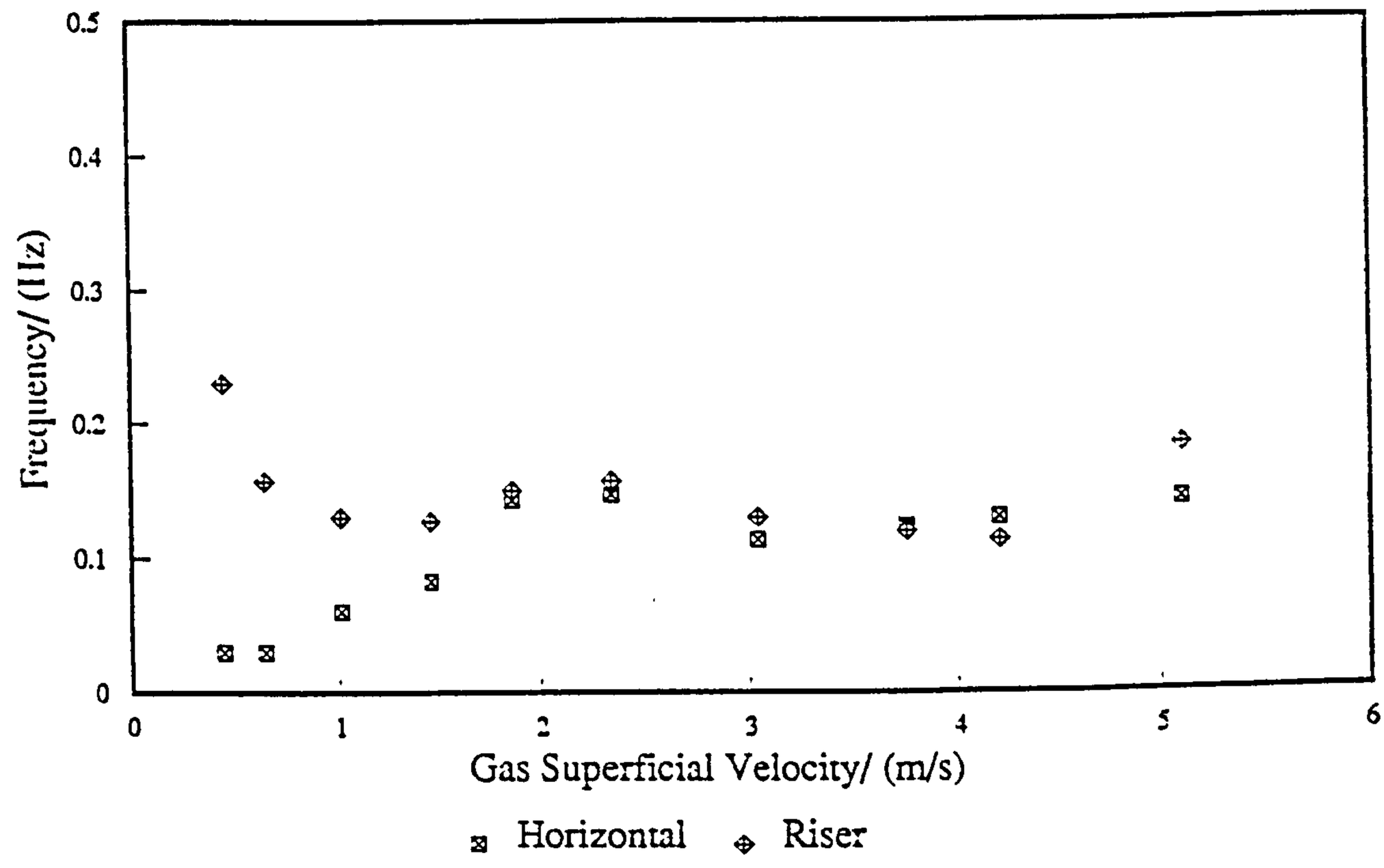


Figure 4.3.6 Slug Frequency at 3rd Wire Probe Position
U_{Ls}=0.271 m/s

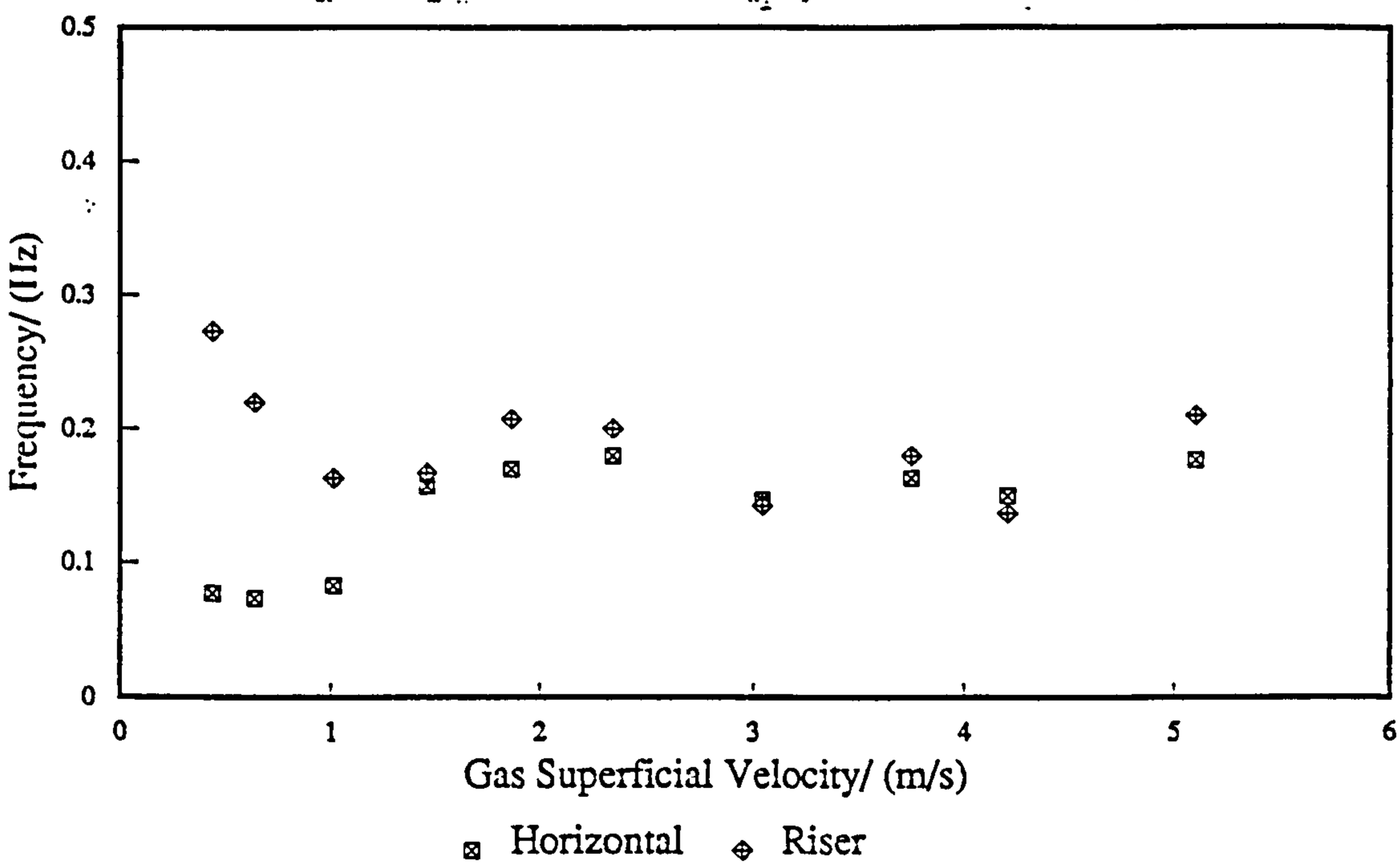


Figure 4.3.7 Slug Frequency at 3rd Wire Probe Position
U_{Ls}=0.32 m/s

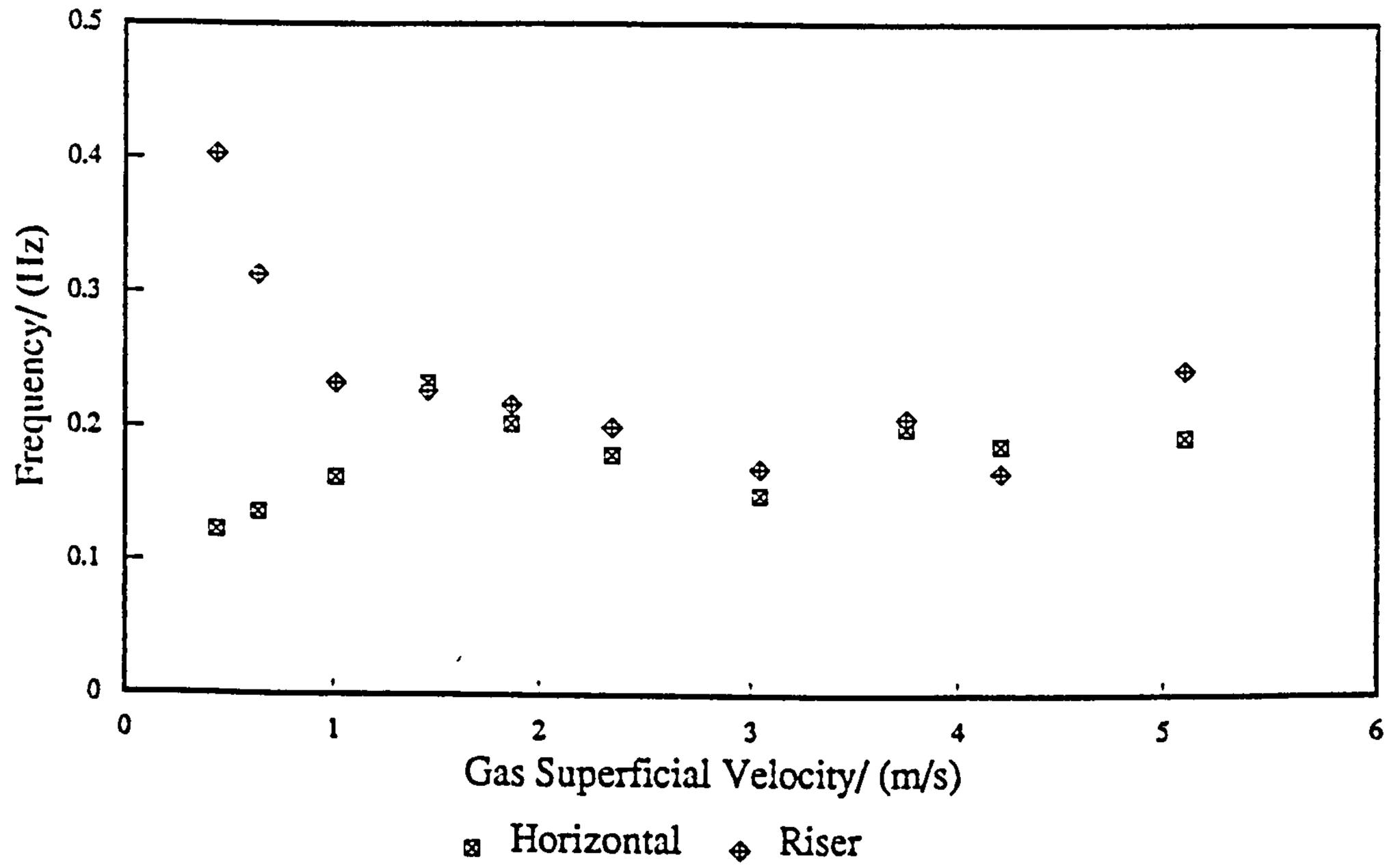


Figure 4.3.8 Slug Frequency at 3rd Wire Probe Position
U_{Ls}=0.391 m/s

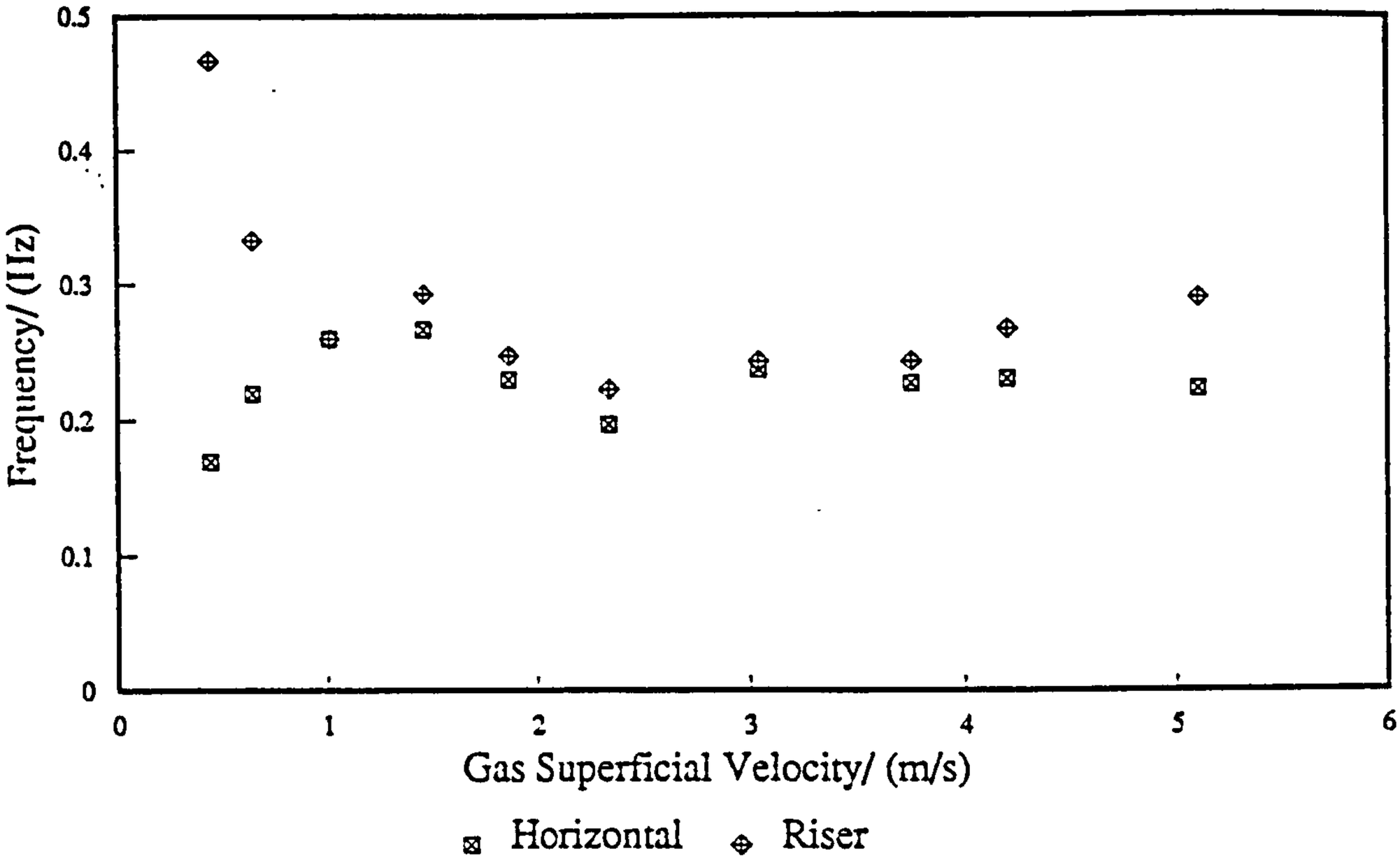


Figure 4.3.9 Slug Frequency at 3rd Wire Probe Position U_{Ls}=0.455 m/s

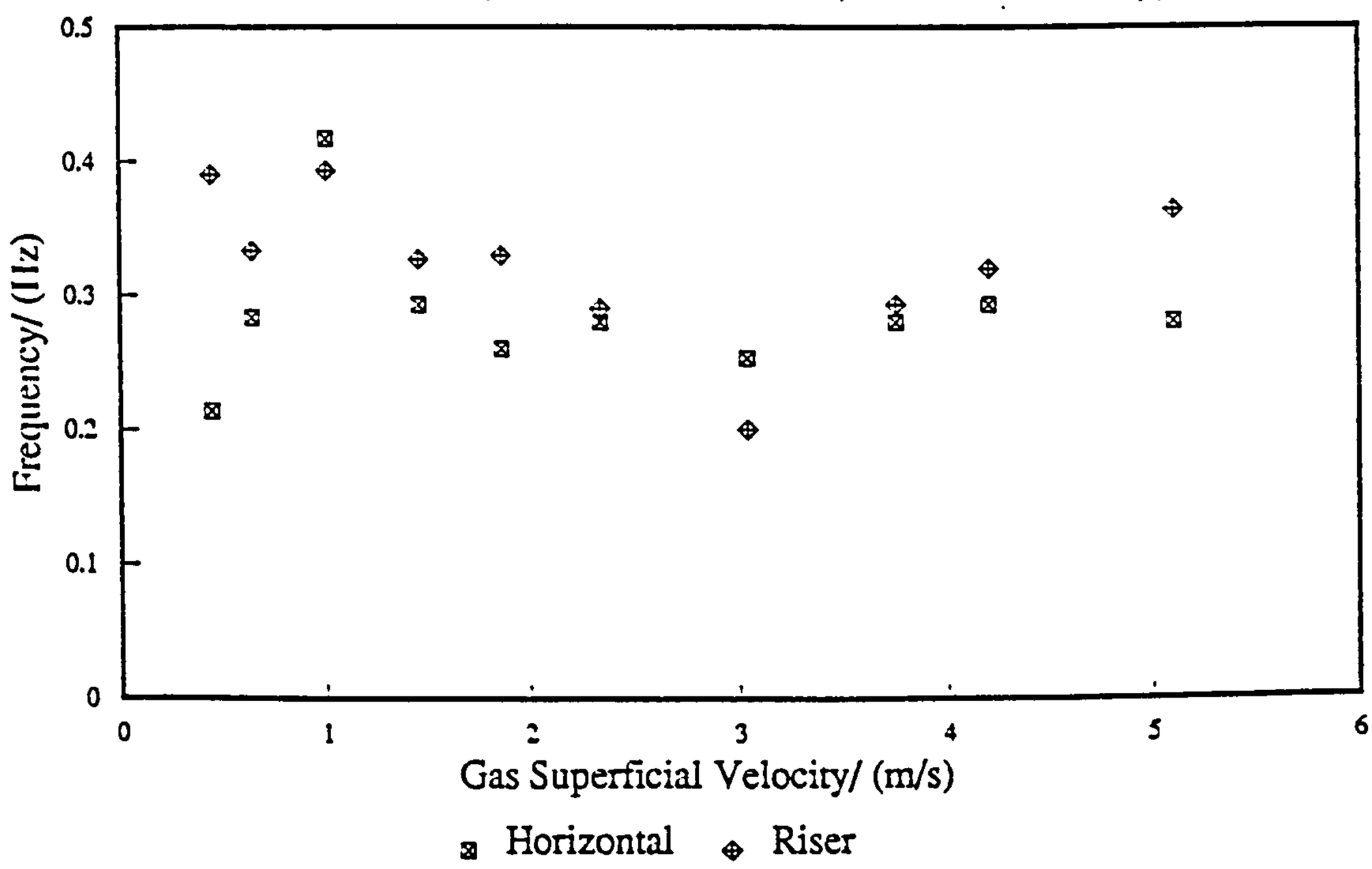


Figure 4.3.10 Slug Frequency at 3rd Wire Probe Position U_{Ls}=0.52 m/s

Figure 4.3.11 Slug Frequency at 3rd Wire Probe Position and Lower Pipe for Riser Configuration
U_{Ls}=0.14 m/s

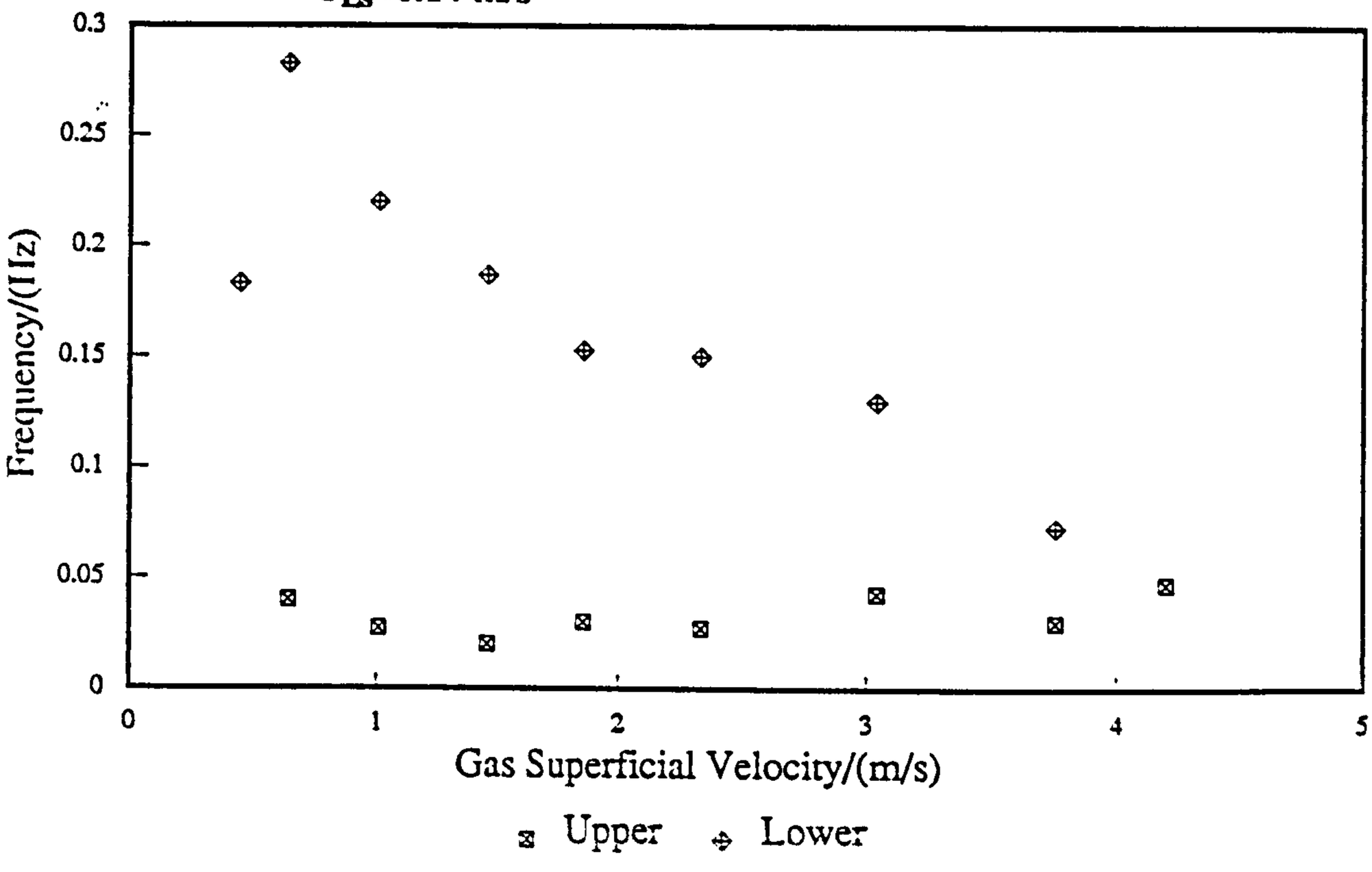


Figure 4.3.12 Slug Frequency at 3rd Wire Probe Position and Lower Pipe for Riser Configuration
U_{Ls}=0.18 m/s

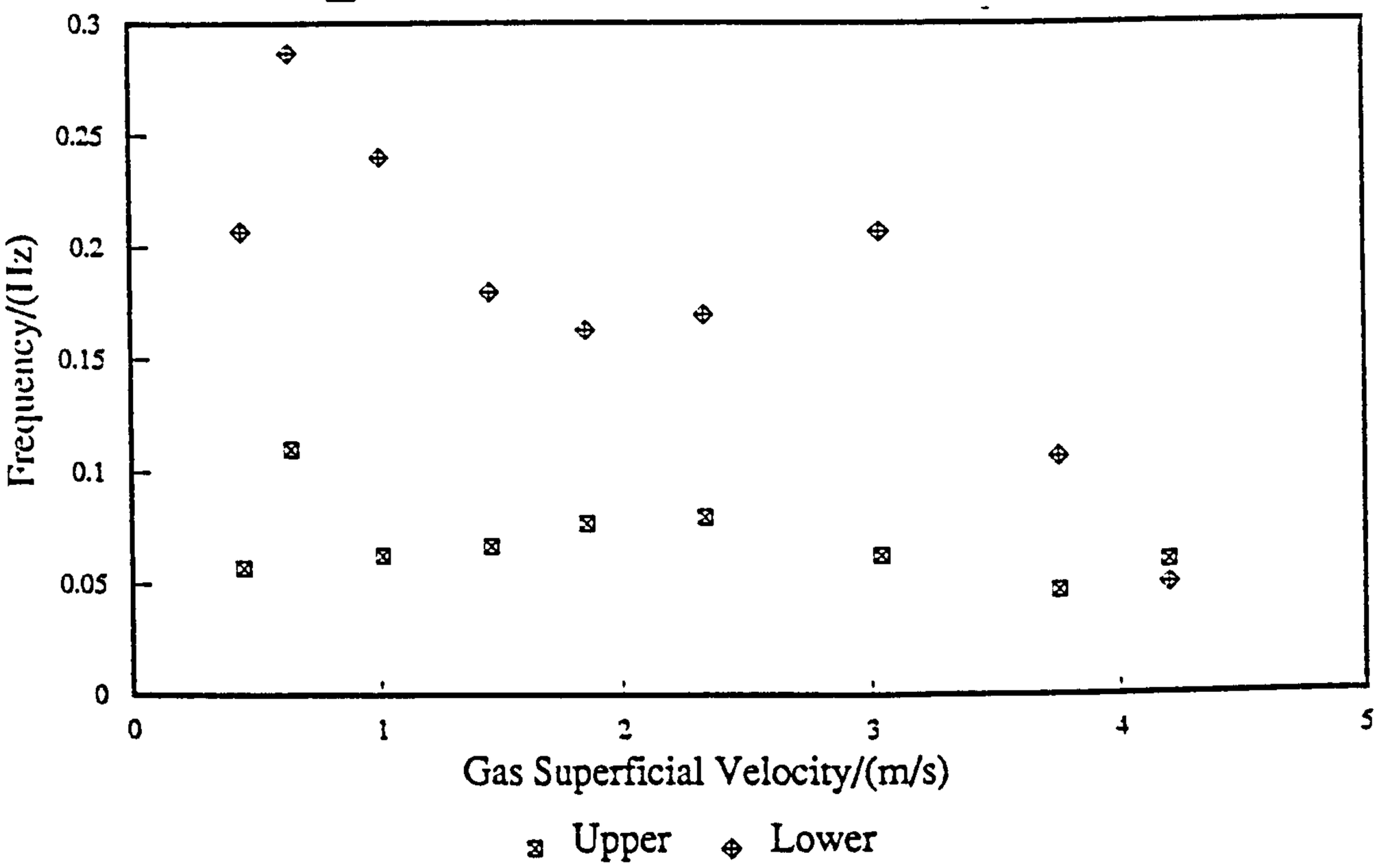


Figure 4.3.13 Slug Frequency at 3rd Wire Probe Position and Lower Pipe for Riser Configuration
U_{Ls}=0.255 m/s

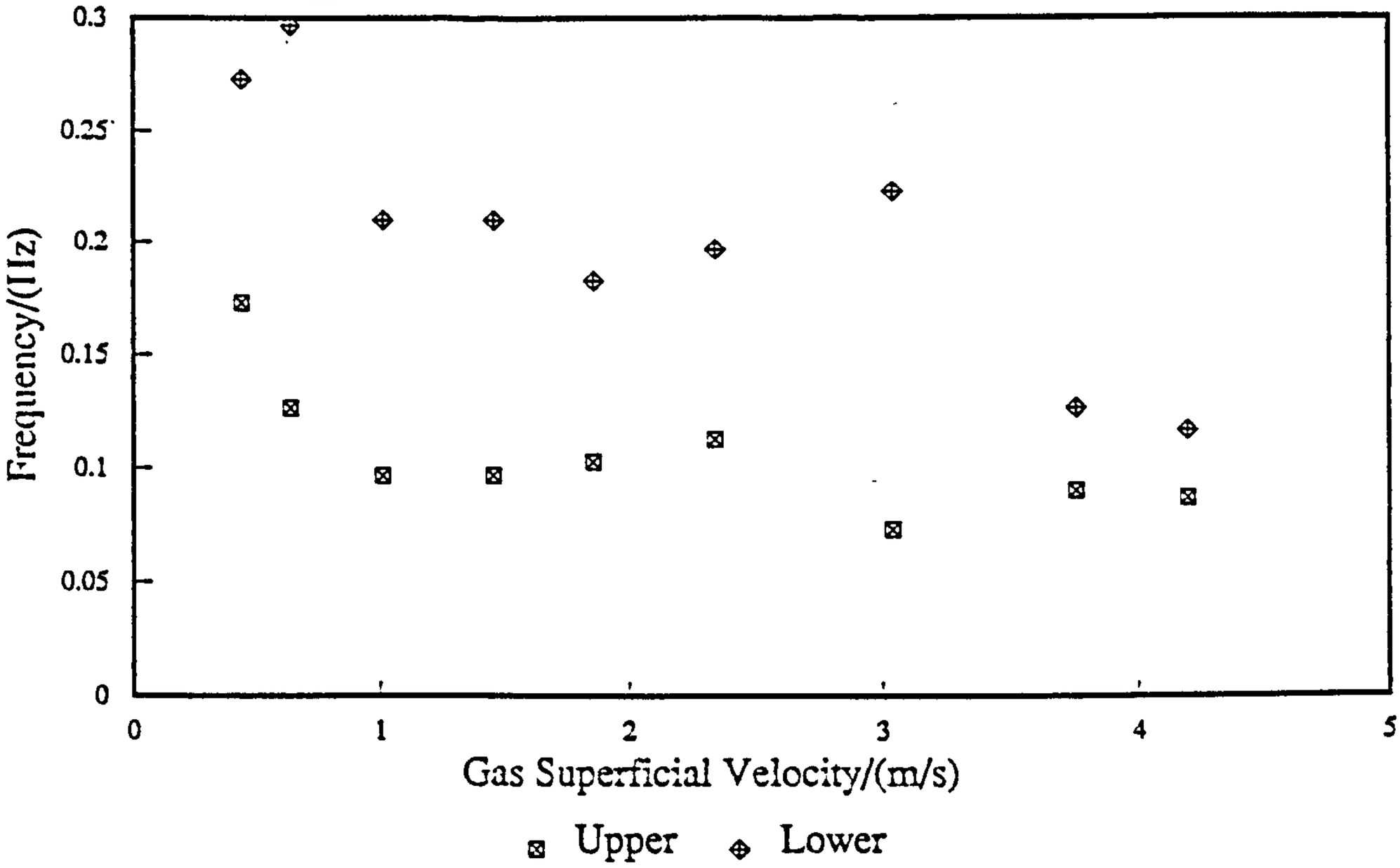


Figure 4.3.14 Slug Frequency at 3rd Wire Probe Position and Lower Pipe for Riser Configuration
U_{Ls}=0.271 m/s

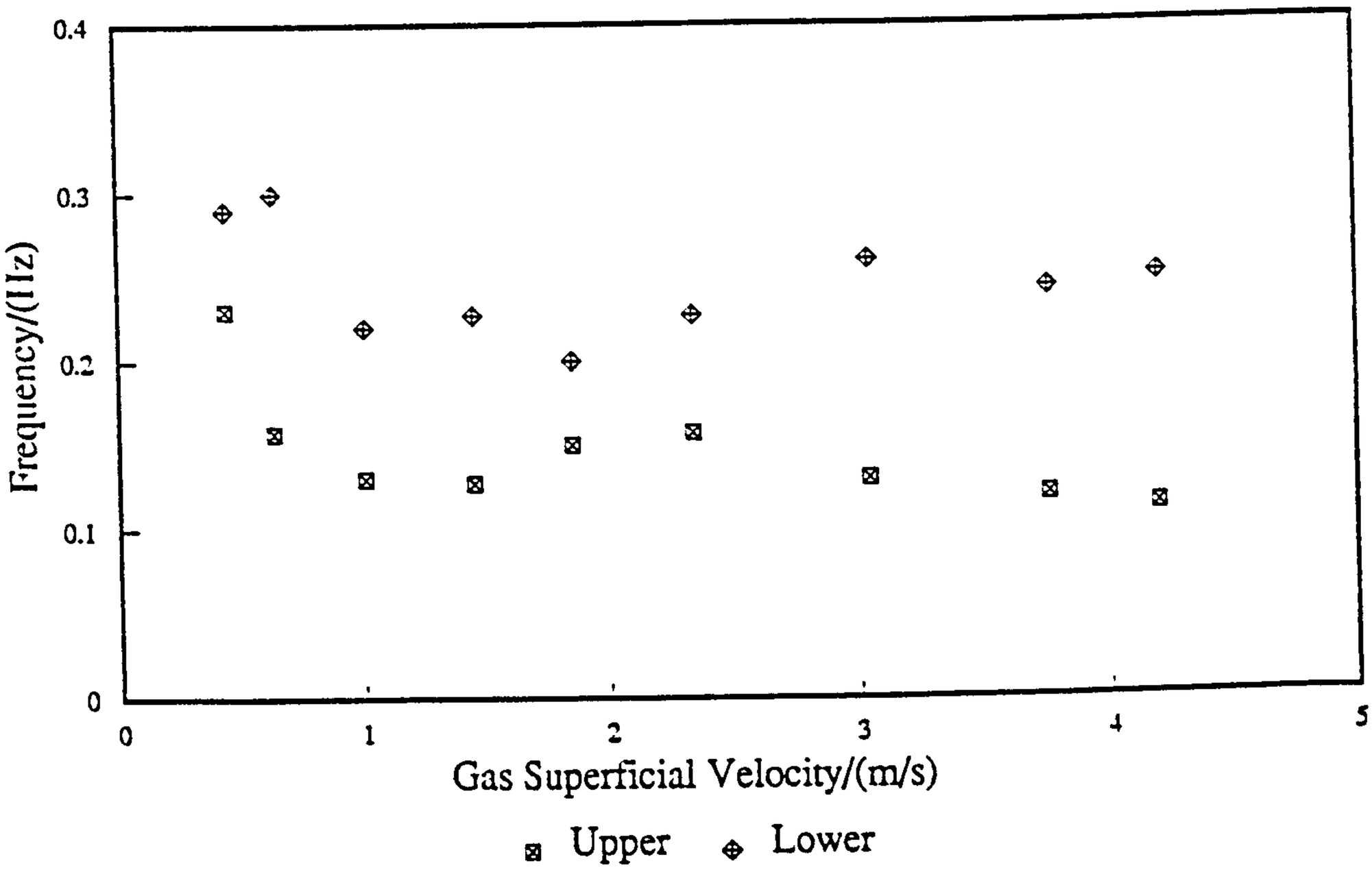


Figure 4.3.15 Slug Frequency at 3rd Wire Probe Position and Lower Pipe for Riser Configuration
U_{Ls}=0.32 m/s

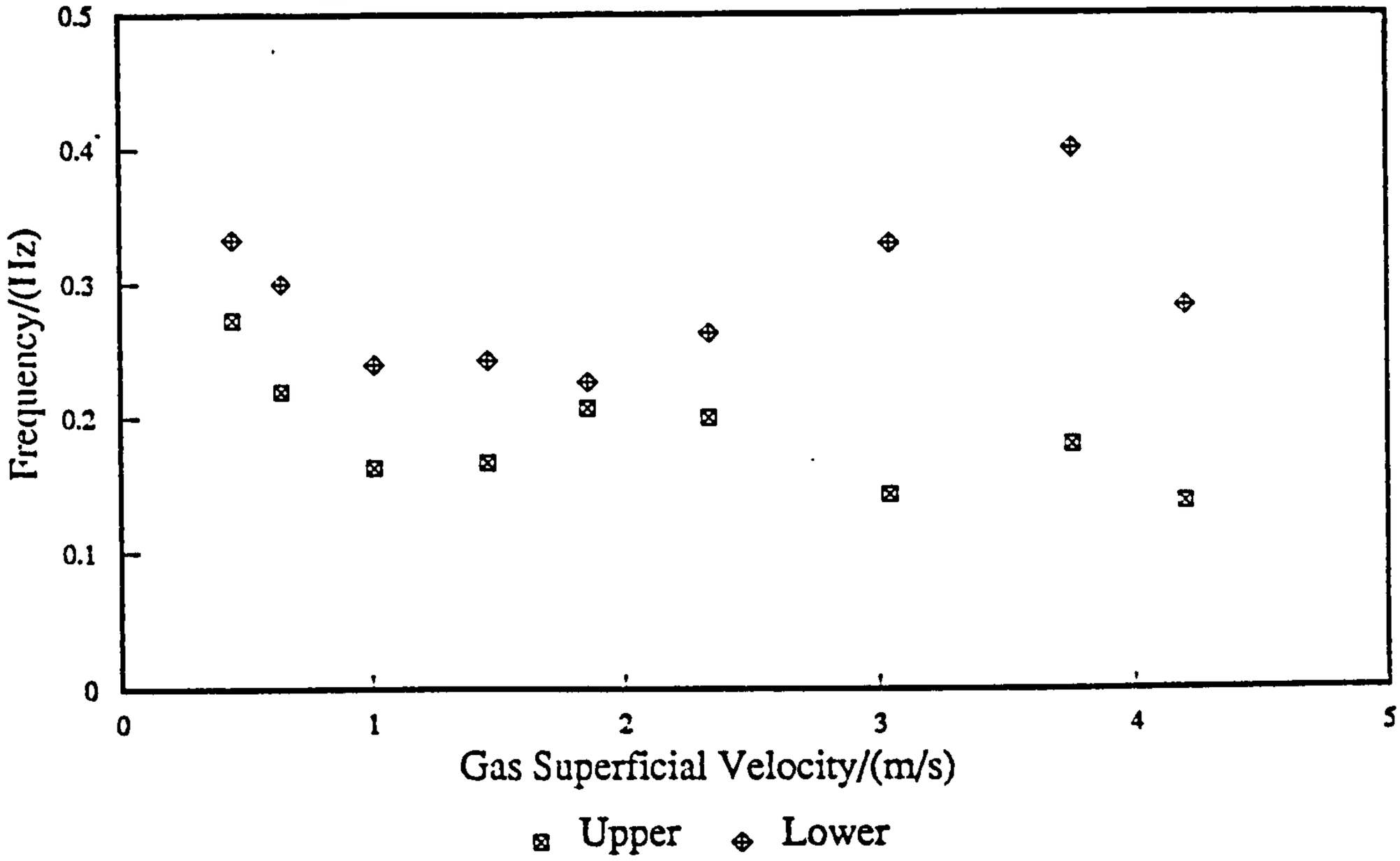


Figure 4.3.16 Slug Frequency at 3rd Wire Probe Position and Lower Pipe for Riser Configuration
U_{Ls}=0.391 m/s

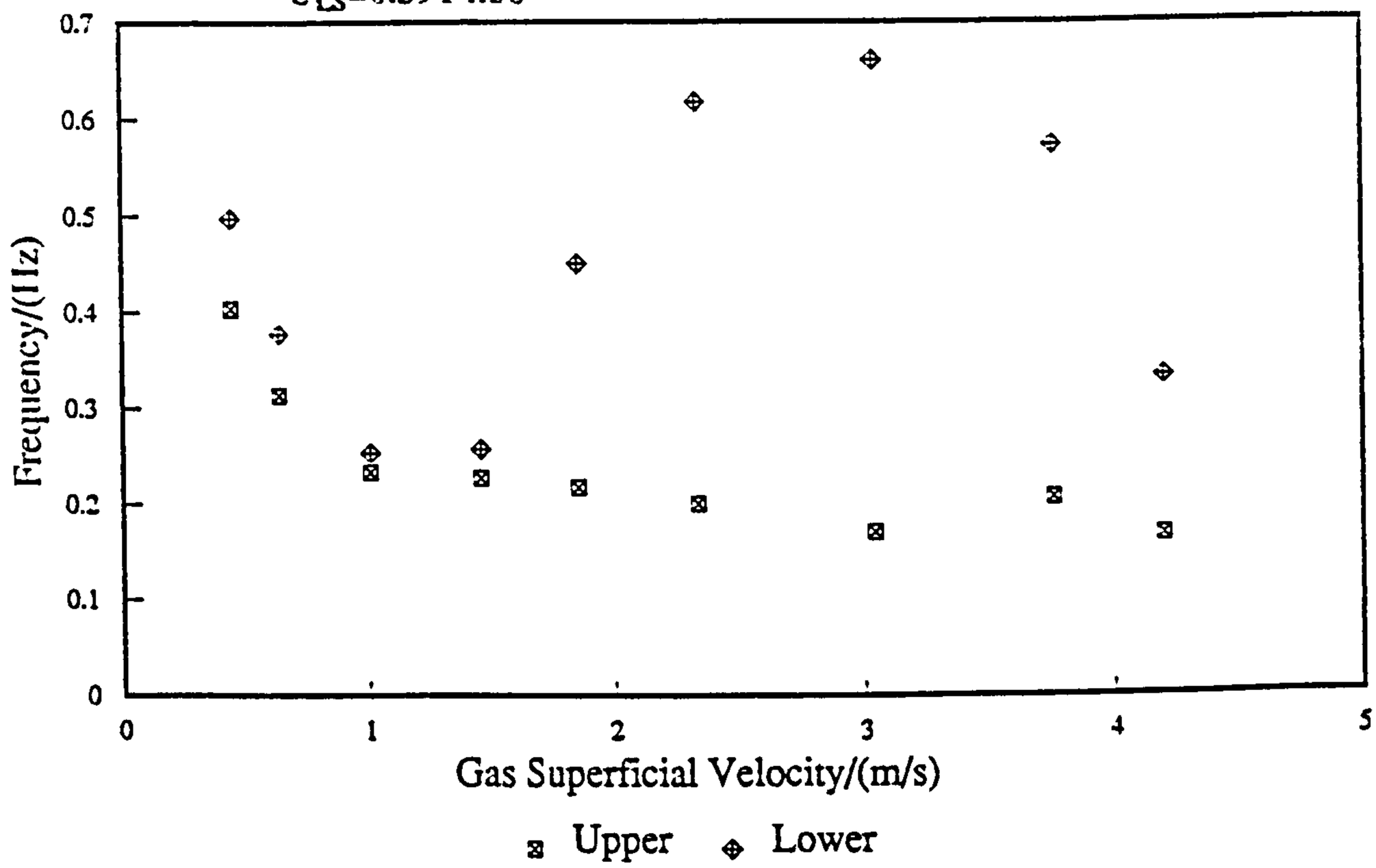


Figure 4.3.17 Slug Frequency at 3rd Wire Probe Position and Lower Pipe for Riser Configuration
U_{Ls}=0.455 m/s

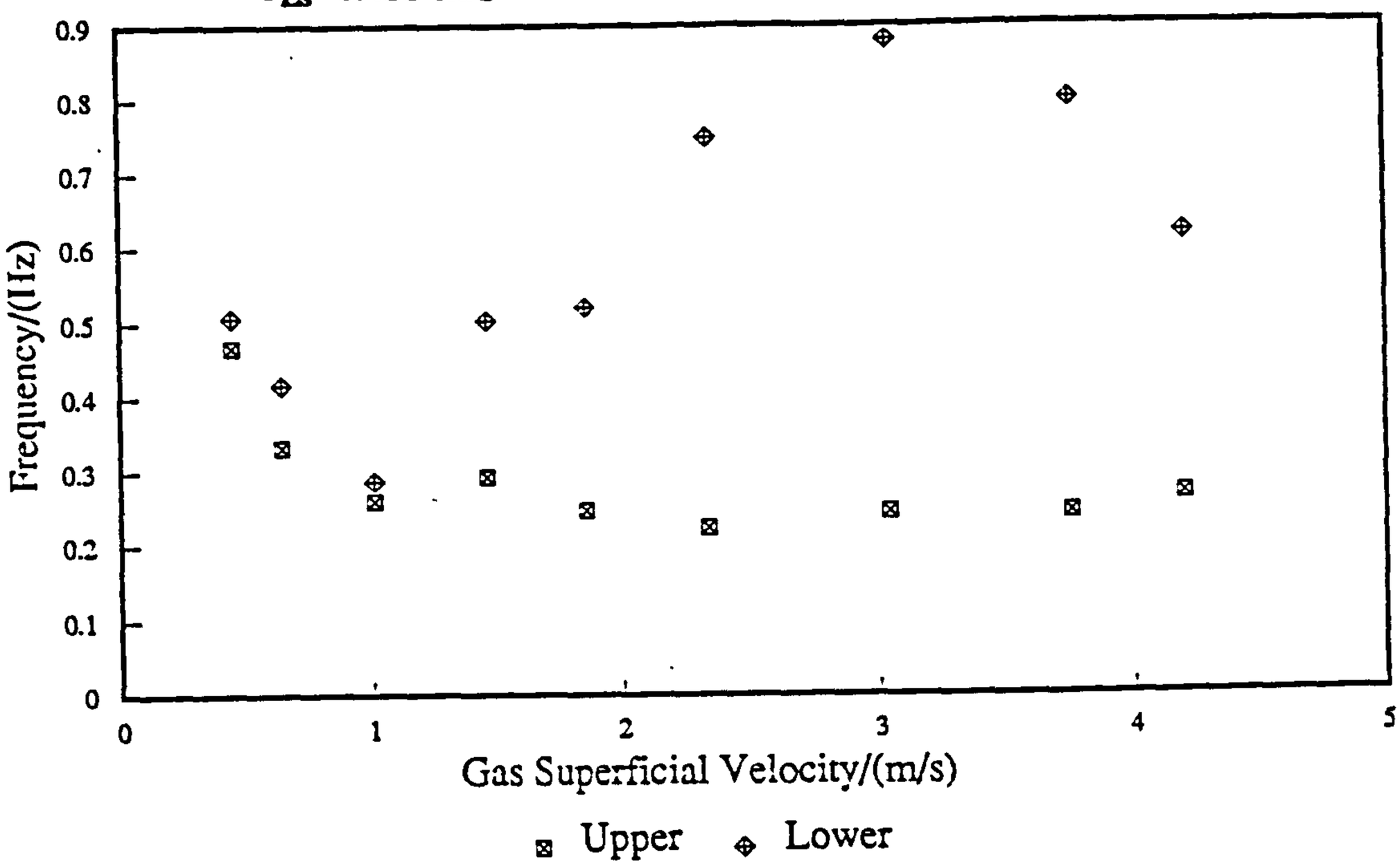


Figure 4.3.18 Slug Frequency at 3rd Wire Probe Position and Lower Pipe for Riser Configuration
U_{Ls}=0.52 m/s

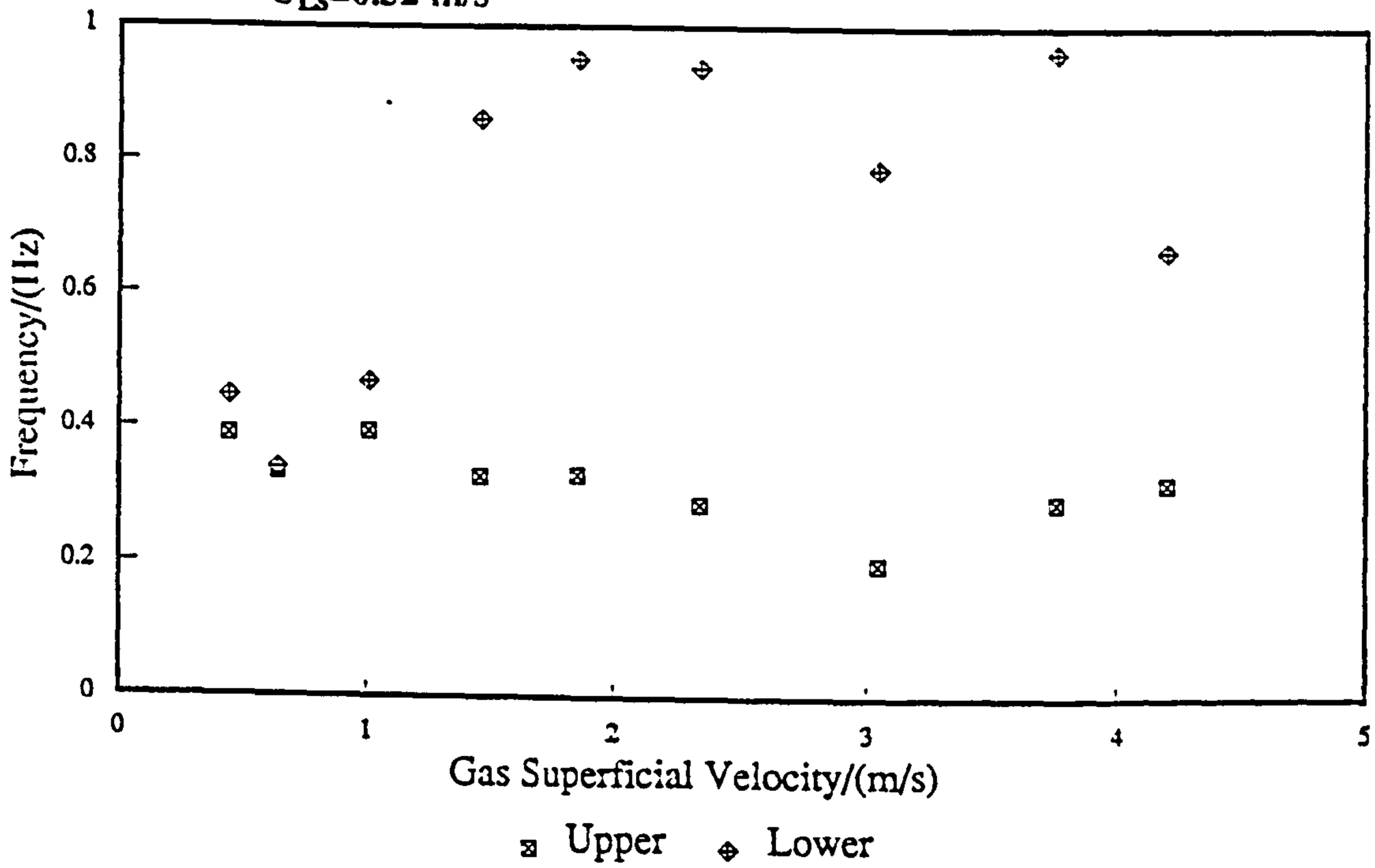


Figure 4.3.19 Slug Front Velocity at Upstream Measurement Location.
U_{Ls}=0.14 m/s

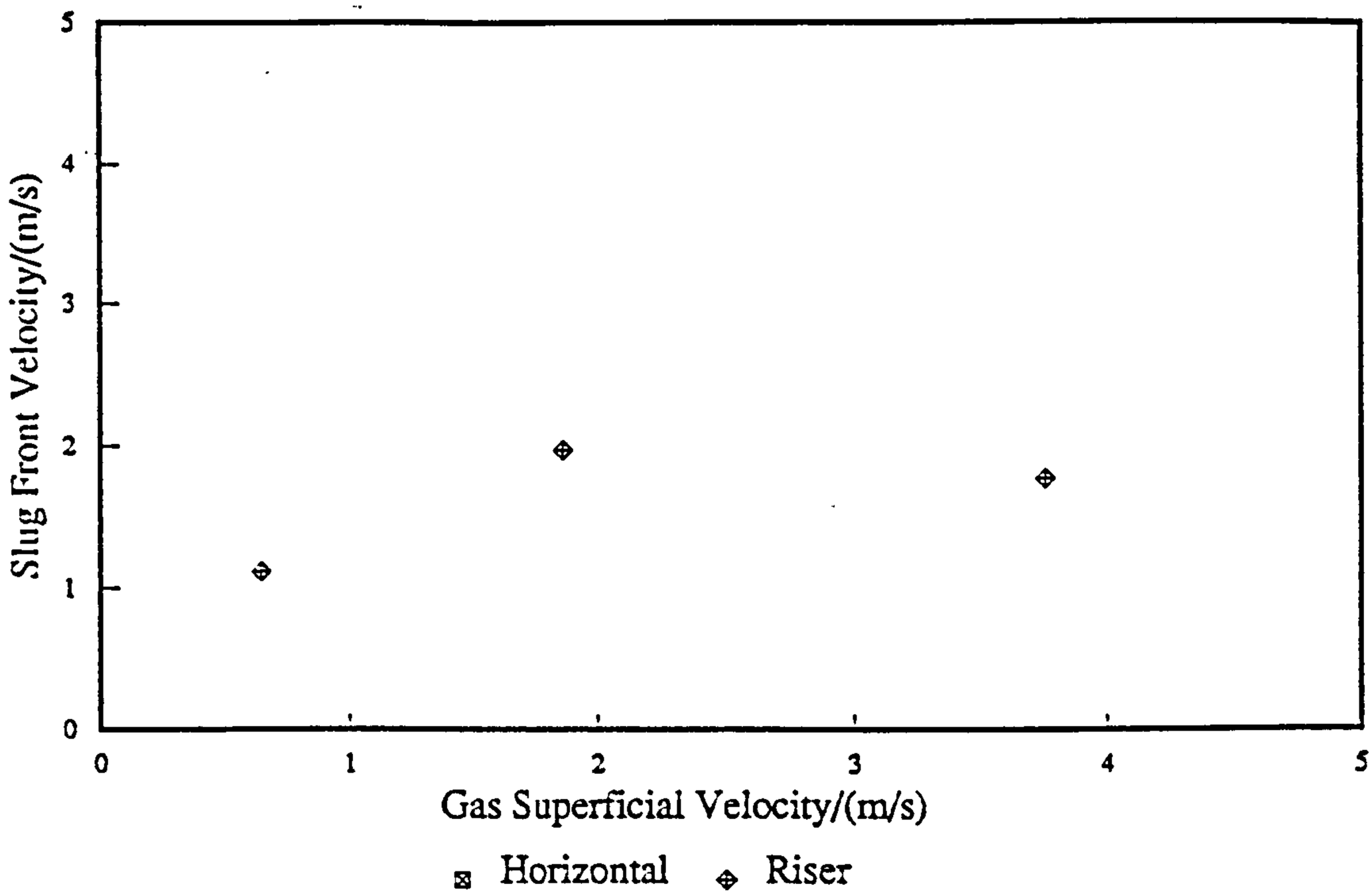


Figure 4.3.20 Slug Front Velocity at Upstream Measurement Location.
U_{Ls}=0.18 m/s

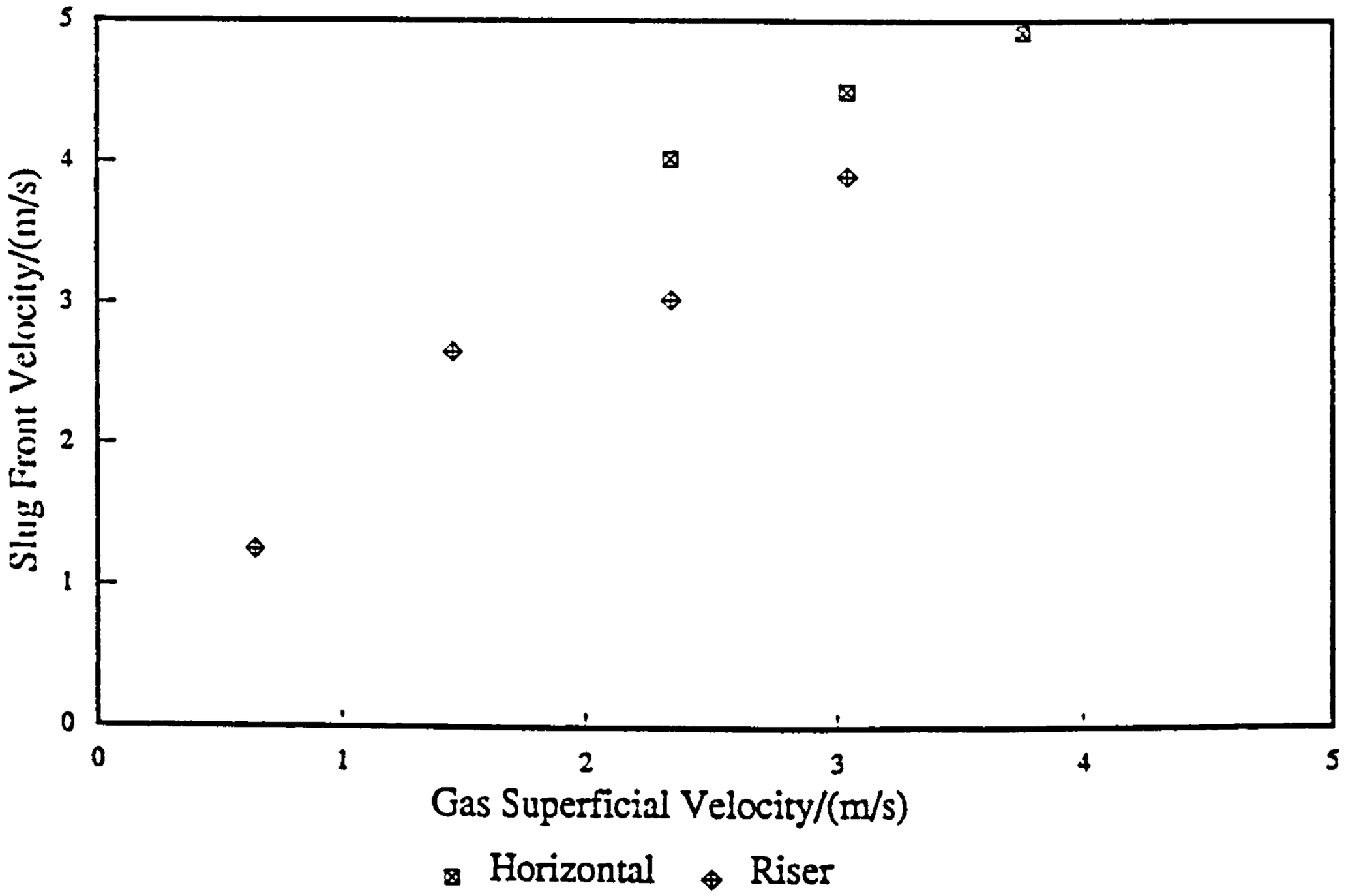


Figure 4.3.21 Slug Front Velocity at Upstream Measurement Location. U_{LS}=0.255 m/s

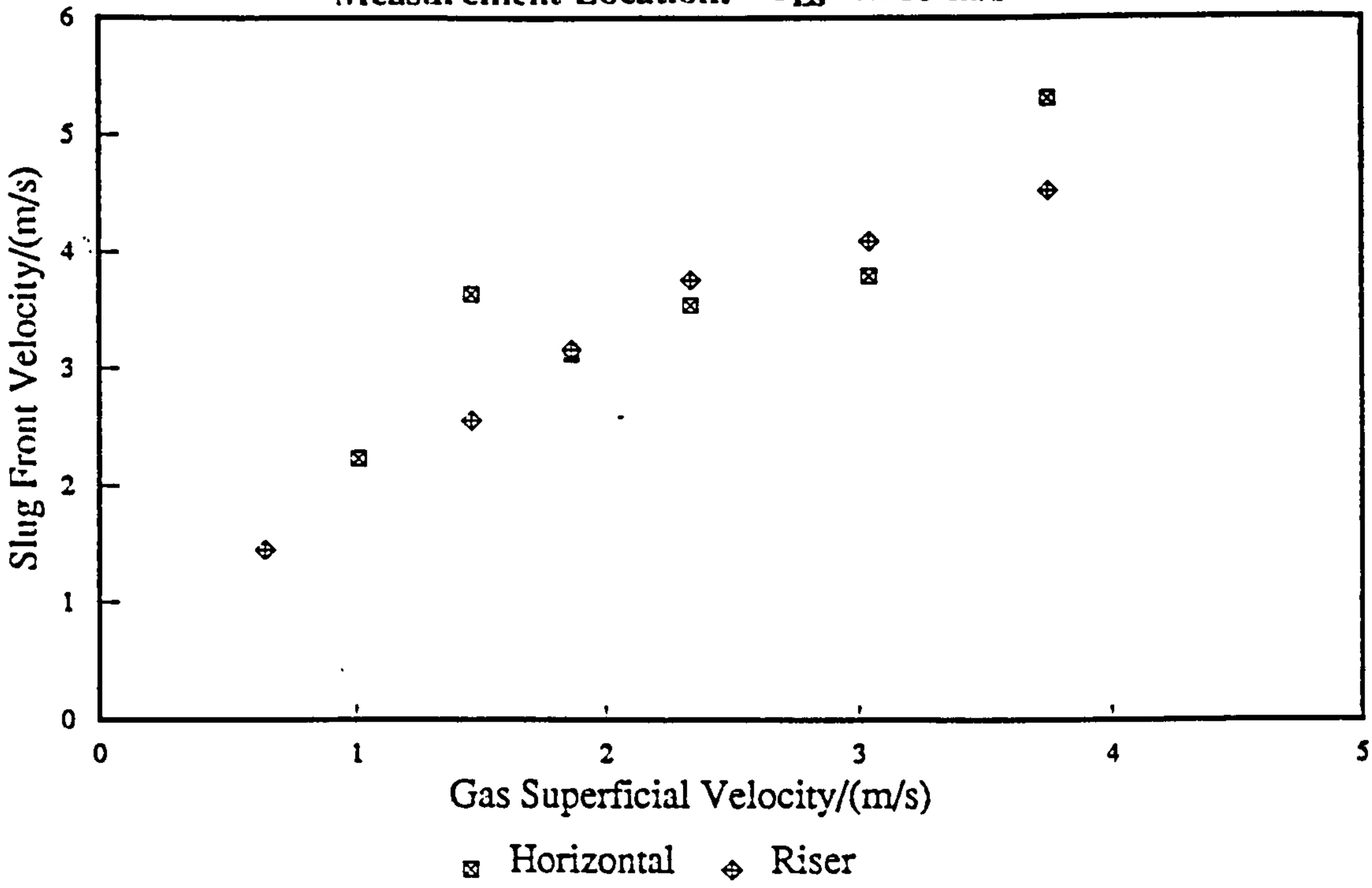


Figure 4.3.22 Slug Front Velocity at Upstream Measurement Location.
U_{LS}=0.271 m/s

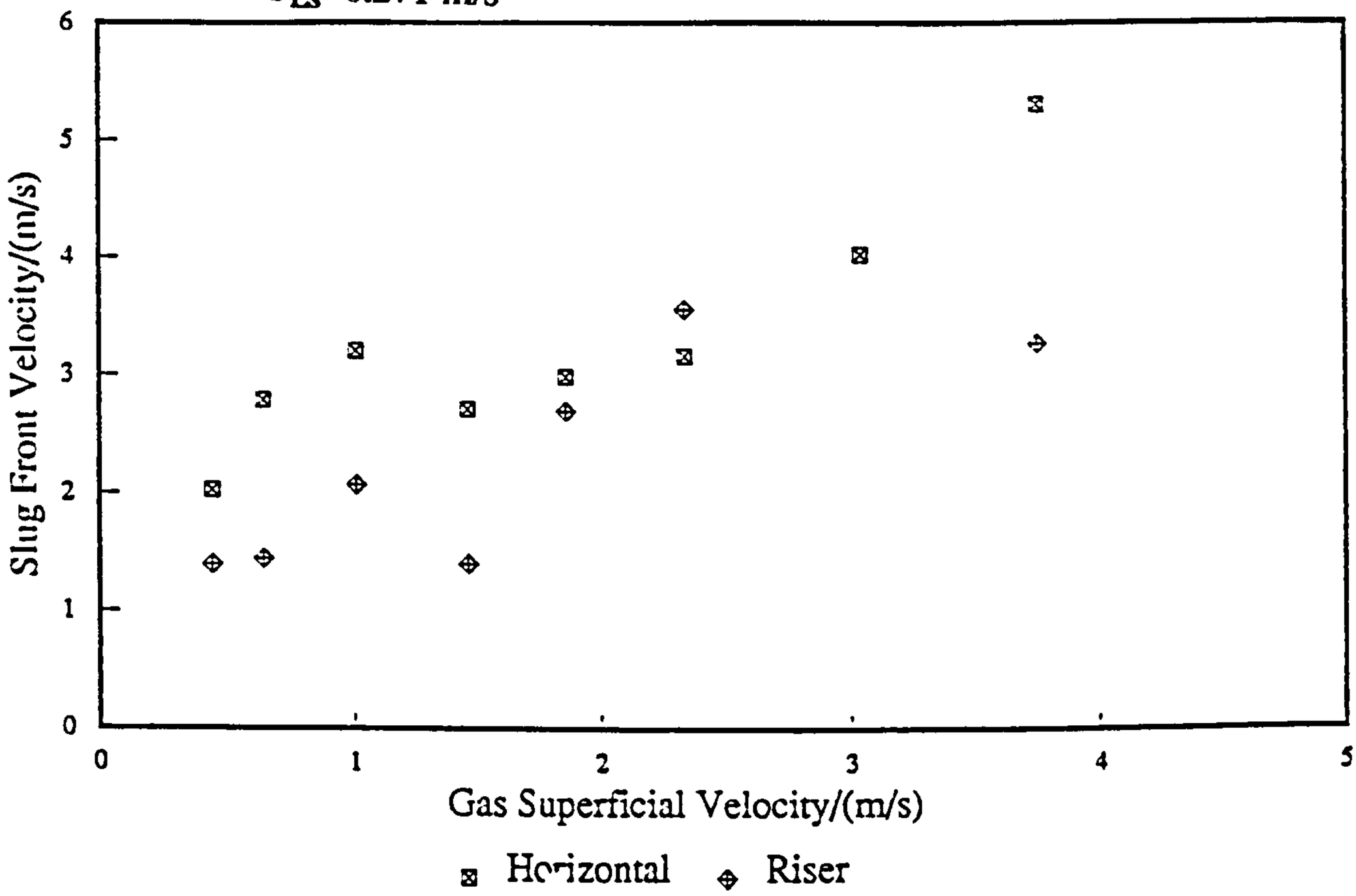


Figure 4.3.23 Slug Front Velocity at Upstream Measurement Location. U_{Ls}= 0.32 m/s.

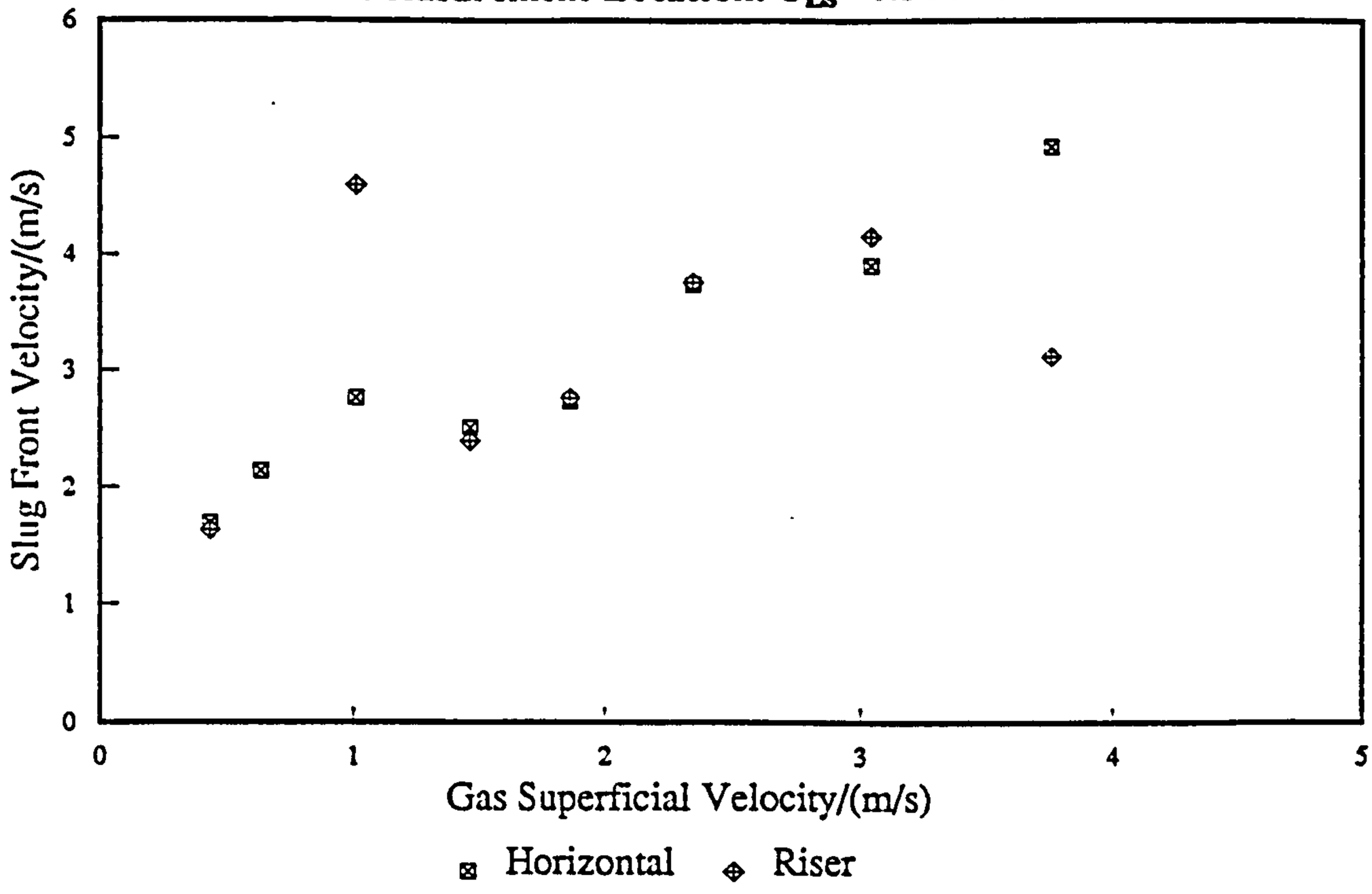


Figure 4.3.24 Slug Front Velocity at Upstream Measurement Location. U_{Ls}= 0.391 m/s.

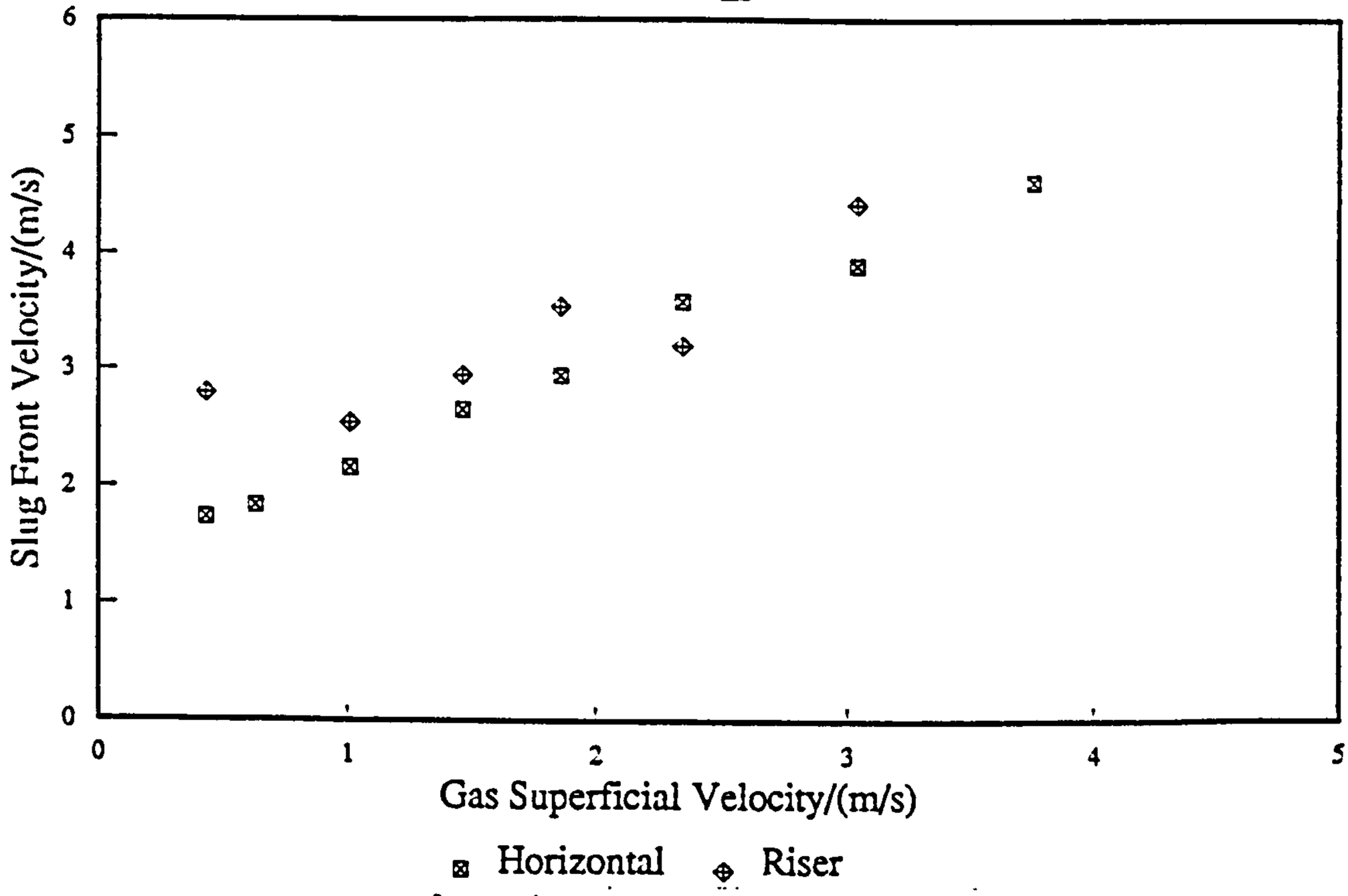


Figure 4.3.25 Slug Front Velocity at Upstream Measurement Location.
U_{Ls}=0.455 m/s

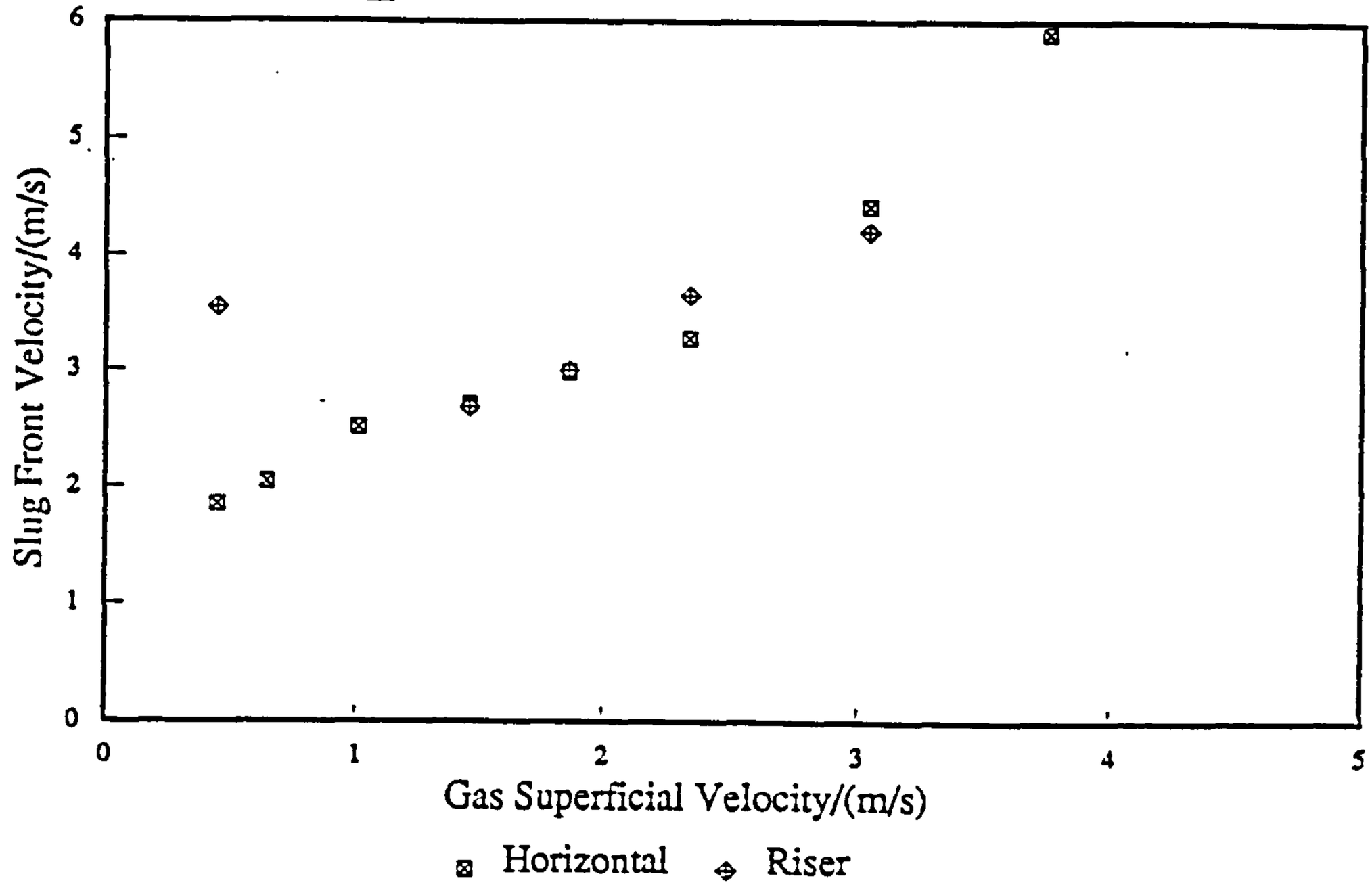


Figure 4.3.26 Slug Front Velocity at Upstream Measurement Location.
U_{Ls}=0.52 m/s

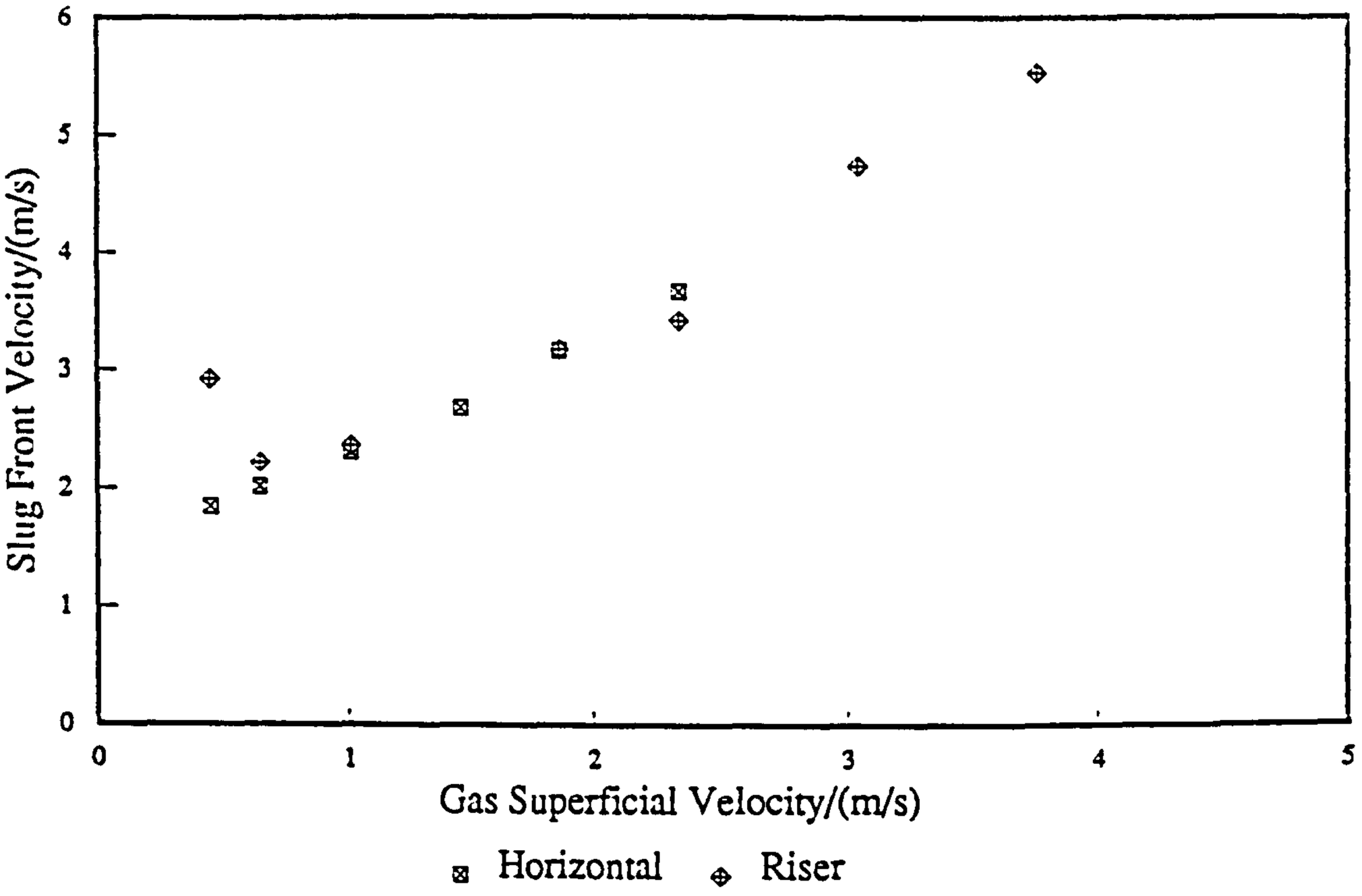


Figure 4.3.27 Slug Front Velocity at Downstream Measurement Location.
U_{Ls}=0.14 m/s

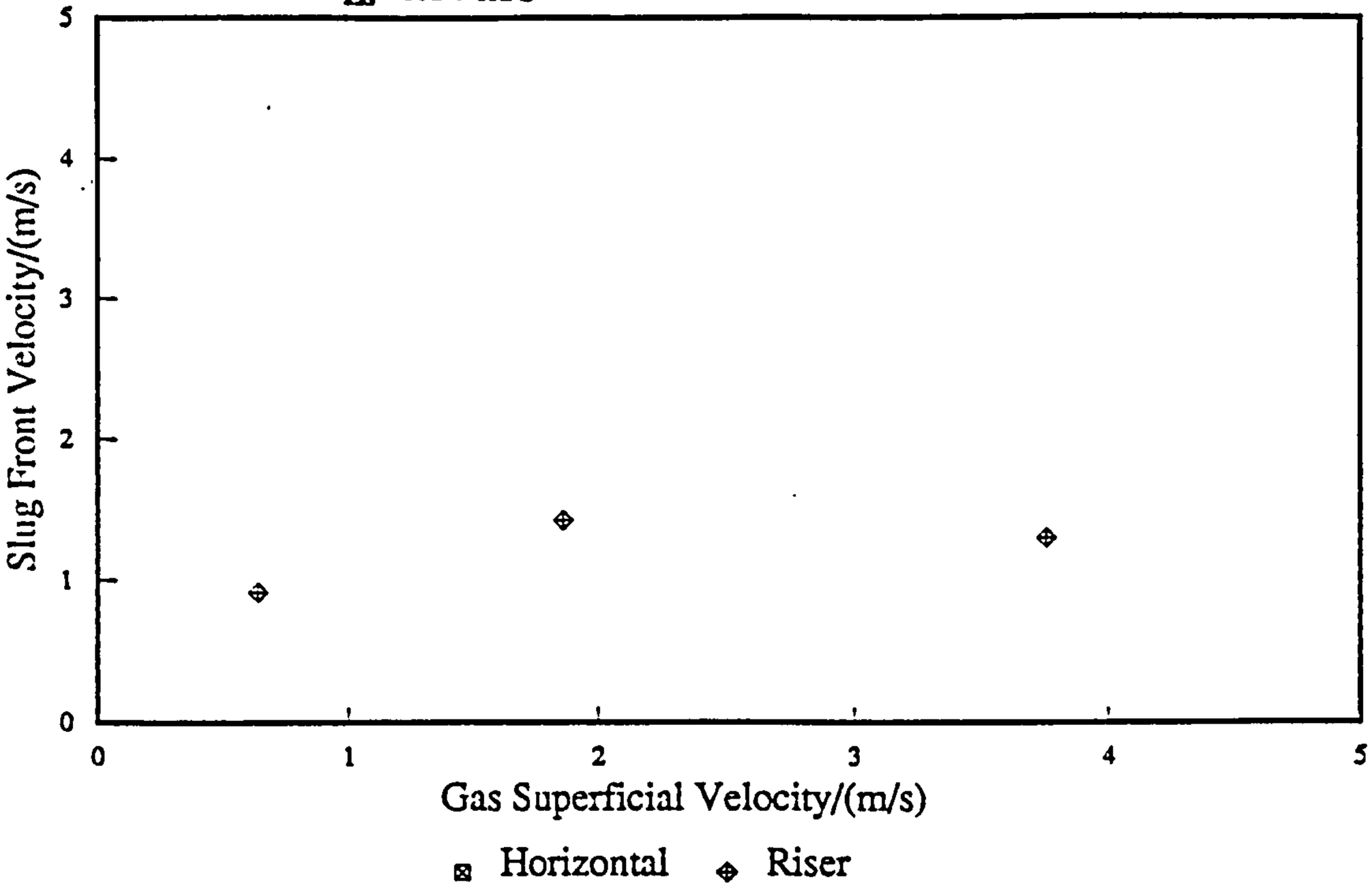


Figure 4.3.28 Slug Front Velocity at Downstream Measurement Location.
U_{Ls}=0.18 m/s

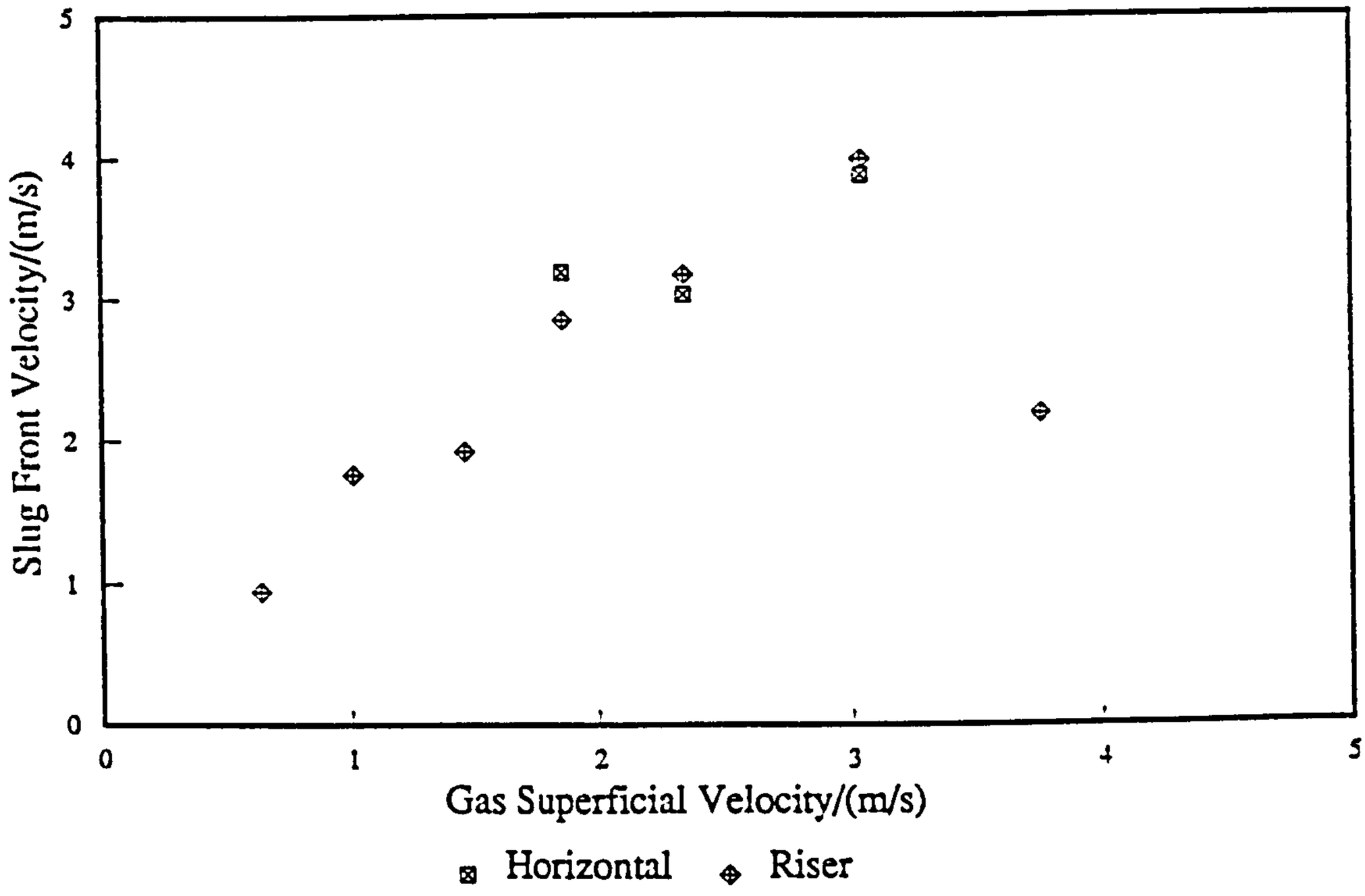


Figure 4.3.29 Slug Front Velocity at Downstream Measurement Location.
U_{Ls}=0.255 m/s

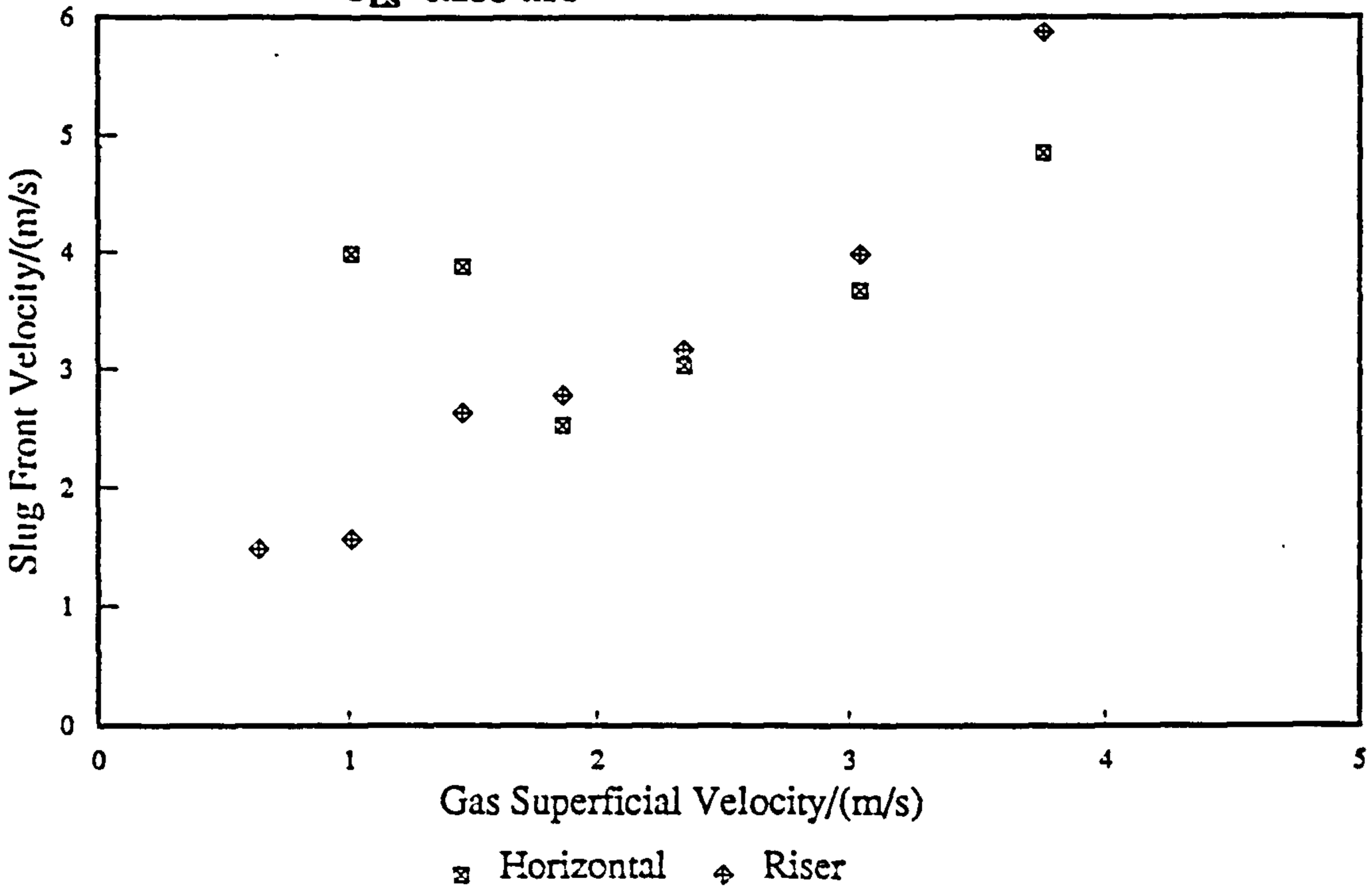


Figure 4.3.30 Slug Front Velocity at Downstream Measurement Location.
U_{Ls}=0.271 m/s

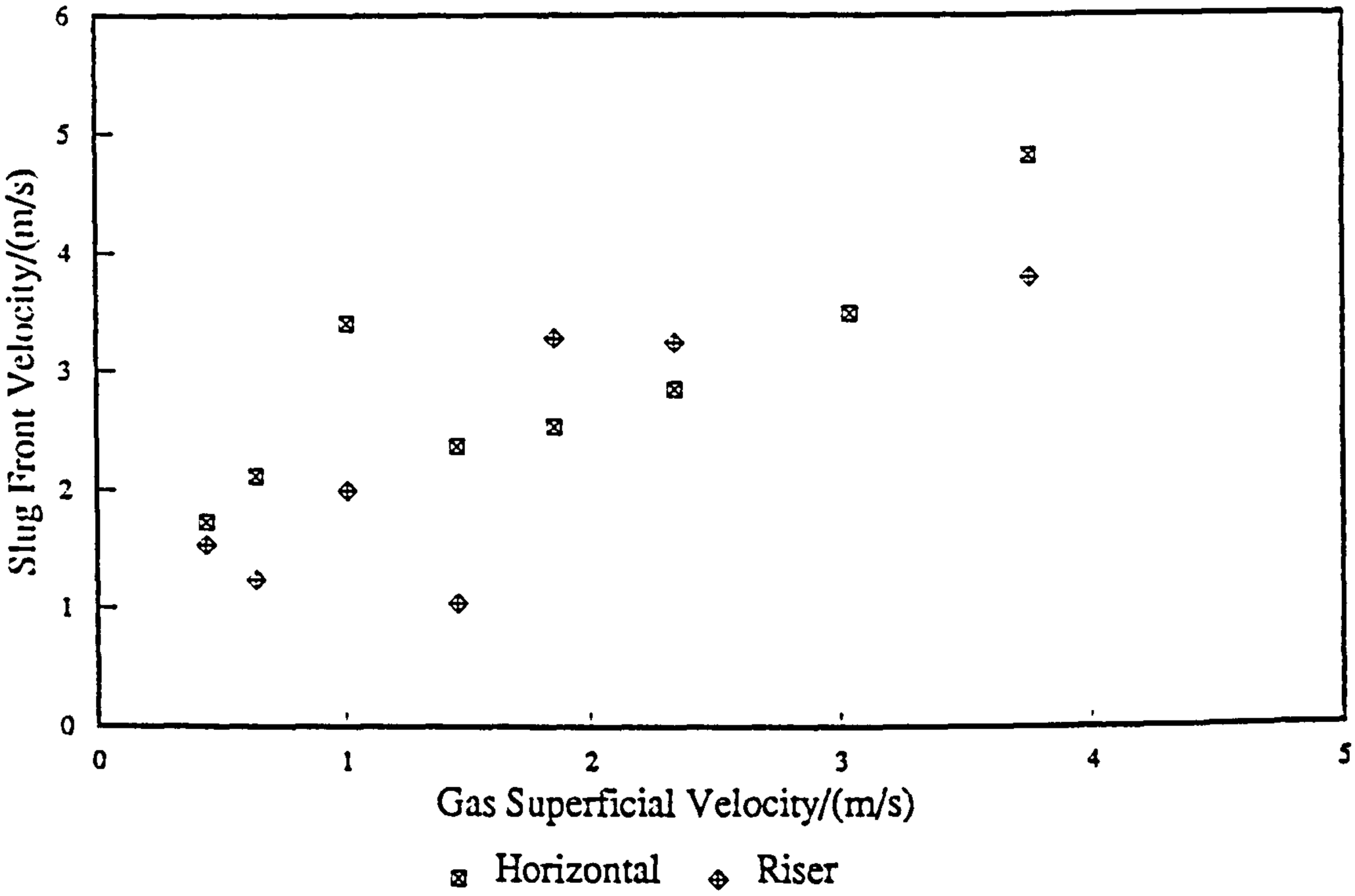


Figure 4.3.31 Slug Front Velocity at Downstream Measurement Location.
U_{Ls}=0.32 m/s

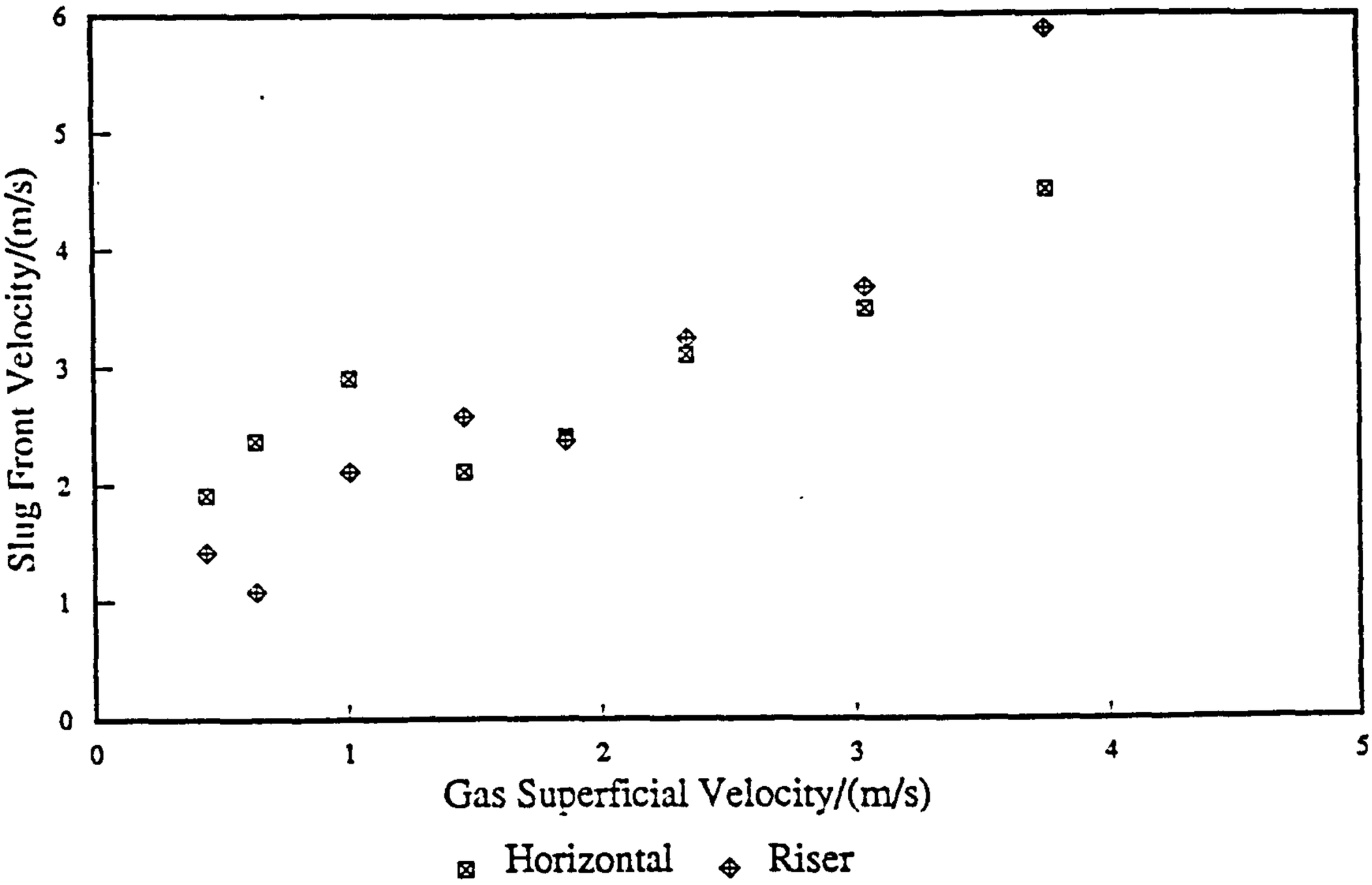


Figure 4.3.32 Slug Front Velocity at Downstream Measurement Location.
U_{Ls}=0.391 m/s

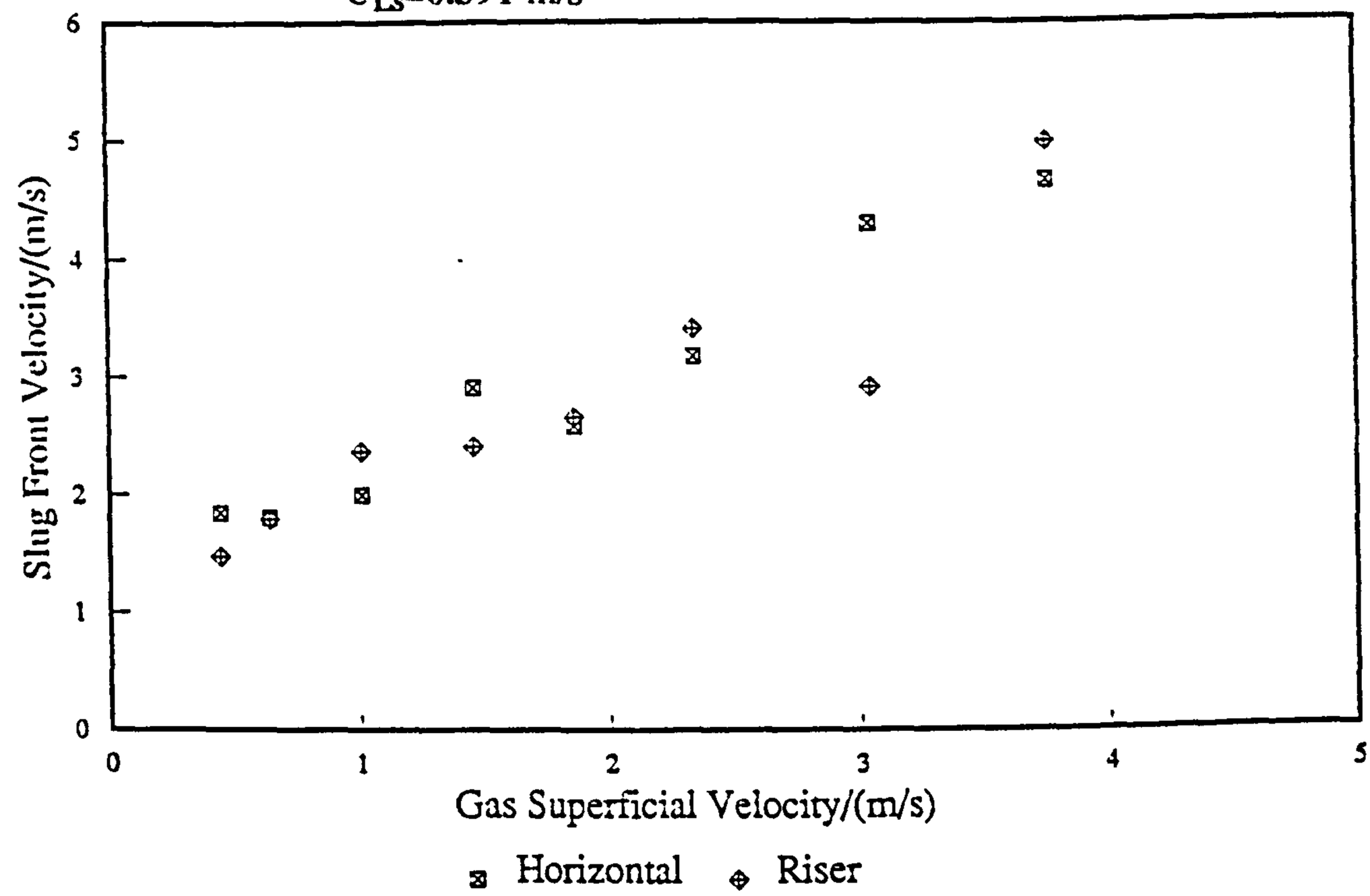


Figure 4.3.33 Slug Front Velocity at Downstream Measurement Location.
U_{Ls}=0.455 m/s

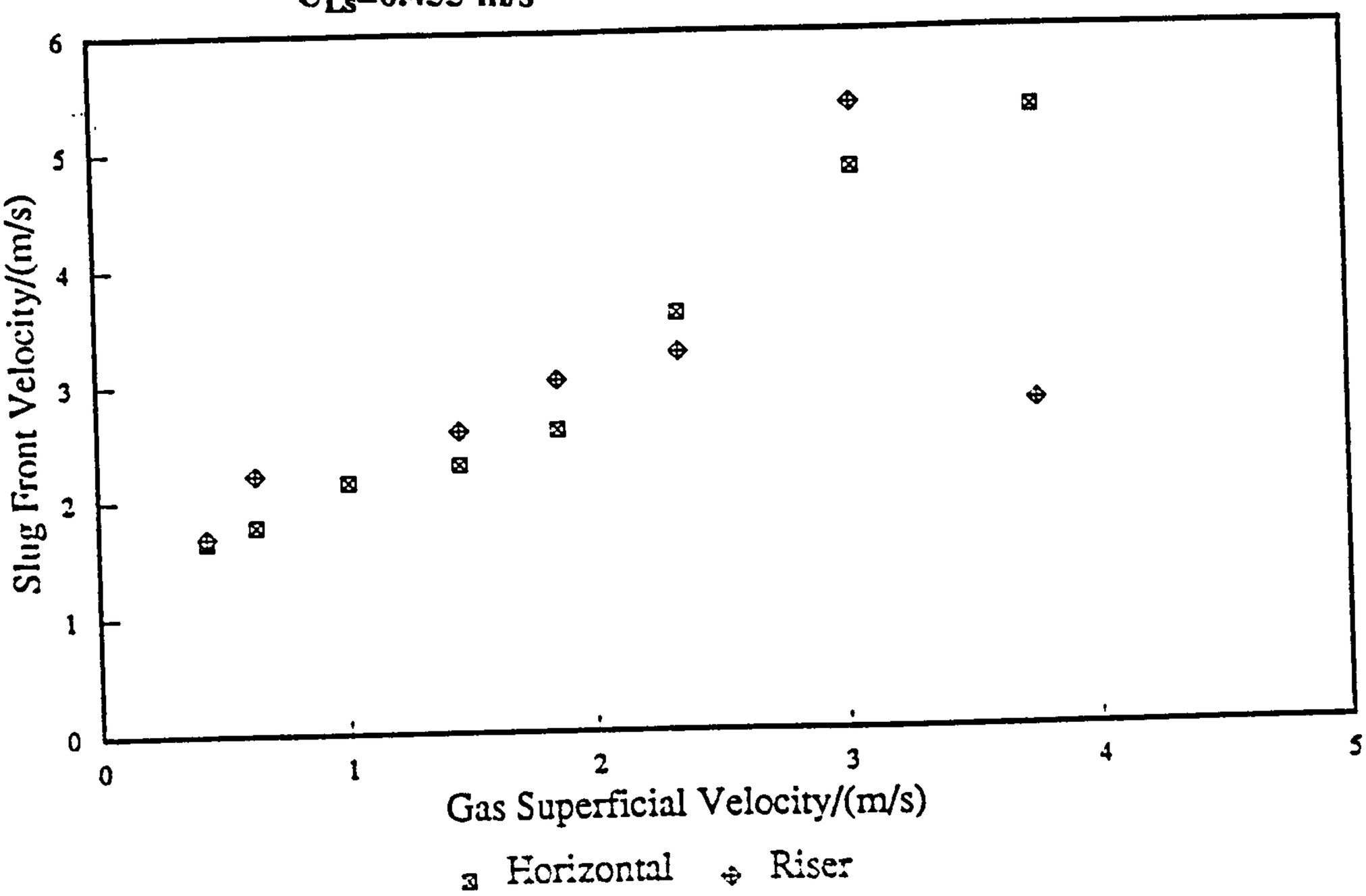
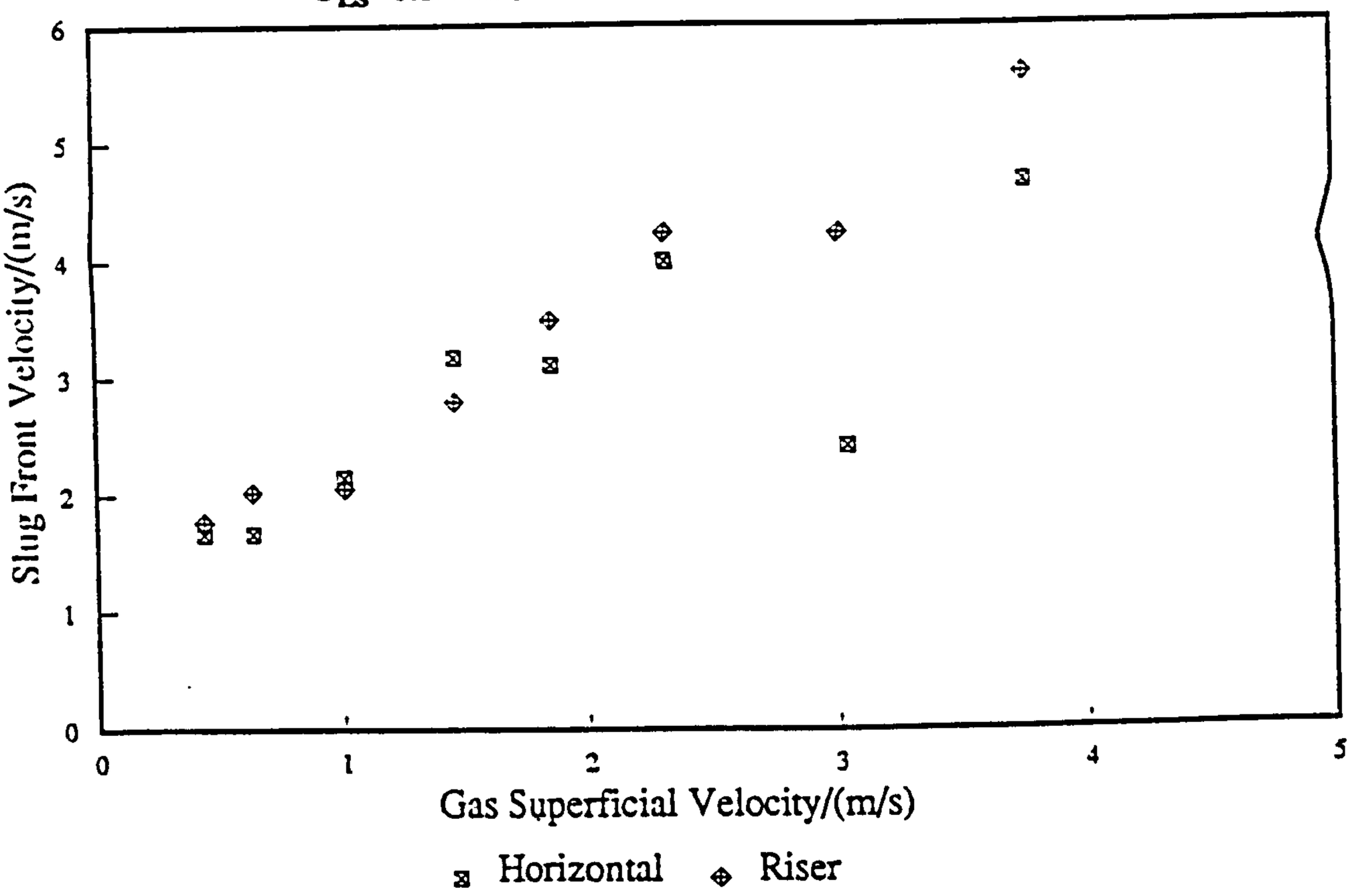


Figure 4.3.34 Slug Front Velocity at Downstream Measurement Location.
U_{Ls}=0.52 m/s



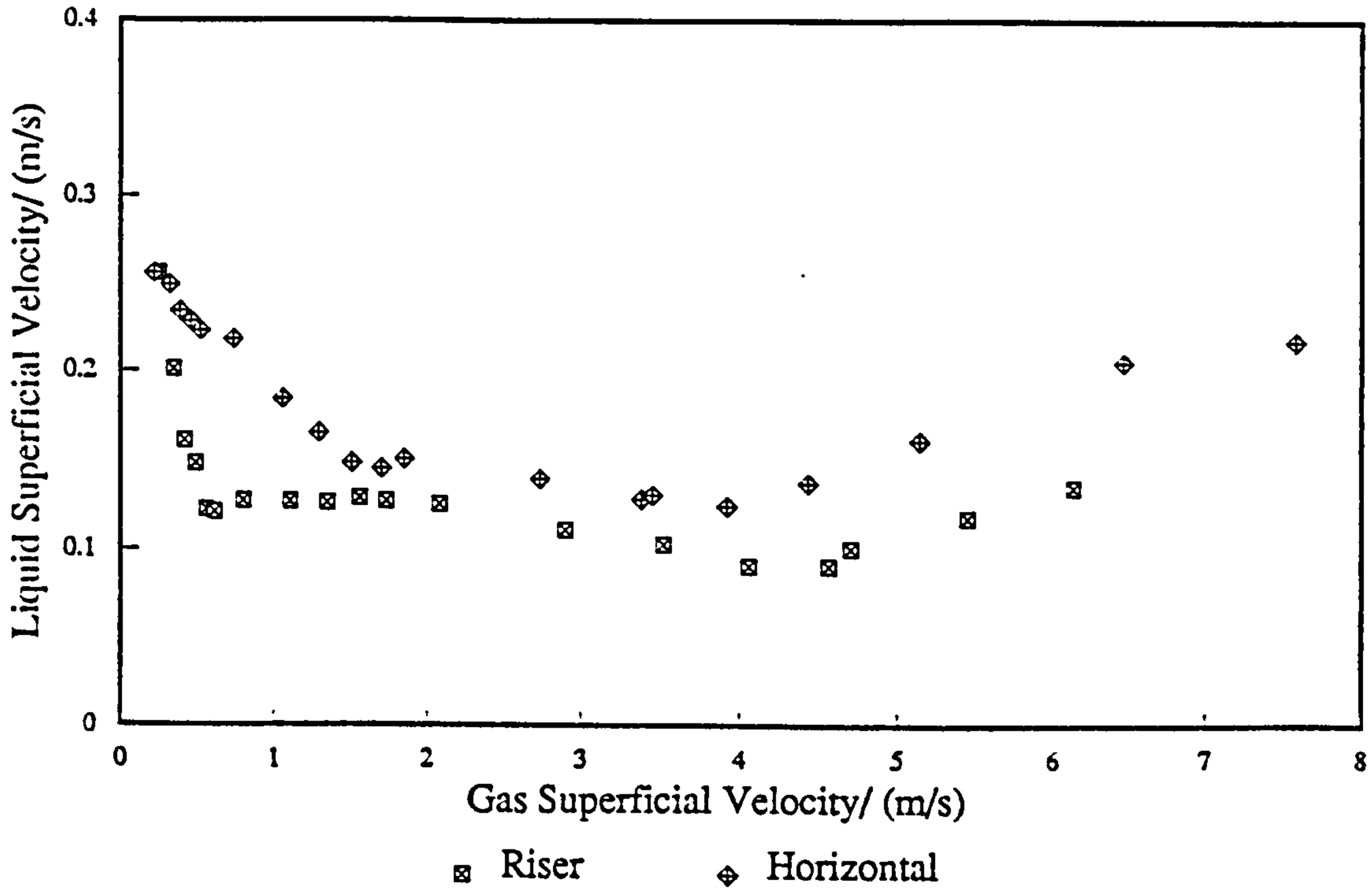


Figure 4.3.35 Experimental Stratified to Intermittent Transition for the Riser and Horizontal Configurations.

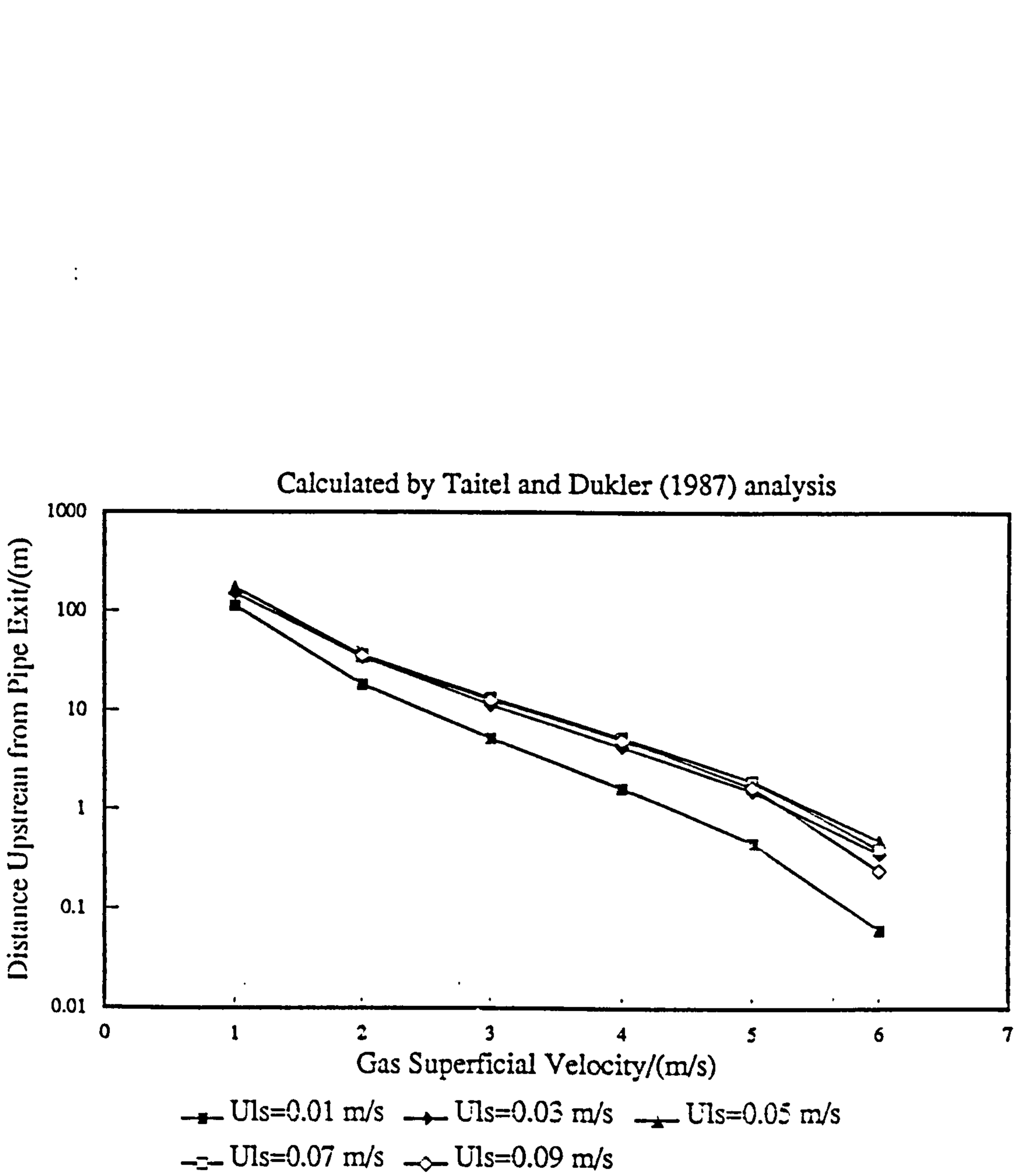


Figure 4.3.36 Upstream distance required for exit effects to be no longer operative.

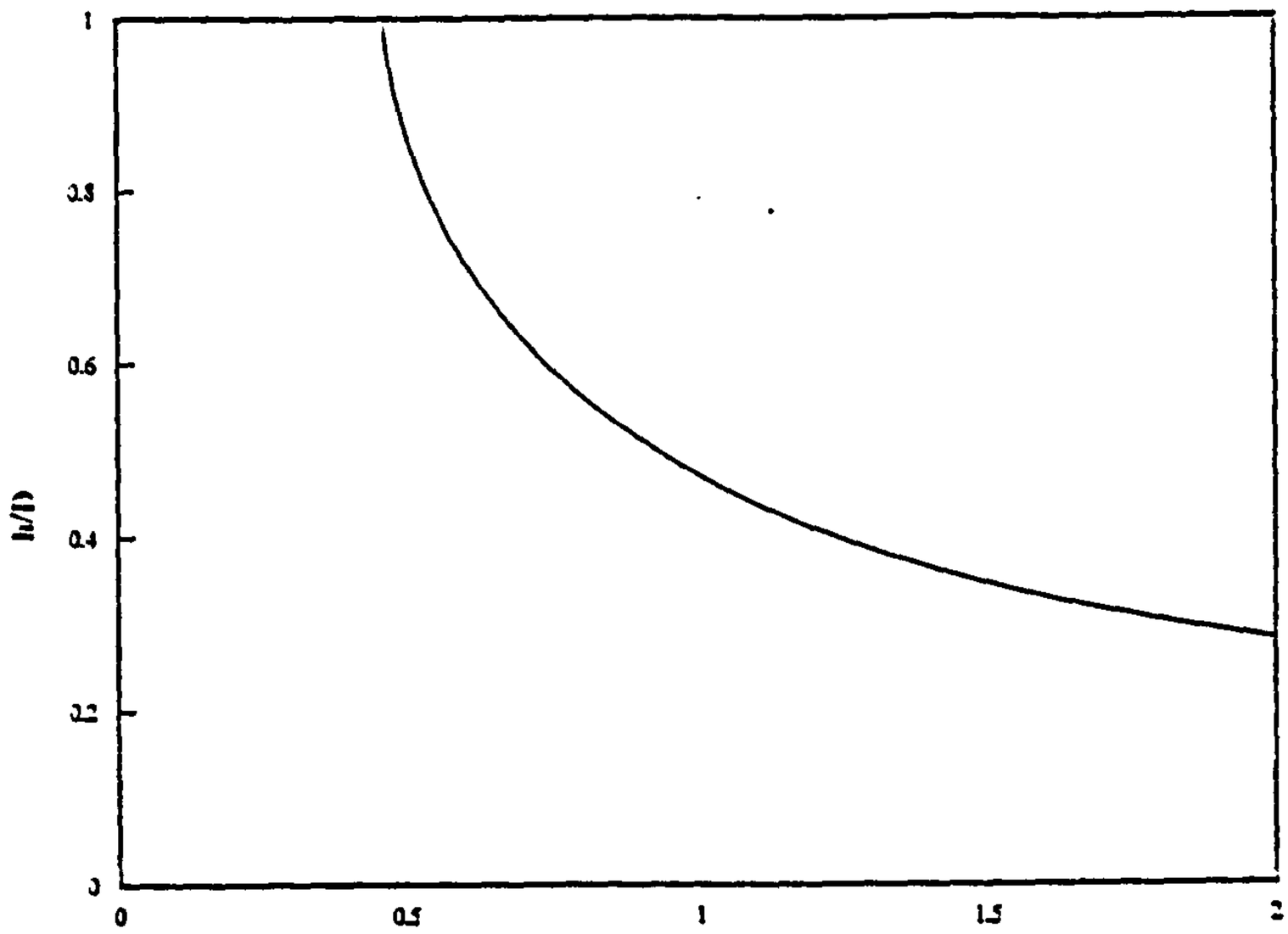


Figure 4.3.37 Minimum liquid film height for stable slug (74mm diameter pipe).

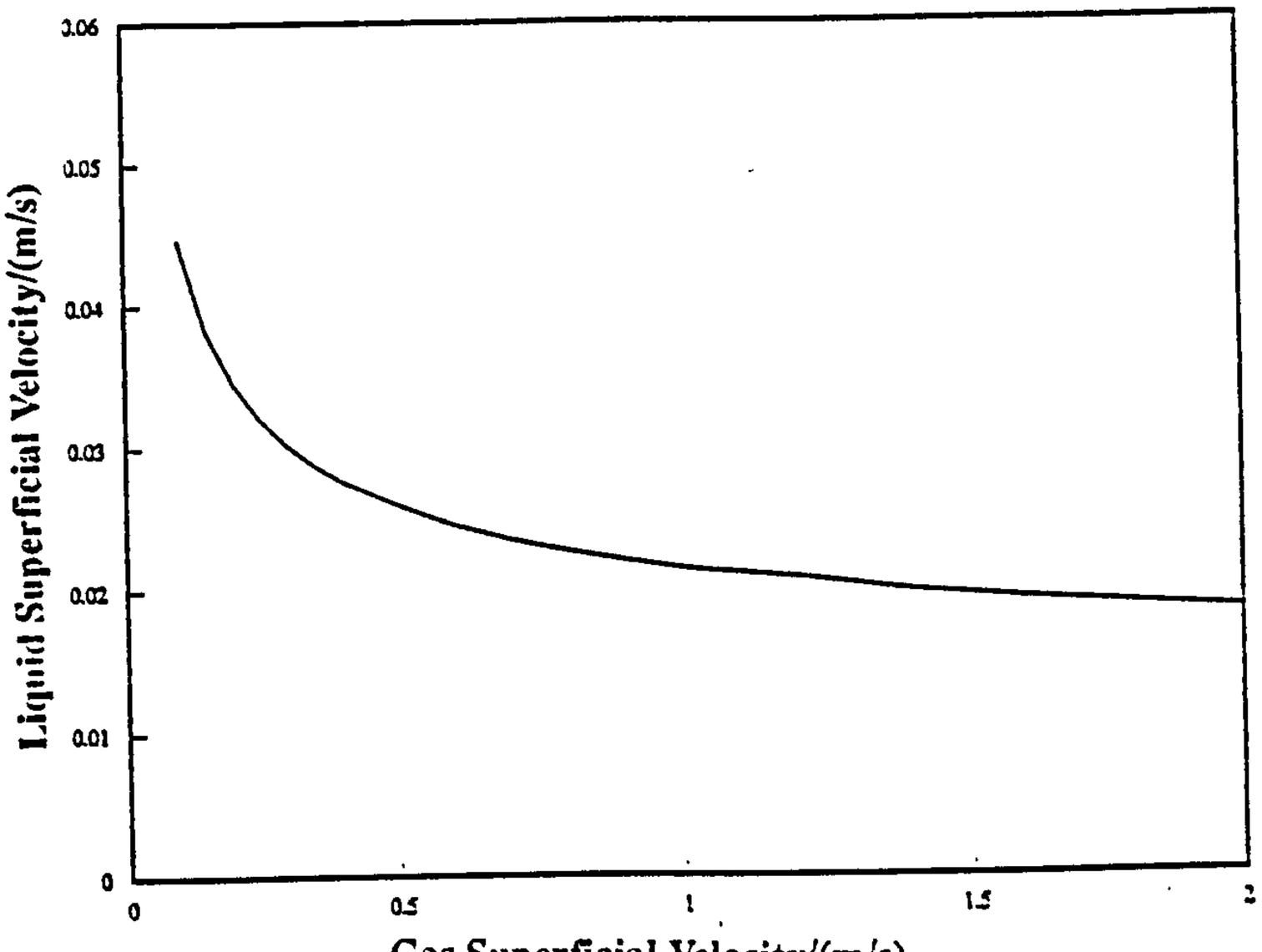


Figure 4.3.38 Minimum liquid superficial velocity for stable slug (74mm diameter pipe).

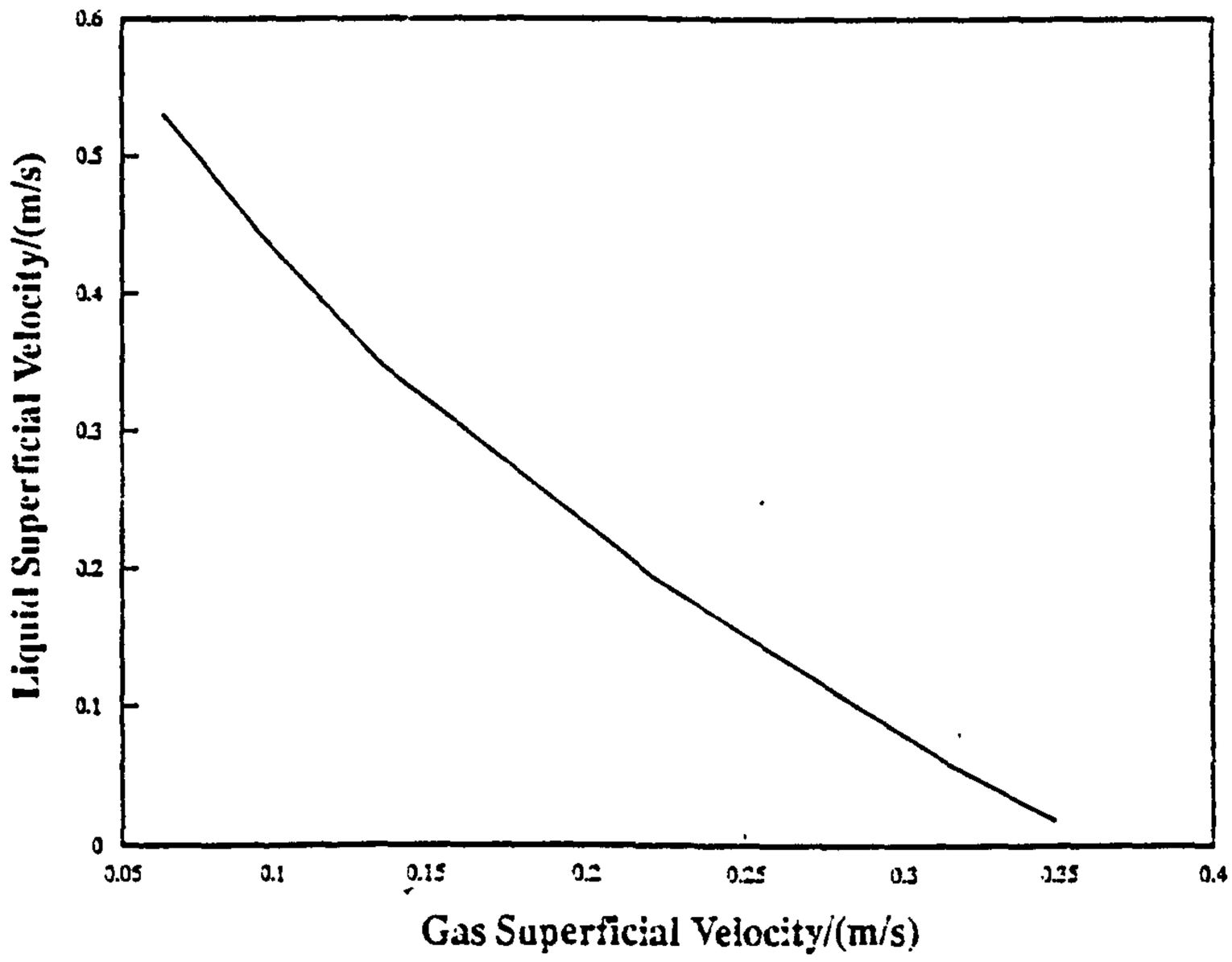


Figure 4.3.39 Liquid superficial velocity limit for slug front criterion (74mm diameter pipe).

4.4 TERRAIN INDUCED SLUGS

Offshore platforms are used to support separator vessels which receive flow from long pipelines containing oil and gas. The flow entering these oil–gas separators is not constant but consists of surges of gas and liquid slugs. Normal slugs are of the order of 25 times the pipe diameter in length. "Terrain induced slugs", formed by liquid collecting at low points in a flowline, can be hundreds of metres in length. A particular example of slugs induced at a low point occurs when a flowline with a downward slope terminates at the riser to a platform. Liquid can form a blockage at the riser base; the blockage growing until the upstream gas pressure is sufficient to blow the liquid into the platform vessel. The liquid slug entering the platform gas–oil separator can be many times the length of the riser, with the potential to cause liquid carryover and liquid level and pressure control problems at the oil–gas separator. These problems can lead to the separator being inoperable at design capacity, resulting in production losses.

In the past, prediction of multiphase flow for the design of oil–gas pipelines has relied on a combination of empirical correlations and simple mechanistic models. Economic and safety considerations have resulted in the need for more detailed prediction of multiphase flow with particular emphasis being placed on transient simulation. One approach to obtain information on transient flow is to use two–fluid codes.

The work described in this Section is an application of the TRAC (Thermal Reactor Analysis Code) code to the simulation of severe slugging. Section 4.4.2 gives a brief description of the TRAC code and in Sections 4.4.3 and 4.4.4 the successful application of the code to the modelling of severe slugging is described. First a discrepancy identified in the review of literature on severe slugging (Section 2.4) is discussed in Section 4.4.1 below.

4.4.1 TRANSITION TO SEVERE SLUGGING

In Chapter 2, three boundaries were identified to delimit the severe slugging flow regime: the transition from stratified flow to normal slug flow in the inclined pipe, transi-

tion to stable flow in the riser, and the transition between severe slugging and semi–severe slugging.

It was noted, in Section 2.4, that while the transition model applied for transition from stratified wavy to intermittent flow in a slightly declined pipe may be derived from theoretical considerations (Taitel and Dukler, 1976), the application of this model to determine a severe slugging boundary has no theoretical basis. However, Schmidt et al (1979), Schmidt et al (1985) and Pots et al (1985) observed that severe slugging only occurred in cases when the flow in the declined pipe was stratified. Thus, if a model like that of Taitel and Dukler (1976) predicted intermittent flow in the declined tube then it was argued that severe slugging would not occur. It should be noted that their experiments were at low pressure and with small bore pipes. Conversely, later work by Fuchs (1987) and Linga (1987) found that severe slugging could occur concurrently with normal slug flow in the inclined pipe. For example, Linga (1987) observed during the riser slug release period two slugs in the line to the riser. The first of these slugs formed the next blockage at the riser base. This implies that the application of the transition criteria of Taitel and Dukler (1976) as a limiting condition is incorrect, assuming the observations of Fuchs (1987) and Linga (1987) are valid. The work of Fuchs (1987) and Linga (1987) was carried out with diesel and nitrogen at elevated pressures in a large diameter pipeline. This discrepancy, which has not been addressed in the literature, is examined in this section.

First it must be noted that if it is assumed that the empirical criterion – ie that severe slugging can only occur if stratified flow exists in the inclined pipe – is true for all pipelines, then the application of a wave instability model, such as Taitel and Dukler (1976), for the transition from stratified to intermittent flow is conservative for pipeline sizing. The slug stability criteria, discussed in Section 4.3, for the transition from intermittent to stratified flow gives transition boundaries at liquid flowrates less than those for a wave instability model.

The work of Linga (1987) suggests that the stratified flow criteria is not true for all pipelines. A possible explanation of this discrepancy may be found by considering the

frequency of slugs in the inclined pipe. If the frequency of normal slugs in the inclined pipe is such that before all the liquid from a slug can drain back down the riser to the riser base, a second slug enters the riser, then liquid will be carried out of the pipe at the riser top by normal slugs. Also a blockage at the riser base may not grow. Conversely, if the frequency of normal slugs in the inclined pipe is such that all the liquid from the first slug has fallen back to the riser base before a second normal slug arrives at the riser base then liquid can build up at the riser base and form the blockage necessary for a severe slug to grow. It is suggested that given a slug frequency correlation for the inclined pipe (specific for each upstream geometry) a transition boundary could be determined for severe slugging in the case where slug flow exists in the inclined tube. This transition boundary would be the locus of flow conditions for which a second slug reaches the riser base just after the liquid shed from the first normal slug has reached the riser base. It has been assumed in the above discussion that a single normal slug would not reach the riser top.

4.4.2 TRAC CODE

Version PF1/MOD1 of the Thermal Reactor Analysis Code (TRAC) was used to simulate severe slugging in this work. TRAC is a "best estimate" code designed for pressurised water reactor (PWR) safety calculations and was developed at Los Alamos National Laboratories. A "best estimate" code contains no deliberate conservatisms.

The code can treat the PWR vessel hydrodynamics in three dimensions and the associated loops in one dimension, modelling the PWR components explicitly. The code is modular and can be used to simulate any system which can be represented in terms of the existing modules. The modules used in the work described in this thesis are:

BREAK: This is a module allowing the pressure to be fixed at a reference point in the system. In PWR calculations it allows the pressure downstream of the break to be fixed, but here it allows the pressure at the pipe exit (separator vessel pressure) to be fixed.

FILL: This module allows fluid flowrates at the inlet to a module to be specified.

PIPE: This module models pipe hydrodynamics in one dimension.

TEE: This module enables a flow mixer or splitter to be modelled.

The code consists of separate continuity and momentum equations for the liquid and vapour, and energy equations for the vapour and mixture. Also there is a non–condensable gas mass equation. Treatment and formulation of the conservation equations in TRAC is covered in detail by Liles et al (1987). A brief summary of the equations will be presented below.

The continuity equations are:

Water:

$$\frac{\partial(1-\varepsilon_G)\varrho_L}{\partial t} + \nabla \cdot [(1-\varepsilon_G)\varrho_L v_L] = \Gamma \qquad (4.4.1)$$

Combined Vapour:

$$\frac{\partial(\varepsilon_G \varrho_G)}{\partial t} + \nabla \cdot (\varepsilon_G \varrho_G v_G) = \Gamma \qquad (4.4.2)$$

Non–condensable gas:

$$\frac{\partial(\varepsilon_G \varrho_a)}{\partial t} + \nabla \cdot (\varepsilon_G \varrho_a v_G) = 0 \qquad (4.4.3)$$

The momentum equations are:

Water:

$$\frac{\partial v_L}{\partial t} + \Delta \cdot v_L = -\frac{1}{\varrho_L}\Delta p - g\sin\theta + (v_G - v_L)|v_G - v_L|\frac{c_i}{(1-\varepsilon_G)\varrho_L}$$

$$-\frac{T}{(1-\varepsilon_G)\varrho_L}(v_{Li} - v_L) - \frac{c_{wL}}{(1-\varepsilon_G)\varrho_L}v_L|v_L| \qquad (4.4.4)$$

Combined vapour:

$$\frac{\partial v_G}{\partial t} + v_G\cdot\nabla v_G = -\frac{1}{\varrho_G}\nabla p - g\sin\theta - \frac{c_i}{\varepsilon_G\varrho_G}(v_G - v_L)|v_G - v_L|$$

$$+\frac{\Gamma}{\varepsilon_G\varrho_G}(v_{Gi} - v_G) - \frac{c_{wG}}{\varepsilon_G\varrho_G}v_G|v_G| \qquad (4.4.5)$$

The energy equations are:

Combined vapour:

$$\frac{\partial(\varepsilon_G\varrho_G u_G)}{\partial t} + \nabla\cdot(\varepsilon_G\varrho_G u_G v_G) = -p\frac{\partial\varepsilon_G}{\partial t} - p\nabla\cdot(\varepsilon_G v_G) \qquad (4.4.6)$$

$$+\dot{q}_{iG} + \Gamma h_{iG} + \dot{q}_{wG}$$

Total energy:

$$\frac{\partial([1-\varepsilon_G]\varrho_L u_L + \varepsilon_G\varrho_G u_G)}{\partial t} + \nabla\cdot([1-\varepsilon_G]\varrho_L u_L v_L + \varepsilon_G\varrho_G u_G v_G) =$$

$$-p\nabla\cdot([1-\varepsilon_G]v_L + \varepsilon_G v_G) + \dot{q}_{wL} + \dot{q}_{wG} \qquad (4.4.7)$$

where u denotes internal energy.

The above time dependant coupled partial differential equations are solved using the stability enhancing two–step (SETS) method. The SETS method consists of a basic

step and a stabilising step and was developed by Mahaffy (1982). The basic step, a semi–implicit equation set, provides information about pressure wave propagation. A stabilizing step is then added to provide information concerning the transport of energy, density and momentum across cell boundaries.

Closure of the above equations requires thermodynamic relations, specification of the interfacial drag coefficient (c_i), wall shear coefficients (c_{wG}, c_{wL}) and for phase change and heat transfer specification of interfacial heat transfer ($\dot{q}_{iG}$), phase change rate (Γ), and wall heat transfer ($\dot{q}_{wG}$ and $\dot{q}_{wL}$). Liles et al (1987) describe the constitutive relationships contained in TRAC. In the work described in this Section the phase change option is switched off and the physical package used is that for air and water.

4.4.3 SIMULATION OF SCHMIDT ET AL (1979) EXPERIMENTS

4.4.3.1 Initial simulation

A TRAC input deck was written to allow TRAC simulations of the experiments of Schmidt et al (1979). A PIPE module represented the declined pipe and riser, and a TEE module the inlet mixer. The cell size and geometry of the test section and riser is shown in Figure 4.4.1. The flow condition of 0.97 m/s gas superficial velocity and 0.34 m/s liquid superficial velocity was chosen for the initial simulation to enable comparison with the simulation of Bendiksen et al (1982) reported in Section 2.4. The riser exit pressure was set at 1 bar using a BREAK module and the flowline declination was 5 degrees. Air and water were the simulation fluids whereas in the experiment, air and kerosine were the respective fluids. The TRAC code is limited in physical property data; a major effort is currently being deployed at the Harwell Laboratory to develop a related code (PLAC) which can handle a wide variety of hydrocarbon properties. The calculations were carried out on the Harwell Laboratory CRAY–2 computer and took an averaged CPU time of 0.79 seconds for 1 second of simulation.

TRAC voidage predictions are shown in Figure 4.4.2. Schmidt et al (1979) did not present any void fraction and pressure data so the TRAC predictions can only be compared with those of Bendiksen et al (1982), Figure 2.4.3. In common with the results obtained

by Bendiksen et al (1982) the magnitude and the frequency of the fluctuations obtained for this TRAC simulation are not consistent with severe slugging. A test was carried out for the sensitivity of the solution to cell size and maximum time step. Simulations with the cell size halved and doubled were run. Figure 4.4.3 compares the voidage at the riser base for the three different cell lengths. An increase in magnitude of the voidage oscillations is observed with decreasing cell size, while the frequency remains about the same. Figure 4.4.4 compares the riser base voidage at a maximum allowable time step of 0.5 seconds and 0.05 seconds. The frequency of the fluctuations are similar for both maximum time steps, but with decreasing maximum time step the amplitude of the oscillation decreases. For inappropriate cell size and maximum time step to be the reason for the inability to predict severe slugging one would expect to observe a large increase in the magnitude of the oscillations and a decrease in oscillation frequency.

If the assumption is made that the numerics of TRAC are able to simulate the hydraulic phenomena of severe slugging, then the simulation failed to predict severe slugging by incorrectly representing the physics of the problem. The parameters affecting the flow regime predictions are discussed below.

(a) Density of the liquid phase. Growth of a severe slug in a riser is a balance between the increase in hydrostatic pressure due to the fluid column and the increase in gas pressure in the inclined pipe section. Because of the limitations of the TRAC physical property package, water physical properties were used in the simulations whereas kerosine was used in the experiments. However the higher the liquid density, the greater is the propensity to severe slugging. Water is denser than kerosine and hence simulating the experiments using the density of kerosine, would not have resulted in a prediction of severe slugging.

(b) Air cavity size upstream of the riser section. The larger the volume of the air cavity upstream of the riser the slower is the rise in pressure in the gas cavity upstream of the pipe blockage. Hence, as the cavity volume

increases severe slugging becomes more likely. Two factors effecting the cavity size are prediction of the voidage in the declined pipe section and correct representation of any gas reservoir upstream of the mixer. The voidage in the inclined section depends on the balance between shear acting on the fluids at the wall–fluid interfaces and the fluid–fluid surface and the force on the fluids due to the component of gravity acting in the direction of flow. At the low gas flowrates in the severe slugging region the interfacial shear and gas–to–wall shear are small. Thus the momentum balance is dominated by the liquid–to–wall shear and gravity. The liquid–to–wall shear would be sensitive to difference in viscosity between kerosine and water but, in fact, the void fraction for the case studied is high (ie the stratified liquid–layer is thin) and the proportional effect of viscosity on void fraction is quite small. A more important effect (ignored in both the initial TRAC calculations reported here and also it is suggested in the work of Bendiksen et al, 1982) was that of the compressible volume in the air supply pipeline to the test section used by Schmidt et al (1979). If the line is not choked then the increase in gas cavity volume will increase the potential for severe slugging.

We see, therefore, that the upstream compressible volume was the most likely cause of the failure of this initial simulation.

4.4.3.2 Final simulation of Schmidt et al (1979) experiments.

Here, we describe calculations carried out taking account of the compressible volume upstream of the mixer in the experiment of Schmidt et al (1979). The length of the air supply pipe was calculated from the rig schematic given by Schmidt et al (1979) as 45.72 m and the pipe bore taken to be 0.05 m. The volume of the air supply pipe was included in the simulation as an air reservoir in the TEE component.

Schmidt et al (1979) described three types of flow regime for their experiments: severe slug type I, severe slug type II, and stable flow. The following flow regime definitions of Schmidt et al (1979) will be used to classify the simulation results.

Severe slug type I: Here, the liquid slug is formed in the inclined pipe as well as the riser. The gas flow through the bend is completely shut off during the build–up phase, and the slugs are practically free of gas, and are substantially longer than the riser.

Severe slug type II: Here, the bulk of the slug is generated in the riser, the gas flowrate being high enough that pockets of gas might break through the bend, giving slightly aerated slugs.

Stable flow: This implies normal slug, annular or bubble flow.

The simulations of three of Schmidt et al's (1979) flow conditions are given below, starting with the flow condition of 0.97 m/s gas superficial velocity and 0.34 m/s liquid superficial velocity which was chosen for the initial simulation described in Section 4.4.3.1.

(a) Severe slug type II

The experiment identified severe slugging type II for a gas superficial velocity of 0.97 m/s and liquid superficial velocity of 0.34 m/s. Figures 4.4.5 and 4.4.6 show the simulation voidage and pressure variations with time at the riser base (cell 42 – see Figure 4.4.1 for cell position). Figures 4.4.7 and 4.4.8 show the voidage and pressure at the riser top (cell 59), and Figure 4.4.9 shows the variation of voidage along the test section prior to slug production (to the separator).

The Figures 4.4.5, 4.4.6, 4.4.7 and 4.4.8 show that the voidage varies in the riser between 0 and 100 % and that the frequency of oscillation is consistent with severe slugging. Figure 4.4.9 illustrates that the maximum slug length is nearly the riser in length and that the slug is mainly generated in the riser. Also Figure 4.4.9 shows slight aeration in the riser section.

Hence this simulation can be classified as severe slugging type II.

(b) Severe slug type I

The experiment identified as severe slugging type I, the flow condition of 0.18 m/s gas superficial velocity and 0.34 m/s liquid superficial velocity. Figures 4.4.10 and 4.4.11 show the simulation voidage and pressure variations with time at the riser base. Figures 4.4.12, 4.4.13 and 4.4.14 show the simulation voidage variation along the test section at different phases in the slugging cycle.

Figures 4.4.10 and 4.4.11 show that the voidage varies between 0 and 70 % at the riser base, and that the frequency of oscillation is consistent with severe slugging. Also the simulation predicts voidages between 0 and 100% at the riser top. Figure 4.4.12 shows the voidage in the test section during the first stage of slug production. While Figure 4.4.13 shows the voidage in the test section prior to the second stage of slug production, and Figure 4.4.14 the voidage just after the second stage of slug production. The figures show that the slug length is significantly greater than the riser length and that slug growth occurs in the inclined section as well as the riser.

Hence this simulation can be classified as severe slugging type I.

(c) Stable flow

The experiment identified as stable flow, the flow condition of 3.4 m/s superficial gas velocity and 0.34 m/s liquid superficial velocity. Figures 4.4.15 and 4.4.16 illustrate the variation of simulation voidage and pressure at the riser base, and Figure 4.4.17 and 4.4.18 the variation at the riser top.

Figures 4.4.15 and 4.4.17 illustrate that the voidage varies between 70 and 90 %. Figures 4.4.16 and 4.4.18 show irregular pressure oscillations the frequency of which are not consistent with severe slugging. No large build–up of liquid is shown by the simulation.

Hence this simulation can be classified as stable flow.

We see, therefore, that the regimes observed by Schmidt et al (1979) can be adequately predicted by the TRAC simulation provided that adequate account is taken of the upstream compressible volume. The general conclusion is that in predicting such transi-

ent behaviour, careful modelling of the full system is necessary. The TRAC code is sufficiently powerful to offer the opportunity of modelling quite complex systems so this requirement provides no major problem once it is realised.

4.4.4 SIMULATION OF POTS ET AL (1985) EXPERIMENTS

The above simulations of the Schmidt et al (1979) experiments provide qualitative support for the ability of TRAC to simulate the occurrence of severe slugging. However, the predictions go further than just predicting the existence of the various regimes. They also give information such as slug length, frequency and velocity. Unfortunately, the paper by Schmidt et al (1979) did not provide information on these detailed characteristics. However, in more recent work, Pots et al (1985), have provided such detailed data and a case reported by these authors has also been investigated in the work reported in this thesis.

The experimental facility of Pots et al (1985) consisted of a 0.05 m internal diameter pipeline of 30 m length connected to a 15 m riser of the same diameter. A gas vessel situated at the test section inlet simulated an extra pipeline length of 120 m. The fluids used in the experiments were air and water or a water/glycerine solution. At the top of the riser gas is released to the atmosphere and the liquid flowrate measured in a storage vessel before the liquid is recycled. Investigations of the effect of pipeline angle, liquid viscosity and gas injection at the riser base were reported.

The following base case severe slugging experiments were simulated using TRAC:

U_{SG} = 0.8 m/s at 1.6 bar, liquid water only, angle = –2 degrees

(i) U_{SL} = 0.18 m/s

(ii) U_{SL} = 0.36 m/s

(iii) U_{SL}= 0.72 m/s

The TRAC simulations used cell lengths of 0.75 m. A PIPE component represented the inclined pipe and riser, and a TEE component the inlet mixer and buffer vessel. FILL

components simulated water and air inlets at constant mass flow and a BREAK component the exit.

Pots et al (1985) used the hydrostatic head in the storage vessel to calculate the slug length, slugging period, liquid production time and the relative slug peak velocity. The relative slug peak velocity is the ratio of the maximum area averaged velocity of the fluid in the slug during the liquid production period to the time averaged velocity of the slug fluid. In order to simulate these measurements, mass flow into the simulation storage vessel, the BREAK component, was used to calculate the simulation results. Output from the TRAC calculations are compared in Table 4.4.1 with the experimental data and model predictions of Pots et al (1979).

		V_{LS} (m/s)		
		0.18	0.36	0.72
SLUG LENGTH (m)	TRAC	25.7	42.4	78.0
	POTS MODEL	36	71	130
	EXP	25	41	58
SLUGGING PERIOD (s)	TRAC	145.8	116.0	127
	POTS MODEL	200	220	170
	EXP	140	110	78
LIQUID PRODUCTION PERIOD (s)	TRAC SLUG	25.4	30.5	46.3
	TRAC TOTAL	40.5	60.6	110.0
	POTS MODEL	39	72	78
	EXP	26	43	48
RELATIVE PEAK SLUG VELOCITY (m/s)	TRAC	4.56	8	1.86
	POTS MODEL	47	33	13
	EXP	88	65	16

Table 4.4.1: Comparison of TRAC calculations with the experimental data and model predictions of Pots et al (1979)

Two values are given for the simulated liquid production time. The first is the time that the slug is producing into the storage vessel, and the second the total liquid production time. One would expect the experimental result to be between the two values. Excellent agreement is found between the TRAC predictions of slug length, slugging period and liquid production time for liquid superficial velocities of 0.18 m/s and 0.36 m/s. These flow conditions are well within the severe slugging region. In the 0.72 m/s case TRAC over predicts the slug length, slugging period and the liquid production time. At all three liquid flow conditions TRAC provides a better prediction of the slugging characteristics than the SLUGFLOW model of Pots et al (1985).

The poor prediction of relative slug peak velocity for all three liquid flow rates is to be expected for two reasons. The first reason is that the peak velocity is a transient of short time and spatial duration in comparison with the slugging frequency and hence may not be simulated using cell lengths of 0.75 m and maximum time steps of 0.5 second. Also the print interval, the time between each output of system variables, was set at 5 seconds for economy. While this is adequate for the capture of low frequency cycles it means the transient could occur in the time between two consecutive prints. The latter reason is the suggested explanation for the increase in predicted relative peak slug velocity between U_{SL} = 0.18 m/s and U_{SL} = 0.36 m/s.

Again, these comparisons indicate the power of the TRAC code to simulate complex, time varying compressible two–phase flows. The wealth of experience developed in the nuclear industry in dealing with such flows (as exemplified by the TRAC code) is ripe for exploitation in the oil industry and other fields.

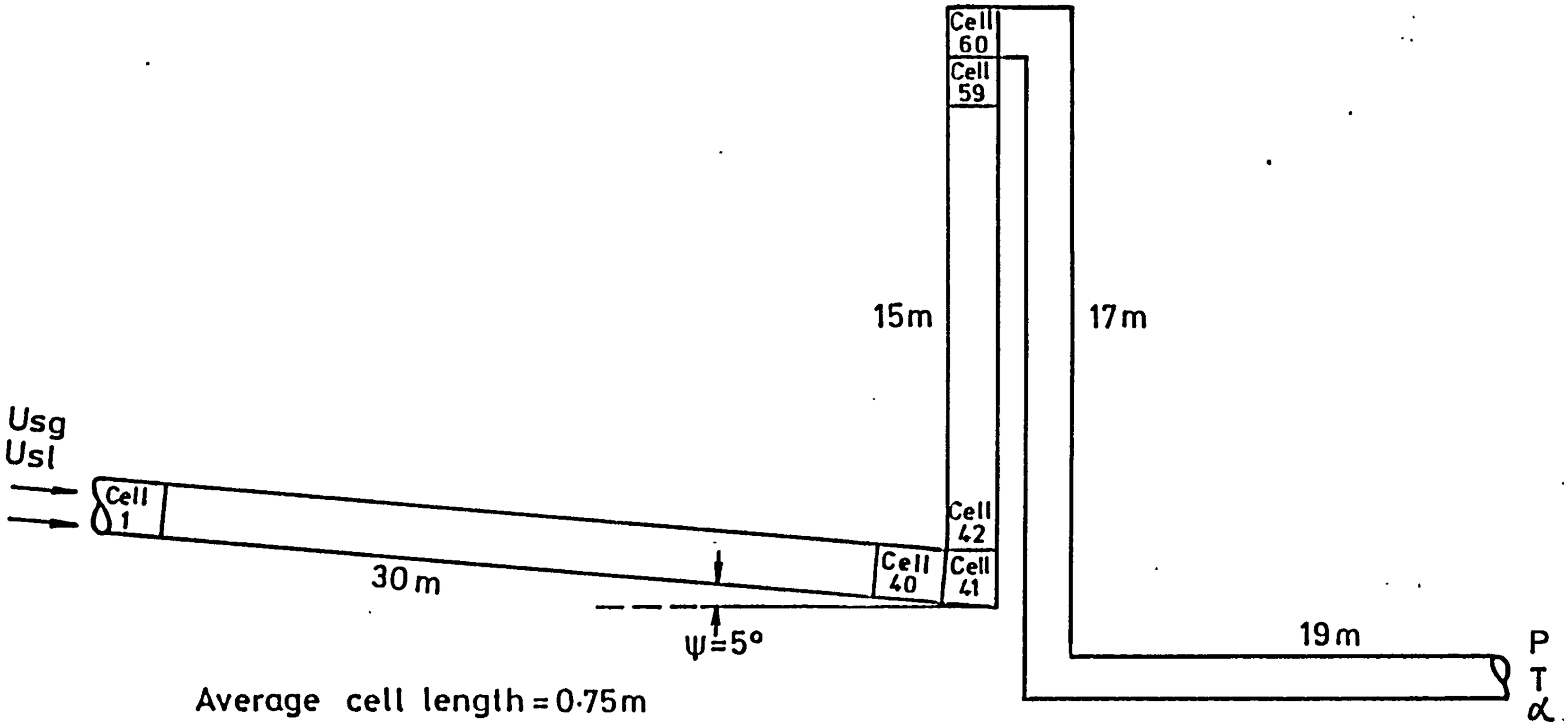


Figure 4.4.1 GEOMETRY OF THE SCHMIDT ET. AL. EXPERIMENT.

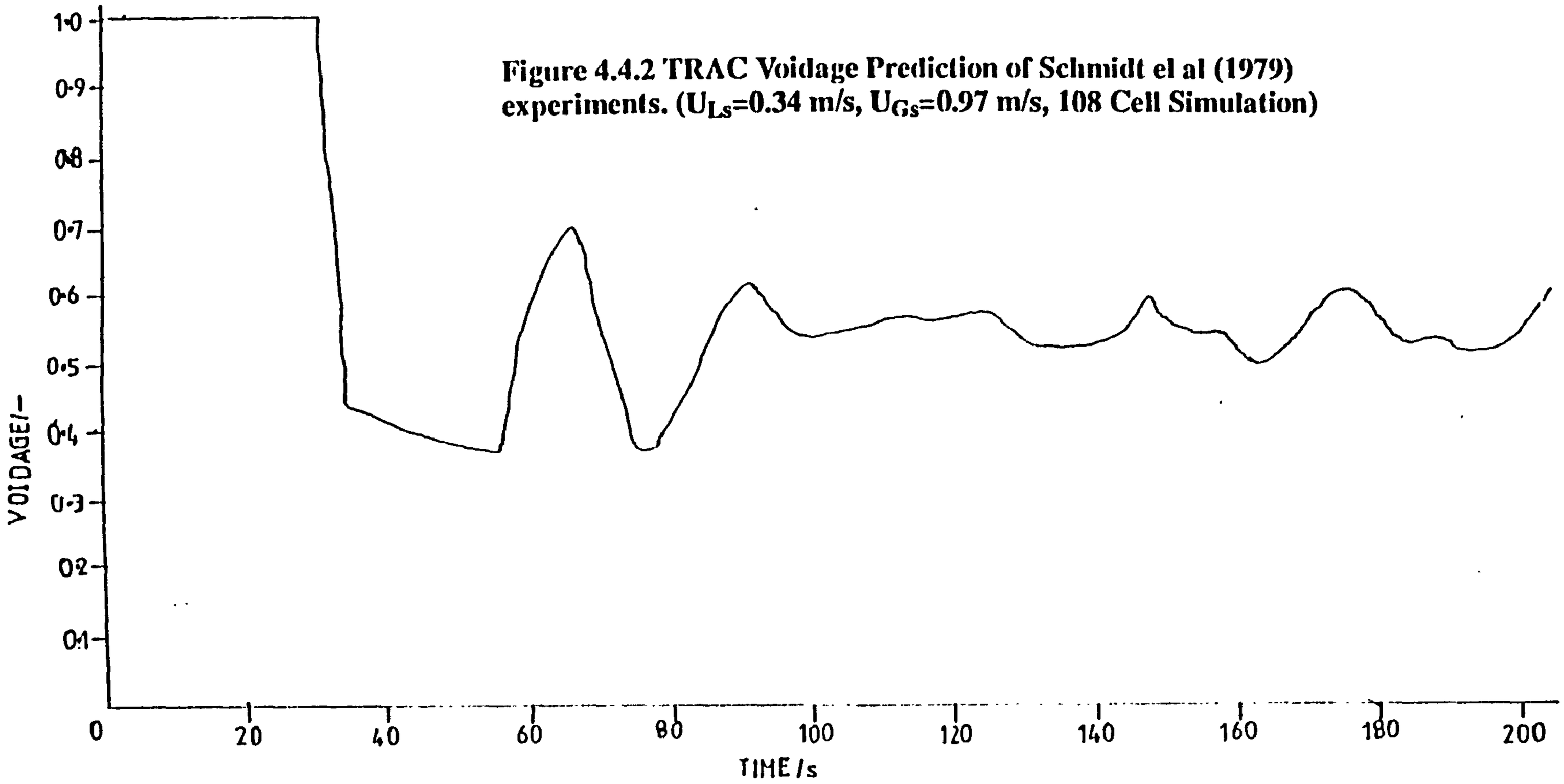
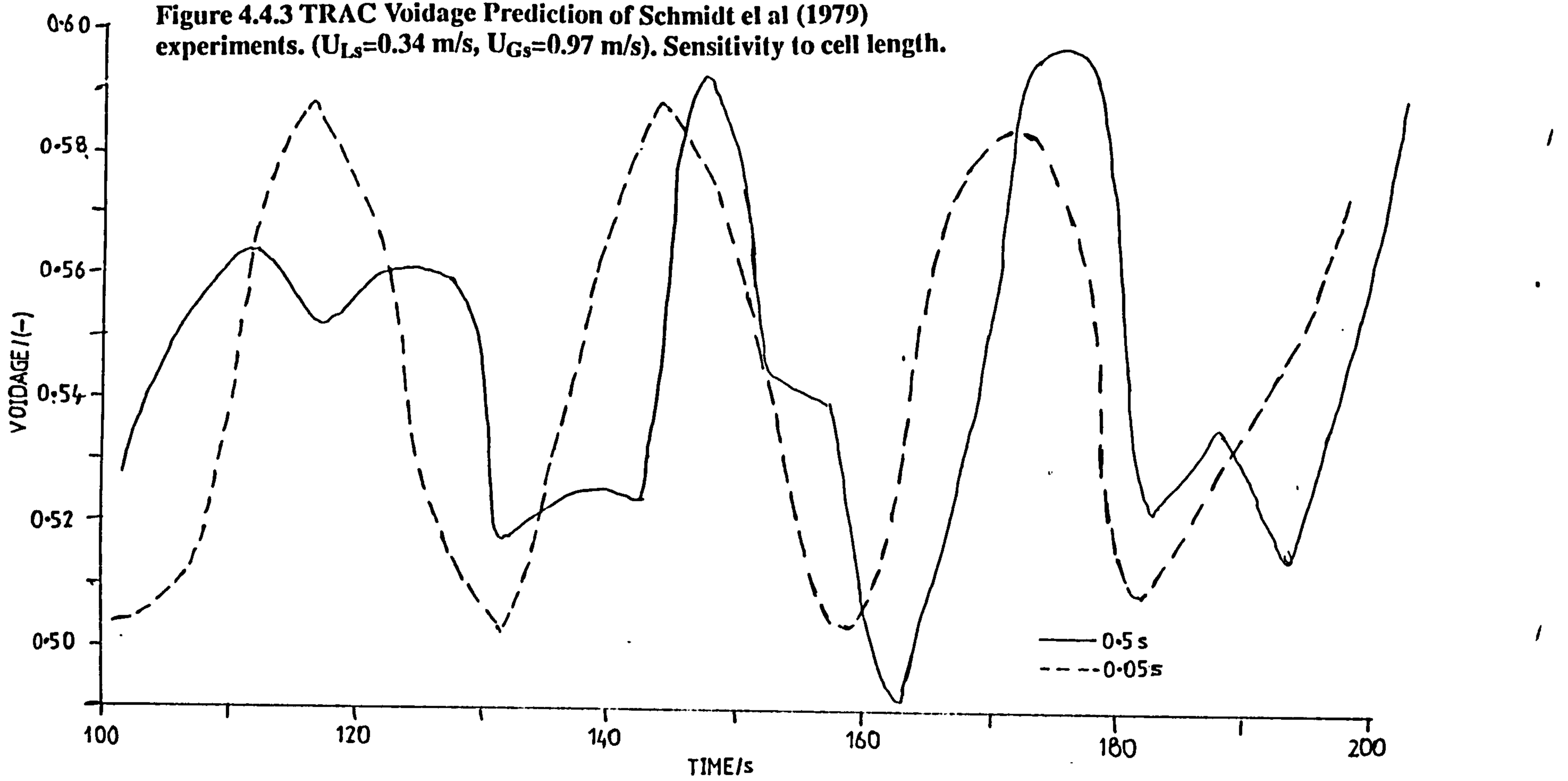


Figure 4.4.2 TRAC Voidage Prediction of Schmidt el al (1979) experiments. (U_{Ls}=0.34 m/s, U_{Gs}=0.97 m/s, 108 Cell Simulation)

Figure 4.4.3 TRAC Voidage Prediction of Schmidt el al (1979) experiments. (U_{Ls}=0.34 m/s, U_{Gs}=0.97 m/s). Sensitivity to cell length.



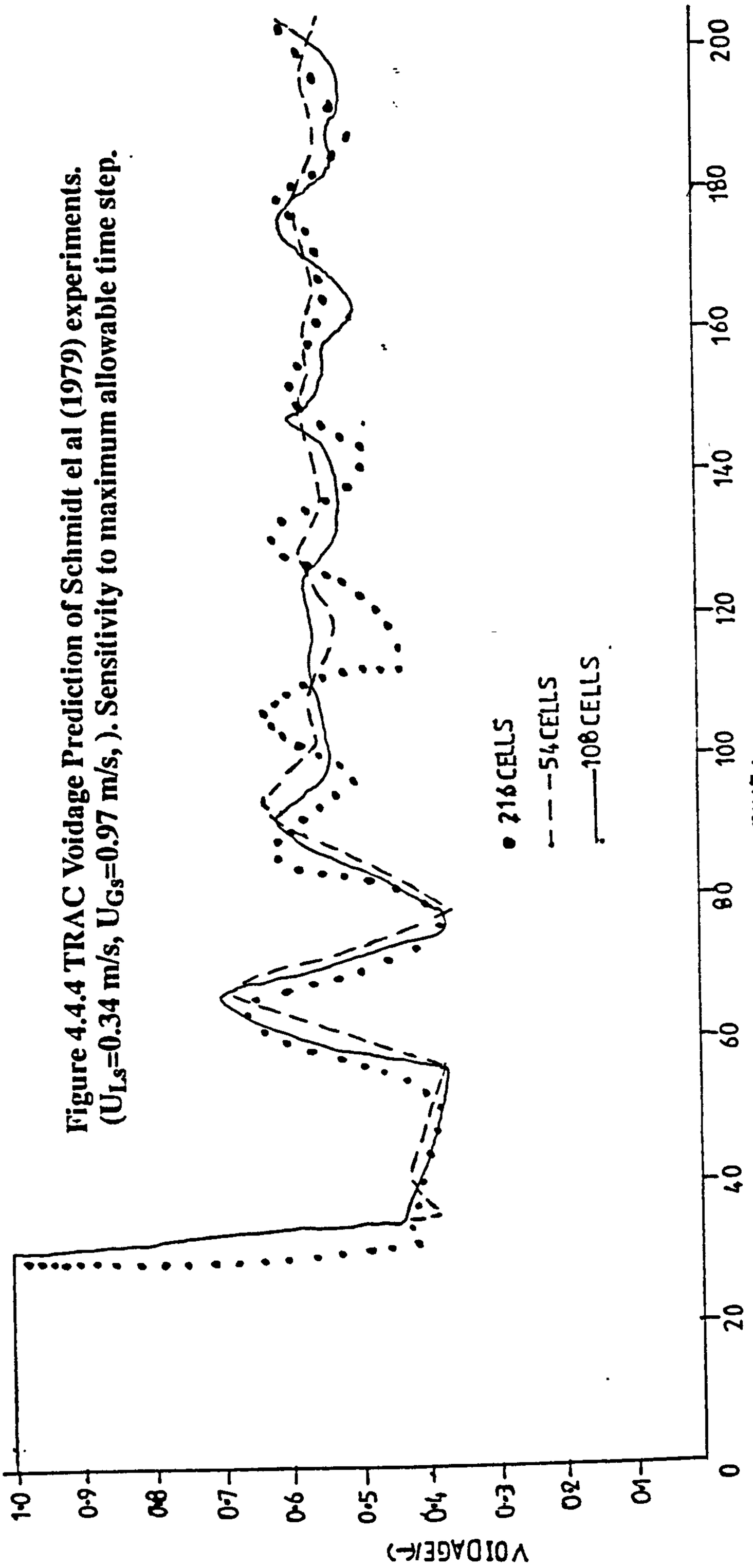


Figure 4.4.4 TRAC Voidage Prediction of Schmidt el al (1979) experiments. (U_{Ls}=0.34 m/s, U_{Gs}=0.97 m/s,). Sensitivity to maximum allowable time step.

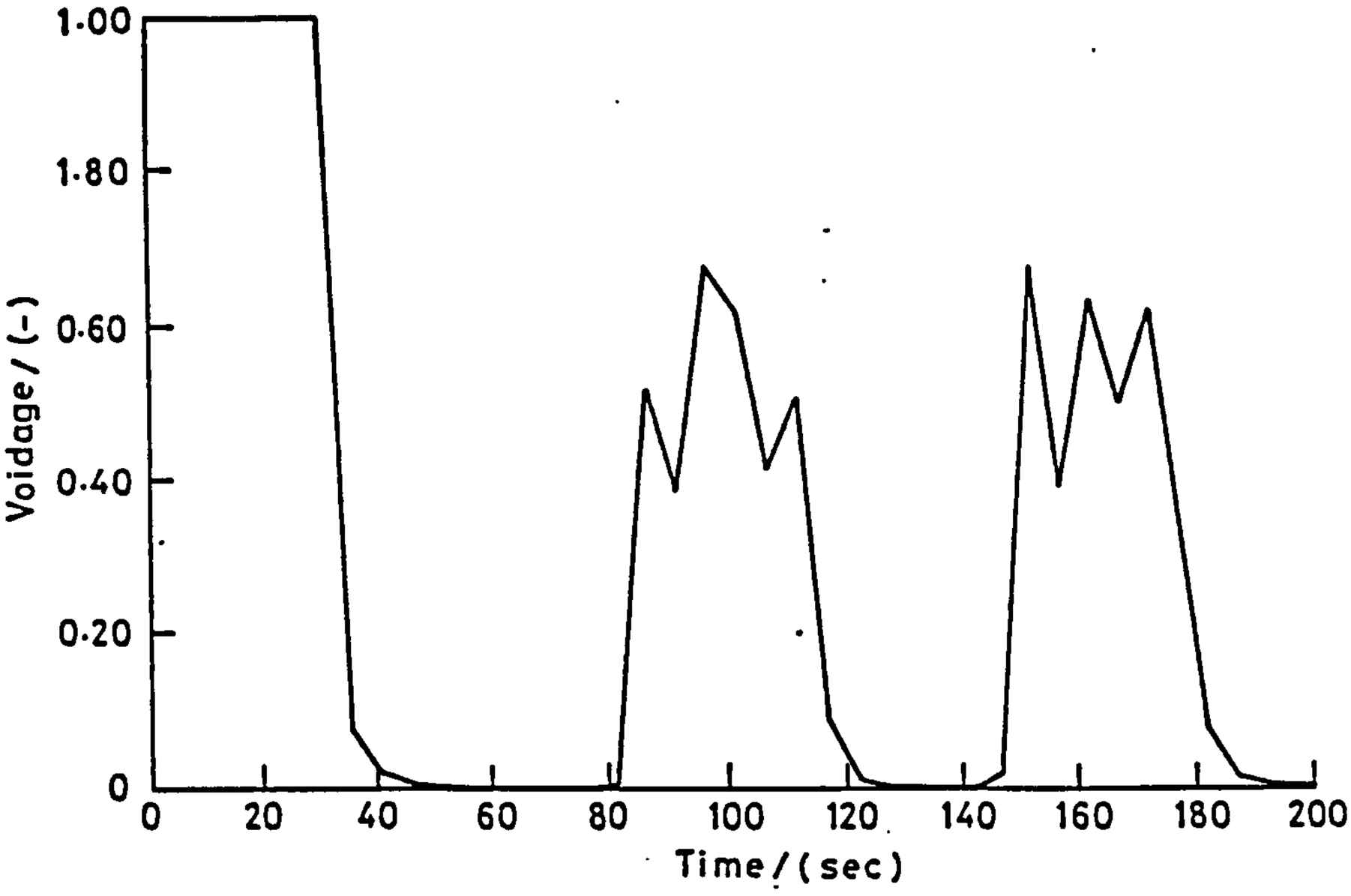


Figure 4.4.5 VOIDAGE VS TIME AT RISER BASE (CELL 42)
Ugs = 0·97 m/s Uls = 0·34 m/s

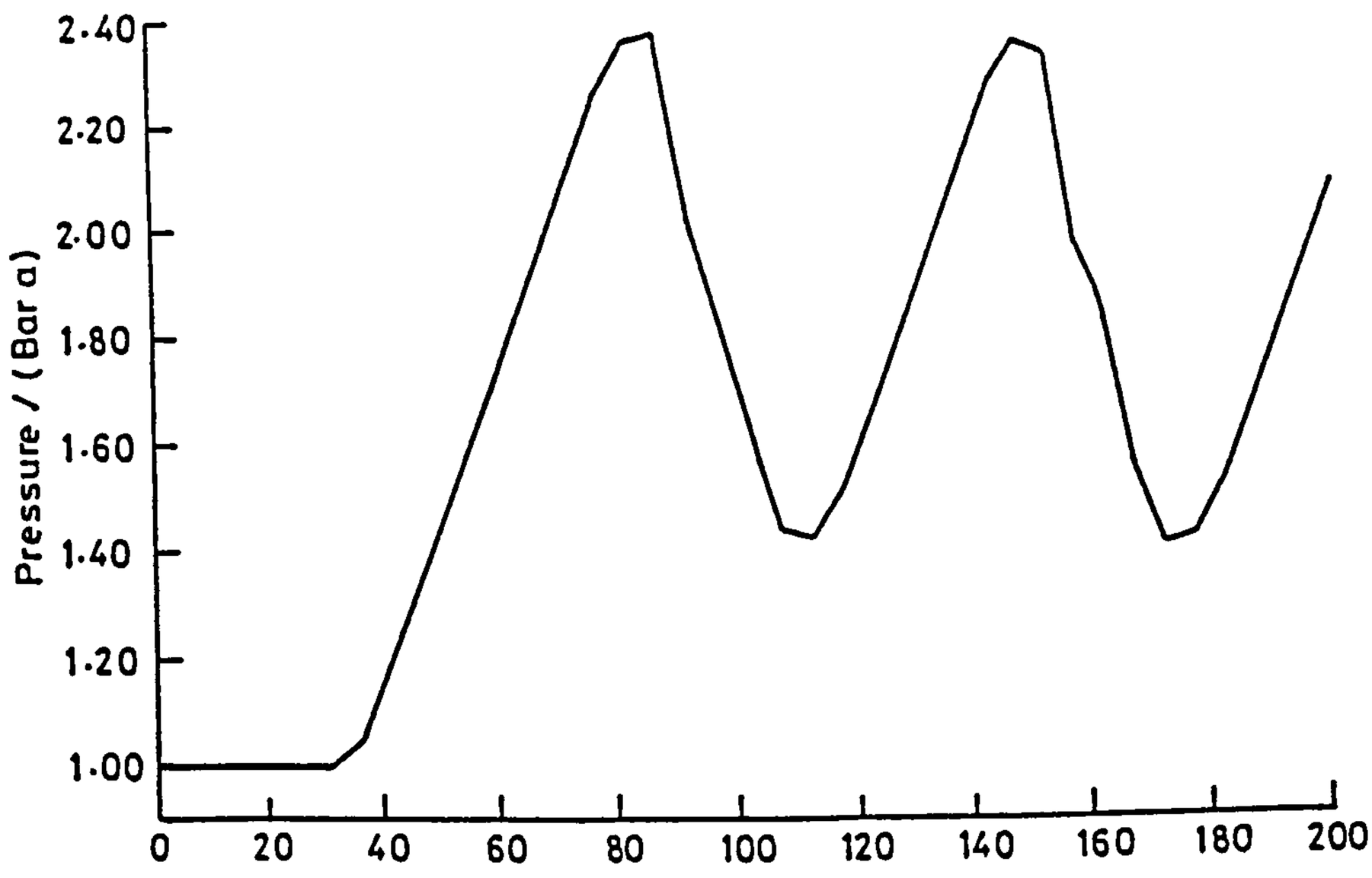


Figure 4.4.6 PRESSURE VS TIME AT RISER BASE (CELL 42)
Ugs = 0·97 m/s Uls = 0·34 m/s

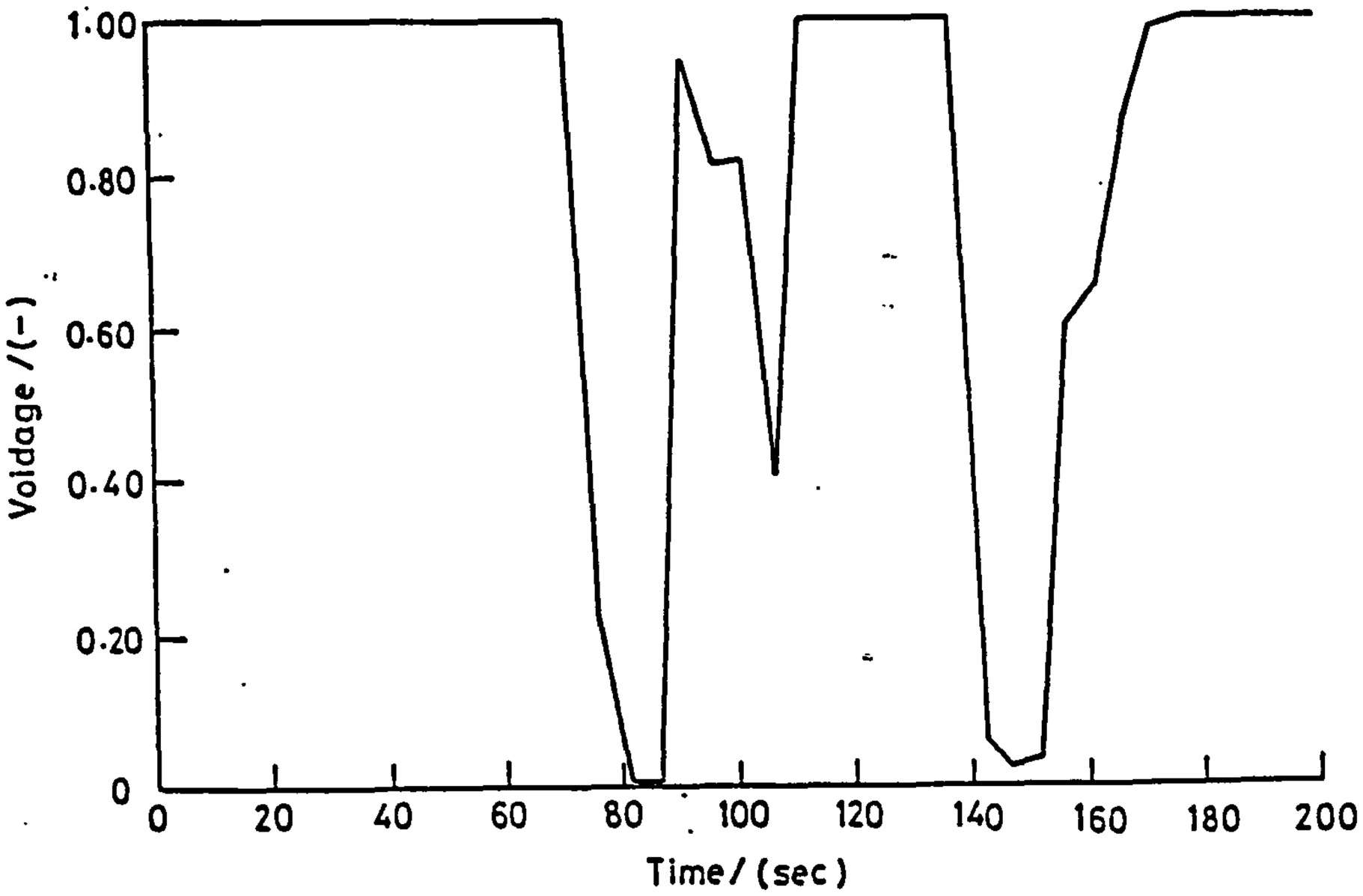


Figure 4.4.7 VOIDAGE VS TIME AT RISER TOP (CELL 59)
Ugs = 0·97 m/s Uls = 0·34 m/s

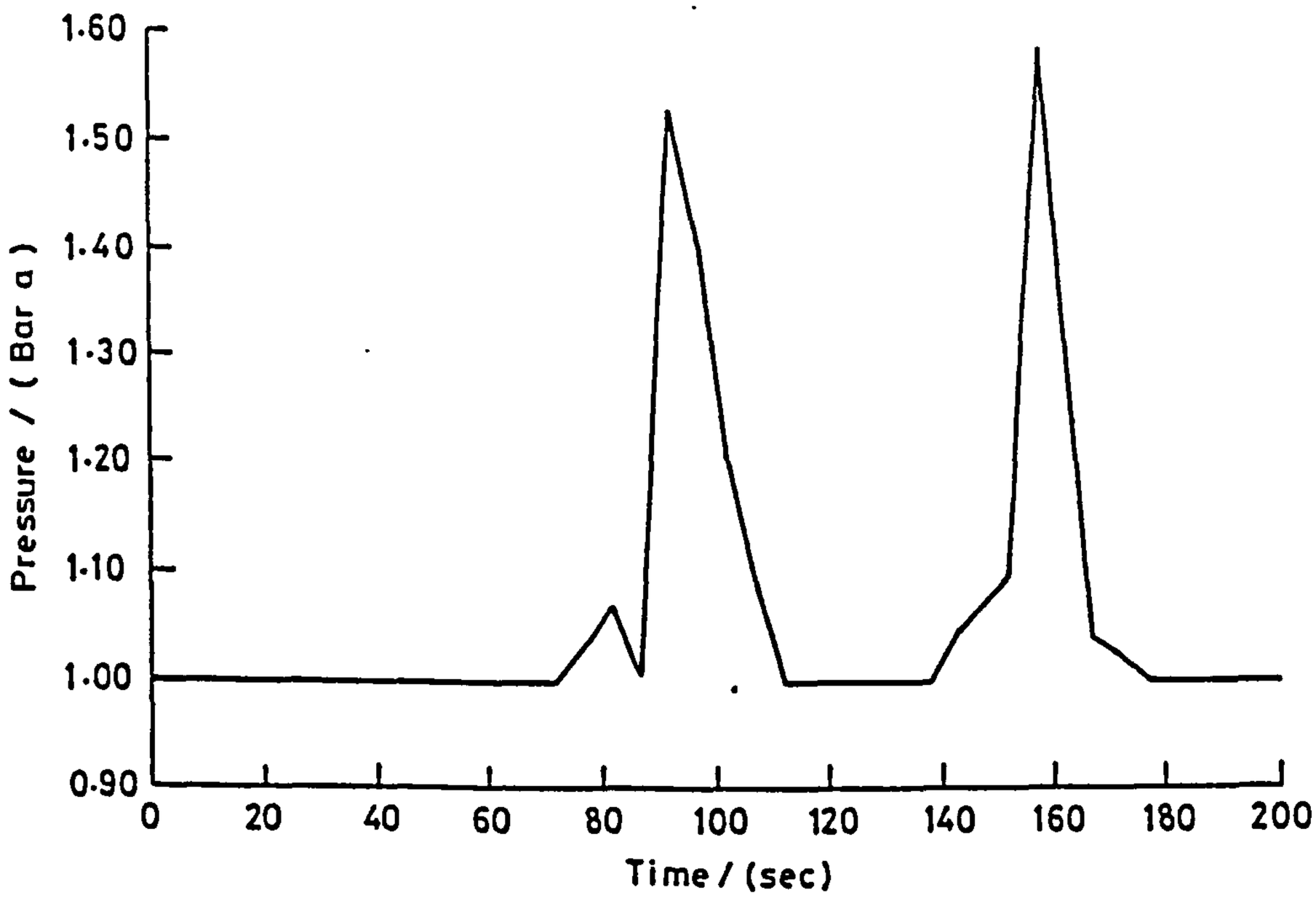


Figure 4.4.8 PRESSURE VS TIME AT RISER TOP (CELL 59)
Ugs = 0·97 m/s Uls = 0·34 m/s

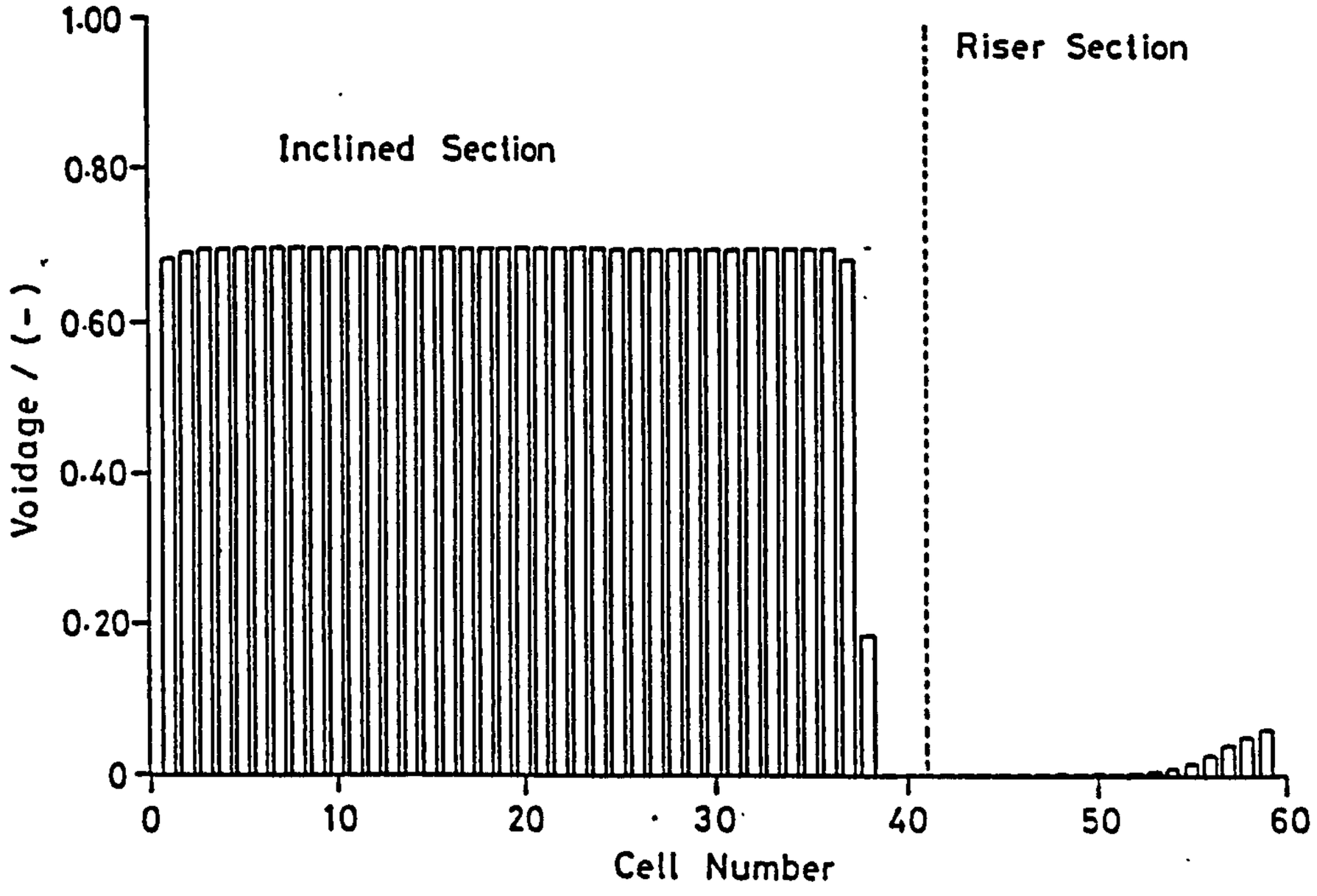


Figure 4.4.9 VOIDAGE ALONG TEST SECTION
Ugs = 0·97 m/s Uls = 0·34 m/s

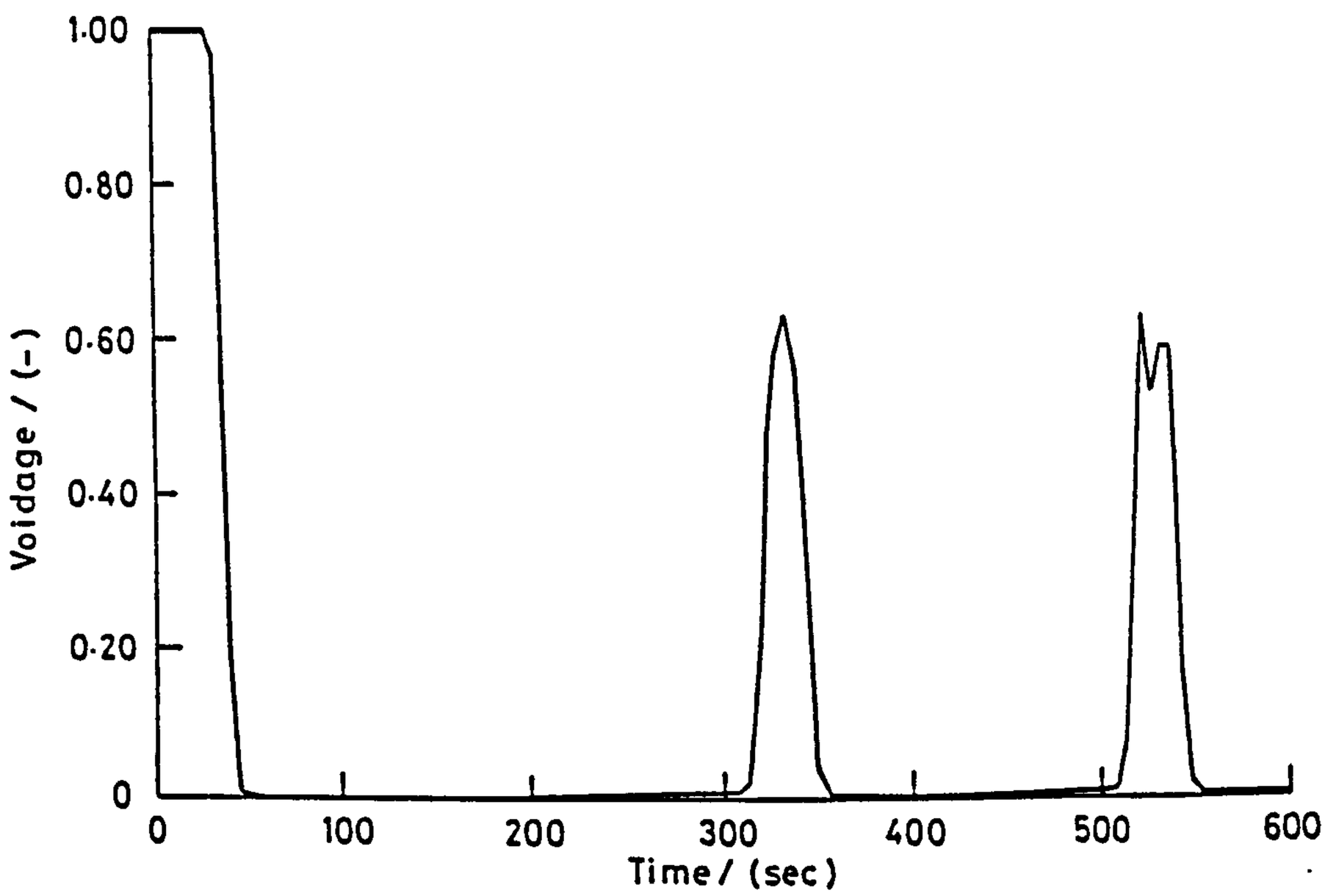


Figure 4.4.10 VOIDAGE VS TIME AT RISER BASE (CELL 42)
Ugs = 0·18 m/s Uls = 0·34 m/s

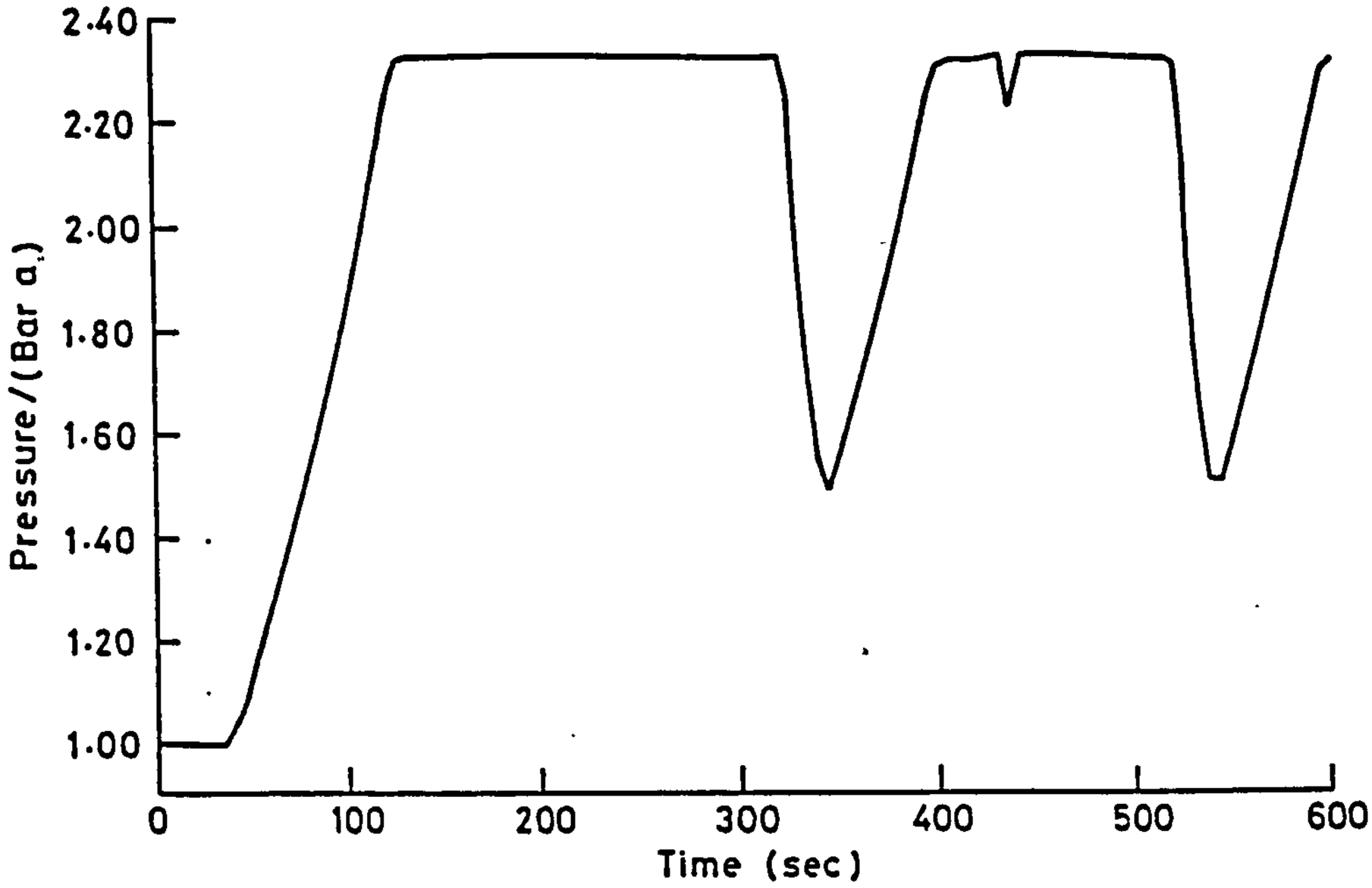


Figure 4.4.11 PRESSURE VS TIME AT RISER BASE (CELL 42)
Ugs = 0·18 m/s Uls = 0·34 m/s

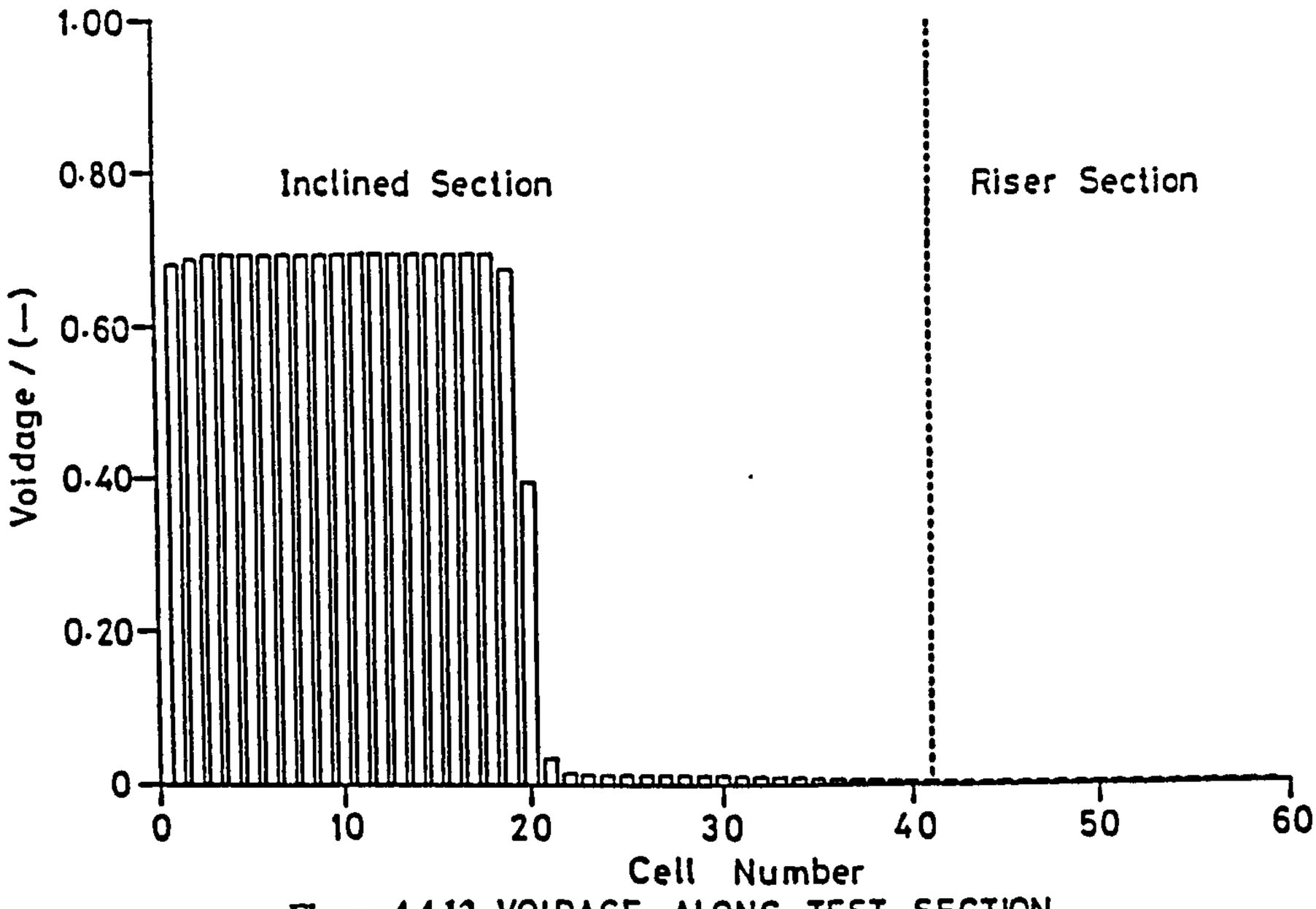


Figure 4.4.12 VOIDAGE ALONG TEST SECTION
Time = 206 secs
Ugs = 0·18 Uls = 0·34

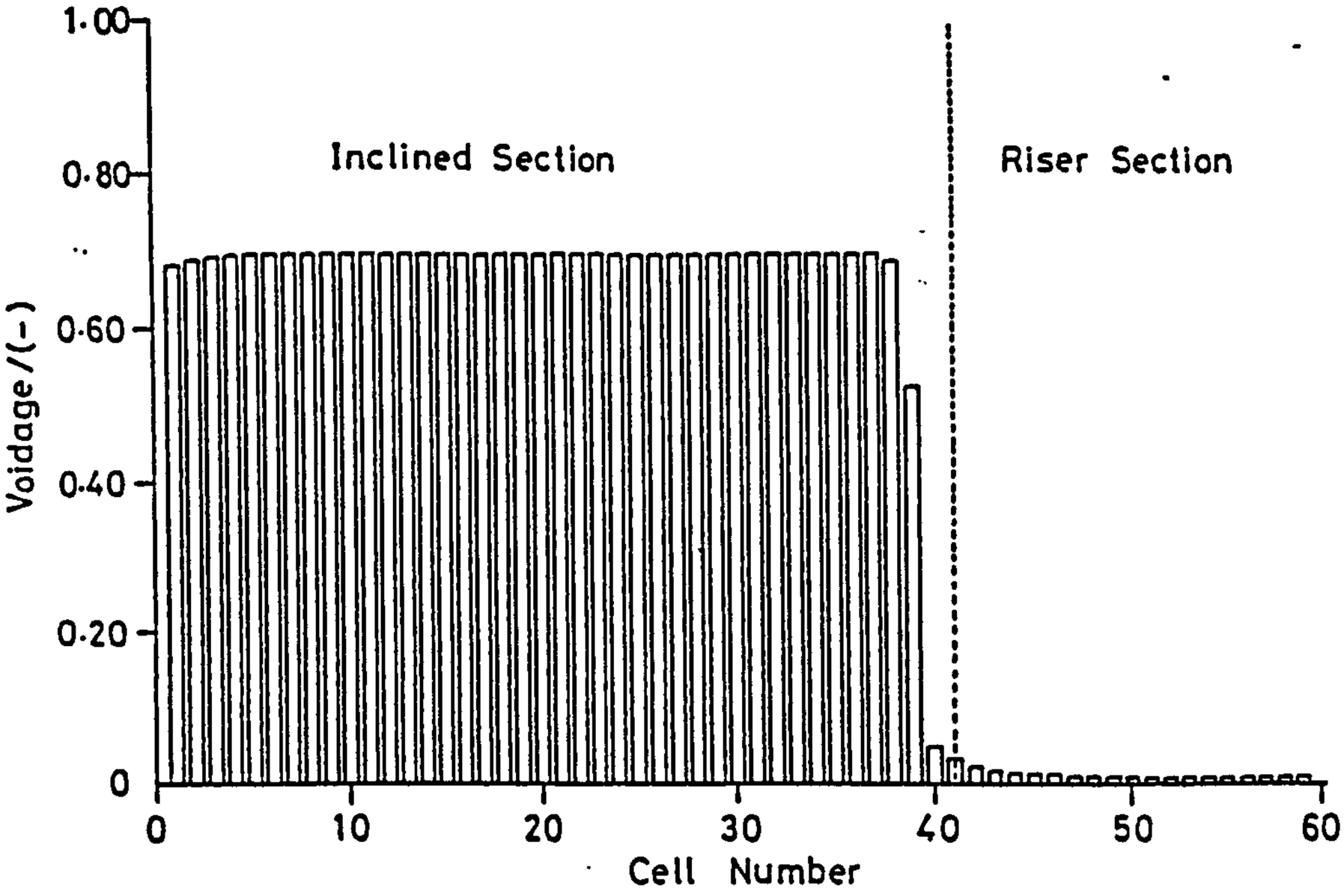


Figure 4.4.13 VOIDAGE ALONG TEST SECTION
TIME = 314 secs
Ugs = 0·18 Uls = 0·34

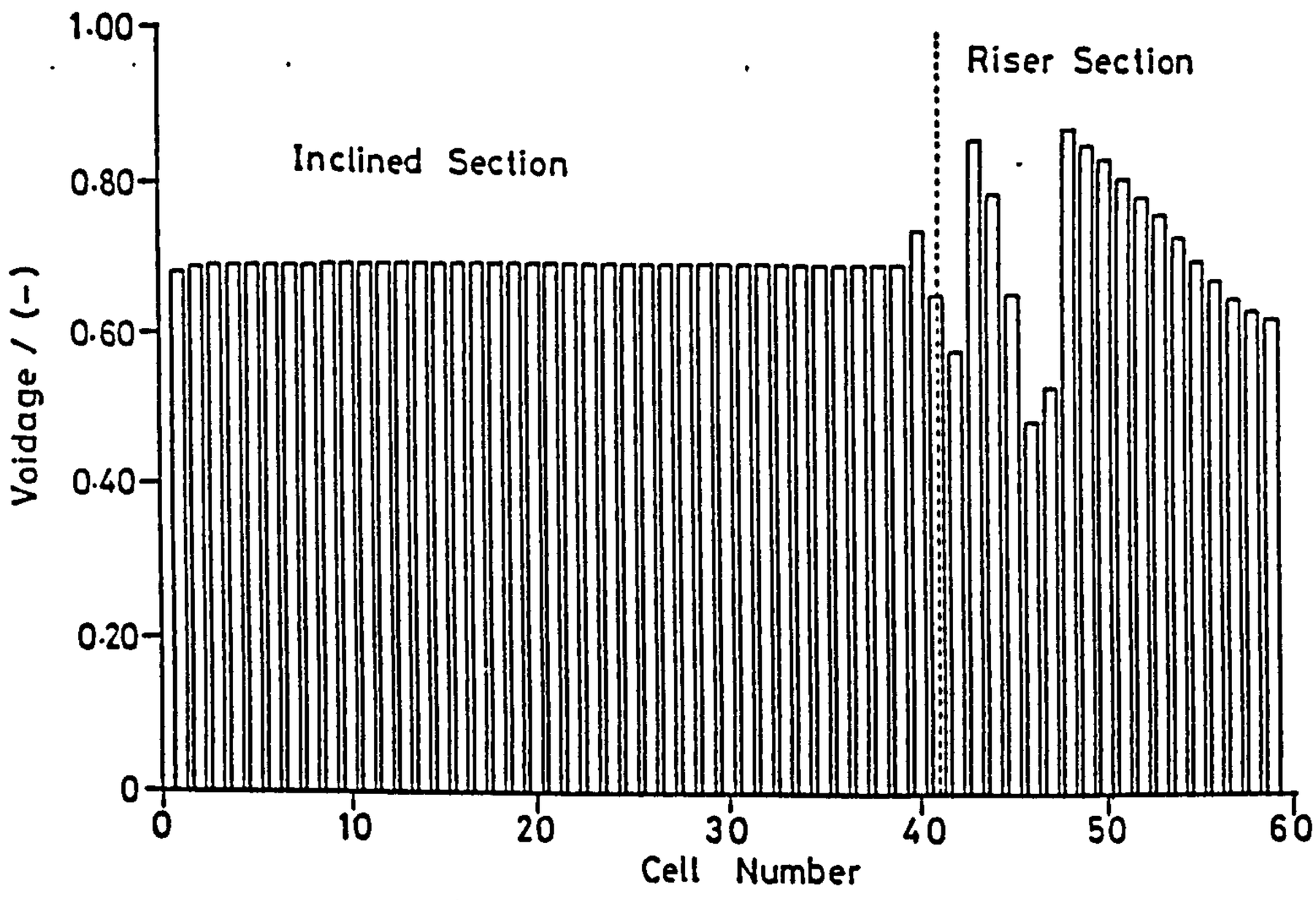


Figure 4.4.14 VOIDAGE ALONG TEST SECTION
TIME = 330 secs
Ugs = 0·18 Uls = 0·34

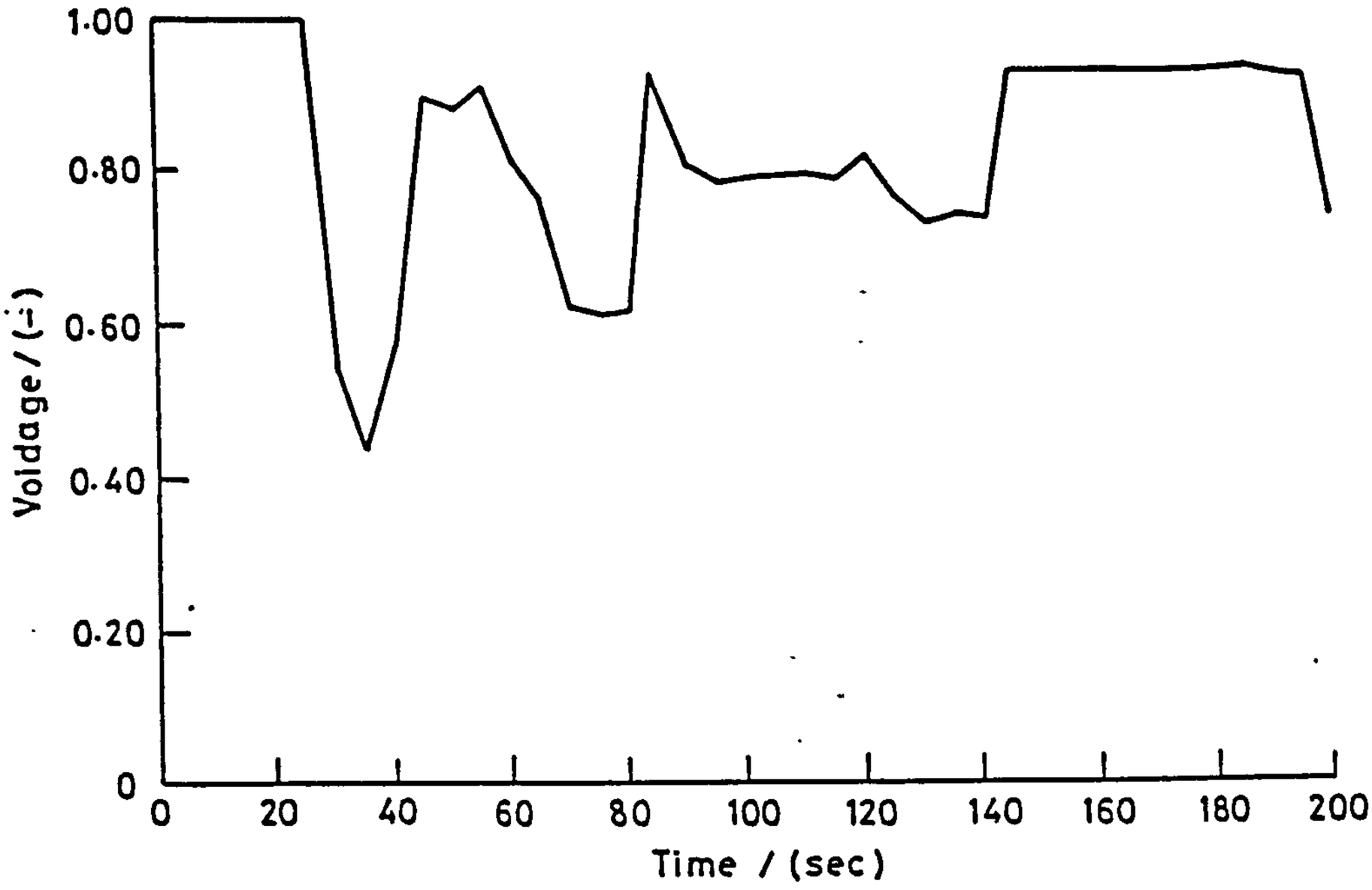


Figure 4.4.15 VOIDAGE VS TIME AT RISER BASE (CELL 42)
Ugs = 3·40 m/s Uls = 0·34 m/s

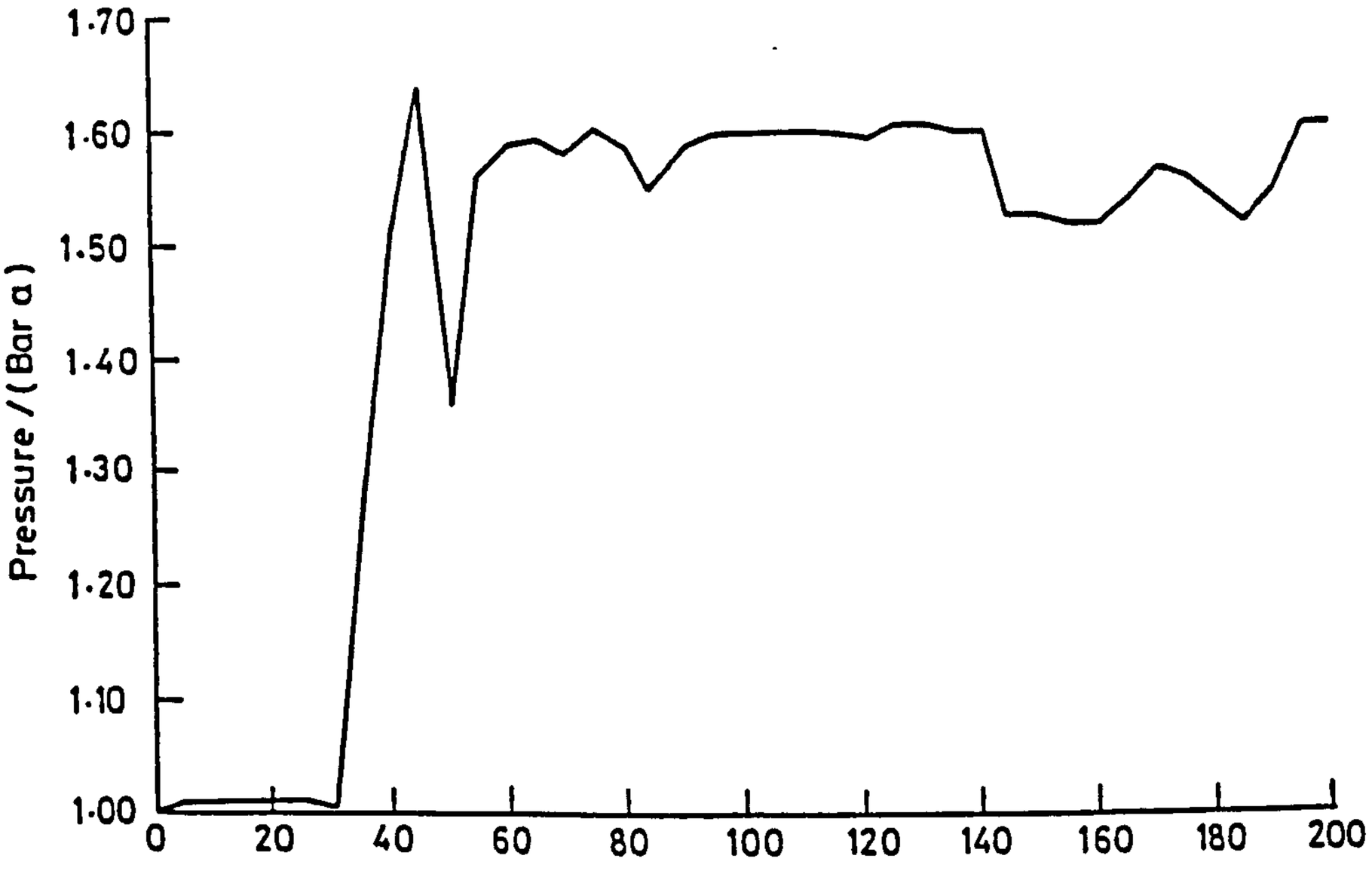


Figure 4.4.16 PRESSURE VS TIME AT RISER BASE (CELL 42)
Ugs = 3·40 m/s Uls = 0·34 m/s

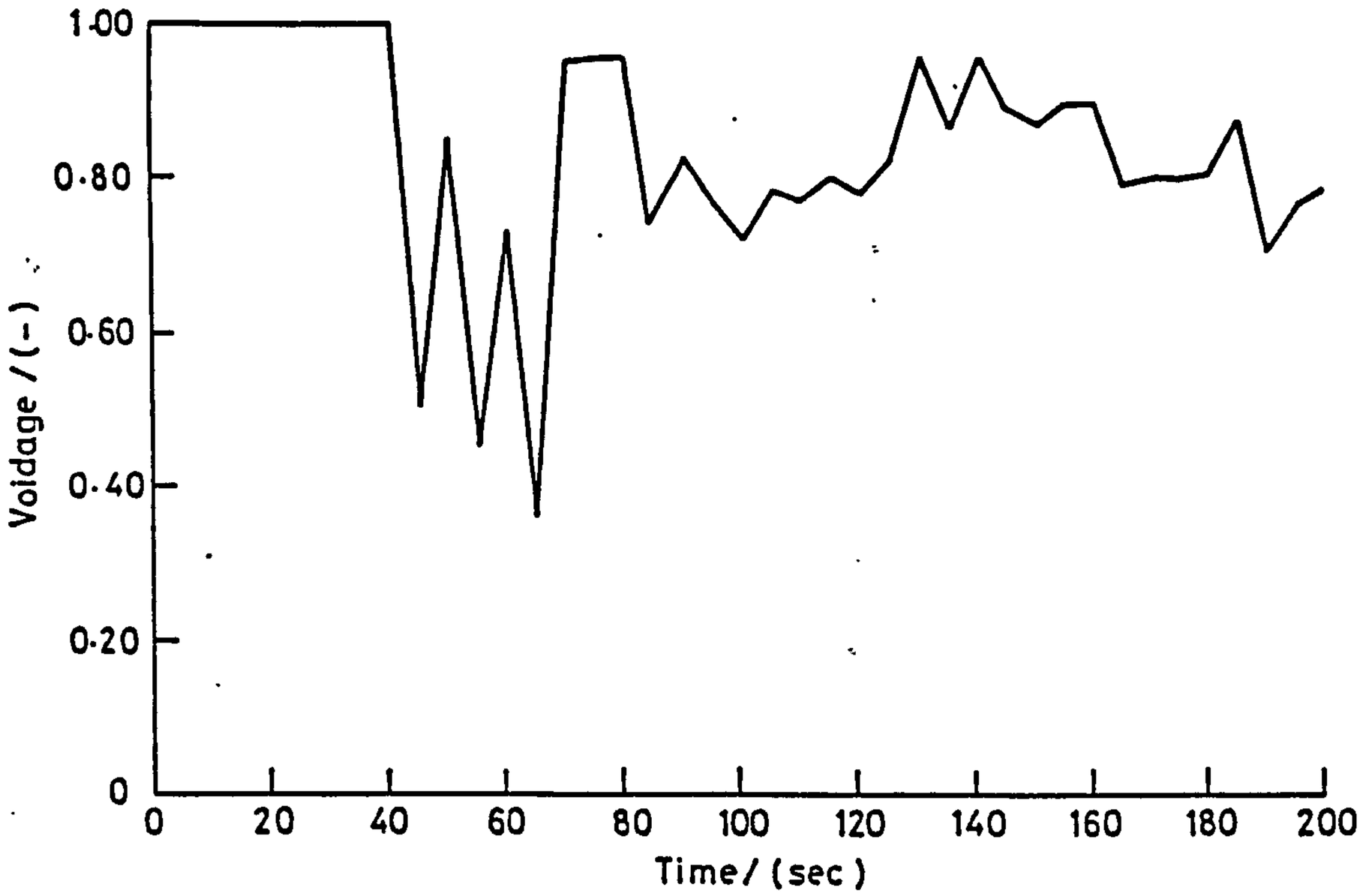


Figure 4.4.17 VOIDAGE VS TIME AT RISER TOP (CELL 59)
Ugs = 3·40 m/s Uls = 0·34 m/s

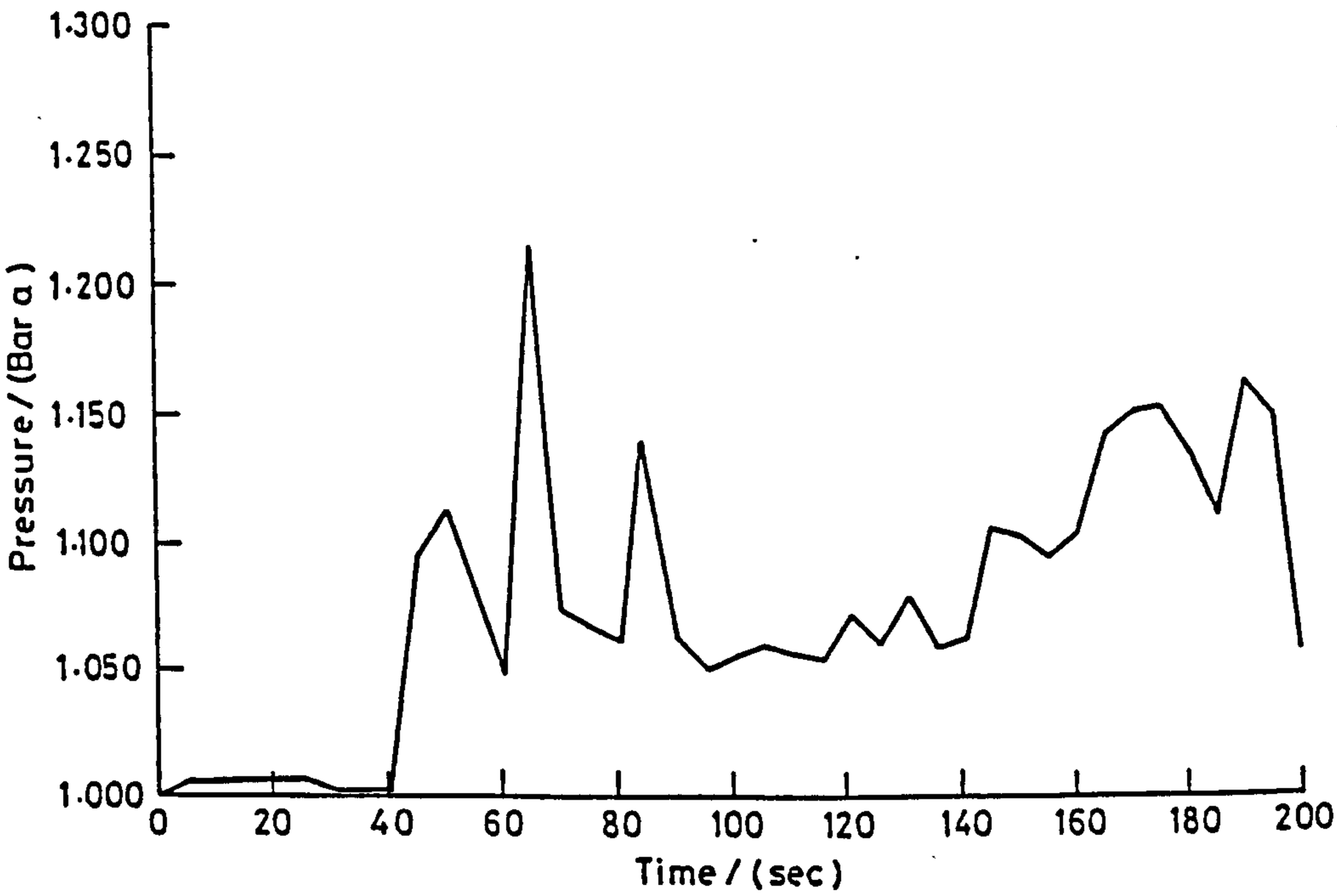


Figure 4.4.18 PRESSURE VS TIME AT RISER TOP (CELL 59)
Ugs = 3·40 m/s Uls = 0·34 m/s

CHAPTER FIVE

ASPECTS OF INTERMITTENT FLOW

New experimental techniques developed for, and critical analysis of, individual aspects of intermittent flow characteristics are discussed in this Chapter. The emphasis of the experimental studies has been to obtain data on quantities which enable the validation/examination of the components of mechanistic models for intermittent flow. This contrasts with the alternative approach of obtaining gross data such as pressure drop to validate a complete mechanistic model of intermittent flow.

In intermittent flow, the slug gathers liquid from the film region ahead of it and sheds liquid from its tail. If the pickup rate exceeds the shedding rate, then the slug grows. Models developed for representing the shedding process are examined in Section 5.1, along with two experiments (see Section 5.1.3 and 5.3.1) specifically addressed at these processes. Another important feature of intermittent flow is the entrapment of gas in the slug body. Section 5.2 presents new visual evidence which indicates the mechanism of this process. In predicting intermittent flows, it is important to know the slug frequency. Usually, empirical correlations are used for this but, clearly, it would be better if the frequency could be predicted from a physical model. Previous attempts at a physical model are assessed in Section 5.4 and the interactions that determine slug frequency discussed.

5.1 SLUG TAIL

A closed mechanistic model of slug flow requires the calculation of the mass picked up from the preceding film at the slug front. In order to obtain this quantity, it is necessary to know the mass flow rate of the liquid and gas in front of the slug in the film/elongated bubble region, and the distribution of fluid across the pipe cross section. Dukler and Hubbard (1975) made the assumption that the gas and liquid are completely separated in the film/elongated bubble region. Hence the liquid volume flow rate in the elongated bubble and the gas volume flow rate in the film are set to zero. The assumption

of Dukler and Hubbard (1975) simplifies the calculation of mass transfer across the slug front, requiring only the knowledge of the film velocity and liquid holdup. Both of these quantities depend upon the process of deceleration in the film behind a slug after shedding takes place. It is therefore necessary, for closure of a mechanistic model, to address the mechanism for shedding at the slug back and the subsequent hydrodynamics of the film. This section uses the above assumption of Dukler and Hubbard (1975) and assesses the models available for slug tail representation.

5.1.1 HYDRODYNAMICS OF THE FILM

Prior to the work of Dukler and Hubbard (1975) the film region was not modelled in detail. Dukler and Hubbard (1975) used a force/momentum balance on the film which takes into account wall shear stress, angle of inclination of the pipe, and the hydrostatic pressure effect. This balance neglected the gas shear at the gas–liquid interface. Maron et al (1982) in their force/momentum balance on the film, take into account gas shear, and also wall friction and the hydrostatic pressure term; however, Maron et al (1982) treated the case of an horizontal rectangular duct and not a round pipe. The analysis necessary to include shear at the gas–liquid interface for a round pipe is examined below.

It will be assumed for the purpose of developing the tail hydrodynamics model that the slug body fluid travels at a uniform velocity. It is convenient to consider the various forces acting on the slug tail in terms of co-ordinates that move with the translational velocity of the slug tail, as shown in Figure 5.1.1. The forces acting on the highlighted control volume are:

(a) The force exerted by the liquid on the gas at the interface, F_i.

(b) The gravitational force, F_G.

(c) The force due to difference in hydrostatic pressure between planes 1 and 2 of the control volume, F_p. It is assumed that the pressure at the gas–liquid interface is constant along the tail profile, and hence contributes no

net force to the control volume.

(d) The force exerted by the wall on the liquid, F_w.

The change of liquid momentum across the control volume must equal the net force experienced:

$$[\varrho_L v_f^2 A_L]_2 - [\varrho_L v_f^2 A_L]_1 = F_w + F_g + F_p - F_i \qquad (5.1.1)$$

where

A_L is the pipe cross–sectional area occupied by the liquid phase.

v_f is the area averaged liquid velocity at position x

ρ_L is the liquid density.

Subscripts 1 and 2 denote entrance and exit planes of the control volume.

Now

$$F_p = [< p > A_L]_1 - [< p > A_L]_2 \qquad (5.1.2)$$

where

<p> denotes the area averaged hydrostatic pressure acting on the liquid area in the plane at right angles to direction x.

Also

$$F_g = \varrho_L A_L g \sin\alpha \, dx \qquad (5.1.3)$$

where

g is the gravitational acceleration.

α is the angle from the horizontal of the pipe axis in the direction of flow.

Substituting Equations 5.1.2 and 5.1.3 in Equation 5.1.1, and allowing dx⇒0:

$$\frac{d(\varrho_L A_L v_f^2)}{dx} = \tau_w S_w + \varrho_L A_L g \sin\alpha + \frac{d(< p > A_L)}{dx} - \tau_i S_i \qquad (5.1.4)$$

where

τ_w is the shear stress acting at the wall–liquid interface.

τ_i is the shear stress acting at the gas–liquid interface.

S_w is the perimeter of the wall–liquid interface.

S_i is the gas–liquid interface width.

The liquid is incompressible so Equation 5.1.4 can be rearranged into the following form:

$$\frac{d(A_L v_f^2)}{dx} = \frac{\tau_w S_w}{\varrho_L} + A_L g \sin\alpha + \frac{1}{\varrho_L}\frac{d(< p > A_L)}{dx} - \frac{\tau_i S_i}{\varrho_L} \qquad (5.1.5)$$

Now consider conservation of mass:

$$v_{f3} A = v_f A_L \qquad (5.1.6)$$

where

v_{f3} is the area averaged liquid velocity at position 3.

A is the pipe cross–sectional area.

The objective of the analysis is to obtain the profile of the slug tail as a function of position. So rearranging Equation 5.1.5 the following equation relating distance to liquid height results:

$$x(h) = \int \frac{\frac{d(A_L v_f^2)}{dh} - \frac{1}{\varrho_L}\frac{d(<p>A_L)}{dh}}{\frac{\tau_w S_w}{\varrho_L} + A_L g \sin\alpha - \frac{\tau_i S_i}{\varrho_L}}\, dh \qquad (5.1.7)$$

Now from Equation 5.1.6 ($A_L\, v_f$) is a constant so Equation 5.1.7 reduces to:

$$x(h) = \int \frac{A_L v_f \frac{dv_f}{dh} - \frac{d(<p>A_L)}{dh}}{\tau_w S_w + \varrho_L A_L g \sin\alpha - \tau_i S_i}\, dh \qquad (5.1.8)$$

The terms comprising the intergrand of Equation 5.1.8 need to be defined. The following standard equations (see Taitel and Dukler, 1976) may be used to calculate the wall–liquid and gas–liquid interfacial shear:

$$\tau_w = \frac{f_L \varrho_L (V_t - v_f)^2}{2} \qquad (5.1.9)$$

$$f_L = \frac{0.046}{\left(\frac{4A_L(V_t - v_f)}{S_w \nu_L}\right)^{0.2}} \qquad (5.1.10)$$

$$\tau_i = \frac{f_i \varrho_G (v_f - v_G)^2}{2} \qquad (5.1.11)$$

$$f_i = \frac{0.046}{\left(\frac{4A_G(v_f - v_G)}{S_w \nu_G}\right)^{0.2}} \qquad (5.1.12)$$

where

f_L is the friction factor for the liquid phase.

f_i is the gas–liquid interfacial friction factor.

V_t is the translational velocity of the slug tail.

ν is the kinematic viscosity of the sub–scripted phase.

Considering Figure 5.1.2 the following relationship for $A_L<p>$ results:

$$A_L < p > = \int_0^h S(y)_i \, \varrho_L g \cos\alpha \, (h - y) \, dy \qquad (5.1.13)$$

$$\Rightarrow \qquad \frac{A_L < p >}{\varrho_L g \cos\alpha} = h \int_0^h S(y)_i \, dy - \int_0^h y S(y)_i \, dy \qquad (5.1.14)$$

now $\frac{dA_L}{dy} = S(y)_i$ so

$$\frac{A_L < p >}{\varrho_L g \cos\alpha} = hA_L - \int_0^h y S(y)_i \, dy \qquad (5.1.15)$$

Let $I = \int_0^h y S(y)_i \, dy$

Now from Figure 5.1.2 it can be seen that

$$S(y)_i = 2\sqrt{Dy - y^2} \qquad (5.1.16)$$

so $I = \int_0^h 2y\sqrt{Dy - y^2} \, dy$

$$= D \int_0^h \sqrt{Dy - y^2} \, dy - \frac{2}{3}\left[(Dy - y^2)^{\frac{3}{2}}\right]_0^h$$

$$= \frac{DA_L}{2} - \frac{2}{3}(Dh - h^2)^{\frac{3}{2}} \qquad (5.1.17)$$

hence $A_L < p > = \varrho_L g \cos\alpha \left[\left(h - \frac{D}{2}\right)A_L + \frac{2}{3}(Dh - h^2)^{\frac{3}{2}}\right]$ (5.1.18)

The derivative of $A_L <p>$ with respect to h is required for Equation 5.1.8. Differentiating Equation 5.1.18 with respect to h the following results:

$$\frac{d(A_L < p >)}{dh} = \varrho_L g A_L \cos\alpha \qquad (5.1.19)$$

The remaining term in Equation 5.1.8 that requires evaluation is dv_f / dh; using Equation 5.1.6 the following term is derived:

$$\frac{dv_f}{dh} = -\frac{A_L S_i v_{f3}}{A_L^2} \qquad (5.1.20)$$

Equations 5.1.6, 5.1.8, 5.1.9, 5.1.10, 5.1.11, 5.1.12, 5.1.19 and 5.1.20 enable the calculation of the profile of the slug tail as a function of position from the rear of the slug.

The inclusion of interfacial shear in the tail representation changes the solution through the intergrand of Equation 5.1.8. The consequences for slug front translational velocity of including interfacial shear in the tail representation are examined below.

In the following discussion all velocities are referenced to a frame moving with the pipe walls, unless explicitly stated otherwise. The height and velocity of the slug tail is necessary for the calculation of the slug front velocity. In the case of the model developed in this section which includes interfacial shear, the film velocity (in a frame of reference moving with the pipe walls) will be greater than that for a model that excludes interfacial shear at a given position behind the slug tail. This statement is true for horizontal pipelines but is only valid for a limited distance from the rear of the slug for inclined pipes. The case of inclined pipes will be discussed latter. The statement results from examination of Equation 5.1.6 which states that the product of the film fluid velocity and the area of the pipe occupied by the pipe is constant. It was noted earlier that by considering conservation of mass Equation 5.1.6 resulted (frame of reference moving with slug tail).

Hence, considering Equation 5.1.6 any increase in final film velocity due to the inclusion of interfacial shear would result in the pipe cross–sectional area occupied by liquid increasing. The purpose behind deriving a slug tail hydrodynamics model is to enable the slug front translational velocity to be calculated.

The following explicit relationship for the slug front translational velocity, V_t is derived in Section 5.3.2.1:

$$V_t = \frac{v_s\varrho_s(1-\varepsilon_s) - \varrho_L v_f(1-\varepsilon_f)}{\varrho_s(1-\varepsilon_s) - \varrho_L(1-\varepsilon_f)} \qquad (5.1.21)$$

where

V_t is the translational velocity of the slug front

v_s is the average slug fluid velocity

v_f is the area averaged liquid film velocity

ε_f is the voidage in the film/elongated bubble region

ε_s is the slug body void fraction

ρ_L is the density of the liquid phase

ρ_s is the density of the slug body fluid.

It can be seen from Equation 5.1.6 that the expression on the top line of Equation 5.1.21 involving the liquid film velocity and voidage will be greater for a slug tail model that includes interfacial shear. This will in turn reduce the value of the top line of Equation 5.1.21 and hence reduce the slug front velocity. The bottom line of Equation 5.1.21 contains a term which is the product of the liquid density and the area of the pipe occupied by the liquid. As stated earlier inclusion of the interfacial shear term in the model of a slug tail results in the increase of the area of the pipe occupied by the liquid tail at a given position from the slug rear. On examination of Equation 5.1.21 it can be seen that the bottom line decreases with increasing slug tail height and hence the slug front velocity increases. The relative effect on the slug front translational velocity of these two competing terms is examined in Figure 5.1.3. The plot shows the slug front translational velocity as a function of film velocity for a liquid slug with a tail translational velocity of 2.4 m/s, a mean fluid velocity of 2 m/s and a constant slug voidages of 1.0, 0.95 and 0.9.

As can be seen from Figure 5.1.3 for the specified flow conditions the effect of including interfacial shear in a tail hydrodynamics model will be to increase the slug front velocity of the preceding slug for gas voidages less than one. This assumes the amount of gas entrained in the slug does not vary with film height/velocity. The faster the liquid film, ie the smaller the length of the elongated bubble between two slugs, the greater will be the effect on slug front translational velocity of inclusion of interfacial shear in tail hydrodynamic models.

The above discussion, as noted earlier in this section, is only partially valid for upwards inclined pipes. For inclined flows the velocity profile of the slug tail depends on the magnitude of the component of gravity acting parallel to the pipe axis. In the case of a model that includes no interfacial shear term the velocity of the film decreases with distance from the slug, reaches zero, and then accelerates in the reverse direction (flows downhill) until the gravity term parallel to the pipe axis and the wall shear are in equilibrium. A model that includes an interfacial shear term may not exhibit this reversal of flow if the inclination of the pipe is such that the interfacial shear can negate the gravity term parallel to the pipe axis.

5.1.2 TAIL TRANSLATIONAL VELOCITY

The slug tail representations described above require as an initial condition the translational velocity of the leading point of the slug tail. Taitel and Dukler (1975) and Maron et al (1982) assumed that the slug is non–growing to gain this information, with the slug tail translational velocity equivalent to the slug front translational velocity. While this representation may be adequate for modelling steady–state slug flow it does not allow models to be formed for flow in short pipelines, the entrance region of long pipelines, or discontinuities in pipeline geometry. In these cases it is necessary to have a method for calculating the slug tail velocity which is independent of the slug front translational velocity.

Figures 5.1.4 and 5.1.5 show a region just upstream of the slug tail leading point in which the liquid profile decreases rapidly. This region seems analogous to the liquid

profile formed when a dam ruptures, with liquid initially being separated at a fixed level from a dry region. Jepson (1987), making this observation, suggested that the tail of a slug could be represented by a dam break and presented the final result of the analysis of Stoker (1957) for slug flow in rectangular ducts. Jepson (1987) also suggested that the work of Stoker (1957) could be applied to circular channels by assuming an equivalent rectangular channel:

$$V_t = U_S + \left(\frac{\pi}{4}\right)^{0.5} (gD)^{0.5} \qquad (5.1.22)$$

In his work on water waves, Stoker (1957) analysed the flow of fluid in rectangular ducts following the rupture of such a dam. Applying the method of characteristics to the shallow water equations, Stoker (1957) was able to obtain analytical solutions for the behaviour of the liquid both upstream and downstream of the initial dam position as a function of time, including the velocity of the wave progressing into the initial liquid layer. The work of Stoker (1957) suggests a method for obtaining the translational velocity of the slug tail, the relevance of this approach depending on the shallow water equations being valid in the region just downstream of the slug.

Gardner (1985) extended the work of Stoker (1957) to the case of circular pipes. Gardner (1985) presented an analytical solution method for the shallow water equations which enables the study of dam breaks in circular tubes. Gardner (1985) aimed to develop a benchmark test for large reactor safety codes and compared his analytical solution for drainage of a tube partially filled with stagnant water, which is suddenly released from one end of the pipe, with simulations using RELAP (a best estimate thermal hydraulics code). The analytical method presented was limited to pipe liquid holdups of 0.85 or less, and hence could not be directly applied to a slug analysis, ie drainage of a tube completely filled with stagnant water. Black et al (1988) continued Gardners aim of benchmark tests for large reactor safety codes, comparing the analytical solution

of Gardner against predictions of the TRAC code. The results obtained, after modification of the TRAC code, showed good agreement with the analytical solution.

The shallow water equations applied by Gardner (1985) for a circular duct are:

$$\frac{\partial A_L}{\partial t} + \frac{\partial u A_L}{\partial x} = 0 \qquad (5.1.23)$$

$$\frac{\partial u}{\partial t} + u\frac{\partial u}{\partial x} + g\frac{\partial h}{\partial x} = 0 \qquad (5.1.24)$$

where

A_L is the crossectional area of the duct occupied by the liquid

u is the area averaged fluid velocity at time t and position x

h is the liquid height at time t and position x.

These equations neglect any source terms such as wall or interfacial shear and assume that the pressure at interface of the liquid and the surrounding fluid is equivalent for both fluids and does not vary with position or time. In the slug tail region where the liquid profile decreases rapidly it does not seem unreasonable to neglect the source terms in comparison with the hydrostatic term in Equation 5.1.23. In addition it will be assumed that over the small tail length considered the change in pressure due to the gas flow is small at the interface of the liquid and gas.

The following presentations are based on Gardner's (1985) analysis but the approach taken enables the study of pipes with liquid holdup greater than 0.85 which is necessary for investigating the application of the dam break analysis to slug flow.

Equation 5.1.23 is rearranged by substituting $dA_L = w\ dh$ where w is the width of the gas–liquid interface:

$$w\frac{\partial h}{\partial t} + A_L\frac{\partial u}{\partial x} + wu\frac{\partial h}{\partial x} = 0 \qquad (5.1.25)$$

adding and subtracting Equation 5.1.25 from 5.1.24 and rearranging gives:

$$\left[\frac{\partial}{\partial t} + \left(u +, - \left(\frac{A_L g}{w}\right)^{0.5}\right]\frac{\partial}{\partial x}\left[u +, - \int\left(\frac{gw}{A_L}\right)^{0.5} dh\right] = 0 \quad (5.1.26)$$

These partial differential equations form an hyperbolic set for which real characteristics exist. The characteristic directions defined by Equation 5.1.26 are:

$$\frac{dx}{dt} = u +, - \left(\frac{A_L g}{w}\right)^{0.5} \qquad (5.1.27)$$

along which the Rieman invariants (see Jeffrey, 1976)

$$u +, - \int\left(\frac{gw}{A_L}\right)^{0.5} dh \qquad (5.1.28)$$

are constant.

Let $c = (A_L g/w)^{0.5}$ and $f(c) = \int\left(\frac{gw}{A_L}\right)^{0.5} dh$. Initially u is zero and therefore there is a positive characteristic of slope c_o in the x,t plane. Consider Figure 5.1.6 which shows a second positive characteristic with two negative characteristics intersecting at points 1 and 2.

Along the straight ($x = c_o t$) positive characteristic the function f(c) is constant. Hence considering the two negative characteristics:

$$u_1 - f(c_1) = -f(c_0)$$

$$u_2 - f(c_2) = -f(c_0) \qquad (5.1.29)$$

and along the second positive characteristic:

$$u_1 + f(c_1) = u_2 + f(c_2) \qquad (5.1.30)$$

The only solution to Equations 5.1.29 and 5.1.30 is:

$$u_1 = u_2 \qquad c_1 = c_2$$

and therefore the second positive characteristic is a straight line of constant water depth along it:

$$\frac{x}{t} = u + c \qquad (5.1.31)$$

and from the negative characteristic.

$$u = f(c) - f(c_0) \qquad (5.1.32)$$

subsituting Equation 5.1.32 into 5.1.31 gives:

$$\frac{x}{t} = c + f(c) - f(c_0) \qquad (5.1.33)$$

Equation 5.1.33 allows the liquid profile to be calculated as a function of distance x at a given value of time t.

The velocity of the leading point of the slug tail is required. In a frame of reference moving at the slug body area averaged fluid velocity this is c_o:

$$c_0 = \left(\frac{gA}{w_0}\right)^{0.5} \qquad (5.1.34)$$

where A = pipe area

w_o = interface width at top of the pipe.

Translating to a frame of reference moving with the pipe wall, the velocity of the leading point of the slug tail is given by:

$$V_t = V_s + \left(\frac{gA}{w_o}\right)^{0.5} \qquad (5.1.35)$$

where V_S is the average velocity of the fluid in the slug body.

As a liquid layer approaches the top of the pipe the interface width tends to zero. Hence V_t tends to infinity. This result is analytically correct but physically absurd. The result is to be expected as a small volume of liquid displaced at the pipe top leads to an infinite uncovering of a line parallel to the tube axis. Thus, in the above form, an area averaged one–dimensional dam break theory for a circular tube cannot represent slug flow.

To calculate the slug tail translational velocity by dam break theory it is preferable to model in three dimensions; no analytical solution being available to the authors knowledge. Such a numerical computation would be expensive for modelling an isolated slug and hence could not be used for multiple slug dynamic calculations. A simple analytical adaption of the above work is presented below to provide an explicit expression for the slug tail translational velocity. The following one–dimensional area averaged equations can be obtained by considering Figure 5.1.1 in the absence of wall friction and interfacial shear (in a frame of reference moving with the pipe walls):

$$\frac{\partial(uA_L)}{\partial t} + \frac{\partial(u^2A_L)}{\partial x} + \frac{1}{\varrho_L}\frac{\partial(< p > A_L)}{\partial x} = 0 \qquad (5.1.36)$$

$$\frac{\partial A_L}{\partial t} + \frac{\partial(uA_L)}{\partial x} = 0 \qquad (5.1.37)$$

where

A is the crossectional area of the duct occupied by the liquid

u is the area averaged fluid velocity at time t and position x

Let $<>_z$ represent a length averaged quantity in a direction perpendicular to the z direction, and h_z liquid height at position z (see Figure 5.1.7). The following assumptions are made about the flow:

$$d(uA_L) = < u >_z h_z dz$$

$$(uA_L) = 2\int_0^R < u >_z h_z dz \qquad (5.1.38)$$

$$dA_L = h_z dz$$

$$A_L = 2\int_0^R h_z dz \qquad (5.1.39)$$

$$d(< p > A_L) = < p >_z h_z dz$$

$$< p >_z = \frac{1}{h_z}\int_0^{h_z} \varrho_L g(h_z - y)dy = \frac{\varrho_L g h_z}{2}$$

$$(< p > A_L) = \varrho_L g \int_0^R h_z^2 dz \qquad (5.1.40)$$

These assumptions allow the fluid velocity and interfacial height to vary parallel to the pipe axis and in the horizontal plane at right angles to the pipe axis. The latter is denoted as the y direction. No coupling is present to allow flow in the z direction to be induced by the hydraulic gradient in the z direction.

Substituting the above in Equation 5.1.37:

$$2\frac{\partial\int_0^R h_z dz}{\partial t} + 2\frac{\partial\int_0^R < u >_z h_z dz}{\partial x} = 0$$

$$\int_0^R \left(\frac{\delta h_z}{\delta t} + \frac{\delta(< u >_z h_z)}{\delta x}\right) dz = 0$$

$$\frac{\partial h_z}{\partial t} + \frac{\partial(< u >_z h_z)}{\partial x} = 0 \qquad (5.1.41)$$

substituting in Equation 5.1.36:

$$\partial\int_0^R < u >_z h_z dz \qquad \partial\int_0^R < u >_z^2 h_z dz \qquad \partial\int_0^R h_z^2 dy$$

$$2\frac{}{\partial t} + 2\frac{}{\partial x} + g\frac{}{\partial x} = 0$$

$$\int_0^R \left(2\frac{\partial(< u >_z h_z)}{\partial t} + 2\frac{\partial(< u >_z^2 h_z)}{\partial x} + g\frac{\partial h_z^2}{\partial x}\right) dz = 0$$

$$\frac{\partial(< u >_z h_z)}{\partial t} + \frac{\partial(< u >_z^2 h_z)}{\partial x} + g h_z \frac{\partial h_z}{\partial x} = 0 \qquad (5.1.42)$$

using Equation 5.1.41 in 5.1.42:

$$\frac{\partial < u >_z}{\partial t} + < u >_z \frac{\partial < u >_z}{\partial x} + g\frac{\partial h_z}{\partial x} = 0 \qquad (5.1.43)$$

Equations 5.1.41 and 5.1.43 can be solved using the method of the last section:

$$\frac{x}{t} = c + 2\sqrt{(gh_z)} \qquad (5.1.44)$$

$$c = \sqrt{(gh_z)}$$

and hence the velocity of the leading point of the slug tail in a frame of reference moving with the pipe walls is $v_s+(gd)^{0.5}$ which is finite. This analysis, as expected, has reduced to that for a dam break in a rectangular channel, with each line of fluid in the y direction at a given cross–section forming a rectangular duct.

Implicit in this work so far has been the assumption that the leading point (the position on the gas–liquid interface of the slug tail which is nearest the slug front) of the slug tail is located at the top of the tube and the flow in the slug body is uniform. Experiments show that the leading point of the slug tail is located below the tube top (see Figures 5.1.4 and 5.1.5) and Kvernvold et al (1984) demonstrated that the liquid velocity profile in the slug body is not uniform.

Obviously a rigourous three dimensional simulation is the ideal method to locate the position of the leading point of the slug tail. As pointed out earlier such a computation would be very expensive and could not be used for multiple slug dynamic calculations; some preliminary work in this direction is reported by Hope (1990). In order to investigate the effect of slug body velocity profile on the velocity of the leading point of the slug tail, without going to a three dimensional simulation, the following assumptions are made about the flow:

(1) The leading point of the slug tail lies on the vertical centre line of the pipe (symmetry)

(2) A boundary layer develops from the mixing zone at the front of the slug to the rear. Maron et al (1982) used the 7 th power law for turbulent flow to represent

the velocity profile in the slug body. The expressions used by Maron et al (1982) for velocity profile (moving co–ordinates) and boundary layer thickness have been applied in this work:

$$\frac{u_y}{V_s} = 1 - \left(\frac{y}{\delta}\right)^{1/7} \qquad (5.1.45)$$

$$\delta = 1.01z\left(\frac{V_s z}{\nu_L}\right)^{-0.2} \qquad (5.1.46)$$

$$z = x - l_m \qquad (5.1.47)$$

where

u_y is the velocity in the horizontal direction at vertical co–ordinate y and axial co–ordinate z.

V_s is the area averaged velocity in the slug body.

x is the axial (horizontal) co–ordinate (from slug front to slug tail).

δ is the boundary layer thickness.

ν_L is the liquid kinematic viscosity.

l_m is the length of the slug mixing region.

(3) The leading point of the slug tail occurs at the point on the vertical centre line where $(gh_y)^{0.5} + u_y$ is a maximum. The velocity u_y is the local fluid velocity at vertical co–ordinate y and is obtained from the boundary layer analysis.

It is interesting to view the liquid profile, calculated from Equation 5.1.44, which results when a tube full of liquid falls into a dry pipe following a rupture of a dam. Figure 5.1.8 shows the variation of interfacial height with axial and radial distance for this solution. This would represent the slug tail profile for flow in a frictionless tube. Obviously it is necessary to perform a two–dimensional analysis to include hydrostatic variation in the radial direction.

Figure 5.1.9 shows the leading point height obtained from the above criteria for a pipe diameter of 76 mm and mean slug velocity of 1 m/s, as a function of boundary layer

thickness. The slug tail leading point height decreases as the boundary layer thickness increases. The latter is equivalent to the slug length increasing. Figure 5.1.10 shows the velocity of the leading point as a function of boundary layer thickness for various pipe radii. Figures 5.1.11 to 5.1.15 show in detail for each pipe radius the variation of the leading point velocity with boundary layer thickness. The velocity of the slug tail decreases as the pipe radius decreases as one would expect. Also the variation of velocity with boundary layer thickness decreases as the pipe radius increases.

In contrast to the unsteady–state models based on dam break theory, Ruder et al (1988) suggested that the tail can be modelled as a "Benjamin bubble". The analysis of Benjamin (1968) enabled the following solution to be obtained by Ruder et al (1988) for the slug tail translational velocity, V_t:

$$V_t = (U_L + U_G) + 0.542(gD)^{0.5} \qquad (5.1.48)$$

5.1.3 PUSHOUT EXPERIMENTS

The steady–state model of Ruder et al (1988) and the models based on dam break theory predict the velocity of a slug tail for an unaerated slug or an aerated slug with the assumption of homogeneous flow in the slug body.

This assumption of homogeneous flow is found on visual observation of intermittent flow not to hold over the complete range of gas flowrates for which intermittent flow exists. It is observed that the leading point of the slug tail progresses through a section of the slug consisting of liquid as the continuous phase with small dispersed bubbles and then reaches a section consisting of a large gas bubble at the top of the pipe with liquid flowing under the bubble. When the leading point of the tail reaches the gas bubble it takes a step jump in position to the front of the ex–gas bubble. The model discussed in the above section are designed to represent the velocity of the slug tail

through a homogeneous region but cannot represent the enhancement of the slug tail velocity due to these jumps in position at large gas bubbles.

In–order to test the validity of the above analysis over a wide range of gas flowrates it is necessary to remove the jump component of slug tail velocity. In natural intermittent flow, calculation of the flow component of tail velocity for validation would require the measurement of the true tail velocity over a given length of pipeline and the subtraction of the distance jumped by the slug tail from this pipeline length. In view of the random nature of intermittent flow this approach would be difficult to implement. The following documents an alternative method of validating the slug tail analysis discussed in Sections 5.1.1 and 5.1.2 above.

5.1.3.1 Experiment

Validation of the analysis requires measurement of the rate of advance of the tail of a section of homogeneous fluid which is advancing down a pipe at a known velocity. To achieve this, liquid ejection or "pushout" experiments, were carried out in which a tube was prefilled with water and this water then ejected (pushed out) by feeding a known flow of air into one end of the tube. The rate of advance of the interface (analogous to the slug tail) could then be measured and the liquid shedding rate determined.

The specific experimental configuration of the 10 m low pressure test rig is shown in Figure 5.1.16. The straight ten metre long test section ends in an inclined section of pipeline, the exit of which has a centre line one diameter above the centre line of the test section. Wire probes located at three positions along the test section are used to monitor the tail position with time. The following experimental sequence was used.

The water pump transfers liquid from the tank to the test section until all air is expelled from the test section and inclined pipe. The pump is switched off and valves linking the test section to the liquid tank closed to prevent air ingress into the test section and inclined pipe. At this point the instrumentation is monitored and the air supply introduced to the entrance of the test section. The air is derived from the site supply and a constant flow is arranged by making the flow across the inlet valve critical. Having set

the position of the valve and the upstream pressure, the flowrate (which is unaffected by the downstream pressure) can be measured by an orifice plate. The air enters the pipe and forms an interface which advances down the pipe. Initially, the liquid accelerates but, eventually, a state is reached at which the interface moves at a steady velocity corresponding to the known air input flowrate plus the shedding rate. This allows the shedding rate to be determined. The interface is detected as it passes each wire probe and the pressure profile behind the liquid slug monitored to determine when the acceleration phase of the experiment is complete. The distance between each set of wire probes is known so given the time taken for the leading point of the air–water interface to pass between two probes the velocity of the simulated slug tail can be calculated.

5.1.3.1 Results

Figure 5.1.17 shows the results taken on the low pressure rig, presenting the tail velocity as a function of gas superficial velocity. Two sets of data are presented corresponding to the calculation of interface velocity between the first and second wire probes and the velocity calculated from the time it takes the interface to pass between the second and third wire probes. As can be seen from Figure 5.1.17, the velocity of the tail increases with gas superficial velocity and that the velocities calculated from the two probe combinations are equivalent.

Pushout experiments were conducted for gas superficial velocities greater than the limit of 2.5 m/s shown in Figure 5.1.17, but, it could not be proved that a steady interface velocity was obtained in the 10 m low pressure test rig. The velocity calculated for the interface between the first and second wire probes and the velocity of the interface between the second and third wire probes were not equivalent. Figure 5.1.18 shows a pressure and wire probe signal recording for a pushout experiment at a gas superficial velocity of 2.8 m/s. As can be seen the interface passes the first wire probe position before a steady pressure is obtained. Hence the less than ideal length of the 10 m low pressure test section limits the pushout results to approximately 2.5 m/s. The

interface velocity at higher gas superficial velocities may be investigated in the future using the longer pipelength of the experimental facility described in Chapter 6.

Models available for representing the processes at the slug tail are compared against the experimental data in Figure 5.1.19. The tail velocity data has been converted to a shedding rate (defined in Section 2.3, Equation 2.3.1) to enable comparison with not only tail translational velocity models, discussed in Section 5.1.2, but, also with the work of Dukler and Hubbard (1975) and Maron et al (1982). As can be seen the relationships for shedding rate developed by Dukler and Hubbard (1975) and Maron et al (1982) do not predict the form or magnitude of the experimental data. Also, the unsteady–state models of Jepson (1987) and Equation 5.1.43 significantly overpredict the experimental shedding rate. The predictions of the steady–state model suggested by Ruder et al (1988) give very good agreement with the experimental data.

In summary, this Section has examined the models available for representing the slug tail. A novel experimental technique has been developed to allow slug tail models to be validated for the case of unaerated slugs. Comparison of the models against experimental data shows that the model of Ruder et al (1988) best represents the shedding rate of the slug tail.

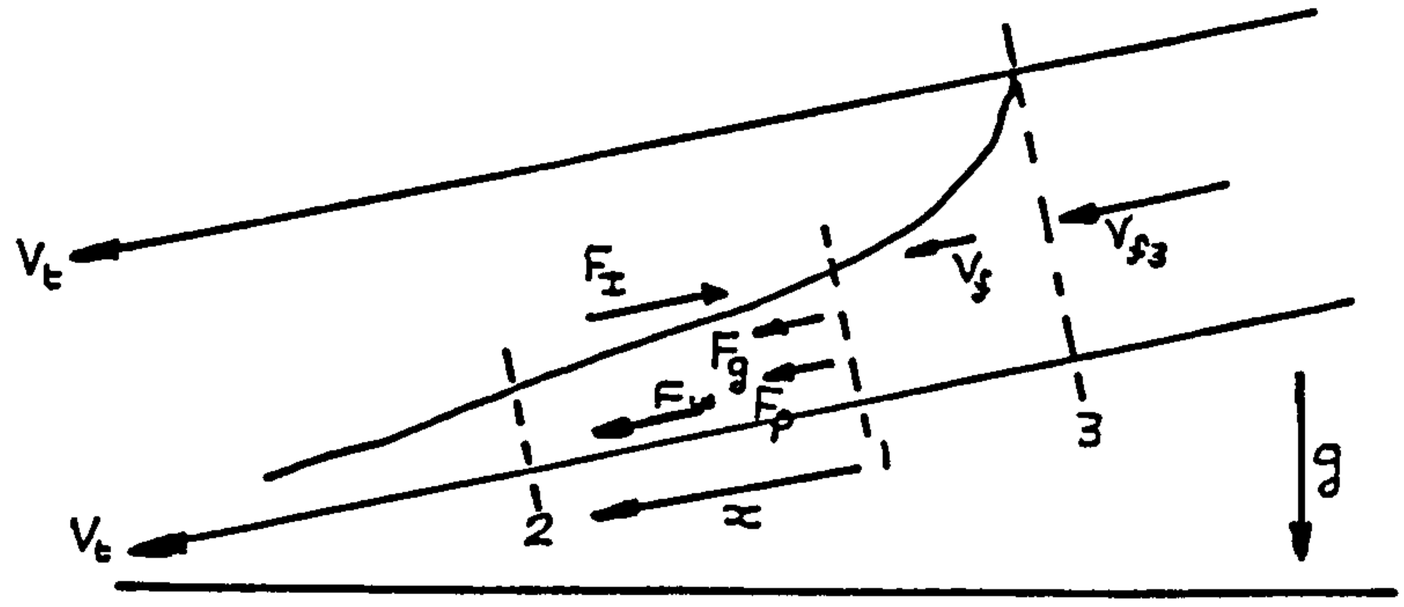


Figure 5.1.1 Forces acting on a slug tail (moving co–ordinates).

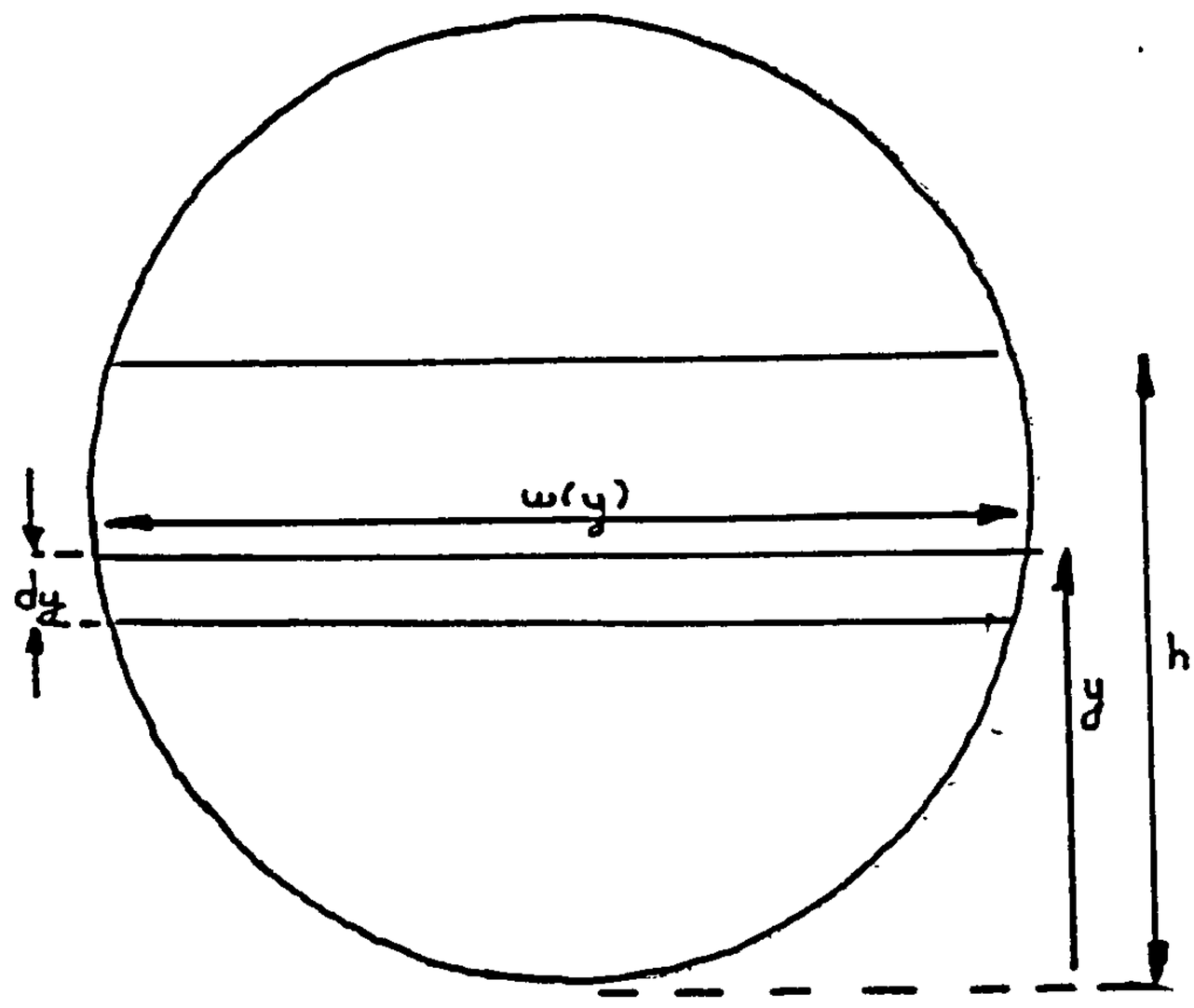


Figure 5.1.2 Definition of y co–ordinate for a circular pipe geometry.

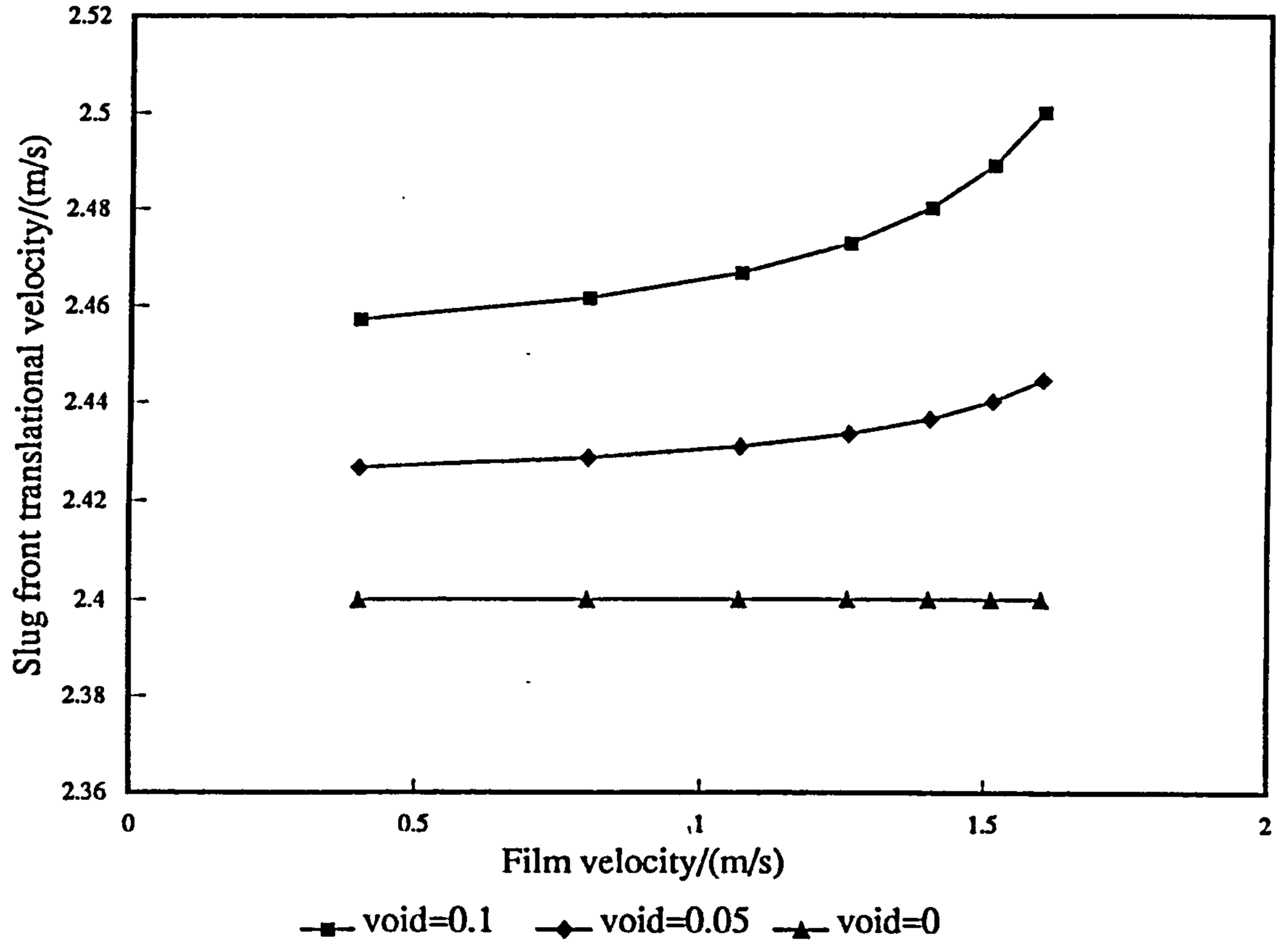


Figure 5.1.3 Effect on slug front translational velocity of interfacial shear

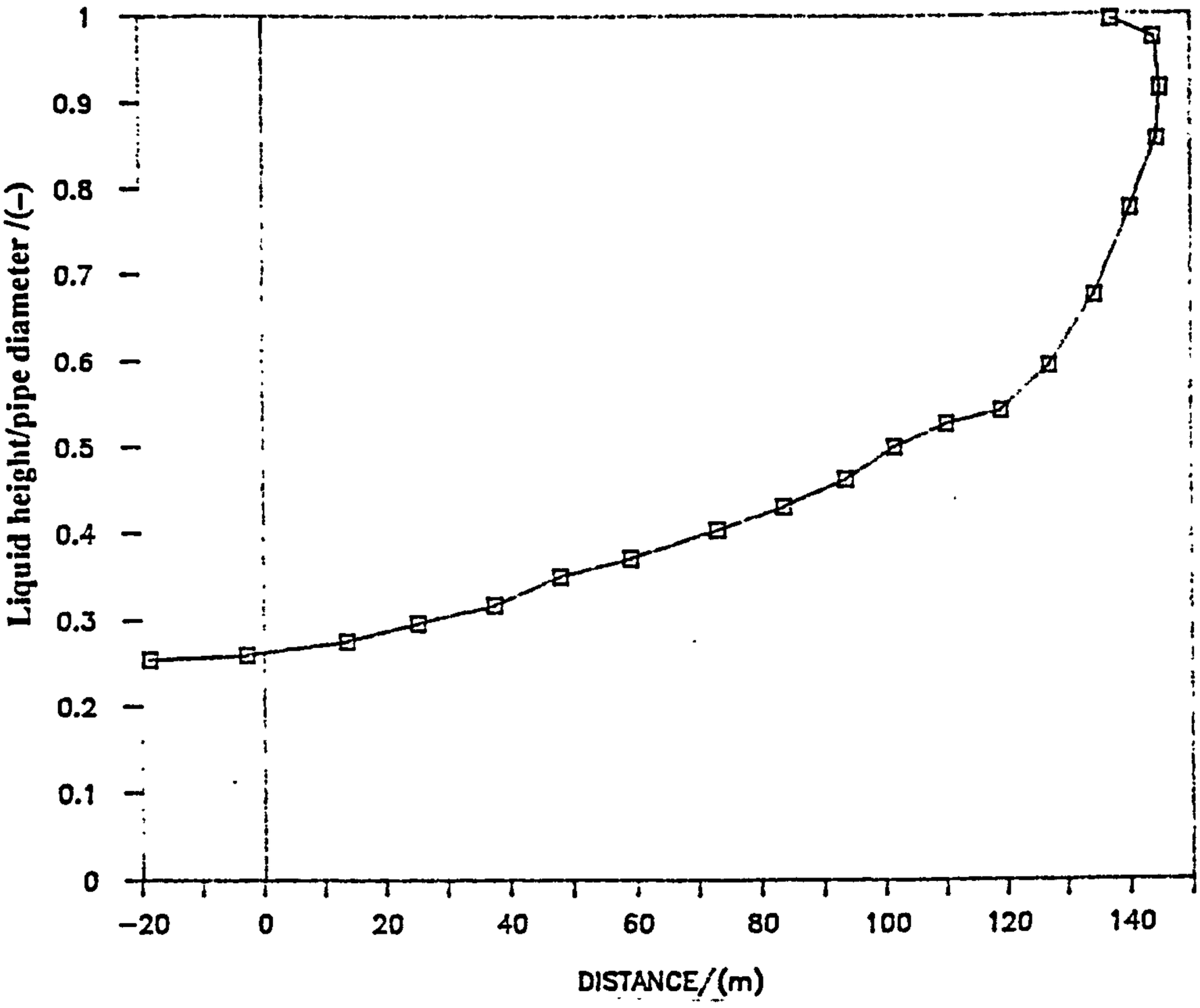


Figure 5.1.4 Experimental slug tail profile

(U_{LS}=0.248 m/s, U_{GS}=2.23 m/s, Frame 5276)

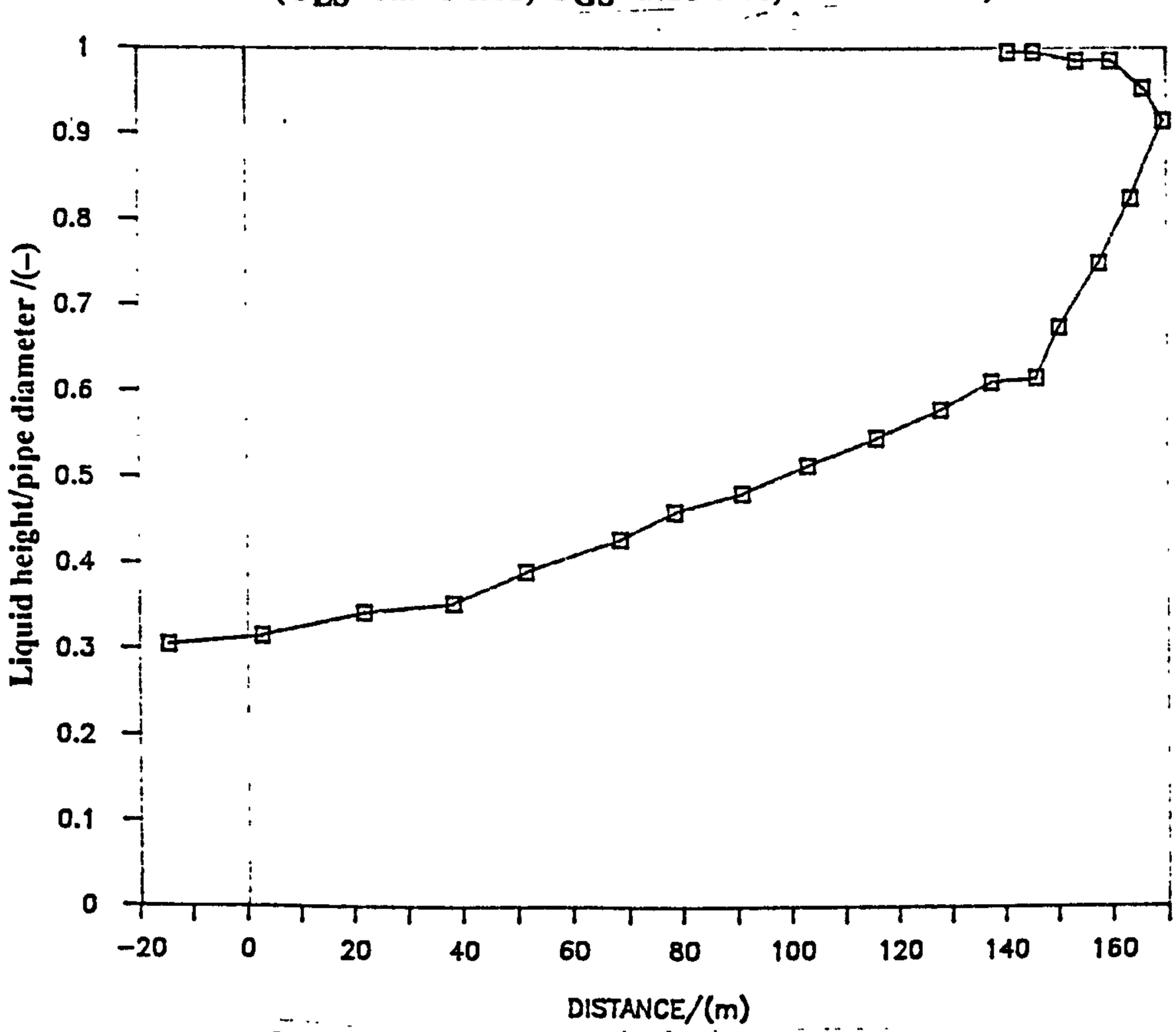


Figure 5.1.5 Experimental slug tail profile

U_{LS}=0.295m/s, U_{GS}=1.84 m/s, Frame 134842)

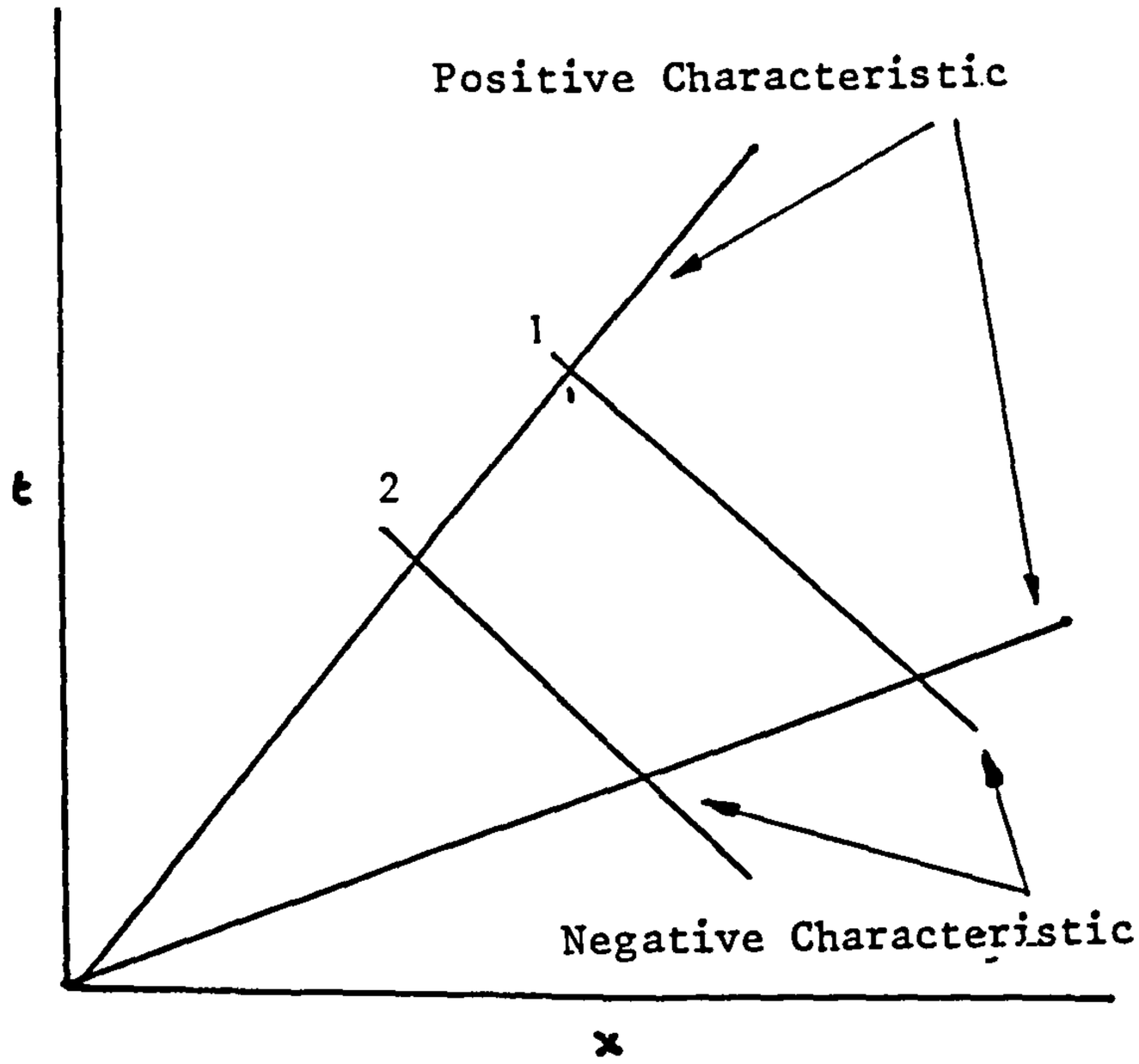


Figure 5.1.6 Representation of characteristics of Equation 5.1.26.

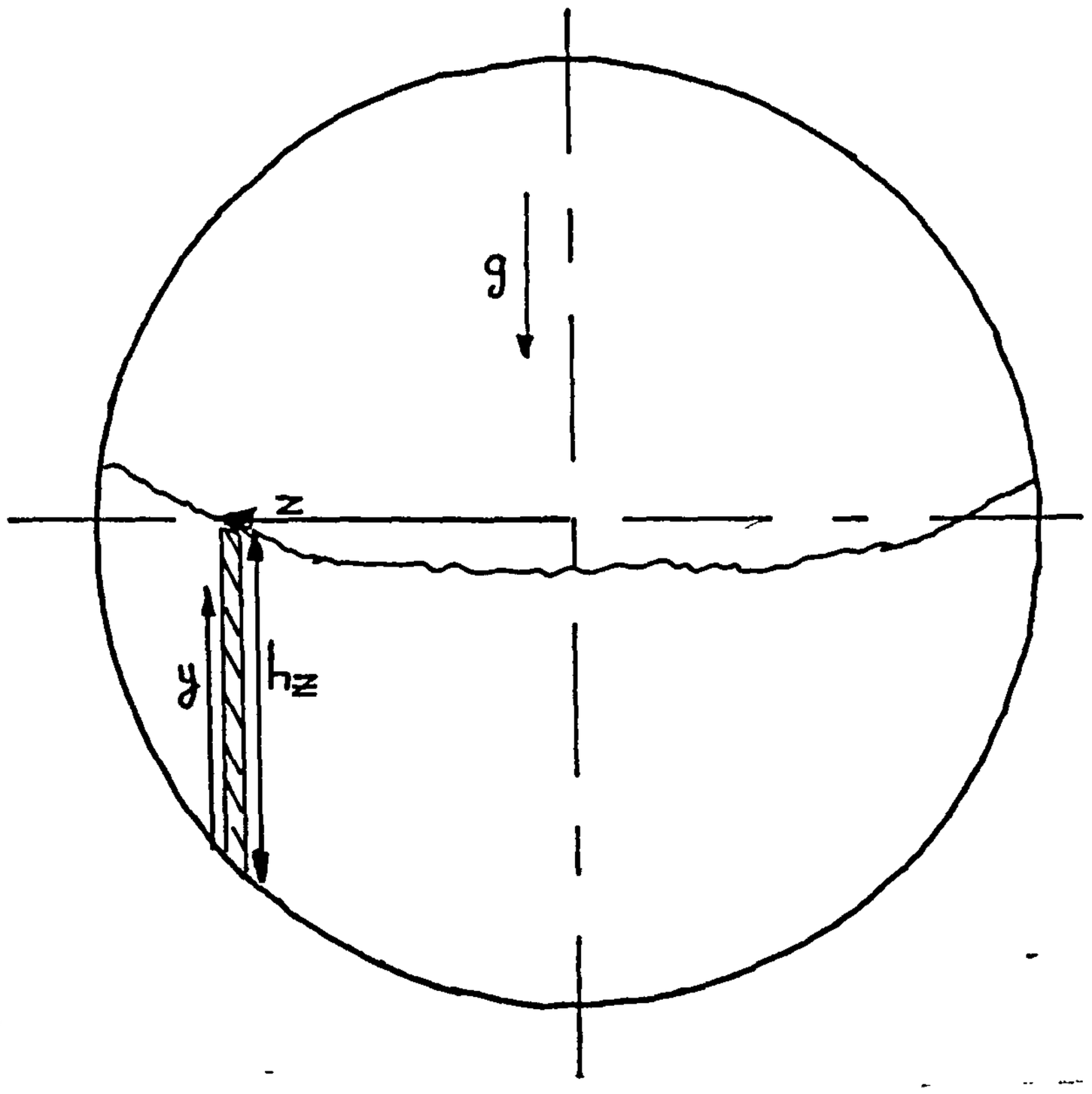


Figure 5.1.7 Definition of flow quantities relative to z co-ordinate for a circular pipe geometry.

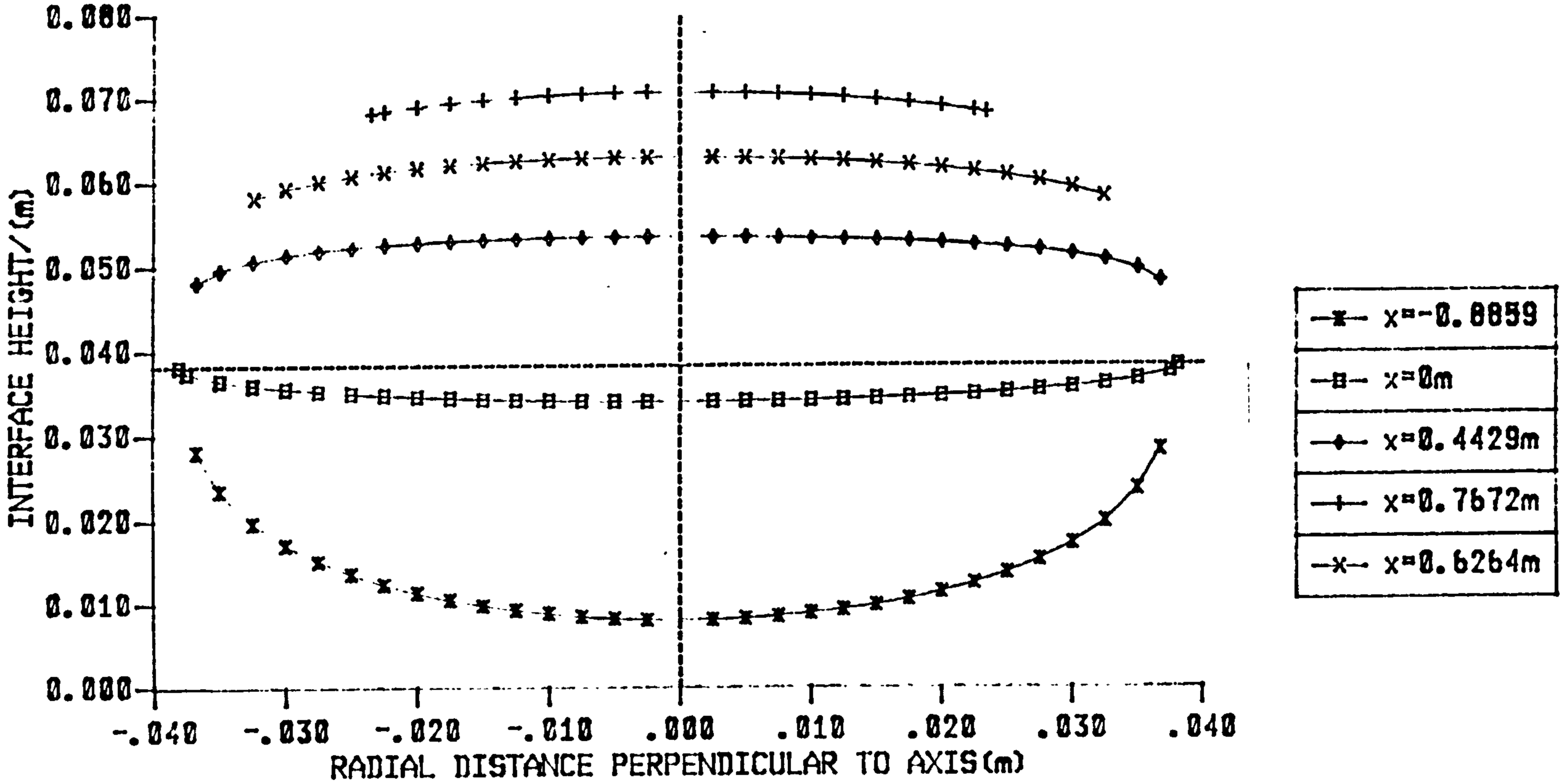


Figure 5.1.8 Variation of interfacial height calculated from Equation 5.1.44 with axial and radial distance

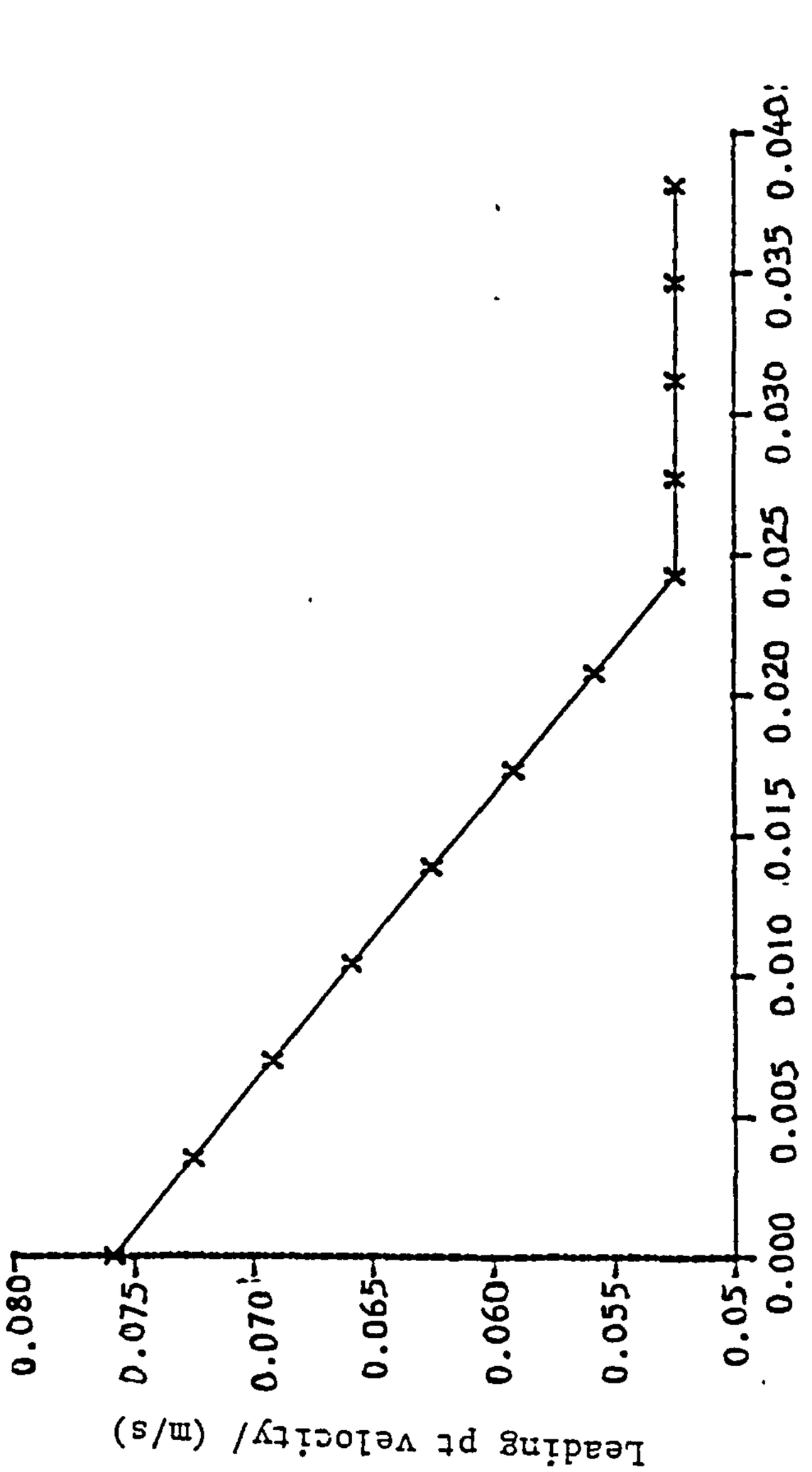


Figure 5.1.9 Slug tail leading point height as a function of boundary layer thickness in the slug body

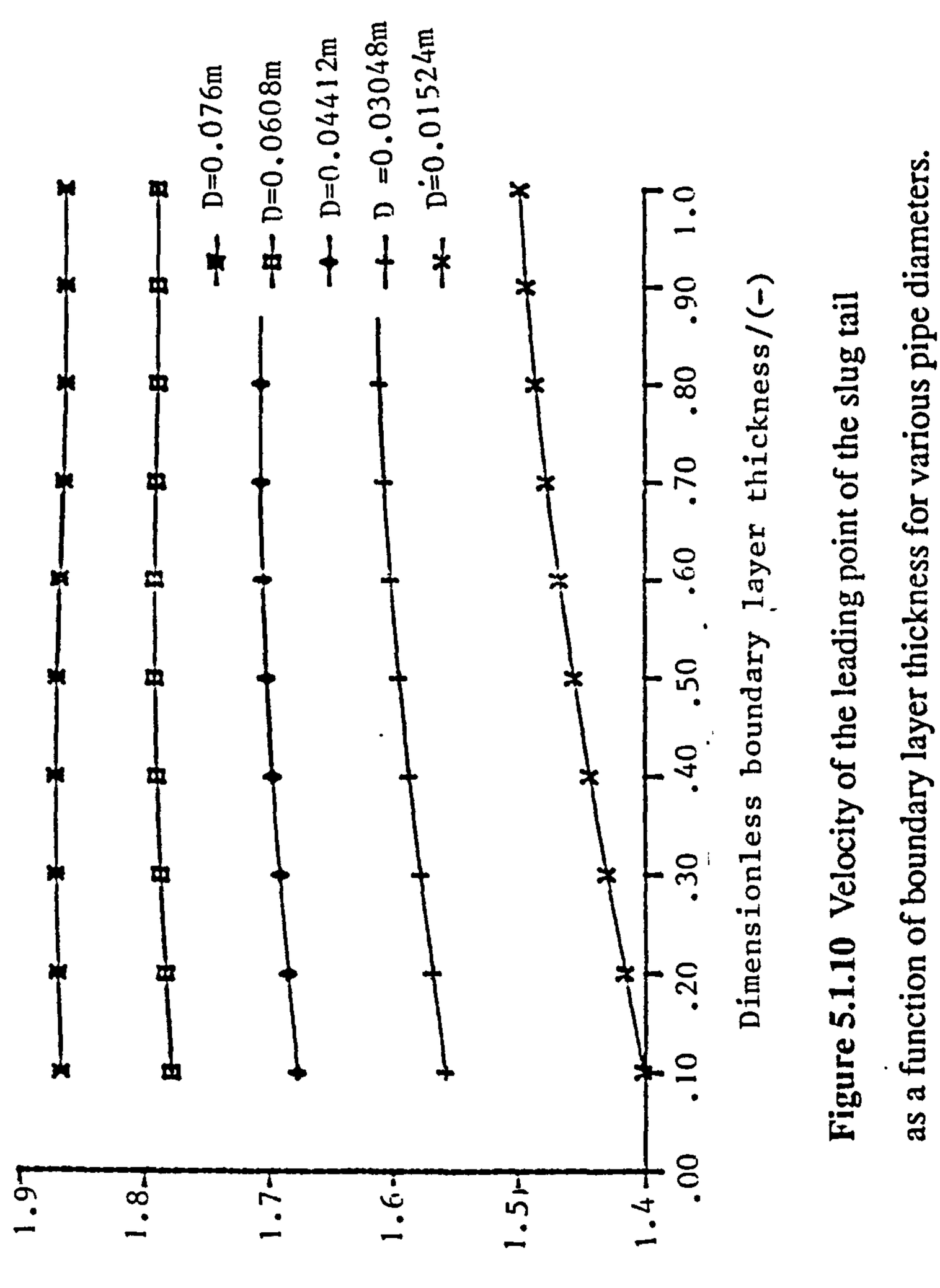


Figure 5.1.10 Velocity of the leading point of the slug tail as a function of boundary layer thickness for various pipe diameters.

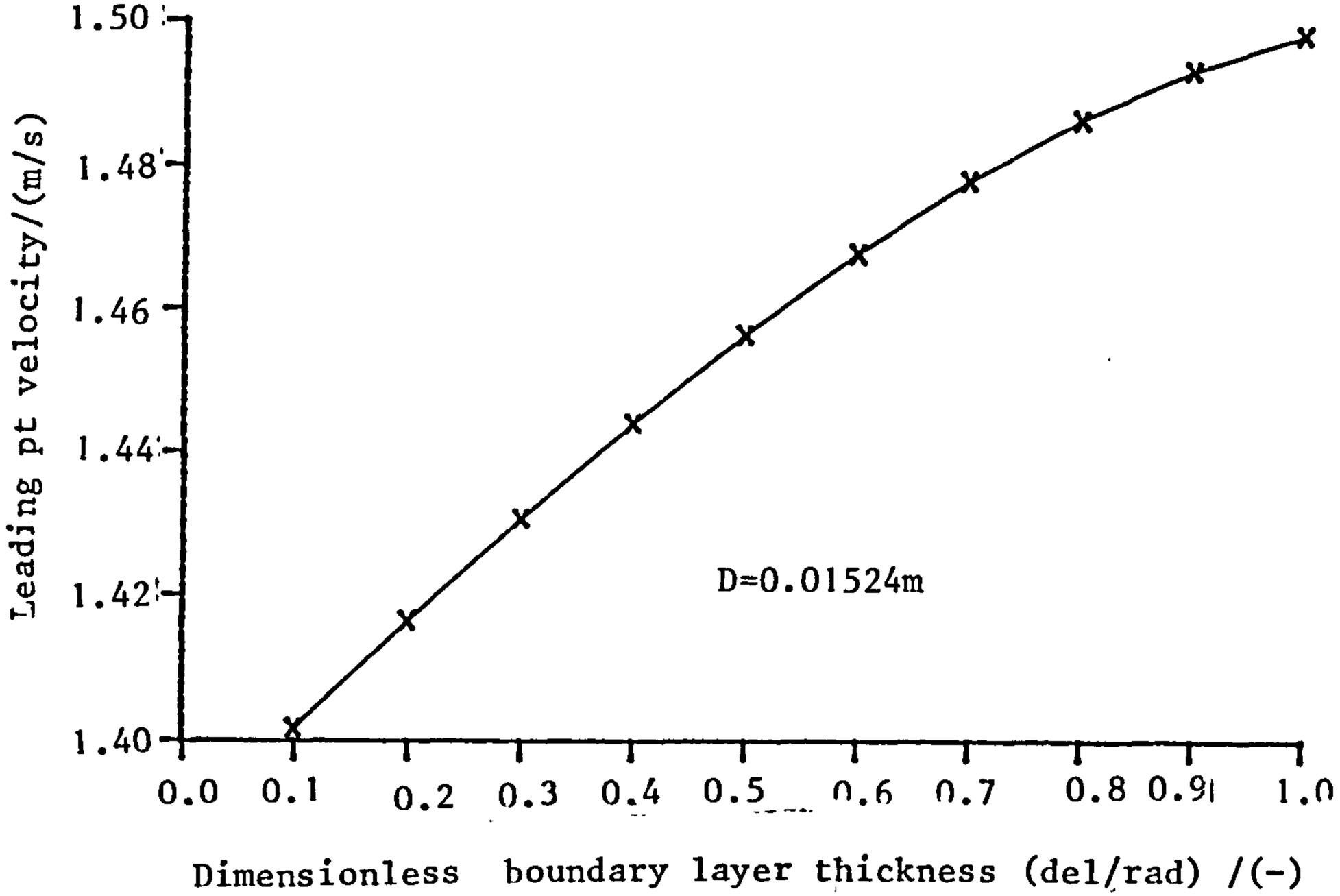


Figure 5.1.11 Variation of the leading point velocity with boundary layer thickness

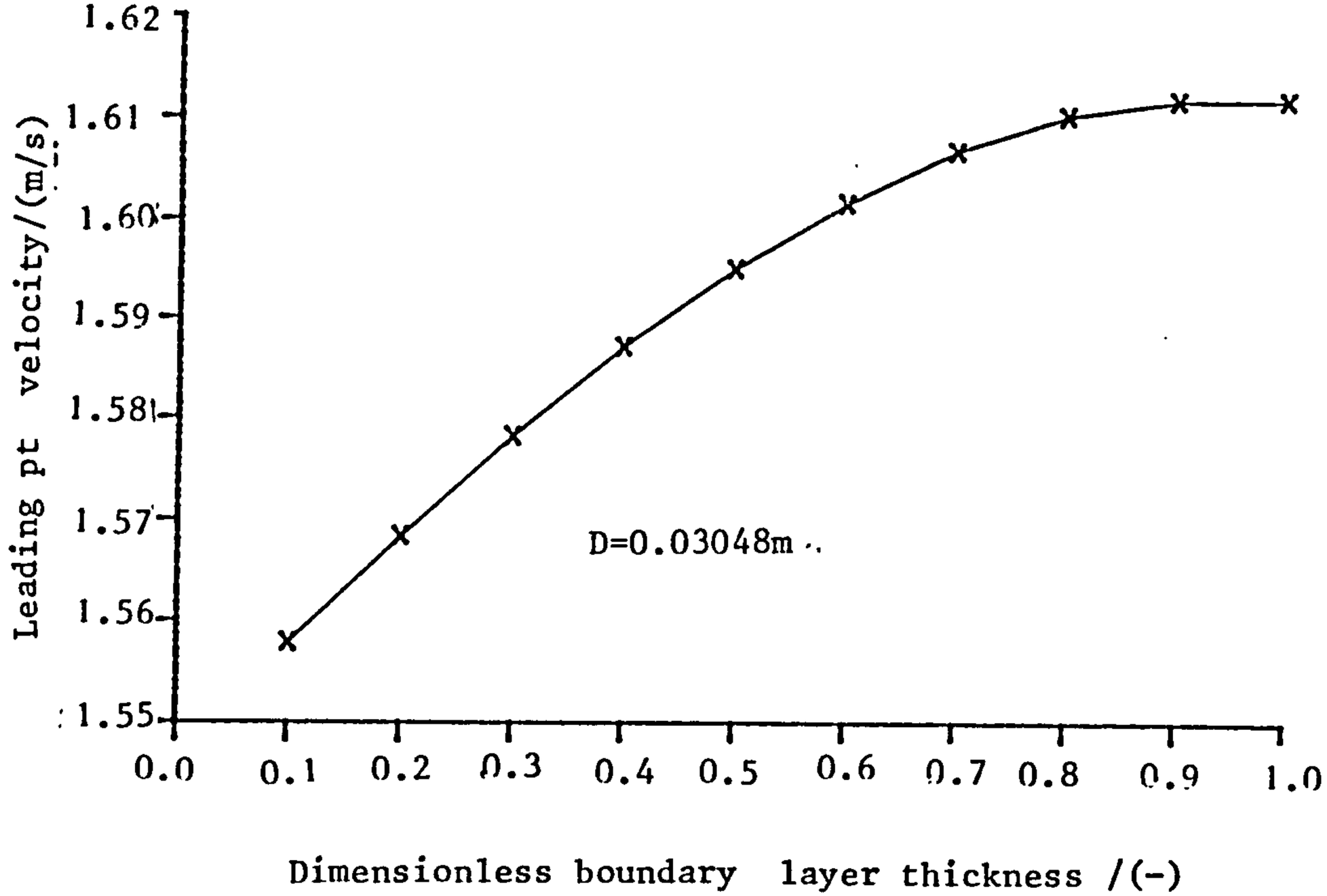


Figure 5.1.12 Variation of the leading point velocity with boundary layer thickness

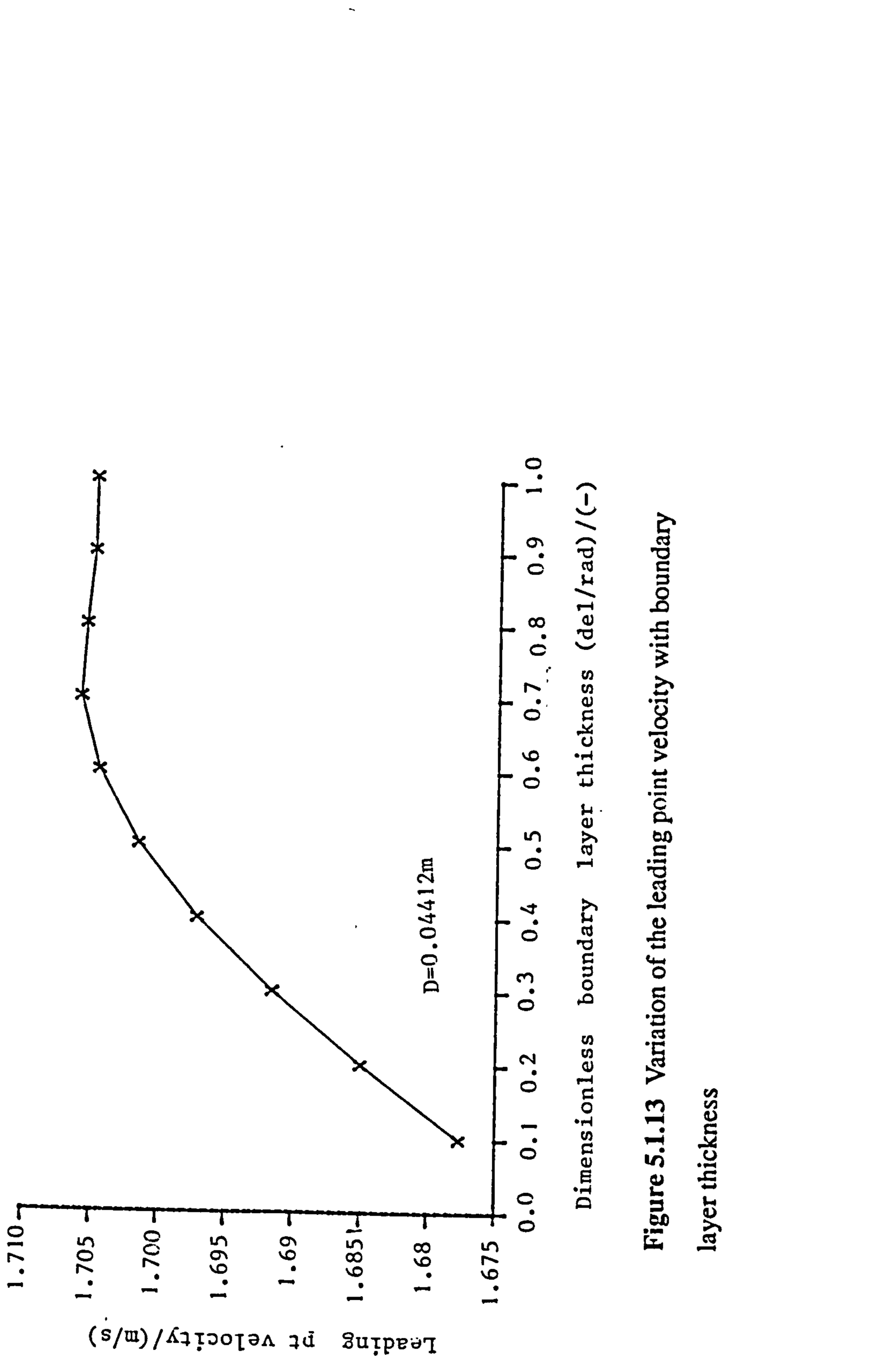


Figure 5.1.13 Variation of the leading point velocity with boundary layer thickness

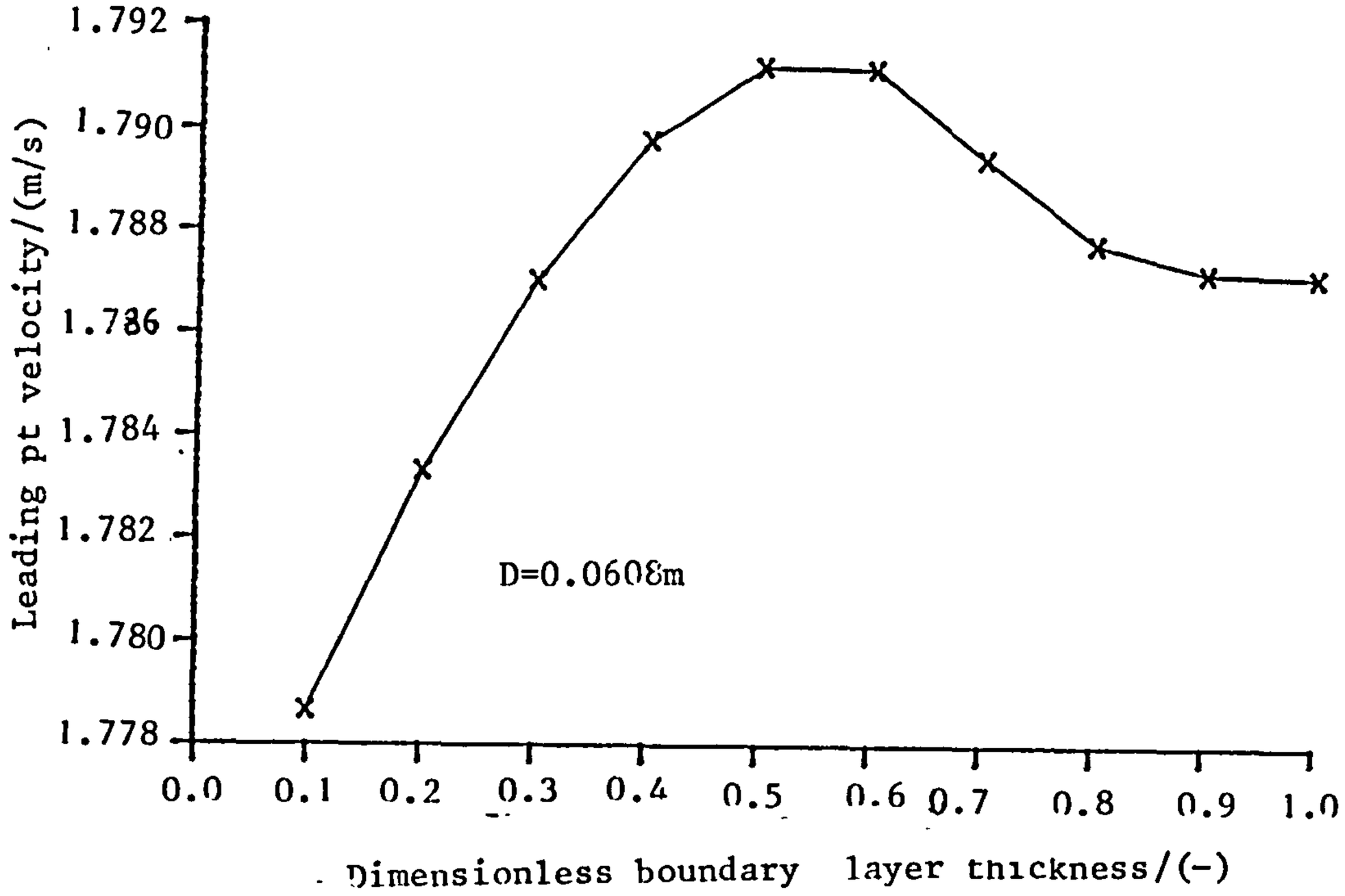


Figure 5.1.14 Variation of the leading point velocity with boundary layer thickness

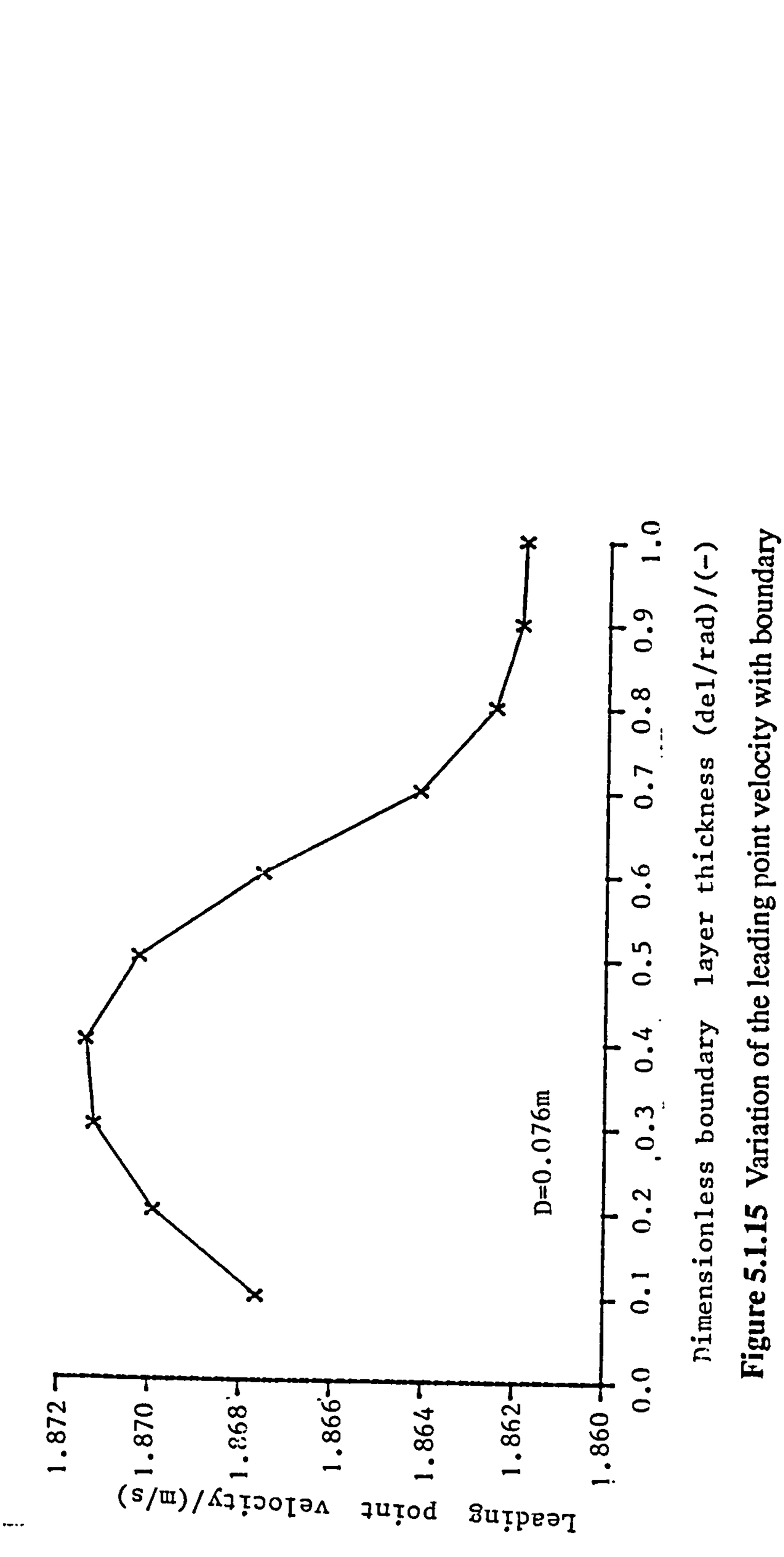


Figure 5.1.15 Variation of the leading point velocity with boundary layer thickness

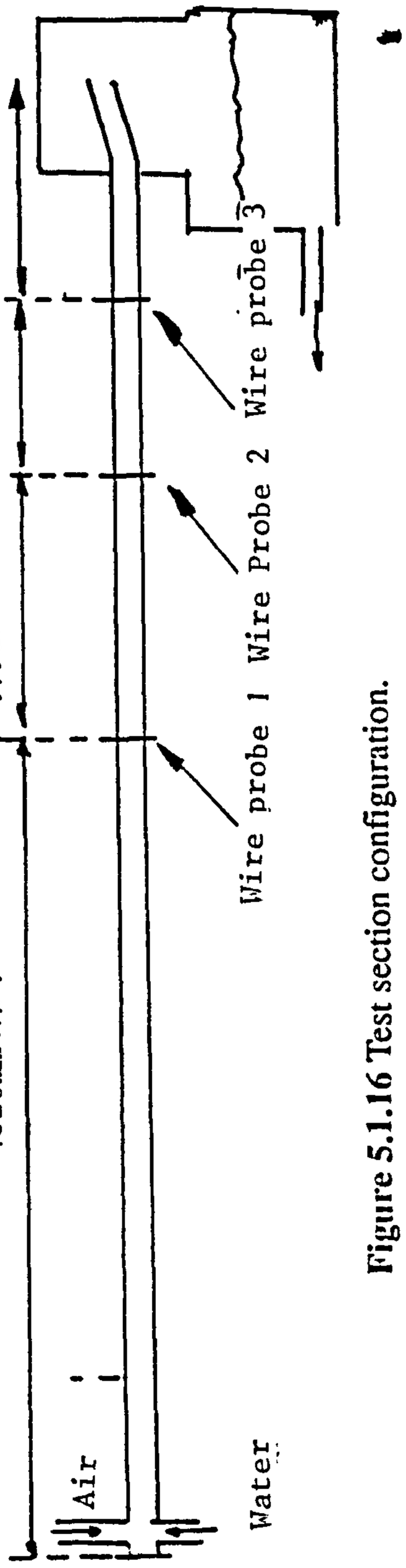


Figure 5.1.16 Test section configuration.

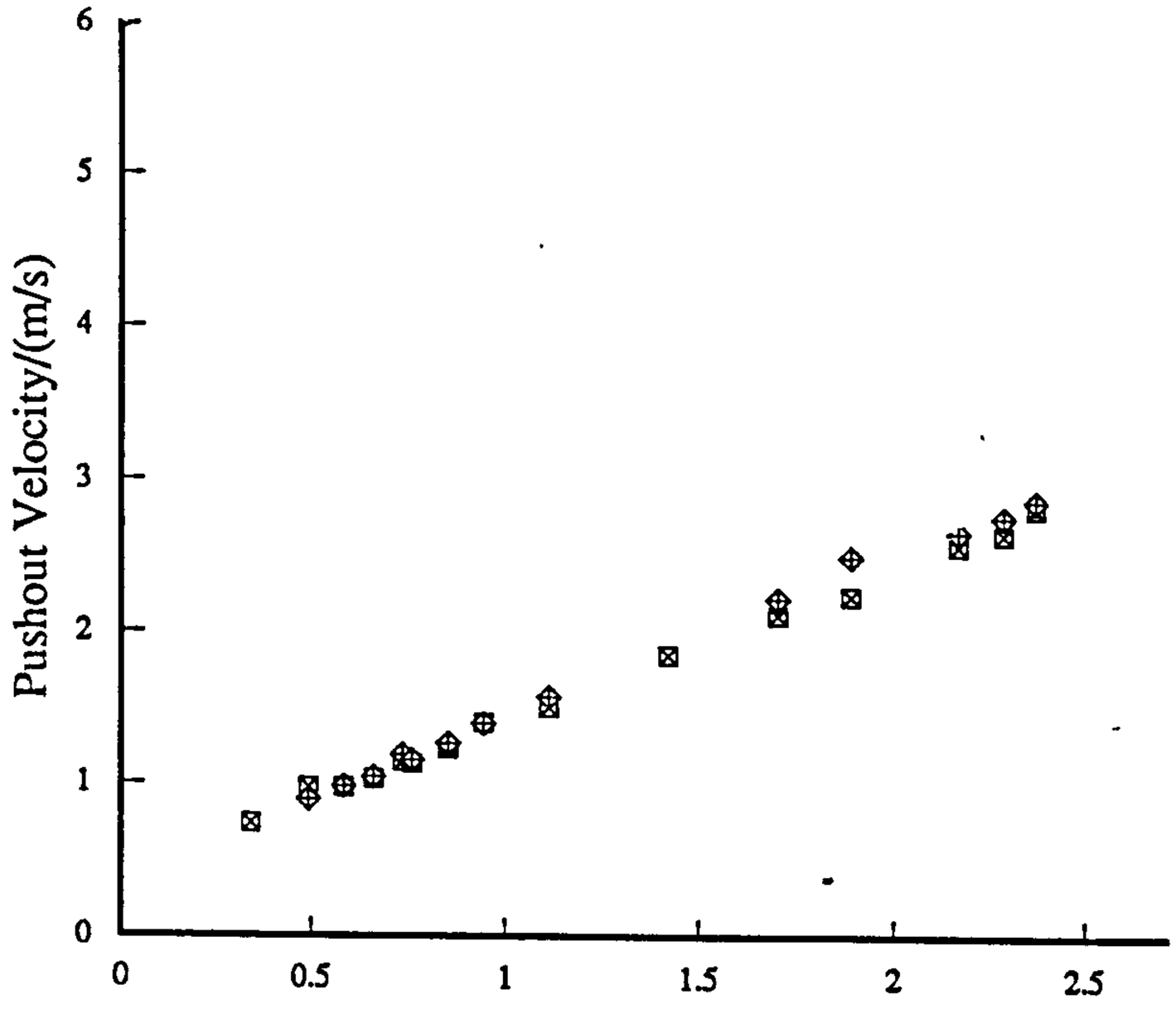


Figure 5.1.17 Interface translational velocity as a function of gas superficial velocity.

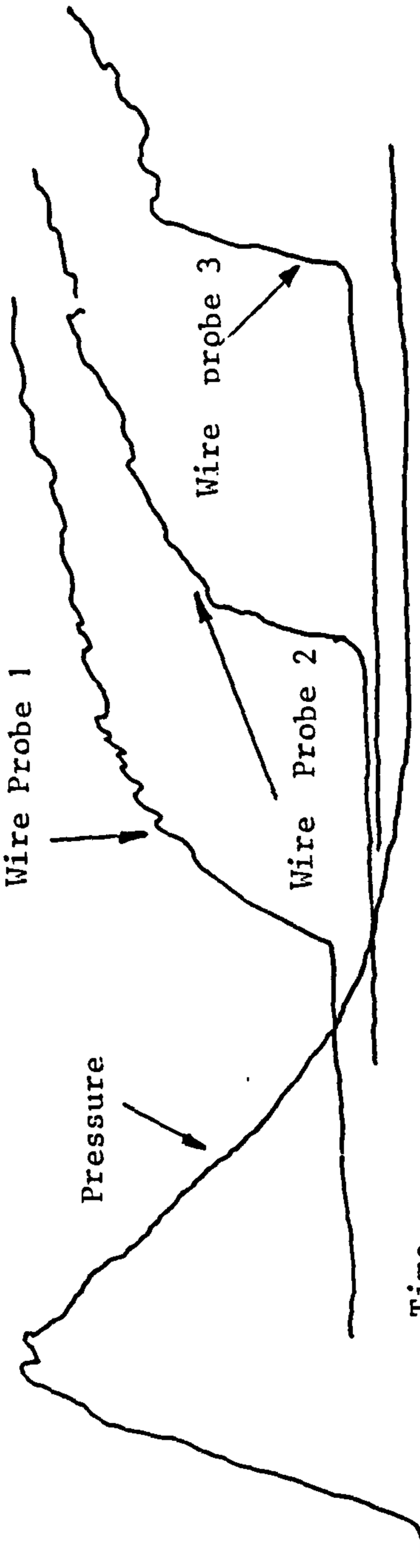


Figure 5.1.18 Pressure and wire probe signal for a gas superficial velocity of 2.8 m/s.

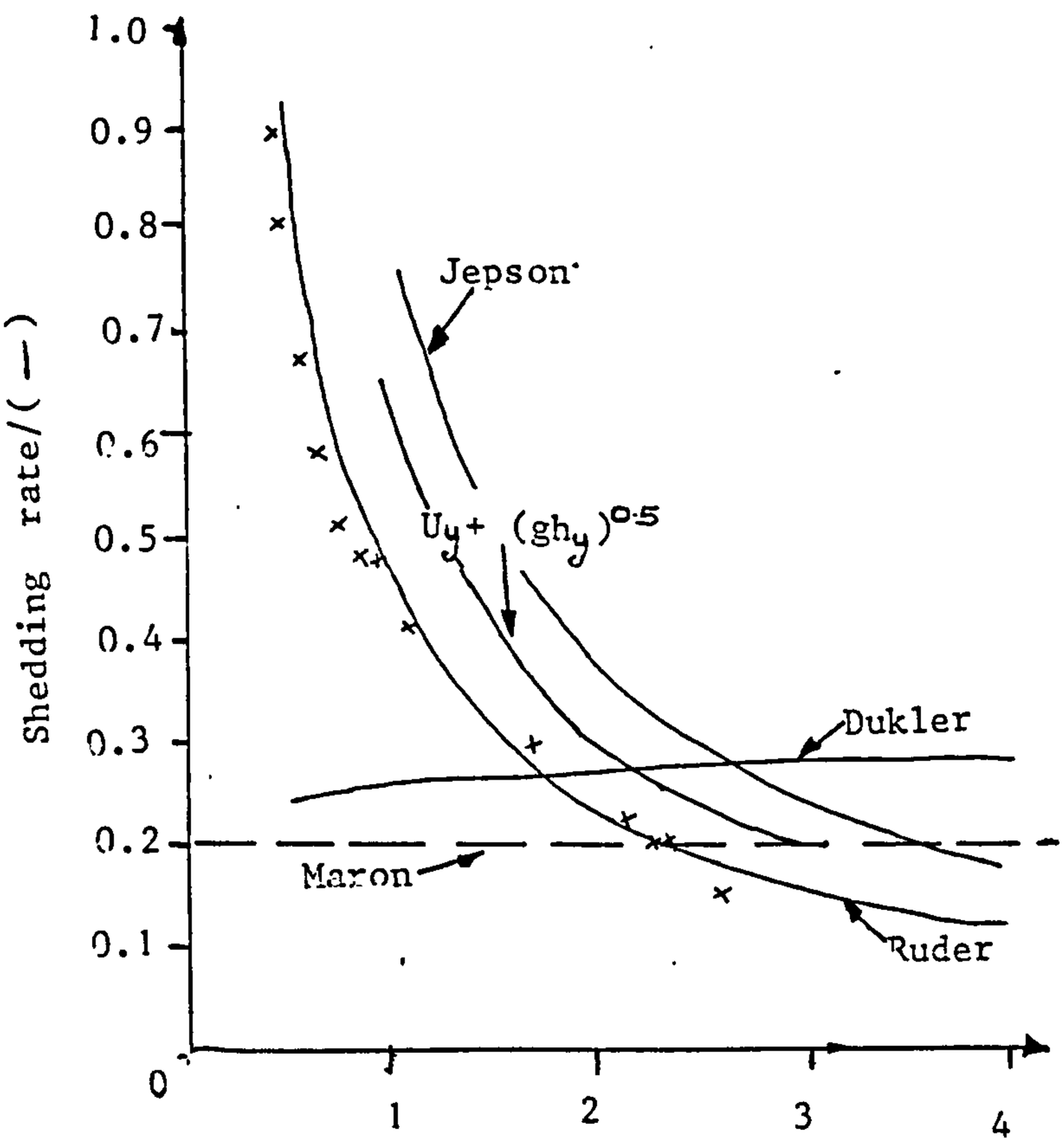


Figure 5.1.19 Comparison of experimental interface shedding rate with various slug tail models.

5.2 SLUG BODY VOIDAGE

Research into an aspect of two–phase flow often initially concentrates on the collection of general experimental data and the production of empirical correlations. Later, separate effects experiments are initiated to elucidate the physics of the problem, and models developed based on postulated mechanisms. Research into slug flow voidage has concentrated on the collection of voidage data and the only model developed to predict voidage has been based on assumptions about the state of the fluid in the slug body. To the author's knowledge, no experimental consideration has been given to the mechanism by which gas enters the slug front and passes back into the slug body. The following section starts to remedy that deficiency.

5.2.1 EXPERIMENT

A brief examination of the gas entrapment mechanism was carried out using the low pressure rig described in Chapter Three. The pipeline was horizontal along its entire length. An high speed video camera and recording equipment operating at 1000 frames/second visualised the flow just downstream of the entrance to the pipeline. A section of FEP tubing surrounded by a box containing water was used to reduce refractive index mismatch.

5.2.2 OBSERVATIONS

The observed mechanism for gas entrapment in the slug is summarised as follows. The slug front induces the formation of a wave in the stratified flow in front of the slug. This wave grows steadily until the slug front has nearly reached the wave position. The wave then grows rapidly (Kelvin–Helmholtz instability) and blocks the tube trapping a "bubble" of air between the wave and slug front. The wave position now becomes the slug front and the bubble passes back into the slug body. This process is cyclic and the frequency of entrapment increases with the gas velocity. Figure 5.2.1 illustrates the above mechanism for one cycle of the entrapment process. Figure 5.2.2 shows three cycles of the entrapment process and the subsequent motion of the entrapped gas in the slug body.

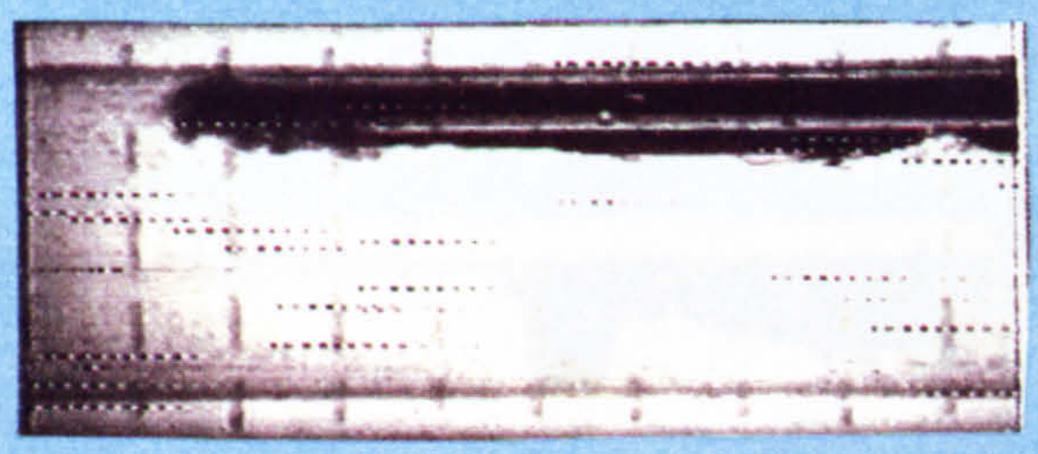
The gas bubble, which rotates clockwise as it enters the slug body, is deformed by a combination of buoyancy and shear forces. The clockwise rotation is imparted on the bubble as it passes through the old slug front. The liquid velocity at the top left hand side of the bubble–liquid interface being approximately the slug translational velocity and the liquid velocity at the bottom bubble–liquid interface being the liquid film velocity. The slug translational velocity exceeds the film velocity and hence a clockwise rotation is imparted on the bubble. The buoyancy forces stretch the bubble upwards and the shear forces deform the bubble axially; the gas nearest the pipe top trailing the gas near the pipe centre since the velocity of the liquid near the pipe wall is smaller than that at the pipe centre. In slugs for which the mixture velocity is low enough for the buoyancy force to completely overcome the turbulence, a developed slug body consists of areas of gas situated at the pipe top separated by liquid. Due to liquid shear during the transport of the gas to the pipe top a gas area forms a pear shape, with the voidage increasing as one moves through a gas area in the direction of the slug tail to slug front.

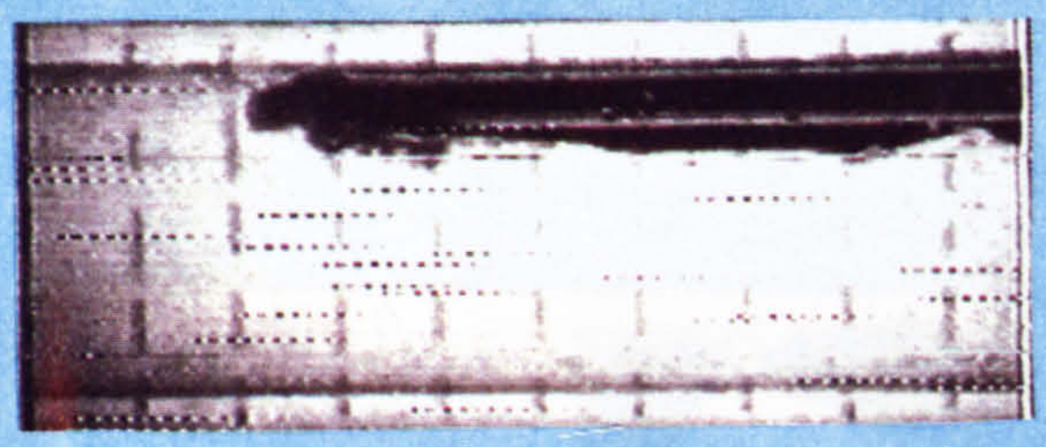
The observations made with the high speed video equipment were for developing slugs growing on the high liquid level near the pipe entrance. It is acknowledged that the observation on the mechanism of gas entrapment may not hold for developed slug flow downstream of the entrance region. However, unaided visual observation of developed slugs showed cyclic gas entrainment at the slug front, the frequency of which increased with the slug translational velocity. The slug body contained pulses of gas, the axial separation and distribution of which depended on the relative magnitude of the buoyancy and turbulence forces. Figure 5.2.3 shows still camera shots of the slug front at 6 m from the pipe inlet. The shutter speed used was 1000 th of a second. These seem to suggest that the same mechanism is taking place between the lower liquid levels of developed slug flow and the slug front.

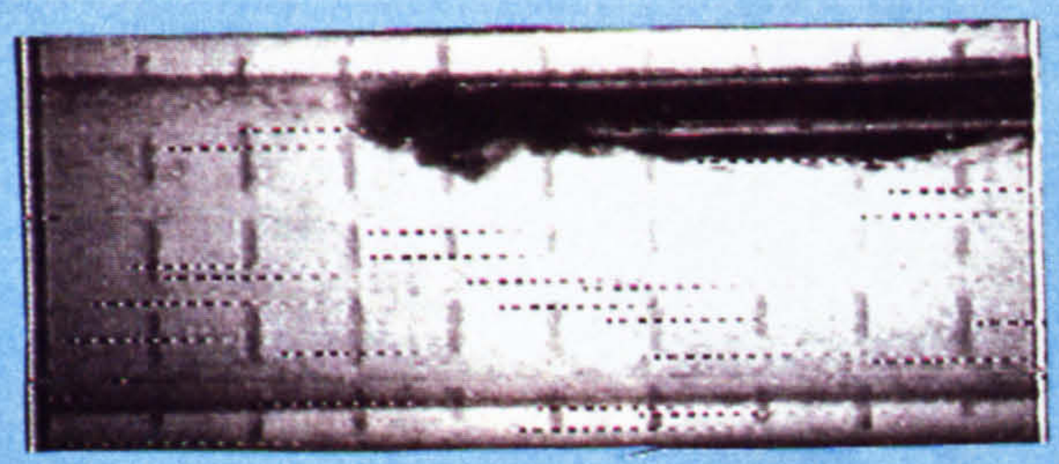
To the present author's knowledge, this is the first time that this cyclic bubble entrapment mechanism has been reported. The use of matched refractive index tube walls give a remarkable increase in the clarity of observations and its use in the present work,

along with the high speed video equipment, may explain the novelty of this observation. It would seem that explanations of voidage based on simplistic turbulence–based models like those of Barnea et al (1985) are not necessarily valid.









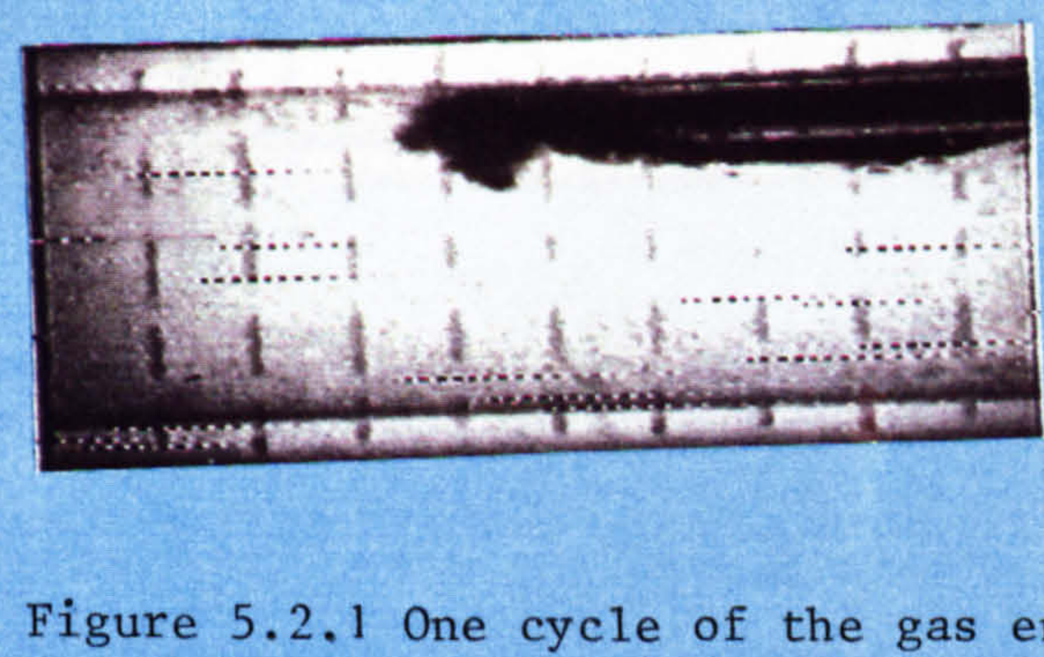
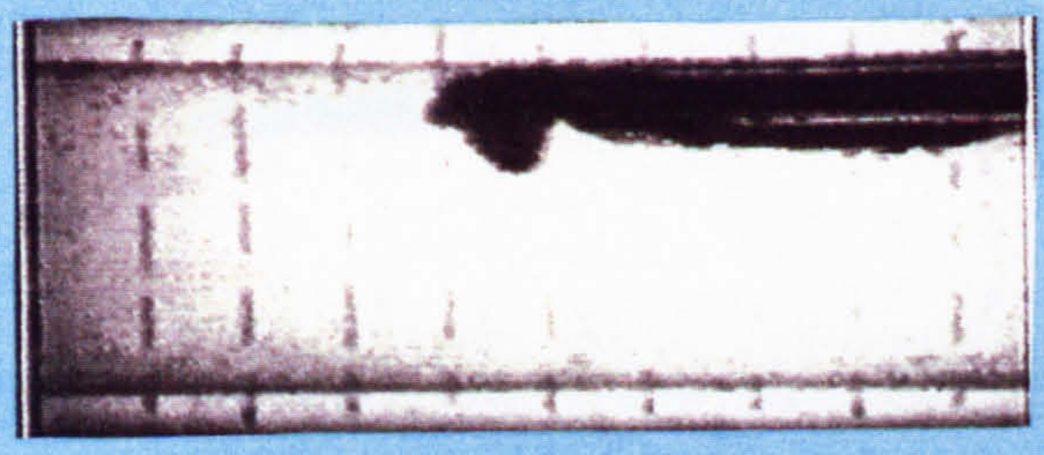
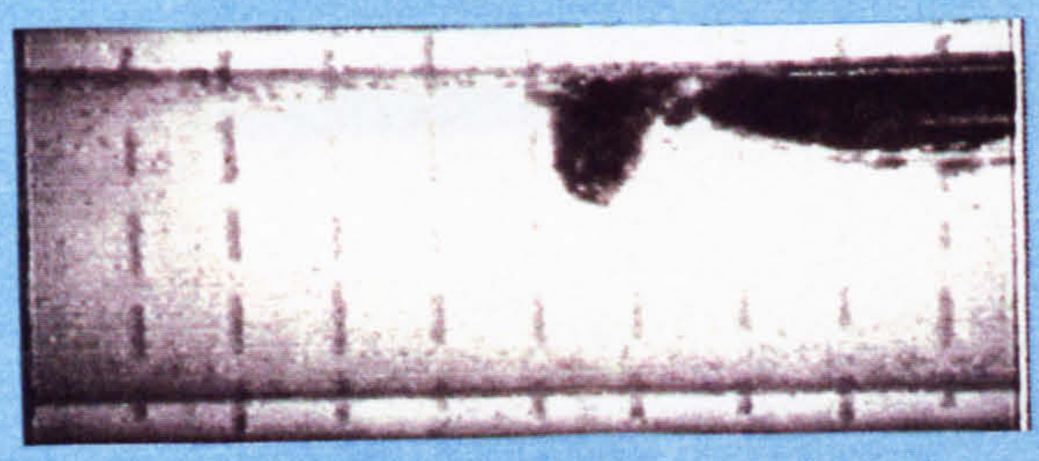


Figure 5.2.1 One cycle of the gas entrapment process. Gas superficial velocity=0.98m/s liquid superficial velocity=0.295m/s.
(continued overleaf)







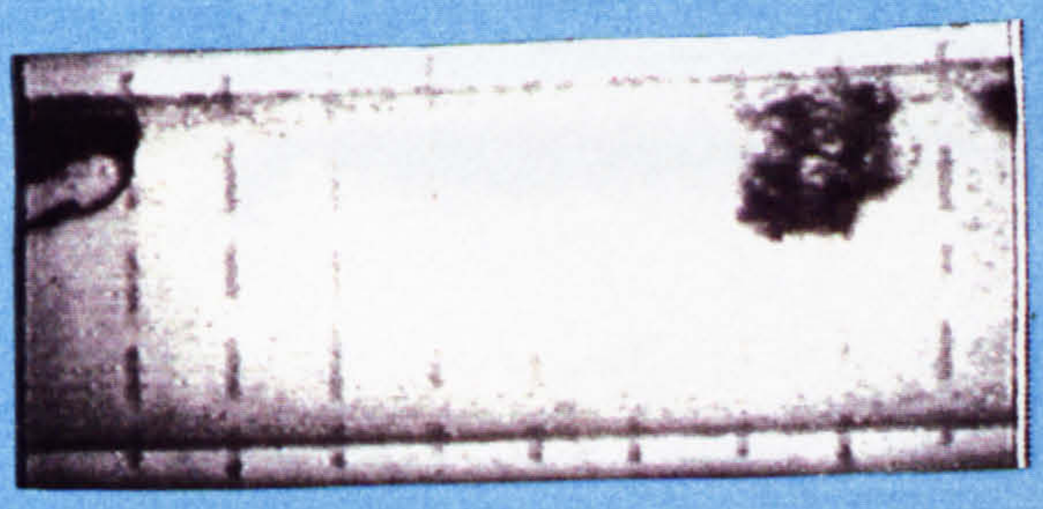


Figure 5.2.1 Continued.

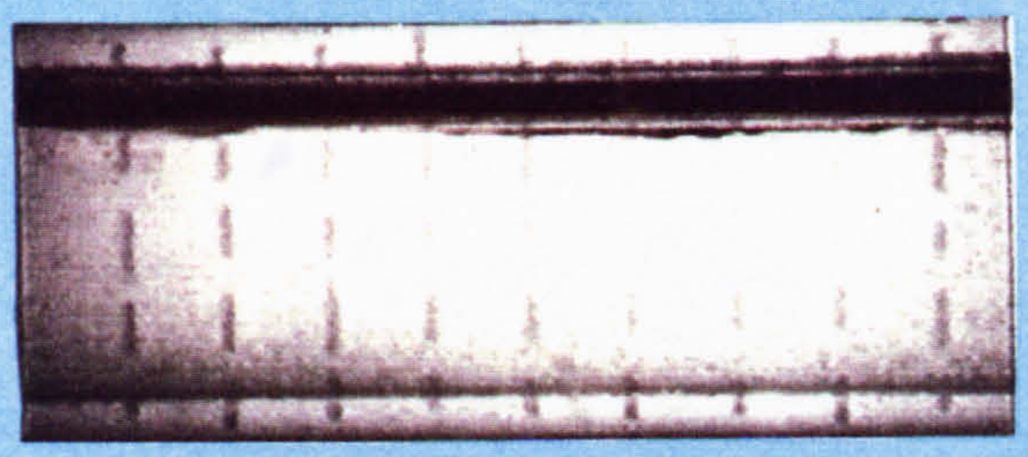


Figure 5.2.2 Three cycles of the gas entrapment process and subsequent motion of the entrapped gas in the slug body. Gas superficial velocity=0.56m/s, liquid superficial velocity=0.295m/s. (Continued overleaf).

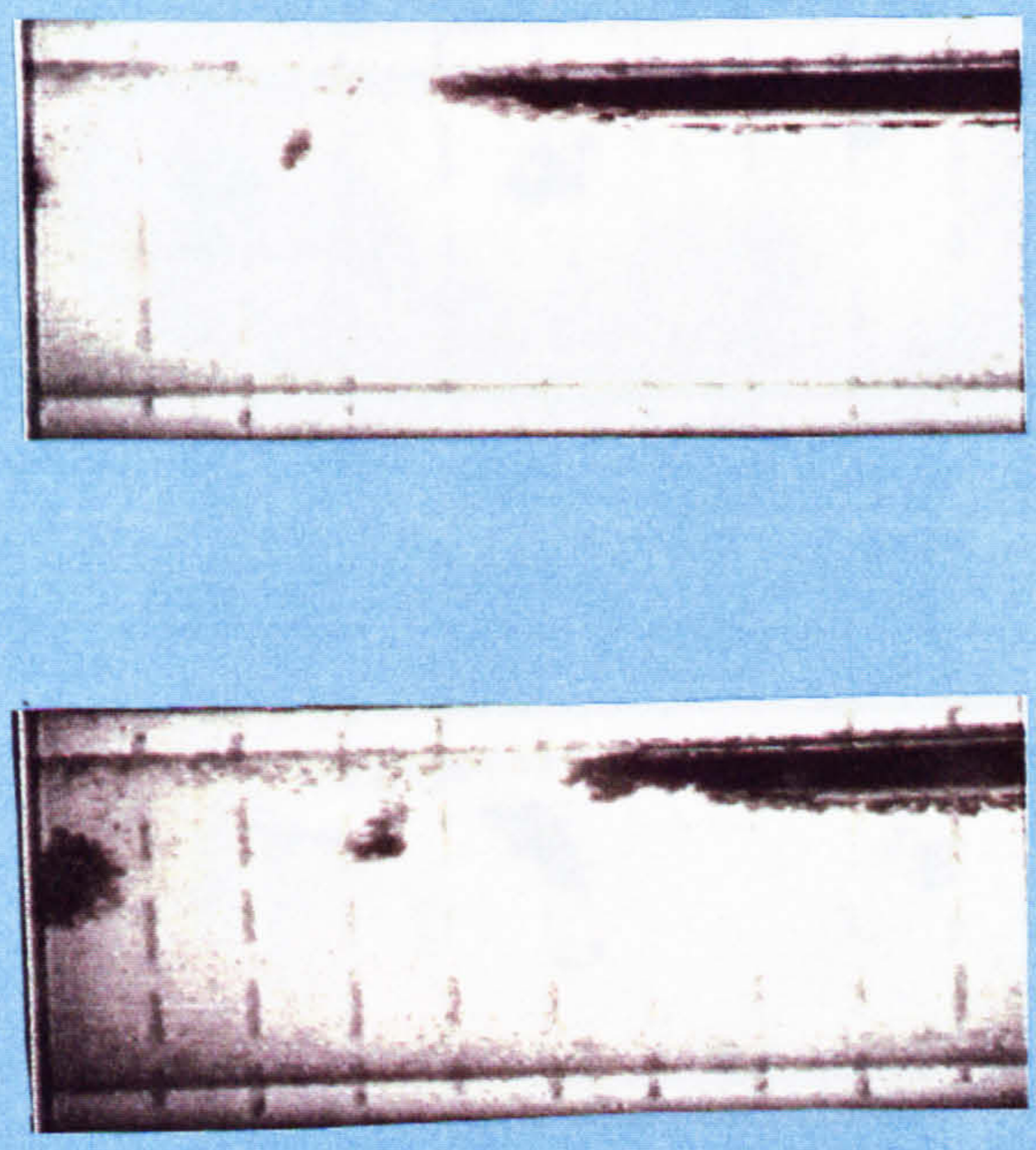
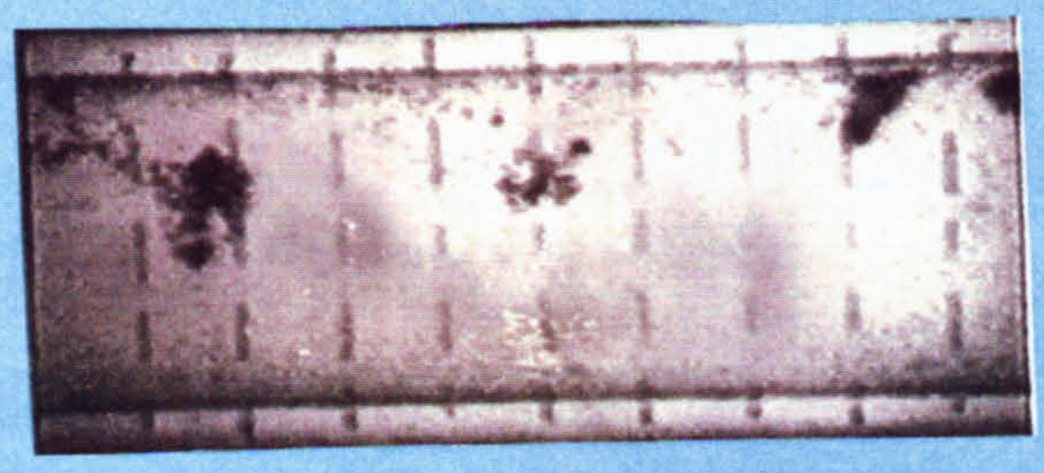
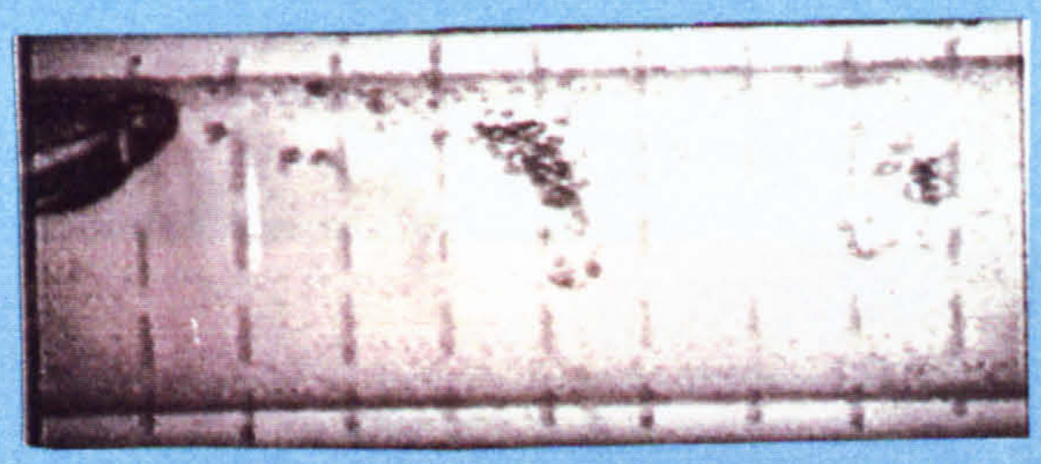
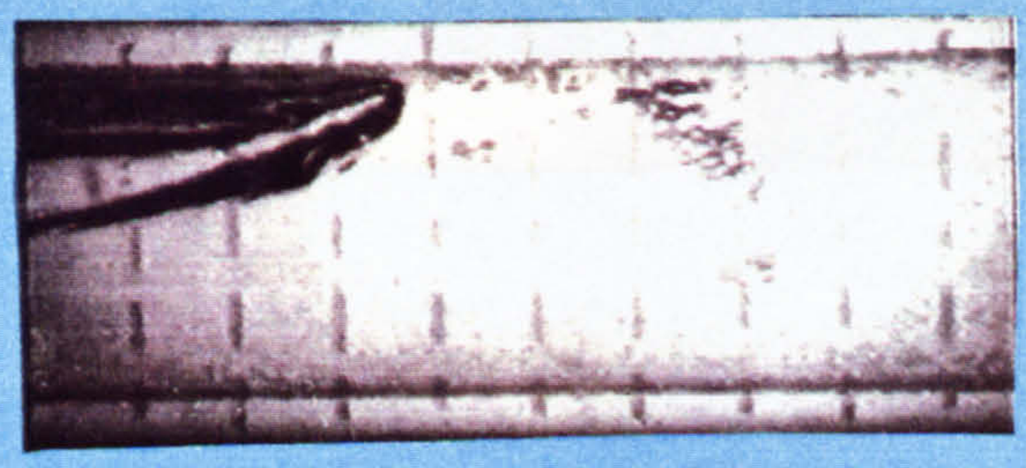


Figure 5.2.2 Continued. (Continued overleaf)







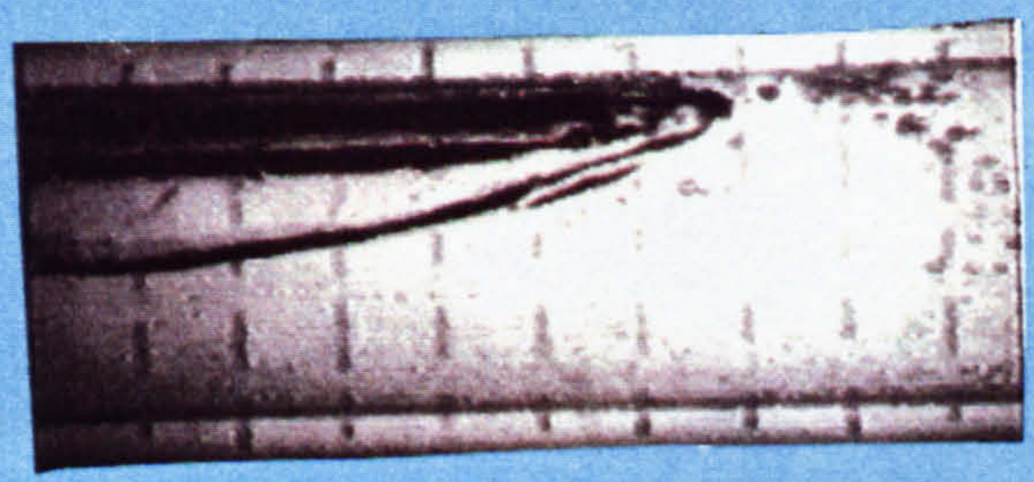


Figure 5.2.2 Continued.

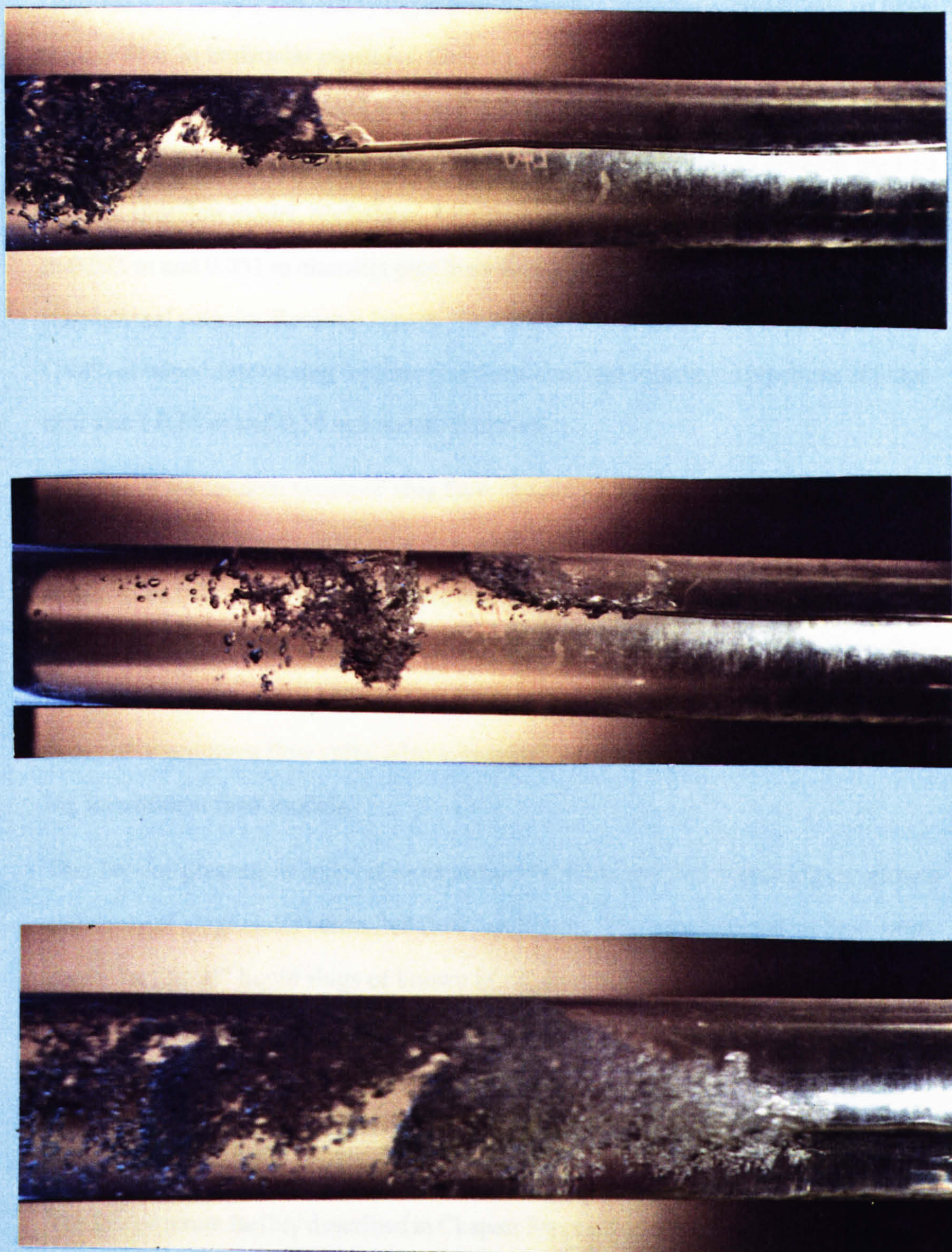


Figure 5.2.3 Slug front entrapment of gas. 6 m from the test section inlet.

5.3 GROWTH AND DECAY OF SLUG UNITS

Over the past thirty years, many experimental studies have been carried out on intermittent flow in horizontal pipelines. Gregory and Scott (1969) obtained data on slug frequency and translational velocity in a 0.01 m diameter pipe. Hubbard and Dukler (1975) used their experimental work in a 0.038 m diameter pipe to develop the first realistic slug flow model. Nicholson, Aziz and Gregory (1978) conducted experiments in 0.025 m and 0.051 m diameter pipelines which yielded data on slug frequency and translational velocity. Recently Jepson, Taylor and Evans (1988) and Taylor and Evans (1989) obtained data on slug frequency and translational velocity in pipelines of industrial size (0.15 m and 0.30 m internal diameter).

Because of the random nature of slug flow, the above workers have used the concept of a time average steady–state slug in analysing their data. The slugs have been assumed to be fully developed and hence non–growing. The characteristics of the intermittent flow, such as slug translational velocity, have been averaged over many slugs for a given flow condition. This approach cannot supply information on the growth and decay of intermittent flow units. Also averaging degrades the value of data for validating intermittent flow models.

This Section presents an innovative experimental technique for examining the growth and decay of slugs under controlled flow conditions. The experimental method introduces "artificial" liquid slugs of known initial length onto a stratified liquid layer of known height. The experimental method is described in Section 5.3.1 and illustrative results given in Section 5.3.2 and 5.3.3.

5.3.1 EXPERIMENT

The low pressure facility described in Chapter 3 was used in this experiment. Two techniques were investigated for introducing "artificial" liquid slugs into the test section.

In the first technique liquid slugs were generated near the test section inlet by locally increasing the liquid flowrate for a short time at a point in an initially stratified flow. The local increase in liquid flowrate was achieved by a piston driving liquid out of a

tube connected to the base of the test section. The piston was driven by the site compressed air supply and the frequency of its up and down motion controlled by two solenoid valves connected to a electronic controller. The amount of liquid introduced into the test section was varied by adjusting the stroke of the piston using a variable stop. Figure 5.3.1 shows the slug generator attached to the test section inlet and Figure 5.3.2 shows the stages in the operation of the piston. It was noted recently, that Pacini et al (1991) applied a similar technique to investigate the onset of slug flow in near–horizontal pipes.

It was found in the present work, that while slugs formed at high gas flowrates and low liquid film heights and at low gas flowrate for high liquid film height, the slug generator was not able to increase the local liquid flowrate sufficiently to form slugs at low gas flowrates and low liquid film heights. Thus a different technique was developed in the present work to remove this limitation at low gas and liquid superficial velocities. This second technique, known as the "artificial slug" experiment, was the method applied to obtain the results presented in this work.

The experiment–specific pipeline geometry for the second technique is given in Figure 5.3.3. The set–up for the artificial slug experiment consists of a short pipe after the mixing section which is lower than the test section. The centre line of the small pipe is one diameter below the centre line of the test section. Both pipes are aligned horizontally and linked by a small riser. The exit of the test section has a weir attached which enables the liquid film height to be specified in the test section.

The experimental technique is illustrated in Figure 5.3.4. The pipe is filled with water and the water pump then switched off, allowing the test section to drain to the level specified by the weir. An inclined manometer measures the liquid film height in the main pipe after drainage has finished. Liquid film height to pipe diameter ratios of 0.135, 0.203, 0.27, 0.324, 0.378, 0.473 and 0.554 were used in the experiments. When the draining is complete the gas flow is turned on and the liquid slug in the small pipe is pushed into the main pipe. The slug travels over the liquid film and exits at the weir. Parallel wire probes are used to obtain the translational velocity of the slug front and

slug tail and pressure transducers monitor the upstream pressure history. The location of the wire probes and pressure transducers relative to the riser as shown in Figure 5.3.1.

5.3.2 TRANSLATIONAL VELOCITY

The translational velocity of the slug tail and slug front were measured as a function of gas flowrate for each film height to pipe diameter ratio.

5.3.2.1 Slug Front

Figures 5.3.5 and 5.3.6 show the translational velocity of the slug front as a function of the gas superficial velocity for each film height to pipe diameter ratio. It can be seen that the translational slug front velocity increases with gas velocity for a given liquid film height and that the slope of the perceived relationship increases with liquid film height. In general, at a given gas superficial velocity the slug front velocity increases with liquid film height. Also, at high gas velocities it is noted that the slope of the plot of slug front translational velocity against gas superficial velocity data (at constant film height) increases.

It will be instructive to derive a mathematical expression for the slug front translational velocity to examine the experimental trends shown. The translational front velocity of a slug is its observed march rate relative to the pipe wall. This velocity is the sum of the mean fluid velocity in the slug relative to the pipe wall and the rate of increase of the slug front position due to pick-up of the liquid film in front of the slug. The following equation represents this relationship:

$$V_t = v_s + \frac{\varrho_L A(1-\varepsilon_f)(V_t - v_f)}{\varrho_s A(1-\varepsilon_s)} \qquad (5.3.1)$$

where

V_t is the translational velocity of the slug front

v_s is the average slug fluid velocity

A is the cross–sectional area of the pipe

v_f is the area averaged liquid film velocity

ε_f is the voidage in the film/elongated bubble region

ε_s is the slug body void fraction

ρ_L is the density of the liquid phase

ρ_s is the density of the slug body fluid.

The following explicit relationship for V_t results on rearranging Equation 5.3.1:

$$V_t = \frac{v_f \rho_s (1 - \varepsilon_s) - \rho_L v_f (1 - \varepsilon_f)}{\rho_s (1 - \varepsilon_s) - \rho_L (1 - \varepsilon_f)} \qquad (5.3.2)$$

This relationship can be simplified by considering the velocity of the film in the experiment. At the start of the experiment the film is stationary and the velocity of the gas above it zero. As the slug of liquid accelerates into the test section the gas in front of it will accelerate, reaching eventually the slug front translational velocity. The gas transfers momentum to the liquid which accelerates. The magnitude of the resulting liquid velocity depends on the time since the artificial slug was initiated, upon the applied gas superficial velocity, upon the liquid–wall interfacial shear, and upon the initial liquid film height. It is suggested that at low gas superficial velocities the momentum transfer will be small and hence the acceleration of the liquid film will be small. At higher gas superficial velocities, while the interaction between the gas and liquid is increased this is counteracted by the smaller time period that is experienced by the film due to faster slug translational velocities. Hence it is postulated that the velocity of the liquid film v_f at a position just in front of a slug was effectively zero in the experiments. It must be noted that this would not be the case for a long pipe.

Substituting $v_f = 0$ into Equation 5.3.2 and noting that $v_s = U_{GS}$ gives:

$$V_t = \frac{U_{GS}}{1 - \frac{\rho_L (1 - \varepsilon_f)}{\rho_s (1 - \varepsilon_s)}} \qquad (5.3.3)$$

Equation 5.3.3 will be used to explain the experimental trends. As can be seen V_t is directly proportional to U_{GS} as found experimentally. The slope of the relationship depending on the film height ($1-\varepsilon_f$) and the degree of aeration of the slug (ρ_s and $(1-\varepsilon_s)$). At low gas superficial velocities the slug can be considered to be pure liquid and so Equation 5.3.3 reduces to:

$$V_t = \frac{U_{GS}}{\varepsilon_f} \qquad (5.3.4)$$

So as the liquid film height increases at constant U_{GS} the slug front translational velocity will increase. In addition at constant film height the translational velocity will increase linearly with gas superficial velocity. This explains the experimental results at low gas superficial velocity

At higher gas superficial velocities slugs are aerated and Equation 5.3.3 holds. Equation 5.3.3 predicts that V_t is a monotonic (though not linear) function of U_{GS} at constant initial film height. This is shown in Figures 5.3.5 and 5.3.6 by the form of the experimental data at higher gas flowrates. In addition the experimental increase of V_t with decreasing ε_f at constant gas superficial velocity is again represented in Equation 5.3.3. It is noted from Figures 5.3.5 and 5.3.6 that there is a change in the gradient of the data points for each value of the initial film height at higher gas superficial velocities. Also the gas velocity at which this change occurs increases with decreasing liquid film height. It is proposed that this gradient increase is due to the aeration of slugs and that the gas velocity at which slug aeration first occurs increases with decreasing film height. It can be seen from Equation 5.3.3 that for a given value of ε_f and U_{GS} the transition from a non–aerated to aerated slug will alter the value of the gradient relating V_t and U_{GS}. This confirms that the change in the gradient of the experimental data may be due to aeration of the slug body.

The fact that the gas superficial velocity at which this gradient change occurs, increases with decreasing liquid film height needs to be explained. As will be seen from the following discussions, more detailed experimental work would be necessary to provide

a greater understanding of this result. An hypothesis which may explain this experimental finding is explored in the following paragraphs.

If we consider the slug front gas entrapment mechanism discussed in Section 5.2, this experimental data may provide further information on the proposed mechanism of gas entrapment. The stability of a disturbance induced in the liquid film by the slug front will depend on the gas flow above it and the size of the disturbance. There will exist a certain gas velocity u_g (actual not superficial) at which a disturbance wave on the interface would grow to block the pipe and trap an air bubble at the slug front. Just in front of the slug, the actual gas velocity will be that of the slug front translational velocity. As noted earlier, V_t increases with increasing liquid film height in front of it.

Let us examine the assumption that the disturbance formed is a small but finite wave. Taitel and Dukler (1976) derived the following stability criterion for a small finite wave:

$$u_G > \left(1 - \frac{h_L}{D}\right)\left[\frac{(\varrho_L - \varrho_G)gA_G}{\varrho_G w}\right]^{0.5} \qquad (5.3.4)$$

where

w is the width of the gas–liquid interface

h_L is the height of the liquid–gas interface referenced to the pipe base.

which predicts that as the liquid film height decreases the slug translational velocity necessary for instability of a small but finite wave increases. Hence, based on Equation (5.3.4), the gas superficial velocity at which the gradient increase occurs will increase with decreasing liquid film height, as the experiment shows.

On further examination of the experimental data shown in Figures 5.3.5 and 5.3.6, it can be seen that the change in gradient for all liquid film heights studied, seems to occur at an approximately constant value of the slug front translational velocity. Equation 5.3.4 would predict that the slug front translational velocity for this gradient change would increase with decreasing liquid height. This prediction disagrees with the ex-

perimental data. In addition the slug front translational velocities necessary for the instability of a small finite wave are large in comparison with the experimental translational velocities at which it is suggested aerated slugs occur. For example in the case of a liquid film height to pipe diameter ratio of 0.554, the slug front translational velocity calculated from Equation 5.3.4 is 6.43 m/s which is far in excess of that required for aerated slugs.

Hence if it is assumed that Equation 5.3.4 correctly calculates the velocity for instability of small finite waves, then the proposed disturbance in front of the slug can not be represented by a small but finite wave. In addition, if it is still proposed that the gas superficial velocity at which the gradient change occurs be explained in terms of the slug front gas entrapment mechanism discussed in Section 5.2, then the following must be noted. The disturbance induced at the slug front must be large to develop at such a low actual gas velocity of approximately 3 m/s. Also that there is a minimum value of the slug front translational velocity (approximately 3 m/s) at which this disturbance occurs which does not depend on the liquid film height in front of the slug. The latter may suggest that there exists a transition in the mechanism of the interaction between the slug front and the liquid film in front of it and perhaps a transition in the flow mechanism within the slug front itself at a slug front translational velocity of approximately 3 m/s.

5.3.2.2 Slug Tail

Figures 5.3.7 and 5.3.8 show the translational velocity of the slug tail as a function of the gas superficial velocity for each film height to pipe diameter ratio. It can be seen that the slug tail translational velocity increases with gas velocity for a given liquid film height and that the slope of the relationship is constant and does not vary with liquid film height. A least squares regressional analysis of all the data points comprising Figures 5.3.7 and 5.3.8 provided the following empirical relationship between the

translational slug tail velocity and the applied gas superficial velocity:

$$V_t = 0.523 + 0.97U_{Gs} \qquad (5.3.5)$$

where V_t is the slug tail translational velocity.

This is the first experimental correlation produced in the literature relating the translational velocity of the slug tail to the area averaged fluid velocity (in the case of these experiments the gas superficial velocity) in the slug body. In addition the technique developed has enabled the environment surrounding the slug to be controlled, reducing the "noise" of the data used in the construction of the correlation. Previous correlations for slug translational velocity have only related the "time averaged" slug translational velocity to the "time averaged" slug body area averaged velocity, assuming steady ie non–growing slugs. The correlation may be used to validate slug tail translational velocity models or steady state slug translational models. The latter is valid because in steady state slug flow the slug front and slug tail velocities are equal.

5.3.3 GROWTH AND DECAY

Figures 5.3.9 to 5.3.15 compare the slug tail and slug front translational velocities as a function of gas superficial for each of the liquid film height to pipe diameter ratios.

As expected at low liquid film height to pipe diameter ratios the slug tail velocity is slightly greater than the slug front velocity over most the range of gas superficial velocities examined, indicating decaying slugs. As the liquid film height to pipe diameter ratio increases, the slug front velocity is greater than the slug tail translational velocity at higher gas superficial velocities. The minimum gas superficial velocity at which the front translational velocity is greater than the tail translational velocity decreases with increasing liquid film to pipe diameter ratios. This minimum gas superficial velocity is the flow condition at which the slugs are stable for a given film height to pipe diameter ratio. Above this gas velocity the slugs will grow in length and, below it, will decay.

It is noted at velocities above this minimum gas velocity, for example see Figure 5.3.15, that the rate of growth of slugs increases with gas superficial velocity.

This Section has presented an innovative experimental technique for examining the growth and decay of slugs under controlled flow conditions. The results, discussed above, indicate the potential of this experimental technique for obtaining the flow conditions for stability of slugs and slug growth/decay rates, avoiding the limitations of the concept of a time average steady–state slug.



Figure 5.3.1 Slug generator on test section.

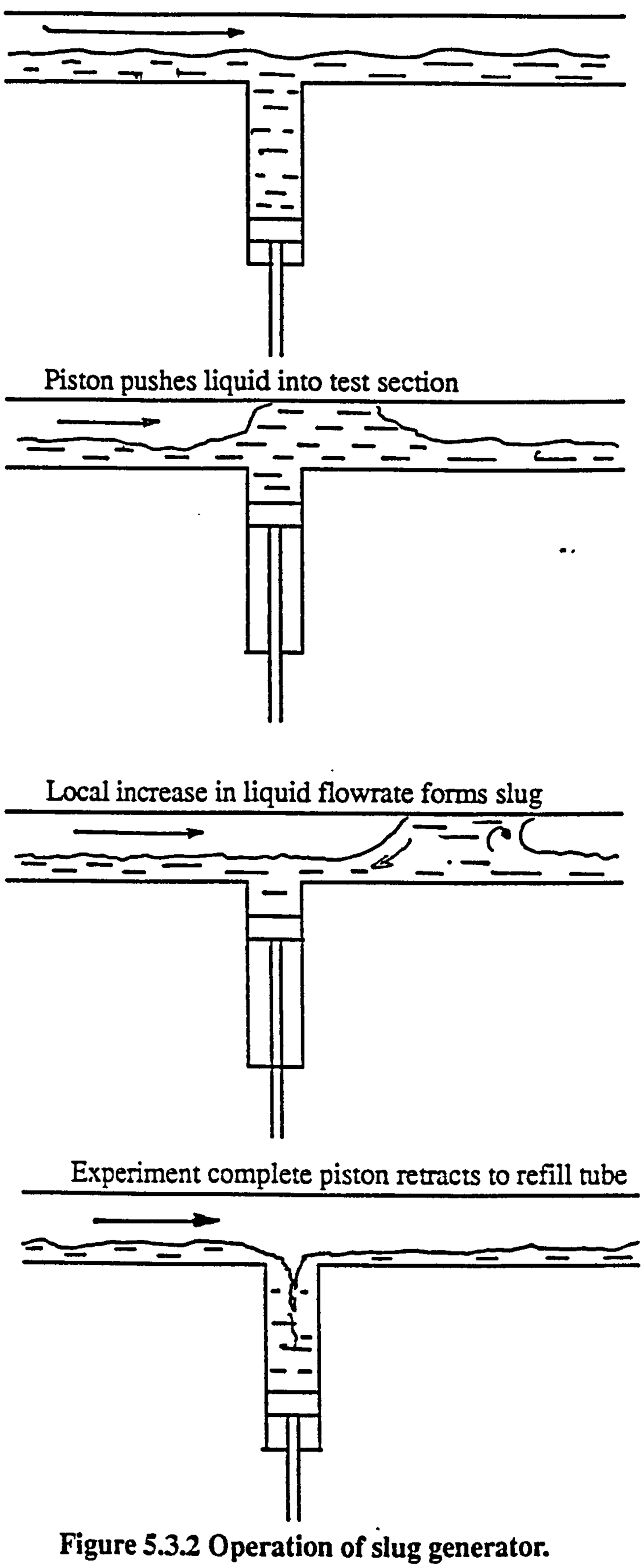


Figure 5.3.2 Operation of slug generator.

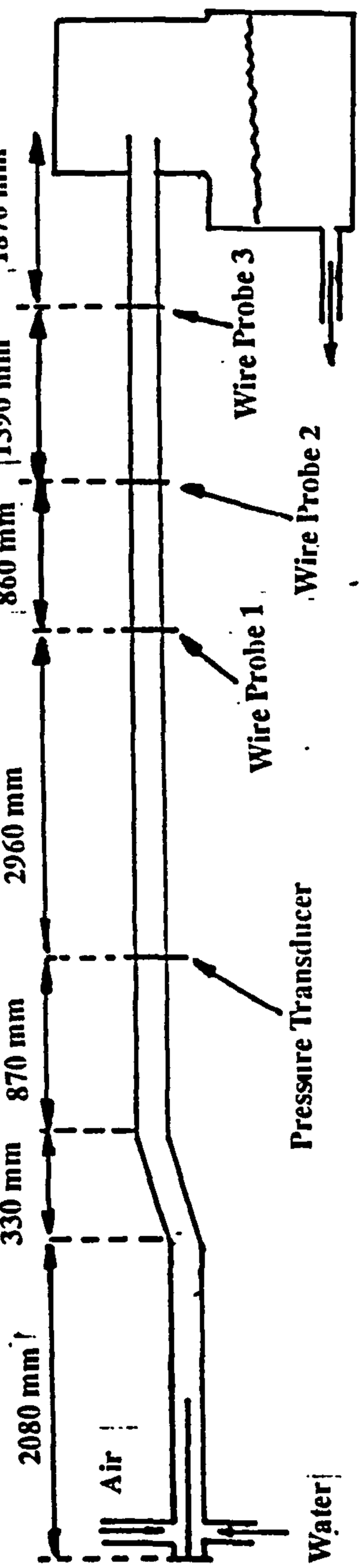
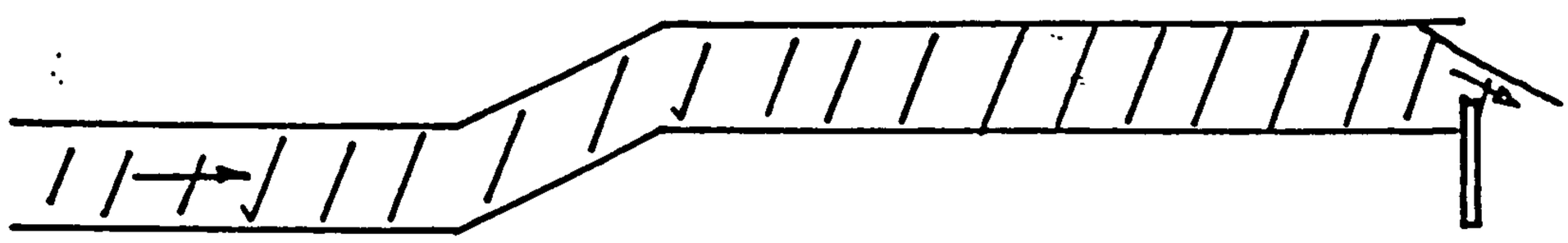
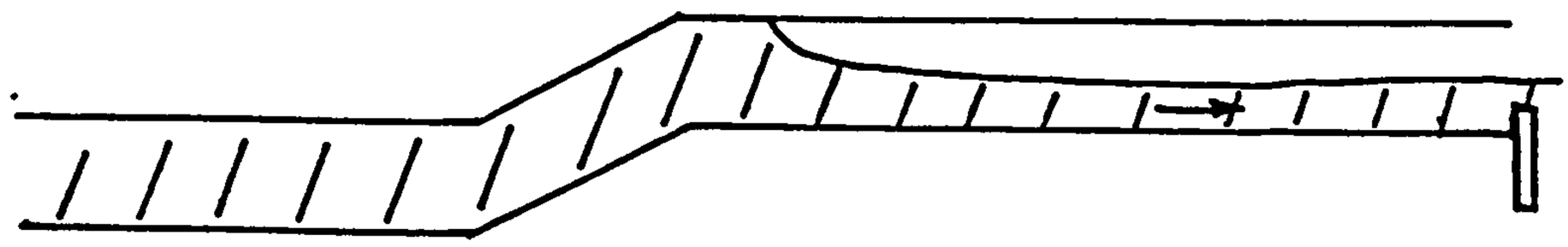


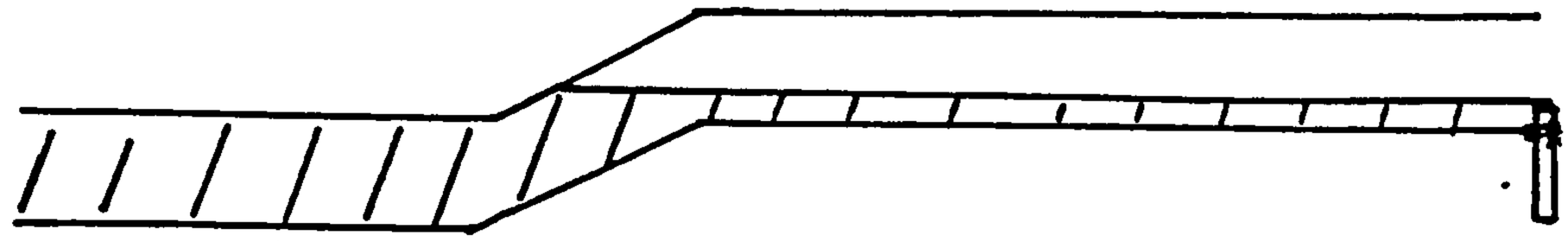
Figure 5.3.3 Test section configuration.



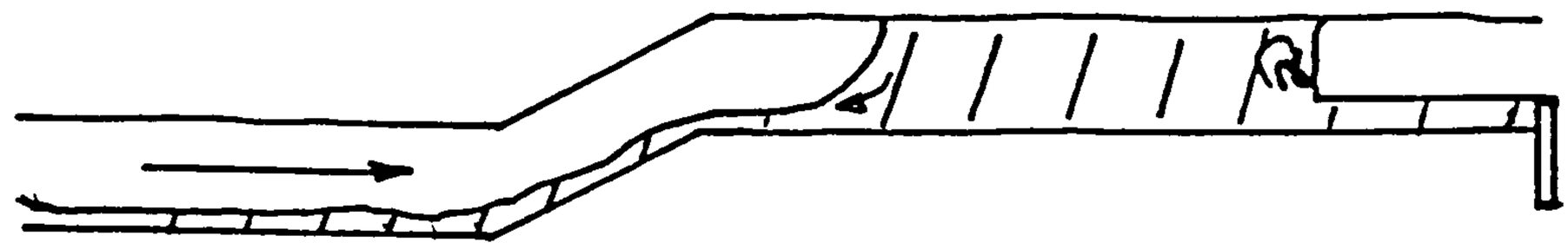
Test section is filled with water.



Pump switched off and liquid drains to level set by weir



Test section ready for introduction of artificial slug



Gas accelerates artificial slug into test section

Figure 5.3.4 Artificial slug experimental method.

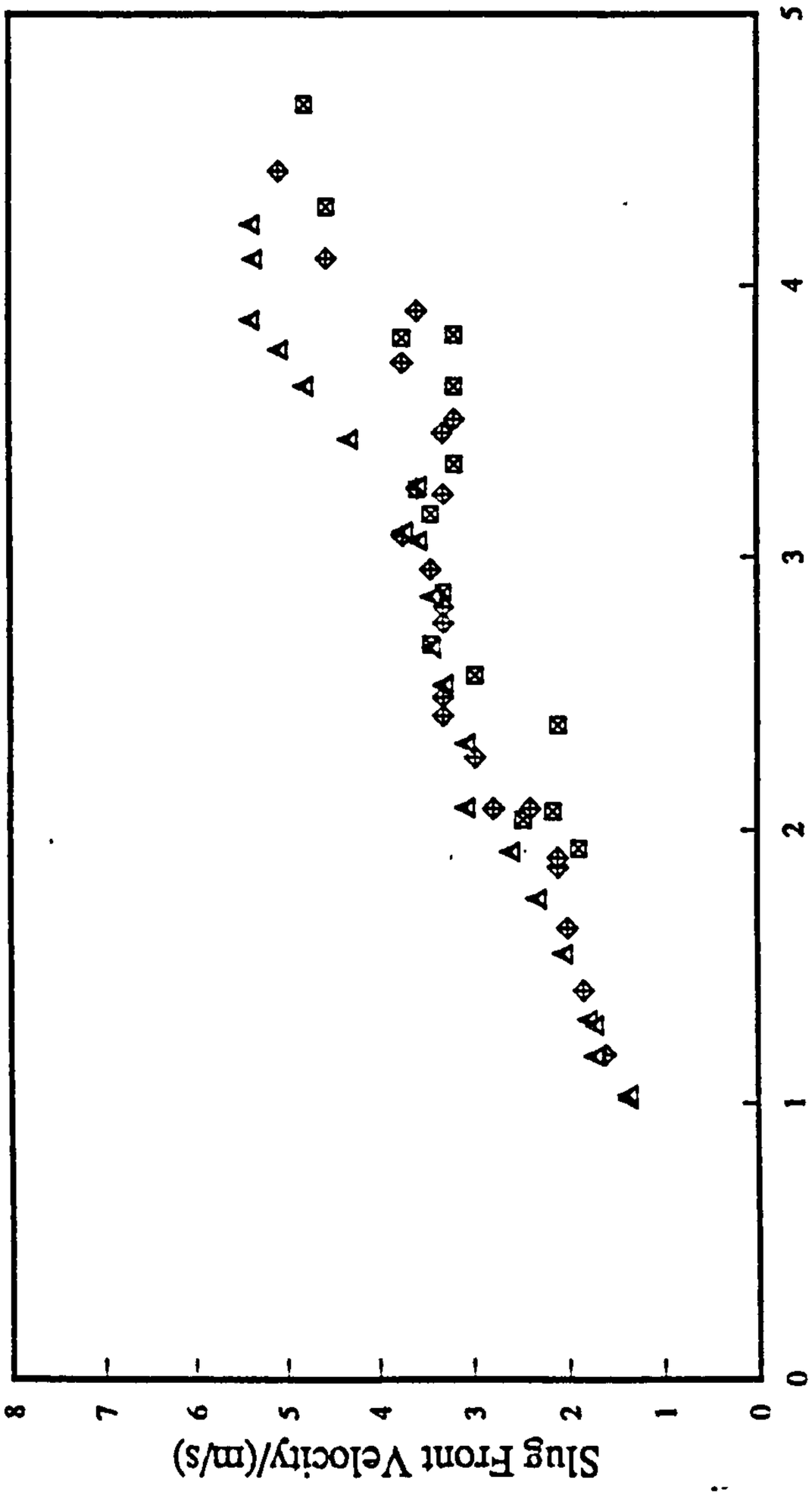


Figure 5.3.5 Slug front translational velocity as a function of gas superficial velocity.

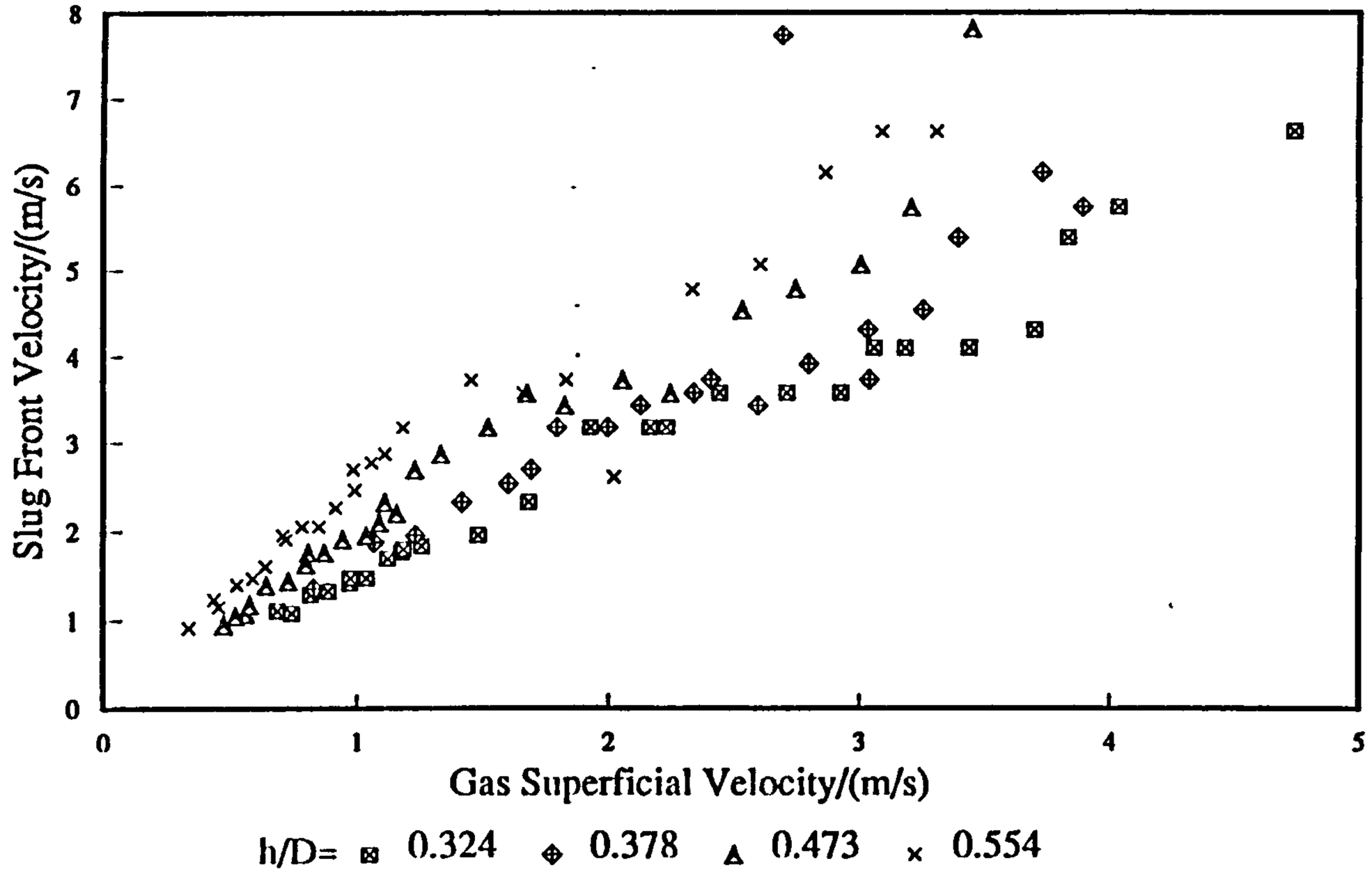


Figure 5.3.6 Slug front translational velocity as a function of gas superficial velocity.

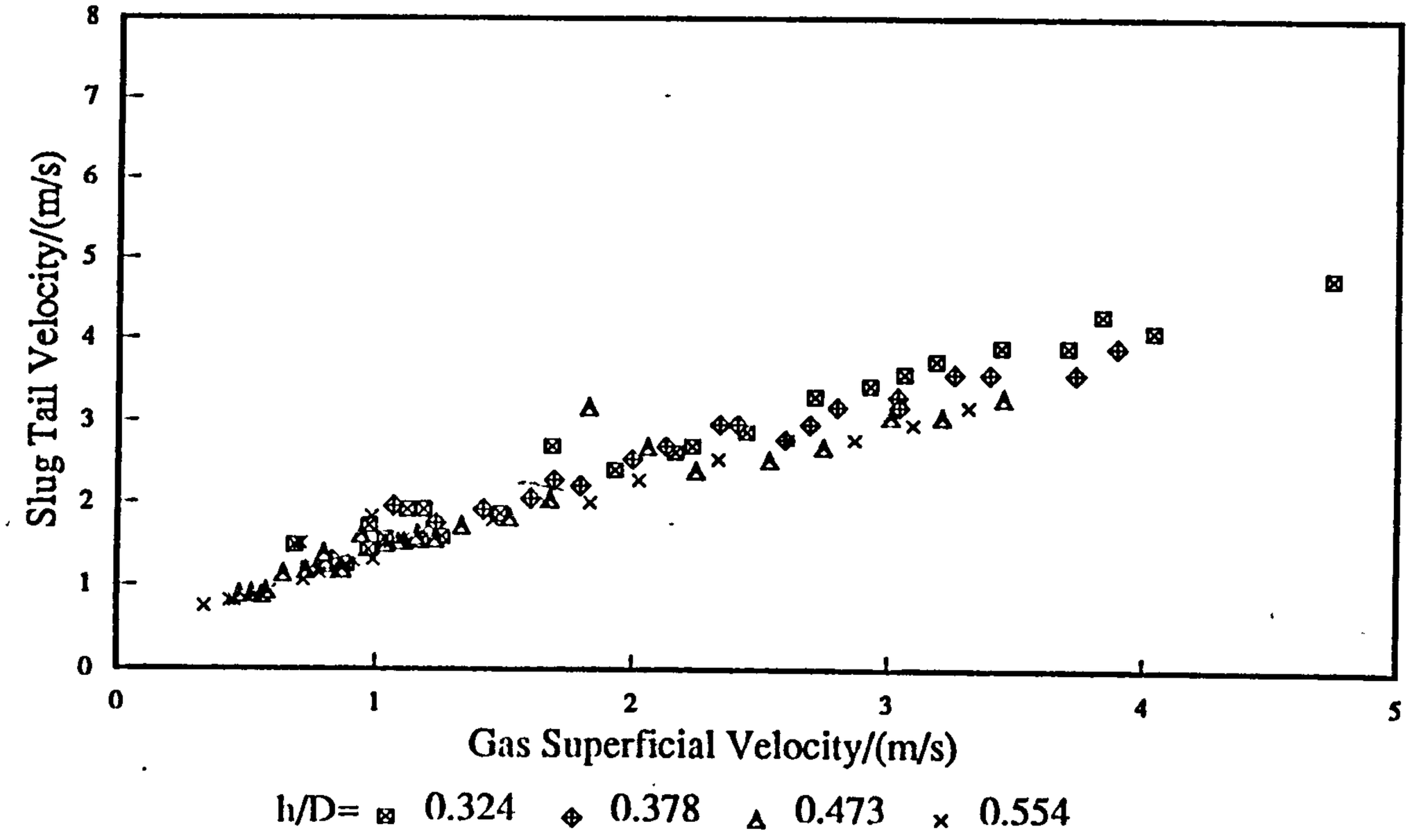


Figure 5.3.7 Slug tail translational velocity as a function of gas superficial velocity.

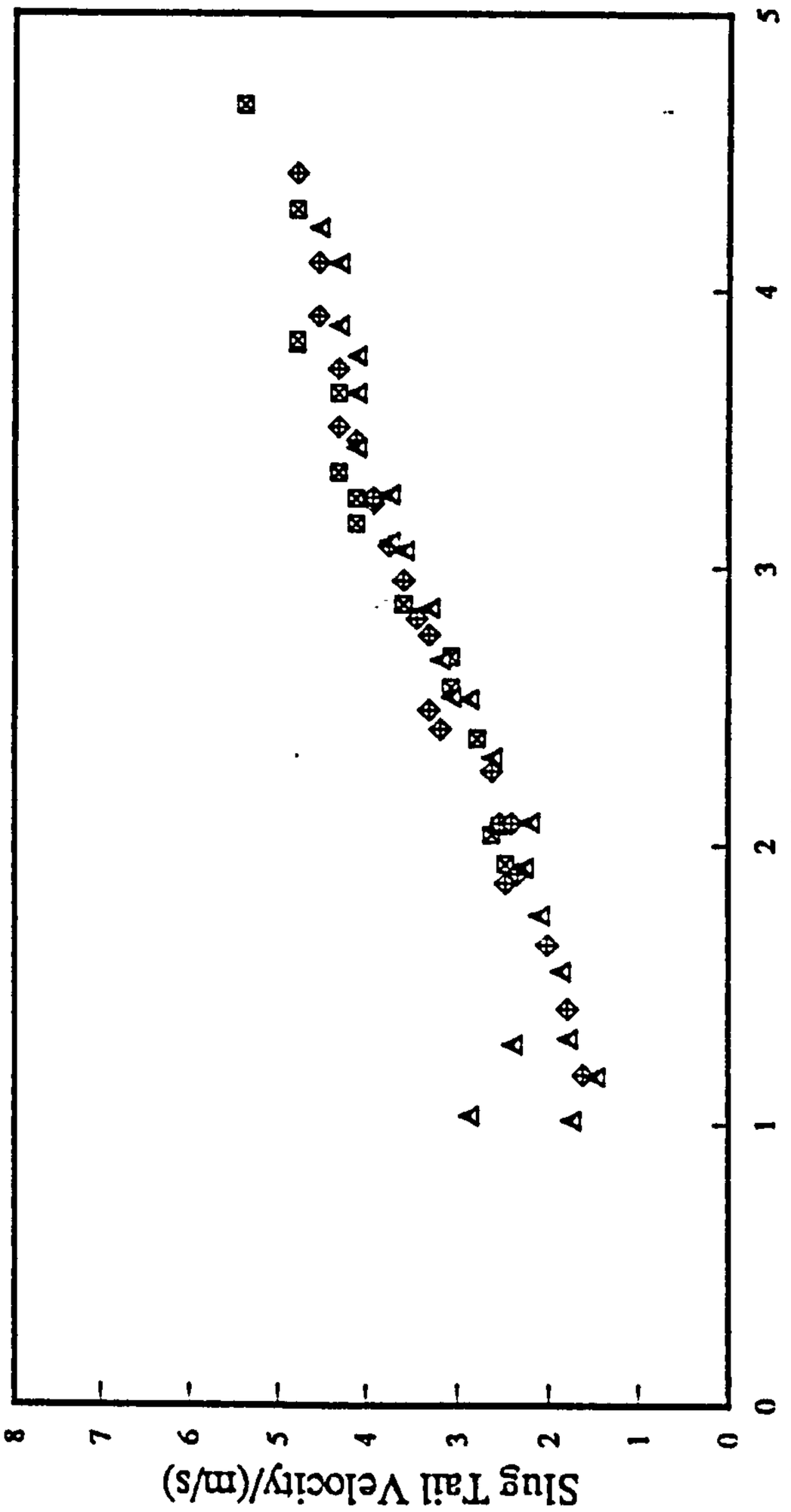


Figure 5.3.8 Slug tail translational velocity as a function of gas superficial velocity.

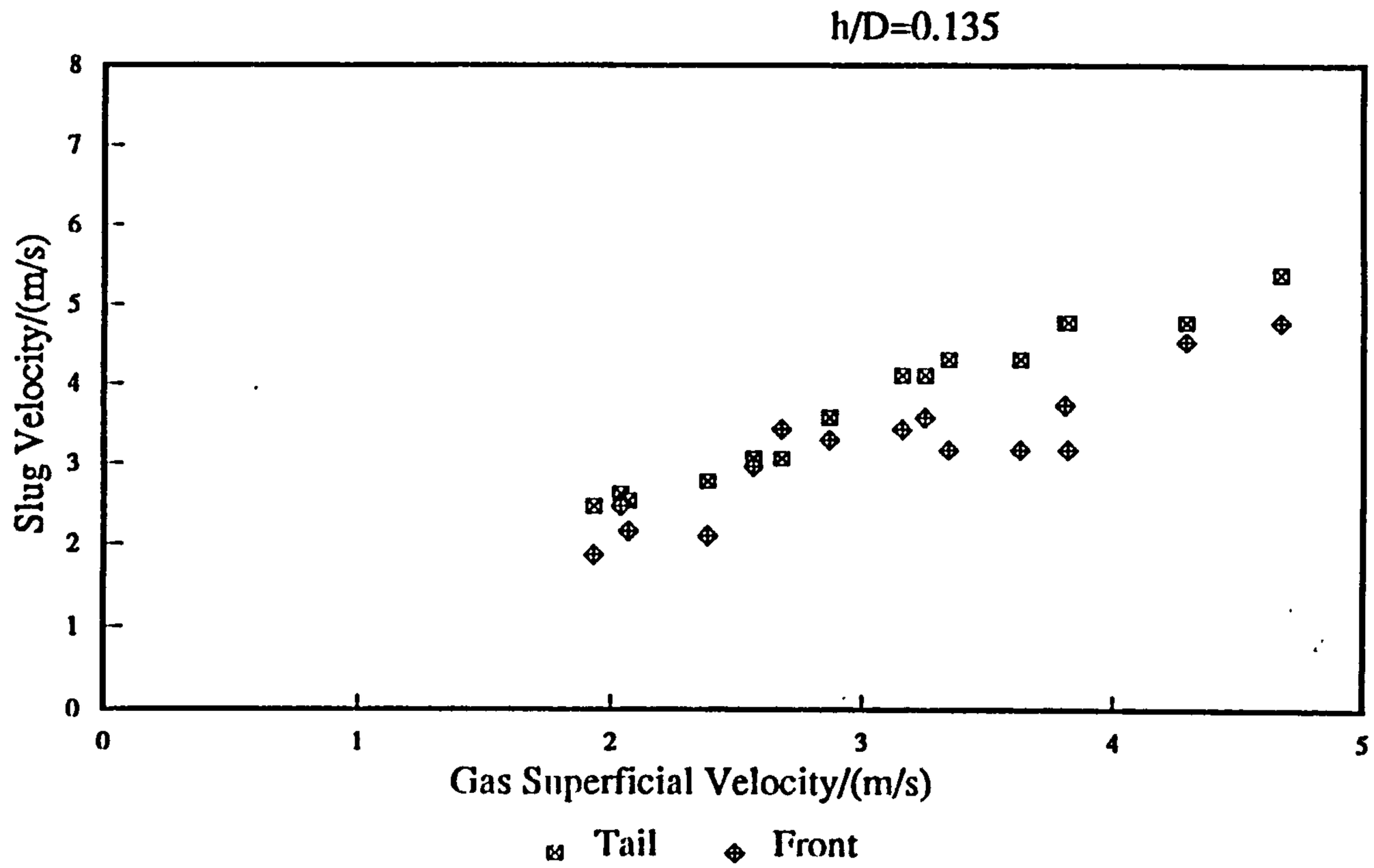


Figure 5.3.9 Comparison of slug tail and slug front translational velocities for h/D=0.135.

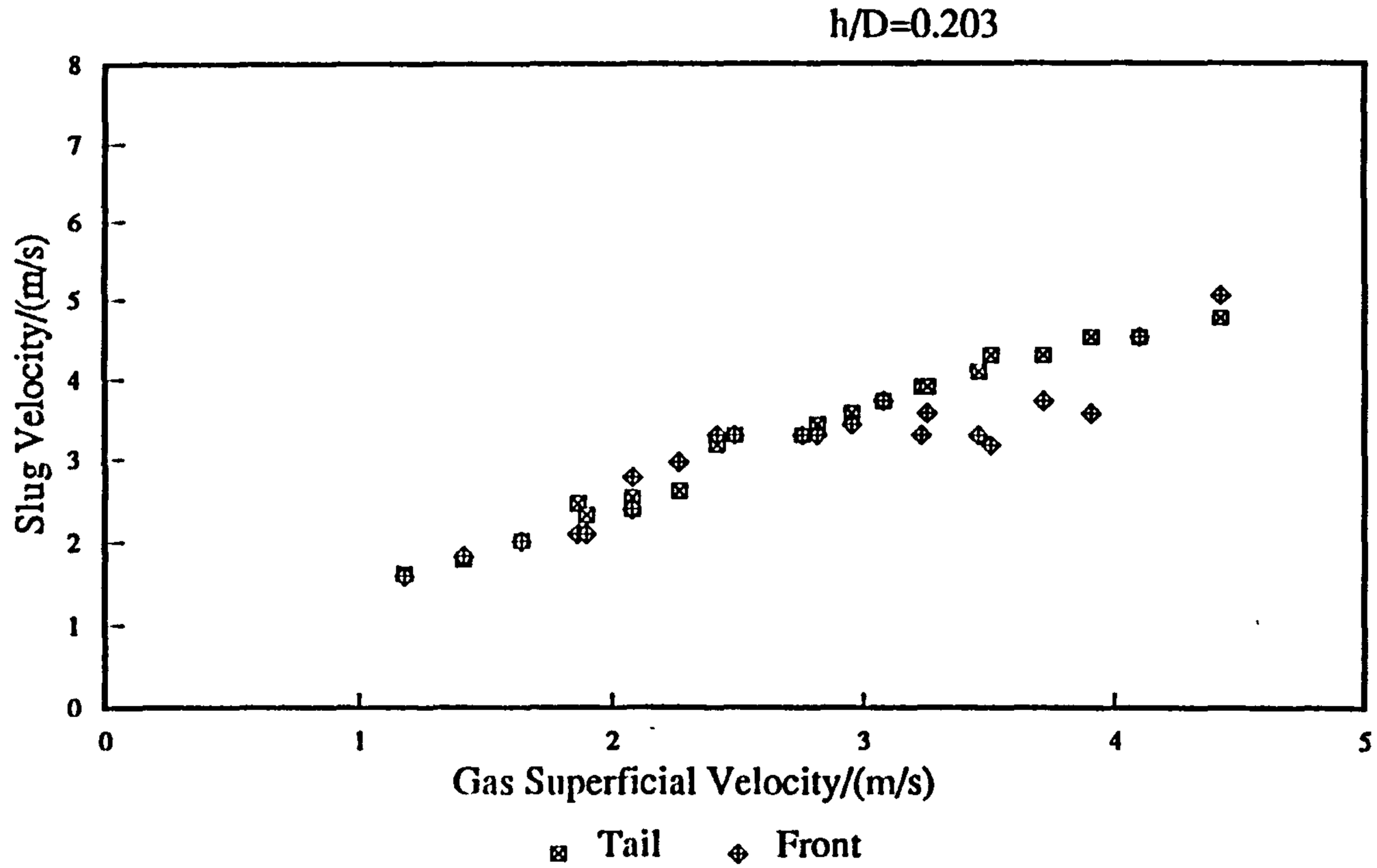


Figure 5.3.10 Comparison of slug tail and slug front translational velocities for h/D=0.203.

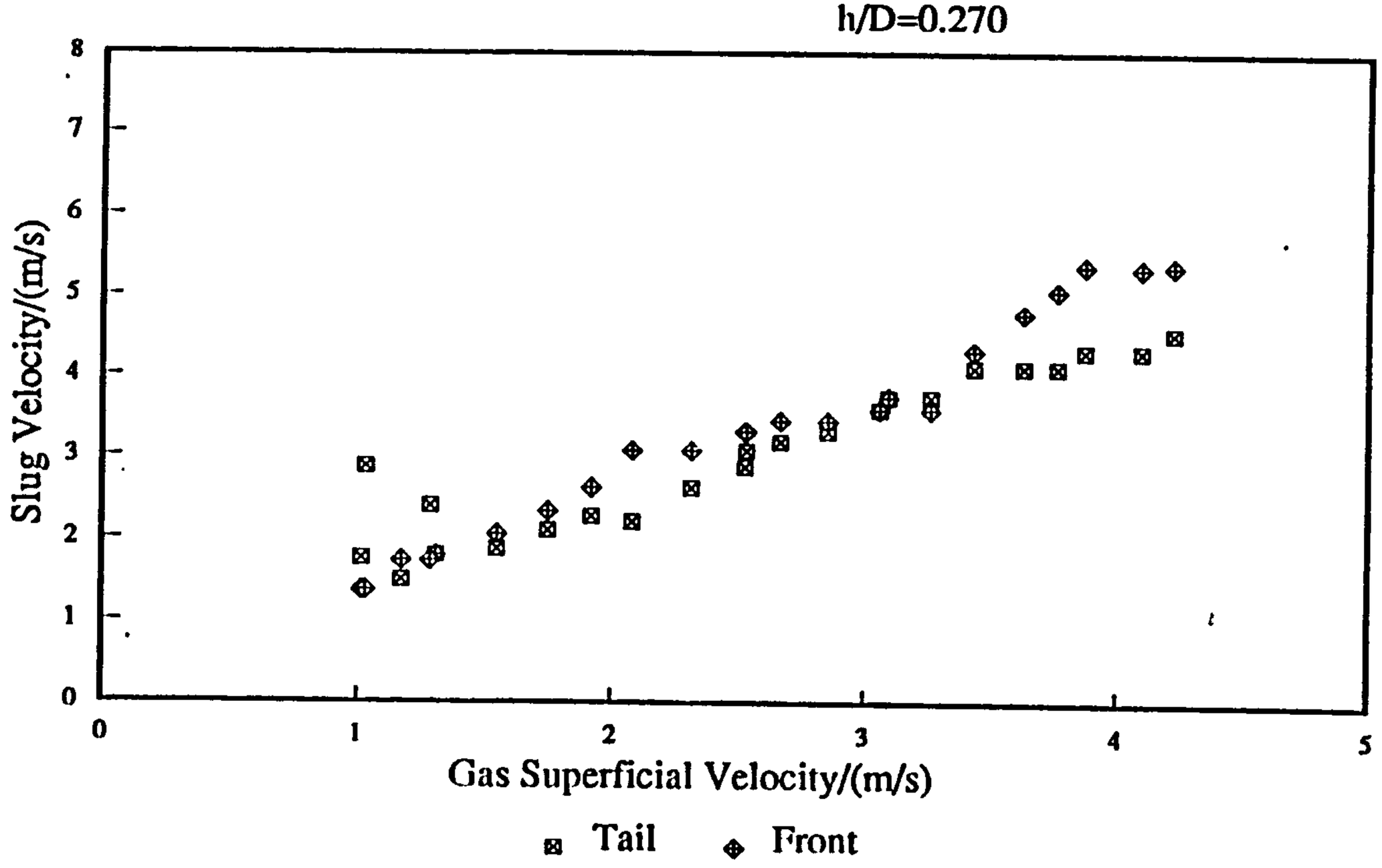


Figure 5.3.11 Comparison of slug tail and slug front translational velocities for h/D=0.270.

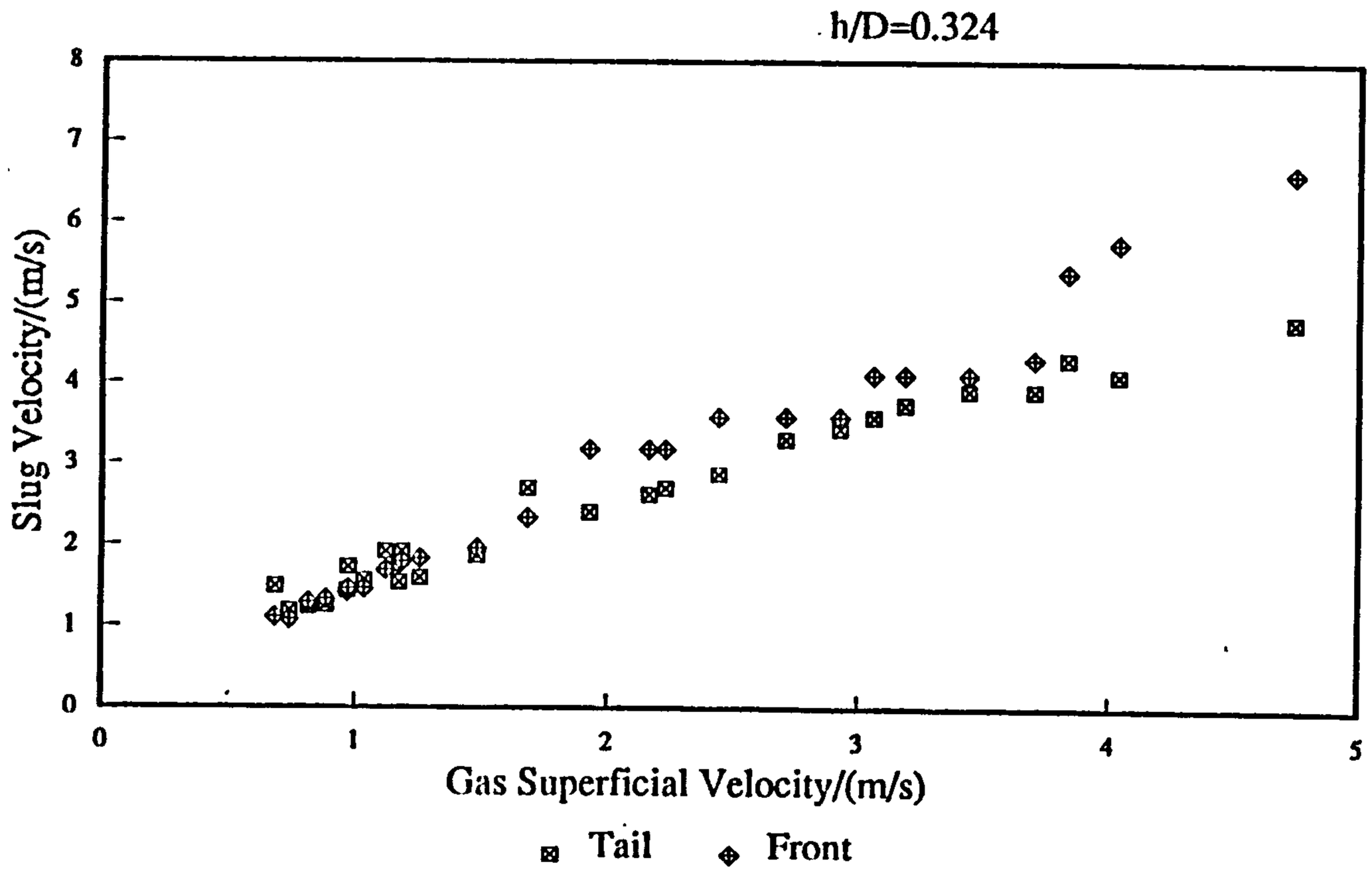


Figure 5.3.12 Comparison of slug tail and slug front translational velocities for h/D=0.324.

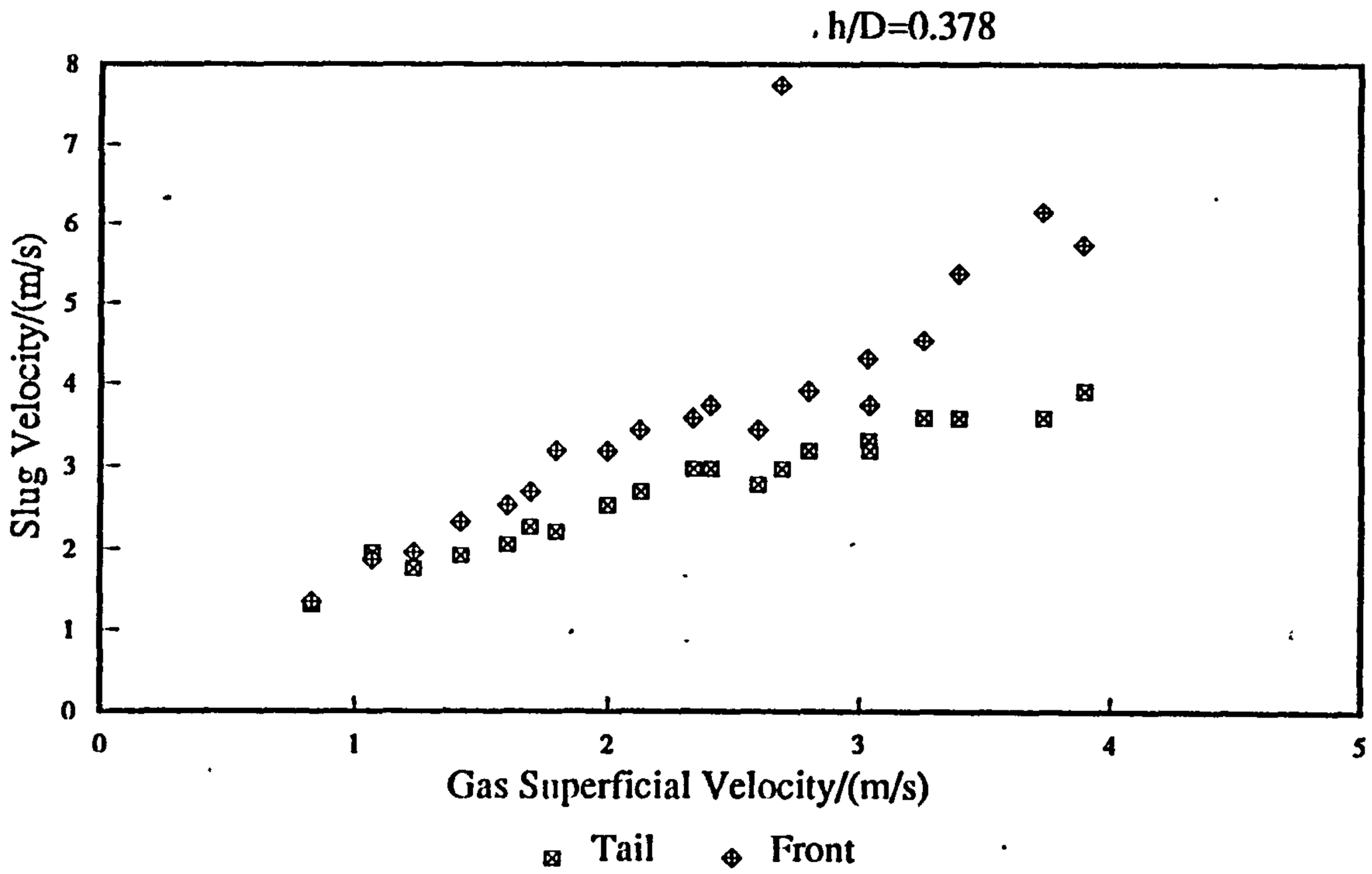


Figure 5.3.13 Comparison of slug tail and slug front translational velocities for h/D=0.378.

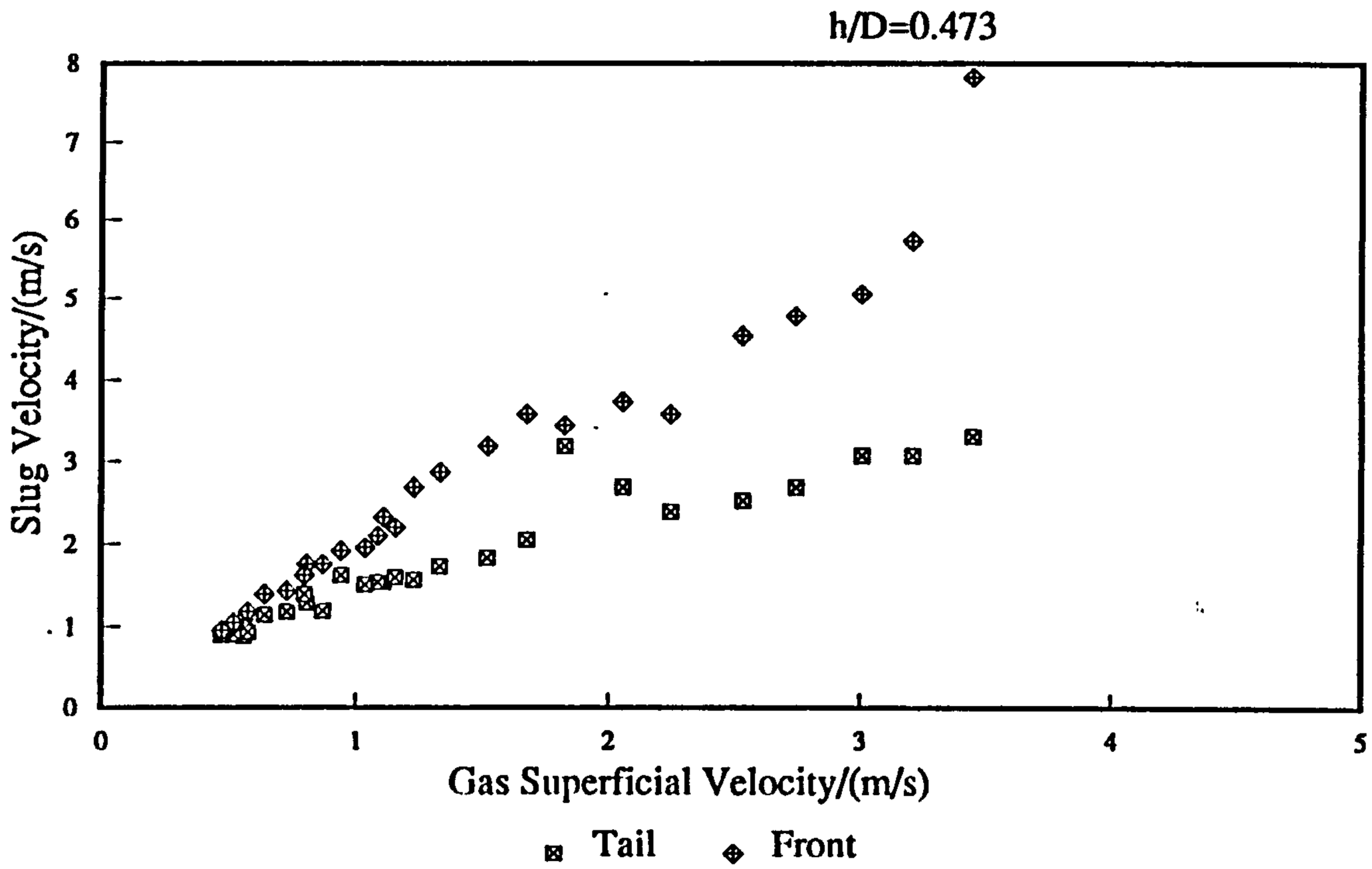


Figure 5.3.14 Comparison of slug tail and slug front translational velocities for h/D=0.473

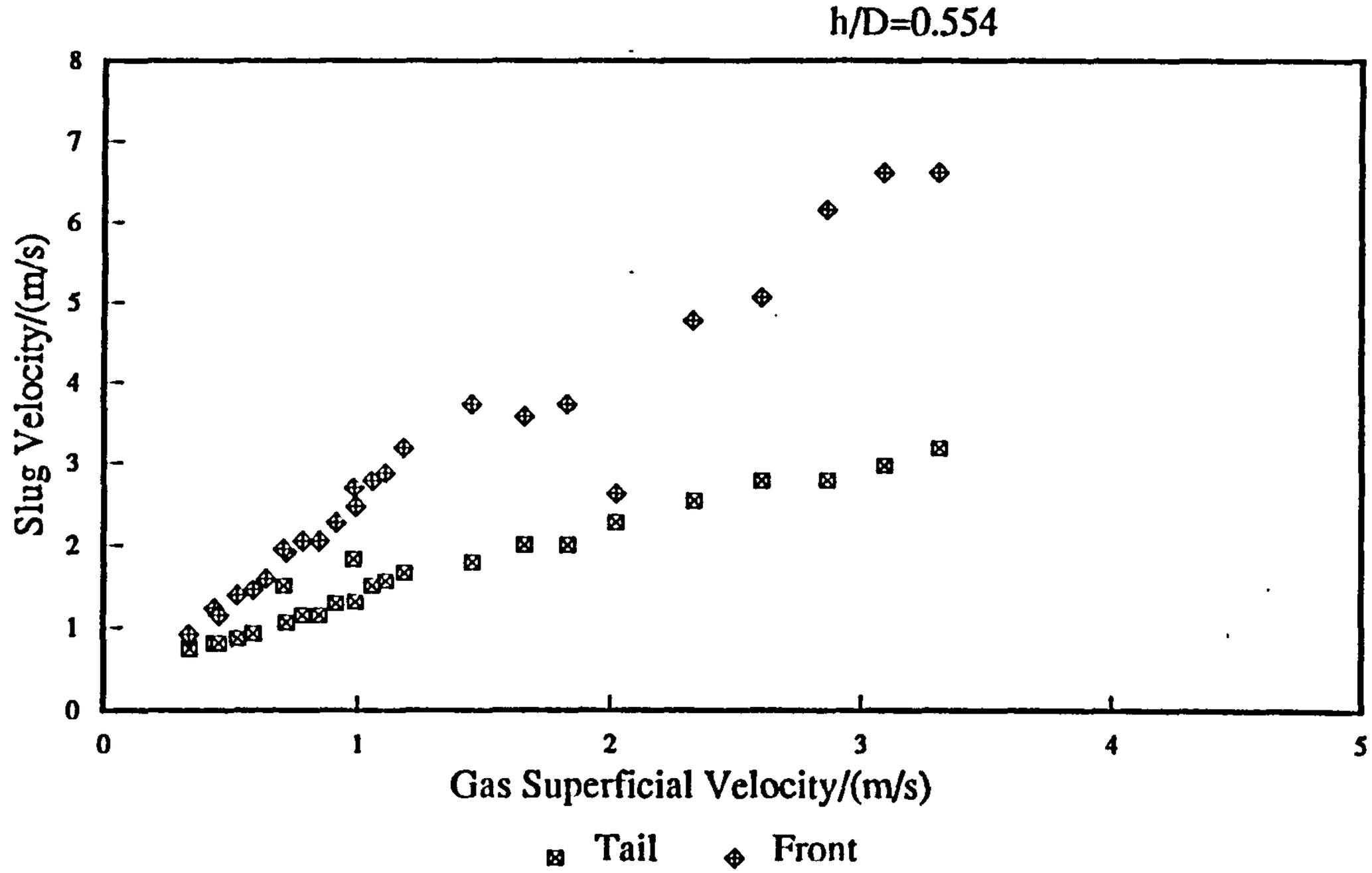


Figure 5.3.15 Comparison of slug tail and slug front translational velocities for h/D=0.554.

5.4 PREDICTION OF SLUG FREQUENCY

The existing mechanistic models of intermittent flow, such as that of Dukler and Hubbard (1975), require the specification of slug frequency for closure. While many authors recorded slug frequency as a function of gas and liquid flowrate, it was not until the work of Gregory and Scot (1969) and Greskovich and Shrier (1972) that "general" correlations for slug frequency appeared in the literature. These correlations do not have any phenomenological basis and are therefore limited to the (narrow) range of pipe size and fluid physical properties of the data on which they were based.

A correlation for slug length, a parameter closely related to slug frequency, was produced by Brill et al (1979) based on data sets covering a wider range of pipe diameters and physical fluid properties. A regression analysis was carried out to enable estimation of mean slug length and hence frequency, for steady flow as a function of superficial mixture velocity and pipe diameter. Brill et al (1979) supplemented the data base available by examining flow in pipelines of large diameter containing petroleum fluids in the Prudhoe Bay Field of Alaska. They noted that slug length could be represented by a log normal distribution, thus enabling designers of slug catchers to make probability assessments of the design slug length for vessel sizing.

Despite the importance of slug frequency for liquid loading calculations the only mechanistic model available in the literature is that of Taitel and Dukler (1977). In fact, researchers seem to have forsaken attempts to develop new approaches to slug frequency prediction. Nevertheless, slug frequency prediction remains an important challenge if a full mechanistic model for slug flow is to be developed.

In the following sections the model of Taitel and Dukler (1977) is reproduced, applied, and the validity of its assumptions assessed. Finally the components necessary for slug frequency prediction are discussed.

5.4.1 TAITEL AND DUKLER (1977) MODEL

The analysis of Taitel and Dukler (1977) is detailed in the following sections and a discussion of the model is presented in light of experimental observation of the slug formation process and an assessment of the assumptions made in the model.

5.4.1.1 The Model

The process of slug formation considered by Taitel and Dukler (1977) is illustrated in Figure 5.4.1. In Figure 5.4.1 (a) a slug has just been formed and moved away to the right, leaving a liquid surface sloping downwards in the direction of flow. The liquid level then begins to rebuild as further liquid enters the channel and eventually reaches an equilibrium level. This equilibrium level is determined by forces at the wall–liquid and gas–liquid interfaces. Waves form on the gas–liquid interface and grow as in Figure 5.4.1 (b). Eventually one wave bridges the pipe (Figure 5.4.1 (c)) and this liquid is accelerated forming a slug. The slug leaves a liquid level less than the equilibrium level just downstream of the slug formation point. The process then repeats itself.

In order to obtain slug frequency it is necessary to calculate the time between successive wave bridges of the pipe. Taitel and Dukler (1977) considered this time to consist of two parts:(1) The time t_1 after the equilibrium level is formed for a wave to bridge the pipe and for liquid to fall to its lowest level and (2), the time t_2 required for this liquid level to rebuild to the equilibrium level. They make the assumption that the wave grows rapidly and that the time (t_1) taken for the bridging to occur and the liquid to fall to its lowest level is negligible. Thus the slug frequency is the reciprocal of the time t_2 for the liquid to rebuild to the equilibrium level. Another important assumption made is that any wave closures occurring before the equilibrium level is reached result in non–persisting slugs.

5.4.1.2 Experimental observations

An examination of the slug initiation process was carried out using the low pressure rig described in Chapter Three. The pipeline was horizontal along its entire length. A cine camera operating at 400 frames/second and a high speed video camera and record-

ing equipment operating at 1000 frames/second visualised the flow just downstream of the entrance to the pipeline. A section of FEP tubing surrounded by a box containing water was used to reduce refractive index mismatch.

The observed process of slug formation agreed for the most part with the model of Taitel and Dukler (1977). The observed time taken for a wave to bridge the pipe was insignificant in comparison with the rebuild time of the liquid level. While this observation agrees with the model, it must be noted that the distance travelled by the growing wave prior to pipe bridging is significant, typically 150 mm. Consequently, the observed fall in the liquid level behind the growing wave varies gradually with distance along the pipe axis, eventually falling to the liquid level defined by the liquid shedding rate from the resulting slug tail. This contrasts with the initial step profile in the liquid level assumed by Taitel and Dukler (1977). Thus the model will overestimate the rebuild time for the liquid level and underestimate the slug frequency. It was also observed with increasing gas flowrate at constant liquid superficial velocity that waves could grow on the rebuilding liquid level and form slugs before the equilibrium level was reached, some of the slugs persisted to the end of the test section. For their model to be implemented Taitel and Dukler (1977) have to assume that any wave closures occurring before the equilibrium level is reached result in non–persisting slugs. This assumption, especially at higher gas flowrates, will result in an underestimate of the slug frequency.

Figures 5.4.2 to 5.4.5 show typical experimental initiation events observed with the high speed video camera. The dashed vertical lines on each frame are shown to indicate scale, adjacent lines being 20 mm apart. The vertical dimension is the pipe diameter of 74 mm.

5.4.1.3 Analysis

Taitel and Dukler (1977) only state the algorithm used to solve their equations. As a precursor to evaluation of the model, and to confirm the original calculations, the solution method was re–derived and is presented here for future researchers. Dukler and Taitel (1977) use the usual one–dimensional flow area averaged conservation equa-

tions. The liquid conservation equations are:

Momentum

$$g\cos\alpha\frac{\partial h}{\partial x} + \frac{\partial u_L}{\partial t} + u_L\frac{\partial u_L}{\partial x} = \frac{-\tau_L S_L}{\varrho_L A_L} + \frac{\tau_i S_i}{\varrho_L A_L} - \frac{1}{\varrho_L}\frac{\partial p}{\partial x} + g\sin\alpha \qquad (5.4.1)$$

Mass

$$\frac{\partial h}{\partial t} + u_L\frac{\partial h}{\partial x} + \frac{A_L}{S_i}\frac{\partial u_L}{\partial x} = 0 \qquad (5.4.2)$$

where

h is the height of the liquid from the pipe base

u_L is the liquid velocity at time t and position x.

τ_L is the shear stress acting at the wall–liquid interface.

τ_i is the shear stress acting at the gas–liquid interface.

S_i is the perimeter of the gas–liquid interface

S_L is the perimeter of the wall–liquid interface

A_L is the pipe area occupied by liquid..

Taitel and Dukler (1977) assume the gas velocity is much greater than the liquid velocity and thus can assume the following quasi steady–state form of the gas conservation equations.

Momentum

$$\frac{\partial p}{\partial x} = \frac{-\tau_G S_G}{A_G} - \frac{\tau_i S_i}{A_G} - \varrho_G\left(\frac{\dot{m}_G}{\varrho_G A_G}\right)\frac{S_i}{A_G}\frac{\partial h}{\partial x} \qquad (5.4.3)$$

Mass

$$A_G u_G \varrho_G = \dot{m}_G = constant \qquad (5.4.4)$$

where

A_G is the pipe area occupied by gas.

τ_G is the shear stress acting at the wall–liquid interface.

u_G is the gas velocity at time t and position x

$\dot{m}_G$ is the gas mass flowrate.

S_G is the perimeter of the wall–liquid interface.

It is assumed that the pressure drop in the gas and liquid is equal at the interface. Thus Equation (5.4.3) can be substituted in Equation (5.4.1) :

$$\frac{\partial u_L}{\partial t} + u_L\frac{\partial u_L}{\partial x} + \frac{\partial h}{\partial x}\left[g\cos\alpha - \frac{\varrho_G}{\varrho_L}\left(\frac{\dot{m}_G}{\varrho_G A_G}\right)^2\frac{S_i}{A_G}\right] =$$

$$-\frac{\tau_L S_L}{\varrho_L A_L} + \frac{\tau_i S_i}{\varrho_L A_L} + \frac{\tau_G S_G}{\varrho_L A_G} + \frac{\tau_i S_i}{\varrho_L A_G} + g\sin\alpha\left(1 - \frac{\varrho_G}{\varrho_L}\right) \qquad (5.4.5)$$

The term $$\frac{\varrho_G}{\varrho_L}\left(\frac{\dot{m}_G}{\varrho_G A_G}\right)^2\frac{S_i}{A_G} \qquad (5.4.6)$$

is called the "Bernoulli effect" by Taitel and Dukler (1977). The physical significance of this term is the creation of unstable waves due to a pressure gradient over the wave, caused by the acceleration of the gas over the wave. As the model of Taitel and Dukler is aimed at calculating a time to reach equilibrium they state that this term can be ignored.

Define:

$$B = g\cos\alpha \qquad (5.4.7)$$

$$S = -\frac{\tau_L S_L}{\varrho_L A_L} + \frac{\tau_i S_i}{\varrho_L A_L} + \frac{\tau_G S_G}{\varrho_L A_G} + \frac{\tau_i S_i}{\varrho_L A_G} + g\sin\alpha\left(1 - \frac{\varrho_G}{\varrho_L}\right) \qquad (5.4.8)$$

Substituting B and S into Equation 5.4.5 the following equations result:

$$\frac{\partial u_L}{\partial t} + u_L\frac{\partial u_L}{\partial x} + B\frac{\partial h}{\partial x} = S \qquad (5.4.9)$$

$$\frac{\partial h}{\partial t} + u_L\frac{\partial h}{\partial x} + \frac{A_L}{S_i}\frac{\partial u_L}{\partial x} = 0 \qquad (5.4.10)$$

In order to obtain a solution of these hyperbolic equations it is necessary to obtain expressions for the characteristic slope:

First add and subtract Equation 5.4.10 from Equation 5.4.9:

$$B\frac{\partial h}{\partial x} + u_L\frac{\partial u_L}{\partial x} + \frac{\partial u_L}{\partial t} +/- \sqrt{\frac{BS_i}{A_L}}\frac{\partial h}{\partial t} +/- u_L\sqrt{\frac{BS_i}{A_L}}\frac{\partial h}{\partial x} +/- \sqrt{\frac{BA_L}{S_i}}\frac{\partial u_L}{\partial x} = S \qquad (5.4.11)$$

rearranging:

$$\left[\frac{\partial}{\partial t} + \left(u_i +/- \sqrt{\frac{BA_L}{S_i}}\right)\frac{\partial}{\partial x}\right]\left[u_L +/- \int\sqrt{\frac{BS_i}{A_L}}dh\right] = S \qquad (5.4.12)$$

Inspecting the above equation the slope of the characteristics are:

$$\frac{dx}{dt} = u_L +/- \sqrt{\frac{BA_L}{S_i}} \qquad (5.4.13)$$

Taitel and Dukler (1977) used the finite difference scheme of Stoker (1957) to solve Equations 5.4.12. Writing the equations separately, we have:

$$\left[\frac{\partial}{\partial t} + \left(u_i + \sqrt{\frac{BA_L}{S_i}}\right)\frac{\partial}{\partial x}\right]\left[u_L + \int\sqrt{\frac{BS_i}{A_L}}dh\right] = S \qquad (5.4.12a)$$

$$\left[\frac{\partial}{\partial t} + \left(u_i - \sqrt{\frac{BA_L}{S_i}}\right)\frac{\partial}{\partial x}\right]\left[u_L - \int\sqrt{\frac{BS_i}{A_L}}dh\right] = S \qquad (5.4.12b)$$

Consider Figure 5.4.6, which defines the nomenclature for specifying a point in the t–x plane:

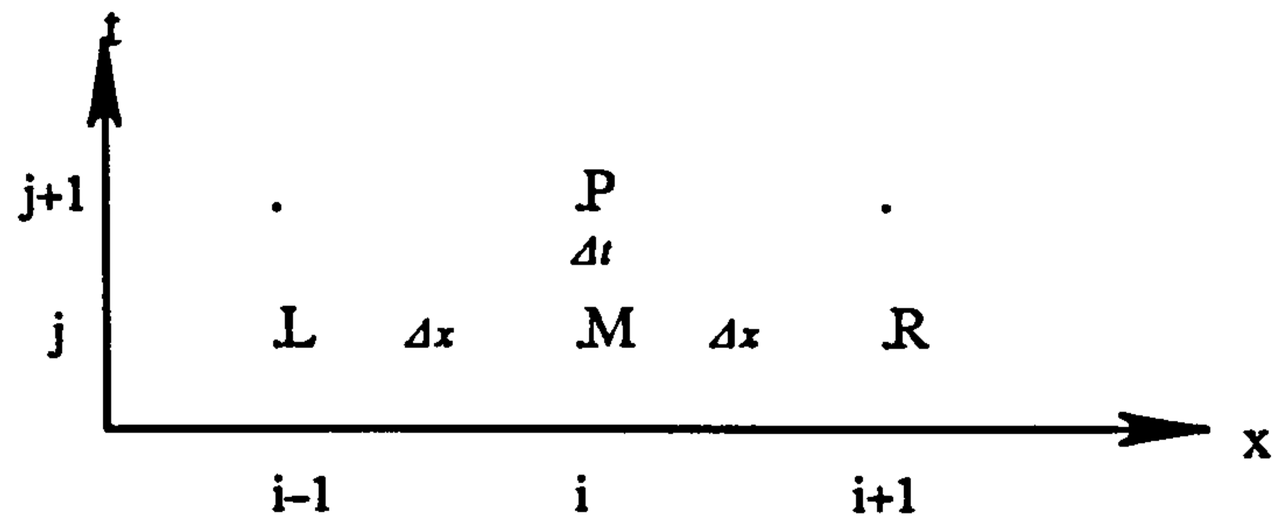


Figure 5.4.6 Nomenclature for location in t–x plane.

In order to advance the values h and u_L from points L,M and R using Equations 5.4.12, U_{Lt} and h_t are replaced by:

$$u_{Lt} = \frac{u_{ij+1} - u_{ij}}{\Delta t} \tag{5.4.14}$$

$$h_t = \frac{h_{ij+1} - h_{ij}}{\Delta t} \tag{5.4.15}$$

in both Equation 5.4.12a and 5.4.12b.

The subscript t denotes the derivative of a quantity with respect to time and the use of subscript x below denotes the derivative of a quantity with respect to co–ordinate x.

To ensure the convergence of the approximations to the exact solutions when t and x tend to zero it is necessary to replace the derivatives u_{Lx} and h_x by formulae which depend on the sign of the characteristic slope.

In the case of Equation 5.4.12a:

$$\frac{dx}{dt} = u_L + \sqrt{\frac{BA_L}{S_i}} \tag{5.4.16}$$

and the characteristic slope is always + ve. So a backward scheme is used for u_{Lx} and h_x:

$$u_{Lx} = \frac{u_{ij} - u_{i-1j}}{\Delta x} \tag{5.4.17}$$

$$h_x = \frac{h_{ij} - h_{i-1j}}{\Delta x} \tag{5.4.18}$$

In the case of Equation 5.4.12b:

$$\frac{dx}{dt} = u_L - \sqrt{\frac{BA_L}{S_i}} \tag{5.4.19}$$

and hence the characteristic slope can be negative or positive. If Equation 5.4.19 is positive then Equations 5.4.17 and 5.4.18 are used. A forward scheme is used for u_{Lx} and h_x if the characteristic slope of Equation 5.4.12b is negative:

$$u_{Lx} = \frac{u_{i+1j} - u_{ij}}{\Delta x} \tag{5.4.20}$$

$$h_x = \frac{h_{i+1j} - h_{ij}}{\Delta x} \tag{5.4.21}$$

So substituting the relevant finite difference scheme equations in Equations 5.4.12a and 5.4.12 two sets of equations for $u_{i,j+1}$ and $h_{i,j+1}$ exist with the set used depending on the sign of the characteristics.

The equations are:

For $\frac{dx}{dt} = u_L - \sqrt{\frac{BA_L}{S_i}} > 0$

$$h_{ij+1} = u_{ij}\frac{\Delta t}{\Delta x}\left[h_{i-1j} - h_{ij} - \frac{A_L}{S_i}\right] + \frac{\Delta t}{\Delta x}\frac{A_L}{S_i}u_{i-1j} + h_{ij} \qquad (5.4.22)$$

$$u_{ij+1} = S\Delta t + u_{ij}\left[1 - u_{ij}\frac{\Delta t}{\Delta x} + u_{i-1j}\frac{\Delta t}{\Delta x}\right] + B\frac{\Delta t}{\Delta x}[h_{i-1j} - h_{ij}] \qquad (5.4.23)$$

and for $\frac{dx}{dt} = u_L - \sqrt{\frac{BA_L}{S_i}} < 0$

$$h_{ij+1} = h_{ij} + u_{ij}\frac{\Delta t}{\Delta x}\sqrt{\frac{A_L}{BS_i}}\left[\frac{u_{i+1j}}{2} + \frac{u_{i-1j}}{2} - u_{ij}\right] - \frac{u_{ij}}{2}\frac{\Delta t}{\Delta x}[h_{i+1j} - h_{i-1j}]$$

$$- \frac{\Delta t}{2\Delta x}\frac{A_L}{S_i}[u_{i+1j} - u_{i-1j}]\frac{\Delta t}{\Delta x}\sqrt{\frac{BA_L}{S_i}}\left[\frac{h_{i+1j}}{2} + \frac{h_{i-1j}}{2} - h_{ij}\right] \qquad (5.4.24)$$

$$u_{ij+1} = S\Delta t + u_{ij} + u_{ij}\frac{\Delta t}{\Delta x}\sqrt{\frac{BS_i}{A_L}}\left[\frac{h_{i-1j}}{2} + \frac{h_{i+1j}}{2} - h_{ij}\right]$$

$$+ \frac{\Delta t}{\Delta x}\sqrt{\frac{BA_L}{S_i}}\left[\frac{u_{i-1j}}{2} + \frac{u_{i+1j}}{2} - u_{ij}\right] + \frac{u_{ij}}{2}\frac{\Delta t}{\Delta x}[u_{i-1j} - u_{i+1j}] + B\frac{\Delta t}{\Delta x}[h_{i-1j} - h_{i+1j}] \qquad (5.4.25)$$

Suitable initial values and boundary conditions make it possible to obtain the values of h and u_L with time and position using Equations 5.4.22 to 5.4.25. The selection of initial values and boundary conditions is discussed below.

Calculation of the time for the film to rebuild to its equilibrium level only requires the definition of the lowest level and equilibrium level conditions. The equilibrium level can easily be obtained for given gas and liquid input by an iterative solution of the fol-

lowing equation:

$$\frac{-\tau_L S_L}{\varrho_L A_L} + \frac{\tau_i S_G}{\varrho_L A_L} + \frac{\tau_G S_G}{\varrho_L A_G} + \frac{\tau_i S_i}{\varrho_L A_G} + g\sin\alpha\left(1 - \frac{\varrho_G}{\varrho_L}\right) = 0 \qquad (5.4.26)$$

This equation is the right hand side of Equation 5.4.5 set to zero. Dukler and Taitel (1977) assume that the lowest liquid level h_s is equivalent to the level below which no waves form at the gas–liquid interface. The model developed by Taitel and Dukler (1976) gives the following condition for this stability level:

$$u_G = \frac{\dot{m}_G}{\varrho_G A_G} = \left(1 - \frac{h_s}{D}\right)\left[\frac{(\varrho_L - \varrho_G) g \cos\alpha\ A_G}{\varrho_G S_i}\right] \qquad (5.4.27)$$

The expression enables h_s to be calculated for specified flowrates. Thus knowing both h_s and h_e the initial values and boundary conditions for the Dukler and Taitel (1977) model are:

$t=0$: $x > x_1$ $h=h_s$, $u_l=u_e$; $x \leq x_1$ $h=h_e$, $u_l=u_e$
$t > 0$: $x=0$ $h=h_e$, $u_l=u_e$

where u_e is the liquid velocity at equilibrium level conditions, h_e is the equilibrium liquid level and h_s is the liquid level from which the film rebuilds.

A computer code was written in fortran for calculating slug frequency from the equations re–derived above for the analysis of Taitel and Dukler (1977). The code includes both the equations for super critical flow (Equations 5.4.22 and 5.4.23) and sub critical flow (Equations 5.4.24 and 5.4.25), even though it is recognised that flowrates in the intermittent regime would mainly be super critical.

5.4.1.4 Consistency Check

This section applies the analysis developed in Section 5.4.1.3 to the example presented in the paper of Taitel and Dukler (1977) to check for consistency with the work of Taitel and Dukler (1977) prior to evaluation of their model.

Taitel and Dukler presented details of a solution for flow in a 3.81 cm diameter pipe at air and water flowrates of 0.09 kg/s and 1.0 kg/s respectively. Figure 5.4.7 shows the liquid profiles calculated in this work at various times, showing the liquid level rebuilding for the case above. At t=0, $x=x_1$ the level was defined as a step change from the equilibrium level of 0.02415 m to the stability level of 0.01238 m. There is a definite time of 1.13095 seconds at which the liquid level overshoots the equilibrium height at a position downstream of x=0. This time is that defined by Taitel and Dukler to be the inverse of slug frequency. The liquid profiles obtained have the same form as those presented by Taitel and Dukler (1977) and the overshoot time of 1.13095 seconds compares well with that of 1.13 seconds given by Taitel and Dukler.

In the code of this work the cell size is specified and does not vary with position or time. The maximum time step that can be chosen for a cell needs to be less than the time set by the characteristic in order to maintain stability of the numerical scheme. At each time step, prior to the calculation of the liquid height and velocity values for the new time, the maximum time step for each cell is calculated from the characteristic slopes and the smallest of these time steps selected. The analysis described in Section 5.4.1.3 is sensitive to cell size and time step. For example, consider a cell size of 0.02 m and the example problem described above. The smallest maximum time step may be reduced by division by a specified number, and then applied for all of the cells. Figure 5.4.8 shows the variation of calculated slug frequency as the number used to reduce the time step is changed. It is shown, in Figure 5.4.8, that the calculated frequency decreases from 0.91 Hz at characteristic time step to 0.884 Hz at one tenth and smaller of the characteristic time step.

5.4.1.5 Model Assessment

The three major assumptions of the model are summarised below:

(a) Bernouli term neglected.

(b) The lowest level h_s is calculated from the criteria for the critical gas velocity for stratified to intermittent flow transition. This choice is arbitrary.

(c) Smooth gas–liquid interface.

The sensitivity of the model of Taitel and Dukler (1977) to each of these assumptions is assessed below. In each case slug frequency calculations are carried out for the example problem of Taitel and Dukler (1977) described in Section 5.4.1.4.

The model neglects the "Bernoulli" term and from a purely mathematical point of view such an action would only be valid if the following condition was true:

$$g\cos\alpha \gg \frac{\varrho_G}{\varrho_L}\left(\frac{\dot{m}_G}{\varrho_G A_G}\right)^2 \frac{S_i}{A_G}$$

The value of gcos α for the example problem above is 9.81, Figure 5.4.9 shows how the value of the Bernoulli term varies along the liquid profile. As can be seen it varies from 48 on the stratified equilibrium level to 4 on the stability level. At no point in the liquid profile is the Bernoulli term insignificant in comparison with gcos α Also for most of the profile:

$$g\cos\alpha < \frac{\varrho_G}{\varrho_L}\left(\frac{\dot{m}_G}{\varrho_G A_G}\right)^2 \frac{S_i}{A_G}$$

which predicts the development of unstable waves on the gas–liquid interface as a result of decreased pressure above a wave due to gas acceleration.

Taitel and Dukler (1977) do not evaluate the magnitude of the Bernoulli term but acknowledge that retention of the term would result in no unique steady state solution.

The time taken for the liquid to rebuild to the equilibrium level after slug formation is dependant on the value chosen for the low liquid level, h_s. The choice by Taitel and Dukler (1977) of the criterion for critical gas velocity for the stratified to intermittent flow transition to calculate h_s is arbitrary and somewhat inconsistent with their model. This inconsistency may be explained by the following argument. As soon as the liquid level starts to rebuild, there will be a liquid level h between h_e and h_s. This liquid level h will be greater than h_s, the level above which the gas–liquid interface will be unstable to small disturbances. Such an instability if formed on the rebuilding liquid level will sweep liquid from the rebuilding level, increasing the time to return to the equilibrium liquid level h_e. In fact, the equilibrium level may never be reached before the next slug is formed. This is examined further in Section 5.4.2.1 below.

The observed experimental fall in the liquid level behind the growing wave varies gradually with distance along the pipe axis, eventually falling to the liquid level defined by the liquid shedding rate from the resulting slug tail. This contrasts with the initial step profile in the liquid level assumed by Taitel and Dukler (1977). Thus, as stated earlier, the model will overestimate the rebuild time for the liquid level and underestimate the slug frequency. Figure 5.4.10 shows the sensitivity of the slug frequency calculations to the stability level. As can be seen, the model of Taitel and Dukler (1977) is very sensitive to the value of h_s.

The other boundary condition specified for the model is the equilibrium level, h_e. The equilibrium level is calculated by solving Equation 5.4.26. Taitel and Dukler (1977) assume a smooth gas–liquid interface, equating the interfacial friction factor f_i to the gas friction factor f_G. This assumption, $f_i=f_G$, can cause large errors in the prediction of stratified flow interface heights if waves exist at the gas–liquid interface. Andritsos and Hanratty (1987) have shown that the ratio of f_i to f_G can be much greater than 1 for air–water stratified flows in a pipe. Figure 5.4.11 shows the variation of h_e, with the value of f_i/f_G. Figure 5.4.12 shows the resulting significant sensitivity of slug frequency to f_i/f_G.

5.4.2 SLUG FREQUENCY MECHANISM

The model of Taitel and Dukler and its associated mathematical analysis has been shown to omit a term in the analysis, which is significant. Also the basis suggested by Taitel and Dukler for calculation of the boundary conditions h_e and h_s needs changing to take account of waves on the interface in the case of h_e and the choice of calculation method for $h_{s,}$, which has been shown to be inappropriate experimentally. Even so, the model of Taitel and Dukler (1977) remains the only mechanistic model available in the literature to the knowledge of the present author.

Determining slug frequency requires an understanding of the mechanisms that determine slug frequency. A new mechanism for slug formation is suggested in Section 5.4.2.1 below and interaction of existing slugs and the slug formation mechanism discussed in Section 5.4.2.2.

5.4.2.1 Slug Initiation Frequency

It was observed that waves could grow on the rebuilding liquid level and form slugs before the equilibrium level was reached, with some of the slugs persisting to the end of the test section. Also in Section 5.4.1.5 it was noted that the gas–liquid interface could be unstable while rebuilding, based on the criterion for critical gas velocity for the stratified to intermittent flow transition (Taitel and Dukler, 1976). These observations suggest the following mechanism, shown in Figure 5.4.13 for representing slug initiation frequency.

It is suggested that there is a position x_e downstream from the pipe inlet at which unstable waves first appear. At this position a wave starts to grow and eventually blocks the pipe at an axial position x_1 downstream of x_e. The liquid blockage is then accelerated by the gas and a slug is formed. The resulting liquid level has a gradient that varies gradually from the equilibrium level at position x_e to a level downstream specified by the amount of liquid shed from the tail of the formed slug. The hydrostatic forces resulting from this liquid gradient rebuild the level downstream of position x_e. While the level is rebuilding unstable waves are still occurring at position x_e and travelling onto

the rebuilding interface. Let us assume that there is an axial distance from the inlet x_u ($x_u>x_e$) where the liquid height is above h_s, the liquid height calculated from the criterion for critical gas velocity for the stratified to intermittent flow transition. Thus for $x_e<x<x_u$ waves grow on the interface and travel downstream. So, an unstable wave will grow on the rebuilding interface, but not necessarily block the tube. If the decrease in liquid height of the interface is greater than the gain in amplitude of the wave as it grows on the re–building interface, then the vertical distance between the top of the pipe and the wave top will increase and no pipe blockage will occur. Conversely, if the gain in amplitude of the wave as it grows on the re–building interface is greater than the decrease in liquid height of the interface then pipe blockage may occur if sufficient growing length is available to the wave. It is also suggested that such a mechanism for slug formation would result in the axial position in the pipe at which a wave blocks the pipe varying for a given flow condition.

Thus, it is suggested that a slug may be formed before the film can rebuild to the equilibrium level downstream of position x_e. It is therefore necessary to represent the growth of a wave on the re–building interface to obtain the slug formation frequency.

5.4.2.2 Slug formation–slug interaction

A pipe blockage formed by the above mechanism will persist as a slug if sufficient liquid is available downstream for it to grow. It is interesting to consider if the presence of slugs downstream of the slug formation position feeds back on the frequency at which slugs are formed.

Consider a flow condition with a gas velocity infinitesimally above the critical gas velocity defining the stratified to intermittent flow transition boundary. Gas and liquid flowrates at the test section inlet are independent of downstream pressure. The pipeline length is such that any slug transit time to the end of the pipe is significantly greater than the stratified layer rebuild time resulting from slug formation. At this point the gas velocity over the stratified flow is just above the critical gas velocity as defined by a criterion for unstable waves such as that of Taitel and Dukler (1976). A slug is formed

and travels down the pipe, with the pressure in the upstream gas cavity reaching a higher (than before the slug formed) steady value, after the initial pressure transient due to the acceleration of the pipe blockage from rest.

This pressure increase will result in the gas velocity over the liquid surface decreasing and hence the liquid level rising due to reduced interfacial shear. The flow geometry upstream of the slug will be stratified. The gas velocity over the slightly higher equilibrium height for the gas–liquid interface will be less than the critical gas velocity (for the new equilibrium height) defining the stratified to intermittent flow transition boundary. Thus no slug will be formed when the level re–builds to the equilibrium level. The exit of the slug from the pipeline releases the gas pressure upstream and the resulting velocity over the liquid interface is greater than that of the initial stratified flow, with a greater liquid height. Hence a new slug is formed. The slug frequency for the above case will not be determined by the time taken to re–build the liquid interface after slug formation but by the transit time for the slug in the pipe. The above assumes that the local values of the liquid superficial velocity which form the stratified to intermittent flow transition boundary increase with decreasing gas superficial velocity.

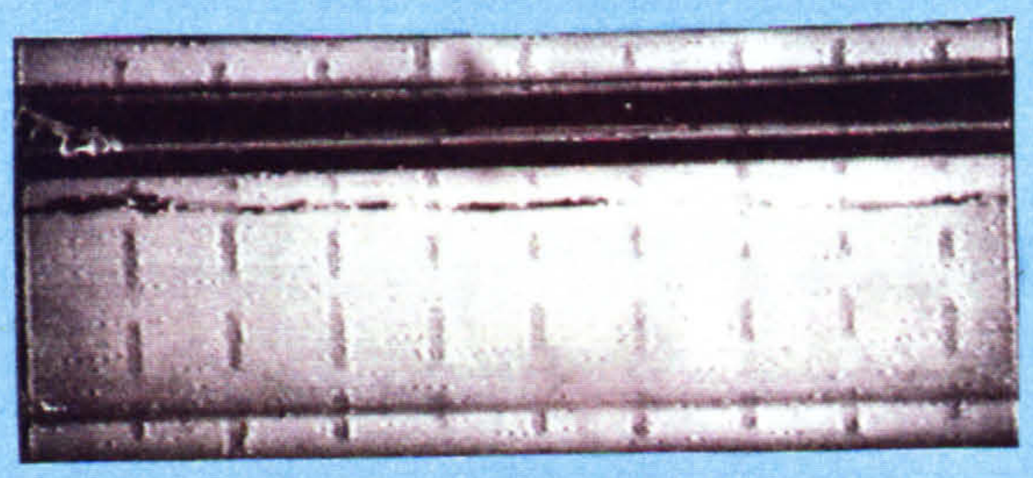
For the same liquid flowrate, consider a flow condition with a gas velocity greater than the critical gas velocity defining the stratified to intermittent flow transition boundary. Again the pipeline length is such that slug transit time to the end of the pipe is significantly greater than the stratified layer rebuild time resulting from slug formation. For this thought experiment consider only the acceleration of the liquid film at the slug front to contribute to the pressure drop, so that the pressure drop due to all steady–state slugs in the pipe are equivalent, irrespective of slug length. For the particular flow condition, let three slugs provide a pressure drop in the pipe sufficient to reduce the gas velocity over the gas–liquid interface below the critical gas velocity for the stratified to intermittent flow transition boundary. Consider an initial condition of stratified flow in the pipe. Keeping the liquid mass flowrate constant, the gas mass flowrate is sharply increased to a gas flowrate which is well above the critical gas velocity defining the stratified to intermittent flow transition boundary. A first slug is formed which quickly

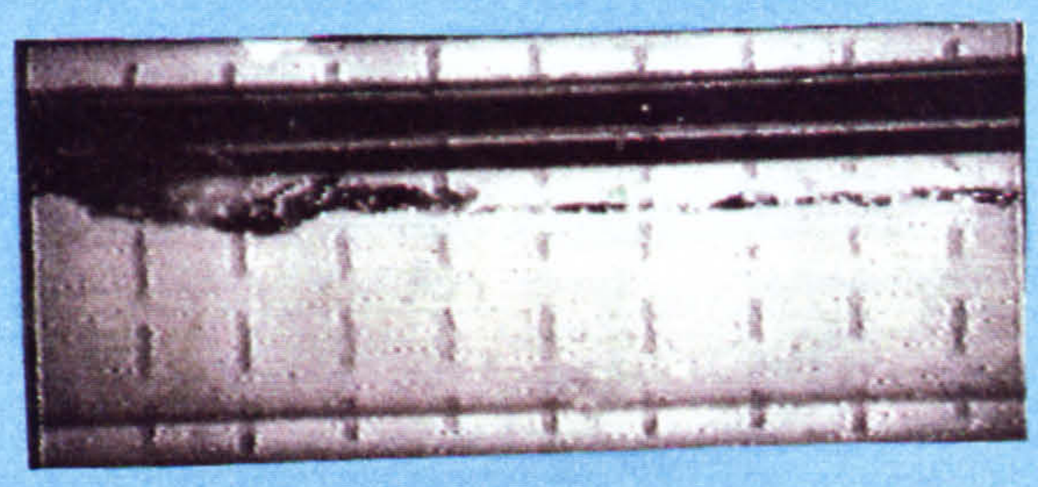
reduces the liquid level in the pipe. A second slug is formed after the liquid level as rebuilt to a sufficient level. Again the liquid level has to re–build before the a third slug can be formed. The increased pressure over the stratified layer due to first and then the second slug will, of course, produce different rebuild times for the formation of the second and third slugs. Thus, there are now travelling in the pipe three slugs closely spaced and the gas velocity over the gas–liquid interface is now below the critical gas velocity for the stratified to intermittent flow transition boundary. Behind the third slug the stratified gas–liquid interface is advancing down the pipe. The first slug exits the pipe and a fourth slug is formed at the inlet, this slug growing rapidly on the long length of stratified flow ahead of it. The second and third slugs exit the pipe soon after the first and a fifth slug and sixth slug form at the inlet. Thus the pattern of slugging observed at the pipe exit will be a long slug followed immediately by two shorter slugs and then a longer period of time before another long slug appears.

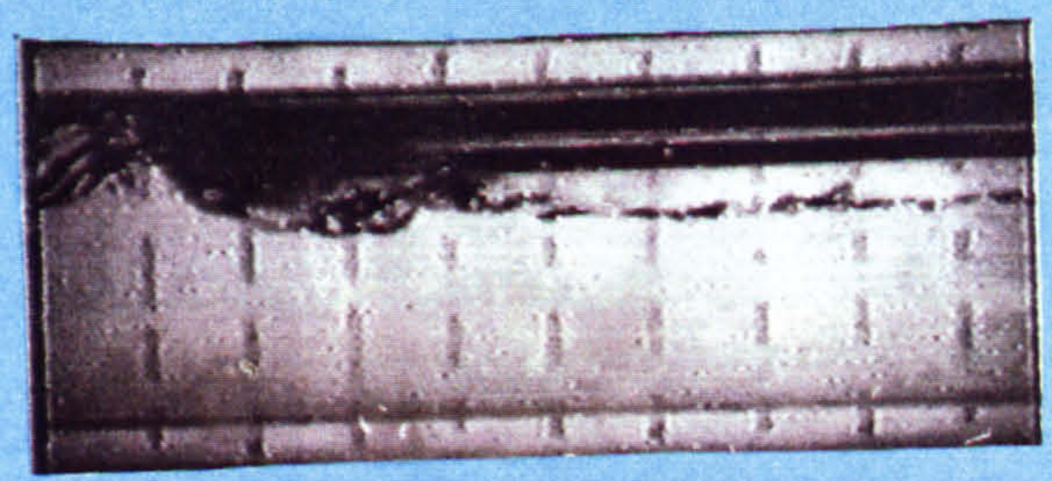
It has been suggested above, that slugs may have a feedback effect on the slug formation frequency. The extent of this feedback will depend on the pipe–length, the amount of pressure drop developed by the slugs in the tube and the gas–liquid flow condition. Development of a mechanistic model for the slug formation mechanism suggested in Section 5.4.2.1 will require a substantial effort. Following such work, the effect on slug frequency of the interaction of preceding slugs and slug formation mechanisms could be examined through the development of a transient model for flow of multiple slugs in a pipeline. Prediction of slug frequency is a major problem that requires significant investment of resources to resolve further.

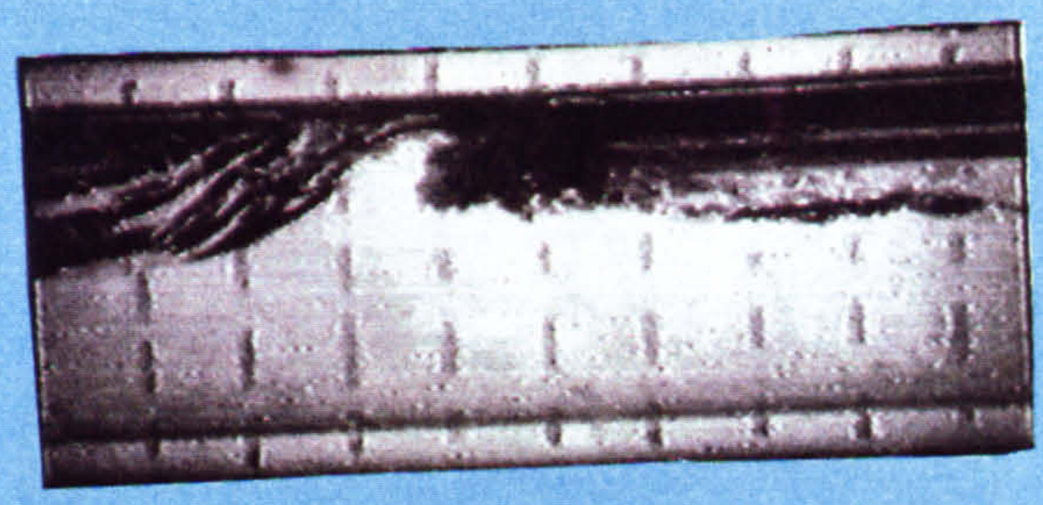


Figure 5.4.1 Process of slug formation (Taitel and Dukler, 1977)









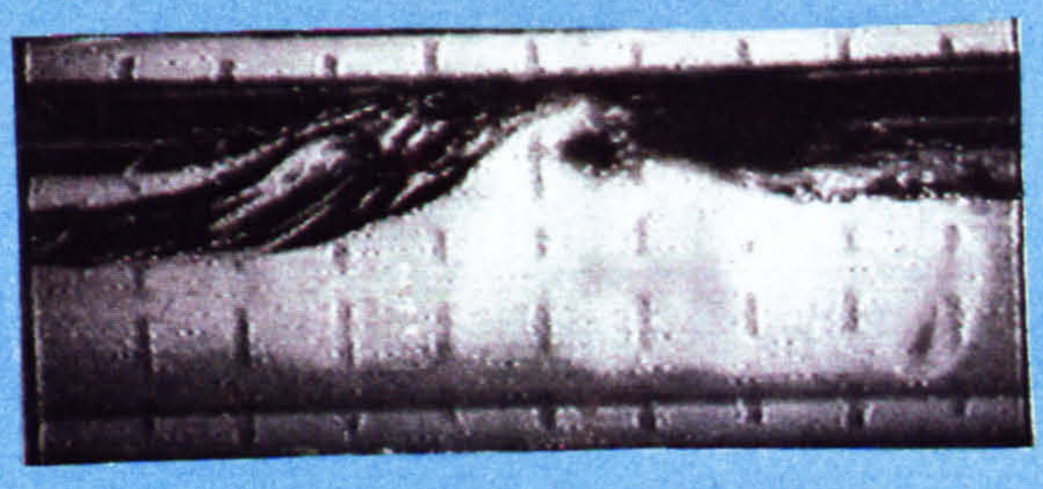


Figure 5.4.2 Slug initiation. (Gas superficial velocity=1.84m/s, liquid superficial velocity=0.295 m/s)
(Continued overleaf)

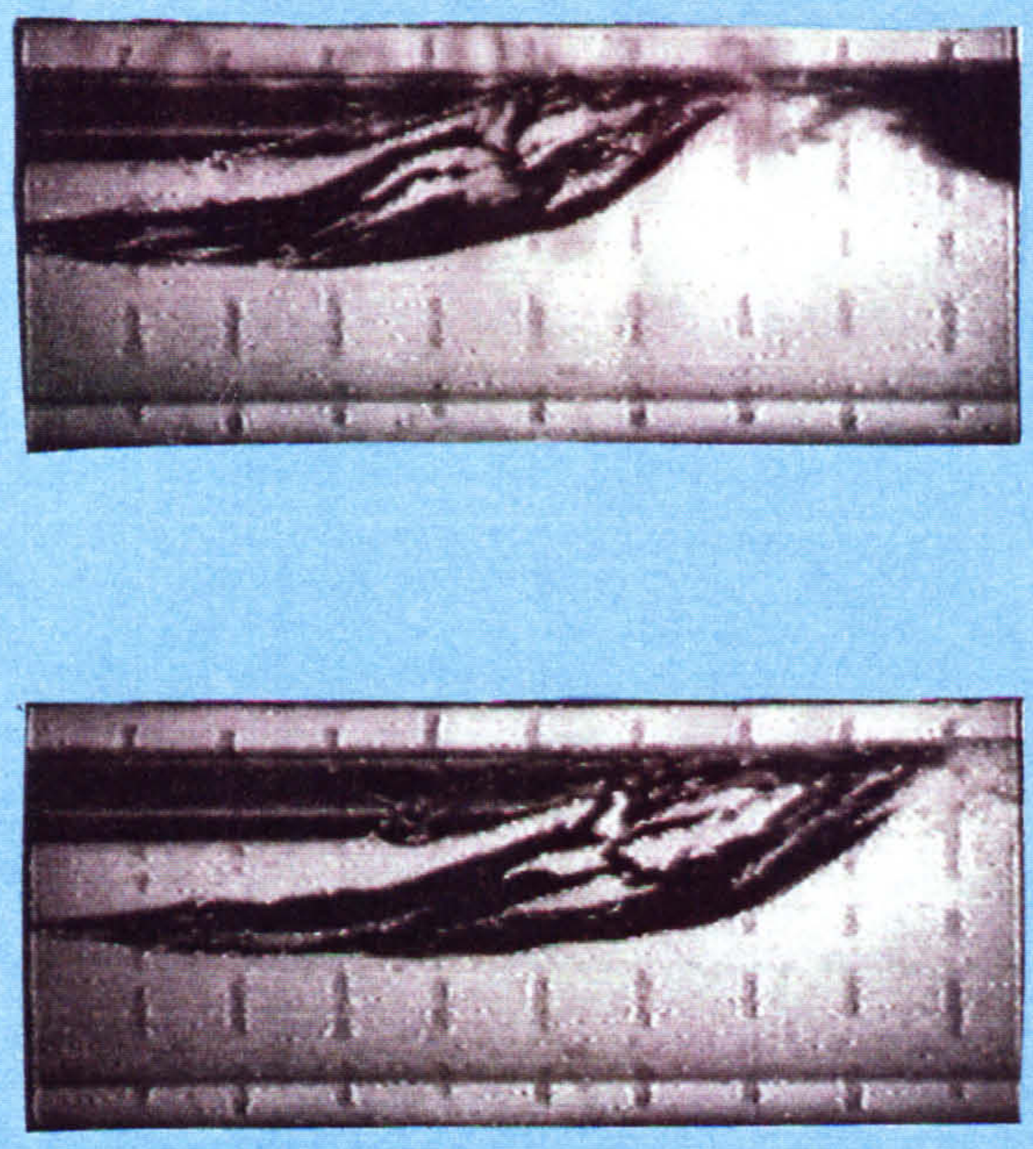


Figure 5.4.2 Continued.

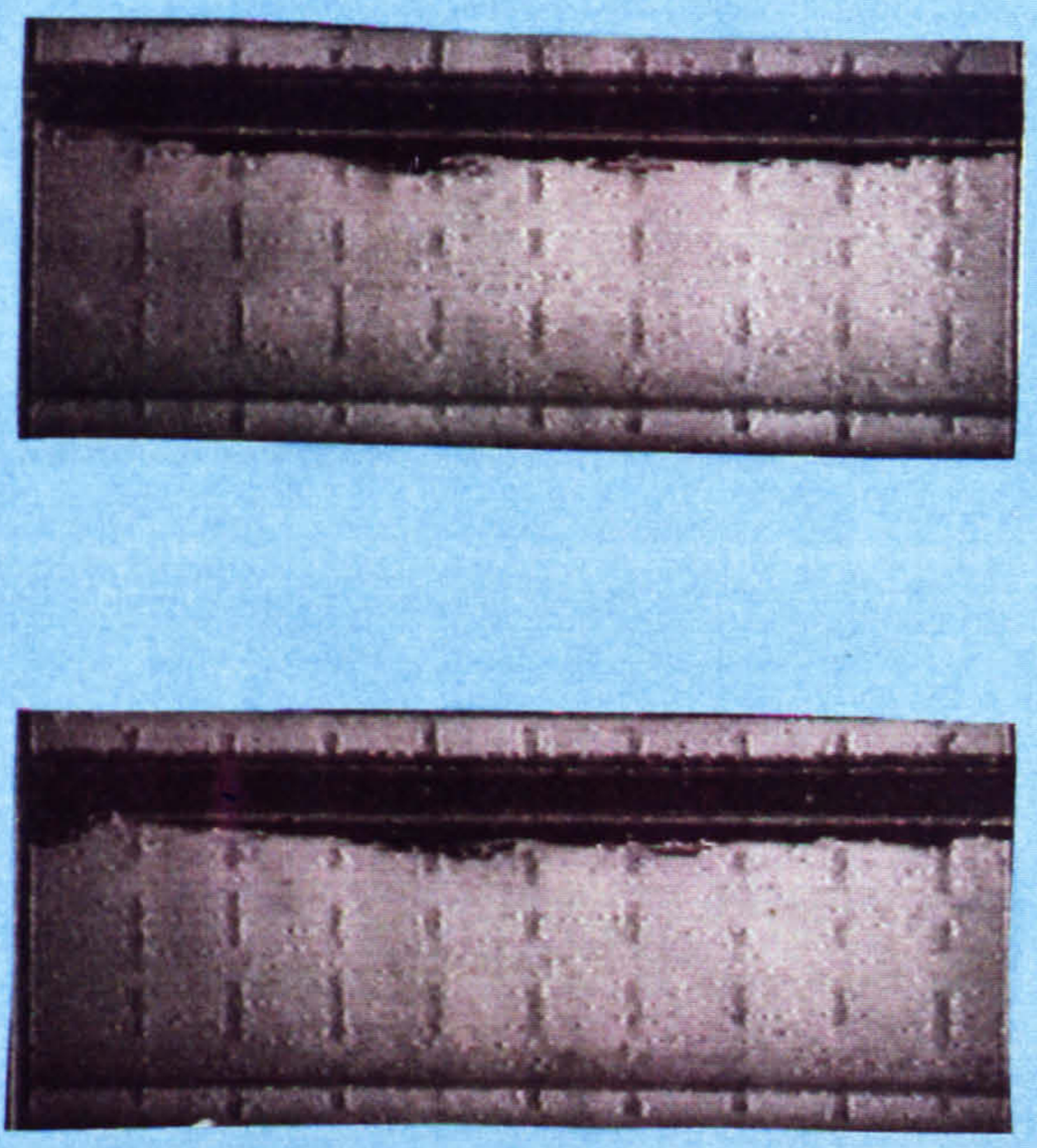
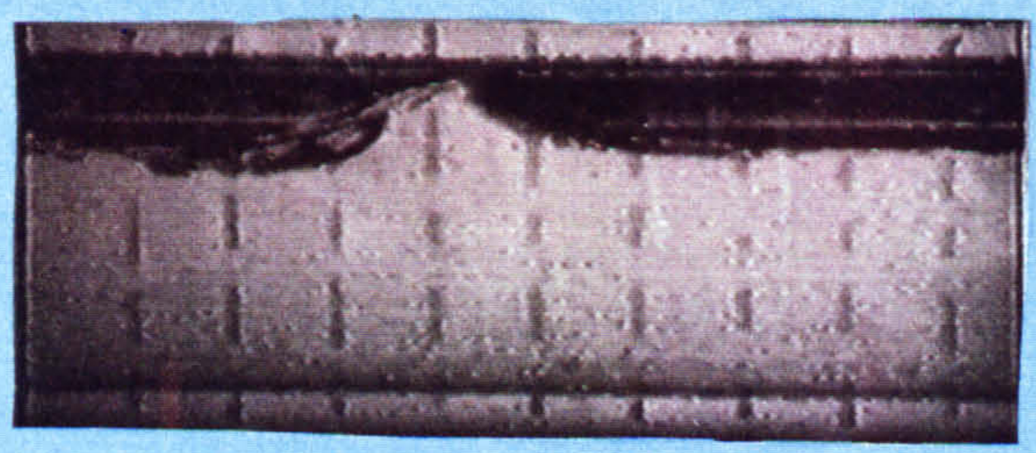
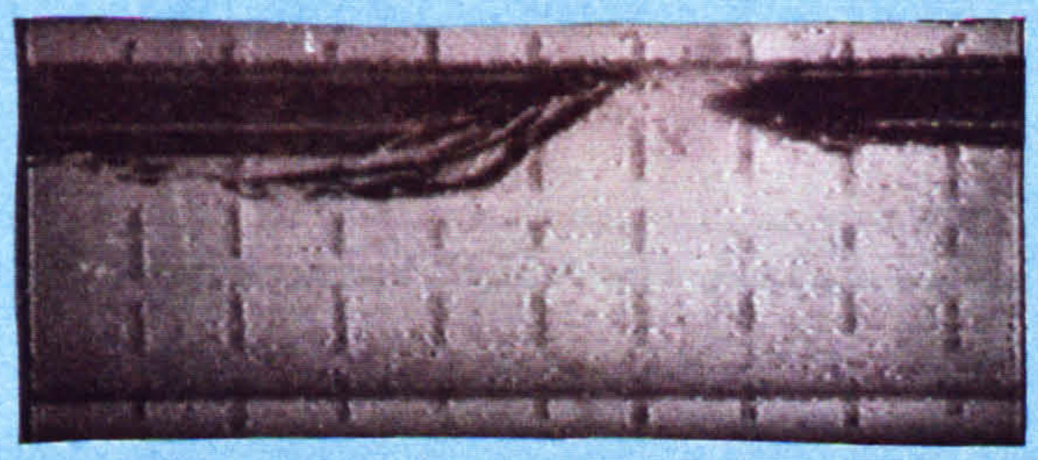
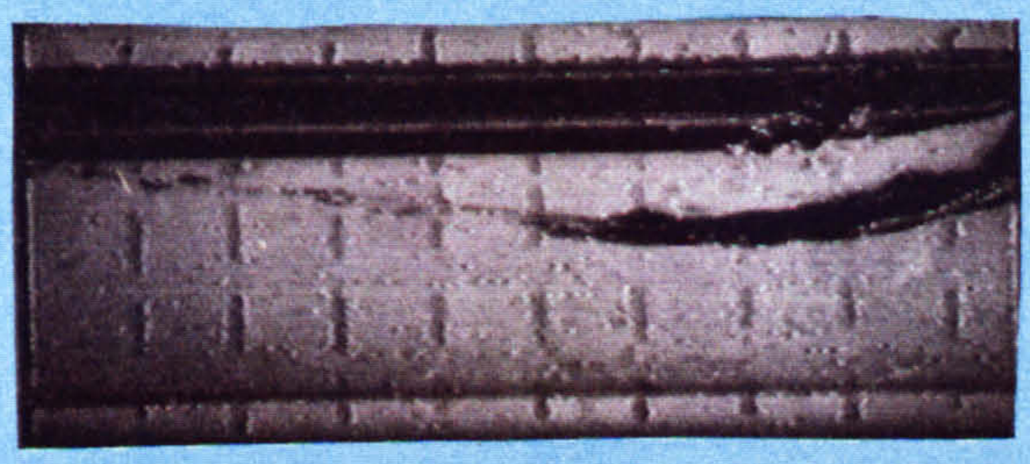


Figure 5.4.3 Slug initiation. (Gas superficial velocity=1.01m/s, liquid superficial velocity=0.411m/s)
(Continued overleaf).







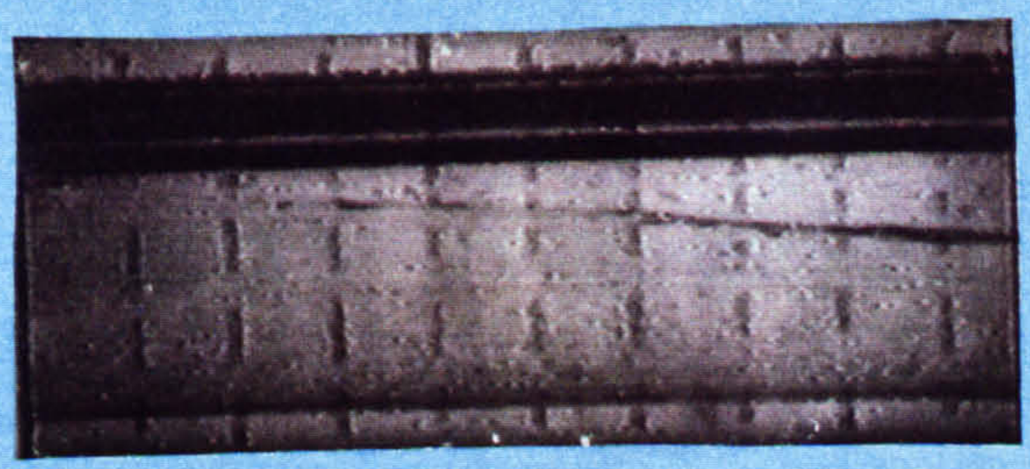


Figure 5.4.3 Continued.

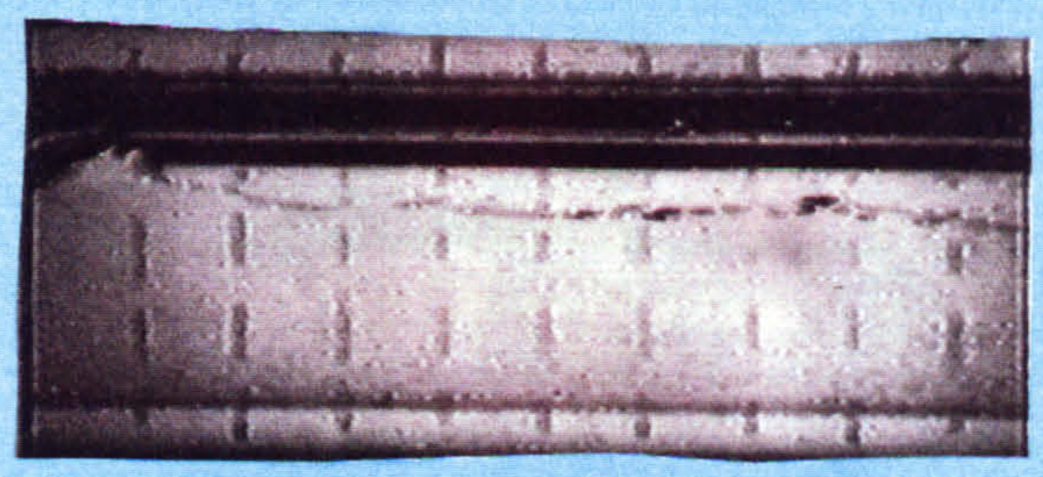


Figure 5.4.4 Slug initiation. (Gas superficial velocity=1.93m/s, liquid superficial velocity=0.248m/s).

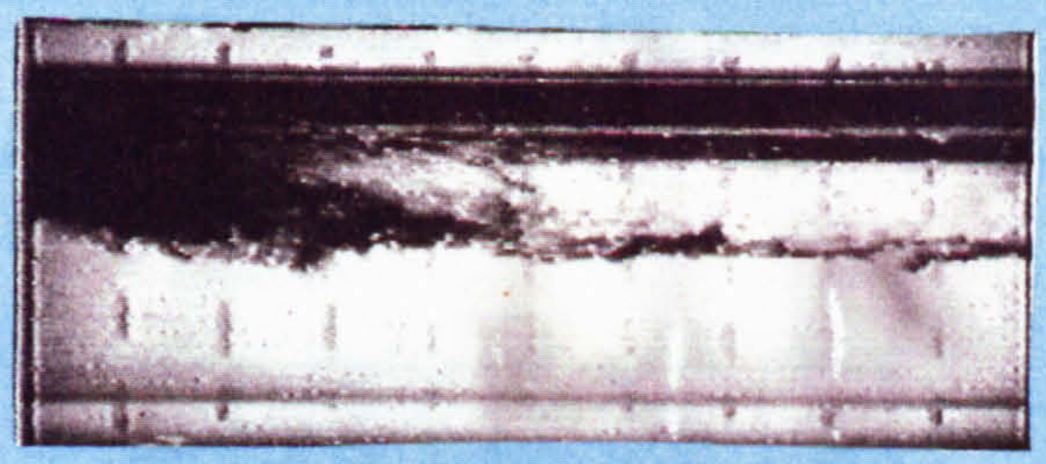


Figure 5.4.5 Slug initiation.
(Gas superficial velocity=2.91m/s,
Liquid superficial velocity=0.209m/s)

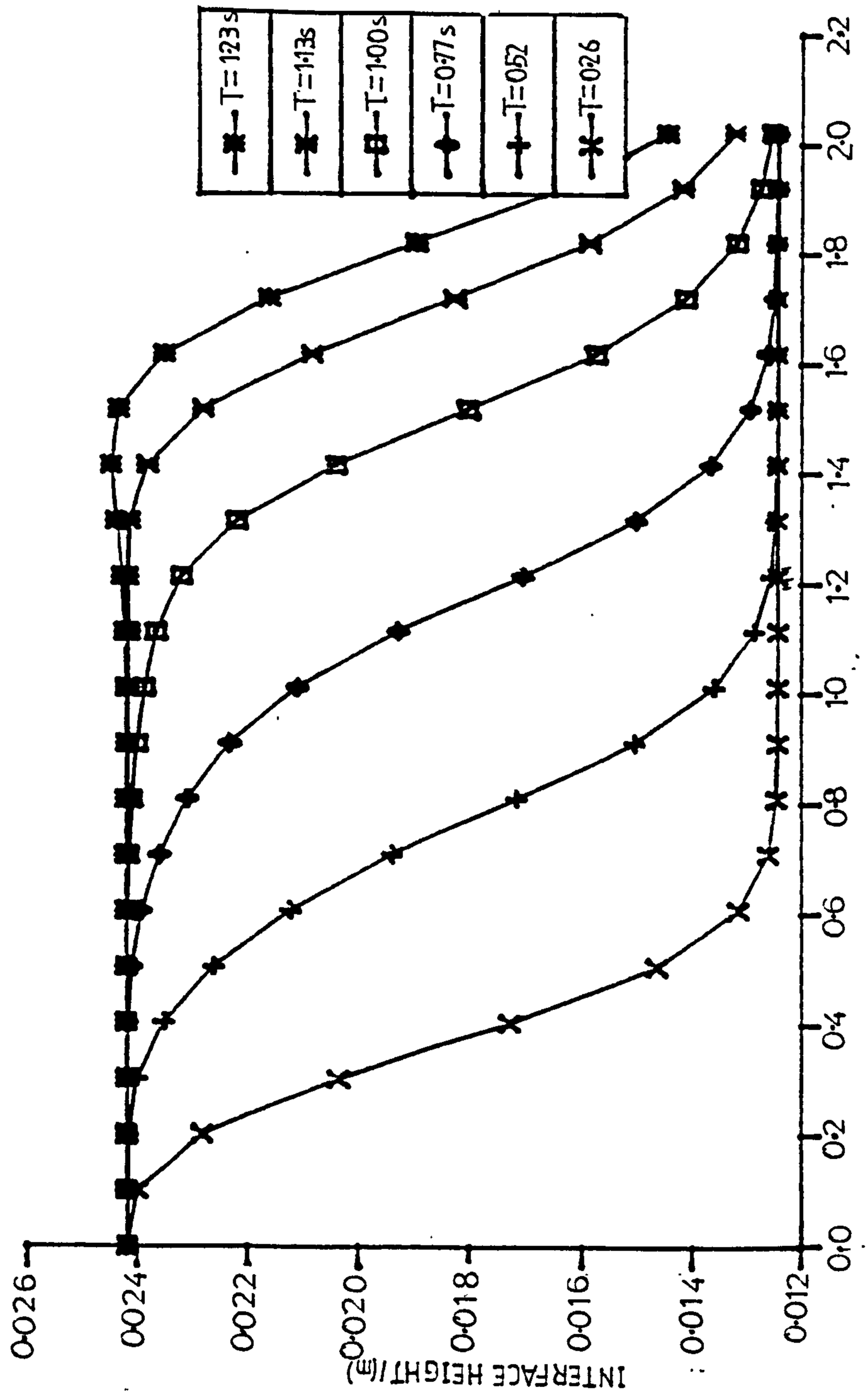


Figure 5.4.7 Liquid rebuild profile for Taitel and Dukler (1977) problem.

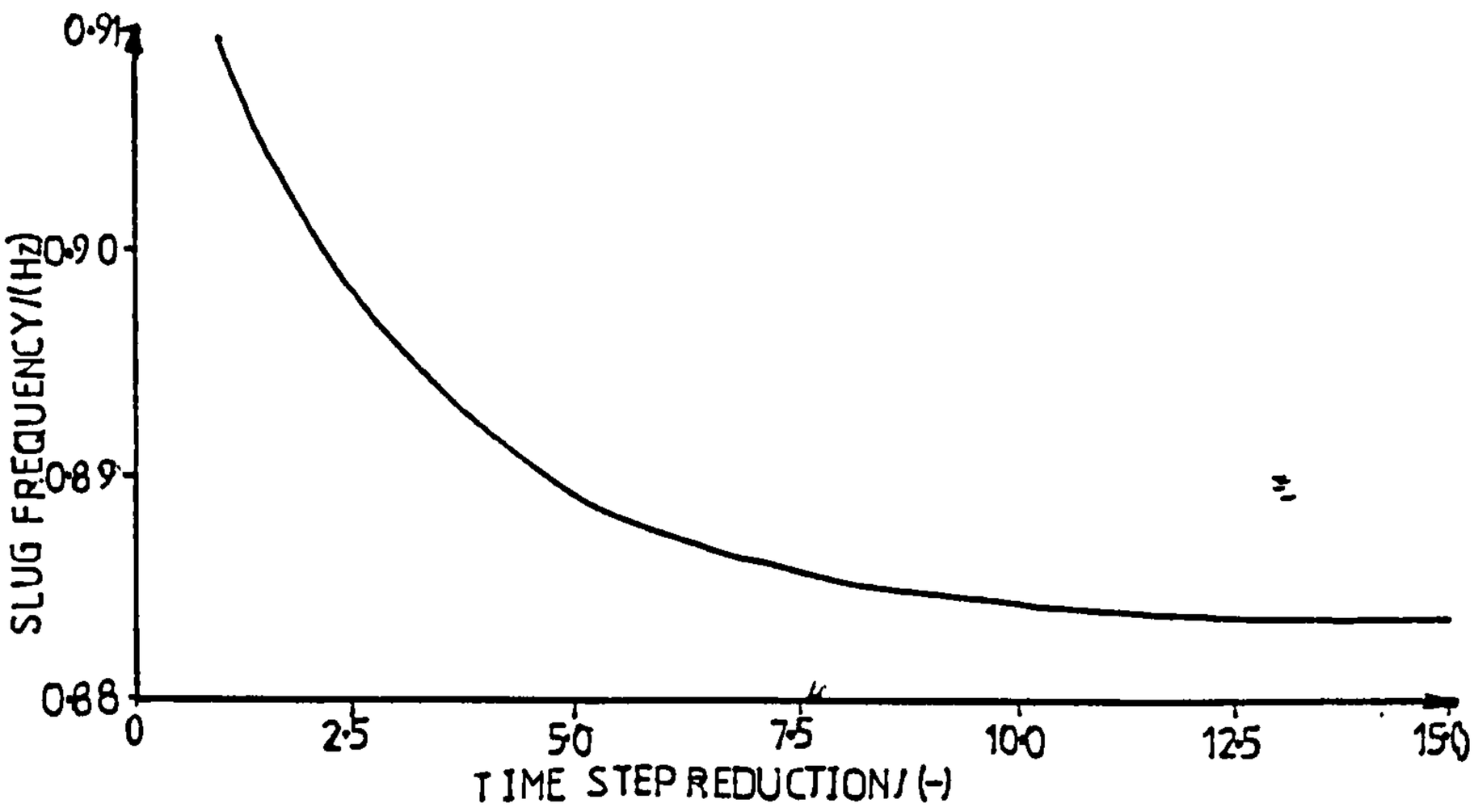


Figure 5.4.8 Variation of slug frequency with time step

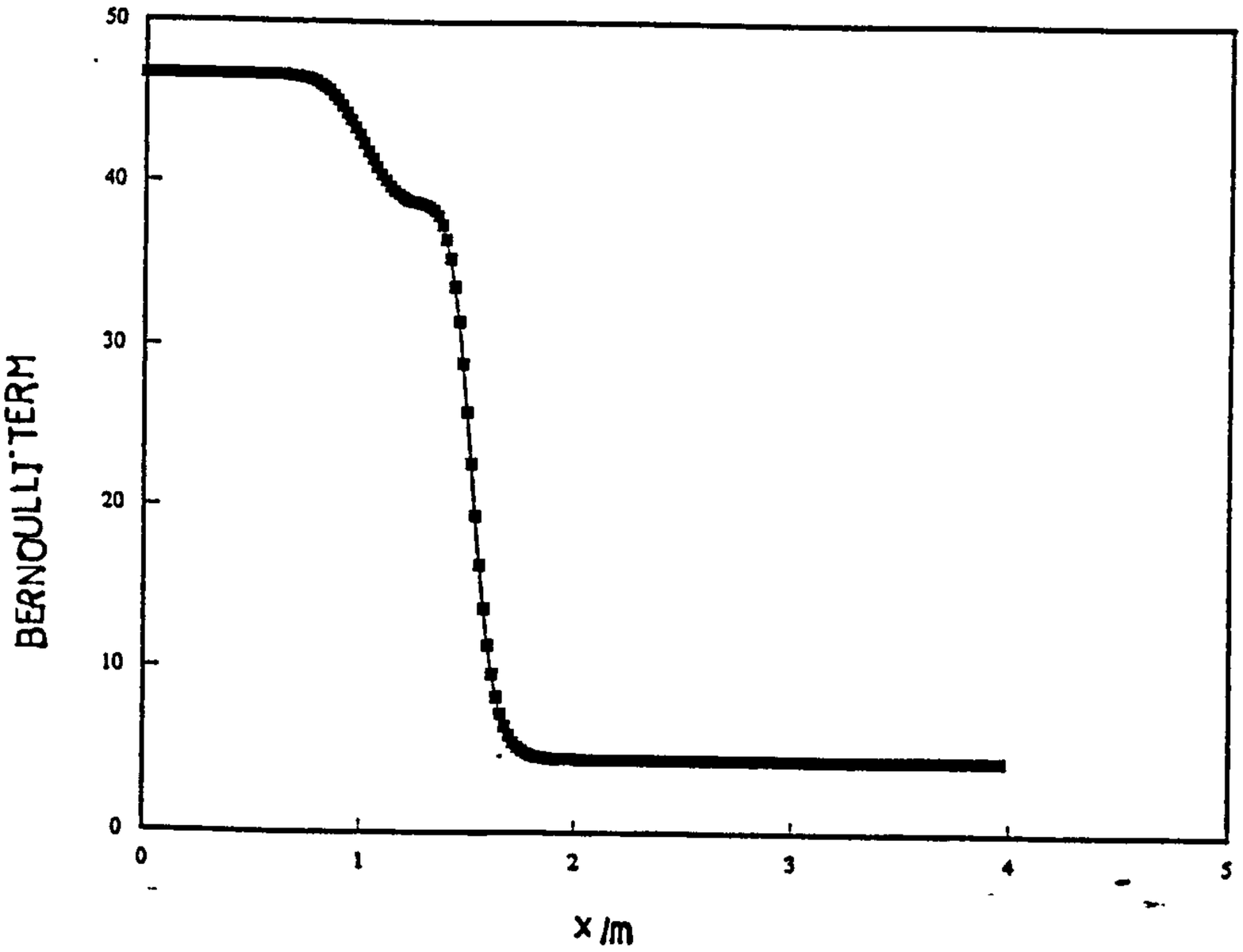


Figure 5.4.9 Bernoulli term variation along liquid profile.

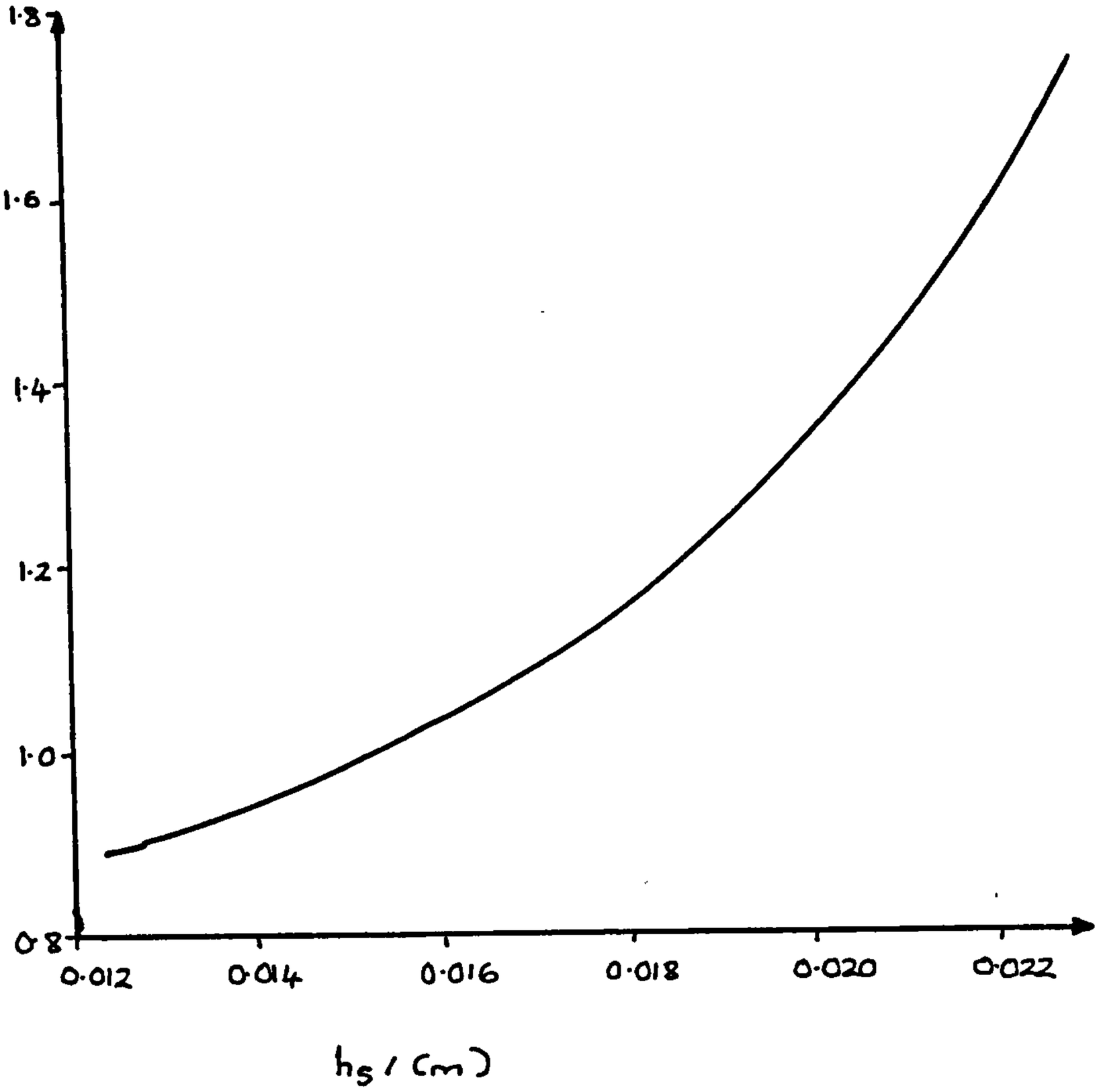


Figure 5.4.10 Sensitivity of slug frequency to stability level.

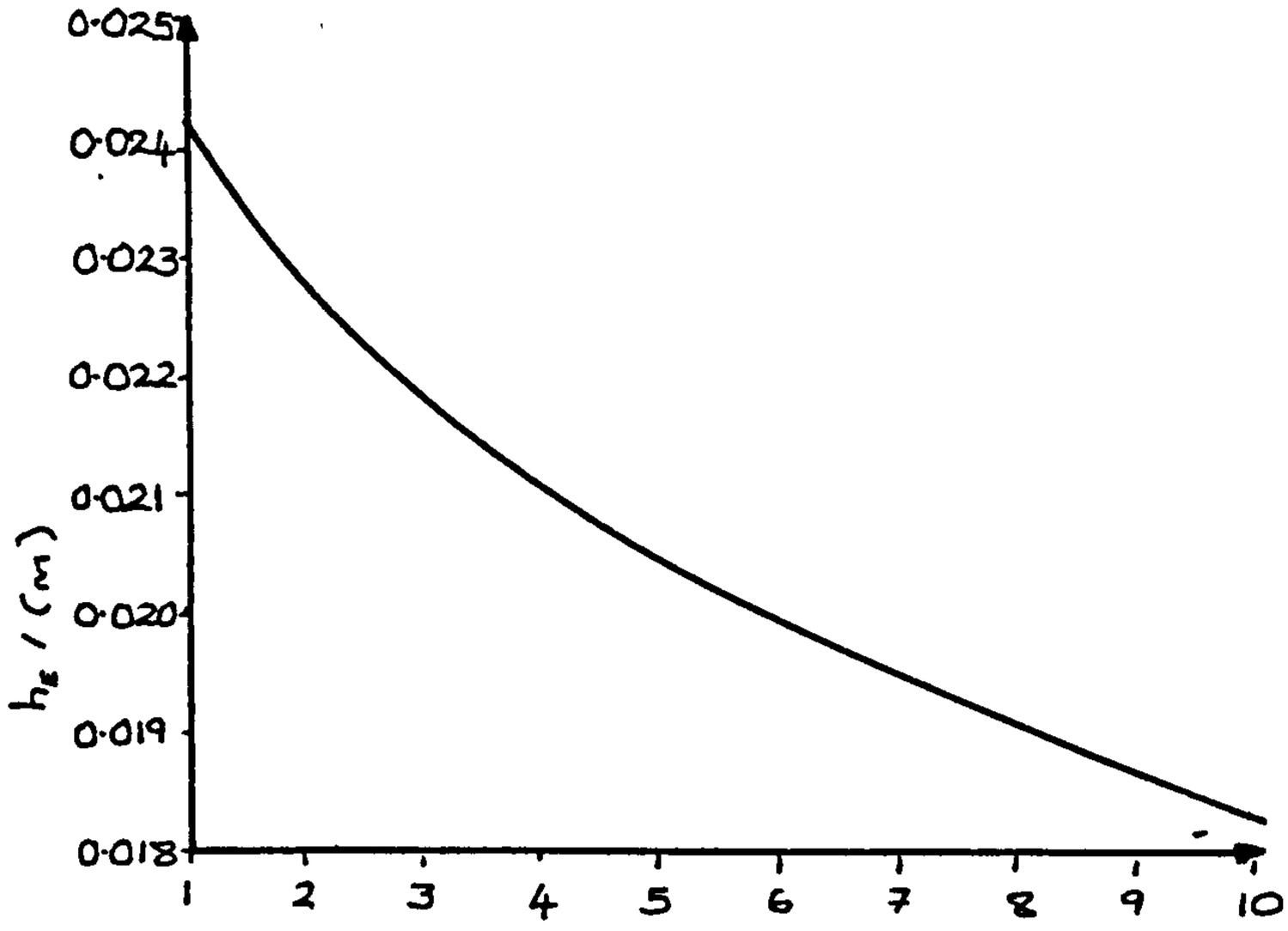


Figure 5.4.11 Variation of equilibrium stratified liquid height with the ratio of interfacial friction factor to gas friction factor.

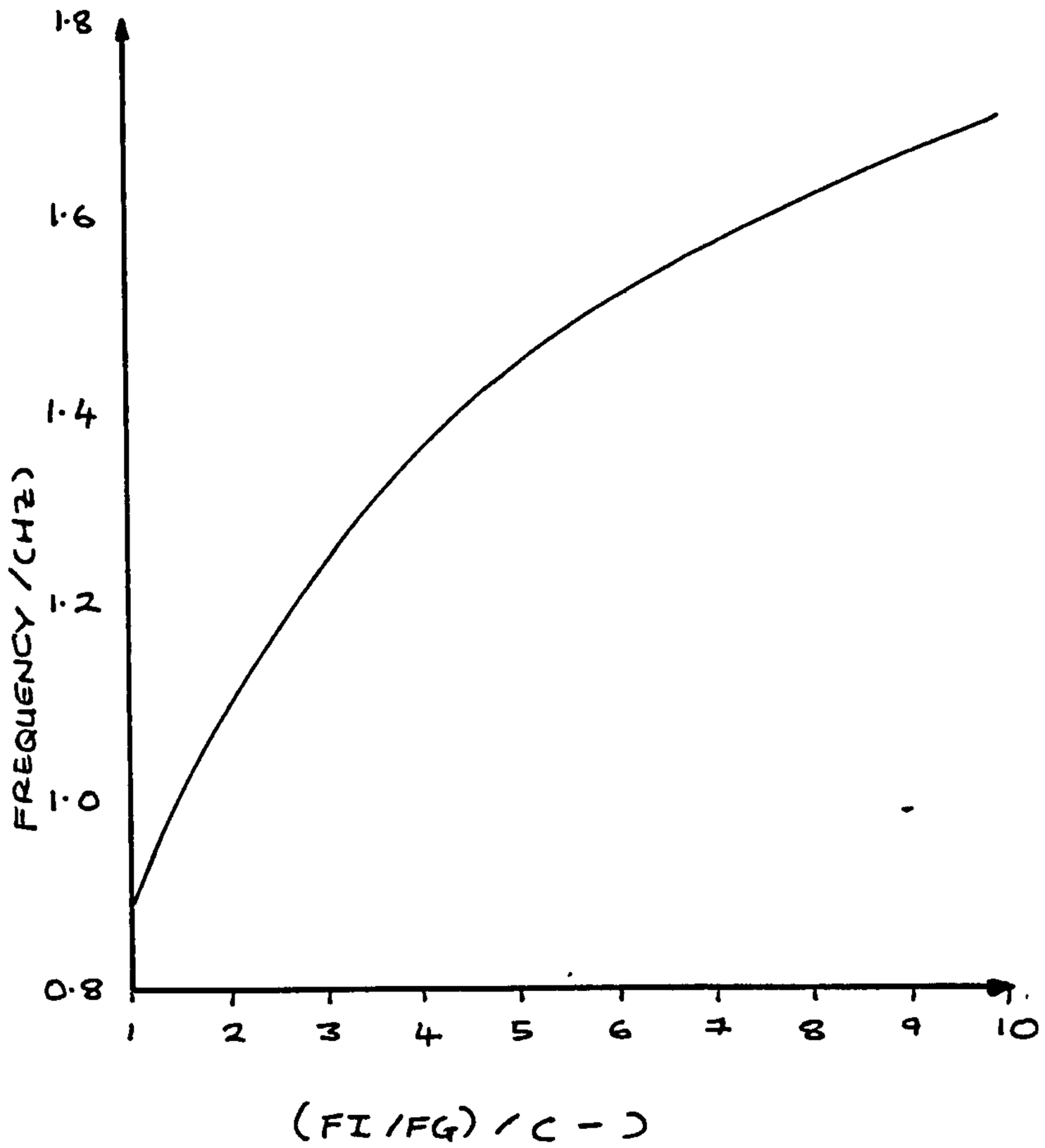
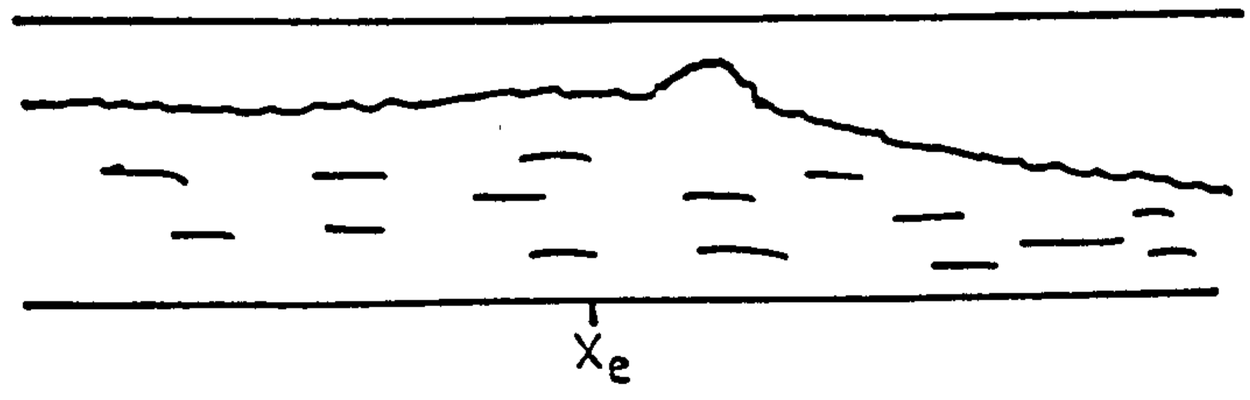
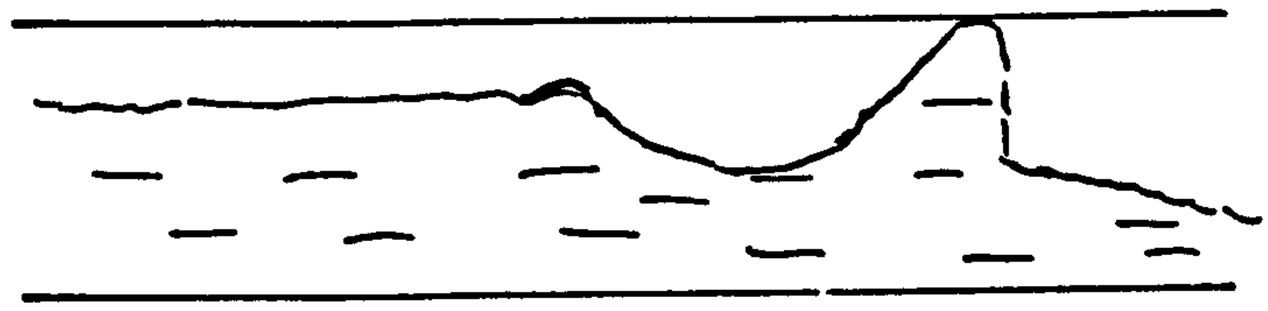


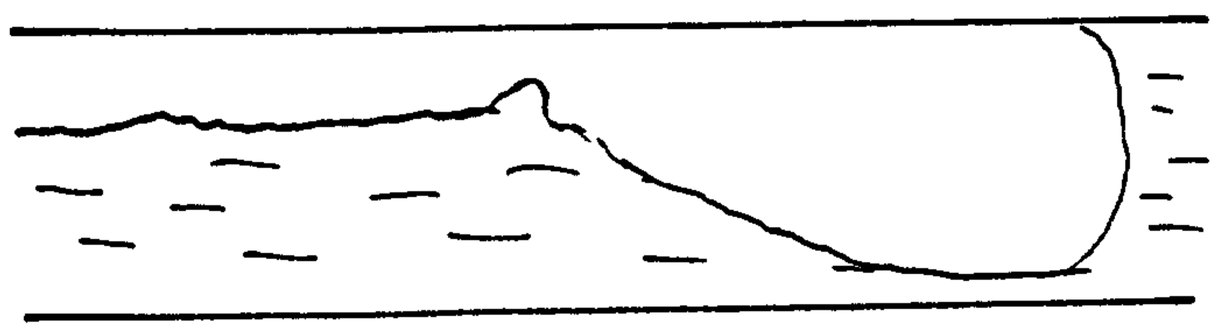
Figure 5.4.12 Sensitivity of slug frequency to the ratio of interfacial friction factor to gas friction factor.



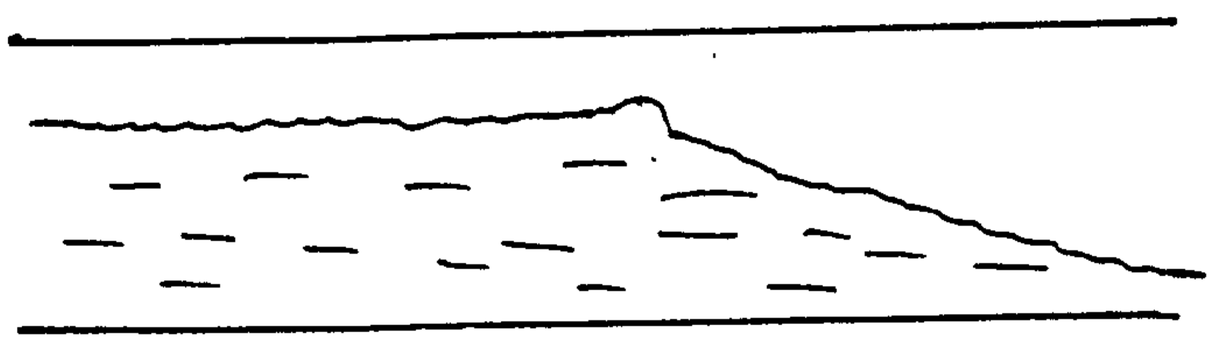
Wave grows on rebuilding level



Wave sweeps up liquid and bridges pipe



Slug formation



Liquid level rebuilds

Figure 5.4.13 Proposed mechanism for slug initiation frequency.

CHAPTER SIX
HIGH PRESSURE MULTIPHASE FLOW RIG

In off-shore oil and gas production, economic evaluation of exploitation strategies for a prospect/existing field requires prediction of the behaviour of the well fluids. Well fluids typically consist of hydrocarbon gases, oil and water. In addition, sand is carried from the reservoir with the well fluids. Over the next decade, exploitation of marginal fields will require the use of long distance multiphase transport lines carrying gas, oil and water. Better understanding of the hydrodynamics of multiphase flows is important for erosion/corrosion control and hydrate protection in such lines. Also the operation of an existing North Sea oil-field well in its decline phase poses significant technical problems for engineers. Particular challenges include high throughput of produced water and sand production. Both of these factors require increased understanding of the phenomena of high pressure multiphase flow. An essential part of this will be the extension of the oil–air, oil–water, and oil–air–water flow databases for pipelines.

A general purpose multiphase flow facility, WASP (Water, Air, Sand, Petroleum) has been designed, constructed and commissioned at Imperial College, London University to allow investigation of the flow of a maximum of four distinct phases. The four phases, water, air, oil and sand can be studied over a wide range of flowrates for pressures up to 50 bar. This facility will be exploited to address the gap between data available from existing experimental rigs, primarily low pressure two phase air–water studies, and that required for industrial conditions, high pressure multiphase operation.

The role of the present author in the development of the WASP facility was to participate in the design and acquisition process (taking sole charge of this from May 1989 to April 1990), to assist in the construction, to prepare the safety case and to organise and carry out the commissioning (from September 1989 to April 1990). In recognition of these roles, the present author was co–author of the first paper on results from the rig (Mendes–Tatsis et al, 1992).

6.1 WASP FACILITY

High pressure multiphase flow facilities are expensive to construct and to operate. To reduce costs the WASP facility was based on the "blow–down" principle. This allows savings by the use of a small compressor to store high pressure air in large tanks. The high pressure air is then blown down through the facility in a controlled manner. The disadvantage of a "blow–down" facility is that the pressure of the air source decreases during operation. However the WASP facility was fortunate in having access to the high pressure tanks of the hypersonic wind tunnel facility of the Department of Aeronautics, Imperial College. These tanks can be operated up to 70 bar and have a volume of 40 m^3. Hence, with such a large storage capacity, useful run times could be obtained for an experimental run at high pressure, and a number of data points obtained for each charge of the air storage tanks by stepping down the pressure for each run. Figure 6.1.1 shows the calculated time limit on a run for a given pressure and gas superficial velocity. Figure 6.1.2 shows the calculated time limit on a run for a given liqũid superficial velocity and a single liquid storage tank of 5 m^3 volume.

6.1.1 FACILITY EQUIPMENT

Figure 6.1.3 shows a basic schematic of the experimental equipment as of March 1990. High pressure air is supplied from large storage tanks to a 74 mm bore test section and is also used to pressurize the oil and water (slurry) tanks to minimise pump head required. The air flows concurrently with the other phases through the test section pipeline which is 42 m in length and can be aligned horizontally or at an incline/decline. Oil and water are pumped from individual tanks, where they are stored under pressure, through a mixing section into the test pipeline. In the mixing section the oil and water are combined with air from the reservoir. The fluid flowrates are metered before the mixing section and the pipeline is instrumented with pressure transducers and voidage probes. In addition a visualisation section is provided at the end of the test pipeline so that flow characteristics can be observed and recorded photographically. After leaving the visualisation section at the end of the test pipeline the multiphase mixture passes

into a slug catcher, which separates the air and liquid phases. Air is vented to atmosphere through a silencer and the liquids pass to a low pressure storage vessel for oil–water separation. Figures 6.1.4–6.1.12 show views of the facility and consist of the following:

Figure 6.1.4 View of high pressure air storage tanks and WASP facility test section.

Figure 6.1.5 View of test section from the inlet section towards the outlet control hut and dump tank. Other pipes shown are the air supply pipes and liquid return line from the dump tank.

Figure 6.1.6 View of oil and water storage tanks at inlet end of the facility, with air control valve located on air supply pipe.

Figure 6.1.7 View of inlet mixer located at the inlet to the test section.

Figure 6.1.8 View of water storage tank, water flow control valve and magflow meter, and pump in its weather–proof box. Box on brick wall contains control solenoid valves for the rig.

Figure 6.1.9 View of air outlet (with silencer) and test section entrance to the facility control hut.

Figure 6.1.10 View of the slug catcher/ air–liquid separator located on the top floor of the control hut.

Figure 6.1.11 View of visualisation section (in containment box) located on the top floor of the control hut.

Figure 6.1.12 View of computer display of facility control system located on ground floor of the control hut.

A number of items of the facility equipment shown in Figures 6.1.4 to 6.1.12 are described below:

Test Section. The test section is a 42 m long, 77.91 mm internal diameter stainless steel tube. Important design features associated with the test section are as follows:

(a) It was important to have continuity of the bore in the tube and the flanged joints are designed to ensure continuity and concentricity of adjacent sections.

(b) Pipes in industrial applications are rarely purely horizontal. Thus, it was important to design in the flexibility to change the angle of inclination of the test section and suitable arrangements of mounting clamps and flexible inlet pipes were installed to achieve this. The pipe was designed to be inclined by 5 degrees in both directions from the horizontal.

Fluid Mixer. This is designed to give essentially parallel flows of the phases at the inlet. Preliminary experiments described in Chapter 4 indicated that slug formation, for instance, may be very sensitive to inlet configuration. This conclusion will be examined in detail using the WASP facility and hence the inlet was designed to enable the 'best' and 'worst' case interactions of the gas and liquid, identified in Chapter 4, to be simulated. An additional consideration was that the inlet had to be generic and handle three phases instead of two. Thus, the mixer was designed for the 'best' case interaction allows input of the air at the top of the pipe in parallel with oil and water streams in the middle and bottom of the pipe respectively.

Visualisation Section. It was considered vital that visualisation of the flow could be achieved. This presents no problems at low pressures, but under the high pressures envisaged for operation of the rig, it presents considerably difficulty. A visualisation section was designed and incorporates a thick walled polycarbonate tube mounted in such

a way to minimise stresses and to ensure geometric continuity with the main test section tube. The visualisation section is shown in Figure 6.1.13 and is normally mounted inside a containment box located on the top floor of the facility control hut.

Slug Catcher/Primary Separator. It is necessary for the gas and liquid phase separation to be carried out at full rig pressure. This minimises feed–back effects caused by back pressure in the separation device. The slug catcher was designed according to available design methods in the literature and was so constructed that the internals can be removed and replaced in order to investigate alternatives.

6.1.2 CONTROL SYSTEM AND INSTRUMENTATION

6.1.2.1 Control

The complexity of the facility operation required an automated control system, which consisted of an ANDS 4400 control unit and ANALOGIC monitor interfaced to a Personal Computer. The facility controls carried out the following main functions:

Inlet Flows: The controls maintained the oil, water and air inlet flows to preset values by monitoring the flowrates and adjusting the air pressure to control valves.

Slug catcher liquid level: The control system maintained the liquid level (using a displacement device) in the slug catcher at a preset level. Liquid is discharged to the dump tank by a control valve.

Test Section Pressure: The test section pressure was controlled by a valve which discharges air from the top of the slug catcher to atmosphere via the silencer.

The software which controls the multiphase rig can be classified into two discrete areas:

Set–up Programme. This provides manual operation of all the actuated valves and motors from the personal computer keyboard with cocurrent display of the state of WASP control variables. This program allows testing and calibration of individual items or sections of the facility and set-up of initial conditions for a facility run. An example of an operation carried out by this programme prior to experimental runs is the transfer of liquid between vessels.

Run Programme. The first action by the programme is to configure the facility valves, experimental conditions and control loops for the specific experiment. Next the programme allows the experiment to be initiated and monitors and displays the control and basic facility operating parameters. The final function of the programme enables the shut down of the experiment in a predetermined safe sequence at the end of a run, or at any time the operator decides an abort is necessary.

6.1.2.2 Instrumentation

The instrumentation of the WASP facility was split into two sections: facility equipment used for monitoring the experiment for control, and experiment specific instrumentation for recording flow characteristics in the test section. The signals from the following facility control measuring equipment are passed to the ANALOGICS monitor:

Air Metering: The air flow is metered by a corner tapping orifice plate designed and installed to the specifications of BS1042. The tappings of the orifice-plate are connected to differential and absolute pressure transducers.

Water Flowrate: The water flowrate is measured using a Danfoss magnetic flow meter covering a range of flowrates from 0 to 1.5 m/s.

Oil Flowrate: The oil flow is metered by a corner tapping orifice plate (for low viscosity fluids) designed and installed to the specifications of BS1042. The tappings of the orifice plate are connected to differential and absolute pressure transducers.

Oil and Water Tank level measurement: Differential pressure transducers are connected between the top and bottom of the tanks.

Slug catcher level measurement: A displacement device is used to measure liquid level in the slug catcher.

Experiment specific instrumentation for recording flow characteristics in the test section, such as differential pressure transducers and wire probes, are connected via amplifiers to the data capture equipment described in Section 3.6 of this work.

6.1.3 SAFETY AND FACILITY DOCUMENTATION.

The safety case for the WASP project had two objectives:

(1) To set up a systematic approach to the design, construction and operation of the rig throughout its life from its conception to the various stages of experiments.

(2) To demonstrate that adequate levels of safety are achieved throughout the entire life of the facility.

In order to achieve these objectives it is necessary first to identify all the potential hazards of the equipment and all the targets which could be harmed. The interaction of the hazards and targets must then be evaluated to enable identification of aspects of the equipment and its operation which need attention with regard to safety and to facilitate the specification of protective methods. Such an assessment needs to quantify the level of hazard to which all identified targets are exposed. It must be recognised that, while in the context of an experimental research programme such assessments can be difficult, they are essential to enable an objective assessment of any future project changes. It must be emphasised that the safety case for any facility depends on the protection of the targets to an acceptable level of safety.

It is not just sufficient to identify high priority interactions but any related decisions concerning the design, manufacture, fitting or operation of the rig should be recorded and available to all future users of a facility. Thus any later modifications and repairs would have available the original safety decisions and related design criteria. It is necessary that any safety case should be up–dated as a project advances. For example, changes in design of equipment may result from the findings at the commissioning stage. The facility for the safety case to be updated during the life time of a project is

particularly important in research projects, as equipment and operational changes will result from experimental evaluation.

This requirement for a safety case that could develop with the research resulted in the following structure being recommended by a safety consultant for the WASP project. A basic safety case sets out the information concerning the equipment and associated hazards, and a current safety case was developed as modifications were made. Comparisons can be made between the current and basic cases so that changes are identified and their impact on the safety of the facility assessed. The basic and current safety cases are contained within the generic safety case. The generic safety case makes an explicit statement that all changes are handled in this way and requires that up–dated operational safety cases are assembled and approved.

The generic safety case document for the WASP rig was edited by the safety consultant. It first set out the objectives of the research project and identified and classified the targets. The six categories of target identified are

1. The environment
2. The surrounding buildings
3. The equipment
4. The occupants of surrounding buildings
5. The employees involved in the construction, testing, commissioning and maintenance of the facility.
6. The employees involved in the operation of the equipment during experimental runs.

In order to assess the amount of protection required by each target it is necessary to identify the potential hazards. Hazards are inherent in the WASP facility and were present during the manufacture, fitting, commissioning, and operation stages of the project. The safety document discussed the hazards under the following headings:

1. Explosion
2. Fire

3. Contamination

4. Impact

5. Nuisances

The categorisation of targets and hazards described above formed the logical basis for an in–depth analysis of the interaction between them. A grading system (low *, medium **, high ***) was used to provide an indication, though subjective, of the seriousness of the selected hazard for a given target. This grading represents both the extent of the consequence and the chance of the interaction occurring. For example the impact of projectiles on the operators is ranked as ***, while the contamination of buildings by liquid jets is marked as *. This subjective assessment was used to identify the critical safety issues, leading to the detail of the implementation of the safety approach.

The generic safety case contains the safety requirements for the design and construction of the facility, detailing the studies carried out to provide safe design and operation. In addition the method by which documentary records are checked, stored and accessed are set out, so that activities which bear on equipment safety are as far as practicable mistake free and to ensure that safety constraints placed on the design and manufacture of equipment are correctly accounted for in future modifications. Also, the practical activities, such as pressure testing carried out to ensure the equipment is adequate for its purpose, were recorded.

The generic safety case details the safety requirements for the operation of the facility considering the following four aspects. The studies carried out to provide safe operation are described; for example the Hazop study carried out in December 1989 for operation with both air–water and air–oil at high pressure. The second aspect detailed was the method by which documents are handled and which documents are necessary for management of the day to day facility operations. The third activity specified the measures, such as inspection and maintenance, necessary for practical confidence in the equipment operation. Finally essential activities such as development and implementation of safety regulations, emergency planning and safety drills are considered in the generic safety document.

The final section dealt with the safety management of the research project specifying how the proposed safety method would be organised to ensure its effective operation throughout the life of the WASP facility.

Safety management depends on the day to day controls specified for a research project. In the case of the WASP facility controls were implemented at two levels:

1. Forms for authorisation and notification of each days operation.
2. An operational safety case for each new combination of operator and experimental programme.

The former required the operator to specify each days operation and to agree the content with the supervisor on a day to day basis. The latter forced an operator to consider the safety aspects of the operation of the rig prior to a programme of work. The purpose of the operational safety case is discussed in this section.

The operational safety case is presented in two main parts. The first part defines the operation of the rig, including the experimental programme, staffing, equipment and operations and administrative procedures. The second section demonstrates the reasoning behind the choice of operational requirements and in this way demonstrates the rationale and level of care which has been used to make decisions with regard to the safety of operation for the particular circumstances prescribed for the operational safety case.

The second section builds on the generic safety case hazard/target interaction work. For example, the first operational safety case, produced by the author of this thesis, limited operation to a high pressure air–water system, which reduces the quantity and quality of the risks. Table 6.1.1 shows the interactions pertinent to high pressure air–water experiments. These interactions are used to highlight a number of attributes (see Tables 6.1.2, 6.1.3, and 6.1.4) in a systematic manner. These attributes provide indicators associated with many aspects of the rig operation and are used to identify the key requirements for the safe operation of the rig.

As an example consider the engineering safeguards necessary to guard against projectiles. The following paragraphs are from the operational safety case for high pressure air–water experiments.

"A projectile results when equipment, fluid or fragmented equipment are accelerated by equipment, gravity or fluid pressure. Fragmentation of equipment can occur due to over pressure in the vessels. Equipment can form a projectile due to faulty assembly."

"The slug catcher, oil vessel and the water vessel are designed in accordance with BS5500. The design pressures are 50 bar and the design temperatures 0 to 50 C. The water and oil vessels are protected by safety relief valves set at 45 bar. An intelligent control interlock between valve V16 and pressure transducer P3 protects the slug catcher. The air supply to the test section shuts off when the pressure in the slug catcher rises above a set value."

"The test section is manufactured in accordance with BS 3351: 1971 for the pipe and BS 1560 Part 2: 1970 for the flanges. The design pressure is 50 bar and the design temperature 38 C. Containment sleeves for the test section flanges will absorb the energy of any jet issuing from the tongue and groove type flanges. Hydrostatic tests on the above equipment have been carried out at a pressure of 75 bar."

"The visualisation section consists of Transpalite SS acrylic pipe with 31 mm wall thickness. While this section has been hydrostatic tested to 60 bar a further measure has been taken to reduce the consequence of brittle fracture of the plastic. A metal box has been constructed around the visualisation section to protect operators from projectiles. In addition operators must wear eye protection when on the second floor of the WASP control hut."

"Two way valves and a bursting disc protect the low pressure return line circuit from over pressurisation. A full rig hydrostatic test was conducted for the high pressure circuit. The hydrostatic test pressure was 625 psig."

The above illustrate the engineering safeguards that resulted from analysis of the hazard/target interactions for high pressure air–water experiments. These are the practi-

cal protective measures resulting from the structured approach to safety described in this section of this thesis.

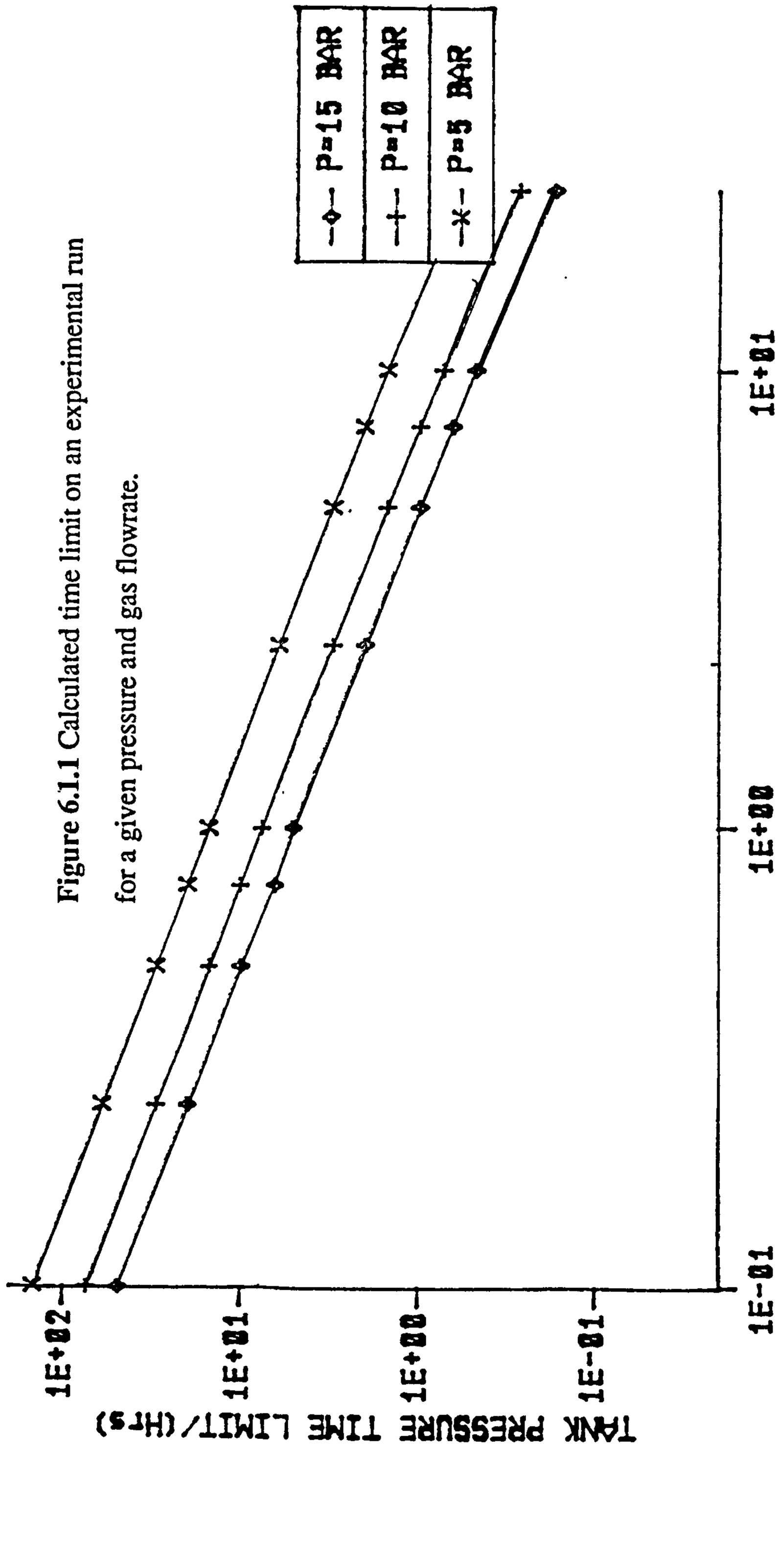


Figure 6.1.1 Calculated time limit on an experimental run for a given pressure and gas flowrate.

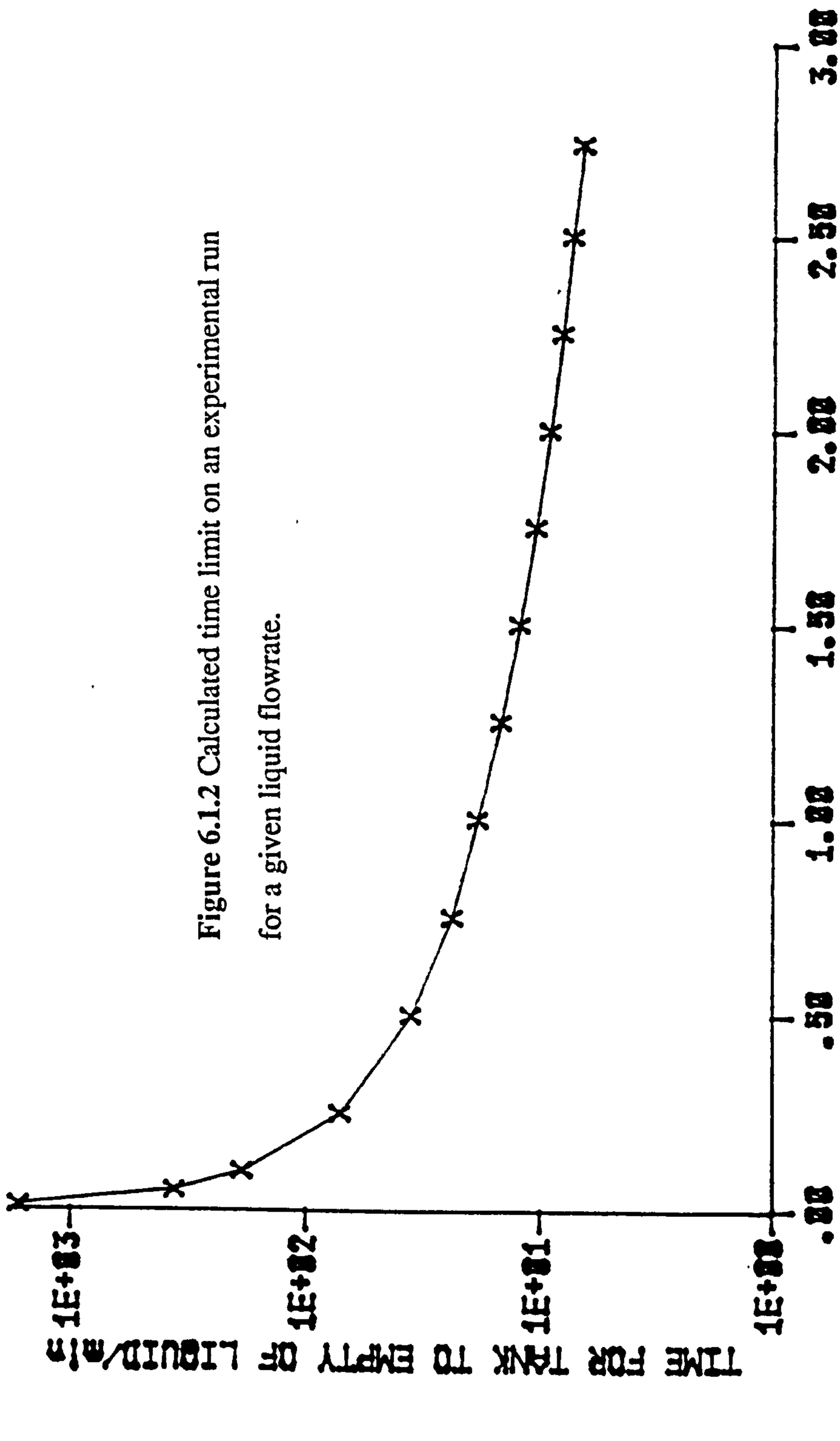


Figure 6.1.2 Calculated time limit on an experimental run for a given liquid flowrate.

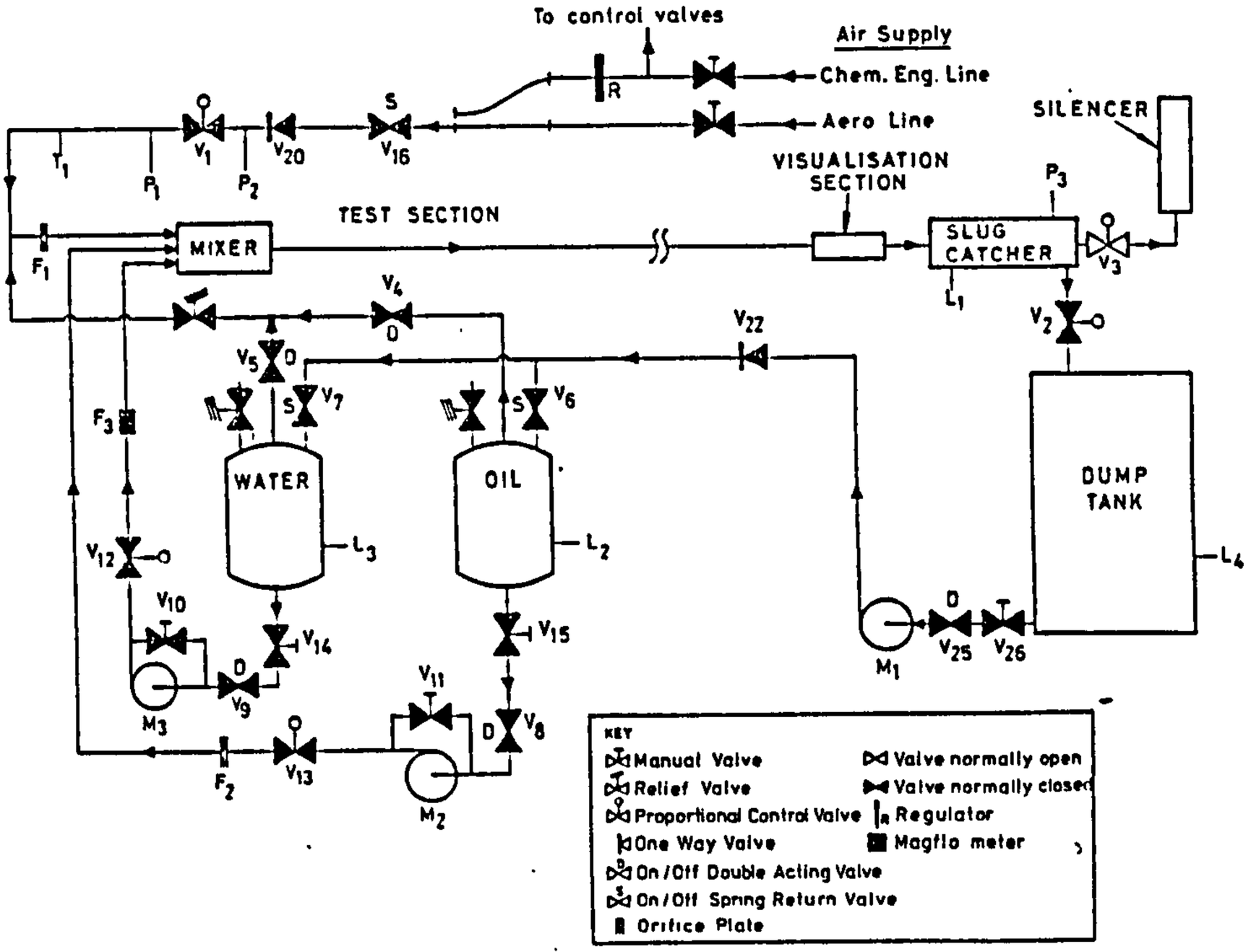


Figure 6.1.3 Basic schematic of WASP facility.



Figure 6.1.4 View of high pressure air storage tanks and WASP facility test section.



Figure 6.1.5 View of the test section from the inlet section towards the outlet control hut and dump tank. Other pipes shown are the air supply pipes and liquid return line from the dump tank.

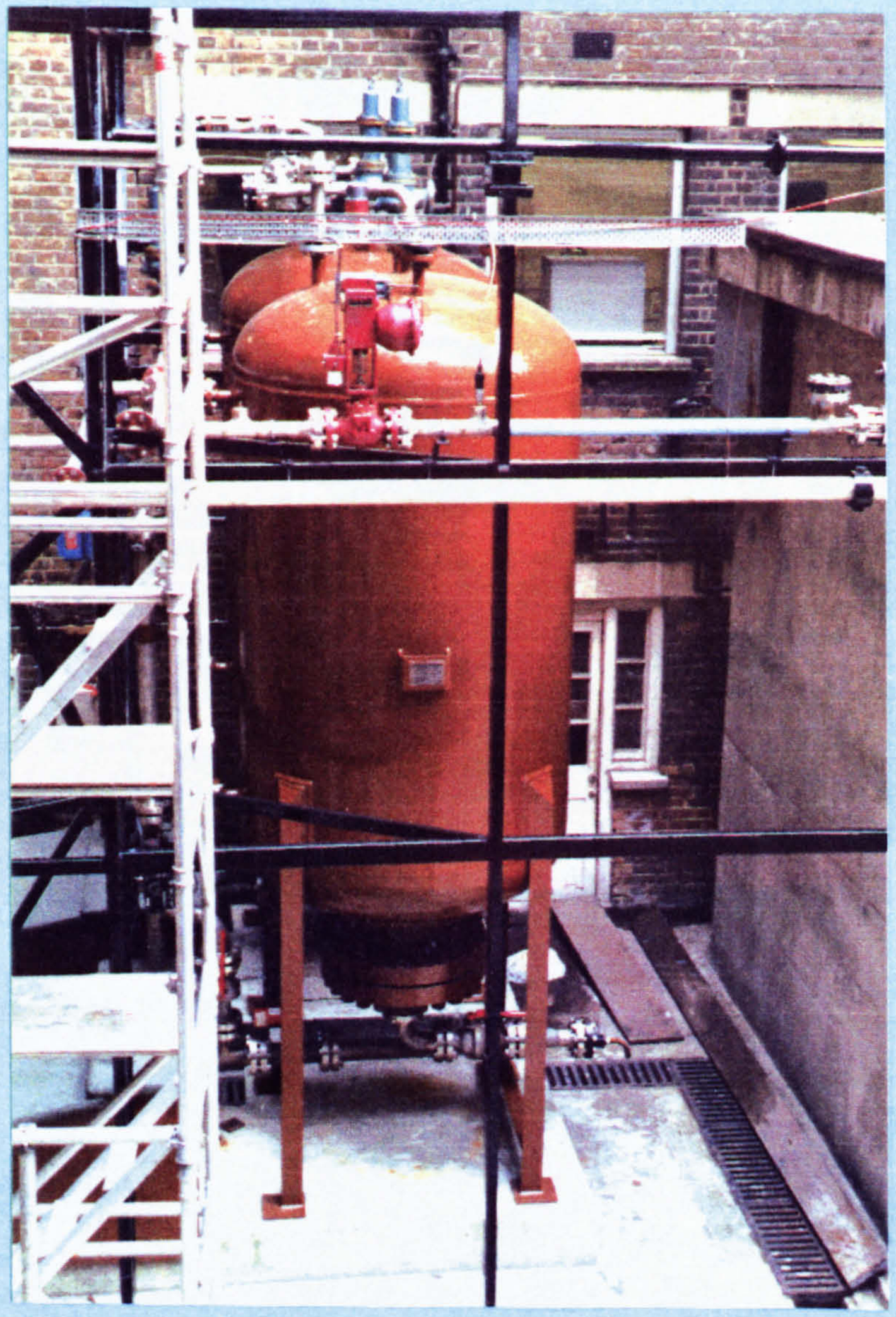


Figure 6.1.6 View of the oil and water storage tanks at the inlet end of the facility, with air control valve located on the air supply pipe.

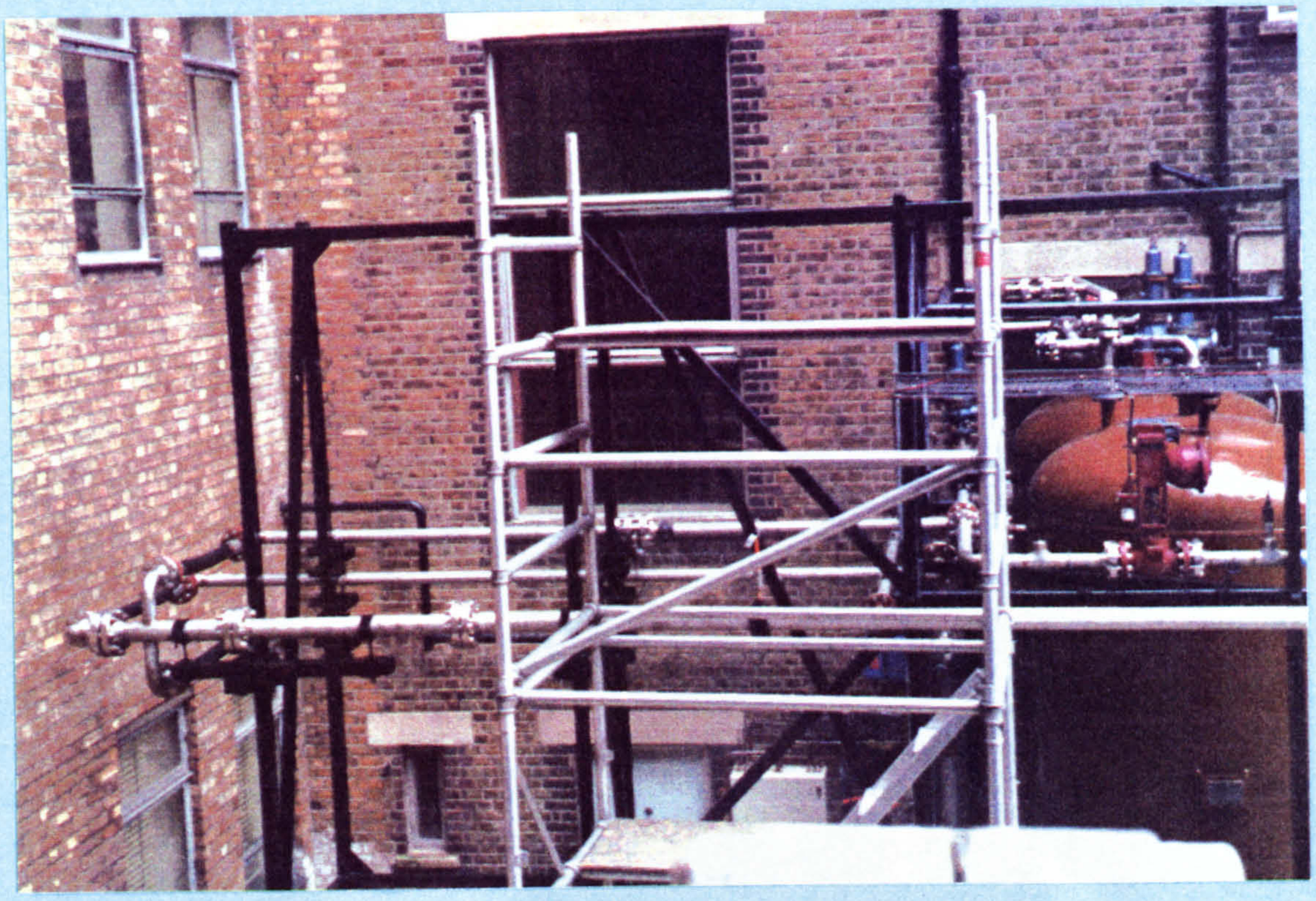


Figure 6.1.7 View of the inlet mixer located at the inlet to the test section.



Figure 6.1.8 View of the water storage tank, water flow control valve and magflow meter, and pump in its weather-proof box. Box on brick wall contains control solenoid valves for the rig.

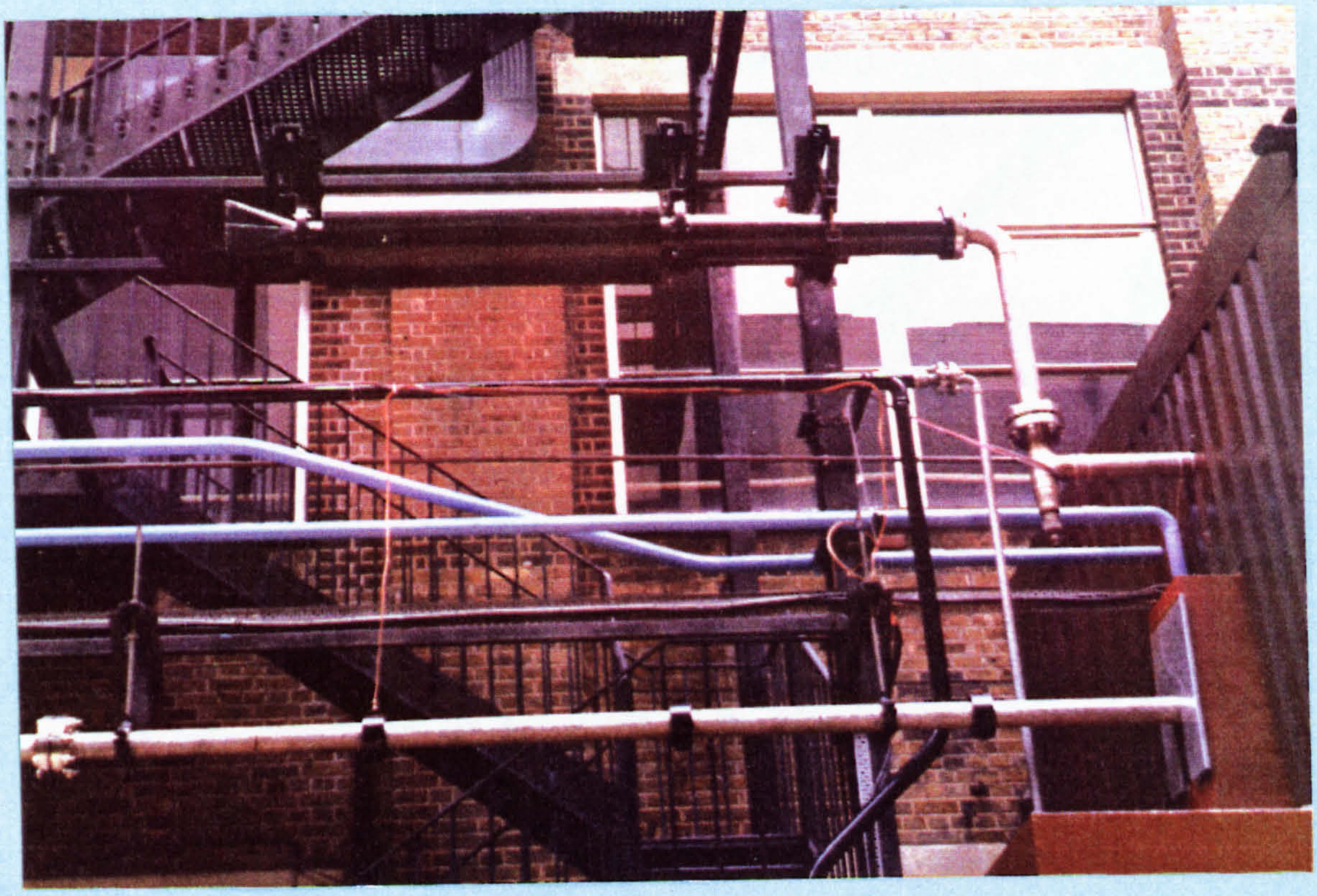


Figure 6.1.9 View of air outlet (with silencer) and test section entrance to the facility control hut.

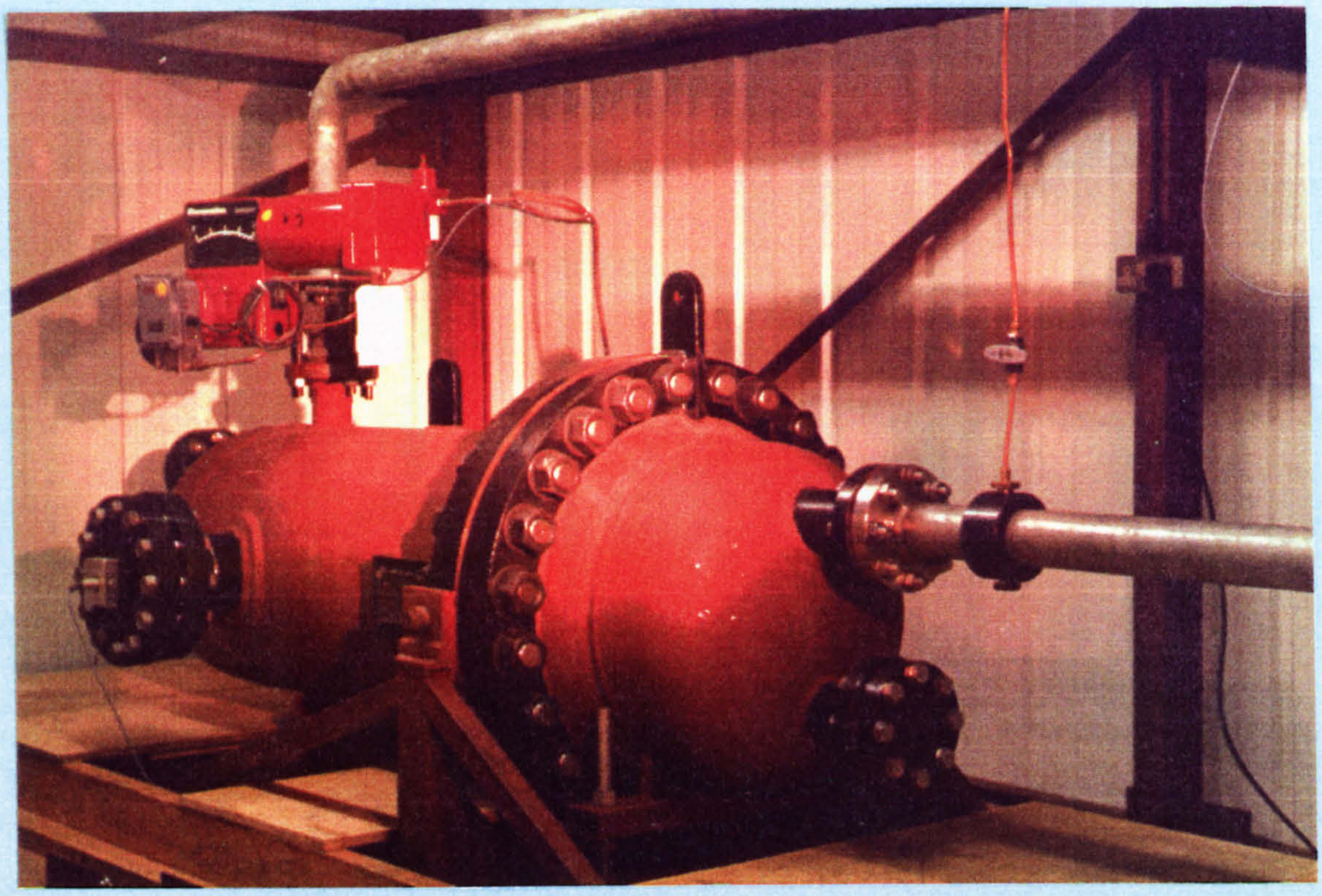


Figure 6.1.10 View of slug catcher/air-liquid separator located on the top floor of the control hut.

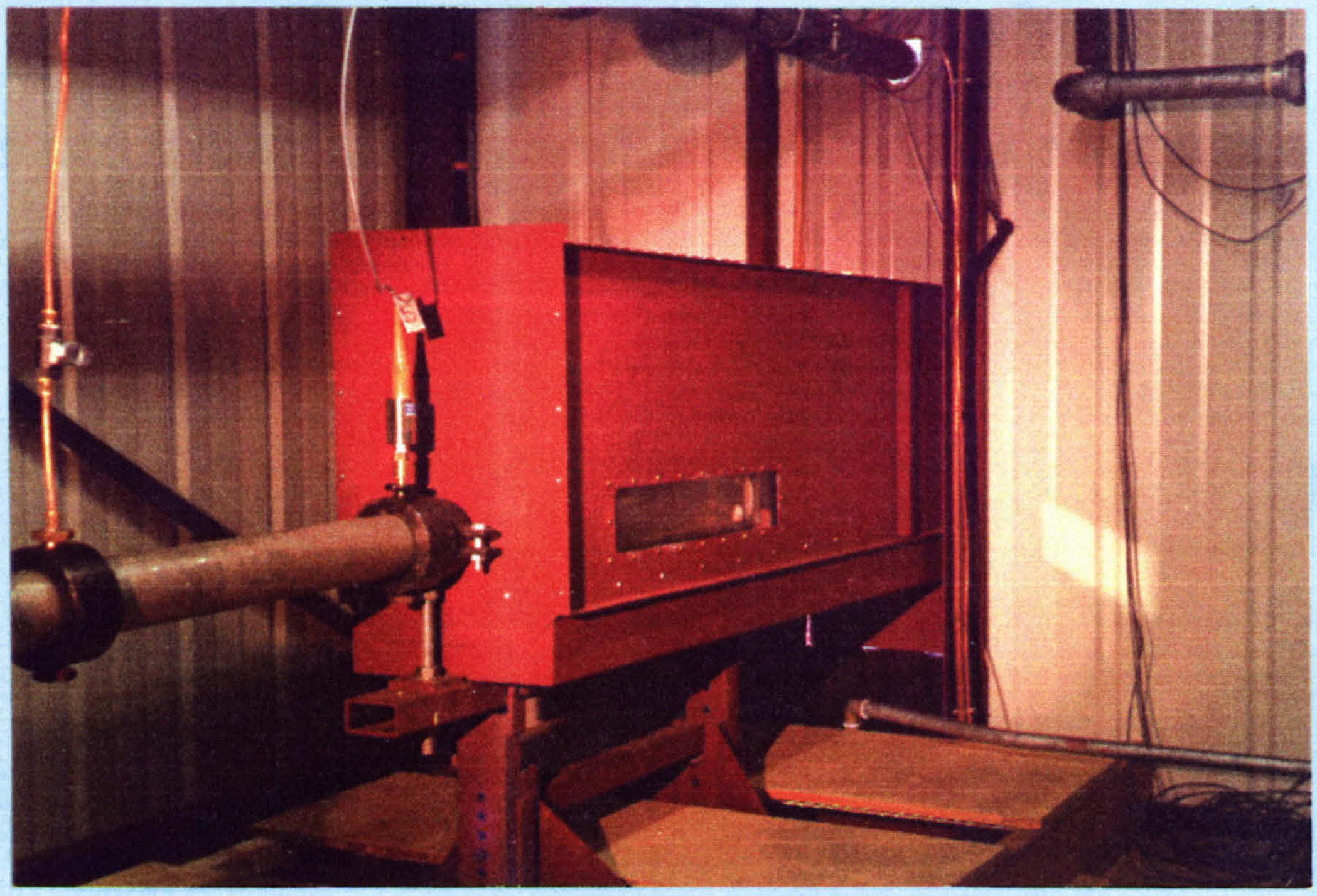


Figure 6.1.11 View of the visualisation section (in containment box) located on the top floor of the control hut.

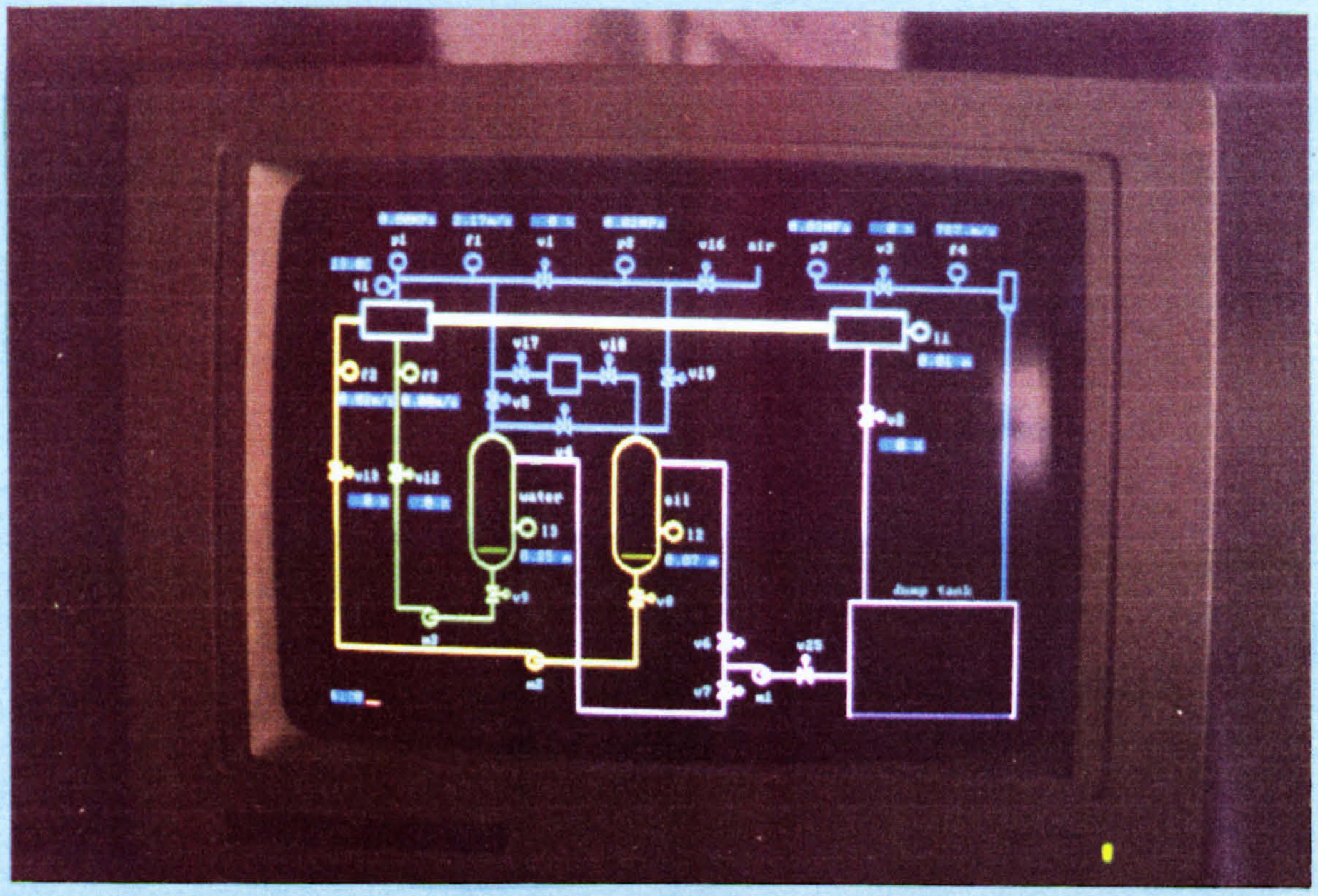


Figure 6.1.12 View of computer display of facility control system located on the ground floor of the control hut.

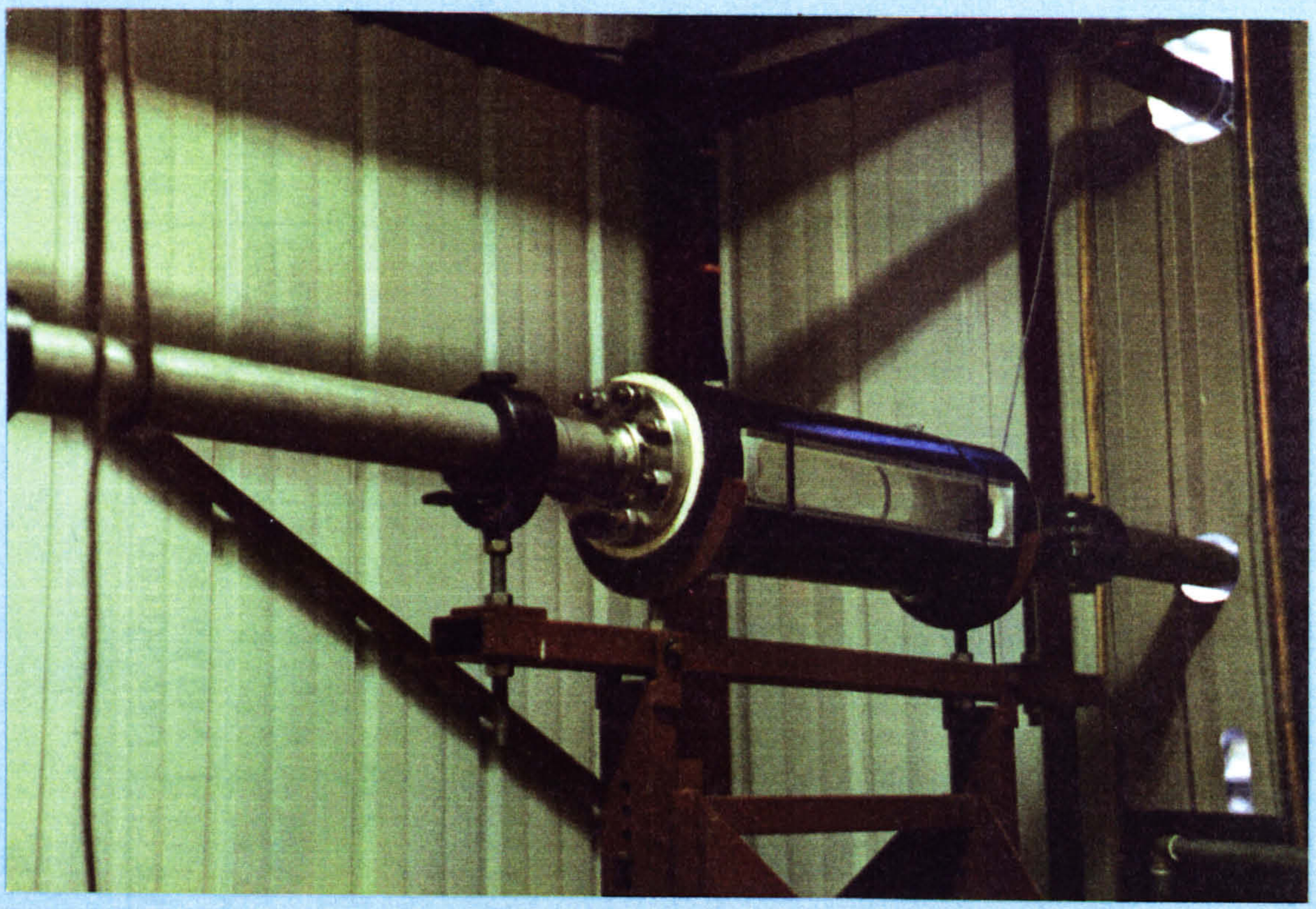


Figure 6.1.13 Visualisation section.

	EXPLOSIONS		FIRES		UNIGNITED RELEASES		MECHAN-ICAL		NUISANCES	
	1 INTER-NAL EX-PLOSION	2 EXTER-NAL EX-PLOSION	3 VAPOUR FIRES	4 LIQUID FIRES	5 CONTA-MINA-TION	6 POLLU-TION	7 PROJEC-TILES	8 FALLING OBJECTS	9 NOISE	10 POLLU-TANT
A ENVIRON-MENT	–	–	–	–	–	–	–	–	*	–
B BUILDINGS	–	–	–	–	–	–	–	–	–	–
C EQUIPMENT	–	–	–	–	–	–	*	* *	–	–
D PUBLIC	–	–	–	–	–	–	*	*	*	–
E EMPLOYEES	–	–	–	–	–	–	* *	***	*	–
F OPERATORS	–	–	–	–	–	–	***	* *	* *	–

Table 6.1.1 Hazard–target interactions pertinent to high pressure air–water experiments on the WASP facility.

PUBLIC ACCESS								1D7	1D8		
PARTS DETACH	3E8	3F7	2C8	2E7	2F8		1C7	1D7	1D8		
LOOSE OBJECTS	3E8		2C8		2F8		1C7		1D8		
KINETIC ENERGY		3F7		2E7				1D7			
PREPARATION NOISE						2F9				1D9	1E9
OPERATION NOISE						2F9				1D9	1E9

Table 6.1.2 Attributes associated with why a hazard poses a threat to a target.

MECHANICAL FAILURE	3E8	3F7	2C8	2E7	2F8		1C7	1D7	1D8		
MAINTENANCE	3E8		2C8		2F8				1D8		
POTENTIAL ENERGY	3E8		2C8		2F8				1D8		
INCREASE INTER-NAL PRESSURE		3F7		2E7			1C7	1D7			
ASSEMBLY ERROR		3F7		2E7			1C7	1D7			
VESSEL CHARGING						2F9				1D9	1E9
DEPRESSURISATION						2F9				1D9	1E9
PUMP OPERATION						2F9				1D9	1E9
VIBRATION						2F9				1D9	1E9

Table 6.1.3 Attributes associated with how a hazard poses a threat to a target.

PRESSURE		3F7		2E7		2F9	1C7	1D7		1D9	1E9
TARGET LOCATION	3E8	3F7	2C8	2E7	2F8	2F9	1C7	1D7	1D8	1D9	1E9
TARGET VULNERABILITY	3E8	3F7	2C8	2E7	2F8	2F9	1C7	1D7	1D8	1D9	1E9
OBJECT/WEIGHT LOCATION/HEIGHT	3E8		2C8		2F8				1D8		
LOCATION OF PROJECTILES		3F7		2E7			1C7	1D7			
VESSEL CAPACITY						2F9				1D9	1E9
CHARGING TIME						2F9				1D9	1E9
VAPOUR FLOWRATE						2F9				1D9	1E9
DURATION OF EXPERIMENTS						2F9				1D9	1E9

Table 6.1.4 Attributes associated with where a hazard poses a threat to a target.

6.2 FACILITY COMMISSIONING

The commissioning of the WASP facility took six months to complete and document. Each part of the rig (valves, instruments, pumps etc) was first operated in isolation, calibrated, performance assessed against design intent and problems rectified. Then sub–systems of the rig were tested at low pressure, and performance adjusted. For example, Figures 6.2.1 and 6.2.2 show sample signals obtained while adjusting the response of the water and air flow metering control systems to changes in set point.

Prior to the testing with the complete facility in operation a complete rig pressure test had to be carried out. Prior to this individual equipment items, such as pipe sections and the visualisation section, had to be hydrostatic pressure tested on site. The procedure was standard for each item of equipment: the pressure was raised to the test pressure (75 bar) and held for one hour at that pressure. Each test was inspected by the Project Director and witnessed by the Chemical Engineering Department Safety Manager. The complete rig pressure took two weeks to prepare and was completed on the 15th December 1989. The test pressure had to be limited to 43 bar due to the test pump having insufficient capacity to make up the liquid lost from leaks around the slug catcher flange at this pressure. This limits the rig working pressure to 29 bar until the slug catcher flange seal is replaced and a new pressure test carried out.

Following the complete rig pressure test, the facility was tested over the full range of air and liquid flowrates, with the rig pressure increased in stages to 20 bar. A number of modifications were made during this final testing and the operating instructions developed. The facility was available for operation with air and water at pressures up to 20 bar at the end of February 1990.

The completion of the commissioning phase was completed just prior to the present author terminating his studies.

Immediately after commissioning, the first series of experiments were carried out (reported recently by Mendes–Tatsis et al, 1992) in which data were obtained on flow patterns for air–water flows at up to 20 bar. This high pressure data was compared with

the flow prediction method of Taitel and Dukler (1976). Figure 6.2.3 shows the comparison made by Mendes–Tatsis et al (1982) with the Taitel and Dukler methods; plotting the Froude number against the Martinelli parameter. The Froude number F_r is defined by Equation 6.2.1 and the Martinelli parameter by Equation 6.2.2

$$F_r = \frac{U_G}{(Dg\cos\alpha)^{0.5}}\left(\frac{\varrho_G}{(\varrho_L - \varrho_G)}\right)^{0.5} \qquad (6.2.1)$$

$$X^2 = \frac{\left(\frac{dp}{dz}\right)_L}{\left(\frac{dp}{dz}\right)_G} \qquad (6.2.2)$$

where $(dp/dz)_L$ and $(dp/dz)_G$ are the frictional pressure gradients for the single–phase flow of the liquid and gas phases flowing alone in the pipe. Examination of Figure 6.2.3 shows a discrepancy between the predicted stratified/intermittent and intermittent/annular boundaries and the experimental data. However, the amount of data reported in the region of the transition boundaries is small and future studies will need to extend the coverage in these regions.

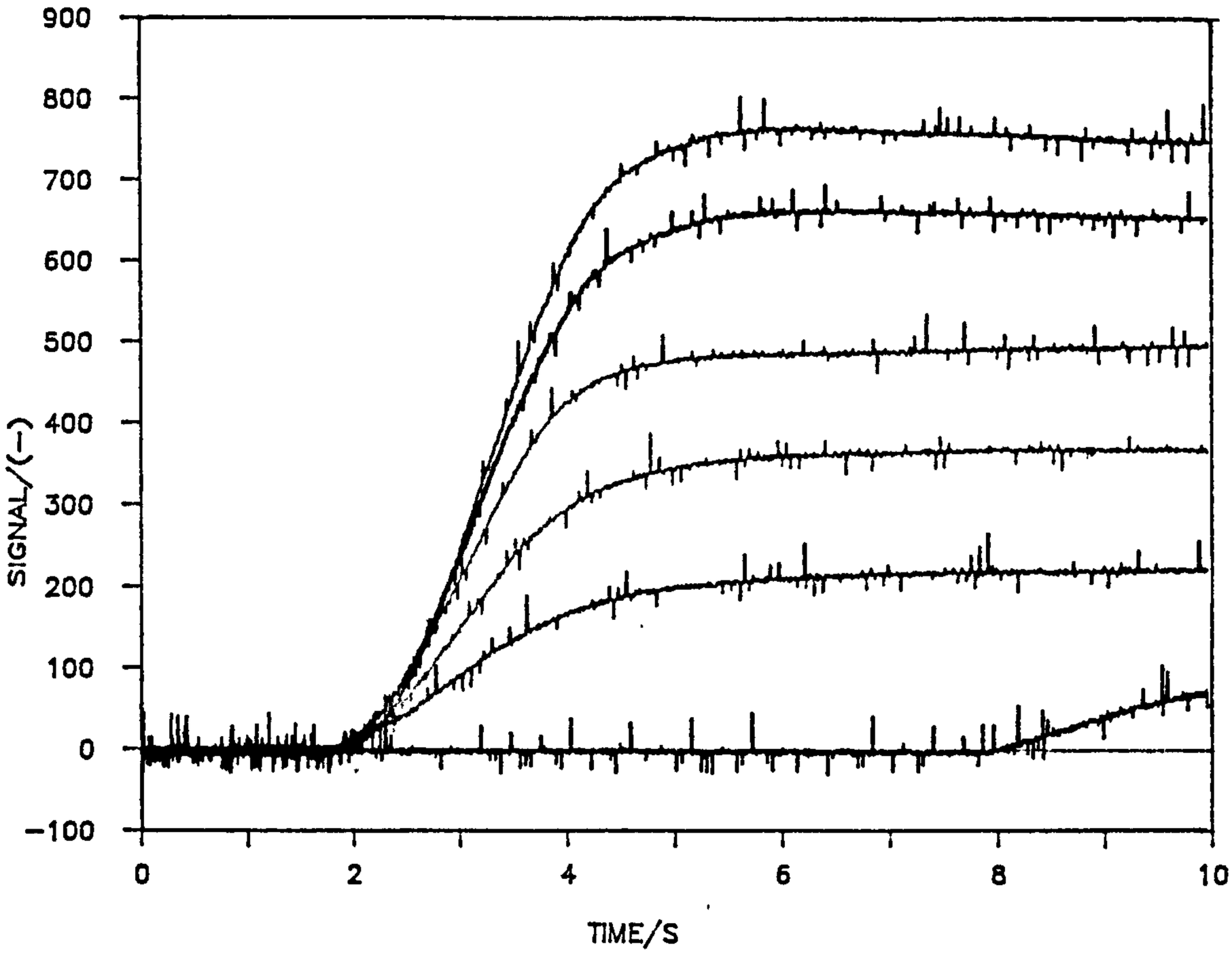


Figure 6.2.1 Sample signals from water metering system.

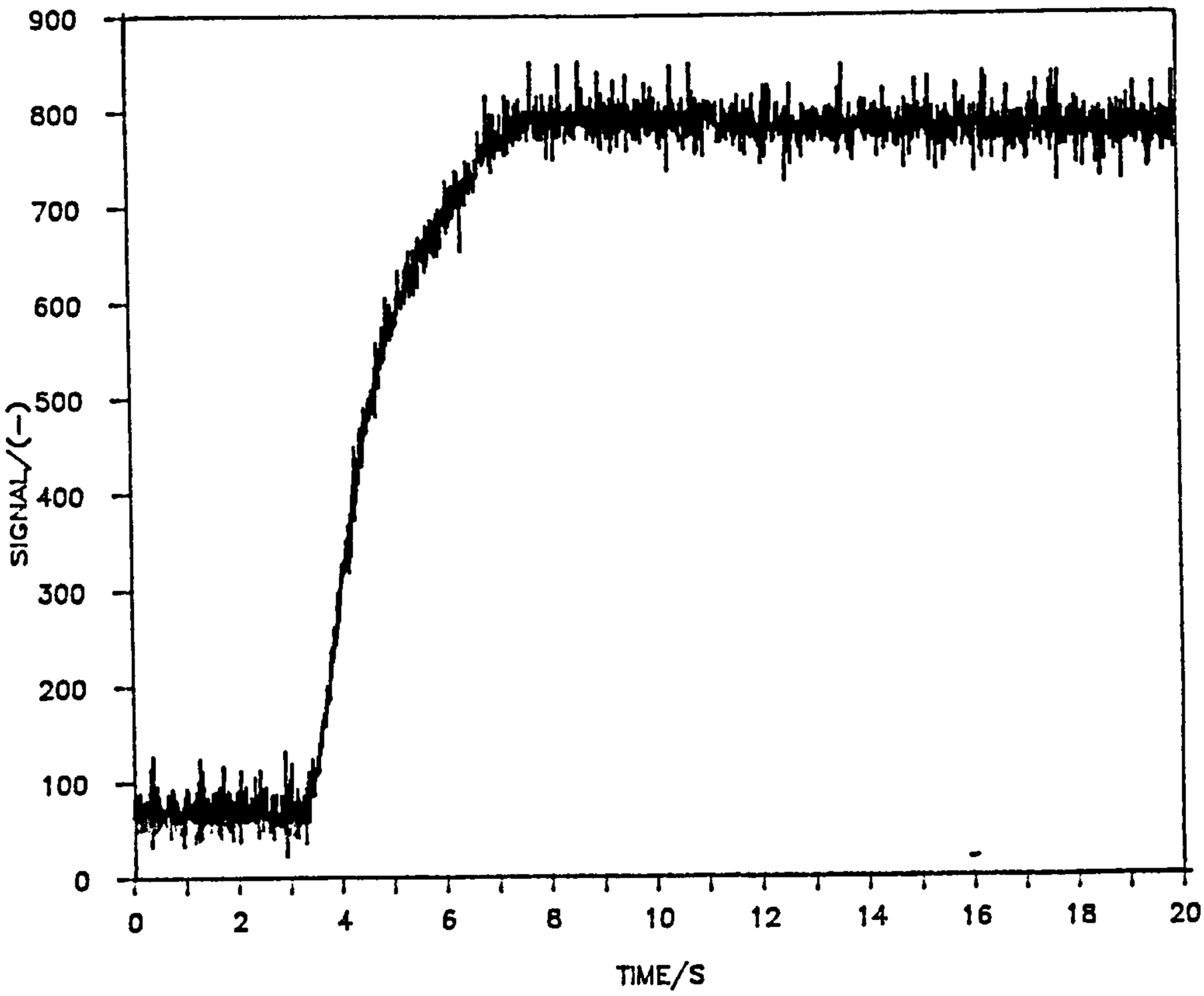


Figure 6.2.2 Sample signal from air metering system.

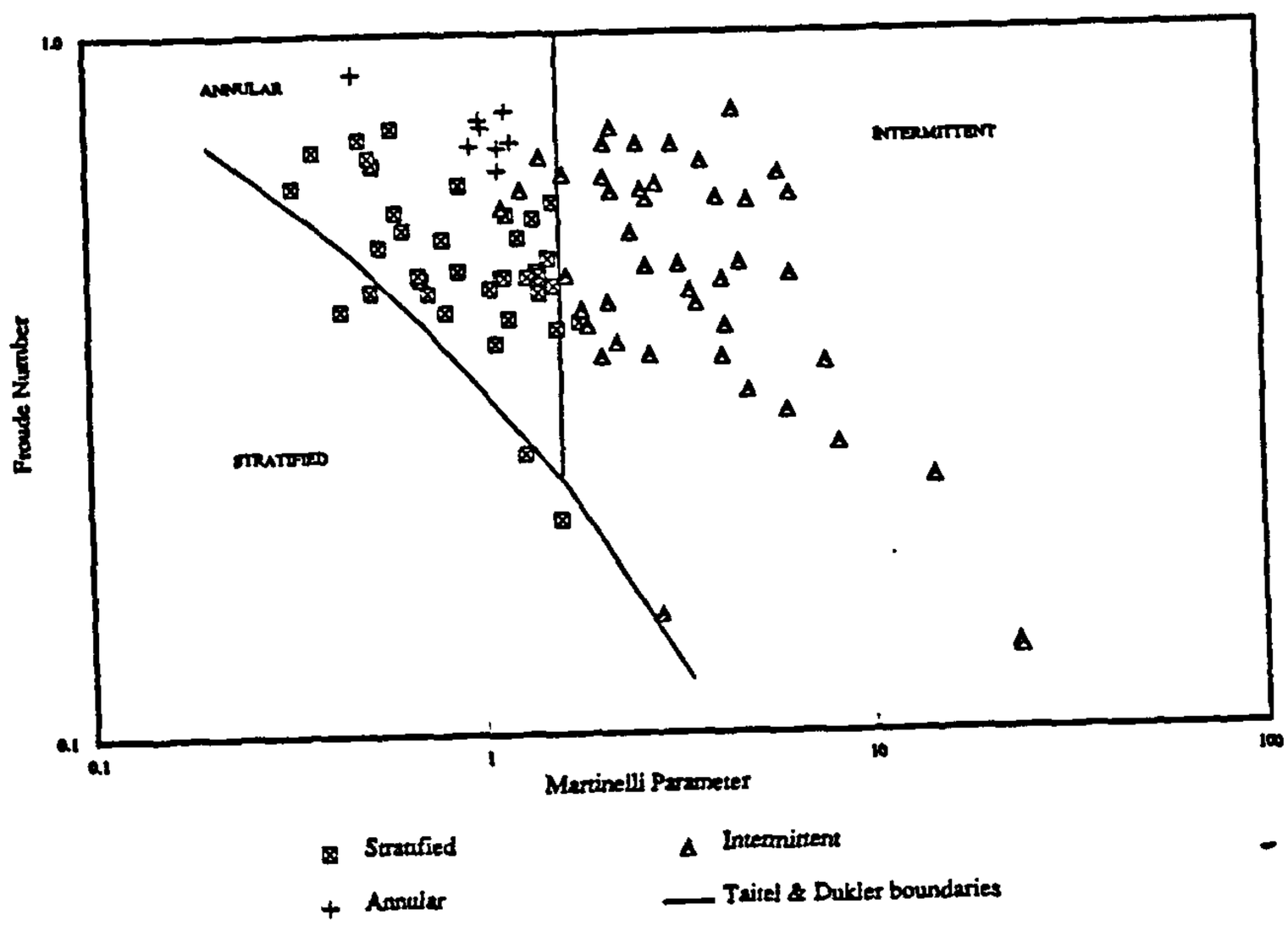


Figure 6.2.3 Flow regime data of Mendes–Tatsis et al (1992)

CHAPTER 7

CONCLUSION AND RECOMMENDATIONS

In Chapter One the general objectives of the present work were stated. In this Chapter progress made against those objectives is summarised and the requirements for future research indicated.

7.1 PIPE GEOMETRY EFFECTS

The stated objective was to investigate the effect of entrance geometry and pipe topography on intermittent flow characteristics.

The influence of pipeline geometry on intermittent characteristics has been studied in the present work, with experimental investigations of the effect of entrance geometry, pipe diameter, and small risers in the flowline. The importance of geometry on intermittent characteristics has been shown to be significant, especially in the economically important case of terrain induced severe slugs.

The present work has shown that the inlet geometry has a significant effect on slug frequency and the stratified to intermittent transition in the developing flow seen in the 10 m low pressure test section. The prediction of the stratified flow to intermittent flow transition boundary is of major importance to designers of multiphase pipelines. In the present studies, comparison with experimental data has shown that the theoretical stratified to intermittent transition criteria of Taitel and Dukler (1976) cannot predict the transition for an engineering scale pipeline. The transition boundary between stratified and intermittent flow has also been shown to be sensitive to the presence of a small riser in an otherwise horizontal pipe. Terrain induced slugs can cause significant operational problems for offshore oil and gas processing facilities. The use of the TRAC code to predict the occurrence and frequency of terrain induced slugs for the geometry of a declined pipe connected to a riser has been successfully demonstrated; this indicates the power of the TRAC code in simulating complex, time varying compressible two–phase flows.

It is recommended that experiments using the facility described in Chapter 6 be carried out to examine the persistence of the differences induced by inlet geometry as a function of pipelength in developing flow and in the developed flow region. It is also recommended that the new facility be used to investigate the transition boundaries to intermittent flow and intermittent flow characteristics in sloping pipes and undulating terrain since these are not yet well characterised. Clearly, the first experiments on the new facility should be with straight horizontal and inclined tubes. However, flow mechanisms should also be studied in the facility with the test section configured to give peaks and valleys.

7.2 ASPECTS OF INTERMITTENT FLOW

The stated objective was to develop novel experimental and theoretical approaches to individual aspects of intermittent flow.

New experimental techniques developed for, and critical analysis of, individual aspects of intermittent flow characteristics were presented in this work.

The models available for representing the slug tail were discussed and a novel experimental technique, the "pushout" experiment, developed to allow slug tail models to be validated for the case of unaerated slugs. Comparison of the models against experimental data shows that the model of Ruder et al (1988) best represents the shedding rate of the slug tail. Another innovative experimental technique, the artificial slug experiment, was developed and used to examine the growth and decay of slugs under controlled flow conditions. The results indicate the potential of this experimental technique for obtaining the flow conditions for stability of slugs and slug growth/decay rates, avoiding the limitations of the concept of a time average steady–state slug.

Also, the use in the present work of matched refractive index tube walls gave a remarkable increase in the clarity of visual observations and, along with the high speed video equipment, enabled a cyclic entrapment process to be observed at the slug front. To the present author's knowledge, this is the first time that this cyclic bubble entrapment mechanism has been reported. It would seem that explanations of voidage based on

simplistic turbulence–based models like those of Barnea et al (1985) are not necessarily valid. The high speed video was also used in the present work to observe slug initiation on an initially stratified gas–liquid interface. This visualisation is recorded in the present work and its implications for slug frequency modelling discussed. It is suggested that not only does the rebuild time of the stratified layer following slug formation determine slug frequency, but that slug frequency is also limited by the pressure developed by preceding slugs.

The artificial slug technique (see Section 5.2) could find many applications in the future; for example, the interaction of two artificial slugs could be used in the longer length of the WASP facility to study intermittent characteristics such as slug voidage. Push–out experiments in the 10 m low pressure test section identified the need for a longer pipe to extend the validity of the technique beyond a gas superficial velocity of approximately 2.5 m/s. It is recommended that the WASP facility be used to examine the shedding rate of the slug tail at higher gas flowrates.

For a complete mechanistic model of intermittent flow it is necessary to develop models for slug frequency and gas entrapment at the slug front. In the future, extensive experimental examination of the gas entrapment mechanism at the slug front should be carried out in the developed region of a pipe to ascertain the range of validity of the gas entrapment mechanism. Prediction of slug frequency is a major problem that requires significant investment of resources to resolve further. Future development of the model of Tailtel and Dukler should first assess the underlying mathematics associated with the stability problems described in the present work and refine the physics of the model. The effect on slug frequency of the interaction of preceding slugs and slug initiation mechanisms could be examined in the future through the development of a transient model for flow of multiple slugs in a pipeline.

7.3 FLUID PROPERTY EFFECTS

The stated objective was to study the effect of pressure and liquid properties on intermittent flow characteristics and the stratified–intermittent flow transition.

As part of the present studies a general purpose multiphase flow facility, WASP (Water, Air, Sand, Petroleum) was designed, constructed and commissioned at Imperial College, London University to allow investigation of the flow of oil, water and air.

While there is a significant amount of literature on gas–liquid flows in horizontal pipes, there is a lack of data at high pressure and for liquids other than water in fully developed flow. For example, most of the data available in the literature on slug initiation and frequency is for low pressure air–water experiments. The limited data available from higher pressure pipelines, indicates that the effect of pressure is very important. For instance, Wu et al (1987) observed that the experimental transition between stratified flow and intermittent flow is at much higher liquid flowrates than predicted by the method of Taitel and Dukler (1976) for gas–condensate flow at 75 bar in a 8 inch pipe. Future work should obtain data with the WASP facility for flow transition, slug frequency, slug velocity and pressure drop for air–water and air–oil flows over a range of pressures. Such data could be used to assess present models and develop new models of two–phase gas–liquid intermittent flow.

REFERENCES

Andreussi P., Paglianti A., Vatistas N., Minervini A. and Bendiksen K. Analysis of slug flow in near horizontal and horizontal pipes. Multiphase Flow Engineering, Memonier Presentate Alle Giorate di Studio di Bologno, 29–30 th September, 1988.

Andritsos N. and Hanratty T. J. Influence of interfacial waves in stratified gas–liquid flows. AIChE J., Vol 33, No 3, pp 444453, March 1987.

Azzopardi B. J., Govan A. H., and Hewitt G. F. Two–phase slug flow in horizontal pipes. Pipelines Symposium, Utrecht, Netherlands, Vol 2, pp 213–226, 6–8 Nov 1985.

Barnea D., Taitel T. and Dukler A. E. Modelling flow pattern transitions for steady upward gas–liquid flow in vertical tubes. AIChE J. , Vol 26, no 3, 1980.

Barnea D. and Brauner N. Holdup of the liquid slug in two–phase intermittent flow. Int. J . Multiphase Flow, Vol II, no 1, pp 43–49, 1985.

Beggs H. D. and Brill J. P. A study of two–phase flow in inclined pipes J. Pet. Tech, Vol 25, pp 607–617, May 1973.

Bendiksen K., Malnes D. and Nuland S. Severe slugging in two–phase flow systems. Selected Topics in Two–phase Flow, Trondheim, Norway, Lecture, pp 38, 29–30 th April 1982.

Bendiksen K.H., and Malnes D. Experimental data on hysterisis effects in the transition from stratified to slug flow in horizontal tubes. Two–Phase Flow Group Meeting, Southampton, UK, Paper A3. pp 13. 4th–7th June 1985.

Benjamin T. B. Gravity currents and related phenomena. J. Fluid Mechanics, Vol 31, pp209–248. 1968.

Black P., Leslie D., and Hewitt G. F. Nuclear Engineering and Design, Vol 108, pp121–136, 1988.

Boe A. Severe slugging characteristics, Two–phase flow lecture series no. 2, Trondheim, March 12–13, 1981

Bonnecaze R. H., Erskine J. R., and Greskovick E. J. Holdup and pressure drop for two–phase slug flow in inclined pipelines, AIChE J, Vol 17, no 5 , 1971

Brotz. Uber die vorausberechnung der absorptiongeshwindig keit von gasen in stro-
mendon flussigkeitsschichten, Chem. Ing. Tech. ,Vol 26, pp 470, 1954.

Brown R. C., Andreussi P., Zanelli S., Can. J. Chem. Eng, Vol 56, pp754–757. 1978.

Coney M. W. E., The analysis of a mechanism of liquid replenishment and draining in horizontal two–phase flow, Int. J. Multiphase Flow, Vol I, pp 647–669, 1974.

Davies R. M. and Taylor G. I. The mechanics of bubbles rising through extended liquids and through liquids in tubes, Proc. Roy. Soc. London, Vol 200, pp 375–390, 1950.

Delhaye J. M. Local measurement techniques for statistical analysis. Chapter 10.3 of Handbook of Multiphase Systems, Ed. G. Hetsroni, Hemisphere Publishing Comp, New York, 1982.

Dukler A.E. and Wicks M. Entrainment and pressure drop in concurrent gas–liquid flow. AICHE J., Vol 6, pp463–468. 1960.

Dukler A. E., Wicks, M. and Cleveland R. G. Frictional pressure drop in two–phase flow: an approach through similarity analysis, AIChE J., Jan 1964.

Dukler A.E. and Hubbard M. G. A model for gas liquid slug flow in horizontal and near horizontal tubes, Ind. Eng. Chem. Fund. , Vol 14, no 4, pp 337, 1975.

Dukler A. E., Barnea D. and Taitel Y. Modelling flow pattern transition for steady upward gas–liquid flow in vertical tubes AIChE J., Vol 26, no 3, 1980.

Dukler A. E., Moalem Maron D. and Brauner N. A physical model for predicting the minimum stable slug length. Chem. Eng. Sci. , Vol 40, no 8, pp 1379–1385, 1985.

Dumitresu D. T. Stromung en einer luftblase in scholten rohr SMM, Vol 23, no 3, pp 139–149, 1943.

Fernandes R. C., Semiat R. and Dukler A. E. Hydrodynamic model for gas–liquid flow in vertical tubes AIChE J., Vol 129, no 6, pp 981, 1983.

Ferschneider G. Ecoulements diphasiques gaz–liquide a pouches et a bouchons en conduites. Revue de l Institut Francais du Petrole, Vol 38, Number 2, 1983.

Fogwell T. W., Window materials for use with flow visualisation techniques. AERE R12313. 1986.

Fuchs P. The pressure limit for terrain slugging. 3rd International Conf. on Multiphase Flow, The Hague, Netherlands, 18–20 May, Paper B4, 1987.

Garcia R. G. Etude experimentale du taux de gaz local en ecoulement diphasique gaz–liquide horizontal en configuration a porches. PhD Thesis, University of Paris. 1980.

Gardner G. C., Drainage of a horizontal pipe. A test for computer codes studying the hot leg of a PWR. CEGB Internal Memorandum TPRD/L/ES/270/M85 (Confidential) 1985.

Govier G. W., Omer M.M. The horizontal pipeline flow of air–water mixtures. Can. J. Chem. Eng, Vol 40, pp 93–104. 1962.

Gregory G. A. and Scott D. S., Correlation of liquid slug velocity and frequency in horizontal co–current gas–liquid slug flow AIChE, Vol 15, no 6, pp 933, 1969.

Gregory G. A., Nicholson, M. K. and Aziz, K. Correlation of the liquid Volume fraction in the slug for horizontal gas–liquid slug flow Int. J. Multiphase Flow, Vol 4, pp 33–39, 1978.

Greskovich E. J. and Shrier A.L. AIChEJ., Vol 17, pp 1214. 1971.

Greskovich E. J. and Shrier A.L. Slug frequency in horizontal gas–liquid slug flow Ind. Eng. Chem, Process Des Develop, Vol II, no 2, pp 317–318, 1972.

Griffith P. and Wallis G. B. Two–phase slug flow, Trans ASME J. Heat Transfer, August 1961.

Hewitt G. F., Martin C. J. and Wilkes N. S. Experimental and modelling studies of annular flow in the region between flow reversal and the pressure drop minimum PhysicoChemical Hydrodynamics, Vol 6, No 1/2, pp 69–86, 1985.

Hewitt G. F. Regime modelling: stratified, plug or slug flows. Workshop on modelling of two–phase flow systems, Univ. of California, Santa Barbara, August 1–15 1986.

Hubbard M. G. PhD thesis, University of Houston, 1965.

Hughmark G. A. Holdup and heat transfer in horizontal slug gas–liquid flow. Chem. Eng. Sci. , Vol 20, pp 1007–1010, 1965.

Jeffrey Quasilinear hyperbolic systems and waves. Pitman Publishing. London. 1976.

Jepson W. P. Transition to slug flow in horizontal conduit. AERE R12813. 1987.

Jepson W. P., Taylor R. E., Evans N. Slug flow and its transitions in large diameter pipes. AERE R12992. 1988.

Kordyban E. S A flow model for two–phase slug flow in horizontal tubes Trans ASME J. Basic Eng, Dec, pp 613, 1961.

KvernVold O., Vindoy V. and Sonivedt T. Velocity distribution in horizontal slug flow Int. J. Multiphase Flow, Vol 10, no 4, pp 441–457, 1984.

Liles D. R. An advanced best estimate computer program for pressurised water reactor thermal–hydraulic analysis Los Alamos, NUREG/CG–3858 LA–10157–MS, 1987.

Lin P. Y., Flow regime transition in horizontal gas–liquid flow. PhD Thesis, Univ. of Illinois. 1985.

Lin P. Y., Hanratty T. J., Int. J. Multiphase Flow, Vol 13, pp 549–563. 1987.

Linga H. Terrain slugging phenomena. Some experimental results obtained at the SINTEF two–phase flow laboratory 3 rd International Conference on Multiphase Flow, The Hague, Netherlands, pp 37–53, 18–20th May 1987.

Mahaffy J. H. A stability enhancing two–step method for fluid flow calculation J. Compt. Phy., Vol 46, pp 329–341, 1982.

Mendes–Tatsis M. A., Hall A. R. W., Davies S. R. and Hewitt G. F. Experimental studies of multiphase flows at high pressure. European Two–phase Flow Group Meeting, Stockholm, June 1–3, Paper F3. 1992.

Miller N. and Mitchie R. E. Measurement of local voidage in liquid gas two–phase flow systems using an universal probe. J. Brit. Nucl. Energy Soc.,9, pp 94–100. 1970.

Miya, M., Properties of roll waves, PhD Thesis, Univ Illinois. 1970.

Moalem Maron D., Yacoub N. and Brauner N. New thoughts on the mechanism of gas–liquid slug flow Letters in Heat Mass Transfer, Vol 9, pp 33–342, 1982.

Moissis R. and Griffith P. Entrance effects in a two–phase slug flow Trans ASME J. Heat Transfer, pp 92, Feb. 1962.

Nicklin D. J., Wilkes J. O. and Davidson J. T. Two–phase flow in vertical tubes Trans. Inst. Chem. Engrs, Vol 40, 1962.

Nicholsen M.K., Aziz K., Gregory G. A. Intermittent two–phase flow in horizontal pipes: Predictive methods. Can. J. Chem. Eng, Vol 56, pp 653–663. 1978.

Nydal O. J. Measurements of void fraction in liquid slugs Multiphase Flow Engineering, Memonier Presentate Alle Giorate di Studio di Bologno, 29–30 th September 1988.

Pacini F., Paglianti A., Andreussi P., A necessary condition for the onset of slug flow in near–horizontal pipes. Proceedings of the 5th International Conference on Multiphase Production, Elsevier Science Publishers, pp 553–564. 1991.

Pots B. F. M., Bromilow I. G. and Konijn M. J. W. F. Severe slug flow in offshore flowline/riser systems SPE 13723, SPE Middle East Oil Technical Conference and Exhibition, pp 347–356, Bahrain, March 11–14 1985.

Ruder Z., Hanratty P. J. and Hanratty T. J. Necessary conditions for the existence of stable slugs Int. J. Multiphase Flow, Vol 15, no 2, pp 209–226, 1989.

Schmidt Z., Brill J.P. and Beggs H. D. Experimental study of severe slugging in a two–phase flow pipeline–riser pipe system SPE 8306, 54 th Annual Fall Technical Conference and Exhibition of the Society of Petroleum Engineers of AIME, pp 407–414, September 23–26 1979.

Schmidt Z., Doty D. R. and Dutta–Roy K. Severe slugging in offshore pipeline riser–pipe systems. Society of Petroleum Engineers Journal, pp 27–38, February 1985.

Sen N. and Ghosal S. Prediction of pressure drop in two–phase co–current gas–liquid horizontal slug flow J. Inst. Eng(India), Vol 63, 1982.

Singh G. and Griffith P. Determination of the pressure drop optimum pipe size for a two–phase slug flow in an inclined pipe. J. Eng. Industry, Vol 92, pp 717–726, Nov 1970.

Stoker J. J. Water Waves Interscience Publishers, New York. 1957.

Taitel Y. and Dukler A. E. A model for predicting flow regime transitions in horizontal and near horizontal gas–liquid flow. AIChE J. , Vol 22, no 1, Jan 1976.

Taitel Y. and Dukler A. E. Model for slug frequency during gas–liquid flow Int. J. Multiphase Flow, Vol 3, pp 588–596, 1977.

Taitel Y. Stability of severe slugging Int. J. Multiphase Flow, Vol 12, no 2, pp 203–217, 1986.

Taitel Y. and Dukler A.E. Effect of pipe length on the transition boundaries for high viscosity liquids. Int. J. Multiphase Flow, Vol 13, pp 577–581 1987.

Taylor R. E., Evans N. Slug flow in a 153 mm diameter horizontal pipe. AERE R–13572. 1989.

Vakilotojjar M. and Javdani K. Bubble frequency in gas–liquid slug flow in vertical tubes. Chem. Eng. Sci. , Vol 35, pp 2356–2358, 1980.

Vermeulen L. R. and Ryan J. T. Two–phase slug flow in horizontal and inclined tubes Can. J. Chem. Eng. , Vol 49, April 1971.

Walklate P. and Martin C. J. The measurements of liquid phase velocity profiles in vertical two–phase flow. 13 th HTFS Res. Symp. , University of Bath, UK, Paper RS499, 13 th September 1983.

Weisman J., Duncan D., Gibson J. and Crawford T., Int. J. Multiphase Flow. Vol 5, pp 437–462. 1979.

Wu H. L., Pots B. F. M., Hollenberg J. F. and Meerhoff R. Flow pattern transitions in two–phase gas/condensate flow at high pressure in an 8–inch horizontal pipe. 3rd International Conf. on Multiphase Flow. The Hague, Netherlands, Paper A2, 18–20 May 1987.

Zuber N. and Hench J. Steady state and transient void fraction of bubbling systems and their operating limit. Part I: steady state operation General Electric Report, 62GL100, 1962.

BIBL
LONDON
UNIV